

DINUCLEAR COMPLEXES OF CU(I), PD(I), PT(I)  
AND RU(I): CATALYSTS FOR THE  
ELECTROCHEMICAL REDUCTION OF CO<sub>2</sub>.

by

Garth Hereward Cripps B.Sc. (Hons.) (Natal)

A thesis submitted in partial fulfilment of the requirements for the degree of Doctor of  
Philosophy in the Faculty of Science, University of Natal, Pietermaritzburg.

School of Chemical and Physical Sciences

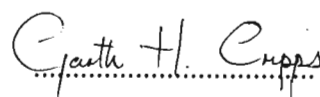
University of Natal

Pietermaritzburg

December 2001

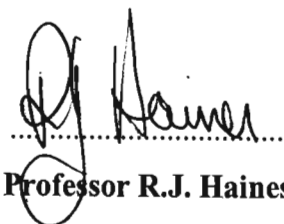
## DECLARATION

I hereby certify that this research is the result of my own investigation that has not already been accepted in substance for any degree and is not being submitted in candidature for any other degree.

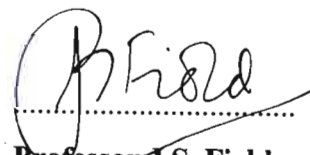


**G.H. Cripps**

We hereby certify that this statement is correct.



**Professor R.J. Haines**  
Supervisor



**Professor J.S. Field**  
Co-Supervisor

School of Chemical and Physical Sciences  
University of Natal  
Pietermaritzburg  
December 2001

## Contents

---

Acknowledgements	5
Summary	6
Abbreviations	9
Structural Formula of Ligands	11
List of Compounds	12
Chapter 1. Introduction	13
1.1. Electrochemical Reduction of Carbon Dioxide	14
1.2. Thermodynamics of the Electrochemical Reduction of Carbon Dioxide	15
1.3. Homogeneous Electrocatalytic Reduction of Carbon Dioxide	16
1.3.1. Copper Complexes as Electrocatalysts	17
1.3.1.(i) $[\text{Cu}_2(\mu\text{-Ph}_2\text{Pbpy})_2(\text{CH}_3\text{CN})_2](\text{PF}_6)_2$	17
1.3.2. Palladium and Platinum Complexes as Electrocatalysts	18
1.3.2.(i) $[\text{PdCl}_2\text{L}_2]$ (L = pyrazole, 4-methylpyridine and 3-methylpyrazole)	18
1.3.2.(ii) $[\text{Pd}(\text{PPh}_3)_2\text{L}]^{2+}$ (L = substituted quinoline, bipyridine and phenanthroline)	19
1.3.2.(iii) $[\text{Pd}(\text{triphos})(\text{solvent})](\text{BF}_4)_2$	20
1.3.2.(iv) $[\text{Pd}_2(\mu\text{-eHTP})(\text{CH}_3\text{CN})_2](\text{BF}_4)_4$	23
1.3.3. Ruthenium Complexes as Electrocatalysts	24
1.3.3.(i) <i>cis</i> - $[\text{Ru}(\text{bpy})_2(\text{CO})\text{H}]^+$	24
1.3.3.(ii) $[\text{Ru}(\text{bpy})_2(\text{CO})\text{Cl}]^+$ and $[\text{Ru}(\text{bpy})_2(\text{CO})_2]^{2+}$	25
1.3.3.(iii) $[\text{Ru}(\text{bpy})(\text{trpy})(\text{CO})]^{2+}$	26
1.3.3.(iv) $[\text{Ru}(\text{bpy})_2(\text{qu})(\text{CO})]^{2+}$	27
1.3.3.(v) $[\text{Ru}(\text{bpy})(\text{napy})_2(\text{CO})_2](\text{PF}_6)_2$	29
1.3.3.(vi) $[\text{Ru}(\text{dmdbbpy})(\text{bpy})_2](\text{PF}_6)_2$ and $[\text{Ru}_2(\mu\text{-dmdbbpy})(\text{bpy})_4](\text{PF}_6)_4$	29
1.3.3.(vii) $[\text{Ru}(\text{H}_2\text{bibzim})(\text{tbbpy})_2]\text{Cl}_2$ , $[\text{Ru}(\text{bibzim})(\text{tbbpy})_2]$ and $[\{\text{Ru}(\text{tbbpy})_2\}_2(\text{bibzim})](\text{PF}_6)_2$	30
1.3.3.(viii) $[\text{Ru}(\text{bpy})(\text{CO})_2]_n$	31
1.4. Aims of this Work	33
Chapter 2. Synthesis and Characterisation of the Heterodifunctional Ligands 6-(diphenylphosphino)-2-(2-quinolyl)pyridine <b>I</b> and 6-[ethyl(phenyl)phosphino]-2,2'-bipyridine <b>II</b>	36
2.1. Introduction	36
2.2. Results and Discussion	38
2.2.1. Synthesis and Characterisation	38
2.2.2. NMR Spectroscopy of the Phosphorus-polypyridyl Ligands	40
2.2.3. Crystal Structure Determination of 6-(diphenylphosphino)-2-(2-quinolyl)pyridine <b>I</b>	50

2.2.4. Cyclic Voltammetry of the Phosphorus-polypyridyl Ligands	51
2.2.5. Extended Hückel Molecular Orbital Calculations	53
2.3. Experimental	55
Chapter 3. Dinuclear Complexes of Copper(I) Bridged by 6-[ethyl(phenyl)phosphino]-2,2'-bipyridine and 6-(diphenylphosphino)-2-(2-quinolyl)pyridine	59
3.1. Introduction	59
3.2. Results and Discussion	59
3.2.1. Synthesis and Characterisation of the Dinuclear Copper Complexes	59
3.2.2. Crystal Structure Determination of $[\text{Cu}_2(\mu\text{-Ph}_2\text{Ppyqn})_2(\text{CH}_3\text{CN})_2](\text{BF}_4)_2$ <b>1</b> and $[\text{Cu}_2\{\mu\text{-Et(Ph)Pbpy}\}_2(\text{CH}_3\text{CN})_2](\text{PF}_6)_2$ <b>2</b>	60
3.2.3. Electrochemical Behaviour of the Dinuclear Copper Complexes	65
3.2.4. Catalytic Properties Towards $\text{CO}_2$ Electrochemical Reduction	70
3.2.5. Extended Hückel Molecular Orbital Calculations	74
3.3. Experimental	79
Chapter 4. Homoleptic Dinuclear Complexes of Palladium(I) and Platinum(I) Bridged by 6-diphenylphosphino-2,2'-bipyridine, 6-(diphenylphosphino)-2-(2-quinolyl)pyridine and 6-[ethyl(phenyl)phosphino]-2,2'-bipyridine	81
4.1. Introduction	81
4.2. Results and Discussion	82
4.2.1. Synthesis and Characterisation of the Dinuclear Complexes	82
4.2.1.(i) $[\text{Pd}_2(\mu\text{-L})_2](\text{BF}_4)_2$ [L = $\text{Ph}_2\text{Pbpy}$ <b>3</b> , $\text{Ph}_2\text{Ppyqn}$ <b>4</b> and $\text{Et(Ph)Pbpy}$ <b>5</b> ]	82
4.2.1.(ii) $[\text{Pt}_2(\mu\text{-L})_2](\text{PF}_6)_2$ [L = $\text{Ph}_2\text{Pbpy}$ <b>6</b> , $\text{Ph}_2\text{Ppyqn}$ <b>7</b> and $\text{Et(Ph)Pbpy}$ <b>8</b> ]	83
4.2.1.(iii) $[\text{PtPd}(\mu\text{-L})_2](\text{PF}_6)_2$ [L = $\text{Ph}_2\text{Pbpy}$ <b>9</b> , $\text{Ph}_2\text{Ppyqn}$ <b>10</b> and $\text{Et(Ph)Pbpy}$ <b>11</b> ]	86
4.2.2. Crystal Structure Determination of $[\text{Pd}_2(\mu\text{-Ph}_2\text{Pbpy})_2](\text{BF}_4)_2$ <b>3</b>	88
4.2.3. Electrochemical Behaviour of the Dinuclear Complexes	91
4.2.3.(i) $[\text{Pd}_2(\mu\text{-L})_2](\text{BF}_4)_2$ [L = $\text{Ph}_2\text{Pbpy}$ <b>3</b> , $\text{Ph}_2\text{Ppyqn}$ <b>4</b> and $\text{Et(Ph)Pbpy}$ <b>5</b> ]	91
4.2.3.(ii) $[\text{Pt}_2(\mu\text{-L})_2](\text{PF}_6)_2$ [L = $\text{Ph}_2\text{Pbpy}$ <b>6</b> , $\text{Ph}_2\text{Ppyqn}$ <b>7</b> and $\text{Et(Ph)Pbpy}$ <b>8</b> ] and $[\text{PtPd}(\mu\text{-L})_2](\text{PF}_6)_2$ [L = $\text{Ph}_2\text{Pbpy}$ <b>9</b> , $\text{Ph}_2\text{Ppyqn}$ <b>10</b> and $\text{Et(Ph)Pbpy}$ <b>11</b> ]	93
4.2.4. Catalytic Properties Towards $\text{CO}_2$ Electrochemical Reduction	98
4.2.5. Extended Hückel Molecular Orbital Calculation On $[\text{Pd}_2(\mu\text{-Ph}_2\text{Pbpy})_2](\text{BF}_4)_2$ <b>3</b>	101
4.3. Experimental	104
Chapter 5. Dinuclear 2,2'-bipyridine Ligand Complexes of Ruthenium(I)	109
5.1. Introduction	109
5.2. Results and Discussion	109
5.2.1. Synthesis and Characterisation of $[\text{Ru}_2(\text{bpy})_2(\text{CO})_4(\text{CH}_3\text{CN})_2](\text{PF}_6)_2$ <b>12</b>	109
5.2.2. Electrochemical Behaviour of $[\text{Ru}_2(\text{bpy})_2(\text{CO})_4(\text{CH}_3\text{CN})_2](\text{PF}_6)_2$ <b>12</b>	114



5.2.2.(i) Oxidation	114
5.2.2.(ii) Reduction	118
5.2.3. Catalytic Properties of $[\text{Ru}_2(\text{bpy})_2(\text{CO})_4(\text{CH}_3\text{CN})_2](\text{PF}_6)_2$ <b>12</b> and the Resulting $[\text{Ru}(\text{bpy})(\text{CO})_2]_n$ Polymer Towards $\text{CO}_2$ Electrochemical Reduction	122
5.2.4. <i>In situ</i> Synthesis of $[\text{Ru}_2(\text{bpy})_2(\text{CO})_4(\text{CH}_3\text{CN})_2](\text{PF}_6)_2$ <b>12</b>	123
5.3. Summary	126
5.4. Experimental	127
Chapter 6. Dinuclear Pyrrole-substituted 2,2'-bipyridine Ligand Complexes of Ruthenium(I)	130
6.1. Introduction	130
6.2. Results and Discussion	133
6.2.1. Synthesis and Characterisation of $[\text{Ru}_2(\text{L})_2(\text{CO})_4(\text{CH}_3\text{CN})_2](\text{PF}_6)_2$ ( $\text{L} = \text{L}_{1-2}$ )	133
6.2.2. Electrochemical Behaviour of $[\text{Ru}_2(\text{L})_2(\text{CO})_4(\text{CH}_3\text{CN})_2](\text{PF}_6)_2$ ( $\text{L} = \text{L}_{1-4}$ )	137
6.2.2.(i) Reduction	137
6.2.2.(ii) Oxidation	142
6.2.2.(iii) Electroactivity of ppyr- $[\text{Ru}_2(\text{L})_2(\text{CO})_4(\text{CH}_3\text{CN})_2](\text{PF}_6)_2$ ( $\text{L} = \text{L}_2$ and $\text{L}_4$ )	144
6.2.3. Catalytic Properties Towards $\text{CO}_2$ Electrochemical Reduction of ppyr- $[\text{Ru}(\text{L})(\text{CO})_2]_n$ ( $\text{L} = \text{L}_2$ and $\text{L}_4$ )	146
6.2.4. $[\text{Ru}_2(\text{CO})_4(\text{CH}_3\text{CN})_6](\text{PF}_6)_2$ - a Potential Precursor for the Electrosynthesis of Mononuclear 2,2'-bipyridine Ligand Complexes of Ruthenium(II)	147
6.2.4.(i) <i>trans</i> ( $\text{CH}_3\text{CN}$ )- $[\text{Ru}(\text{bpy})(\text{CO})_2(\text{CH}_3\text{CN})_2]^{2+}$	147
6.2.4.(ii) <i>trans</i> ( $\text{CH}_3\text{CN}$ )- $[\text{Ru}(\text{L}_1)(\text{CO})_2(\text{CH}_3\text{CN})_2]^{2+}$	149
6.2.4.(iii) Catalytic Properties Towards $\text{CO}_2$ Electrochemical Reduction of ppyr- $[\text{Ru}(\text{L}_1)(\text{CO})_2]_n$	153
6.3. Summary	153
6.4. Experimental	154
Chapter 7. Dinuclear Complexes of Ruthenium(I) Bridged by 6-diphenylphosphino-2,2'-bipyridine and 6-(diphenylphosphino)-2-(2-quinolyl)pyridine	157
7.1. Introduction	157
7.2. Results and Discussion	159
7.2.1. Synthesis and Characterisation of the Dinuclear Ruthenium Complexes	159
7.2.2. Crystal Structure Determination of <i>cis</i> ( $\text{Ph}_2\text{Ppyqn}$ )- $[\text{Ru}_2(\mu\text{-Ph}_2\text{Ppyqn})_2(\text{CO})_2(\text{CH}_3\text{CN})_2](\text{PF}_6)_2$ , <i>cis</i> ( $\text{Ph}_2\text{Ppyqn}$ )- <b>19</b>	162
7.2.3. Cyclic Voltammetry of the Dinuclear Ruthenium Complexes	169
7.2.4. Catalytic Properties Towards $\text{CO}_2$ Electrochemical Reduction	175
7.2.5. Extended Hückel Molecular Orbital Calculations	177
7.3. Experimental	182

Chapter 8. Conclusions	186
Appendix A. General Experimental Details	191
A.1. Instrumentation	191
A.2. Experimental Techniques	191
A.3. Crystal Structure Determination	191
A.3.1. Data Collection	191
A.3.2. Structural Solution Refinement	192
A.4. Electrochemistry	192
A.4.1. Cyclic Voltammetry	193
A.4.2. Electrocatalytic Experiments	194
A.4.3. UV-vis Spectroelectrochemical Measurements	194
A.5. Extended Hückel Molecular Orbital Calculations	195
A. 6. Sources of Chemicals	196
A.6.1. Commercially Available Chemicals	196
A.6.2. Compounds Synthesised by Published Methods	196
Appendix B. Supporting Information	197
B.1. Crystallographic Supporting Information	197
B.1.1. Ph <sub>2</sub> Ppyqn I	197
B.1.2. [Cu <sub>2</sub> (μ-Ph <sub>2</sub> Ppyqn) <sub>2</sub> (CH <sub>3</sub> CN) <sub>2</sub> ](BF <sub>4</sub> ) <sub>2</sub> <b>1</b>	200
B.1.3. [Cu <sub>2</sub> {μ-Et(Ph)Pbpy} <sub>2</sub> (CH <sub>3</sub> CN) <sub>2</sub> ](PF <sub>6</sub> ) <sub>2</sub> <b>2</b>	205
B.1.4. [Pd <sub>2</sub> (μ-Ph <sub>2</sub> Pbpy) <sub>2</sub> ](BF <sub>4</sub> ) <sub>2</sub> <b>3</b>	210
B.1.5. [Ru <sub>2</sub> (bpy) <sub>2</sub> (CO) <sub>4</sub> (CH <sub>3</sub> CN) <sub>2</sub> ](PF <sub>6</sub> ) <sub>2</sub> ·(CH <sub>3</sub> CN) <sub>2</sub> <b>12</b> .	214
B.1.6. <i>cis</i> (Ph <sub>2</sub> Ppyqn)-[Ru <sub>2</sub> (μ-Ph <sub>2</sub> Ppyqn) <sub>2</sub> (CO) <sub>2</sub> (CH <sub>3</sub> CN) <sub>2</sub> ](PF <sub>6</sub> ) <sub>2</sub> , <i>cis</i> (Ph <sub>2</sub> Ppyqn)- <b>19</b>	218
B.2. Extended Hückel Molecular Orbital Calculations	231
B.2.1. Ph <sub>2</sub> Pbpy	231
B.2.2. Ph <sub>2</sub> Ppyqn I	234
B.2.3. Et(Ph)Pbpy II	237
B.2.4. [Cu <sub>2</sub> (μ-Ph <sub>2</sub> Pbpy) <sub>2</sub> (CH <sub>3</sub> CN) <sub>2</sub> ](PF <sub>6</sub> ) <sub>2</sub> , [Cu <sub>2</sub> (μ-Ph <sub>2</sub> Ppyqn) <sub>2</sub> (CH <sub>3</sub> CN) <sub>2</sub> ](BF <sub>4</sub> ) <sub>2</sub> <b>1</b> and [Cu <sub>2</sub> {μ-Et(Ph)Pbpy} <sub>2</sub> (CH <sub>3</sub> CN) <sub>2</sub> ](PF <sub>6</sub> ) <sub>2</sub> <b>2</b> .	240
B.2.5. [Pd <sub>2</sub> (μ-Ph <sub>2</sub> Pbpy) <sub>2</sub> ](BF <sub>4</sub> ) <sub>2</sub> <b>3</b>	243
B.2.6. <i>cis</i> (Ph <sub>2</sub> Pbpy)-[Ru <sub>2</sub> (μ-Ph <sub>2</sub> Pbpy) <sub>2</sub> (CO) <sub>2</sub> (EtCN) <sub>2</sub> ](PF <sub>6</sub> ) <sub>2</sub> and [Ru <sub>2</sub> (μ-Ph <sub>2</sub> Ppyqn) <sub>2</sub> (CO) <sub>2</sub> (CH <sub>3</sub> CN) <sub>2</sub> ](PF <sub>6</sub> ) <sub>2</sub> , <i>cis</i> (Ph <sub>2</sub> Ppyqn)- <b>19</b>	245
References	249

## Acknowledgements

There are a number of people to whom I express my thanks for the time and help that they willingly gave;

Professor Raymond J. Haines, for the supervision and support he provided throughout this project.

Professors John S. Field, I appreciate greatly his advice and encouragement.

Dr. Orde Q. Munro, whose advice on computational chemistry was indispensable, but more for answering the inevitable daily knock on his door and ensuing questions with insight and useful discussion.

Dr. Alain Deronzier, who welcomed me into LEOPR. (I hope you manage to visit South Africa one day!)

Dr. Sylvie Chardon, for her significant contribution to this thesis and for making my stay in Grenoble such a memorable one. Je vous remercie. Le chef a toujours raison.

Dr. Shawn Gouws, for his timely help while I was at LEOPR.

Philippe Da Costa, for his willing assistance with the preparative-scale electrolysis experiments.

Dr. Murray Low, for his help with the electrochemical aspects of this project.

Mr. Martin Watson, who showed great patience in training myself to operate the NMR spectrometers.

Miss Niyum S. Ramesar, for her help in solving the X-ray structures.

Mr. Paul Forder, who readily produced glassware at short notice.

Jean McKensie and Jan Gertenbach, for helping to proof read this thesis.

Mrs Karen Kader, for her speed typing.

Mssrs. Les Mayne, Darryl Leibrandt and Chris Morewood, of the Mechanical Instrument Workshop, for their essential technical assistance.

I would also like to thank the John Wakeford Scholarship Trust, the NRF, the French Ambassador to South Africa and De Beers Industrial Diamonds for the generous financial support they provided.

Thank you to Barbara for her companionship.

Most of all I would like to thank my family - Ruth, Ryan and Lesley Cripps. My gratitude to you is profound.

## Summary

The work described in this thesis concerns the synthesis of dinuclear complexes of Cu(I), Pd(I), Pt(I) and Ru(I) and the investigation of their electrochemical properties with the view to their use as novel catalysts for the electrochemical reduction of carbon dioxide.

Chapter 1 provides an introduction to the electrochemical reduction of carbon dioxide. The catalysis of this reaction by copper, palladium and ruthenium complexes, in particular those containing polypyridyl ligands, is reviewed.

The synthesis and characterisation of the novel tridentate ligands 6-(diphenylphosphino)-2-(2-quinolyl)pyridine **I** (Ph<sub>2</sub>Ppyqn) and 6-[ethyl(phenyl)phosphino]-2,2'-bipyridine **II** [Et(Ph)Pbpy] are reported in Chapter 2. These phosphorus-polypyridyl ligands are prepared by the nucleophilic substitution of the appropriate halogen-substituted  $\alpha$ -diimine [6-bromo-2-(2-quinolyl)pyridine and 6-chloro-2,2'-bipyridine] with lithium diphenylphosphide and lithium ethyl(phenyl)phosphide respectively. The electrochemical properties of **I** and **II** as well as those of the closely related ligand, 6-diphenylphosphino-2,2'-bipyridine (Ph<sub>2</sub>Pbpy), are examined. Extended Hückel Molecular Orbital calculations performed on the ligands provide a description of their redox active orbitals.

The synthesis of the dinuclear complexes [Cu<sub>2</sub>( $\mu$ -Ph<sub>2</sub>Ppyqn)<sub>2</sub>(CH<sub>3</sub>CN)<sub>2</sub>](BF<sub>4</sub>)<sub>2</sub> **1** and [Cu<sub>2</sub>{ $\mu$ -Et(Ph)Pbpy}<sub>2</sub>(CH<sub>3</sub>CN)<sub>2</sub>](PF<sub>6</sub>)<sub>2</sub> **2** is described in Chapter 3. The crystal structures of **1** and **2** have been determined and reveal a distorted tetrahedral geometry about the copper atoms, the phosphorus-polypyridyl ligands bridging the metal centres in a head-to-tail arrangement. The electrochemical properties of **1** and **2** as well as those of the previously reported complex [Cu<sub>2</sub>( $\mu$ -Ph<sub>2</sub>Pbpy)<sub>2</sub>(CH<sub>3</sub>CN)<sub>2</sub>](PF<sub>6</sub>)<sub>2</sub>, are studied by cyclic voltammetry. On a cyclic voltammetric time scale all of the above copper(I) complexes are reversibly reduced in four one-electron steps to complexes in which the copper atoms are formally in the -1 oxidation state. Extended Hückel Molecular Orbital calculations show that the site of reduction is primarily the  $\alpha$ -diimine fragment of the phosphorus-polypyridyl ligand. Cyclic voltammetric studies indicate that the triply reduced form of **1** and the doubly reduced form of **2** catalyse the electrochemical reduction of carbon dioxide. On an electrosynthetic time scale the reduction products of **1**, **2** and [Cu<sub>2</sub>( $\mu$ -Ph<sub>2</sub>Pbpy)<sub>2</sub>(CH<sub>3</sub>CN)<sub>2</sub>](PF<sub>6</sub>)<sub>2</sub> are chemically unstable under both Ar and CO<sub>2</sub> atmospheres.

The synthesis, characterisation and electrochemical properties of the homoleptic complexes [Pd<sub>2</sub>( $\mu$ -L)<sub>2</sub>](BF<sub>4</sub>)<sub>2</sub> [L = Ph<sub>2</sub>Pbpy **3**, Ph<sub>2</sub>Ppyqn **4** and Et(Ph)Pbpy **5**], [Pt<sub>2</sub>( $\mu$ -L)<sub>2</sub>](PF<sub>6</sub>)<sub>2</sub> [L = Ph<sub>2</sub>Pbpy **6**, Ph<sub>2</sub>Ppyqn **7** and Et(Ph)Pbpy **8**] and [PdPt( $\mu$ -L)<sub>2</sub>](PF<sub>6</sub>)<sub>2</sub> [L = Ph<sub>2</sub>Pbpy **9**, Ph<sub>2</sub>Ppyqn **10** and Et(Ph)Pbpy **11**] are reported in Chapter 4. The structure of **3** has been confirmed by single-crystal X-ray crystallography: the Pd(I) atoms are square-planar and are

bridged by the Ph<sub>2</sub>Pbpy ligands in a head-to-tail arrangement. While the dipalladium complexes **3 - 5** are irreversibly reduced, the diplatinum complexes **6 - 8** and the heterodinuclear complexes **9 - 11** are reversibly reduced in four discrete one-electron steps to the formally M(-1) species. Cyclic voltammetric studies show that the triply reduced forms of complexes **6 - 11** catalyse the electrochemical reduction of carbon dioxide. On an electrosynthetic time scale, in the presence of both Ar and CO<sub>2</sub>, the reduction products of **6 - 11** decompose.

The synthesis, characterisation and electrochemical properties of the dinuclear 2,2'-bipyridyl ligand complex of Ru(I), [Ru<sub>2</sub>(bpy)<sub>2</sub>(CO)<sub>4</sub>(CH<sub>3</sub>CN)<sub>2</sub>](PF<sub>6</sub>)<sub>2</sub> **12** are described in Chapter 5. The crystal structure of **12** reveals an octahedral coordination geometry about the ruthenium centres. The molecule adopts a conformation about the Ru-Ru bond in which the equatorial 2,2'-bipyridyl ligands approach an eclipsing of one another. The electrochemical oxidation of **12** is irreversible and leads to formation of the Ru(II) mononuclear complex *cis*(CH<sub>3</sub>CN)-[Ru(bpy)(CO)<sub>2</sub>(CH<sub>3</sub>CN)<sub>2</sub>](PF<sub>6</sub>)<sub>2</sub> **13**. The irreversible two-electron reduction of **12** results in the formation of the Ru(0) polymer [Ru(bpy)(CO)<sub>2</sub>]<sub>n</sub>. The complete oxidation of [Ru(bpy)(CO)<sub>2</sub>]<sub>n</sub> can be accomplished in two, one-electron steps, leading firstly to **12** and then secondly to **13**. The Ru(0) polymer derived from **12** is an effective electrocatalyst for the reduction of CO<sub>2</sub> to carbon monoxide.

The synthesis of the dinuclear pyrrole-substituted 2,2'-bipyridine ligand complexes of Ru(I), [Ru<sub>2</sub>(L)<sub>2</sub>(CO)<sub>4</sub>(CH<sub>3</sub>CN)<sub>2</sub>](PF<sub>6</sub>)<sub>2</sub> [L = L<sub>1-4</sub> **14 - 17**; L<sub>1</sub> = 4-(4-pyrrol-1-ylbutyl)-4'-methyl-2,2'-bipyridine; L<sub>2</sub> = 4,4'-bis((3-pyrrol-1-ylpropyloxy)carbonyl)-2,2'-bipyridine; L<sub>3</sub> = 4,4'-bis(4-pyrrol-1-ylbutyl)-2,2'-bipyridine; L<sub>4</sub> = 4,4'-bis(13-pyrrol-1-yltridecyl)-2,2'-bipyridine] is described in Chapter 6. The complexes **14 - 17** undergo an irreversible two-electron reduction to the respective Ru(0) polymers [Ru(L)(CO)<sub>2</sub>]<sub>n</sub> (L = L<sub>1-4</sub>). Their anodic electrochemistry shows that they are irreversibly oxidized. Anodic electropolymerisation of **15** and **17** gives rise to the polypyrrole films ppyr-[Ru<sub>2</sub>(L)<sub>2</sub>(CO)<sub>4</sub>(CH<sub>3</sub>CN)<sub>2</sub>](PF<sub>6</sub>)<sub>2</sub> (L = L<sub>2</sub> and L<sub>4</sub>) containing pendant dinuclear Ru(I) complexes. The subsequent reduction of the Ru(I) centres in the polypyrrole films leads to the immobilised Ru(0) polymers ppyr-[Ru(L)(CO)<sub>2</sub>]<sub>n</sub> (L = L<sub>2</sub> and L<sub>4</sub>). Also described in Chapter 6 is the electrochemical synthesis of the mononuclear Ru(II) complexes *trans*(CH<sub>3</sub>CN)-[Ru(L)(CO)<sub>2</sub>(CH<sub>3</sub>CN)<sub>2</sub>]<sup>2+</sup> (L = bpy and L<sub>1</sub>). Anodic electropolymerisation of *trans*(CH<sub>3</sub>CN)-[Ru(L<sub>1</sub>)(CO)<sub>2</sub>(CH<sub>3</sub>CN)<sub>2</sub>]<sup>2+</sup> leads to the efficient formation of the polypyrrole film ppyr-[Ru(L<sub>1</sub>)(CO)<sub>2</sub>(CH<sub>3</sub>CN)<sub>2</sub>]<sup>2+</sup> containing pendant mononuclear Ru(II) complexes. The subsequent two-electron reduction of the Ru(II) centres leads to the polypyrrole-supported Ru(0) polymer ppyr-[Ru(L<sub>1</sub>)(CO)<sub>2</sub>]<sub>n</sub>. The Ru(0) polymers ppyr-[Ru(L)(CO)<sub>2</sub>]<sub>n</sub> (L = L<sub>1</sub>, L<sub>2</sub> and L<sub>4</sub>), supported in polypyrrole matrices, are shown to be electrocatalysts towards the reduction of CO<sub>2</sub>.



The synthesis, characterisation and electrochemical studies of the previously reported complex *cis*(Ph<sub>2</sub>Pbpy)-[Ru<sub>2</sub>(μ-Ph<sub>2</sub>Pbpy)<sub>2</sub>(CO)<sub>2</sub>(CH<sub>3</sub>CN)<sub>2</sub>](PF<sub>6</sub>)<sub>2</sub>, *cis*(Ph<sub>2</sub>Pbpy)-**18** and of the novel complex *cis*(Ph<sub>2</sub>Ppyqn)-[Ru<sub>2</sub>(μ-Ph<sub>2</sub>Ppyqn)<sub>2</sub>(CO)<sub>2</sub>(CH<sub>3</sub>CN)<sub>2</sub>](PF<sub>6</sub>)<sub>2</sub>, *cis*(Ph<sub>2</sub>pyqn)-**19** are described in Chapter 7. The structure of *cis*(Ph<sub>2</sub>Ppyqn)-**19** has been determined by single-crystal X-ray crystallography and confirms that the Ph<sub>2</sub>Ppyqn ligands occupy mutually *cis* positions about the octahedral Ru(I) atoms, bridging the metal centres in a head-to-tail fashion. In contrast to *cis*(Ph<sub>2</sub>Ppyqn)-**19**, which is reversibly reduced to the formally Ru(-1) species, *cis*(Ph<sub>2</sub>Pbpy)-**18** exhibits one irreversible reduction peak. Extended Hückel Molecular Orbital calculations are performed on the complexes and show the redox orbitals to be of both metal and ligand character. It is evident from the cyclic voltammetric studies that the singly reduced form of *cis*(Ph<sub>2</sub>Pbpy)-**18** and the triply reduced form of *cis*(Ph<sub>2</sub>Ppyqn)-**19** catalyse the electrochemical reduction of carbon dioxide. However, preparative electrolysis experiments show that the reduced forms of *cis*(Ph<sub>2</sub>Pbpy)-**18** and **19** are chemically unstable on an electrosynthetic time-scale in the presence of CO<sub>2</sub>.

A comparison of the electrochemical behaviour of the complexes studied in this work is made in Chapter 8. In general, where the site of electron addition is metal based the reduction is observed to be irreversible. On the other hand, ligand based reduction processes are reversible. The interaction of the phosphorus-polypyridyl complexes with carbon dioxide occurs over a narrow range of potentials, varying from -1.95 V {for [Cu<sub>2</sub>(μ-Ph<sub>2</sub>Pbpy)<sub>2</sub>(CH<sub>3</sub>CN)<sub>2</sub>](PF<sub>6</sub>)<sub>2</sub>] to -2.15 V vs. Ag/Ag<sup>+</sup> [for [Pt<sub>2</sub>{μ-Et(Ph)Pbpy}<sub>2</sub>](PF<sub>6</sub>)<sub>2</sub> **8**]. This is not inconsistent with an outer-sphere mechanism for the reduction of CO<sub>2</sub> by these complexes. On the other hand the diplatinum complex [Pt<sub>2</sub>(μ-Ph<sub>2</sub>Ppyqn)<sub>2</sub>](PF<sub>6</sub>)<sub>2</sub> **7** catalyses the reduction of carbon dioxide at a somewhat different potential of -1.86 V vs. Ag/Ag<sup>+</sup>. It is speculated that the activation of CO<sub>2</sub> by this complex involves an inner-sphere mechanism. As the reduced forms of the phosphorus-polypyridyl complexes are not stable in the presence of CO<sub>2</sub> on an electrosynthetic time scale their use as practical catalysts for the electrochemical reduction of CO<sub>2</sub> is not viable.

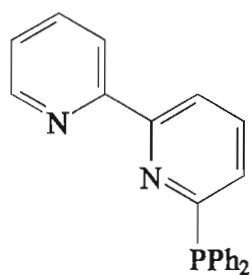
## Abbreviations

Ar	aromatic group
bpy	2,2'-bipyridine
CV	cyclic voltammogram
COSY	Correlated Spectroscopy
dba	dibenzylideneacetone
dmbbbpy	2,2'-bis(1-methylbenzimidazol-2-yl)-4,4'-bipyridine
dmbpy	4,4'-dimethyl 2,2'-bipyridine
DMF	<i>N,N</i> -dimethylformamide
dmpm	bis(dimethylphosphino)methane
dppm	bis(diphenylphosphino)methane
EHMO	Extended Hückel Molecular Orbital
etdp	(RO) <sub>2</sub> PNEtP(OR) <sub>2</sub> ; R = Me, Et, Pr <sup><i>i</i></sup> or Ph
Et	ethyl
EtCN	proprionitrile
Et <sub>2</sub> O	diethylether
Et(Ph)Pbpy	6-[ethyl(phenyl)phosphino]-2,2'-bipyridine
GC	gas chromatography
HOMO	highest occupied molecular orbital
h	hour
H <sub>2</sub> bibzim	1,1'-bibenzimidazole
L <sub>1</sub>	4-(4-pyrrol-1-ylbutyl)-4'-methyl-2,2'-bipyridine
L <sub>2</sub>	4,4'-bis((3-pyrrol-1-ylpropyloxy)carbonyl)-2,2'-bipyridine
L <sub>3</sub>	4,4'-bis(4-pyrrol-1-ylbutyl)-2,2'-bipyridine
L <sub>4</sub>	4,4'-bis(13-pyrrol-1-yltridecyl)-2,2'-bipyridine
LUMO	lowest unoccupied molecular orbital
M <sup>+</sup>	molecular ion
Me	methyl
me <sub>2</sub> Ppy	2-(dimethylphosphino)pyridine
napy	1,8-naphthyridine
NMR	Nuclear Magnetic Resonance
NOE	Nuclear Overhauser Effect
NOESY	Nuclear Overhauser Effect Spectroscopy
Ph	phenyl

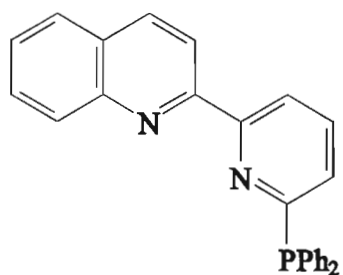
phen	1,10-phenanthroline
Ph <sub>2</sub> Pbpy	6-diphenylphosphino-2,2'-bipyridine
Ph <sub>2</sub> Pphen	6-diphenylphosphino-1,10-phenanthroline
Ph <sub>2</sub> Ppy	2-(diphenylphosphino)pyridine
(Ph <sub>2</sub> P) <sub>2</sub> py	2,6-bis(diphenylphosphino)pyridine
Ph <sub>2</sub> Ppyqn	6-(diphenylphosphino)-2-(2-quinolyl)pyridine
Ph <sub>2</sub> Pquin	2-(diphenylphosphino)quinoline
P,N,N	phosphorus-polypyridyl ligand
Ppyr	polypyrrole
Pr <sup>i</sup>	<i>iso</i> -propyl
py	pyridine
qu	quinoline
R	alkyl group
RDE	rotating disc electrode
rt	room temperature
SLUMO	second lowest unoccupied molecular orbital
tbbpy	4,4'-di- <i>tert</i> -butyl-2,2'-bipyridine
TBAP	tetrabutylammonium perchlorate
THF	tetrahydrofuran
TLUMO	third lowest unoccupied molecular orbital
TMS	tetramethylsilane
trpy	2,2':6',2'-terpyridine
X	halide



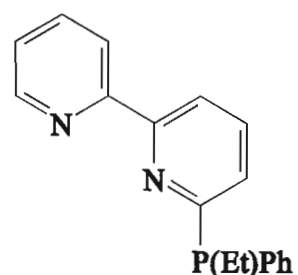
## Structural Formula of Ligands



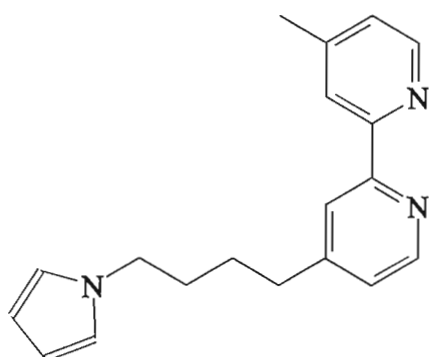
$\text{Ph}_2\text{Pbpy}$



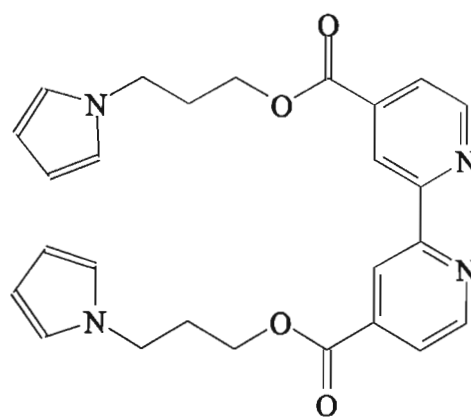
$\text{Ph}_2\text{Ppyquin I}$



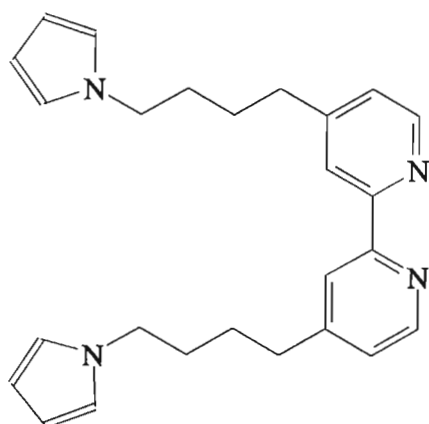
$\text{Et(Ph)Pbpy II}$



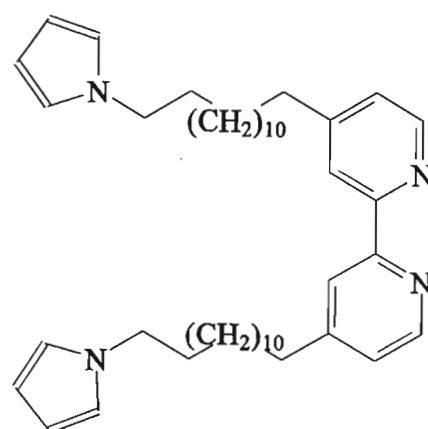
$\text{L}_1$



$\text{L}_2$



$\text{L}_3$



$\text{L}_4$

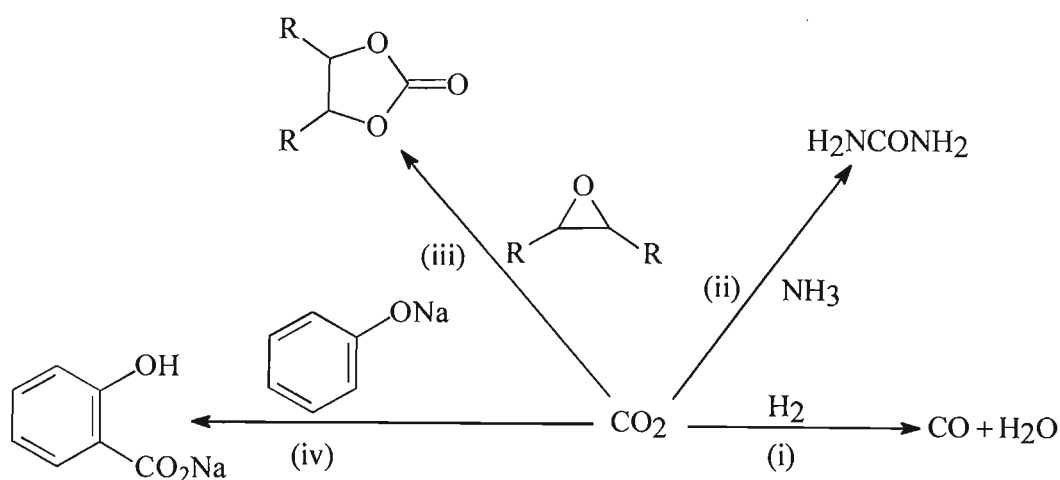
## List of Compounds

I	6-(diphenylphosphino)-2-(2-quinolyl)pyridine
II	6-[ethyl(phenyl)phosphino]-2,2'-bipyridine
III	2-(ethylsulfanyl)quinoline
IV	2-(ethylsulfinyl)quinoline
1	$[\text{Cu}_2(\mu\text{-Ph}_2\text{Ppyqn})_2(\text{CH}_3\text{CN})_2](\text{BF}_4)_2$
2	$[\text{Cu}_2\{\mu\text{-Et(Ph)Pbpy}\}_2(\text{CH}_3\text{CN})_2](\text{PF}_6)_2$
3	$[\text{Pd}_2(\mu\text{-Ph}_2\text{Pbpy})_2](\text{BF}_4)_2$
4	$[\text{Pd}_2(\mu\text{-Ph}_2\text{Ppyqn})_2](\text{BF}_4)_2$
5	$[\text{Pd}_2\{\mu\text{-Et(Ph)Pbpy}\}_2](\text{BF}_4)_2$
6	$[\text{Pt}_2(\mu\text{-Ph}_2\text{Pbpy})_2](\text{PF}_6)_2$
7	$[\text{Pt}_2(\mu\text{-Ph}_2\text{Ppyqn})_2](\text{PF}_6)_2$
8	$[\text{Pt}_2\{\mu\text{-Et(Ph)Pbpy}\}_2](\text{PF}_6)_2$
9	$[\text{PtPd}(\mu\text{-Ph}_2\text{Pbpy})_2](\text{PF}_6)_2$
10	$[\text{PtPd}(\mu\text{-Ph}_2\text{Ppyqn})_2](\text{PF}_6)_2$
11	$[\text{PtPd}\{\mu\text{-Et(Ph)Pbpy}\}_2](\text{PF}_6)_2$
12	$[\text{Ru}_2(\text{bpy})_2(\text{CO})_4(\text{CH}_3\text{CN})_2](\text{PF}_6)_2$
13	<i>cis</i> ( $\text{CH}_3\text{CN}$ )- $[\text{Ru}(\text{bpy})(\text{CO})_2(\text{CH}_3\text{CN})_2](\text{PF}_6)_2$
14	$[\text{Ru}_2(\text{L}_1)_2(\text{CO})_4(\text{CH}_3\text{CN})_2](\text{PF}_6)_2$
15	$[\text{Ru}_2(\text{L}_2)_2(\text{CO})_4(\text{CH}_3\text{CN})_2](\text{PF}_6)_2$
16	$[\text{Ru}_2(\text{L}_3)_2(\text{CO})_4(\text{CH}_3\text{CN})_2](\text{PF}_6)_2$
17	$[\text{Ru}_2(\text{L}_4)_2(\text{CO})_4(\text{CH}_3\text{CN})_2](\text{PF}_6)_2$
18	$[\text{Ru}_2(\mu\text{-Ph}_2\text{Pbpy})_2(\text{CO})_2(\text{CH}_3\text{CN})_2](\text{PF}_6)_2$
19	$[\text{Ru}_2(\mu\text{-Ph}_2\text{Ppyqn})_2(\text{CO})_2(\text{CH}_3\text{CN})_2](\text{PF}_6)_2$

## Chapter 1. Introduction

The artificial fixation of carbon dioxide has long attracted the interest of chemists. This has primarily been for two reasons. Firstly, the petrochemical industry is based on a source of carbon that is almost exclusively fossilized matter - mineral oil, natural gas and coal. As these resources are limited there has been a significant effort to find alternative ones. Carbon dioxide represents a ubiquitous if dilute potential source of C<sub>1</sub> feedstocks that could be used for producing fuels, chemicals and materials. Secondly, since the beginning of industrialization in the second half of the last century increasing anthropogenic CO<sub>2</sub> emissions have contributed to an elevated concentration of atmospheric CO<sub>2</sub>, this becoming a growing concern with respect to global climate change. The potentially serious environmental threat posed by uncontrolled CO<sub>2</sub> emissions has further focussed research on its mitigation and use.<sup>1,2,3</sup>

The chemical industry does already possess experience in utilizing carbon dioxide as a raw material in four commercial processes (Scheme 1.1).<sup>4</sup> In the industrial synthesis of methanol (10 Mt/a) from H<sub>2</sub>/CO/CO<sub>2</sub> mixtures (ICI process), the direct hydrogenation of CO<sub>2</sub> plays an important role (i). Urea (80 Mt/a) is commonly produced by reacting ammonia and CO<sub>2</sub> over a zinc catalyst at moderate temperatures and high pressures (ii). In a reaction discovered by IG Farben cyclic organic carbonates are synthesised from CO<sub>2</sub> and ethylene oxide (iii). Salicylic acid (25 000 t/a) is produced from the carboxylation of sodium phenolate using the Kolbe-Schmitt process (iv).



**Scheme 1.1.** Industrial syntheses utilising carbon dioxide.

From a safety aspect CO<sub>2</sub> is an ideal raw material. In comparison to the widely used C<sub>1</sub> starting materials carbon monoxide (CO) and phosgene (COCl<sub>2</sub>), it is practically non-toxic and can be stored, transported and handled without problems.<sup>4</sup> Technology exists for the separation and concentration of carbon dioxide; of principle importance in this context is absorption in aqueous solutions of amines.<sup>5</sup>

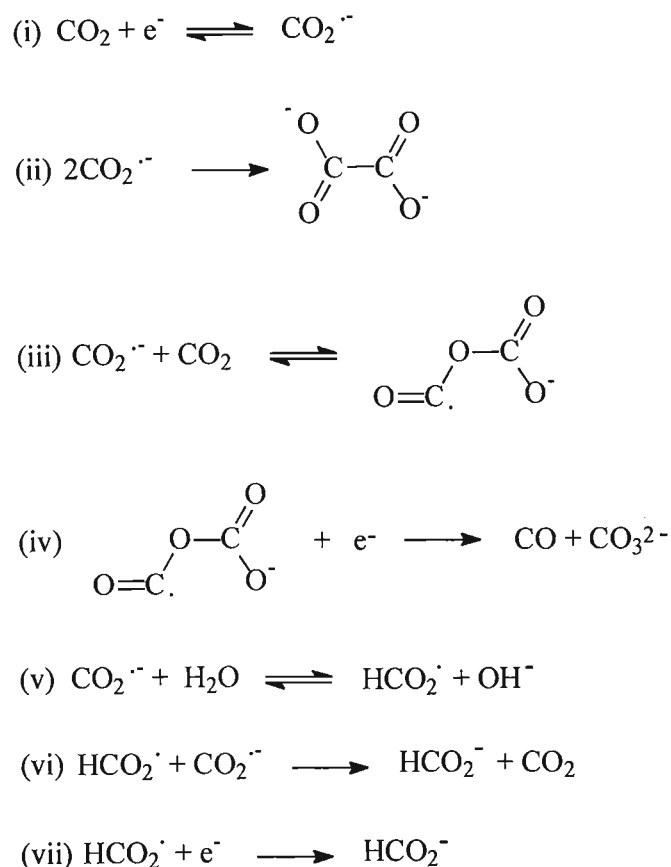
However, beyond the industrial uses described, the utilization of carbon dioxide as a source of chemical carbon is limited. This can be ascribed to the thermodynamic stability of CO<sub>2</sub>, which constitutes the thermodynamic end product of many commercial and natural processes. The exploitation of CO<sub>2</sub> as a source of carbon therefore necessitates an input of energy, either directly, such as in an electrode process, or by its reaction with a compound of high free energy content, for example, by hydrogenation with molecular hydrogen. Hydrogen is produced industrially by the involvement of the water-gas-shift reaction, where CO<sub>2</sub> is the ultimate oxygen sink (Equation 1.1). This paradox means alternative strategies for carbon dioxide conversion must be considered, among which electrochemical reduction is of fundamental interest.



### 1.1. Electrochemical Reduction of Carbon Dioxide

The electrochemical reduction of carbon dioxide can yield C<sub>1</sub>, C<sub>2</sub> and C<sub>4</sub> oxygenated products, for example carbon monoxide, formate, formic acid, formaldehyde, methanol, methane and oxalate.<sup>6,7</sup> The product distribution obtained is chiefly a function of the solvent and cathode material, with the metal often playing a catalytic role through chemisorption of CO<sub>2</sub>, intermediates or products.<sup>6,7</sup> At inert (or outer-sphere) electrodes, such as Pb, Hg and Tl, where the electrochemical reduction can be described as direct, carbon monoxide and oxalate are formed in aprotic solvents. The reduction of carbon dioxide in aqueous media with a Pb cathode produces formate as the sole product, while a Hg electrode affords both formate and oxalate.<sup>6,7</sup> Savéant *et al.* proposed that the formation of the products may be explained in terms of the generation of CO<sub>2</sub><sup>•-</sup> and its subsequent evolution in the reaction medium.<sup>6,7</sup> The radical anion CO<sub>2</sub><sup>•-</sup> can react via three competing reaction pathways, leading to the formation of oxalate, CO and formate (Scheme 1.2). Oxalate results from the dimerisation of two anion radicals [step (ii)]. Carbon monoxide is formed via oxygen-carbon coupling of CO<sub>2</sub><sup>•-</sup> with CO<sub>2</sub> to form a radical anion complex (iii), followed by the transfer of an electron from the electrode (iv). In the

presence of a proton source, formate may arise by protonation of  $\text{CO}_2^{\cdot-}$  to form the neutral radical  $\text{HCO}_2\cdot$  (v), followed by an additional electron transfer from a  $\text{CO}_2^{\cdot-}$  radical (vi) or the electrode surface (vii).



**Scheme 1.2.** Mechanism for the direct electrochemical reduction of carbon dioxide.

## 1.2. Thermodynamics of the Electrochemical Reduction of Carbon Dioxide

The two, four, six and eight electron reduction products of carbon dioxide are listed in Table 1.1. The nature of the product has a strong influence on its thermodynamic accessibility from  $\text{CO}_2$ . As the number of electrons involved in the reduction process increases the redox potential becomes less negative.

Although the thermodynamic potentials for the electrochemical reduction of  $\text{CO}_2$  to the products shown are at accessible potentials, the difficulty in coordinating multiple electron and proton additions to the site of reduction results in the reduction processes being kinetically hindered. Furthermore, and most significantly, a large cathodic potential is required for the initial one electron reduction of carbon dioxide to its radical anion, a typical value for this couple being  $-2.21$  V (vs. SCE) in DMF (Hg electrode).<sup>8</sup> Thus it is evident that electrocatalysts must be

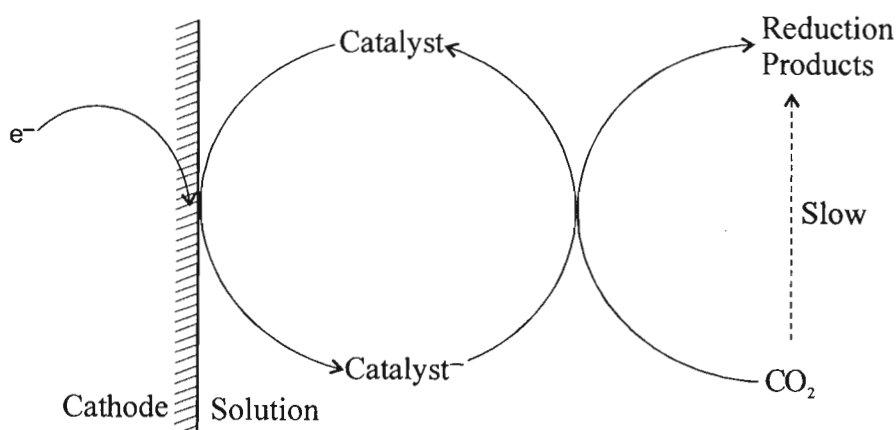
developed to facilitate the process of electron transfer if the electrochemical reduction of carbon dioxide is to become a viable proposition.

**Table 1.1.** The standard  $\Delta G^\circ$  (25°C, pH = 0) and corresponding  $E^\circ$  values for the two, four, six and eight electron reductions of  $\text{CO}_2$  (g) in aqueous solution.<sup>9</sup>

Reaction	$\Delta G^\circ/\text{kJ}\cdot\text{mol}^{-1}$	$E^\circ/\text{V vs. NHE}$
$2\text{CO}_2(\text{g}) + 2\text{H}^+ + 2\text{e}^- = \text{H}_2\text{C}_2\text{O}_4$	+91.8	-0.475
$\text{CO}_2(\text{g}) + 2\text{H}^+ + 2\text{e}^- = \text{HCOOH}(\text{aq})$	+38.4	-0.199
$\text{CO}_2(\text{g}) + 2\text{H}^+ + 2\text{e}^- = \text{CO}(\text{g}) + \text{H}_2\text{O}$	+19.9	-0.103
$\text{CO}_2(\text{g}) + 4\text{H}^+ + 4\text{e}^- = \text{HCHO}(\text{aq}) + \text{H}_2\text{O}$	+27.5	-0.071
$\text{CO}_2(\text{g}) + 6\text{H}^+ + 6\text{e}^- = \text{CH}_3\text{OH}(\text{aq}) + \text{H}_2\text{O}$	-17.3	+0.030
$\text{CO}_2(\text{g}) + 8\text{H}^+ + 8\text{e}^- = \text{CH}_4(\text{g}) + 2\text{H}_2\text{O}$	-130.8	+0.169

### 1.3. Homogeneous Electrocatalytic Reduction of Carbon Dioxide

The general principle of homogeneous redox catalysis is schematically presented in Scheme 1.3. Homogeneous transition metal electrocatalysts function by being reversibly reduced at the electrode surface. Carbon dioxide then coordinates to the reduced metal complex in solution and electron transfer takes place. The oxidised catalyst returns to the electrode and the cycle begins again.<sup>10</sup> The oxidised transition metal complex is reduced at a lower potential than the substrate. Thus the redox catalyst lowers the kinetic barrier, or overpotential, of reduction bringing the potential of reduction closer to the thermodynamic values.

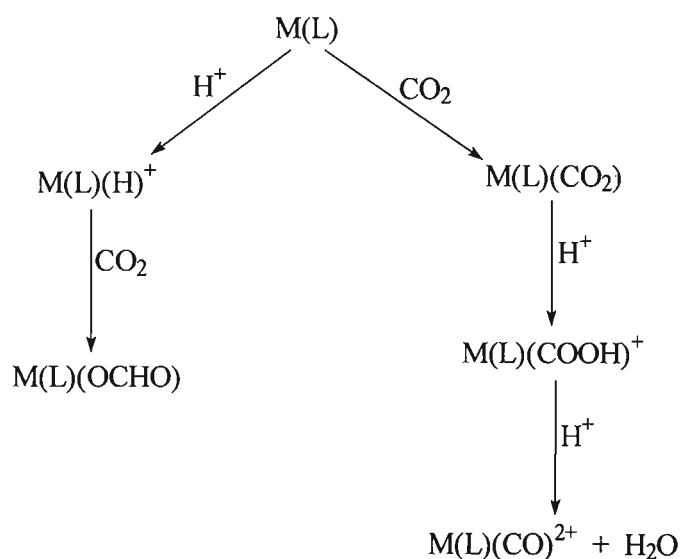


**Scheme 1.3.** Mediation of the electrochemical reduction of carbon dioxide by a transition metal redox catalyst.

The reduction of  $\text{CO}_2$  catalysed by homogeneous electrocatalysts commonly gives rise to either formate or CO together with  $\text{H}_2$  formation.<sup>3</sup> For some catalysts a high selectivity for  $\text{CO}_2$

over the more thermodynamically favoured reduction of protons to  $H_2$  has been attained, current efficiencies of close to a 100 % having been obtained even in acidic conditions. This selectivity arises from the reaction of 17-electron intermediates with  $CO_2$  in preference to  $H^+$ .

The nature of the  $CO_2$  reduction product formed also shows a dependence on the selectivity of the reduced forms of the catalyst for  $CO_2$  versus  $H^+$ .<sup>3</sup> Scheme 1.4 illustrates the two possible competing pathways. Initial reaction of the low-valent metal complex with  $CO_2$  results in a  $M-CO_2$  complex, protonation of which yields a metallocarboxylic acid; C–O bond cleavage then leads to CO and  $H_2O$  or  $OH^-$ . Alternatively the catalyst reacts with protons to form a metal hydride; its subsequent reaction with  $CO_2$  leads to formate.



**Scheme 1.4.** Possible reaction pathways arising from the competing interaction of low-valent catalysts with protons or  $CO_2$ .<sup>3</sup>

The aim of this work is the synthesis of copper, palladium, platinum and ruthenium complexes as potential homogeneous electrocatalysts for the reduction of carbon dioxide. Selected homogeneous electrocatalysts of these transition metals are now reviewed to provide a background to our approach to the design of potential new catalysts.

### 1.3.1. Copper Complexes as Electrocatalysts

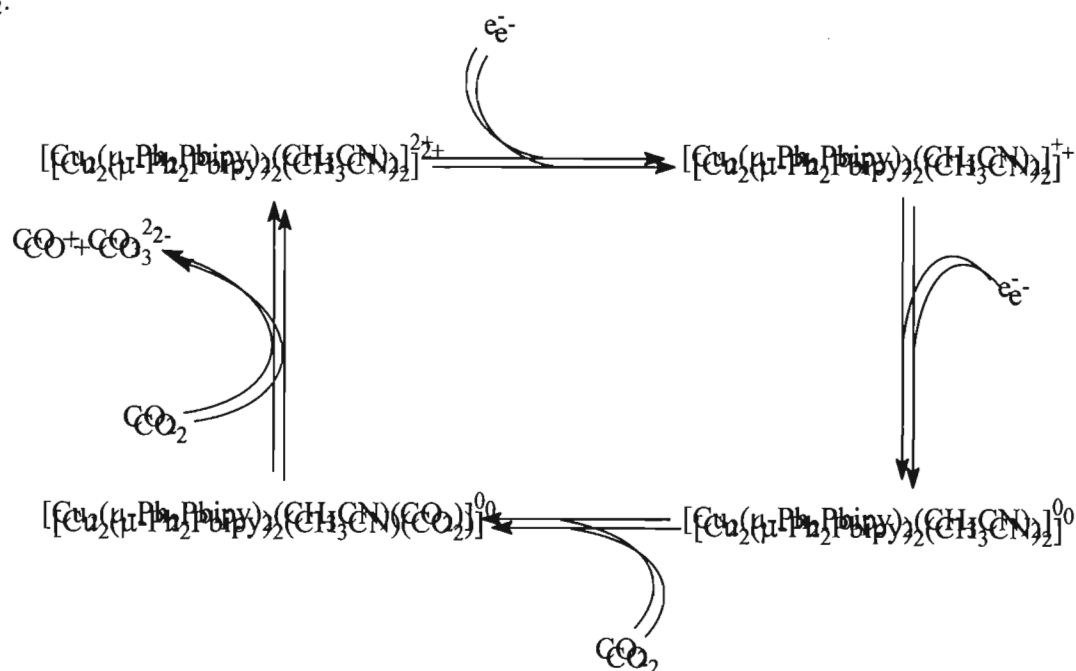
#### 1.3.1.(i) $[Cu_2(\mu-Ph_2Pbpy)_2(CH_3CN)_2](PF_6)_2$

The dicopper complex  $[Cu_2(\mu-Ph_2Pbpy)_2(CH_3CN)_2](PF_6)_2$  [ $Ph_2Pbpy = 6$ - (diphenylphosphino)-2,2'-bipyridyl] has been shown to catalyse the reductive disproportionation of  $CO_2$  to CO and  $CO_3^{2-}$ .<sup>11</sup> Although the complex undergoes two discrete one-electron



reductions at  $-1.35$  and  $-1.53$  V vs. SCE, it significantly functions as a two-electron electrocatalyst, catalysing the net transfer of two electrons to  $\text{CO}_2$  at  $-1.6$  V vs. SCE.

The proposed catalytic cycle for the reduction of  $\text{CO}_2$  catalysed by  $[\text{Cu}_2(\mu\text{-Ph}_2\text{Pbpy})_2(\text{CH}_3\text{CN})_2](\text{PF}_6)_2$  is presented in Scheme 1.5. The first two steps are considered to be the heterogeneous electron transfers that lead to the highly reduced metal complex capable of binding  $\text{CO}_2$ . The rate determining step is the coordination of the  $\text{CO}_2$  to the metal by the substitution of a solvent molecule. The exact mechanism of the reductive disproportionation in the final step is unclear. It may involve the ‘head-to-tail’ dimerisation of two  $\text{CO}_2$  molecules followed by collapse to  $\text{CO}$  and  $\text{CO}_3^{2-}$  that is too rapid to be observed. Infrared spectroelectrochemical measurements performed on the copper dimer system imply that a  $\text{CO}_3^{2-}$  complex is formed as an intermediate in the reaction of the reduced dimer with two molecules of  $\text{CO}_2$ .<sup>11</sup>



**Scheme 1.5.** Proposed catalytic cycle for the reduction of carbon dioxide catalysed by  $[\text{Cu}_2(\mu\text{-Ph}_2\text{Pbpy})_2(\text{CH}_3\text{CN})_2](\text{PF}_6)_2$ .

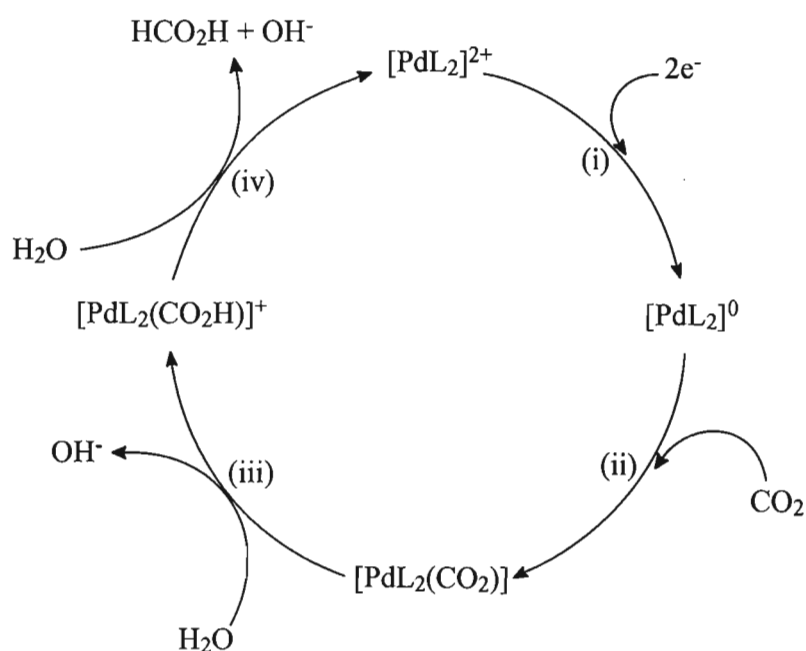
### 1.3.2. Palladium and Platinum Complexes as Electrocatalysts

#### 1.3.2.(i) $[\text{PdCl}_2\text{L}_2]$ (L = pyrazole, 4-methylpyridine and 3-methylpyrazole)

The pyridine- and pyrazole-substituted complexes of palladium(II)  $[\text{PdCl}_2\text{L}_2]$  (L = pyrazole, 4-methylpyridine and 3-methylpyrazole) catalyse the electrochemical reduction of  $\text{CO}_2$  to formic acid in a water-acetonitrile solution at  $-1.10$  V vs.  $\text{Ag}/\text{Ag}^+$ .<sup>12</sup>



A possible reduction mechanism is presented in Scheme 1.6. The complexes undergo a quasi-reversible, two-electron reduction to the formally palladium(0) product,  $[\text{PdL}_2]^0$ , at potentials between  $-0.35$  and  $-1.20$  V vs.  $\text{Ag}/\text{Ag}^+$ . The loss of the halide ligand provides a potential coordination site to which the  $\text{CO}_2$  can bind. The authors believe that the pyridine and pyrazole ligands act as electron acceptor sites at accessible potentials. In step (ii), carbon dioxide binds to the electron-rich complex, forming an intermediate in which it is speculated that the  $\text{CO}_2$  is carbon-bound. Protonation (iii) of the complexed  $\text{CO}_2$  leads to a bound formate anion in  $[\text{PdL}_2(\text{CO}_2\text{H})]^+$ , which rapidly dissociates (iv) to give  $[\text{PdL}_2]^{2+}$  for re-entry into the reduction cycle.



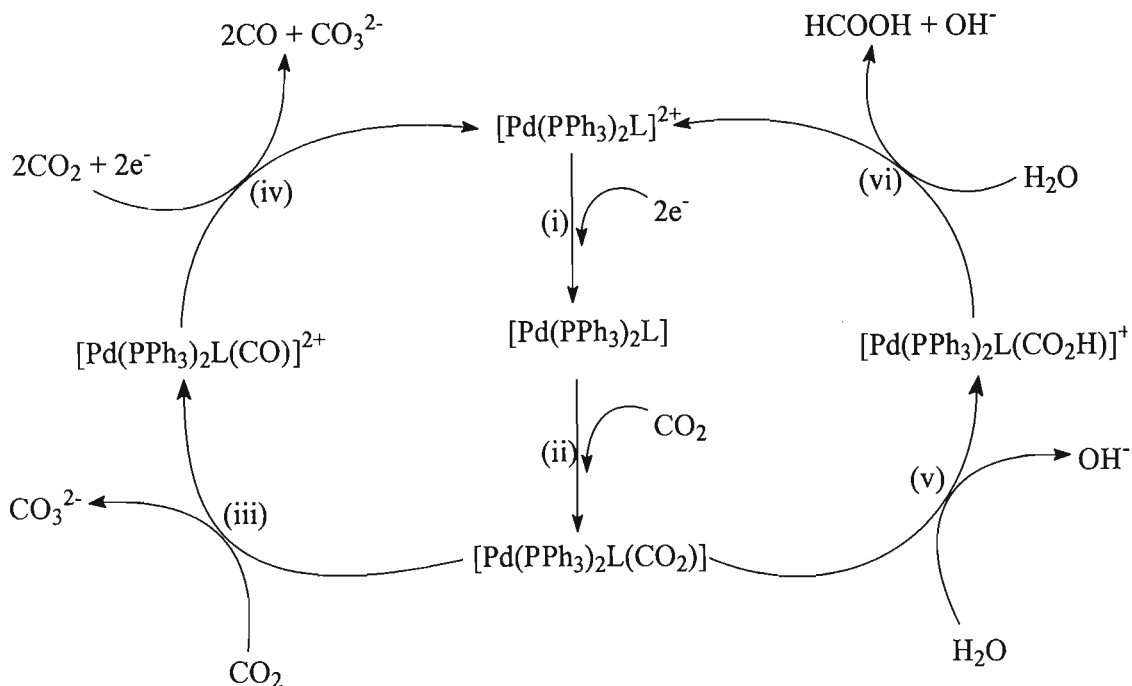
**Scheme 1.6.** Proposed mechanism for the catalytic reduction of  $\text{CO}_2$  to formic acid by pyridine- and pyrazole-substituted complexes of palladium.

### 1.3.2.(ii) $[\text{Pd}(\text{PPh}_3)_2\text{L}]^{2+}$ (L = substituted quinoline, bipyridine and phenanthroline)

Ogura *et al.* have further investigated a series of quinoline, bipyridine and phenanthroline ligand-substituted palladium complexes as catalysts.<sup>13</sup> The complexes  $[\text{Pd}(\text{PPh}_3)_2\text{L}]\text{X}_2$  (L = 2-methyl-8-hydroxyquinoline, 2-quinoxalinol, 1-hydroxyisoquinoline, 3-hydroxyisoquinoline, 4,4'-dimethyl-2,2'-bipyridine or 4-methyl-1,10-phenanthroline; X = Cl or  $\text{ClO}_4$ ) catalyse the reduction of  $\text{CO}_2$  to CO under anhydrous conditions at  $-1.30$  V vs.  $\text{Ag}/\text{Ag}^+$ . In an acetonitrile-water solution the reduction products were CO and  $\text{HCOOH}$ .

A probable reaction mechanism is shown in Scheme 1.7. As for the pyridine and pyrazole palladium species, the electrocatalytic reduction of  $\text{CO}_2$  was triggered by an initial two-electron reduction of the complex (i). The reduced metal complex, stabilized by the heteroaromatic rings,

is believed to react with  $\text{CO}_2$  to afford a five coordinate intermediate,  $[\text{Pd}(\text{PPh}_3)_2\text{L}(\text{COO})]$ , where the  $\text{CO}_2$  is  $\sigma$ -bonded (ii). Under anhydrous conditions, subsequent oxide abstraction by  $\text{CO}_2$  leads to  $[\text{Pd}(\text{PPh}_3)_2\text{L}(\text{CO})]^{2+}$  and  $\text{CO}_3^{2-}$  (iii). The former further catalyses the reductive disproportionation of  $\text{CO}_2$  to  $\text{CO}$  and  $\text{CO}_3^{2-}$  (iv). In the presence of water the  $\sigma$ - $\text{CO}_2$  complex  $[\text{Pd}(\text{PPh}_3)_2\text{L}(\text{COO})]$  is protonated (v), leading to a second intermediate that further reacts with water to give  $\text{HCO}_2^-$  and the regenerated catalyst (vi).



**Scheme 1.7.** Proposed catalytic mechanism for the reduction of  $\text{CO}_2$  mediated by quinoline, bipyridine and phenanthroline ligand-substituted palladium(II) complexes.

### 1.3.2.(iii) $[\text{Pd}(\text{triphos})(\text{solvent})](\text{BF}_4)_2$

DuBois *et al.* have focussed their research on palladium complexes coordinated by a tridentate phosphine ligand and a solvent molecule such as  $[\text{Pd}(\text{triphos})(\text{solv})](\text{BF}_4)_2$  [triphos, for example =  $\text{PhP}(\text{CH}_2\text{CH}_2\text{PPh}_2)_2$ ,  $\text{PhP}(\text{CH}_2\text{CH}_2\text{PCy}_2)_2$  or  $\text{PhP}(\text{CH}_2\text{CH}_2\text{PEt}_2)_2$ ; solv =  $\text{CH}_3\text{CN}$  or DMF].<sup>14</sup> A number of these catalysts operate at relatively positive potentials, exhibiting high activity and selectivity for the electrochemical reduction of  $\text{CO}_2$  to  $\text{CO}$ . Thus  $[\text{Pd}(\text{etp})(\text{CH}_3\text{CN})](\text{BF}_4)_2$  [etp =  $\text{PhP}(\text{CH}_2\text{CH}_2\text{PPh}_2)_2$ ] electrocatalyses the reduction of  $\text{CO}_2$  in acidic-acetonitrile solutions at  $-1.18$  V vs. ferrocene. Polyphosphine ligands were chosen over the monodentate analogues in an effort to prevent undesirable side reactions resulting from the phosphine ligand dissociation. The incorporation of a weakly bound acetonitrile ligand into the triphosphine metal complexes provides, through its dissociation, a possible vacant site for coordination of the substrate molecule.

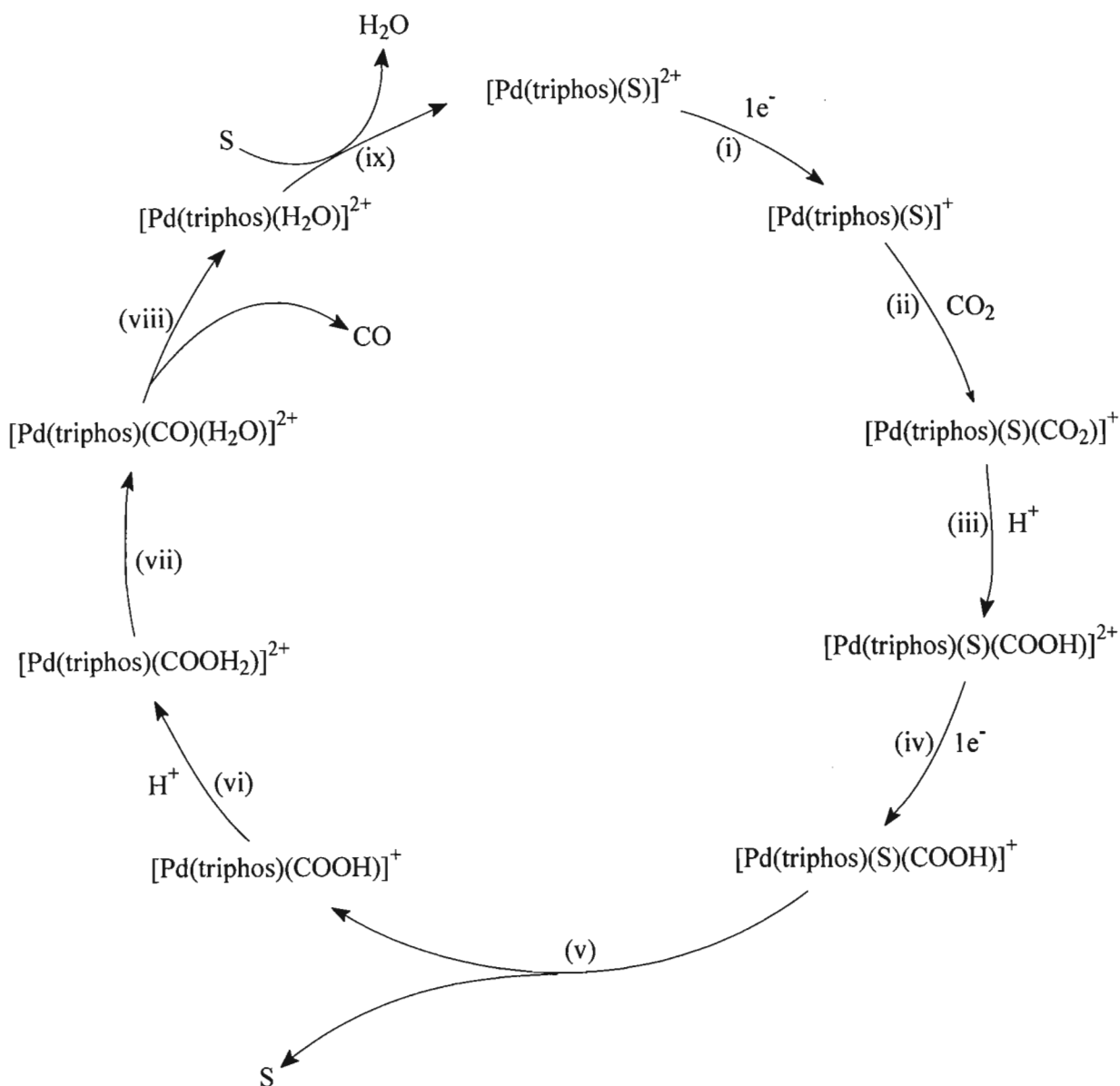
The complexes undergo a quasi-reversible two-electron reduction, the product of which mediates the electrochemical reduction of CO<sub>2</sub> to CO in an acetonitrile-HBF<sub>4</sub> solution. In dry acetonitrile the Pd(0) complexes do not react rapidly with CO<sub>2</sub>. In contrast, the isoelectronic platinum complex [Pt(triphos)(PEt<sub>3</sub>)](BF<sub>4</sub>)<sub>2</sub> interacts strongly with CO<sub>2</sub> upon reduction.<sup>14</sup> The authors attribute this difference in the ability of the metal(0) complex to bind CO<sub>2</sub> to the increased nucleophilicity of the Pt complex, as evidenced by it being reduced at a potential 0.2 V more negative than the analogous Pd complex. However, the Pt complex displays no catalytic activity in the presence of acid.

The structurally related bis(diphosphine) metal complexes [M(dppe)<sub>2</sub>](BF<sub>4</sub>)<sub>2</sub> [M = platinum and palladium, dppe = bis(1,2-diphenylphosphine)ethane] lack any catalytic activity.<sup>14</sup> Moreover, the addition of an excess of monodentate phosphine ligand, where the phosphine is P(OMe)<sub>3</sub>, PEt<sub>3</sub>, P(CH<sub>2</sub>OH)<sub>3</sub>, or PPh<sub>3</sub>, retards the catalytic activity of the palladium(II) triphosphine complexes.<sup>15</sup> These observations emphasize the importance of a ligand dissociation step to form the solvated complexes before the catalytic cycle can be entered.

The catalytic cycle proposed for this process is shown in Scheme 1.8. The first two steps in the cycle are the successive one-electron reductions of the palladium(II) complex followed by reaction of the reduced species with CO<sub>2</sub>. Significantly a five-coordinate palladium(I) complex is shown to be the transition state, formed by the approach of the CO<sub>2</sub> along an axis perpendicular to the plane of the catalyst.<sup>16</sup> Steps (iii) to (vi) involve the protonation of the bound CO<sub>2</sub>, electron transfer and solvent loss, leading to the activated complex [Pd(triphos)(COOH<sub>2</sub>)]<sup>2+</sup>. The precise sequence of these steps is not known. The dissociation of the solvent molecule produces a vacant coordination site that may be filled by the oxygen atom of CO<sub>2</sub>, resulting in the formation of a η<sup>2</sup> complex. This mode of coordination is possibly required for cleavage of the carbon-oxygen bond in step (vii). The subsequent steps, (viii) and (ix), consisting of CO loss and displacement of water by solvent, complete the catalytic cycle. The rate-determining step depends upon the acid concentration. At low acid concentrations it is the cleavage of the C–O bond to form CO and water, while at high acid concentrations the reaction of the Pd(I) species with CO<sub>2</sub> is the rate determining reaction.

A close relationship between the ligand structure and the catalytic activity of the complexes exists.<sup>15,17,18</sup> The nature of the tridentate donor set plays a critical role in determining the reaction pathway. Thus the series of complexes [Pd(PXP)(CH<sub>3</sub>CN)](BF<sub>4</sub>)<sub>2</sub> (PXP = tridentate ligand where X = C, N, O, S, or As) in which the central phosphorus atom of the tridentate ligand is substituted with C, N, O, S, or As atoms, showed no catalytic activity in the reduction of carbon dioxide.<sup>17</sup> Likewise, the palladium complexes in which the terminal phosphorus atoms have been substituted with N or S atoms failed to catalyse the electrochemical reduction of

CO<sub>2</sub>.<sup>15</sup> Any variation from the simple triphosphine donor set is detrimental with respect to CO<sub>2</sub> reduction.



**Scheme 1.8.** Proposed catalytic cycle for the reduction of CO<sub>2</sub> to CO by the  $[\text{Pd}(\text{triphos})(\text{solvent})](\text{BF}_4)_2$  complexes.

Catalytic activity of the palladium complexes is further dependent upon the nature of the substituents on the phosphorus atoms of the triphosphine ligands. A comparison of the catalytic rate constants for the complexes  $[\text{Pd}(\text{triphos})(\text{CH}_3\text{CN})](\text{BF}_4)_2$  [triphos =  $\text{RP}(\text{CH}_2\text{CH}_2\text{PR}'_2)_2$ ; R = phenyl; R' = phenyl, ethyl or cyclohexyl] shows that the more electron-rich alkyl groups promote the reaction of the Pd(I) complex with CO<sub>2</sub>.<sup>15</sup>

By systematically varying the number of methylene groups bridging the phosphorus atoms of the triphosphine ligand and hence its chelate bite, a further relationship between the

structure of the ligand and the reactivity of the metal complexes can be established.<sup>18</sup> In particular the initial binding of CO<sub>2</sub> to the palladium(I) complex has been shown to be faster for catalysts containing triphosphine ligands with two-carbon backbones than for those containing three.<sup>15</sup> This has been ascribed to the former having a high-lying d<sub>z<sup>2</sup></sub> orbital that promotes the reaction with CO<sub>2</sub>.<sup>15</sup>

The triphosphine ligands have also been altered by substituting pendant phosphonium groups onto either the central or terminal phosphorus atoms.<sup>19</sup> These positively charged ligands confer water solubility on their metal complexes and enable them to be immobilized upon cation-exchange resins. The use of water-soluble catalysts offers the environmental benefits of using water to replace organic solvents and, for an electrochemical process, a much lower resistance across the cell that improves the energy efficiency of the process. The palladium(II) complexes of these ligands, [Pd(triphos<sup>+</sup>)(CH<sub>3</sub>CN)](BF<sub>4</sub>)<sub>3</sub> {triphos<sup>+</sup> = [(Bu<sub>3</sub>PCH<sub>2</sub>CH<sub>2</sub>)P(CH<sub>2</sub>CH<sub>2</sub>PEt<sub>2</sub>)<sub>2</sub>]<sup>+</sup> and [Me<sub>3</sub>PCH<sub>2</sub>CH<sub>2</sub>)P(CH<sub>2</sub>CH<sub>2</sub>PEt<sub>2</sub>)<sub>2</sub>]<sup>+</sup>} catalyse the electrochemical reduction of CO<sub>2</sub> to CO in acidic dimethylformamide solutions in the same manner as the analogous simple triphosphine complexes do. The central and terminal phosphorus atoms have also been modified with hydroxypropyl, dialkylamine and (diethoxyphosphoranyl)ethyl functional groups to generate water-soluble catalysts.<sup>20</sup> Although the [Pd(triphos)(CH<sub>3</sub>CN)](BF<sub>4</sub>)<sub>2</sub> complexes of these modified ligands mediate the electrochemical reduction of CO<sub>2</sub> to CO in dimethylformamide and buffered aqueous solutions they are unstable under the electrochemical conditions.

#### 1.3.2.(iv) [Pd<sub>2</sub>(μ-eHTP)(CH<sub>3</sub>CN)<sub>2</sub>](BF<sub>4</sub>)<sub>4</sub>

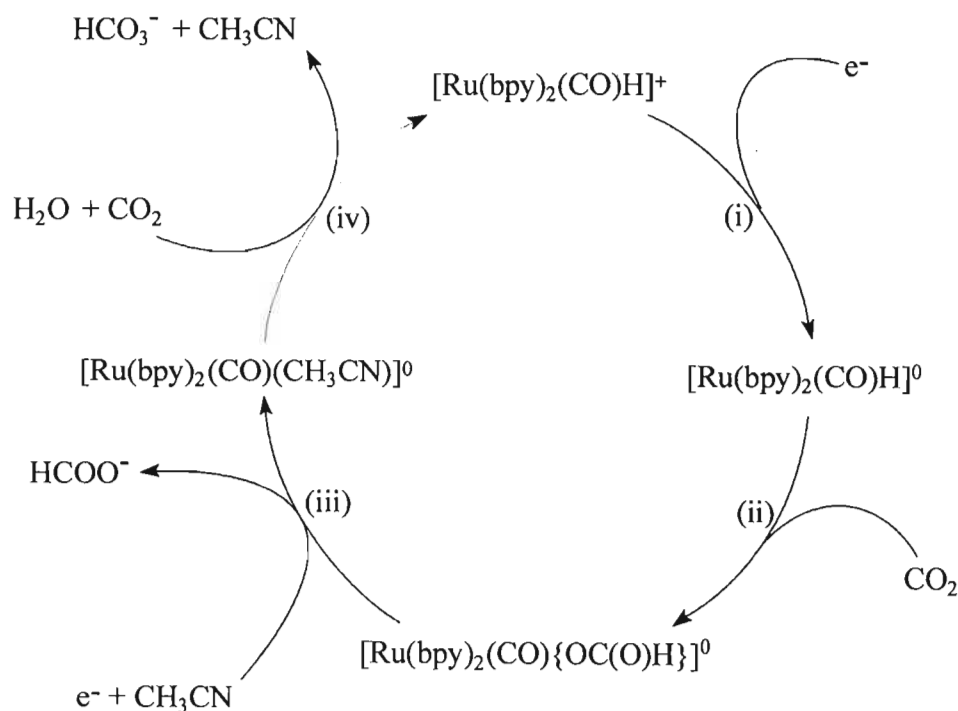
DuBois has described the catalytic activity of the palladium(II) complex [Pd<sub>2</sub>(μ-eHTP)(CH<sub>3</sub>CN)<sub>2</sub>](BF<sub>4</sub>)<sub>4</sub> [eHTP = (Et<sub>2</sub>PCH<sub>2</sub>CH<sub>2</sub>)<sub>2</sub>PCH<sub>2</sub>P(CH<sub>2</sub>CH<sub>2</sub>PEt<sub>2</sub>)<sub>2</sub>], which is a dinuclear analogue of the [Pd(triphos)(CH<sub>3</sub>CN)](BF<sub>4</sub>)<sub>2</sub> complexes.<sup>21</sup> Controlled potential electrolysis of acidified dimethylformamide solution of the former under CO<sub>2</sub> at -1.3 V vs. ferrocene showed that the reduced form of [Pd<sub>2</sub>(μ-eHTP)(CH<sub>3</sub>CN)<sub>2</sub>](BF<sub>4</sub>)<sub>4</sub> catalyses the electrochemical reduction of CO<sub>2</sub> to CO. Significantly the catalytic rate of CO<sub>2</sub> reduction for [Pd<sub>2</sub>(μ-eHTP)(CH<sub>3</sub>CN)<sub>2</sub>](BF<sub>4</sub>)<sub>4</sub> is at least three orders of magnitude greater than that of the mononuclear analogue at a similar potential. This has been accounted for in terms of a cooperative interaction between the two palladium sites and CO<sub>2</sub> during the catalytic cycle, in which one palladium centre binds to the carbon atom of the CO<sub>2</sub> while the second bonds to an oxygen atom.<sup>21</sup>

### 1.3.3. Ruthenium Complexes as Electrocatalysts

A number of closely related *bis*  $\alpha$ -diimine ruthenium(II) complexes have been shown to be catalysts for the electrochemical reduction of carbon dioxide. These include  $[\text{Ru}(\text{bpy})_2(\text{CO})_2]^{2+}$ ,  $[\text{Ru}(\text{bpy})_2(\text{CO})\text{Cl}]^+$ ,<sup>22,23,24</sup> *cis*- $[\text{Ru}(\text{bpy})_2(\text{CO})\text{H}]^+$ ,<sup>23,25</sup>  $[\text{Ru}(\text{bpy})_2(\text{qu})(\text{CO})]^{2+}$  (qu = quinoline),<sup>26</sup>  $[\text{Ru}(\text{bpy})(\text{trpy})(\text{CO})]^{2+}$  (trpy = 2,2':6',2''-terpyridine),<sup>27</sup>  $[\text{Ru}(\text{bpy})(\text{napy})_2(\text{CO})_2](\text{PF}_6)_2$ ,<sup>28</sup> *cis*- $[\text{Ru}(\text{bpy})_2(\text{py})\text{Cl}]^+$  (py = pyridine), *cis*- $[\text{Ru}(\text{bpy})_2(\text{solv})\text{Cl}]^{2+}$  (solv = CH<sub>3</sub>CN or DMF) and *cis*- $[\text{Ru}(\text{bpy})_2\text{Cl}_2]$ .<sup>23</sup> The catalytic properties of these complexes will now be briefly reviewed.

#### 1.3.3.(i) *cis*- $[\text{Ru}(\text{bpy})_2(\text{CO})\text{H}]^+$

The CV of *cis*- $[\text{Ru}(\text{bpy})_2(\text{CO})\text{H}]^+$  has been shown to consist of two reversible redox processes at  $E_{1/2} = -1.45$  and  $-1.65$  V vs. a saturated sodium chloride calomel reference electrode (SSCE), which arise from the sequential reduction of the two bipyridyl ligands.<sup>25</sup> The CV of a CO<sub>2</sub>-saturated acetonitrile solution of *cis*- $[\text{Ru}(\text{bpy})_2(\text{CO})\text{H}]^+$  showed a dramatic increase in peak current at both reduction waves. Controlled-potential electrolysis at potentials from  $-1.3$  to  $-1.6$  V of the complex in CO<sub>2</sub>-saturated CH<sub>3</sub>CN/H<sub>2</sub>O solutions revealed that *cis*- $[\text{Ru}(\text{bpy})_2(\text{CO})\text{H}]^+$  catalyses the electrochemical reduction of carbon dioxide to the formate anion and CO.

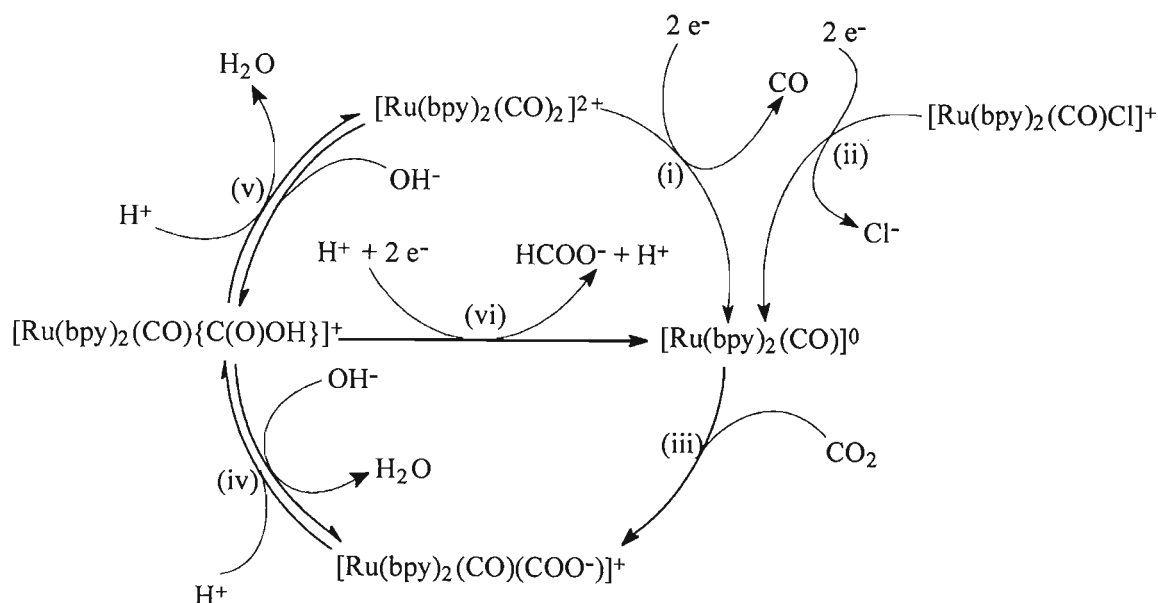


**Scheme 1.9.** Proposed mechanism for the electrochemical reduction of CO<sub>2</sub> catalysed by *cis*- $[\text{Ru}(\text{bpy})_2(\text{CO})\text{H}]^+$ .

A mechanism proposed by Meyer *et al.* for the reaction that leads to the formate anion is given in Scheme 1.9.<sup>25</sup> The first step (i) is the one electron bipyridyl-based reduction of  $[\text{Ru}(\text{bpy})_2(\text{CO})\text{H}]^+$ . This enhances the electron density in the complex, activating the Ru-H bond towards  $\text{CO}_2$  insertion (ii). The singly reduced formate complex  $[\text{Ru}(\text{bpy})_2(\text{CO})\{\text{OC}(\text{O})\text{H}\}]^0$ , undergoes a second reduction leading to the loss of the formate anion and to the formation of the acetonitrile complex (iii). The reduction of water to reform the hydride completes the catalytic cycle (iv).

### 1.3.3.(ii) $[\text{Ru}(\text{bpy})_2(\text{CO})\text{Cl}]^+$ and $[\text{Ru}(\text{bpy})_2(\text{CO})_2]^{2+}$

The complex  $[\text{Ru}(\text{bpy})_2(\text{CO})\text{Cl}]^+$  undergoes two successive one-electron reductions in a DMF solution; one reversible reduction at  $-1.24$  V and an irreversible reduction at  $-1.48$  V *vs.* SCE, which is followed by a chemical reaction.<sup>22</sup> The cyclic voltammogram of  $[\text{Ru}(\text{bpy})_2(\text{CO})_2]^{2+}$  shows an irreversible two electron reduction at  $-0.95$  V.<sup>22</sup> The CVs of both  $[\text{Ru}(\text{bpy})_2(\text{CO})\text{Cl}]^+$  and  $[\text{Ru}(\text{bpy})_2(\text{CO})_2]^{2+}$  in  $\text{CO}_2$ -saturated DMF are essentially the same as those of the complexes under  $\text{N}_2$ , but show a strong enhancement in current around  $-1.40$  V *vs.* SCE. The controlled-potential electrolysis of a  $\text{CO}_2$ -saturated DMF/ $\text{H}_2\text{O}$  (pH 6.0) solution containing  $[\text{Ru}(\text{bpy})_2(\text{CO})\text{Cl}]^+$  or  $[\text{Ru}(\text{bpy})_2(\text{CO})_2]^{2+}$  at  $-1.50$  V shows that the complexes mediate the electrochemical reduction of  $\text{CO}_2$  to CO. In a  $\text{CO}_2$ -saturated alkaline DMF/ $\text{H}_2\text{O}$  (pH 9.5) solution, electrolysis gives not only CO but also  $\text{HCOO}^-$ .



**Scheme 1.10.** Mechanism of electrochemical reduction of  $\text{CO}_2$  to CO and  $\text{HCO}_2^-$  catalysed by  $[\text{Ru}(\text{bpy})_2(\text{CO})\text{Cl}]^+$  and  $[\text{Ru}(\text{bpy})_2(\text{CO})_2]^{2+}$ .

A possible mechanism for the reduction of CO<sub>2</sub> in this system is presented in Scheme 1.10.<sup>22</sup> The complex [Ru(bpy)<sub>2</sub>(CO)<sub>2</sub>]<sup>2+</sup> undergoes an irreversible two-electron reduction to give the twenty electron complex [Ru(bpy)<sub>2</sub>(CO)<sub>2</sub>]<sup>0</sup>. Carbon monoxide dissociates from this, generating the 18 electron pentacoordinate complex [Ru(bpy)<sub>2</sub>(CO)]<sup>0</sup> (i). The two electron reduction of [Ru(bpy)<sub>2</sub>(CO)Cl]<sup>+</sup> results in the dissociation of Cl<sup>-</sup> to afford the same reactive intermediate (ii). Carbon dioxide reacts with the latter to produce [Ru(bpy)<sub>2</sub>(CO)(COO<sup>-</sup>)]<sup>+</sup> (iii), proceeding through [Ru(bpy)<sub>2</sub>(CO)(η<sup>1</sup>-CO<sub>2</sub>)].<sup>29,30</sup> The CO<sub>2</sub> adduct is easily converted to [Ru(bpy)<sub>2</sub>(CO)<sub>2</sub>]<sup>2+</sup> through [Ru(bpy)<sub>2</sub>(CO){η<sup>1</sup>-C(O)OH}]<sup>2+</sup> in acidic conditions according to the equilibrium reactions (iv) and (v).<sup>31</sup> On the other hand in weakly alkaline conditions [Ru(bpy)<sub>2</sub>(CO){C(O)OH}]<sup>+</sup> exists as the predominant species, which undergoes a two electron reduction involving the participation of a proton to give HCOO<sup>-</sup> with regeneration of the pentacoordinate intermediate [Ru(bpy)<sub>2</sub>(CO)]<sup>0</sup> (vi).

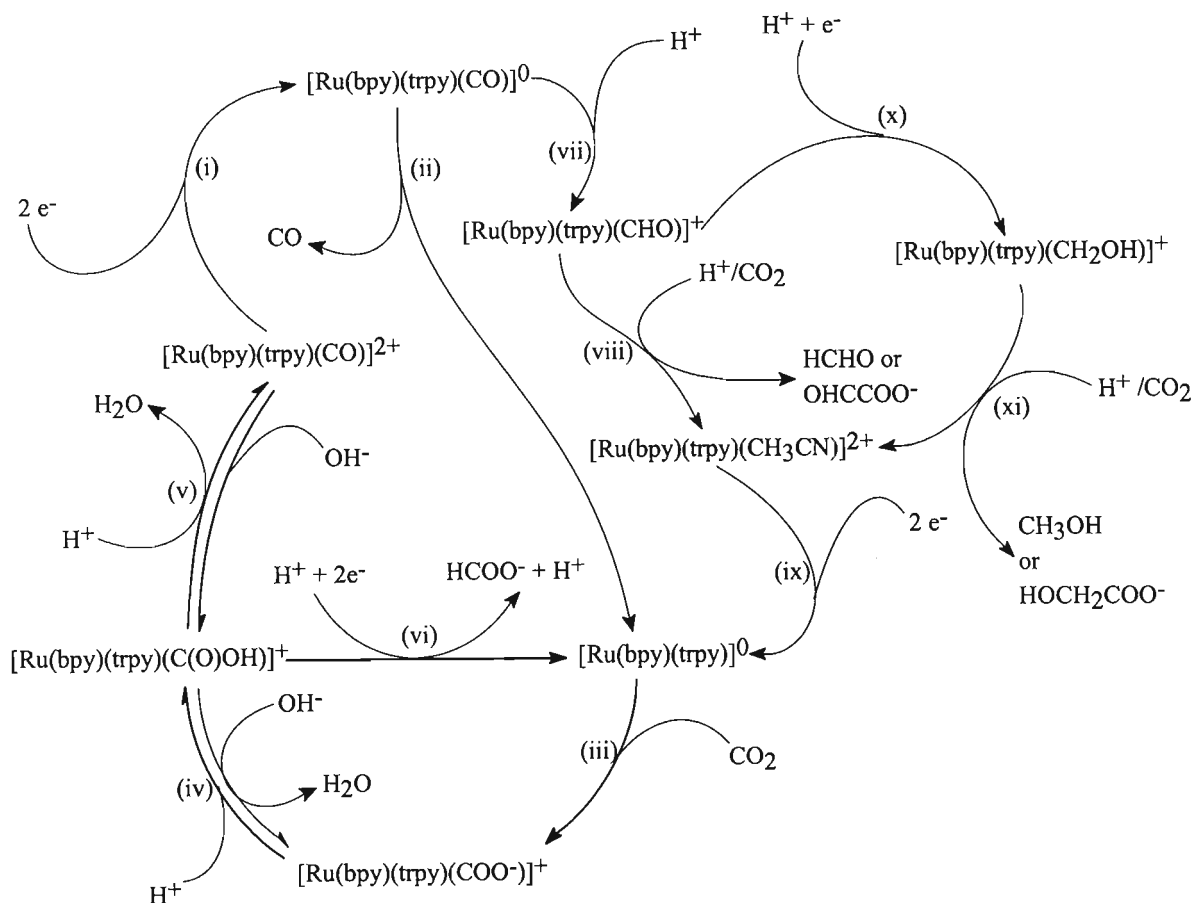
### 1.3.3.(iii) [Ru(bpy)(trpy)(CO)]<sup>2+</sup>

The complex [Ru(bpy)(trpy)(CO)]<sup>2+</sup> is remarkable in that it has the ability to catalyse the four- and six-electron reduction of CO<sub>2</sub> coupled with carbon-carbon bond formation.<sup>27</sup> In contrast to [Ru(bpy)<sub>2</sub>(CO)<sub>2</sub>]<sup>2+</sup>, which undergoes an irreversible two-electron reduction resulting in the dissociation of the carbonyl ligand, [Ru(bpy)(trpy)(CO)]<sup>2+</sup> is reversibly reduced in two steps to [Ru(bpy)(trpy)(CO)]<sup>0</sup> at -20°C.<sup>27</sup> The controlled-potential electrolysis of [Ru(bpy)(trpy)(CO)]<sup>2+</sup> at -1.75 V vs. Ag/Ag<sup>+</sup> in a CO<sub>2</sub>-saturated C<sub>2</sub>H<sub>5</sub>OH/H<sub>2</sub>O solution at -20°C produced HC(O)H, CH<sub>3</sub>OH, H(O)CCOOH and HOCH<sub>2</sub>COOH together with CO and HCOOH. Under similar conditions the electrochemical reduction of CO<sub>2</sub> in the presence of [Ru(bpy)<sub>2</sub>(CO)<sub>2</sub>]<sup>2+</sup> gave only CO and HCOOH.

A mechanism for the electrochemical reduction of CO<sub>2</sub> catalysed by [Ru(bpy)(trpy)(CO)]<sup>2+</sup> is presented in Scheme 1.11.<sup>27,32</sup> The achievement of the multi-electron reduction of CO<sub>2</sub> by [Ru(bpy)(trpy)(CO)]<sup>2+</sup> is ascribed to the stability of [Ru(bpy)(trpy)(CO)]<sup>0</sup> at -20°C. Thus while Ru-CO bond cleavage spontaneously occurs in [Ru(bpy)<sub>2</sub>(CO)<sub>2</sub>]<sup>0</sup>, [Ru(bpy)(trpy)(CO)]<sup>0</sup> is protonated to [Ru(bpy)(trpy)(CHO)]<sup>+</sup>. This reaction is outlined in step (vii) of Scheme 1.10. The reduction of [Ru(bpy)(trpy)(CHO)]<sup>+</sup> in protic media will afford HC(O)H (viii) or [Ru(bpy)(trpy)(CH<sub>2</sub>OH)]<sup>+</sup> (x), the latter of which is a possible precursor to CH<sub>3</sub>OH, as shown in step (xi). The products H(O)CCOOH and HOCH<sub>2</sub>COOH possibly arise from the carboxylation of [Ru(bpy)(trpy)(CHO)]<sup>+</sup> (viii) and [Ru(bpy)(trpy)(CH<sub>2</sub>OH)]<sup>+</sup> (xi) respectively. At room temperature [Ru(bpy)(trpy)(CO)]<sup>0</sup> is thermally labile, the key intermediate in the multi-electron reduction pathway, [Ru(bpy)(trpy)(CHO)]<sup>+</sup>, cannot be formed and thus the



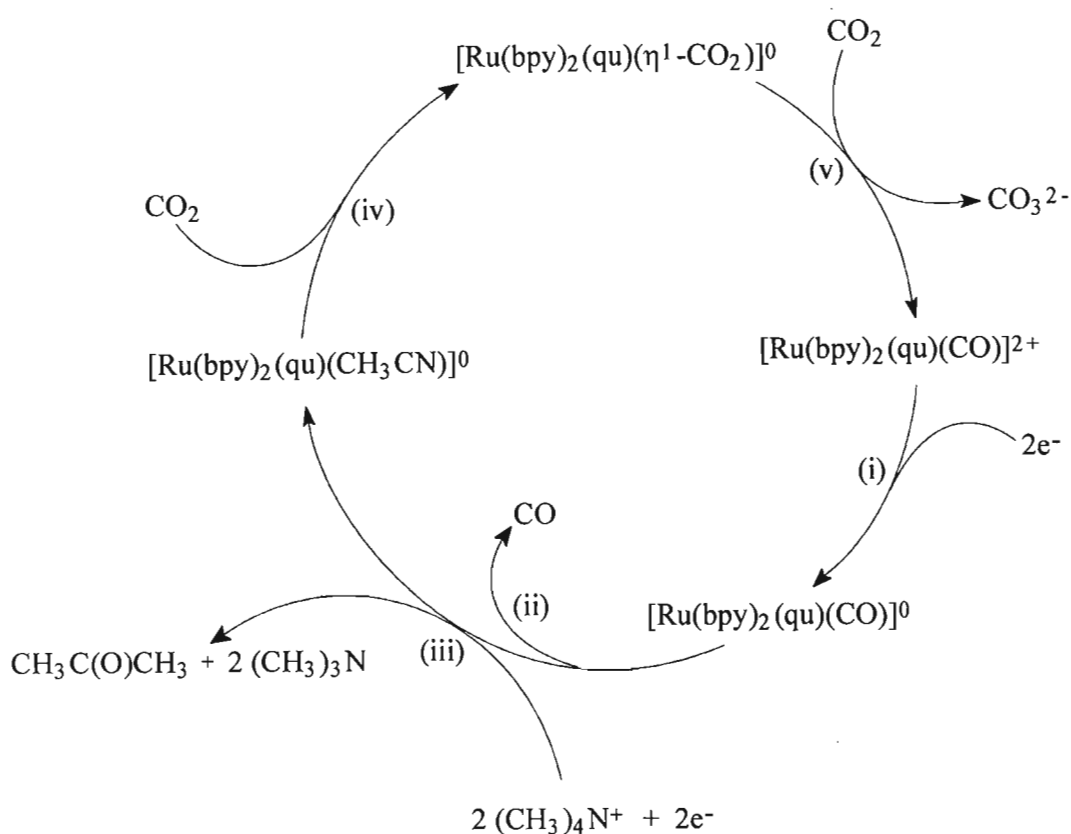
ruthenium complex only catalyses the reduction of CO<sub>2</sub> to HCOOH and CO. The mechanism of this reaction is shown in steps (ii) - (v) and is the same as that previously described for [Ru(bpy)<sub>2</sub>(CO)<sub>2</sub>]<sup>2+</sup>.



**Scheme 1.11.** Mechanism for the electrochemical reduction of CO<sub>2</sub> catalysed by [Ru(bpy)(trpy)(CO)]<sup>2+</sup>.

### 1.3.3.(iv) [Ru(bpy)<sub>2</sub>(qu)(CO)]<sup>2+</sup>

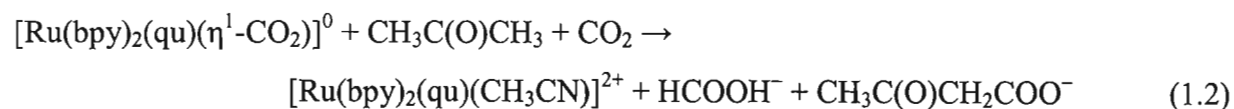
The cyclic voltammogram of [Ru(bpy)<sub>2</sub>(qu)(CO)]<sup>2+</sup> shows three reversible one-electron redox waves at -1.11, -1.37 and -1.65 V vs. Ag/AgCl in acetonitrile under a N<sub>2</sub> atmosphere.<sup>26</sup> In the presence of CO<sub>2</sub> the cyclic voltammogram of [Ru(bpy)<sub>2</sub>(qu)(CO)]<sup>2+</sup> shows a strong cathodic current at a potential just negative of the cathodic wave for the [Ru(bpy)<sub>2</sub>(qu)(CO)]<sup>1+/0</sup> couple, suggesting high reactivity of the reduced form of the complex with CO<sub>2</sub>. The controlled-potential electrolysis of [Ru(bpy)<sub>2</sub>(qu)(CO)]<sup>2+</sup> at -1.50 V vs. Ag/AgCl in CO<sub>2</sub>-saturated CH<sub>3</sub>CN using LiBF<sub>4</sub> as a supporting electrolyte showed that the reduced complex catalysed the reductive disproportionation of CO<sub>2</sub> to CO and CO<sub>3</sub><sup>2-</sup>. On the other hand, the same controlled-potential electrolysis, but using Me<sub>4</sub>NBF<sub>4</sub> as a supporting electrolyte, predominantly produced CO. In addition HCOOH<sup>-</sup>, CH<sub>3</sub>C(O)CH<sub>3</sub> and CH<sub>3</sub>C(O)CH<sub>2</sub>COO<sup>-</sup> are produced as minor products, with



the concomitant formation of  $\text{Me}_3\text{N}$ . The supporting electrolyte  $\text{Me}_4\text{NBF}_4$  functions as a methylating agent of the carbonyl moiety resulting from the reductive disproportionation of  $\text{CO}_2$ .

**Scheme 1.12.** Mechanism for the electrocatalytic reduction of  $\text{CO}_2$  mediated by  $[\text{Ru}(\text{bpy})_2(\text{qu})(\text{CO})]^{2+}$ .

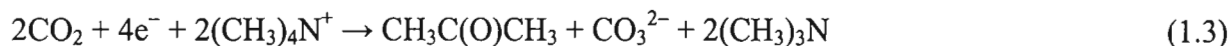
A proposed mechanism is given in Scheme 1.12.<sup>26</sup> The two-electron reduction of  $[\text{Ru}(\text{bpy})_2(\text{qu})(\text{CO})]^{2+}$ , step (i), induces the double methylation of the carbonyl ligand by the supporting electrolyte to produce  $\text{CH}_3\text{C}(\text{O})\text{CH}_3$  (iii). Alternatively, a spontaneous Ru–CO bond cleavage will occur in  $[\text{Ru}(\text{bpy})_2(\text{qu})(\text{CO})]^0$ , producing CO (ii). It is believed the resulting  $\text{CH}_3\text{C}(\text{O})\text{CH}_3$  undergoes abstraction of its  $\alpha$ -proton by  $[\text{Ru}(\text{bpy})_2(\text{qu})(\eta^1\text{-CO}_2)]^0$  followed by carboxylation. Thus both  $\text{CH}_3\text{C}(\text{O})\text{CH}_2\text{COO}^-$  and  $\text{HCOOH}^-$  are formed under a  $\text{CO}_2$  atmosphere.



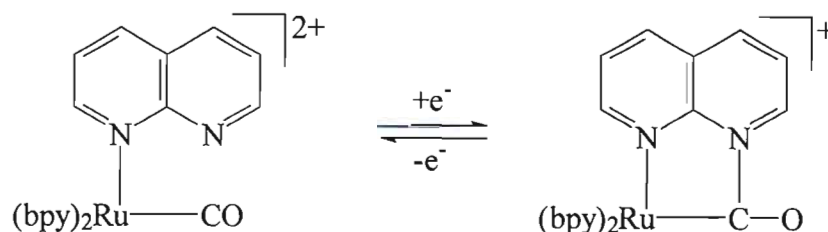
The complex  $[\text{Ru}(\text{bpy})_2(\text{qu})(\text{CH}_3\text{CN})]^0$  catalyses the reductive disproportionation of  $\text{CO}_2$ , proceeding via  $[\text{Ru}(\text{bpy})_2(\text{qu})(\eta^1\text{-CO}_2)]^0$  and the subsequent oxide abstraction by  $\text{CO}_2$ , as shown in steps (iv) and (v).

### 1.3.3.(v) $[\text{Ru}(\text{bpy})(\text{napy})_2(\text{CO})_2](\text{PF}_6)_2$

The 1,8-naphthyridine coordinated Ru(II) complex  $[\text{Ru}(\text{bpy})(\text{napy})_2(\text{CO})_2](\text{PF}_6)_2$  selectively catalyses the electrochemical reduction of  $\text{CO}_2$  to acetone in the presence of  $(\text{CH}_3)_4\text{NBF}_4$ .<sup>28,33</sup> The CV of  $[\text{Ru}(\text{bpy})(\text{napy})_2(\text{CO})_2](\text{PF}_6)_2$  in DMSO +  $(\text{CH}_3)_4\text{NBF}_4$  ( $0.1 \text{ molL}^{-1}$ ) displays two irreversible cathodic waves at  $E_{\text{pc}} = -0.76$  and  $-0.98 \text{ V}$  followed by three quasi-reversible waves at  $E_{\text{pc}} = -1.44$ ,  $-1.58$  and  $-1.94 \text{ V}$  vs.  $\text{Ag}/\text{Ag}^+$ . In the presence of  $\text{CO}_2$  a strong catalytic current is seen at potentials more negative than  $-1.4 \text{ V}$ . Controlled potential electrolysis of  $[\text{Ru}(\text{bpy})(\text{napy})_2(\text{CO})_2](\text{PF}_6)_2$  at  $-1.6 \text{ V}$  in  $\text{CO}_2$  saturated DMSO +  $\text{LiBF}_4$  ( $0.1 \text{ molL}^{-1}$ ) produced the two-electron reduction products  $\text{CO}$  and  $\text{CO}_3^{2-}$ . Under the same experimental conditions, but using  $(\text{CH}_3)_4\text{NBF}_4$  in place of  $\text{LiBF}_4$ , acetone was generated with traces of  $\text{CO}$ , the electrolyte functioning as a methylating agent according to Equation 1.3.



The first two one-electron reductions of  $[\text{Ru}(\text{bpy})(\text{napy})_2(\text{CO})_2](\text{PF}_6)_2$  are based on the monodentate napy ligands and lead to the formation of a  $\text{Ru}-\text{C}(\text{O})-\text{N}-\text{N}$  ring by nucleophilic attack of the non-bonded napy nitrogen atom on the carbonyl carbon atom (Scheme 1.13).<sup>28,34</sup> This metallocyclisation is key to the formation of acetone as it suppresses the reductive cleavage of the  $\text{Ru}-\text{CO}$  bond.

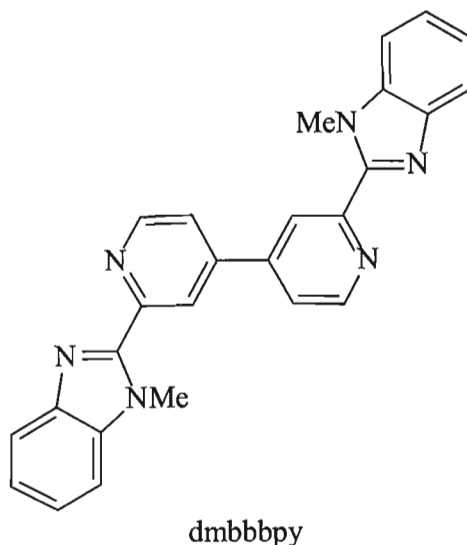


**Scheme 1.13.** Intramolecular nucleophilic attack by the non-bonded nitrogen of monodentate napy to form a five-membered ring.

### 1.3.3.(vi) $[\text{Ru}(\text{dmdbbpy})(\text{bpy})_2](\text{PF}_6)_2$ and $[\text{Ru}_2(\mu\text{-dmdbbpy})(\text{bpy})_4](\text{PF}_6)_4$

The mono and dinuclear ruthenium(II) complexes  $[\text{Ru}(\text{dmdbbpy})(\text{bpy})_2](\text{PF}_6)_2$  [ $\text{dmdbbpy} = 2,2'$ -bis(1-methylbenzimidazol-2-yl)-4,4'-bipyridine] and  $[\text{Ru}_2(\mu\text{-dmdbbpy})(\text{bpy})_4](\text{PF}_6)_4$  have

been reported to catalyse the electrochemical reduction of carbon dioxide to  $\text{HCO}_2\text{H}$ ,  $\text{CO}$  and  $\text{C}_2\text{O}_4^{2-}$ .<sup>35</sup> The unsymmetrical chelating ligand serves to not only accumulate the electrons necessary for  $\text{CO}_2$  reduction but also to create a reaction site by the opening of the chelate ring.

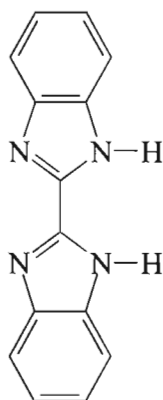


The CV of  $[\text{Ru}(\text{dmbbbpy})(\text{bpy})_2](\text{PF}_6)_2$  consists of three reversible one-electron reductions at  $E_{1/2} = -1.45, -1.75$  and  $-1.99$  V (vs.  $\text{Ag}/\text{AgCl}$ ). Similarly,  $[\text{Ru}_2(\mu\text{-dmbbbpy})(\text{bpy})_4](\text{PF}_6)_4$  shows three reversible redox couples with a small positive shift (0.2 V) for the first dmbbbpy based reduction. Introduction of  $\text{CO}_2$  into the acetonitrile solutions of  $[\text{Ru}(\text{dmbbbpy})(\text{bpy})_2](\text{PF}_6)_2$  and  $[\text{Ru}_2(\mu\text{-dmbbbpy})(\text{bpy})_4](\text{PF}_6)_4$  results in an increase in cathodic current at potentials more negative than  $-1.60$  and  $-1.50$  V respectively. Controlled-potential electrolysis of  $[\text{Ru}(\text{dmbbbpy})(\text{bpy})_2](\text{PF}_6)_2$  and  $[\text{Ru}_2(\mu\text{-dmbbbpy})(\text{bpy})_4](\text{PF}_6)_4$  at  $-1.65$  and  $-1.55$  V, carried out in  $\text{CO}_2$ -saturated acetonitrile, yielded  $\text{C}_2\text{O}_4^{2-}$ . The similar electrochemical reduction of  $\text{CO}_2$  in the presence of  $\text{H}_2\text{O}$  produced predominantly  $\text{HCO}_2^-$  with trace amounts of  $\text{CO}$ . Significantly, the reduced forms of  $[\text{Ru}(\text{bpy})_2\text{L}]^{2+}$  ( $\text{L} = \text{bpy}$  and 2-pyridyl-1-methylbenzimidazole) have no ability to catalyse the electrochemical reduction of  $\text{CO}_2$ . The authors believe that the two-electron reduction of the dmbbbpy complexes causes dechelation of the unsymmetrical ligand. The resultant five coordinate Ru and monodentate  $\text{dmbbbpy}^-$  provides two binding sites for the  $\text{CO}_2$  substrate, thereby facilitating the coupling reaction of  $\text{CO}_2$  to afford oxalate.

### 1.3.3.(vii) $[\text{Ru}(\text{H}_2\text{bibzim})(\text{tbbpy})_2]\text{Cl}_2$ , $[\text{Ru}(\text{bibzim})(\text{tbbpy})_2]$ and $[\{\text{Ru}(\text{tbbpy})_2\}_2(\text{bibzim})](\text{PF}_6)_2$

The benzimidazole containing ruthenium polypyridyl complex  $[\text{Ru}(\text{H}_2\text{bibzim})(\text{tbbpy})_2]\text{Cl}_2$  ( $\text{tbbpy} = 4,4'$ -di-*tert*-butyl-2,2'-bipyridine,  $\text{H}_2\text{bibzim} = 1,1'$ -bibenzimidazole), its deprotonated analogue  $[\text{Ru}(\text{bibzim})(\text{tbbpy})_2]$  and the dinuclear,

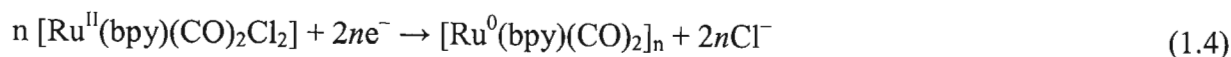
deprotonated complex  $[\{\text{Ru}(\text{tbbpy})_2\}_2(\text{bibzim})](\text{PF}_6)_2$  have been reported to be active catalysts for the electrochemical reduction of  $\text{CO}_2$ .<sup>36</sup> The complexes all exhibit two reversible one-electron reductions while the protonated complex  $[\text{Ru}(\text{H}_2\text{bibzim})(\text{tbbpy})_2]\text{Cl}_2$  shows a more complex redox behaviour. In the presence of  $\text{CO}_2$  an increase in cathodic current is seen for the second reduction step. From the degree of current enhancement, the activity of the complexes increases two-fold from  $[\text{Ru}(\text{H}_2\text{bibzim})(\text{tbbpy})_2]\text{Cl}_2$  to  $[\text{Ru}(\text{bibzim})(\text{tbbpy})_2]$ , while the dimer complex is further more active. Deprotonation of the bibenzimidazole ligand enhances its  $\sigma$ -donor properties and increases the electron density on the metal centre. Preliminary investigations bear out this difference in activity; exhaustive electrolysis experiments of the complexes in  $\text{CO}_2$  saturated  $\text{CH}_3\text{CN}$  show that  $[\text{Ru}(\text{H}_2\text{bibzim})(\text{tbbpy})_2]\text{Cl}_2$  produces oxalate and  $\text{CO}$  with current efficiencies of *ca.* 10 and 1-2 % respectively, in comparison to 43 and 1-2 % for  $[\text{Ru}(\text{bibzim})(\text{tbbpy})_2]$ .



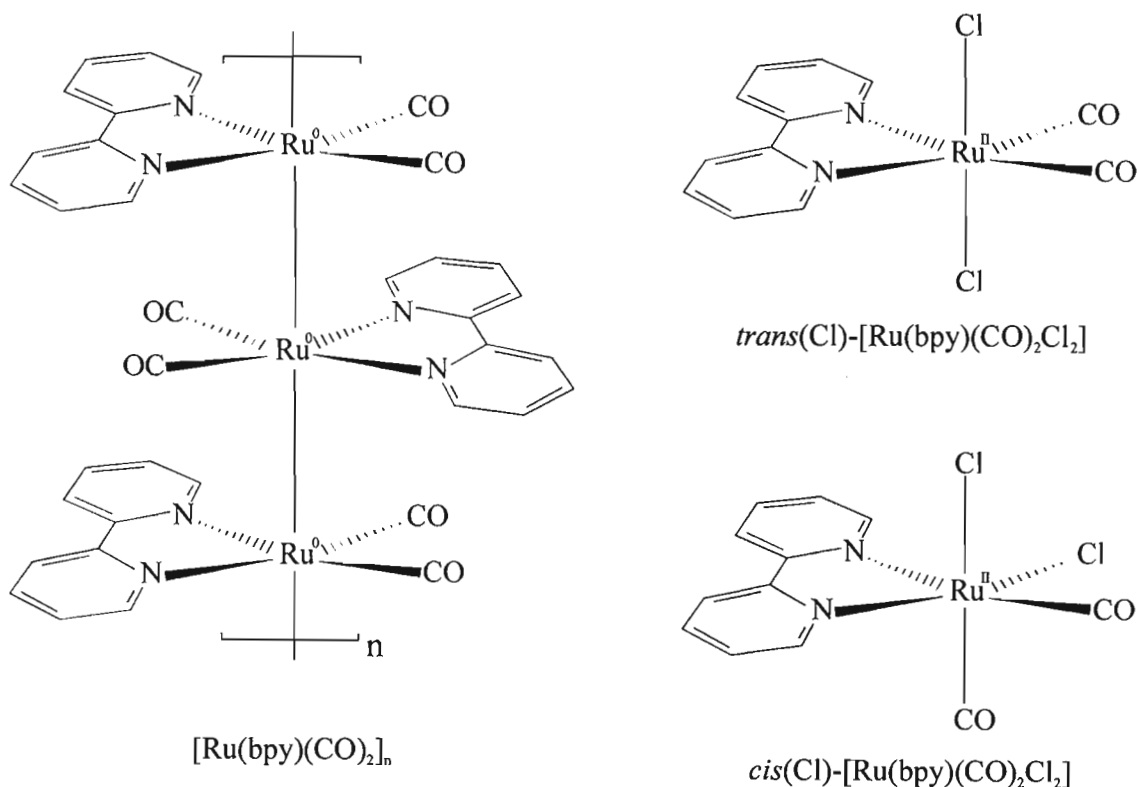
$\text{H}_2\text{bibzim}$

### 1.3.3.(viii) $[\text{Ru}(\text{bpy})(\text{CO})_2]_n$

The mono(bipyridine) complex *trans*(Cl)- $[\text{Ru}(\text{bpy})(\text{CO})_2\text{Cl}_2]$  is known to act as an efficient homogeneous catalyst for the electrochemical reduction of carbon dioxide.<sup>23,24,37</sup> For instance, in aqueous acetonitrile solution *trans*(Cl)- $[\text{Ru}(\text{bpy})(\text{CO})_2\text{Cl}_2]$  catalyses the electrochemical reduction of  $\text{CO}_2$  at  $-1.30$  V vs. SCE to  $\text{CO}$  with an 88% current efficiency.<sup>24</sup> In addition, it has been shown beyond doubt that the formation of an electroactive  $[\text{Ru}(\text{bpy})(\text{CO})_2]_n$  polymeric film, formed upon reduction of  $[\text{Ru}(\text{bpy})(\text{CO})_2\text{Cl}_2]$ ,<sup>38,39</sup> is key to the electrocatalytic behaviour of this complex.<sup>37,40,41,42</sup> Electropolymerisation of the Ru(II) monomer results from the overall addition of two electrons per mole of  $[\text{Ru}(\text{bpy})(\text{CO})_2\text{Cl}_2]$  and is associated with the loss of both chloride ligands (Equation 1.4).



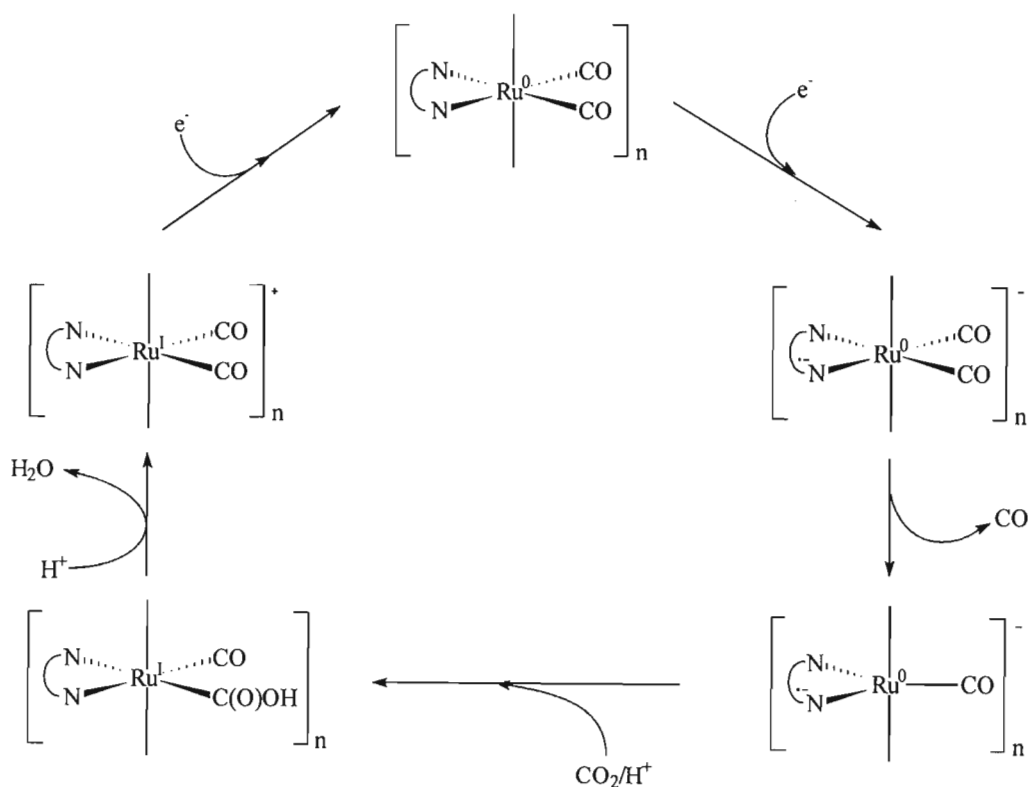
The resulting dark blue, strongly adherent film formed on the electrode surface is composed of an 'open' cluster polymer  $[\text{Ru}(\text{bpy})(\text{CO})_2]_n$  based upon extended  $\text{Ru}^0\text{-Ru}^0$  bonds.<sup>38</sup> The formation of the  $\text{Ru}(0)$  polymer is independent of the stereochemistry of the  $\text{Ru}(\text{II})$  monomer precursor, both *cis*(Cl)- and *trans*(Cl)- $[\text{Ru}(\text{bpy})(\text{CO})_2\text{Cl}_2]$  giving rise to the same  $[\text{Ru}(\text{L})(\text{CO})_2]_n$  polymer upon reduction.<sup>43</sup> The method has general applicability: through the two-electron reduction of the appropriate  $\text{Ru}(\text{II})$  precursor  $[\text{Ru}(\text{L})(\text{CO})_2\text{X}_2]$  (L = substituted 2,2'-bipyridyl or phenanthroline derivative; X = Cl or Br) diverse  $[\text{Ru}(\text{L})(\text{CO})_2]_n$  films have been prepared.<sup>39,44</sup>



Carbon- $[\text{Ru}(\text{bpy})(\text{CO})_2]_n$  modified electrodes are efficient electrocatalysts for the selective reduction of  $\text{CO}_2$  to CO (97% current efficiency) at  $-1.55$  V vs. SCE in aqueous acetonitrile.<sup>37</sup> Significantly,  $[\text{Ru}(\text{bpy})(\text{CO})_2]_n$  catalyses the reduction  $\text{CO}_2$  to CO in pure aqueous electrolyte with the same selectivity (> 97 %) at a moderate applied potential.<sup>40,42</sup>

A mechanism for the electrocatalytic reaction based upon the proposed  $\text{Ru}(0)$  polymeric structure is shown in Scheme 1.14.<sup>40</sup> The one-electron reduction of a  $[\text{Ru}(\text{bpy})(\text{CO})_2]$  unit in the  $\text{Ru}(0)$  polymer gives an unstable 19 electron species  $[\text{Ru}(\text{bpy}^{\cdot-})(\text{CO})_2]^-$ ; this liberates CO to form the pentacoordinate species  $[\text{Ru}(\text{bpy}^{\cdot-})(\text{CO})]^-$ . The reaction of  $[\text{Ru}(\text{bpy}^{\cdot-})(\text{CO})]^-$  with  $\text{CO}_2$  in the presence of  $\text{H}_2\text{O}$  leads to the intermediate  $[\text{Ru}(\text{bpy})(\text{CO})\{\text{C}(\text{O})\text{OH}\}]$ . C-O bond cleavage results in the formation of  $\text{H}_2\text{O}$  and  $[\text{Ru}(\text{bpy})(\text{CO})_2]^+$ , which is reduced back to  $[\text{Ru}(\text{bpy})(\text{CO})_2]$  to continue the cycle.

Notably,  $[\text{Ru}(\text{L})(\text{CO})_2]_n$  catalysts containing bipyridyl ligands substituted by electron-withdrawing groups give  $\text{HCOO}^-$  as the major product with current efficiencies of 90 %.<sup>42</sup> Conversely, the 4,4'-dimethyl-2,2'-bipyridine substituted analogue primarily leads to CO. The selectivity of the catalyst for CO or  $\text{HCOO}^-$  formation can therefore be controlled by choice of the appropriately substituted bipyridyl ligand. The nature of the intermediate formed by the reaction of the pentacoordinate species  $[\text{Ru}(\text{L}^-)(\text{CO})]_n^-$  with  $\text{CO}_2$  and  $\text{H}_2\text{O}$  dictates whether CO or  $\text{HCOO}^-$  is produced. The preliminary formation of a metal hydride followed by insertion of  $\text{CO}_2$  leads to the formate form  $\text{M}-\text{O}-\text{C}(\text{O})\text{H}$  from which  $\text{HCOO}^-$  is generated. Carbon monoxide originates from the metalcarboxylic acid form  $\text{M}-\text{C}(\text{O})\text{OH}$  generated by reaction of  $\text{CO}_2$  with the intermediate  $[\text{Ru}(\text{L}^-)(\text{CO})]_n^-$  anion followed by protonation.



**Scheme 1.14.** Proposed mechanism for the electrochemical reduction of  $\text{CO}_2$  catalysed by  $[\text{Ru}(\text{bpy})(\text{CO})_2]_n$ .

#### 1.4. Aims of this Work

A number of conclusions can be drawn from the examples reviewed;

A key feature in many of the catalysts is the utilisation of polypyridyl ligands, which can function not only as ‘electron reservoirs’ but can stabilise the metal in a low oxidation state necessary to trigger the binding of carbon dioxide to it.

Provision is made in the complexes for the formation of a vacant site for coordination of the substrate during the catalytic cycle. This is achieved either through the incorporation of a weakly bound solvent ligand e.g. acetonitrile in  $[\text{Cu}_2(\mu\text{-Ph}_2\text{Pbpy})_2(\text{CH}_3\text{CN})_2](\text{PF}_6)_2$ , or the dissociation of a ligand initiated by the reduction of the complex e.g. the loss of  $\text{Cl}^-$  from  $[\text{Ru}(\text{bpy})_2(\text{CO})\text{Cl}]^+$  to form the coordinatively unsaturated species  $[\text{Ru}(\text{bpy})_2(\text{CO})]^0$ . Alternatively, though coordinatively saturated, the square-planar palladium catalysts are able to form a five coordinate intermediate.

The presence of a proton source in the electrochemical medium is pivotal in determining the catalytic pathway. The stepwise reduction of  $\text{CO}_2$  to  $\text{CH}_4$  essentially involves the breakage of C–O bonds and the formation of C–H bonds. It is therefore not unexpected that a number of these catalysts are only active in protic media. Under anhydrous conditions the complexes reviewed catalyse the electrochemical reduction of  $\text{CO}_2$  to  $\text{CO}$ ,  $\text{CO}_3^{2-}$  and  $\text{C}_2\text{O}_4^{2-}$ . In protic solvents,  $\text{CO}$  and  $\text{HCOOH}^-$  are the chief products of electrocatalytic reduction. This reflects the products formed by the direct electrochemical reduction of carbon dioxide in aprotic and protic media.

The structure of the ligands plays a crucial role in the activity of the electrocatalysts. This is well illustrated by considering the closely related ruthenium catalysts  $[\text{Ru}(\text{bpy})_2(\text{CO})_2]^{2+}$ ,  $[\text{Ru}(\text{bpy})_2(\text{qu})(\text{CO})]^{2+}$  and  $[\text{Ru}(\text{bpy})(\text{trpy})(\text{CO})]^{2+}$ ; while the former two complexes catalyse the two-electron reduction of  $\text{CO}_2$ , the latter mediates four- and six-electron reductions. In the palladium complexes  $[\text{Pd}(\text{triphos})(\text{solv})](\text{BF}_4)_2$  described by DuBois, any variation of the donor set from the tridentate phosphine inactivates the electrocatalyst.

The vast majority of homogeneous electrocatalysts mediate the two-electron reduction of carbon dioxide, the four- and six-electron reduction catalysed by  $[\text{Ru}(\text{bpy})(\text{trpy})(\text{CO})]^{2+}$  being a rare exception. The multi-electron reduction of carbon dioxide coupled with C–C bond formation remains a fundamental challenge in the activation of carbon dioxide. Ruthenium,<sup>45</sup> palladium,<sup>46</sup> platinum<sup>47</sup> and copper<sup>48</sup> cathodes are effective materials for the generation of hydrocarbons and alcohols from  $\text{CO}_2$ . The synthesis of dinuclear complexes of these metals is therefore of interest as they may mimic these heterogeneous catalysts in the homogeneous phase. Dinuclear transition metal complexes with bridging carbon dioxide ligands have been extensively studied as intermediates in the activation of carbon dioxide.<sup>49,50</sup> The binding of carbon dioxide to dinuclear complexes is believed to be enhanced by cooperative effects between the two metals and the substrate.<sup>21</sup> Moreover, the close proximity of the metal centres in dinuclear catalysts may allow for C–C bond formation. However, besides the copper, palladium and ruthenium complexes described above and the iron(0) porphyrin - Lewis acid cation



bimetallic systems reported by Savéant *et al.*,<sup>51</sup> few other dinuclear transition metal complexes have been explored as redox catalysts. The aim of this work is therefore the synthesis of low-valent, dinuclear complexes of copper, palladium, platinum and ruthenium containing phosphine and  $\alpha$ -diimine ligands that are potential electrocatalysts for the electrochemical reduction of carbon dioxide.

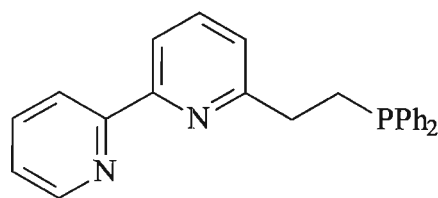
## Chapter 2. Synthesis and Characterisation of the Heterodifunctional Ligands 6-(diphenylphosphino)-2-(2-quinoly)pyridine I and 6-[ethyl(phenyl)phosphino]-2,2'-bipyridine II

---

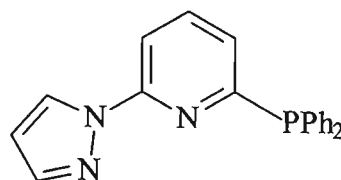
### 2.1. Introduction

Transition metal complexes of difunctional ligands containing both phosphorus(III) and nitrogen donor atoms are of topical interest, particularly with regard to the development of novel catalysts.<sup>52,53</sup> As a consequence of the distinctive electronic properties of the soft phosphorus and hard nitrogen atoms these ligands are expected to exhibit a coordination chemistry beyond that of the traditional diphosphorus and dinitrogen donor ligands. For example, their unsymmetrical nature facilitates the formation of heterodinuclear complexes. Furthermore, the hard nitrogen donor of some P,N ligands in certain chelate complexes is easily displaced from the metal centre. This hemilabile behaviour may be taken advantage of to generate a free coordination site during a catalytic cycle.<sup>54</sup> There is particular interest in transition metal complexes containing a chelating P,N ligand for use in asymmetric catalysis, as these ligands allow for precise control of the coordination sphere during a catalytic cycle.<sup>55</sup>

In comparison to pyridylphosphines,<sup>56</sup> polypyridylphosphines have received little attention. Ziessel *et al.* have prepared a number of aromatic polyimines substituted with the diphenylphosphine group.<sup>57</sup> Of particular relevance is the recently synthesised 6-(2-diphenylphosphinoethyl)-2,2'-bipyridine.<sup>58,59</sup> Initial studies show this ligand displays either P-monodentated, bridging or meridional coordinating behaviour towards ruthenium(II) and rhodium(III) ions. The 2-(diphenylphosphino)-6-(pyrazol-1-yl)pyridine ligand represents a further addition to this class of P,N ligands.<sup>60</sup>



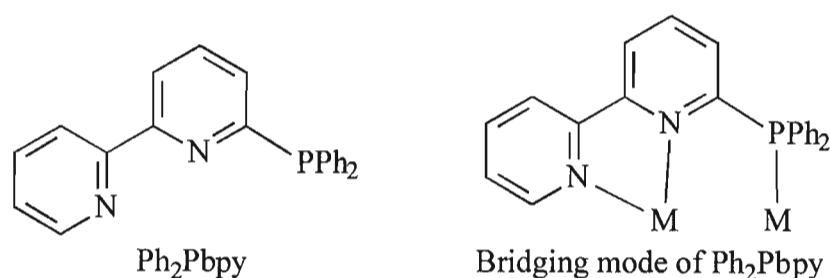
6-(2-diphenylphosphinoethyl)-2,2'-bipyridine



2-(diphenylphosphino)-6-(pyrazol-1-yl)pyridine

Of the P,N ligands whose coordination behaviour has been examined, considerable attention has been devoted to 2-(diphenylphosphino)pyridine ( $\text{Ph}_2\text{Ppy}$ ).<sup>128</sup> This ligand possesses a rigid, short bite and has been used as a bridging ligand to stabilise dinuclear and, in particular, heterodinuclear complexes.<sup>61</sup> The novel phosphorus-bipyridyl hybrid ligand, 6-

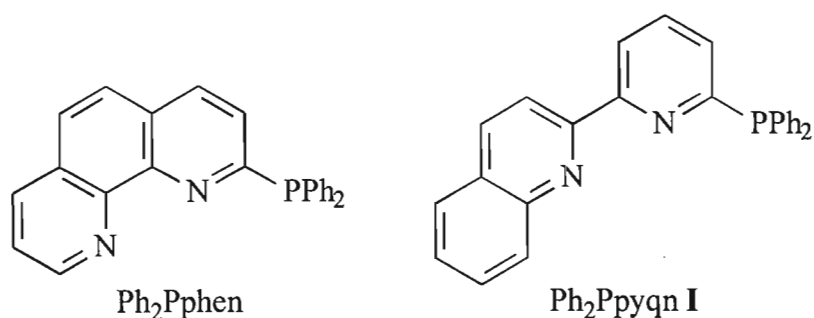
diphenylphosphino-2,2'-bipyridine ( $\text{Ph}_2\text{Pbpy}$ ),<sup>62</sup> can be considered as the tridentate equivalent of  $\text{Ph}_2\text{Ppy}$  in terms of its coordination properties. It is a composite of probably the two most ubiquitous ligands in coordination chemistry, triphenylphosphine and 2,2'-bipyridine. It was envisaged that this ligand would show a strong propensity to promote the formation of dinuclear complexes. The synthesis of a range of ruthenium(I), silver(I), and copper(I) dinuclear compounds bridged by  $\text{Ph}_2\text{Pbpy}$  prove that this is indeed so.<sup>101,129,185</sup> In these complexes  $\text{Ph}_2\text{Pbpy}$  adopts a bridging coordination mode, with the bipyridyl fragment chelating to the first metal and the phosphorus completing the bridge to the second. The 2,2'-bipyridyl ligand is remarkable for its ability to stabilize a transition metal through a wide range of formal oxidation states.<sup>63</sup> Thus the union of 2,2'-bipyridine with triphenylphosphine results in a potentially bridging ligand designed to stabilise and curtail the fragmentation of dinuclear complexes during a redox process.



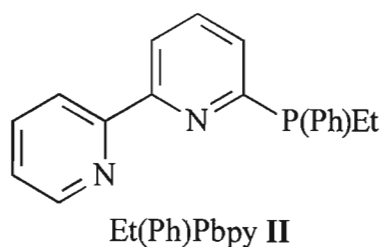
The  $\text{Ph}_2\text{Pbpy}$  ligand is the key to our approach to the synthesis of dinuclear homogeneous electrocatalysts for the electrochemical reduction of carbon dioxide. In order to enhance the possible electrocatalytic properties of the complexes of the ligand, the molecular architecture of  $\text{Ph}_2\text{Pbpy}$  was deliberately altered in a number of ways. These are now described.

$\alpha$ -Diimines, such as 2,2'-bipyridine and 1,10-phenanthroline, are able to stabilise metals in very low formal oxidation states by accepting electron density into their  $\pi^*$ -orbitals. By virtue of its extended conjugation the 1,10-phenanthroline analogue of  $\text{Ph}_2\text{Pbpy}$ , 6-diphenylphosphino-1,10-phenanthroline ( $\text{Ph}_2\text{Pphen}$ ), would be expected to possess a  $\pi^*$  orbital of lower energy. Thus the ability of the ligand to function as an electron reservoir may be strengthened. This ligand has been prepared and characterised.<sup>64</sup> However, initial results show that in contrast to the analogous  $\text{Ph}_2\text{Pbpy}$  complexes, those of  $\text{Ph}_2\text{Pphen}$  display no reversible electrochemistry.

In 6-(diphenylphosphino)-2-(2-quinolyl)pyridine **I** ( $\text{Ph}_2\text{Ppyqn}$ ), the inclusion of a quinoline fragment extends the degree of conjugation while retaining the arrangement of donor atoms found in  $\text{Ph}_2\text{Pbpy}$ . Complexes of  $\text{Ph}_2\text{Ppyqn}$  may exhibit less negative reduction potentials than those of  $\text{Ph}_2\text{Pbpy}$  as it would be expected to be a stronger  $\pi$ -accepting ligand.<sup>65</sup>



It is well known that carbon dioxide forms complexes with transition metal ions in low oxidation states.<sup>66</sup> On a qualitative basis there is a more favourable electrostatic interaction between the weakly electrophilic CO<sub>2</sub> and an electron rich metal.<sup>67</sup> In conformance with this a large number of transition metal carbon dioxide complexes that have been characterised contain alkyl phosphines as spectator ligands.<sup>68</sup> The basicity of the phosphine in 6-[ethyl(phenyl)phosphino]-2,2'-bipyridine **II** [Et(Ph)Pbpy], and therefore the electron density on the metal to which it is bonded, is increased by the presence of the alkyl group. Transition metal complexes of this ligand would be expected to react more readily with CO<sub>2</sub>. Furthermore the soft phosphorus in Et(Ph)Pbpy would provide effective stabilisation to low-valent metal centres.



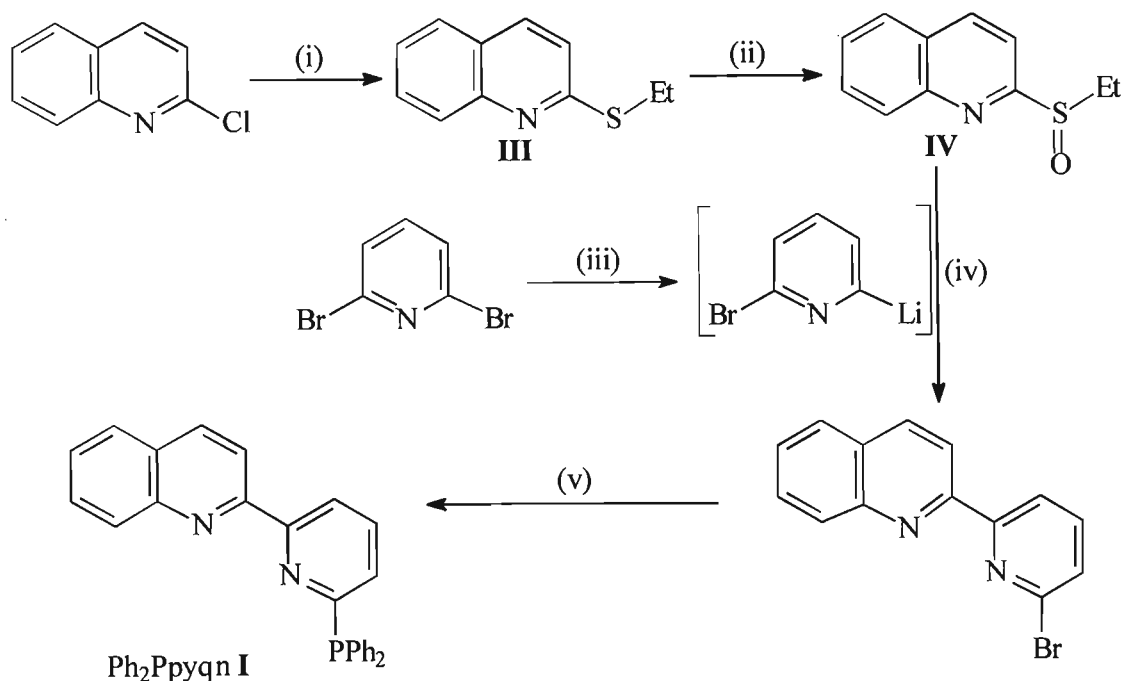
The synthesis and characterisation of the two phosphorus-polypyridyl ligands **I** and **II** are described in this chapter. The electrochemical properties of these ligands and Ph<sub>2</sub>Pbpy are examined.

## 2.2. Results and Discussion

### 2.2.1. Synthesis and Characterisation

Scheme 2.1 summarises the synthesis of **I**. Several methods for the preparation of sulfides, such as 2-(ethylsulfanyl)quinoline **III**, are reported in the literature. For example, **III** has been prepared by the reaction of 2-thiolquinoline in 10% NaOH with ethyl sulfate.<sup>69</sup> Several pyridyl sulfides and 2-(methylsulfanyl)quinoline have been synthesized from the respective mercapto-substituted heteroaromatics and the corresponding alkyl halides.<sup>70,71</sup> However, in this study, the reaction of 2-thiolquinoline with EtX (X = Br, I) in acetonitrile, in the presence of

triethylamine as a base, was shown to furnish **III** in unsatisfactory yields. The sulfide **III** was therefore prepared via the nucleophilic displacement of 2-chloroquinoline by sodium ethanethiolate. This type of reaction is usually carried out in HMPA,<sup>72</sup> but acceptable yields of **III** were achieved in DMF.



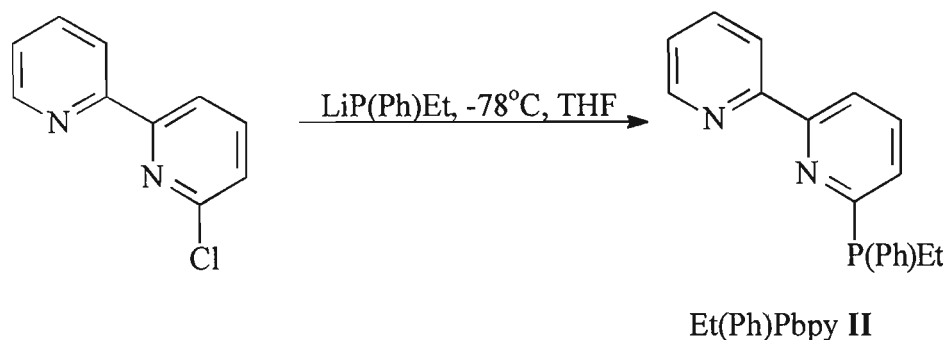
**Scheme 2.1.** Preparation of Ph<sub>2</sub>Ppyqn I. (i) NaSEt, DMF; (ii) H<sub>2</sub>O<sub>2</sub>, AcOH; (iii) BuLi, -78°C, THF; (iv) -78°C, THF; (v) LiPPh<sub>2</sub>, THF, -78°C.

Of the number of oxidising agents available for the preparation of sulfoxides from sulfides,<sup>73</sup> two were examined: *m*-chloroperbenzoic acid and hydrogen peroxide. The use of *m*-chloroperbenzoic acid in dichloromethane, even with careful control of the reaction temperature and stoichiometry, resulted chiefly in the over-oxidation of the sulfide to the corresponding sulfone. Selective oxidation of the sulfide to the S-monoxide was achieved by the reaction of **III** with hydrogen peroxide in acetic acid, leading to the sulfoxide **IV** in a 70 % yield.

The  $\alpha$ -diimine, 6-bromo-2-(2-quinolyl)pyridine, was prepared by the ligand coupling reaction between **IV** and a lithiopyridine intermediate, generated by lithium-halogen exchange of 2,6-dibromopyridine with butyl lithium, as described by S. Oae *et al.*<sup>74</sup> The intermolecular cross coupling methodology developed by Oae *et al.* presented the most facile preparation of the unsymmetrical heteroaromatic, which was furthermore halogenated in the desired position.<sup>75</sup>

In the final step of the synthesis, lithium diphenylphosphide, prepared from the reaction of diphenylphosphine with butyl lithium, was quenched with 6-bromo-2-(2-quinolyl)pyridine in THF at -78°C. An acid-base purification step followed by repeated washing with hexane to

remove unreacted 6-bromo-2-(2-quinolyl)pyridine and finally recrystallisation from chloroform/hexane gave **I** in a 44% yield.



**Scheme 2.2.** Reaction of 6-chloro-2,2'-bipyridine with lithium ethylphenylphosphide.

Scheme 2.2 summarises the reaction used to synthesise Et(Ph)Pbpy **II**. The LiP(Ph)Et was prepared by the reaction of ethyldiphenylphosphine with two molar equivalents of lithium in THF followed by selective quenching of the PhLi that forms in this reaction with 2-chloro-2-methylpropane.<sup>76</sup> Treatment of LiP(Ph)Et with 6-chloro-2,2'-bipyridine<sup>62</sup> in THF at  $-78^{\circ}\text{C}$  afforded **II** as a racemic mixture. The product was purified by means of fractional distillation with a final yield of 42 %.

The GC-MS spectral data of the new ligands are consistent with their proposed structures, molecular ions of 390 and 292 amu being observed for **I** and **II** respectively. Further conformation comes from examination of the fragmentation patterns, these showing the stepwise cleavage of phenyl and diphenylphosphide (for **I**), and ethyl(phenyl)phosphide (for **II**) fragments from the molecule. The microanalytical data for **I** are consistent with the formulation of the compound. Unfortunately, the highly air-sensitive nature of **II** prevented the attainment of an acceptable microanalytical result.

### 2.2.2. NMR Spectroscopy of the Phosphorus-polypyridyl Ligands

For reasons of convenience the NMR data for ligand **II** is discussed first. The NMR spectral data of **II** along with the atom numbering scheme are presented in Table 2.1. The trivalent phosphorus atom in **II** possesses a lone pair of electrons and is described as a tetrahedral, chiral centre.<sup>77</sup> As such, the methylene carbon bonded to it is prochiral and has two non-equivalent, diastereotopic protons, labelled  $\text{H}_a$  and  $\text{H}_b$ . These two methylene protons are likely to have different averaged environments and consequently different chemical shifts. Thus in the  $^1\text{H}\{-^{31}\text{P}\}$  NMR spectrum of **II** the  $\text{PCH}_2\text{CH}_3$  protons exhibit what may be approximated as an  $\text{ABX}_3$  signal multiplicity. This is illustrated in Figure 2.1 which depicts the methylene proton

resonances of the PCH<sub>2</sub>CH<sub>3</sub> fragment. The diastereotopic shift is sufficient to separate each overlapping doublet of quartets that are seen at 2.48 and 2.15 ppm. A vicinal coupling constant, <sup>2</sup>J(H<sub>a</sub>H<sub>b</sub>), of 13.69 Hz, and geminal couplings, <sup>3</sup>J(H<sub>a</sub>H) and <sup>3</sup>J(H<sub>b</sub>H), of 7.81 and 7.57 Hz respectively are observed. The latter values are reflected in the resonances of the protons of the methyl group, which occur as a pseudo-triplet at 1.18 ppm.

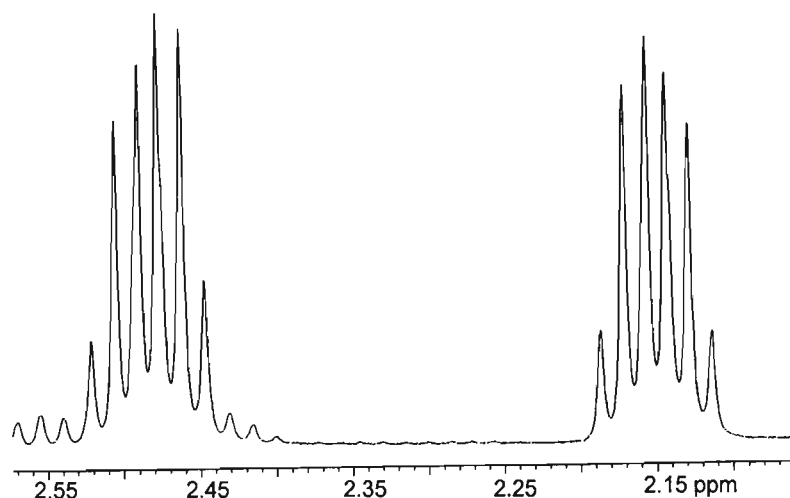


**Figure 2.1.** Expanded <sup>1</sup>H-<sup>31</sup>P} NMR spectrum of Et(Ph)Pbpy **II** depicting the methylene proton resonances of the PCH<sub>2</sub>CH<sub>3</sub> fragment.

The ABX<sub>3</sub> spectral pattern is further split by heteronuclear spin-spin interactions of <sup>1</sup>H with <sup>31</sup>P, resulting in the <sup>1</sup>H NMR spectrum illustrated in Figure 2.2. Each methylene proton exhibits a ‘doublet of quartets of doublets’, while the methyl protons are observed as a doublet of triplets. The presence of the lone pair on the phosphorus(III) atom means the one, two and three bond couplings are particularly sensitive to the bond orientation about the P–C bond in acyclic phosphines.<sup>78,79</sup> The strong stereochemical dependence of the magnitude of proton-phosphorus coupling is manifested by the significant difference in the vicinal couplings of <sup>2</sup>J(PH<sub>a</sub>) 0.98 and <sup>2</sup>J(PH<sub>b</sub>) 2.69 Hz. In comparison to the vicinal phosphorus-hydrogen coupling, the geminal coupling of 17.34 Hz seems anomalous. However, this is also observed for P(CH<sub>2</sub>CH<sub>3</sub>)<sub>3</sub>, where vicinal and geminal phosphorus-hydrogen coupling constants of 0.5 and 13.7 Hz respectively are observed.<sup>80</sup> The small <sup>2</sup>J(PH) coupling constants observed for three coordinate alkyl organophosphorus compounds are in contrast to the large values of opposite signs obtained for cyclic three coordinate phosphorus compounds. The small values for acyclic phosphines have been interpreted as being the average of the positive and negative values caused by free rotation about the C–P bond.<sup>81</sup>

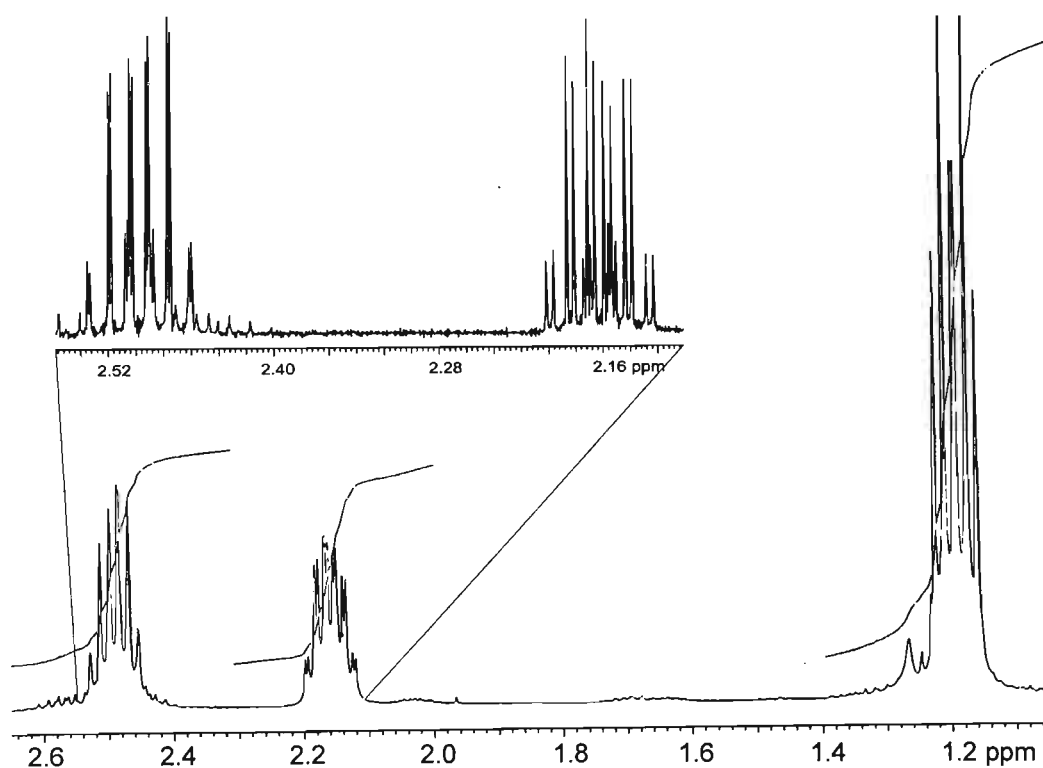


**Figure 2.2.** Expanded  $^1\text{H}$  NMR spectrum of  $\text{Et}(\text{Ph})\text{Pbpy II}$  depicting the  $\text{PCH}_2\text{CH}_3$  resonances.

The  $^1\text{H}$  NMR spectral pattern of the bipyridyl moiety of **II** (Figure 2.3) was essentially first-order and was interpreted as such. Similarities existed between it and the proton NMR spectrum of 2,2'-bipyridine.<sup>82,83</sup> It is established that the proton in the  $\beta$ -position to the nitrogen is well shielded and consequently appears at higher fields. Hence the doublet of doublets at 7.24 ppm, which is further split by three bond phosphorus-hydrogen coupling of 1.95 Hz, is due to 5-H. The multiplet at 7.28 ppm displays a principal splitting of 7.45 and 4.87 Hz. The latter value is characteristic of geminal coupling to a proton  $\alpha$ - to the nitrogen and the resonances at 7.28 ppm are therefore assigned to the  $\beta$ -proton 5'-H. The coupling constant of 4.87 Hz is reflected in the doublet of doublets at 8.66 ppm and this resonance is due to the  $\alpha$ -proton 6'-H. This is consistent with the precedent set by substituted pyridines in which the  $\alpha$ -proton appears at lowest field and couples to the  $\beta$ -proton with a smaller magnitude.

In pyridines substituted in the 2-position the 3-proton is deshielded by electronegative substituents.<sup>82</sup> The doublet of doublets at 8.52 and 8.27 ppm are accordingly assigned to 3'-H and 3-H respectively. A comparison of the coupling between protons on non-adjacent carbons, namely C-5 and C-5', allows the two protons to be logically differentiated. The doublet of triplets at 7.62 ppm exhibits a phosphorus-hydrogen coupling of 2.44 Hz in the  $^1\text{H}$  NMR spectrum of **II**, and is assigned to 4-H. The remaining proton, 4'-H is observed as a ddd at 7.79 ppm.



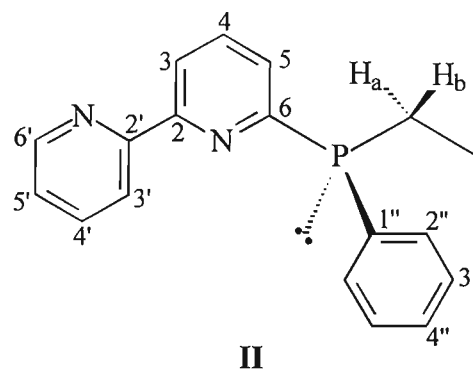


**Table 2.1.** NMR spectral data of Et(Ph)Pbpy **II**.<sup>a, b, c</sup>

H: 8.66 (1H, dd,  $J$  4.87 and 1.23, 6'-H), 8.52 (1H, dd,  $J$  7.81 and 0.93, 3'-H), 8.27 (1H, dd,  $J$  7.81 and 1.04, 3-H), 7.79 (1H, ddd,  $J$  7.81, 7.45 and 1.23, 4'-H), 7.62 (1H, dt,  $J$  7.81 and  $^4J(\text{PH})$  2.44, 4-H), 7.58 (2H, m, Ph), 7.35 (3H, m, Ph), 7.28 (1H, ddd,  $J$  7.45, 4.87 and 0.93, 5'-H), 7.24 (1H, ddd,  $J$  7.81, 1.04 and  $^3J(\text{PH})$  1.95, 5-H), 2.48 (1H, ddq,  $^2J(\text{H}_a\text{H}_b)$  13.69,  $^3J(\text{H}_a\text{H})$  7.81 and  $^2J(\text{PH})$  0.98,  $\text{H}_a$ ), 2.15 (1H, ddq,  $^2J(\text{H}_a\text{H}_b)$  13.69,  $^3J(\text{H}_b\text{H})$  7.57 and  $^2J(\text{PH})$  2.69,  $\text{H}_b$ ), 1.18 (3H, ddd,  $^3J(\text{PH})$  17.34,  $^3J(\text{H}_a\text{H})$  7.81 and  $^3J(\text{H}_b\text{H})$  7.57,  $\text{PCH}_2\text{CH}_3$ ).

$^{13}\text{C}-\{^1\text{H}\}$ : 164.58 (d,  $^1J(\text{PC})$  2.94, C-6), 156.52 (s, C-2'), 156.00 (d,  $^3J(\text{PC})$  6.85, C-2), 149.23 (s, C-6'), 137.52 (d,  $^1J(\text{PC})$  13.21, C-1'), 137.00 (s, C-4'), 136.25 (d,  $^3J(\text{PC})$  5.38, C-4), 134.21 (d,  $^2J(\text{PC})$  19.56, C-2'), 129.41 (d,  $^4J(\text{PC})$  0.98, C-4'), 128.67 (d,  $^3J(\text{PC})$  7.83, C-3'), 128.15 (d,  $^2J(\text{PC})$  25.92, C-5), 123.88 (s, C-5'), 121.45 (s, C-3'), 119.31 (s, C-3), 20.38 (d,  $^1J(\text{PC})$  8.32,  $\text{PCH}_2\text{CH}_3$ ), 10.45 (d,  $^2J(\text{PC})$  16.63,  $\text{PCH}_2\text{CH}_3$ )

$^{31}\text{P}-\{^1\text{H}\}$ : -7.9 (s)

<sup>a</sup> Recorded in  $\text{CDCl}_3$  at 298 K. Data given as chemical shift ( $\delta$ ) (number of equivalent nuclei (by integration), multiplicity,  $J/\text{Hz}$ , assignment), s = singlet, d = doublet, t = triplet, m = multiplet. <sup>b</sup>  $\text{Me}_4\text{Si}$  was used as an internal reference for  $^1\text{H}$  (500 MHz) and  $^{13}\text{C}$  (125 MHz) spectra. <sup>c</sup>  $^{31}\text{P}-\{^1\text{H}\}$  (32.2 MHz) spectra were measured against  $(\text{CH}_3\text{O})_3\text{P}$  ( $\delta_{\text{P}} = 141.0$ ) as a secondary reference and are quoted relative to 85% phosphoric acid.

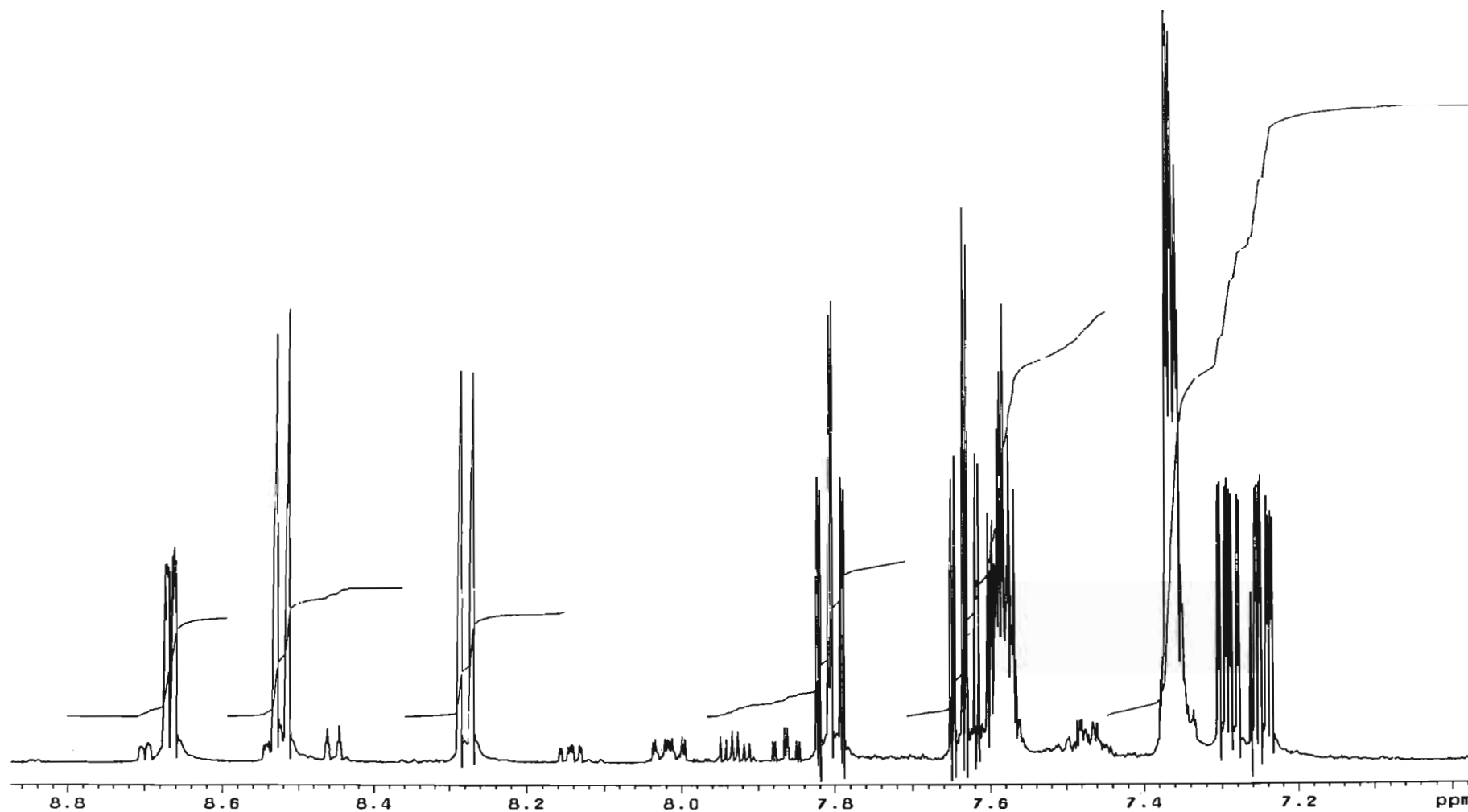


**Figure 2.3.** Expanded  $^1\text{H}$  NMR spectrum of Et(Ph)Pbpy II depicting the aromatic resonances.

**Table 2.2.** Comparison of the  $^{13}\text{C}$  chemical shifts of the phenyl ring carbon atoms in  $\text{Ph}_2\text{Ppyqn}$  **I** and  $\text{Et}(\text{Ph})\text{Pbpy}$  **II** and those of  $\text{PPh}_3$  and  $\text{P}(\text{Ph})_2\text{Et}$ . The  $^{13}\text{C}$ - $^{31}\text{P}$  coupling constants are given in parentheses.

	$\delta_{\text{C}}/\text{ppm}$ ( $J(\text{PC})/\text{Hz}$ )			
	<b>I</b>	$\text{PPh}_3$	<b>II</b>	$\text{P}(\text{Ph})_2\text{Et}$
C-1''	136.52(10.76)	137.8(12.5)	137.52(13.21)	140.2(14.9)
C-2''	134.22(19.83)	134.0(19.7)	134.21(19.56)	133.3(18.9)
C-3''	128.50(7.34)	128.8(6.8)	128.67(7.83)	128.9(6.5)
C-4''	128.32(0.98)	128.5(0.3)	129.41(0.98)	128.8

Table 2.2 above lists the  $^{13}\text{C}$  chemical shifts reported for free  $\text{P}(\text{Ph})_2\text{Et}$  and compares these with those recorded for **II**; also given are the  $^{13}\text{C}$ - $^{31}\text{P}$  coupling constants.<sup>84</sup> As an inspection of the listings shows, there is a good correlation between the chemical shifts and coupling constants which allows these carbons to be assigned with an acceptable degree of certainty. Indeed, the good correlation extends to the phenyl carbons of  $\text{PPh}_3$  and **I**.

**Table 2.3.** Comparison of the  $^{13}\text{C}$  chemical shifts of carbon atoms C-2' to C-6' of  $\text{Et}(\text{Ph})\text{Pbpy}$  **II** with those of 2,2'-bipyridine.

	$\delta_{\text{C}}/\text{ppm}$	
	<b>II</b>	2,2'-bipyridine
C-2'	156.52	156.40
C-3'	121.45	121.40
C-4'	137.00	137.20
C-5'	123.88	124.00
C-6'	149.23	149.40

Table 2.3 provides a comparison of the  $^{13}\text{C}$  chemical shifts of the pyridyl carbon atoms C-2' to C-6' in **II** with those reported for 2,2'-bipyridyl.<sup>85</sup> The close agreement shown in Table 2.3 is the basis of the assignment. The absence of any phosphorus-carbon coupling enabled these resonances to be differentiated from those associated with the C atoms of the phosphine substituted pyridyl ring. The latter were assigned as follows. Carbons C-2, C-3 and C-4, found at 156.00, 119.31 and 136.25 ppm respectively, show similar chemical shifts to the corresponding carbons in 2,2'-bipyridyl (see Table 2.2). The quaternary carbon signal of C-2 and the methine signal of C-4 are split by phosphorus-carbon spin-spin interactions and exhibit coupling constants of 6.85 and 5.38 Hz respectively. The chemical shifts of C-6 and C-5 are moved down field from their values in 2,2'-bipyridyl by the phosphine substituent at position 6, appearing at

164.58 and 128.15 ppm. Both the quaternary carbon and methine resonances of C-6 and C-5 are coupled to the phosphorus with spin-spin coupling constants of 2.94 and 25.92 Hz.

The NMR spectral data of **I** is presented in Table 2.4, with the  $^1\text{H}$  NMR spectrum shown in Figure 2.4. The proton resonances for the quinoline fragment of **I** reflect an ABX system for the heteroaromatic ring and an ABCD system for the benzoid ring.<sup>86</sup> Protons 4'-H and 3'-H are readily identified as doublets at 8.18 and 8.47 ppm, exhibiting a mutual coupling constant of 8.55 Hz. As in **II** and 2,2'-bipyridine, the 3'-H proton is deshielded by the 2-substituent and is shifted down field from the value observed in quinoline.<sup>86,87</sup> The proton 4'-H is slightly broadened by coupling to 5'-H and cross ring coupling to 8'-H.

The doublet of 4'-H overlaps with a second broad doublet due to 8'-H centred at 8.16 ppm. This low field signal, broadened by *meta*, *para* and cross ring coupling to 4'-H, is characteristic of 8'-H. A comparison with the 200 MHz  $^1\text{H}$  NMR spectra of **I**, where the two doublets no longer overlap with one another, confirms that there are two doublets present and validates the coupling constants given in Table 2.4. The resonance of proton 5'-H appears as a well-defined doublet of doublets centred at 7.82 ppm.

The multiplets centred at 7.72 and 7.54 ppm have a mutual coupling constant of 6.88 Hz. The magnitude of this coupling is noticeably smaller than that of the remaining hydrogens on adjacent carbons and is characteristic of coupling between hydrogens at positions 6' and 7' on the quinoline ring.<sup>86</sup> Correlation of the coupling constants with those of protons 5'-H and 8'-H allows for the assignment of 6'-H and 7'-H to the signals at 7.72 and 7.54 ppm respectively.

The three pyridyl ring protons 3-H, 4-H and 5-H are rationally assigned on the basis of their splitting patterns; in the  $^1\text{H}\{-^{31}\text{P}\}$  NMR spectrum of **I** the 5-H and 3-H resonances appear as doublets of doublets at 8.58 and 7.20 ppm respectively, while 4-H is seen as a triplet centred at 7.75 ppm. In the  $^1\text{H}$  NMR spectrum of **I** the resonances of protons 5-H and 4-H are further split by coupling to the phosphorus atom and exhibit coupling constants of  $^3\text{J}(\text{PH})$  1.22 and  $^4\text{J}(\text{PH})$  2.20 Hz respectively. As is observed in **II**, the signal due to 3-H is shifted down field, while that of 5-H is shifted up field.

As in **II**, there is a strong correlation between the  $^{13}\text{C}$  chemical shifts and  $^{13}\text{C}\text{-}^{31}\text{P}$  coupling constants of the phenyl carbons in **I** and those in the related tertiary phosphine  $\text{PPh}_3$  (Table 2.2).<sup>88</sup> Likewise, by comparison with the  $^{13}\text{C}$  chemical shifts recorded for quinoline, those of the quinoline fragment in **I** could be partially assigned (Table 2.5). The C-4a' carbon resonance is masked by the down field resonance of the doublet assigned to C-3''. The observation of a signal due to this quaternary carbon was however possible in a 200 MHz  $^{13}\text{C}$  NMR spectrum of **I** as the two signals no longer overlapped and thus its presence was confirmed.

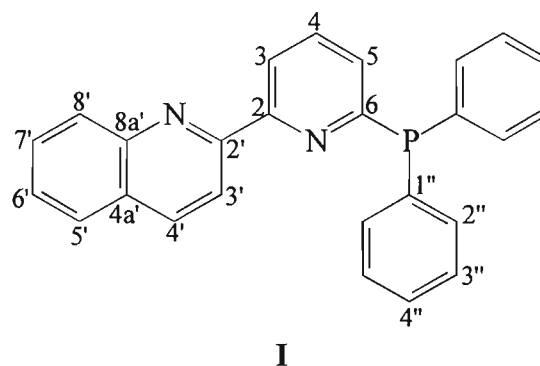


**Table 2.4.** NMR spectral data of Ph<sub>2</sub>Ppyqn I.<sup>a, b, c</sup>

H: 8.58 (1H, ddd, J 7.81, 1.10 and <sup>5</sup>J(PH) 0.73, 3-H), 8.47 (1H, d, J 8.55, 3'-H), 8.18 (1H, d, J 8.55, 4'-H), 8.16 (1H, br d, J 8.34, 8'-H), 7.82 (1H, dd, J 8.12 and 1.41, 5'-H), 7.75 (1H, td, J 7.81 and <sup>4</sup>J(PH) 2.20, 4-H), 7.72 (1H, ddd, J 8.12, 6.88 and 1.22, 6'-H), 7.54 (1H, ddd, J 8.34, 6.88 and 1.41, 7'-H), 7.43 (4H, m, Ph), 7.30 (6H, m, Ph), 7.20 (1H, ddd, J 7.81, 1.10 and <sup>3</sup>J(PH) 1.22, 5-H).

<sup>13</sup>C-<sup>1</sup>H: 162.71 (d, <sup>1</sup>J(PC) 3.91, C-6), 156.37 (d, <sup>3</sup>J(PC) 11.74, C-2), 156.07 (s, C-2'), 147.78 (s, C-8a'), 136.57 (s, C-4'), 136.57 (d, <sup>3</sup>J(PC) 7.83, C-4), 136.52 (d, <sup>1</sup>J(PC) 10.76, C-1''), 134.22 (d, <sup>2</sup>J(PC) 19.83, C-2''), 129.71 and 129.42 (s, C-7', C-8'), 128.97 (s, C-5'), 128.50 (d, <sup>3</sup>J(PC) 7.34, C-3''), 128.47 (s, C-4a'), 128.32 (d, <sup>4</sup>J(PC) 0.98, C-4''), 127.58 (s, C-5), 126.69 (s, C-6'), 120.21 (s, C-3'), 119.37 (s, C-3).

<sup>31</sup>P-<sup>1</sup>H: -3.6 (s)

<sup>a</sup> Recorded in CDCl<sub>3</sub> at 298 K. Data given as chemical shift (δ) (number of equivalent nuclei (by integration), multiplicity, J/Hz, assignment), s = singlet, d = doublet, t = triplet, m = multiplet. <sup>b</sup> Me<sub>4</sub>Si was used as an internal reference for <sup>1</sup>H (500 MHz) and <sup>13</sup>C (125 MHz) spectra. <sup>c</sup> <sup>31</sup>P-<sup>1</sup>H (32.2 MHz) spectra were measured against (CH<sub>3</sub>O)<sub>3</sub>P (δ<sub>P</sub> = 141.0) as a secondary reference and are quoted relative to 85% phosphoric acid.

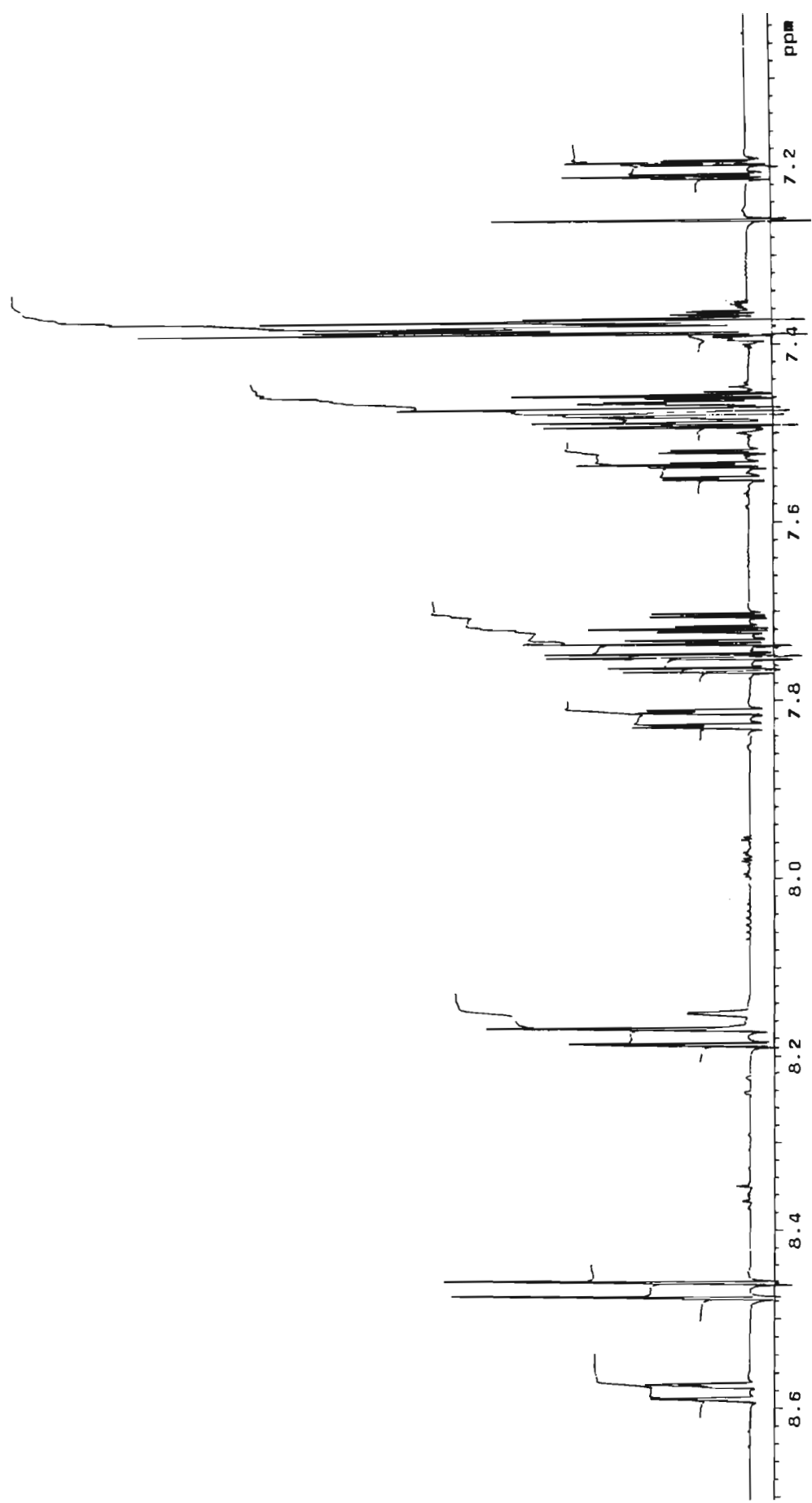


Figure 2.4.  $^1\text{H}$  NMR spectrum of  $\text{Ph}_2\text{Ppyqn I}$ .

Carbons C-2, C-3 and C-4 exhibit signals at 156.37, 119.37 and 136.57 ppm respectively, chemical shifts that are similar to those of the corresponding carbons in 2,2'-bipyridyl and **II**, the latter exhibiting resonances at 156.00 (C-2), 119.31 (C-3) and 136.25 ppm (C-4). The quaternary signal of C-2 and the methine signal of C-4 are split by phosphorus-carbon couplings of 11.74 and 7.83 Hz respectively. The signal of C-6, the position at which the pyridyl ring is substituted by the phosphine, is significantly shifted down field and is split by a  $^{13}\text{C}$ - $^{31}\text{P}$  coupling of 3.91 Hz. The resonance due to carbon C-5 appears as a singlet at 127.58 ppm. Interestingly there is no evidence of a spin-spin interaction of this carbon with phosphorus.

**Table 2.5.** Comparison of the  $^{13}\text{C}$  chemical shifts of carbon atoms C-2' to C-8a' of  $\text{Ph}_2\text{Ppyqn}$  **I** with those of quinoline.

	$\delta_{\text{C}}/\text{ppm}$	
	<b>I</b>	quinoline
C-2'	156.07	150.9
C-3'	120.21	121.7
C-4'	136.57	136.1
C-4a'	128.47	128.9
C-5'	128.97	128.5
C-6'	126.69	127.0
C-7'	129.42	129.9
C-8'	129.71	130.5
C-8a'	147.78	149.3

As has been previously discussed, the ultraviolet and NMR spectroscopic data obtained for 2,2'-bipyridyl are consistent with a *trans*-planar conformation of the molecule in solution.<sup>83,89,90</sup> Indeed, this is the conformation found for the molecule in the solid state.<sup>91</sup> In this arrangement the existence of a van der Waals interaction between the lone pair of the nitrogen and proton 3-H contributes significantly to the deshielding of that proton as evidenced in the NMR spectrum. The deshielding of the equivalent proton in **I** and **II** to a lower field resonance together with the *transoid* near-planar conformations observed for **I** (Section 2.2.3.) and  $\text{Ph}_2\text{Pbpy}$  in the solid state, suggest that **I** and **II** also adopt a *transoid* arrangement in solution. This will not impair the chelating ability of the ligand as in solution there is the possibility of free rotation about the interannular C-C bond, allowing for the *cisoid* arrangement required for the chelating bonding mode.

The  $^{31}\text{P}\{-^1\text{H}\}$  NMR spectra of **I** and **II** exhibited a sharp singlet at -3.6 and -7.9 ppm respectively. This is in the vicinity one would expect for a tertiary phosphine. The substitution of

a phenyl group with an alkyl group shifts the resonance of **II** up field compared to that recorded at  $-3.7$  ppm for  $\text{Ph}_2\text{Pbpy}$ .<sup>62</sup>

### 2.2.3. Crystal Structure Determination of 6-(diphenylphosphino)-2-(2-quinolyl)pyridine **I**

The molecular structure of **I** is depicted in Figure 2.5, while selected interatomic distances and angles are listed in Table 2.6. The molecules exist as discrete entities in the crystal, there being no unusual intermolecular contact distances. A *transoid* conformation is adopted in the solid state for the isolated ligand as is found for both  $\text{Ph}_2\text{Pbpy}$  and 2,2'-bipyridine itself.<sup>62,91</sup> The pyridine and quinoline rings are almost co-planar with the dihedral angle between the mean planes defined by the non-hydrogen atoms of the two heteroaromatic rings being  $8.8^\circ$ . The phosphorus does not deviate significantly from the mean plane defined by the non-hydrogen atoms of the quinoline and pyridine rings, this distance being  $0.30 \text{ \AA}$ . The C–P–C bond angles range from  $101.9$  to  $104.6^\circ$  describing a pyramidal geometry about the phosphorus atom. The P $\cdots$ N(1) distance of  $2.643(8) \text{ \AA}$  defines a short 'bite' of the potentially bridging fragment essentially equivalent to that of  $\text{Ph}_2\text{Pbpy}$  [ $2.655(2) \text{ \AA}$ ].<sup>62</sup>

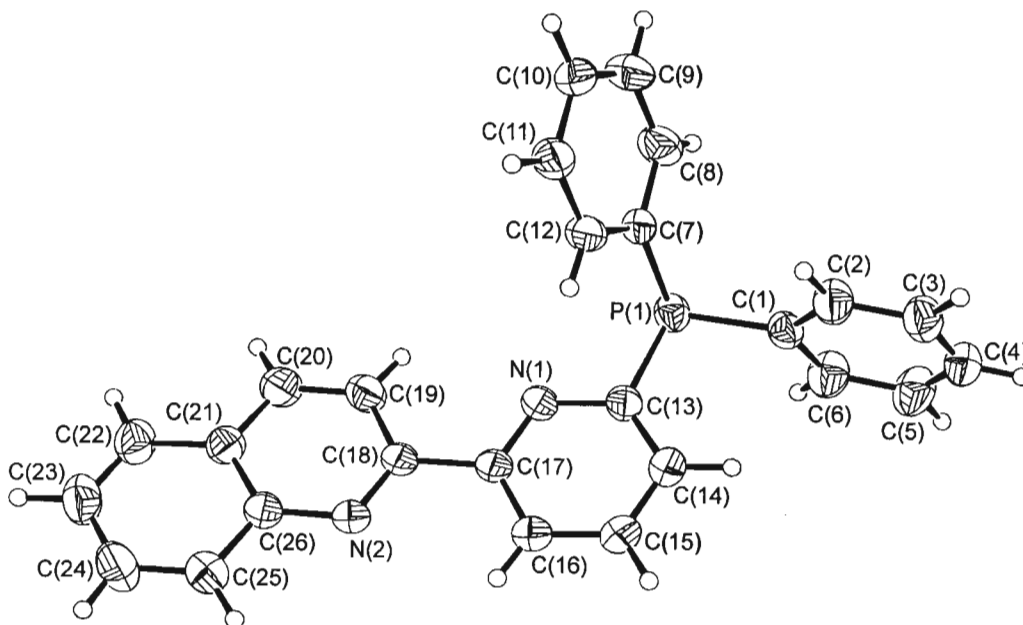


**Figure 2.5.** Perspective view of  $\text{Ph}_2\text{Ppyqn}$  **I**. Non-hydrogen atoms are represented as 40% probability thermal ellipsoids.



**Table 2.6.** Selected interatomic distances(Å) and angles(°) for Ph<sub>2</sub>Ppyqn I.

P(1)-C(7)	1.825(2)	N(1)-C(13)	1.342(2)
P(1)-C(1)	1.827(2)	N(2)-C(18)	1.318(2)
P(1)-C(13)	1.835(2)	N(2)-C(26)	1.363(2)
N(1)-C(17)	1.339(2)		
C(7)-P(1)-C(1)	104.55(8)	C(8)-C(7)-P(1)	117.2(2)
C(7)-P(1)-C(13)	101.87(8)	N(1)-C(13)-C(14)	122.1(2)
C(1)-P(1)-C(13)	102.22(8)	N(1)-C(13)-P(1)	111.7(2)
C(17)-N(1)-C(13)	118.5(2)	C(14)-C(13)-P(1)	126.2(2)
C(18)-N(2)-C(26)	117.9(2)	N(1)-C(17)-C(16)	122.3(2)
C(6)-C(1)-P(1)	116.6(2)	N(1)-C(17)-C(18)	116.4(2)
C(2)-C(1)-P(1)	125.8(2)	N(2)-C(18)-C(19)	123.3(2)
C(12)-C(7)-P(1)	124.7(2)		

#### 2.2.4. Cyclic Voltammetry of the Phosphorus-polypyridyl Ligands

The strong correlation that exists between the electronic structure of heterocyclic  $\alpha$ -diimine ligands and the electrochemical properties of their metal complexes is well documented.<sup>92,93</sup> To provide a basis for the understanding of the electrochemical behaviour of their metal complexes, the electrochemical properties of the phosphorus-polypyridyl ligands I, II and Ph<sub>2</sub>Pbpy were examined. Ph<sub>2</sub>Pbpy was synthesized and characterized as previously described by Haines *et al.*<sup>62</sup>

**Table 2.7.** Cyclic voltammetric data for Ph<sub>2</sub>Pbpy, Ph<sub>2</sub>Ppyqn I and Et(Ph)Pbpy II.<sup>a</sup>

Ligand	$E_{pa}^{ox}$	$E_{1/2}^{0/-}/V$ ( $\Delta E_p/mV$ )	$E_{pc}^{red}$	$E_{pa}^{red}$
2,2'-bipyridine <sup>b</sup>	-	-2.77	-3.29 <sup>c</sup>	
2,2'-biquinoline <sup>b</sup>	-	-2.29	-2.73	
Ph <sub>2</sub> Ppyqn I	1.08	-2.20(65)	-2.77	-2.57
Ph <sub>2</sub> Pbpy	1.16	-2.46(70)	-3.03	
Et(Ph)Pbpy II	0.95	-2.49(125)	-3.15	

<sup>a</sup> Potentials vs. Ag/Ag<sup>+</sup>, scan rate 100 mV s<sup>-1</sup>,  $T = 298$  K, measured in CH<sub>3</sub>CN (0.1 M TBAP) using a Ag/AgCl wire pseudo-reference electrode. Definitions:  $E_{pa}^{ox}$ ,  $E_{pa}^{red}$  = anodic and cathodic peak potentials of chemically irreversible oxidation and reductions respectively;  $E_{1/2} = (E_{pc} + E_{pa})/2$ ;  $\Delta E_p = E_{pc} - E_{pa}$ . <sup>b</sup> From reference 95, measured in THF. <sup>c</sup>  $E_{1/2}^{-/-2}$  of reversible wave.

The redox data of the P,N,N ligands Ph<sub>2</sub>Pbpy, **I** and **II** are summarised in Table 2.7. The CV of **I** shown in Figure 2.6 is typical of the form observed for the three ligands that are found to undergo two one-electron reductions.

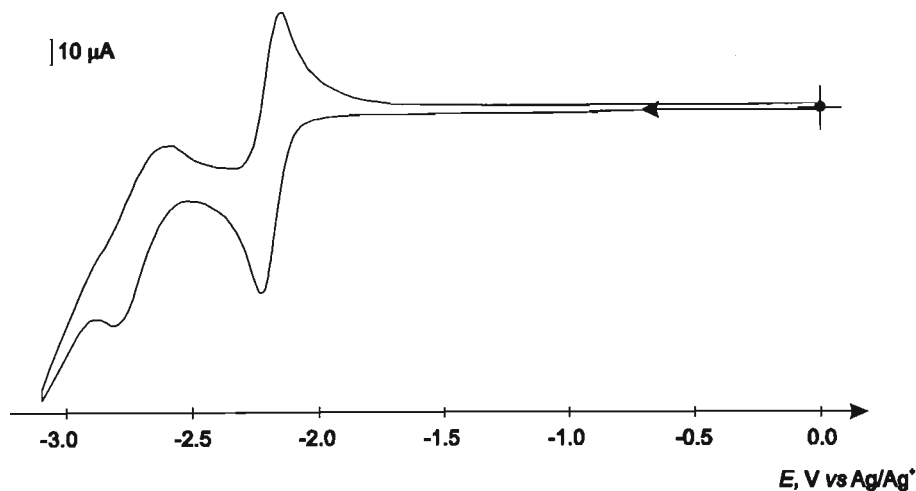


**Figure 2.6.** CV of Ph<sub>2</sub>Ppyqn **I**, measured in CH<sub>3</sub>CN (0.1 M TBAP). (Pt electrode,  $r = 1.0$  mm;  $\nu = 100$  mVs<sup>-1</sup>)

In both Ph<sub>2</sub>Pbpy and **I** the first reduction wave meets the criteria for a fully reversible couple;<sup>94</sup> the separation of the anodic and cathodic peak potentials  $\Delta E_p$  is close to that of 58 mV expected for a one-electron reduction and is seen to be independent of scan rate; the ratio of the anodic to cathodic peak current  $i_{pa}/i_{pc}$  is unity; and a linear relationship is observed between the peak current  $i_p$  and the square-root of the scan rate  $\nu^{1/2}$ . The ease with which the ligands are reduced follows a trend that one would intuitively anticipate. Thus **I**, containing a more extended  $\pi$  system than Ph<sub>2</sub>Pbpy and **II**, is reduced at the most anodic potential. The reduction of **II** occurs at the most cathodic potential as expected in view of the substitution of a phenyl by the more electron-donating ethyl group. However, the difference in the reduction potentials for Ph<sub>2</sub>Pbpy and **II** of 30 mV is barely significant.

The first reduction couple of **II** shows a peak-to-peak separation of 125 mV, which is significantly larger than that expected for a reversible one-electron process. Furthermore  $\Delta E_p$  is dependent upon  $\nu$ , ranging from 100 ( $\nu = 20$  mVs<sup>-1</sup>) to 195 mV ( $\nu = 500$  mVs<sup>-1</sup>) and this reduction wave is described as electrochemically quasi-reversible. An  $i_{pa}/i_{pc}$  of unity as well as the absence of any additional oxidation waves in the cathodic CV of **II** implies that the first reduction is at least chemically reversible. In contrast to Ph<sub>2</sub>Pbpy, which displays a chemically and electrochemically reversible one-electron reduction, the substitution of a phenyl ring by a more electron donating alkyl group in **II** hinders the rate of heterogeneous charge transfer.

The second one-electron reduction step showed no corresponding anodic response in the CVs of Ph<sub>2</sub>Pbpy and **II**, and thus is chemically irreversible. The CV of Ph<sub>2</sub>Pbpy showed a further broad and ill-defined anodic peak at *ca.* -1.5 V on the reverse scan. This corresponds to the oxidation of the decomposition product formed subsequent to the second irreversible reduction. The second reduction step of **I** displays some degree of chemical reversibility with a small anodic peak being observed (Figure 2.6). In none of the P,N,N ligands did the reversibility of the second reduction improve upon lowering the temperature of the solution to -38 °C.

The reductive electrochemistry of Ph<sub>2</sub>Pbpy, **I** and **II** parallels that of a number of polypyridyl ligands examined by Vlček *et al.*<sup>95</sup> For example, at 298 K 2,2'-bipyridine undergoes two one electron reductions of which the first is fully reversible, while the second is chemically irreversible. The authors were able to show that 2,2'-bipyridine actually undergoes two chemically fully reversible reduction steps to the corresponding dianion by cyclic voltammetric measurements at -74°C. Although at room temperature the second reduction of 2,2'-bipyridine is irreversible, at low temperatures chemical reactions coupled with the transfer of charge from the electrode are considerably slowed down. It was only at this temperature that the deactivation of the dianion by reaction with proton donors in the solution could be prevented. Thus it is reasonable to speculate that trace amounts of proton donors present in the solvent are responsible for the irreversibility of the second reduction, and that this is not an intrinsic property of the P,N,N molecules.

With regard to the oxidative electrochemistry of Ph<sub>2</sub>Pbpy, **I** and **II** a broad and irreversible oxidation wave is observed in their CVs when the potential is scanned in an anodic direction; the  $E_{pa}$  values are given in Table 2.6. Triphenylphosphine is shown to undergo an irreversible oxidation of the phosphorus at  $E_{pa} = 1.00$  V in dry acetonitrile.<sup>96,97</sup> The irreversible wave displayed by the phosphorus-polypyridyl ligands is ascribed to the oxidation of their phosphine centre. The lower oxidation potential of **II** relative to those of Ph<sub>2</sub>Pbpy and **I** is consistent with the increased electron density on the alkyl substituted phosphine.

### 2.2.5. Extended Hückel Molecular Orbital Calculations

The energies and charge distributions of the lower unoccupied molecular orbitals of the ligands were determined by Extended Hückel Molecular Orbital (EHMO) calculations. The geometry-optimised molecular structures of the ligands, in which the heteroaromatic rings are envisaged as being coplanar, were used in the calculations. As indicated by the <sup>1</sup>H NMR spectroscopic and X-ray crystal structure analyses, the heteroaromatic rings of the free ligands adopt a *trans*-coplanar arrangement both in solution (*vide infra*) and the solid state.<sup>185</sup> On the

other hand, the ligands adopt a *cis*-coplanar arrangement when bonded to a metal in the chelating mode. Thus, both the *cis* and *trans* configurations were examined. The details of these calculations are presented in the Appendix. In each case a simplification was made in that it was assumed that the anions would have the same molecular geometry as the ground state structures.

The energies of the lower unoccupied molecular orbitals are given in Table 2.8. There is a discernable correlation between the energies of the lowest unoccupied molecular orbitals (LUMOs) and the  $E_{1/2}$  values of the relevant reduction wave. Thus in the *trans* conformation, **I** possesses a LUMO noticeably lower in energy than those of Ph<sub>2</sub>Pbpy and **II**, consistent with it having the least cathodic first reduction potential of the three ligands. That there is no noticeable difference in the LUMO energies for *trans*-Ph<sub>2</sub>Pbpy and *trans*-**II** is also consistent with the very small difference in their first reduction potentials (Table 2.7). In contrast, the LUMO of *cis*-**I** does not differ markedly in energy from the equivalent orbitals in Ph<sub>2</sub>Pbpy and **II**. Although there is no immediate explanation for this, the difference in energy of the LUMO between the two possible forms is pertinent as it is in the *cis* conformation that **I** will coordinate to a metal centre.

**Table 2.8.** Calculated energies of the lower unoccupied molecular orbitals of the free P,N,N ligands Ph<sub>2</sub>Pbpy, Ph<sub>2</sub>Ppyqn **I** and Et(Ph)Pbpy **II** in both the *trans*- and *cis*-coplanar geometries.

Ligand	Eigenvalues of Molecular Orbitals/eV	
	LUMO	SLUMO
<i>trans</i> -Ph <sub>2</sub> Pbpy	-9.31	-9.08
<i>cis</i> -Ph <sub>2</sub> Pbpy	-9.33	-8.93
<i>trans</i> -Ph <sub>2</sub> Ppyqn <b>I</b>	-9.68	-9.11
<i>cis</i> -Ph <sub>2</sub> Ppyqn <b>I</b>	-9.30	-9.14
<i>trans</i> -Et(Ph)Pbpy <b>II</b>	-9.31	-9.03
<i>cis</i> -Et(Ph)Pbpy <b>II</b>	-9.32	-8.91

The spatial distribution of the LUMO and second lowest unoccupied molecular orbital (SLUMO) of Ph<sub>2</sub>Pbpy, depicted in Figure 2.7, are typical of those found in all three phosphorus-polypyridyl ligands. Both the LUMO and SLUMO are almost exclusively located on the  $\alpha$ -diimine moiety of the molecule. This is borne out in the small difference in the  $E_{1/2}^{0/-}$  values of Ph<sub>2</sub>Pbpy and **II** (Table 2.7), confirming that the substitution of a phenyl ring on the phosphine by an alkyl group does not significantly perturb the energy of the LUMO.

The strong similarity between the electrochemical behaviour of the P,N,N ligands and 2,2-bipyridine, together with the results of the EHMO calculations, show that the phosphorus-

polypyridyl ligands are able to accept two electrons into the  $\pi^*$  orbitals of the  $\alpha$ -diimine fragment. The electrochemical properties they display are in essence those of the  $\alpha$ -diimine moiety, the phosphine moiety not being expected to play a significant role in determining the electronic properties of the electroactive part of the molecule.

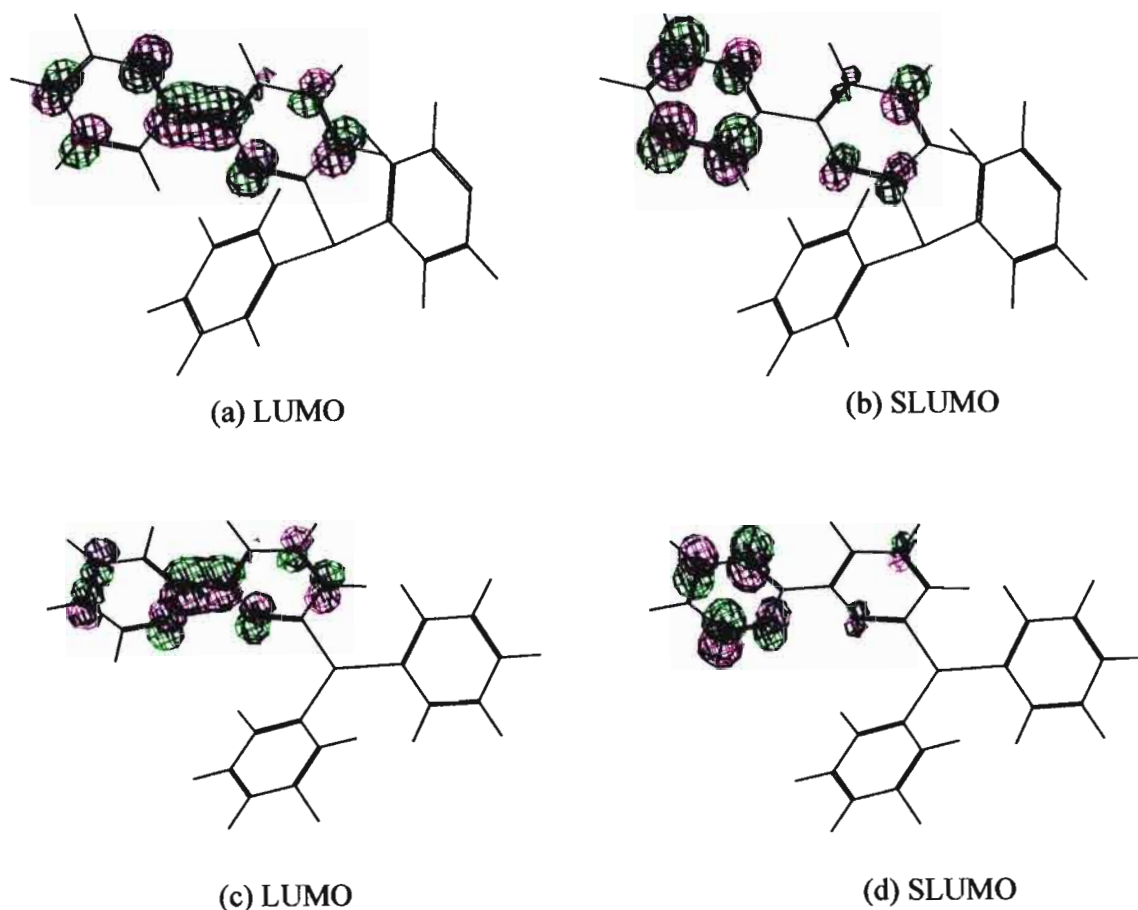


**Figure 2.7.** Pictorial representation of the (a) LUMO and (b) SLUMO of *trans*-Ph<sub>2</sub>Pbpy and the (c) LUMO and (d) SLUMO of *cis*-Ph<sub>2</sub>Pbpy.

### 2.3. Experimental

**2-(Ethylsulfanyl)quinoline III.** 2-Chloroquinoline (5.00 g, 30.6 mmol) and sodium ethanethiolate (2.96 g, 35.1 mmol) were dissolved in freshly dried DMF (20 cm<sup>3</sup>) and the solution maintained at 0 °C for 1h, after which it was allowed to warm to room temperature and left to react for a further 11 h. The reaction mixture was poured onto ice and the suspension formed extracted with petroleum ether (40 - 60 °C) (3 x 100 cm<sup>3</sup>). The organic fractions were combined, washed with water (2 x 20 cm<sup>3</sup>) and brine (2 x 20 cm<sup>3</sup>), dried over MgSO<sub>4</sub> and the solvent removed under reduced pressure. Chromatography of the resulting residue on silica gel (CHCl<sub>3</sub>, R<sub>f</sub> 0.8) followed by fractional distillation (0.50 mmHg, 102 °C) gave the sulfide as a

very pale yellow oil (3.9 g, 67%). (Found: C, 69.57; H, 5.66; N, 7.31. Calc. for  $C_{11}H_{11}NS$ : C, 69.80; H, 5.86; N, 7.40%);  $\delta_H$  (200 MHz,  $CDCl_3$ ,  $SiMe_4$ ) 7.95 (1H, ddd, J 8.39, 1.25 and 0.72 Hz, 8-H), 7.87 (1H, dd, J 8.64 and 0.42 Hz, 4-H), 7.70 (1H, dd, J 7.97 and 1.39 Hz, 5-H), 7.64 (1H, ddd, J 8.39, 7.26 and 1.39 Hz, 7-H), 7.41 (1H, ddd, J 7.97, 7.26 and 1.25 Hz, 6-H), 7.22 (1H, d, J 8.64 Hz, 3-H), 3.32 (2H, q, J 7.21 Hz,  $CH_3CH_2S$ ) 1.42 (3H, t, J 7.21 Hz,  $CH_3CH_2S$ );  $\delta_c$  (50 MHz,  $CDCl_3$ ,  $SiMe_4$ ) 159.40 (C-2), 148.32 (C-8a), 135.15 (C-4), 129.49 (C-5), 127.95 and 127.56 (C-7, C-8), 125.81 (C-4a), 125.07 (C-6), 120.91 (C-3), 24.12 ( $SCH_2CH_3$ ), 14.60 ( $SCH_2CH_3$ );  $m/z$  (EI) 189 ( $M^+$ , 87%) .

**2-(Ethylsulfinyl)quinoline IV.** To a stirred solution of 2-(ethylsulfonyl)quinoline (3.88 g, 20.5 mmol) in glacial acetic acid (15  $cm^3$ ) was added drop wise 1.15 equivalents of hydrogen peroxide (100 vols) (2.43  $cm^3$ , 23.6 mmol). The solution was maintained at room temperature for 24 h, neutralised with  $Na_2CO_3$  and extracted with  $CHCl_3$  (3 x 30  $cm^3$ ). The organic extracts were combined, washed with water (2 x 10  $cm^3$ ) and brine (10  $cm^3$ ), dried over  $MgSO_4$  and the solvent removed under reduced pressure. Purification of the remaining residue by flash chromatography using gradient elution, the solvent composition being varied from 1:5 ( $R_f$  0.1) to 1:1 EtOAc-hexane, furnished the pure sulfoxide as a white solid (2.96 g, 70%), m.p. 63°C, (Found: C, 64.24; H, 5.36; N, 6.58. Calc. for  $C_{11}H_{11}ONS$ : C, 64.36; H, 5.40; N, 6.82%);  $\delta_H$  (200 MHz,  $CDCl_3$ ,  $SiMe_4$ ) 8.42 (1H, dd, J 8.55 and 0.83 Hz, 4-H), 8.11 (1H, d, J 8.55 Hz, 3-H), 8.10 (1H, dddd, J 8.49, 1.40, 0.83 and 0.55 Hz, 5-H), 7.92 (1H, ddd, J 8.14, 1.57 and 0.55 Hz, 8-H), 7.81 (1H, ddd, J 8.49, 6.91 and 1.57 Hz, 6-H), 7.64 (1H, ddd, J 8.14, 6.91 and 1.40 Hz, 7-H), 3.16 (2H, m,  $SCH_2CH_3$ ), 1.26 (3H, t, J 7.42 Hz,  $SCH_2CH_3$ );  $\delta_c$  (50 MHz,  $CDCl_3$ ,  $SiMe_4$ ) 165.07 (C-2), 148.19 (C-8a), 138.80 (C-4), 131.41 (C-5), 129.88 (C-6), 128.79 and 128.48 (C-7, C-8), 128.46 (C-4a), 116.74 (C-3), 48.21 ( $SCH_2CH_3$ ), 5.79 ( $SCH_2CH_3$ );  $m/z$  (EI) 205 ( $M^+$ , 8%).

**6-(Diphenylphosphino)-2-(2-quinoly)pyridine I.** Butyl lithium (1.81M hexane solution) (4.72  $cm^3$ , 8.54 mmol) was added drop wise to a stirred solution of diphenylphosphine (1.59 g, 8.54 mmol) in dry THF (15  $cm^3$ ) held at  $-78^\circ C$ . The resulting orange solution was allowed to warm to room temperature and refluxed for 3 h, it was then cooled and transferred by cannula to a dropping funnel. To a rapidly stirring suspension of 6-bromo-2-(2-quinoly)pyridine (2.12 g, 7.43 mmol) in THF (30  $cm^3$ ) maintained at  $-78^\circ C$ , the above solution was added drop wise over 25 min. The reaction mixture was allowed to warm to room temperature and stirred for 8 h. The solvent was then removed under vacuum and  $CHCl_3$  (15  $cm^3$ ) added to the residue. First concentrated HCl (30-33%) (2.5  $cm^3$ ), then 3 M HCl (7.5  $cm^3$ ) were added drop wise to the stirred  $CHCl_3$  suspension. The yellow precipitate that formed was filtered and washed with

CHCl<sub>3</sub> (2 x 5 cm<sup>3</sup>). To a rapidly stirred suspension of this solid in CHCl<sub>3</sub> (15 cm<sup>3</sup>) at 0°C, was added concentrated ammonia solution (25%), drop wise, until a pH of 10 was attained. The organic layer was separated and the aqueous layer further washed with CHCl<sub>3</sub> (2 x 5 cm<sup>3</sup>). The organic fractions were combined, dried (MgSO<sub>4</sub>) and the solvent removed under reduced pressure. The solid obtained was washed with hexane (3 x 20 cm<sup>3</sup>), and then recrystallised twice from CHCl<sub>3</sub>/hexane to give a white crystalline product (1.28 g, 44%), m.p. 159°C (Found: C, 79.53; H, 4.79; N, 7.00. Calc. for C<sub>26</sub>H<sub>19</sub>N<sub>2</sub>P: C, 79.99; H, 4.91; N, 7.18 %);  $\lambda_{\max}/\text{nm}$  (CH<sub>3</sub>CN) 208 (sh) ( $\epsilon/\text{dm}^3 \text{ mol}^{-1} \text{ cm}^{-1}$  45 900), 213 (sh) (43 600), 219 (sh) (38 200), 251 (41 600), 322 (sh) (8 180) and 336 (sh) (4 680);  $\nu_{\max}/\text{cm}^{-1}$  (KBr) 1598w, 1563w (sh), 1550s, 1504w, 1480w, 1438s, 1424s, 1069w, 810s, 755w (sh), 742s, 699s and 506w;  $m/z$  (EI) 390 (M<sup>+</sup>, 100%), 313 (42, M<sup>+</sup>-C<sub>6</sub>H<sub>5</sub>), 205 (30, M<sup>+</sup>-P(C<sub>6</sub>H<sub>5</sub>)<sub>2</sub>), 185 (24, P(C<sub>6</sub>H<sub>5</sub>)<sub>2</sub>).

**6-[Ethyl(phenyl)phosphino]-2,2'-bipyridine II.** A suspension of finely cut lithium (24.7 mg, 35.7 mmol) and PPh<sub>2</sub>Et (3.32 g, 15.5 mmol) in dry THF (20 cm<sup>3</sup>) was sonicated in an ultrasound bath for 5 h at 25°C. The resulting dark red solution was transferred by cannula to a second flask. To this, at 0°C, was added drop wise 2-chloro-2-methylpropane (1.70 cm<sup>3</sup>) in THF (5 cm<sup>3</sup>). The reaction mixture was stirred at room temperature for 1 h. Subsequently its temperature was lowered to -78°C and a solution of 6-chloro-2,2'-bipyridine (2.95 g, 15.5 mmol) in THF (25 cm<sup>3</sup>) added drop wise over 15 min. The reaction mixture was allowed to warm to room temperature and stirred for 12 h. The solvent was removed under vacuum, then CH<sub>2</sub>Cl<sub>2</sub> (50 cm<sup>3</sup>) followed by deaerated H<sub>2</sub>O (20 cm<sup>3</sup>) added to the residue. The suspension was briefly stirred to ensure all the residue dissolved. The organic layer was separated, and the remaining aqueous layer washed with CH<sub>2</sub>Cl<sub>2</sub> (20 cm<sup>3</sup>). The CH<sub>2</sub>Cl<sub>2</sub> layers were combined and dried over MgSO<sub>4</sub>. Removal of the solvent *in vacuo* yielded a light yellow oil that contained in addition to the product, small amounts of oxidized product and unreacted 6-chloro-2,2'-bipyridine. The crude oil was purified using a Kugelrohr apparatus; the product, oxidized product and 6-chloro-2,2'-bipyridine distilling over at 160°C (0.1 mmHg), the latter two were then fractionated from the product at 100°C (0.1 mmHg) over a period of three days, leading to an almost colourless oil (1.90 g, 42%).  $\lambda_{\max}/\text{nm}$  (CH<sub>2</sub>Cl<sub>2</sub>) 223 ( $\epsilon/\text{dm}^3 \text{ mol}^{-1} \text{ cm}^{-1}$  21 600), 239 (17 200), 247 (sh) (15 700) and 280 (15 000);  $\nu_{\max}/\text{cm}^{-1}$  (film) 3056w, 2964w, 2932w, 1590w (sh), 1578s (sh), 1557s, 1474w, 1450w, 1435w (sh), 1424s, 1160w, 1094w, 989w, 776s, 746s, 698s, 665w, 635w, 621w, 482vs and 464vs;  $m/z$  (EI) 292 (M<sup>+</sup>, 47%), 215 (100, M<sup>+</sup>-C<sub>6</sub>H<sub>5</sub>), 155 (21, M<sup>+</sup>-PC<sub>8</sub>H<sub>8</sub>).

**X-ray Data Collection and Structure Solution for I.** Colourless, cube-shaped crystals of **I** were grown by the slow evaporation of a chloroform solution of the compound. Details of the crystal data, data collection and structure refinement of **I** are summarized in Table 2.9, while the complete crystallographic data are presented in Appendix B. Supporting Information.

**Table 2.9.** Crystal data and structure refinement parameters for Ph<sub>2</sub>Ppyqn **I**.

Formula	C <sub>26</sub> H <sub>19</sub> N <sub>2</sub> P
FW/amu	390.40
<i>a</i> /Å	17.591(4)
<i>b</i> /Å	10.693(4)
<i>c</i> /Å	11.358(3)
$\alpha$ /°	90
$\beta$ /°	107.56(2)
$\gamma$ /°	90
<i>U</i> /Å <sup>3</sup>	2037(2)
Crystal system, space group	Monoclinic, P2 <sub>1</sub> /c
<i>Z</i>	4
<i>D<sub>c</sub></i> /g cm <sup>3</sup>	1.273
F(000)	816
$\mu$ /mm <sup>-1</sup>	0.149
Power and current settings	55 kV, 25 mA
Increment/°	1.00
Crystal dimensions/mm	1.35 x 0.77 x 0.65
$\lambda$ (Mo K $\alpha$ )/Å	0.71069
Temperature/K	293(2)
$\theta$ range for collected data/°	2.26 to 29.96
Index ranges	-1 ≤ <i>h</i> ≤ 24 -1 ≤ <i>k</i> ≤ 15 -15 ≤ <i>l</i> ≤ 15
Total reflections collected	7046
Completeness to 2 $\theta$	99.8%
Absorption correction	Semi-empirical
Relative transmission coefficients (I)	0.9996 and 0.9475
Unique data	5892 ( <i>R</i> <sub>int</sub> = 0.0227)
Unique observed data [ <i>I</i> > 2 $\sigma$ ( <i>I</i> )]	4072
Refinement method	Full-matrix least-squares on <i>F</i> <sup>2</sup>
Data / restraints / parameters	5892 / 0 / 339
Goodness-of-fit (based on <i>F</i> <sup>2</sup> )	1.093
Extinction coefficient	0.0107(11)
Max( $\Delta\rho$ )/e.Å <sup>-3</sup>	0.381
Min( $\Delta\rho$ )/e.Å <sup>-3</sup>	-0.322
Final <i>R</i> indices [ <i>I</i> > 2 $\sigma$ ( <i>I</i> )]	<i>R</i> <sub>1</sub> = 0.0453, <i>wR</i> <sub>2</sub> = 0.1087
<i>R</i> indices (all data)	<i>R</i> <sub>1</sub> = 0.0788, <i>wR</i> <sub>2</sub> = 0.1380



## Chapter 3. Dinuclear Complexes of Copper(I) Bridged by 6-[ethyl(phenyl)phosphino]-2,2'-bipyridine and 6-(diphenylphosphino)-2-(2-quinolyl)pyridine

---

### 3.1. Introduction

A review of the literature reveals a number of ligand-bridged dinuclear copper(I) complexes which have been conveniently prepared from the copper(I) precursor  $[\text{Cu}(\text{CH}_3\text{CN})_4]^+$ , and a P,N or P,P type bidentate ligand. In a typical example, treatment of  $[\text{Cu}(\text{CH}_3\text{CN})_4](\text{BF}_4)$  with an equimolar amount of bis(diphenylphosphino)methane (dppm) in acetonitrile affords  $[\text{Cu}_2(\mu\text{-dppm})_2(\text{CH}_3\text{CN})_4](\text{BF}_4)_2$ .<sup>98</sup> Similarly, reaction of copper(I) tetrakisacetonitrile with 2,6-bis(diphenylphosphino)pyridine  $[(\text{Ph}_2\text{P})_2\text{py}]$  in acetonitrile gives  $[\text{Cu}_2\{\mu\text{-}(\text{Ph}_2\text{P})_2\text{py}\}_3](\text{PF}_6)_2$ .<sup>99</sup> By varying the solvent and molar ratios, Guineno *et al.* prepared a range of dinuclear copper(I) complexes bridged by  $\text{Ph}_2\text{Ppy}$  e.g., treatment of  $[\text{Cu}(\text{CH}_3\text{CN})_4]\text{BF}_4$  with  $\text{Ph}_2\text{Ppy}$  at room temperature in acetonitrile and dichloromethane gave  $[\text{Cu}_2(\mu\text{-Ph}_2\text{Ppy})_2(\text{CH}_3\text{CN})_4](\text{BF}_4)_2$  and  $[\text{Cu}_2(\mu\text{-Ph}_2\text{Ppy})_2(\text{CH}_3\text{CN})_2](\text{BF}_4)_2$  respectively.<sup>100</sup> Of most relevance to this study is the facile preparation of  $[\text{Cu}_2(\mu\text{-Ph}_2\text{Pbpy})_2(\text{CH}_3\text{CN})_2](\text{PF}_6)_2$  by the treatment of  $[\text{Cu}(\text{CH}_3\text{CN})_4]\text{PF}_6$  with one mole equivalent of  $\text{Ph}_2\text{Pbpy}$ .<sup>101</sup> As described in this chapter, the analogous  $\text{Et}(\text{Ph})\text{Pbpy}$  and  $\text{Ph}_2\text{Ppyqn}$  ligand-bridged dinuclear copper(I) complexes are synthesized by this method.

### 3.2. Results and Discussion

#### 3.2.1. Synthesis and Characterisation of the Dinuclear Copper Complexes

Treatment of an acetonitrile solution of  $[\text{Cu}(\text{CH}_3\text{CN})_4]^+$  with one equivalent of L [L =  $\text{Ph}_2\text{Ppyqn}$  or  $\text{Et}(\text{Ph})\text{Pbpy}$ ] at room temperature, and precipitation of the product after 24 h by the addition of diethyl ether, led to an orange crystalline product. The  $^1\text{H}$  NMR spectra recorded in  $\text{CD}_2\text{Cl}_2$  exhibit aromatic resonances from 8.90 to 6.70 ppm characteristic of the polypyridyl ligands as well as a singlet at 1.97 ppm assigned to the methyl protons of the acetonitrile ligand. Broad single peaks, at 9.0 (L =  $\text{Ph}_2\text{Ppyqn}$ ) and 10.0 ppm [L =  $\text{Et}(\text{Ph})\text{Pbpy}$ ], downfield to that recorded for the free ligands are observed in the  $^{31}\text{P}\text{-}\{^1\text{H}\}$  NMR spectra. This featureless broad band can be expected of a phosphorus donor atom bonded to a copper nucleus with an unsymmetrical charge distribution due to quadrupolar relaxation.<sup>79</sup> The infrared spectrum, recorded as a KBr disc, exhibits very strong absorption bands at 1085 and 838  $\text{cm}^{-1}$  typical of the  $\text{BF}_4^-$  and  $\text{PF}_6^-$  counter ions respectively. Elemental analysis for % C, H and N was consistent

with the formulation of the compounds as  $[\text{Cu}_2(\mu\text{-Ph}_2\text{Ppyqn})_2(\text{CH}_3\text{CN})_2](\text{BF}_4)_2$  **1** and  $[\text{Cu}_2\{\mu\text{-Et(Ph)Pbpy}\}_2(\text{CH}_3\text{CN})_2](\text{PF}_6)_2$  **2**. This was subsequently confirmed by means of single crystal X-ray structure determinations.

### 3.2.2. Crystal Structure Determination of $[\text{Cu}_2(\mu\text{-Ph}_2\text{Ppyqn})_2(\text{CH}_3\text{CN})_2](\text{BF}_4)_2$ **1** and $[\text{Cu}_2\{\mu\text{-Et(Ph)Pbpy}\}_2(\text{CH}_3\text{CN})_2](\text{PF}_6)_2$ **2**

The structure of the dications  $[\text{Cu}_2(\mu\text{-Ph}_2\text{Ppyqn})_2(\text{CH}_3\text{CN})_2]^{2+}$  and  $[\text{Cu}_2\{\mu\text{-Et(Ph)Pbpy}\}_2(\text{CH}_3\text{CN})_2]^{2+}$  together with their atomic numbering schemes are depicted in Figures 3.1 and 3.2 respectively. Selected interatomic distances and angles for the dications are given in Table 3.1.

**Table 3.1.** Selected interatomic distances (Å) and angles (°) for  $[\text{Cu}_2(\mu\text{-Ph}_2\text{Ppyqn})_2(\text{CH}_3\text{CN})_2](\text{BF}_4)_2$  **1** and  $[\text{Cu}_2\{\mu\text{-Et(Ph)Pbpy}\}_2(\text{CH}_3\text{CN})_2](\text{PF}_6)_2$  **2**.

	<b>1</b>	<b>2</b>
Cu···Cu <sup>a</sup>	3.045(4)	3.028(2)
Cu–N(3)	2.02(2)	1.994(6)
Cu–N(1)	2.10(2)	2.082(5)
Cu–N(2)	2.13(2)	2.109(5)
Cu–P	2.217(4)	2.203(2)
N(3)–Cu–N(1)	113.4(6)	104.3(2)
N(3)–Cu–N(2)	101.9(6)	100.3(2)
N(1)–Cu–N(2)	78.1(6)	78.4(2)
N(3)–Cu–P <sup>a</sup>	133.5(4)	129.2(2)
N(1)–Cu–P <sup>a</sup>	110.5(5)	122.6(2)
N(2)–Cu–P <sup>a</sup>	101.4(4)	106.6(2)
N(3)–Cu–Cu <sup>a</sup>	86.1(4)	83.9(2)
N(1)–Cu–Cu <sup>a</sup>	91.9(4)	90.4(2)
N(2)–Cu–Cu <sup>a</sup>	169.1(5)	168.7(2)
P <sup>a</sup> –Cu–Cu <sup>a</sup>	77.7(2)	77.94(6)

<sup>a</sup> Symmetry transformations used to generate equivalent atoms:  $(-x-1/2, -y-1/2, z)$  and  $(-x+3/2, y, -z+1/2)$  for **1** and **2** respectively.

Both molecules contain a crystallographically imposed centre of symmetry midway between the copper ions. The phosphorus-polypyridyl ligands bridge the copper atoms in a head-to-tail manner. Each metal atom has coordinated to it the phosphorus atom of the first bridging ligand, the chelating polypyridyl fragment of the second and an acetonitrile molecule.

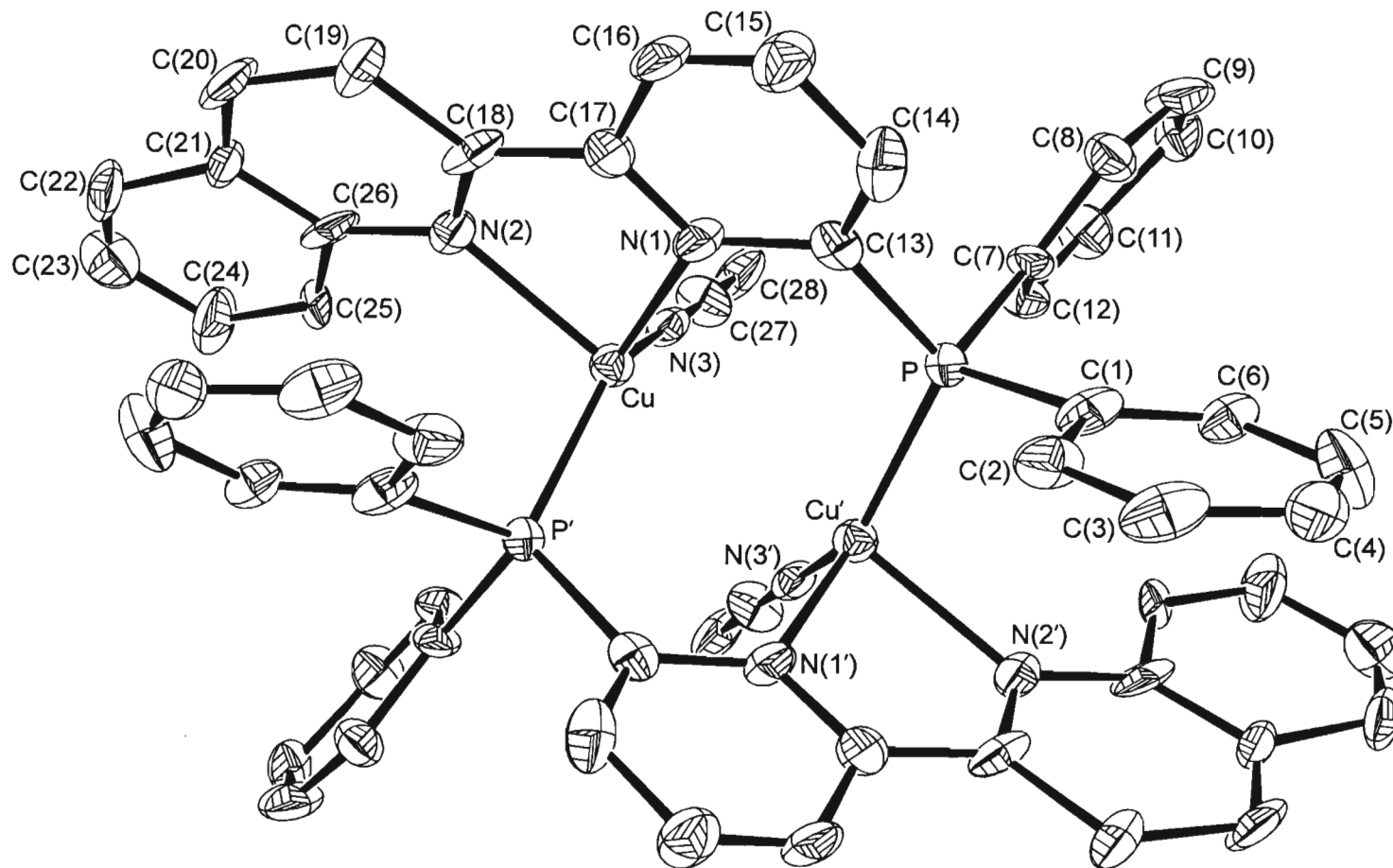


**Figure 3.1.** Perspective view of the dication  $[\text{Cu}_2(\mu\text{-Ph}_2\text{Ppyqn})_2(\text{CH}_3\text{CN})_2]^{2+}$ . The atoms are represented by their 20% probability thermal ellipsoids.

In order to accommodate the small-bite chelating fragment a significant distortion of the tetrahedral geometry about the metal atoms is observed in **1** and **2**. The Cu–P and Cu–N bond lengths listed in Table 3.1 do not differ markedly from those observed in the analogous Ph<sub>2</sub>Pbpy-bridged dicopper(I) complex, [Cu<sub>2</sub>(μ-Ph<sub>2</sub>Pbpy)<sub>2</sub>(CH<sub>3</sub>CN)<sub>2</sub>](PF<sub>6</sub>)<sub>2</sub>, where the Cu–P distance is 2.191(3) Å and the Cu–N bond lengths are 2.070(9) [Cu–N(1)], 2.106(9) [Cu–N(2)] and 2.073(9) Å [Cu–N(3)].<sup>101</sup>

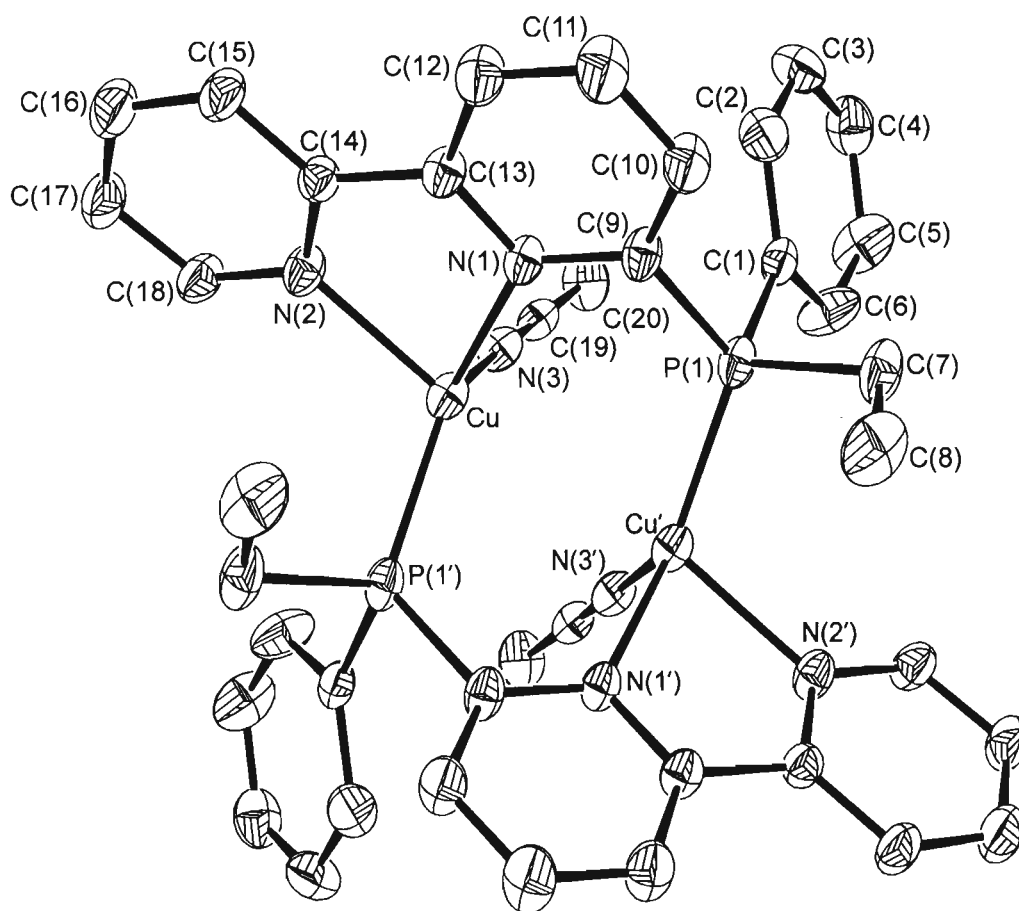


**Figure 3.2.** Perspective view of the dication [Cu<sub>2</sub>{μ-Et(Ph)Pbpy}<sub>2</sub>(CH<sub>3</sub>CN)<sub>2</sub>]<sup>2+</sup>. The atoms are represented by their 20% probability thermal ellipsoids.

A comparison of the molecular structures reveals an interesting conformational difference between the [Cu<sub>2</sub>(μ-Ph<sub>2</sub>Pbpy)<sub>2</sub>(CH<sub>3</sub>CN)<sub>2</sub>]<sup>2+</sup> dication on one hand and the [Cu<sub>2</sub>{μ-Et(Ph)Pbpy}<sub>2</sub>(CH<sub>3</sub>CN)<sub>2</sub>]<sup>2+</sup> and [Cu<sub>2</sub>(μ-Ph<sub>2</sub>Ppyqn)<sub>2</sub>(CH<sub>3</sub>CN)<sub>2</sub>]<sup>2+</sup> dications on the other. In the latter two species the bridging ligands are coordinated *cis* to one another, whereas in the former they are seen to adopt a *trans* arrangement. This is depicted in Figure 3.3, where the conformations of the [Cu<sub>2</sub>{μ-Et(Ph)Pbpy}<sub>2</sub>(CH<sub>3</sub>CN)<sub>2</sub>]<sup>2+</sup> and [Cu<sub>2</sub>(μ-Ph<sub>2</sub>Pbpy)<sub>2</sub>(CH<sub>3</sub>CN)<sub>2</sub>]<sup>2+</sup> dications are compared. Furthermore the Cu⋯Cu distance is shortened from 3.941(2) Å in [Cu<sub>2</sub>(μ-Ph<sub>2</sub>Pbpy)<sub>2</sub>(CH<sub>3</sub>CN)<sub>2</sub>](PF<sub>6</sub>)<sub>2</sub> to 3.045(4) and 3.0291(16) Å in **1** and **2** respectively.

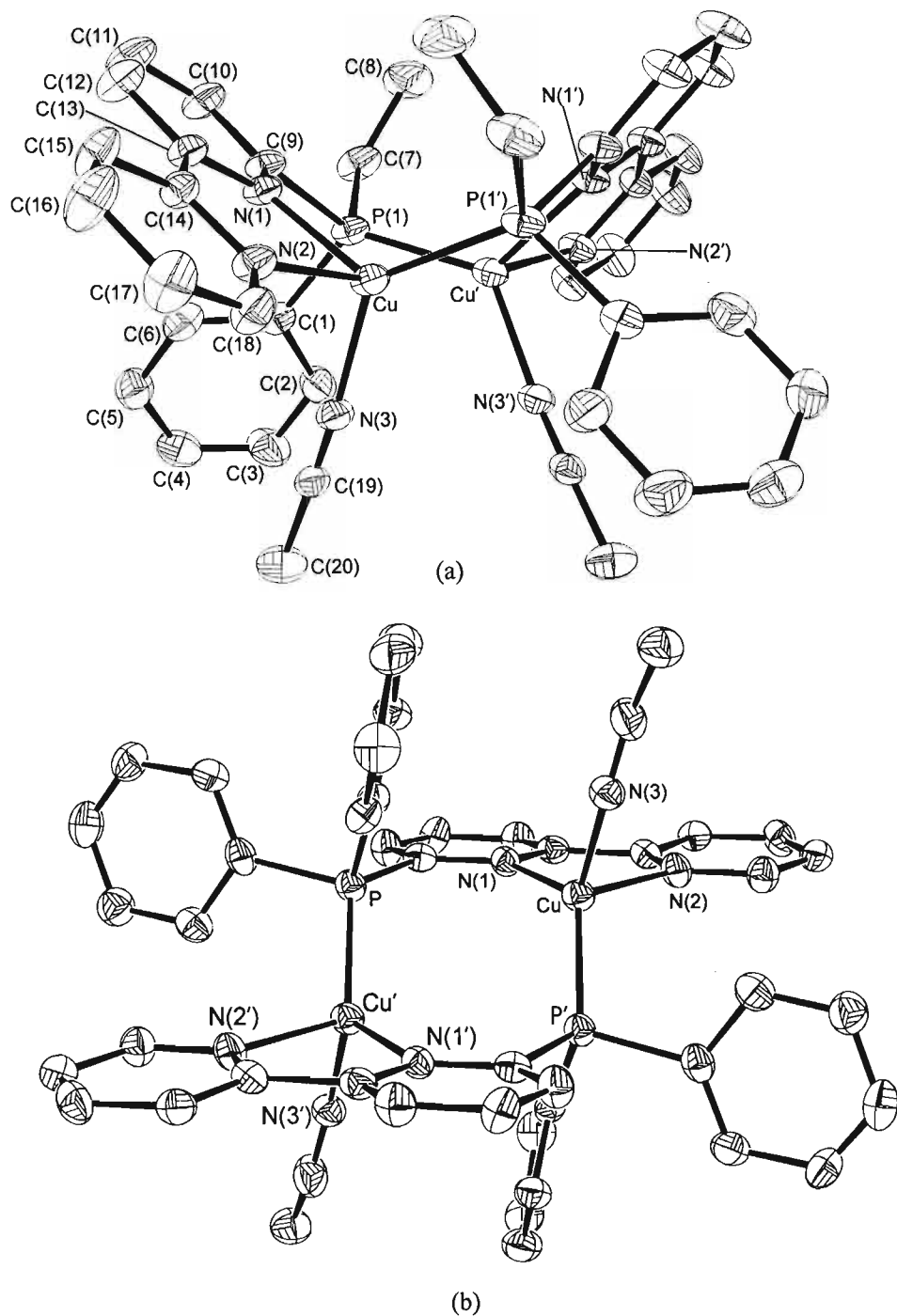


**Figure 3.3.** Perspective views of the dications (a)  $[\text{Cu}_2\{\mu\text{-Et(Ph)Pbpy}\}_2(\text{CH}_3\text{CN})_2]^{2+}$  and (b)  $[\text{Cu}_2(\mu\text{-Ph}_2\text{Pbpy})_2(\text{CH}_3\text{CN})_2]^{2+}$  illustrating the *cis* and *trans* disposition of the phosphorus-polypyridyl ligands respectively.

The core bonding atoms of the complexes give rise a  $\text{Cu}_2\text{P}_2\text{N}_2\text{C}_2$  eight-membered ring. It is the variation in the framework of this ring that results in the different structures. As illustrated in Figure 3.4, a chair-conformation of the eight-membered ring is adopted in  $[\text{Cu}_2(\mu\text{-$

$\text{Ph}_2\text{Pbpy})_2(\text{CH}_3\text{CN})_2](\text{PF}_6)_2$ . In contrast, the cations of **1** and **2** are found to have an alternative twisted-boat arrangement of this ring.

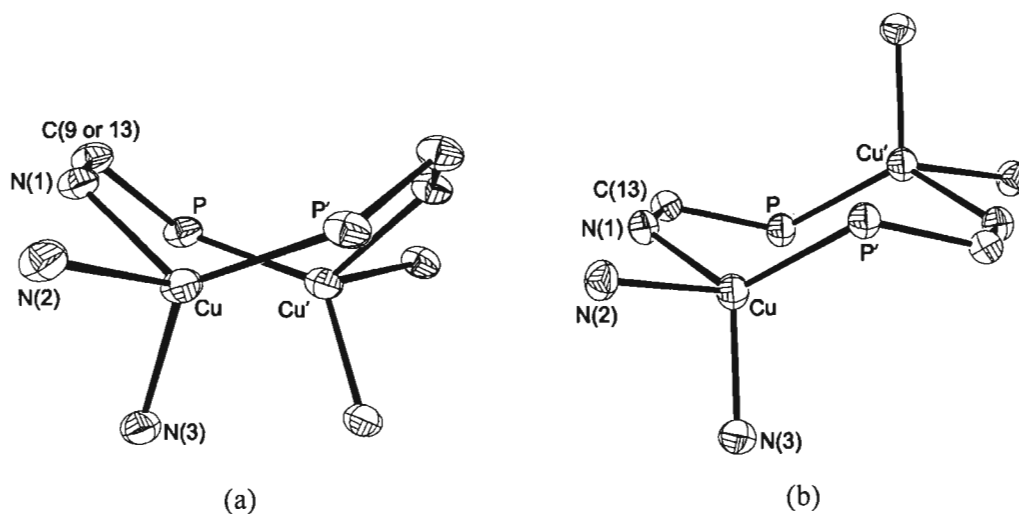


**Figure 3.4.** (a) Twisted-boat conformation of the eight-membered ring found in **1** and **2**. (b) Chair conformation found in  $[\text{Cu}_2(\mu\text{-Ph}_2\text{Pbpy})_2(\text{CH}_3\text{CN})_2](\text{PF}_6)_2$ . The coordinated nitrogen atom of the acetonitrile ligand is labelled N(3).

In comparison the eight-membered  $\text{Cu}_2\text{P}_2\text{N}_2\text{C}_2$  ring in  $[\text{Cu}_2(\mu\text{-Ph}_2\text{Ppy})_2(\text{CH}_3\text{CN})_2](\text{PF}_6)_2$ , in which the copper atoms have an irregular trigonal geometry, has a ‘staggered’ or chair conformation very similar to that of  $[\text{Cu}_2(\mu\text{-Ph}_2\text{Pbpy})_2(\text{CH}_3\text{CN})_2](\text{PF}_6)_2$ .<sup>102</sup> The closely related phosphorus-polypyridyl ligand-bridged complex  $[\text{Cu}_2(\mu\text{-Ph}_2\text{Pphen})_2(\text{CH}_3\text{CN})_2](\text{PF}_6)_2$  similarly possesses a chair conformation.<sup>64</sup> On the other hand, the conformation of the eight-membered  $\text{Cu}_2\text{P}_4\text{C}_2$  ring in  $[\text{Cu}_2(\mu\text{-dppm})_2(\text{CH}_3\text{CN})_4](\text{ClO}_4)_2$  is described by Gimeno *et al.* as eclipsed and is analogous to that found in **1** and **2**. This conformation is also observed in other ligand bridged dinuclear complexes having a four coordinate copper(I) atom and a stronger precedent seems to have been set for it.<sup>60,103</sup> For example, the eight-membered  $\text{Cu}_2\text{P}_4\text{C}_2$  ring in  $[\text{Cu}_2(\mu\text{-dppm})_2(\text{S}_2\text{CT})_2]$  ( $\text{S}_2\text{CT}$  = dithio-*o*-toluate)<sup>104</sup> and the  $\text{Cu}_2\text{N}_2\text{C}_4$  ring in  $[\text{Cu}_2(\mu\text{-vpy})_2(\text{vpy})_2](\text{ClO}_4)_2$  ( $\text{vpy}$  = 2-vinylpyridine)<sup>105</sup> both assume chair conformations.

The reaction of  $[\text{Cu}_2(\mu\text{-Ph}_2\text{Pbpy})_2(\text{CH}_3\text{CN})_2]^{2+}$  with halide ions and sodium ethanethiolate in solution at room temperature readily affords the substitution products  $[\text{Cu}_2(\mu\text{-Ph}_2\text{Pbpy})_2(\mu\text{-X})](\text{PF}_6)$  ( $\text{X} = \text{Br}$  and  $\text{I}$ ) and  $[\text{Cu}_2(\mu\text{-Ph}_2\text{Pbpy})_2(\mu\text{-SEt})](\text{PF}_6)$  respectively.<sup>129</sup> Crystal structure determinations of these compounds reveal that the eight-membered rings adopt twisted-boat conformations as opposed to the chair conformations of the parent complexes. This suggests that the conformation of the molecule may readily change between the two possibilities. Similarly, the chair-conformation of the eight-membered  $\text{Cu}_2\text{P}_2\text{N}_2\text{C}_2$  ring in  $[\text{Cu}_2(\mu\text{-$

$\text{Ph}_2\text{Pphen})_2(\text{CH}_3\text{CN})_2](\text{PF}_6)_2$  readily converts to the twisted-boat configuration upon the introduction of the diethyldithiocarbamate bridging ligand in  $[\text{Cu}_2(\mu\text{-Ph}_2\text{Pphen})_2\{\mu\text{-S}_2\text{CN}(\text{Et})_2\}_2](\text{PF}_6)$ .<sup>64</sup>

The labile acetonitrile ligands, which can be considered as the active sites of the molecule, are *cis* to one another in the twisted-boat conformation. Furthermore, the two metal centres are in closer proximity than in comparison to the chair conformation, presenting the possibility of cooperative effects between the two metals during a catalytic cycle. Thus the conformation of the cyclic framework in these related complexes in solution may play an important role in their catalytic behaviour. The factors governing which conformation the eight-membered  $\text{Cu}_2\text{P}_2\text{N}_2\text{C}_2$  ring preferentially forms are not immediately obvious. The inherent stability of a particular conformation, and thus its preferential formation in a given complex, may stem from the unique steric nature of its phosphorus-polypyridyl ligand.

### 3.2.3. Electrochemical Behaviour of the Dinuclear Copper Complexes

The electrochemistry of  $[\text{Cu}_2(\mu\text{-Ph}_2\text{Pbpy})_2(\text{CH}_3\text{CN})_2](\text{PF}_6)_2$  has been described previously, the complex being reported as undergoing two one-electron reductions.<sup>11,129</sup> The closely related complexes **1** and **2** were found to possess a richer electrochemistry and therefore that of  $[\text{Cu}_2(\mu\text{-Ph}_2\text{Pbpy})_2(\text{CH}_3\text{CN})_2](\text{PF}_6)_2$  was re-examined. The redox properties of the complexes are summarised in Tables 3.2 and 3.3.

**Table 3.2.** Cyclic voltammetric data for the dicopper complexes  $[\text{Cu}_2(\mu\text{-L})_2(\text{CH}_3\text{CN})_2](\text{PF}_6)_2$  [**L** =  $\text{Ph}_2\text{Ppyqn}$  **1**,  $\text{Et}(\text{Ph})\text{Pbpy}$  **2** and  $\text{Ph}_2\text{Pbpy}$ ].<sup>a</sup>

Complex	$E_{1/2}/V(\Delta E_p/\text{mV})$			
	$E_{1/2}^{+2/+}$	$E_{1/2}^{+0}$	$E_{1/2}^{0/-}$	$E_{1/2}^{-/-2}$
$[\text{Cu}_2(\mu\text{-Ph}_2\text{Ppyqn})_2(\text{CH}_3\text{CN})_2](\text{PF}_6)_2$ <b>1</b>	-1.66(100) <sup>b</sup>		-2.04(75)	-2.23(85)
$[\text{Cu}_2(\mu\text{-Ph}_2\text{Pbpy})_2(\text{CH}_3\text{CN})_2](\text{PF}_6)_2$	-1.68(75)	-1.88(75)	-2.18(75)	-2.34(70)
$[\text{Cu}_2\{\mu\text{-Et}(\text{Ph})\text{Pbpy}\}_2(\text{CH}_3\text{CN})_2](\text{PF}_6)_2$ <b>2</b>	-1.72(70)	-1.91(50)	-2.23(50)	-2.40(80)

<sup>a</sup> Potentials vs.  $\text{Ag}/\text{Ag}^+$ , measured in  $\text{CH}_3\text{CN}$  (0.1 M TBAP) using a  $\text{Ag}/\text{AgCl}$  wire pseudo-reference electrode, scan rate  $100 \text{ mV s}^{-1}$ ,  $T = 298 \text{ K}$ . Definitions:  $E_{1/2} = (E_{pc} + E_{pa})/2$ ;  $\Delta E_p = E_{pc} - E_{pa}$ .<sup>b</sup> Overall transfer of  $2e^-$ , where the half-wave potential corresponds to the average of the two,  $E_{1/2} = (E_{1/2}^{+2/+} + E_{1/2}^{+0})/2$ .

The cathodic CV of **2**, depicted in Figure 3.5, is very similar to that observed for  $[\text{Cu}_2(\mu\text{-Ph}_2\text{Pbpy})_2(\text{CH}_3\text{CN})_2](\text{PF}_6)_2$ . It consists of four successive reduction waves which are essentially chemically and electrochemically reversible;  $i_{pa}/i_{pc} \sim 1$ ,  $i_p$  shows a linear relationship with  $\nu^{1/2}$

when  $\nu$  is varied from 20 to 500  $\text{mVs}^{-1}$ ,  $\Delta E_p$  is what one would expect for a reversible one-electron reduction and is independent of  $\nu$ . Comparison of the current response in the RDE voltammogram of each of the complexes with that of a known amount of ferrocene measured *in situ*, shows that the four reduction steps each consist of a one electron transfer, ultimately leading to formally dicopper(-1) complexes.

When the potential scan is held beyond the fourth wave ( $E_\lambda$  of  $-2.48$  and  $-2.58$  V for  $[\text{Cu}_2(\mu\text{-Ph}_2\text{Pbpy})_2(\text{CH}_3\text{CN})_2]^{2+}$  and **2** respectively) for *ca.* 30 seconds the return scan shows the appearance of a new small anodic peak at  $-0.66$  V. This is in the region one would expect for a copper stripping peak, consistent with a demetallation of the complexes and the concurrent deposition of elemental copper onto the electrode surface. This anodic wave is however absent in the return scan when the potential is held just beyond the third wave ( $E_\lambda$  of  $-2.34$  and  $-2.41$  V for  $[\text{Cu}_2(\mu\text{-Ph}_2\text{Pbpy})_2(\text{CH}_3\text{CN})_2]^{2+}$  and **2** respectively) for *ca.* 30 seconds. These qualitative observations show that while the fourth reduction product may appear stable on the time scale of cyclic voltammetric measurements at scan rates of  $20 \text{ mVs}^{-1}$ , over a longer time period it is only the triply reduced species that are chemically stable.

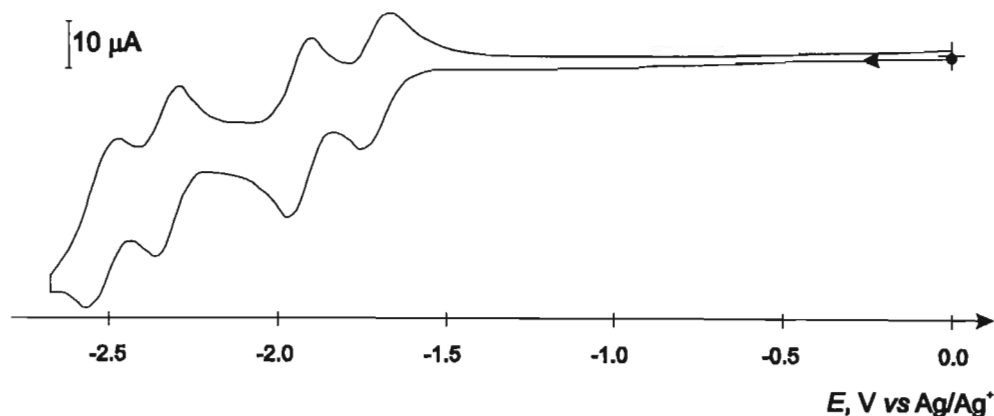


**Figure 3.5.** Cyclic voltammogram of  $[\text{Cu}_2\{\mu\text{-Et(Ph)Pbpy}\}_2(\text{CH}_3\text{CN})_2](\text{PF}_6)_2$  **2**, measured in  $\text{CH}_3\text{CN}$  (0.1 M TBAP). (Pt electrode,  $r = 1.0$  mm;  $\nu = 100 \text{ mVs}^{-1}$ )

As illustrated in Figure 3.6, the cathodic CV of **1** exhibits three reduction waves. No additional peaks are observed when the scan is extended to  $-2.90$  V. The cathodic to anodic peak separation of each redox couple showed no significant variation when the scan rate was varied from 20 to 500  $\text{mV s}^{-1}$ . The peak current  $i_p$  is linearly related to  $\nu^{1/2}$  and the estimated  $i_{pa}/i_{pc}$  was unity for each couple. These observations demonstrate the chemical and electrochemical reversibility of each couple. When the potential scan was held beyond the third wave ( $E_\lambda$  of



-2.58 V) for *ca.* 30 s the form of the CV was unchanged, indicating that the ultimate reduction product is stable on a time scale beyond that of the cyclic voltammetric measurement.

The current response in the RDE voltammogram of **1** shows unequivocally that the first reduction step involves a two-electron transfer, the second and third reductions each being a one-electron transfer process. The anodic to cathodic peak splitting for a one-step, simultaneous two-electron transfer process is expected to be 28.3 mV. The  $\Delta E_p$  splitting of this two electron redox couple is a 100 mV. The form of the first reduction wave is therefore more typical of that expected for two consecutive one-electron transfer processes where the difference in the two standard potentials is not large enough to resolve the two waves. That the energy required for the second electron transfer is only slightly more than the first suggests the presence of two structurally similar redox centres in the molecule which do not interact to any significant extent.

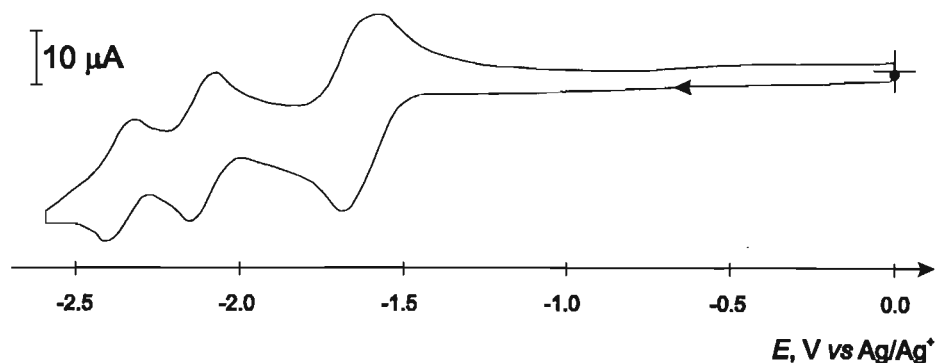


**Figure 3.6.** CV of  $[\text{Cu}_2(\mu\text{-Ph}_2\text{Ppyqn})_2(\text{CH}_3\text{CN})_2](\text{PF}_6)_2$  **1**, measured in  $\text{CH}_3\text{CN}$  (0.1 M TBAP). (Pt electrode,  $r = 1.0$  mm;  $\nu = 100$   $\text{mVs}^{-1}$ )

The exhaustive electrolysis in acetonitrile of  $[\text{Cu}_2(\mu\text{-L})_2(\text{CH}_3\text{CN})_2](\text{PF}_6)_2$  ( $\text{L} = \text{Ph}_2\text{Ppyqn}$  **1**,  $\text{Ph}_2\text{Pbpy}$  and  $\text{Et}(\text{Ph})\text{Pbpy}$  **2**) at the potential of their first reduction peak show that the singly reduced complexes are unstable on an electrochemical time scale. While no sign of the original complex is seen in CVs recorded after exhaustive reduction, the appearance of several new redox systems in them reflects the formation of a number of decomposition products. In view of the complexity of these, their full characterisation was not undertaken. In each case a dominant peak whose reduction potential corresponds to that of the first reduction of the respective free P,N,N ligand is observed. Furthermore, a reddish coloured copper deposit is observed on the surface of the working electrode. These observations are characteristic of the behaviour of most Cu(I) complexes under such conditions, their reduction leading to the dissociation of Cu(0) from the ligand to give a Cu deposit on the electrode surface and free ligand in solution.<sup>106,107</sup>

Nevertheless, the reversibility exhibited by the Cu(I) complexes here in their cyclic voltammetry is noteworthy given that the electrochemical reduction of  $d^{10}$  copper(I) complexes

is often characterized by the dissociation of the zero-valent metal from the ligand subsequent to reduction. Thus the one-electron reductions of  $[\text{Cu}(\text{bpy})_2]^+$  and  $[\text{Cu}(\text{PPh}_3)_4]^+$  lead to the formation of copper metal and free ligand in solution.<sup>108,109</sup> This electrochemical demetallation has been prevented by the use of electron deficient ligands in the complex which accept the reducing electron into their low lying empty molecular orbitals.<sup>110,111</sup> The reversible electrochemical behaviour displayed by  $[\text{Cu}_2(\mu\text{-Ph}_2\text{Pbpy})_2(\text{CH}_3\text{CN})_2](\text{PF}_6)_2$ , **1** and **2** therefore indicates that the primary site of reduction is ligand based. The sequence of reduction of the metal complexes parallels that of the free ligands, demonstrating the similar electronic character of the redox orbital in each case. A comparison of the separation between successive reduction waves for the free ligands and their complexes supports this interpretation. Thus, the free ligands exhibit separations between their first and second reduction potentials that range from 540 (Ph<sub>2</sub>Pbpy) to 600 mV [Et(Ph)Pbpy] and which closely match the differences between the first and third  $E_{1/2}$  values on one hand, and the second and fourth  $E_{1/2}$  values on the other, observed for  $[\text{Cu}_2(\mu\text{-Ph}_2\text{Pbpy})_2(\text{CH}_3\text{CN})_2](\text{PF}_6)_2$  and **2** (*cf.* data in Tables 2.6 and 3.2). Likewise, the separations between the averaged half-wave potential of the first two reductions of **1** and the third and fourth reduction potentials are 380 and 570 mV respectively. Thus it appears that the overall four-electron reduction process consists of the addition of one electron to each polypyridyl fragment in turn followed by the addition of a second electron to each polypyridyl fragment in turn.

A reversible  $\text{Cu}^{I/0}$  redox couple is alternatively achieved in 1,10-phenanthroline catenates of Cu(I) whereby the ligands encase the  $\text{Cu}^0$  generated by reduction, thus preventing demetallation.<sup>112,113</sup> A parallel can be drawn with the bridging phosphorus-polypyridyl ligands, where the inter-locking phosphorus bridging moieties fix the copper atoms into the coordination sphere preventing their dissociation from the reduced ligands. It is the combination of this property with the electron acceptor capability of the  $\alpha$ -diimine fragment that probably accounts for the unusual stability of the reduced forms of the P,N,N ligand-bridged complexes.

The stability of the Cu(I) 1,10-phenanthroline catenates to electrochemical reduction has also been ascribed to the geometrical distortion of the tetrahedral coordination brought about by their particular topography.<sup>114</sup> Zacharias *et al.* found that the electrochemical reversibility of the  $\text{Cu}^{I/0}$  redox couple observed for a series of Cu(I) 2,9 substituted 1,10-phenanthroline complexes parallels the steric bulk of the substituents and hence the distortion observed in the complex. As noted, the final reduction product of **1** was observed to be chemically more stable than those of  $[\text{Cu}_2(\mu\text{-Ph}_2\text{Pbpy})_2(\text{CH}_3\text{CN})_2](\text{PF}_6)_2$  and **2**. It can be concluded that, in addition to having stronger

$\pi$  acceptor properties, the  $\alpha$ -diimine fragment of the Ph<sub>2</sub>Ppyqn ligand, by providing steric bulk at the  $\alpha$ -position, further stabilises the dicopper(-1) species to fragmentation.

In contrast to [Cu( $\mu$ -L)(CH<sub>3</sub>CN)]<sub>2</sub>(PF<sub>6</sub>)<sub>2</sub> [L = Ph<sub>2</sub>Ppyqn **1**, Ph<sub>2</sub>Pbpy and Et(Ph)Pbpy **2**], the analogous P,N,N ligand-bridged adduct [Cu<sub>2</sub>( $\mu$ -Ph<sub>2</sub>Pphen)<sub>2</sub>(CH<sub>3</sub>CN)<sub>2</sub>](PF<sub>6</sub>)<sub>2</sub> is irreversibly reduced at  $E_{pc} = -1.48$  V vs. FeCp<sub>2</sub><sup>0/+</sup> in CH<sub>3</sub>CN + 0.1 M TBAP.<sup>64</sup> Yet Ph<sub>2</sub>Pphen, derived from 1,10-phenanthroline, would be expected to be a good electron-acceptor ligand as a consequence of its planarity and increased conjugation. In point of fact, the potential of the irreversible reduction of [Cu<sub>2</sub>( $\mu$ -Ph<sub>2</sub>Pphen)<sub>2</sub>(CH<sub>3</sub>CN)<sub>2</sub>](PF<sub>6</sub>)<sub>2</sub> is 350 mV more positive than the first reduction of [Cu<sub>2</sub>( $\mu$ -Ph<sub>2</sub>Pbpy)<sub>2</sub>(CH<sub>3</sub>CN)<sub>2</sub>](PF<sub>6</sub>)<sub>2</sub>. The P,N,N ligands Ph<sub>2</sub>Ppyqn, Ph<sub>2</sub>Pbpy and Et(Ph)Pbpy differ from Ph<sub>2</sub>Pphen in that they possess rotational freedom about the interannular C–C bond of their pyridyl rings. As a result, these ligands will have a coordinative flexibility absent in the rigid Ph<sub>2</sub>Pphen, allowing them to better accommodate the changes in the redox state of their complexes. Evidently the steric properties of the ligands play an equally important role as their electronic properties in determining the electrochemical behaviour of their Cu(I) complexes.

The phosphorus-polypyridyl ligand-bridged dicopper(I) complexes undergo an irreversible one-electron oxidation step in the region of 0.75 V. The anodic CV of [Cu<sub>2</sub>( $\mu$ -Ph<sub>2</sub>Pbpy)<sub>2</sub>(CH<sub>3</sub>CN)<sub>2</sub>](PF<sub>6</sub>)<sub>2</sub>, shown in Figure 3.7, is typical of this. A reverse cathodic response, corresponding to the first oxidation process, is observed at 0.35 and 0.34 V in the CVs of [Cu<sub>2</sub>( $\mu$ -Ph<sub>2</sub>Pbpy)<sub>2</sub>(CH<sub>3</sub>CN)<sub>2</sub>]<sup>2+</sup> and **2** respectively, but is absent in the case of **1**. The relative stabilisation of the Cu(I) centres in **1**, **2** and [Cu<sub>2</sub>( $\mu$ -Ph<sub>2</sub>Pbpy)<sub>2</sub>(CH<sub>3</sub>CN)<sub>2</sub>](PF<sub>6</sub>)<sub>2</sub> is a reflection of the electron donor-acceptor properties of the P,N,N ligands, the irreversible oxidation potential of **1** being the most anodic, that of **2** the most cathodic.

**Table 3.3.** Oxidative cyclic voltammetric data of the dicopper complexes [Cu<sub>2</sub>( $\mu$ -L)<sub>2</sub>(CH<sub>3</sub>CN)<sub>2</sub>](PF<sub>6</sub>)<sub>2</sub> [L = Ph<sub>2</sub>Ppyqn **1**, Et(Ph)Pbpy **2** and Ph<sub>2</sub>Pbpy].<sup>a</sup>

Complex	$E_{pa}^{ox I}$	$E_{pc}^{ox I}$	RER <sup>b</sup> of Cu <sup>I</sup>
[Cu <sub>2</sub> ( $\mu$ -Ph <sub>2</sub> Ppyqn) <sub>2</sub> (CH <sub>3</sub> CN) <sub>2</sub> ](PF <sub>6</sub> ) <sub>2</sub> <b>1</b>	0.92	-	2.57
[Cu <sub>2</sub> ( $\mu$ -Ph <sub>2</sub> Pbpy) <sub>2</sub> (CH <sub>3</sub> CN) <sub>2</sub> ](PF <sub>6</sub> ) <sub>2</sub>	0.83	0.42	2.49
[Cu <sub>2</sub> { $\mu$ -Et(Ph)Pbpy} <sub>2</sub> (CH <sub>3</sub> CN) <sub>2</sub> ](PF <sub>6</sub> ) <sub>2</sub> <b>2</b>	0.72	0.41	2.37

<sup>a</sup> Potentials vs. Ag/Ag<sup>+</sup>, measured in CH<sub>3</sub>CN (0.1 M TBAP) using a Ag/AgCl wire pseudo-reference electrode, scan rate 100 mV s<sup>-1</sup>,  $T = 298$  K. Definitions:  $E_{pa}^{ox}$ ,  $E_{pc}^{ox}$  = anodic and cathodic peak potentials respectively of chemically irreversible oxidation. <sup>b</sup> Redox existence range =  $E_{pa}^{ox I} - E_{1/2}^{+2/+}$ .

A change in coordination geometry is often associated with the Cu<sup>II/I</sup> redox couple, the d<sup>10</sup> Cu(I) ion preferentially forming tetracoordinate, tetrahedral complexes whilst the d<sup>9</sup> Cu(II) ion is normally pentacoordinate.<sup>115</sup> This difference in the coordination number of the oxidation states has been exploited to stabilise Cu(I) through the use of 2,2'-bipyridine and 1,10-phenanthroline ligands substituted in the 6,6' and 2,9 positions.<sup>111,112,116,117</sup> Bulky groups at these stereoactive positions favour the formation of a 4-coordinate geometry, thereby increasing the Cu<sup>II/I</sup> redox potential. The redox existence range (RER) is the difference between the Cu<sup>II/I</sup> and Cu<sup>I/0</sup> redox potentials and is a measure of the stabilisation of the +1 oxidation state. The RER of [Cu(bpy)<sub>2</sub>]<sup>+</sup> is 0.56 V,<sup>113</sup> while that of [Cu(bfp)<sub>2</sub>]<sup>+</sup> [bfp = 2,9-bis-(trifluoromethyl)-1,10-phenanthroline] is 2.77 V - the highest value reported for a [Cu(N,N)<sub>2</sub>]<sup>+</sup> system.<sup>116</sup> The RERs of the P,N,N Cu(I) complexes, ranging from 2.37 V for **2** to 2.57 V for **1** (Table 3.3), show a comparatively high stabilisation of Cu(I) and are striking in view of the labile acetonitrile ligand at each metal. This must stem from the efficient electron-acceptor character of the P,N,N ligands combined with the steric bulk of their 6-phosphino substituents, augmented in Ph<sub>2</sub>Ppyqn by the additional quinoline moiety.

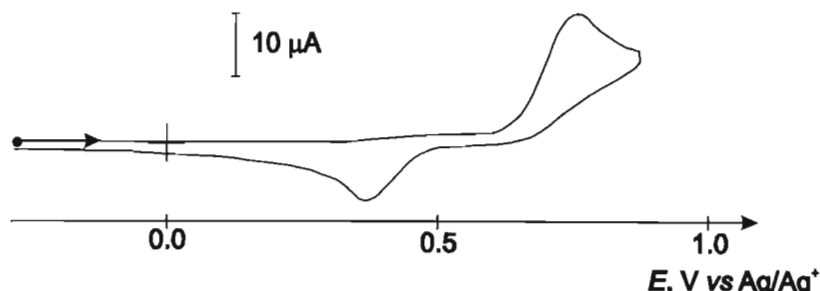


**Figure 3.7.** CV of [Cu<sub>2</sub>(μ-Ph<sub>2</sub>Pbpy)<sub>2</sub>(CH<sub>3</sub>CN)<sub>2</sub>](PF<sub>6</sub>)<sub>2</sub>, measured in CH<sub>3</sub>CN (0.1 M TBAP). (Pt electrode, r = 1.0 mm; ν = 100 mVs<sup>-1</sup>)

### 3.2.4. Catalytic Properties Towards CO<sub>2</sub> Electrochemical Reduction

The electrocatalytic properties of [Cu<sub>2</sub>(μ-Ph<sub>2</sub>Pbpy)<sub>2</sub>(CH<sub>3</sub>CN)<sub>2</sub>](PF<sub>6</sub>)<sub>2</sub> have been previously reported, this complex catalysing the reductive disproportionation of CO<sub>2</sub> to CO and CO<sub>3</sub><sup>2-</sup>.<sup>11</sup> For comparison with the closely related complexes **1** and **2**, the electrocatalytic properties of [Cu<sub>2</sub>(μ-Ph<sub>2</sub>Pbpy)<sub>2</sub>(CH<sub>3</sub>CN)<sub>2</sub>](PF<sub>6</sub>)<sub>2</sub> were re-examined under the same experimental conditions.

The CVs of [Cu<sub>2</sub>(μ-Ph<sub>2</sub>Pbpy)<sub>2</sub>(CH<sub>3</sub>CN)<sub>2</sub>](PF<sub>6</sub>)<sub>2</sub> and **2** recorded under CO<sub>2</sub> display the same features, illustrated in Figure 3.8, as have been already described for [Cu<sub>2</sub>(μ-Ph<sub>2</sub>Pbpy)<sub>2</sub>(CH<sub>3</sub>CN)<sub>2</sub>](PF<sub>6</sub>)<sub>2</sub>.<sup>11</sup> When the switching potential  $E_{\lambda}$  is just beyond the first reduction peak the form of the couple is unperturbed by the presence of CO<sub>2</sub>. If the value of  $E_{\lambda}$  is such that

the potential scan is reversed after the second reduction an enhancement in current is observed at the onset of the second cathodic peak. On the return scan neither anodic peaks are present. These observations are indicative of the formally direduced  $[\text{Cu}_2(\mu\text{-L})_2(\text{CH}_3\text{CN})_2]^0$  [ $\text{L} = \text{Ph}_2\text{Pbpy}$  and  $\text{Et}(\text{Ph})\text{Pbpy}$  **2**] complexes catalysing the electrochemical reduction of  $\text{CO}_2$  in a coupled two-electron process, as shown for  $[\text{Cu}_2(\mu\text{-Ph}_2\text{Pbpy})_2(\text{CH}_3\text{CN})_2](\text{PF}_6)_2$ .<sup>11</sup>

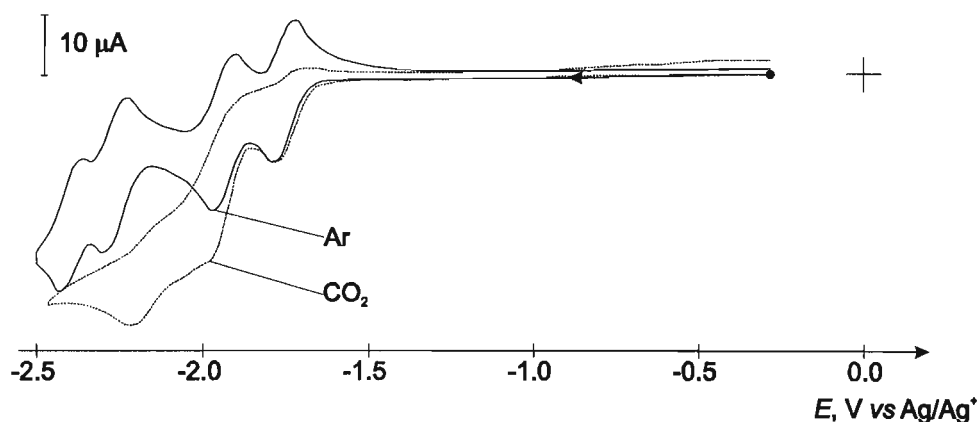


**Figure 3.8.** CVs of  $[\text{Cu}_2(\mu\text{-Ph}_2\text{Pbpy})_2(\text{CH}_3\text{CN})_2](\text{PF}_6)_2$  in  $\text{CO}_2$  and Ar saturated acetonitrile (0.1 M TBAP) solution. (Pt electrode,  $r = 1.0$  mm;  $\nu = 100$   $\text{mVs}^{-1}$ ).

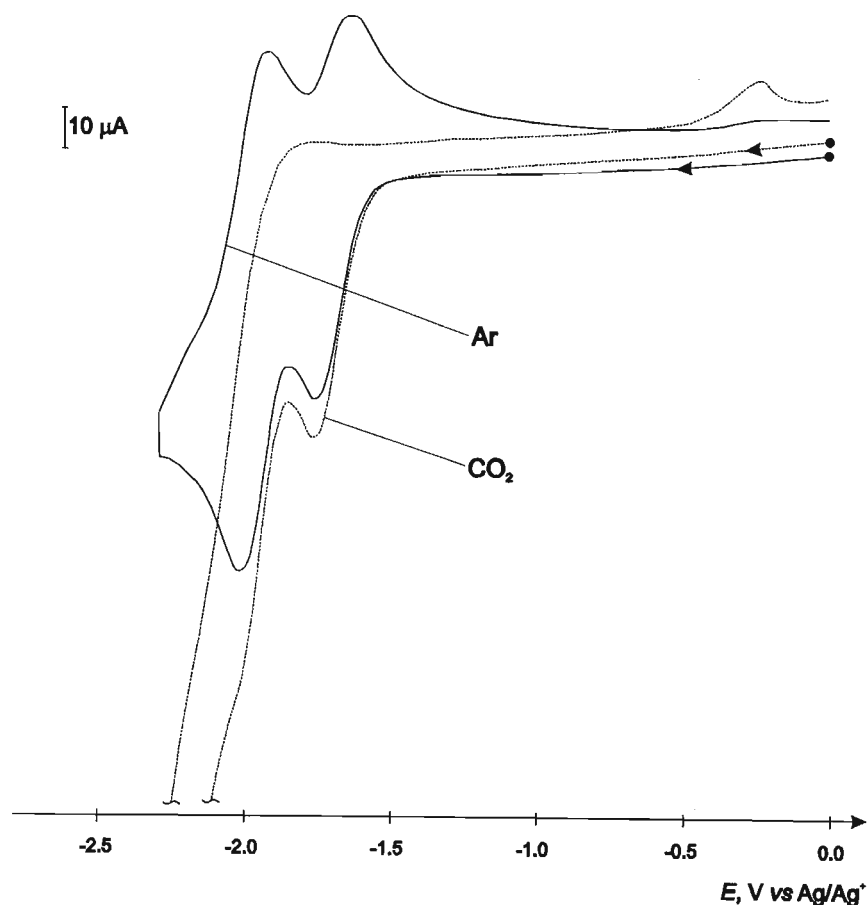


**Figure 3.9.** CVs of  $[\text{Cu}_2\{\mu\text{-Et}(\text{Ph})\text{Pbpy}\}_2(\text{CH}_3\text{CN})_2](\text{PF}_6)_2$  **2** in  $\text{CO}_2$  and Ar saturated acetonitrile (0.1 M TBAP) solution with water (0.5 %) present. (Pt electrode,  $r = 1.0$  mm;  $\nu = 100$   $\text{mVs}^{-1}$ ).

A marked enhancement in the catalytic current is observed upon the addition of trace amounts of water (0.5 %) to the solution of the complexes. This is illustrated in Figure 3.9, which shows the CV of **2** recorded under argon and CO<sub>2</sub> both in the presence of water. Of significance is the appearance of a small copper stripping peak at *ca.* 0.6 V on the reverse scan in the presence of CO<sub>2</sub>. On this basis it is doubtful that the complex will survive a bulk electrolysis experiment carried out in the presence of both CO<sub>2</sub> and water. On the other hand the original form of the CV is regained on purging the solution with argon indicating, as expected, that there is no stoichiometric reaction of CO<sub>2</sub> with the dicationic starting material but only with its reduced form, **2**<sup>0</sup>. The CVs of [Cu<sub>2</sub>(μ-Ph<sub>2</sub>Pbpy)<sub>2</sub>(CH<sub>3</sub>CN)<sub>2</sub>](PF<sub>6</sub>)<sub>2</sub> recorded under argon and CO<sub>2</sub> in the presence of water display the same features as those of **2**, illustrated in Figure 3.9.

The electrochemical behaviour of **1** in the presence of CO<sub>2</sub>, illustrated in Figure 3.10, contrasts that of [Cu<sub>2</sub>(μ-L)<sub>2</sub>(CH<sub>3</sub>CN)<sub>2</sub>](PF<sub>6</sub>)<sub>2</sub> [L = Ph<sub>2</sub>Pbpy and Et(Ph)Pbpy **2**] in that the doubly reduced complex does not exhibit such a marked variation of *i*<sub>cat</sub> under CO<sub>2</sub>. This is apparent from the less significant current enhancement consequent to the appearance of the first two-electron reduction peak. Moreover, the ratio of the peak currents *i*<sub>pa</sub>/*i*<sub>pc</sub> of the first redox process remains close to unity for this wave. It is only when the potential scan is extended to the third one-electron reduction peak that a reaction occurs between the complex and CO<sub>2</sub>, as evidenced by a current enhancement beginning at -2.0 V and the absence of the return anodic response. The form of the first redox couple still remains essentially unperturbed, with *i*<sub>pa</sub>/*i*<sub>pc</sub> ~ 1. These observations imply that it is only the triply reduced dicopper complex that catalyses the electrochemical reduction of carbon dioxide.

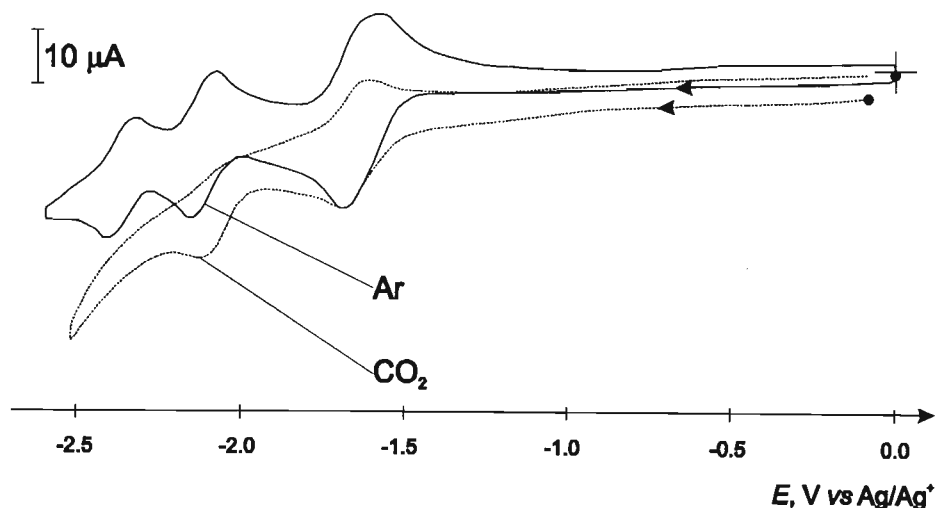


**Figure 3.10.** CVs of [Cu<sub>2</sub>(μ-Ph<sub>2</sub>Ppyqn)<sub>2</sub>(CH<sub>3</sub>CN)<sub>2</sub>](PF<sub>6</sub>)<sub>2</sub> **1** in CO<sub>2</sub> and Ar saturated acetonitrile (0.1 M TBAP) solution. (Pt electrode, *r* = 1.0 mm; *v* = 100 mVs<sup>-1</sup>).

In the presence of trace quantities of water (0.5 %) the CV of **1** in an acetonitrile solution saturated with CO<sub>2</sub> showed a drastic enhancement in current just beyond the first reduction wave, beginning at about -2.0 V (see Figure 3.11). Furthermore no anodic peaks were observed in the return scan, suggesting that the reduced complex had been completely deoxidised to its original form by its interaction with CO<sub>2</sub>. Unfortunately, the subsequent CVs ran during the experiment showed that the complex deteriorates in the presence of water as proven by the appearance of a copper stripping peak.

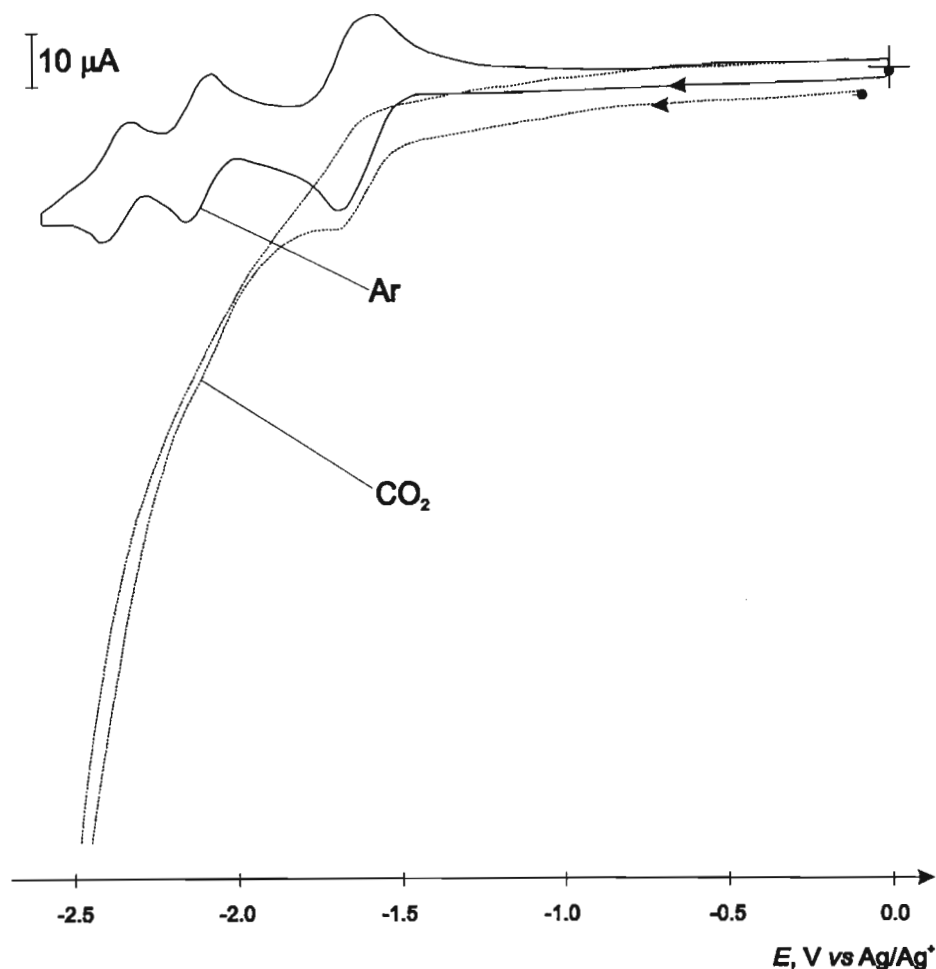


**Figure 3.11.** CVs of  $[\text{Cu}_2(\mu\text{-Ph}_2\text{Ppyqn})_2(\text{CH}_3\text{CN})_2](\text{PF}_6)_2$  **1** in CO<sub>2</sub> and Ar saturated acetonitrile (0.1 M TBAP) solution with water (0.5 %) present. (Pt electrode,  $r = 1.0$  mm;  $\nu = 100$  mVs<sup>-1</sup>).

The electrocatalytic properties of the complexes were further examined by preparative electrolysis in the presence of CO<sub>2</sub>. A summary of representative examples of these experiments is presented in Table 3.4. The experimental conditions used in these electrolysis experiments are those reported by Haines *et al.*<sup>11</sup> a pure anhydrous CH<sub>3</sub>CN + 0.1 M TBAP electrolyte, a 0.3 mM concentration of complex and a Pt gauze electrode, while the applied potentials used were slightly cathodic of the second reduction peak of the respective complexes.

In accordance with the observed instability of the first reduction product under argon, the complexes decompose during the preparative scale electrolysis experiments in the presence of CO<sub>2</sub>. This is proven firstly by a rapid colour change of the electrolyte as soon as a potential is applied to the working electrode. During the course of the electrolysis the solution becomes progressively lighter in colour, leading eventually to an almost clear solution. Concurrently formation of a black deposit is observed on the electrode surface. After the electrolysis each solution was thoroughly purged with Ar and CVs recorded. These confirmed that the starting complex was not present in solution. As has been described, it is likely that the reduction of the Cu(I) complexes leads to the dissociation of Cu(0) from the ligand and its deposition on the electrode surface. Indeed, CVs of the Pt gauze and carbon felt electrodes recorded after electrolysis showed large oxidation peaks at *ca.* -0.60 V characteristic of surface copper. During the catalytic experiments performed with [Cu<sub>2</sub>(μ-Ph<sub>2</sub>Pbpy)<sub>2</sub>(CH<sub>3</sub>CN)<sub>2</sub>](PF<sub>6</sub>)<sub>2</sub> the current shows a steady increase. Given that Cu electrodes have been reported to be heterogeneous catalysts towards the electrochemical reduction of CO<sub>2</sub>,<sup>48</sup> this increase in current is attributable to the reduction of CO<sub>2</sub> catalysed by Cu(0) on the electrode surface. Even under the carefully controlled experimental conditions used here it is evident that the complexes decompose upon reduction in the presence of CO<sub>2</sub>. Their use as practical electrocatalytic systems is therefore not viable.

**Table 3.4.** Summary of preparative scale electrocatalysis experiments carried out on the Cu(I) dinuclear complexes [Cu<sub>2</sub>(μ-L)<sub>2</sub>(CH<sub>3</sub>CN)<sub>2</sub>](PF<sub>6</sub>)<sub>2</sub> [L = Ph<sub>2</sub>Ppyqn **1**, Ph<sub>2</sub>Pbpy and Et(Ph)Pbpy **2**].

Complex	E <sub>app</sub> / V	<i>i</i> / mA (change in <i>i</i> per 10 C)	Coulombs / C	Faradaic Yield	
				CO	HCOO <sup>-</sup>
[Cu <sub>2</sub> (μ-Ph <sub>2</sub> Pbpy) <sub>2</sub> (CH <sub>3</sub> CN) <sub>2</sub> ](PF <sub>6</sub> ) <sub>2</sub> <sup>a</sup>	-1.90	2.4 (+1.8)	66	1	29
[Cu <sub>2</sub> (μ-Ph <sub>2</sub> Pbpy) <sub>2</sub> (CH <sub>3</sub> CN) <sub>2</sub> ](PF <sub>6</sub> ) <sub>2</sub> <sup>b</sup>	-1.96	2.3 (+0.5)	22	1	9
[Cu <sub>2</sub> {μ-Et(Ph)Pbpy} <sub>2</sub> (CH <sub>3</sub> CN) <sub>2</sub> ](PF <sub>6</sub> ) <sub>2</sub> <b>2</b> <sup>b</sup>	-1.95	1.7 (-0.4)	24	4	10
[Cu <sub>2</sub> (μ-Ph <sub>2</sub> Ppyqn) <sub>2</sub> (CH <sub>3</sub> CN) <sub>2</sub> ](PF <sub>6</sub> ) <sub>2</sub> <b>1</b> <sup>b</sup>	-1.85	1.6 (-0.2)	27	12	20

<sup>a</sup> Working electrode Pt gauze. <sup>b</sup> Working electrode carbon felt.

### 3.2.5. Extended Hückel Molecular Orbital Calculations

The redox properties of transition metal complexes can be adequately described in terms of localised molecular orbital (MO) configurations.<sup>118</sup> In the localised MO approximation the molecular orbitals of the transition metal complex are labelled as either metal or ligand



according to their predominant localisation. Thus, oxidation and reduction processes are viewed as either metal or ligand centred, depending on the relative contributions of the metal or ligand to the HOMO and LUMO respectively. To gain some understanding of the nature of their redox processes EHMO calculations were performed on the phosphorus-polypyridyl ligand-bridged dicopper(I) complexes to establish the energies and localisations of their frontier molecular orbitals.<sup>†</sup> The results of these are summarised in Table 3.5, while the MO coefficients of the copper and coordinating  $\alpha$ -diimine nitrogen and phosphorus atoms of  $[\text{Cu}_2(\mu\text{-Ph}_2\text{Pbpy})_2(\text{CH}_3\text{CN})_2](\text{PF}_6)_2$ , **1** and **2** are given in the supporting information.

**Table 3.5.** Calculated energies of the frontier MOs and the relative percent atomic contribution<sup>a</sup> of the metal, phosphine and  $\alpha$ -diimine atoms to them, of  $[\text{Cu}_2(\mu\text{-L})_2(\text{CH}_3\text{CN})_2](\text{PF}_6)_2$  [L = Ph<sub>2</sub>Ppyqn **1**, Ph<sub>2</sub>Pbpy and Et(Ph)Pbpy **2**].

Complex	Molecular Orbital	Eigenvalue /eV	Percent Relative Atomic Contribution		
			Cu	$\alpha$ -diimine	phosphine
$[\text{Cu}_2(\mu\text{-Ph}_2\text{Pbpy})_2(\text{CH}_3\text{CN})_2]^{2+}$	HOMO	-11.62	28	61	6
	LUMO	-9.78	2	90	8
	SLUMO	-9.62	3	90	7
<b>1</b>	HOMO	-11.3	35	54	5
	LUMO	-9.96	1	97	1
	SLUMO	-9.89	1	97	1
<b>2</b>	HOMO	-11.23	37	52	6
	LUMO	-9.65	1	95	4
	SLUMO	-9.57	2	94	4

<sup>a</sup>Atomic contributions do not add up to 100 % since atomic contributions to the MOs of less than 1 % are neglected.

The relative ordering of the energies of the HOMOs and LUMOs agrees qualitatively with the sequence of  $E_{1/2}^{+2/+}$  values of the complexes determined by cyclic voltammetry (Table 3.2). The relative percent atomic contributions show the HOMO to contain significant contributions from both the metal and  $\alpha$ -diimine fragments, while the lower unoccupied MOs are almost exclusively  $\alpha$ -diimine in nature. This supports the assignments of the reductions as ligand-based electron transfers.

<sup>†</sup> The limitations of the EHMO method, elaborated upon in Appendix A, Section A.5, mean that caution needs to be exercised in using the results of the calculations.

In comparing the electrochemical reduction potentials of the free ligands (Table 2.7) with those of their corresponding dicopper complexes, it is evident that the ligand based reductions of the complexes (Table 3.2) occur at a less negative potential. The  $\pi$ -acceptor orbitals are therefore stabilised upon coordination to the metal. A comparison of the eigenvalues of the LUMOs of the free ligands, given in Table 2.7, with those of the complexes shows that the latter are indeed lower in energy. This may be ascribed to the loss of negative charge from the ligand upon coordination, which occurs by  $\sigma$ -donation through the chelating nitrogen atoms.<sup>93</sup>

The forms of the frontier MOs are pictorially presented in Figures 3.12 and 3.13, using  $[\text{Cu}_2(\mu\text{-Ph}_2\text{Pbpy})_2(\text{CH}_3\text{CN})_2](\text{PF}_6)_2$  and **1** as illustrative examples. The HOMO and lower unoccupied MOs are of  $\sigma$ - and  $\pi$ -symmetry respectively. In contrast to the spatial distribution of the LUMO in  $[\text{Cu}_2(\mu\text{-Ph}_2\text{Pbpy})_2(\text{CH}_3\text{CN})_2](\text{PF}_6)_2$  and **2**, which extends over both P,N,N ligands, that in **1** is to a large extent localised on one of the P,N,N ligands. Moreover the SLUMO of **1** is likewise concentrated on the second P,N,N ligand. In  $[\text{Cu}_2(\mu\text{-Ph}_2\text{Pbpy})_2(\text{CH}_3\text{CN})_2](\text{PF}_6)_2$  and **2** the electron of the first one-electron reduction would thus be delocalised over both ligands and its presence would be expected to perturb the addition of the second electron. The first reduction in **1**, however, is almost spatially isolated on one of the ligands and would have no significant effect on the addition of a second electron to the second, essentially non-interacting, redox centre. (This assumes that the relative magnitude of the orbital splitting and spin pairing energy is such that the second electron is placed in the SLUMO.) These conclusions are borne out by the CVs measured for the complexes; thus  $[\text{Cu}_2(\mu\text{-Ph}_2\text{Pbpy})_2(\text{CH}_3\text{CN})_2](\text{PF}_6)_2$  and **2** exhibit two distinctive first and second reduction waves while in **1** these cathodic waves overlap one another.

Two limiting cases can be used to describe the redox orbitals of transition metal complexes containing multiple  $\alpha$ -diimine ligands; (i) single-ring delocalisation, where the electrons are localised on individual chelate rings, or (ii) multi-ring delocalisation, in which they are delocalised over all the ligands in the reduced complex. The distribution of the lower unoccupied MOs described above and the reductive pattern displayed by the complexes suggest that the redox orbitals of **1** tend towards the former limiting case, while those of  $[\text{Cu}_2(\mu\text{-Ph}_2\text{Pbpy})_2(\text{CH}_3\text{CN})_2](\text{PF}_6)_2$  and **2** fit more the multi-ring delocalisation description.

The one electron nature of the first oxidation is counter-intuitive to what one would expect from a dinuclear complex containing two non-bonded metal centres. It suggests the removal of an electron from a HOMO significantly delocalised over the entire molecule, rather than from one isolated on each metal centre. The forms of the calculated HOMOs are indeed in accordance with this model.

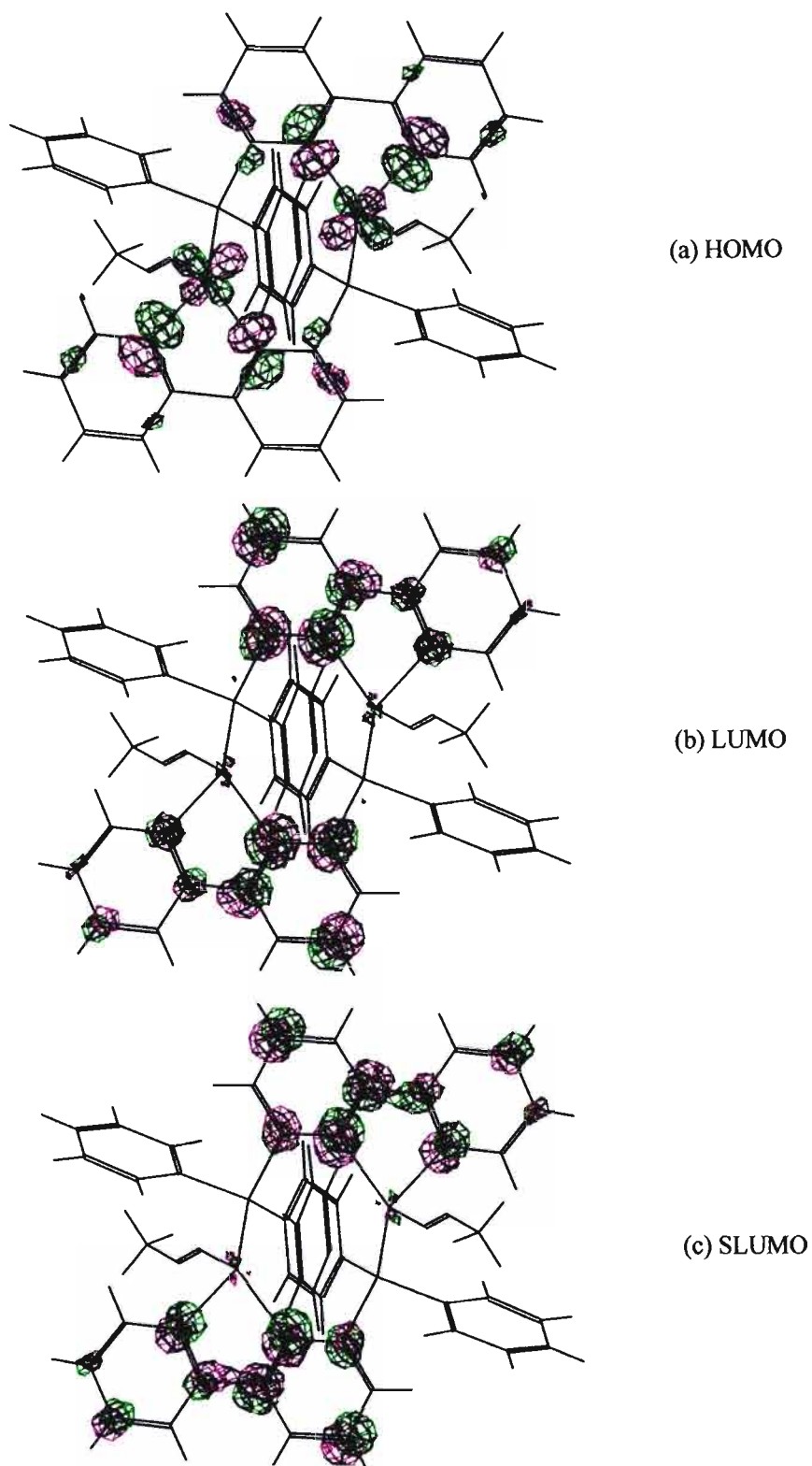


**Figure 3.12.** Molecular orbital representation for the (a) HOMO, (b) LUMO and (c) SLUMO of [Cu<sub>2</sub>(μ-Ph<sub>2</sub>Pbpy)<sub>2</sub>(CH<sub>3</sub>CN)<sub>2</sub>](PF<sub>6</sub>)<sub>2</sub>.

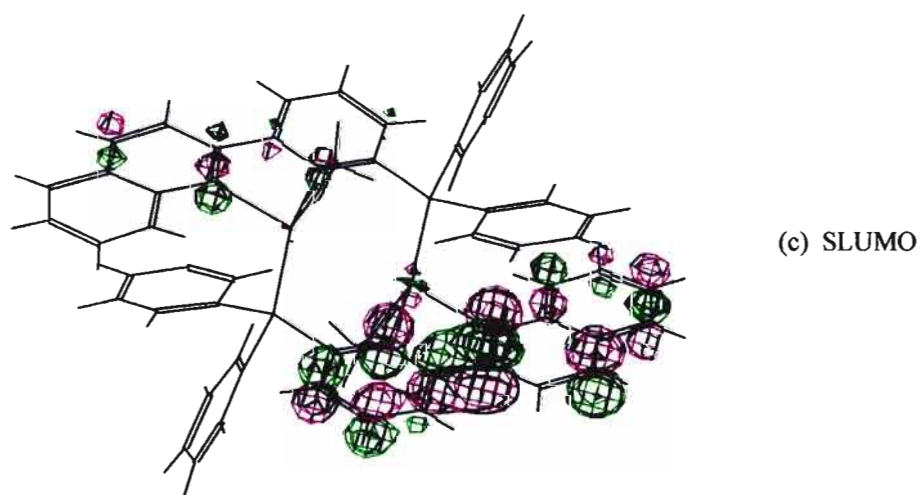
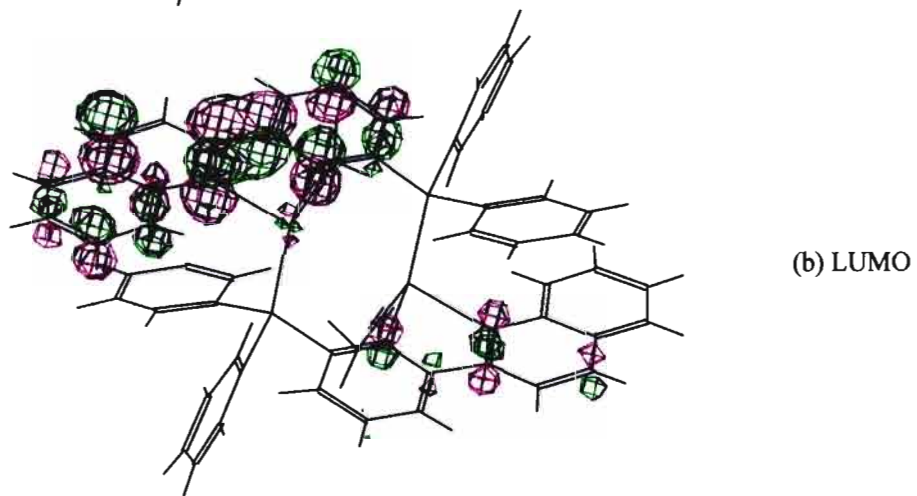
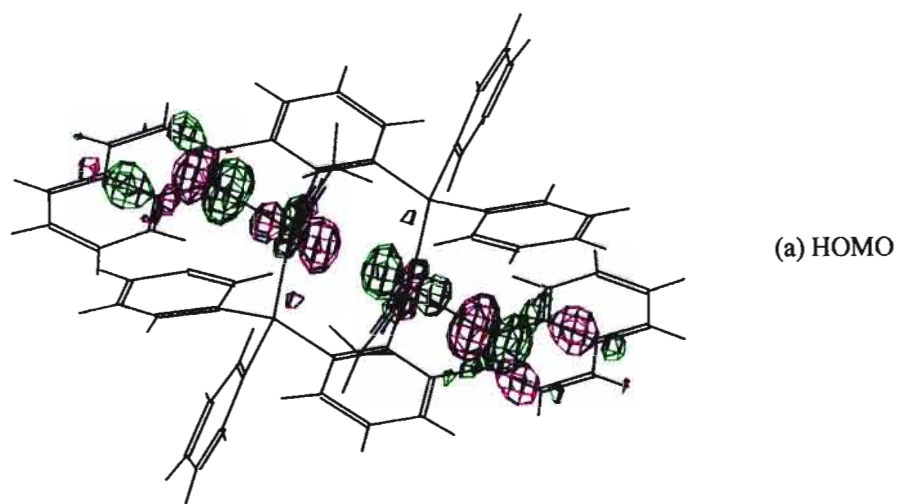


**Figure 3.13.** Molecular orbital representation for the (a) HOMO, (b) LUMO and (c) SLUMO of  $[\text{Cu}_2(\mu\text{-Ph}_2\text{Ppyqn})_2(\text{CH}_3\text{CN})_2](\text{PF}_6)_2$  **1**.

### 3.3. Experimental

**[Cu<sub>2</sub>(μ-Ph<sub>2</sub>Ppyqn)<sub>2</sub>(CH<sub>3</sub>CN)<sub>2</sub>](BF<sub>4</sub>)<sub>2</sub> 1.** A solution of [Cu(CH<sub>3</sub>CN)<sub>4</sub>](BF<sub>4</sub>)<sup>119</sup> (0.21 g, 0.67 mmol) and Ph<sub>2</sub>Ppyqn (0.26 g, 0.67 mmol) in CH<sub>3</sub>CN (15 cm<sup>3</sup>) was maintained at room temperature for 24 h. Subsequently the solution was filtered through glass microfibre and reduced in volume to *ca.* 8 cm<sup>3</sup> *in vacuo*. The crude product was precipitated by the addition of excess Et<sub>2</sub>O. This was recrystallised by the slow diffusion of Et<sub>2</sub>O into a CH<sub>3</sub>CN solution of the crude material, to afford the dicopper complex as orange crystals (0.48 g, 62 %). (Found: C, 57.67; H, 3.72; N, 7.13. Cu<sub>2</sub>C<sub>56</sub>H<sub>44</sub>N<sub>6</sub>P<sub>2</sub>B<sub>2</sub>F<sub>8</sub> requires C, 57.80; H, 3.81; N, 7.22 %); λ<sub>max</sub>/nm (CH<sub>3</sub>CN) 262 (ε/dm<sup>3</sup> mol<sup>-1</sup> cm<sup>-1</sup> 71 100), 306 (sh) (31 000), 334 (sh) (26 400) and 400 (sh) (4720); ν<sub>max</sub>/cm<sup>-1</sup> (KBr) 1510w, 1438s, 1085 vs (BF<sub>4</sub>), 806s, 784w, 762w (sh), 740w, 698w, 558s and 526w; δ<sub>H</sub> (200 MHz, CD<sub>2</sub>Cl<sub>2</sub>, CDHCl<sub>2</sub>) 8.90 to 6.70 (36H, br m), 6.15 (2H, m), 1.97 (6H, s, CH<sub>3</sub>CN); δ<sub>P</sub> (32.2 MHz, CD<sub>2</sub>Cl<sub>2</sub>, 85% H<sub>3</sub>PO<sub>4</sub>) 9.0 (br s).

**[Cu<sub>2</sub>{μ-Et(Ph)Pbpy}<sub>2</sub>(CH<sub>3</sub>CN)<sub>2</sub>](PF<sub>6</sub>)<sub>2</sub> 2.** This complex was prepared using the same procedure as for [Cu<sub>2</sub>(μ-Ph<sub>2</sub>Ppyqn)<sub>2</sub>(CH<sub>3</sub>CN)<sub>2</sub>](BF<sub>4</sub>)<sub>2</sub>. Thus reaction of [Cu(CH<sub>3</sub>CN)<sub>4</sub>](PF<sub>6</sub>)<sup>120</sup> (0.63 g, 1.7 mmol) with Et(Ph)Pbpy (0.49 g, 1.7 mmol) in CH<sub>3</sub>CN (20 cm<sup>3</sup>) yielded the complex as orange crystals (1.37 g, 75 %). (Found: C, 44.45; H, 3.51; N, 7.58. Cu<sub>2</sub>C<sub>40</sub>H<sub>40</sub>N<sub>6</sub>P<sub>4</sub>F<sub>12</sub> requires C, 44.33; H, 3.72; N, 7.75 %); λ<sub>max</sub>/nm (CH<sub>3</sub>CN) 246 (ε/dm<sup>3</sup> mol<sup>-1</sup> cm<sup>-1</sup> 35 200), 292 (29 700) and 463 (sh) (900); ν<sub>max</sub>/cm<sup>-1</sup> (KBr) 1600w, 1587w (sh), 1557w, 1483w, 1440s, 1419w (sh), 838vs (PF<sub>6</sub>), 774s, 747s (sh), 696w, 616w and 558s; δ<sub>H</sub> (200 MHz, CD<sub>2</sub>Cl<sub>2</sub>, CHDCl<sub>2</sub>) 8.48 (6H, m), 8.32 (2H, m), 8.15 (2H, t), 7.77 (2H, m), 7.65 (2H, m), 7.33 (8H, m), 6.98 (2H, m), 2.30 (4H, m, PCH<sub>2</sub>CH<sub>3</sub>), 1.96 (6H, s, CH<sub>3</sub>CN), 0.96 (6H, m, PCH<sub>2</sub>CH<sub>3</sub>); δ<sub>P</sub> (32.2 MHz, CD<sub>2</sub>Cl<sub>2</sub>, 85% H<sub>3</sub>PO<sub>4</sub>) 10.0 (br s).

**X-ray Data Collection and Structure Solution for 1 and 2.** Orange crystals of **1** (eight-side polyhedron shaped) and **2** (diamond shaped) were grown by the slow vapour diffusion of diethyl ether into an acetonitrile solution of the complex. Details of the crystal data, data collection and structure refinement of **1** and **2** are summarized in Table 3.6, while their complete crystallographic data is presented in Appendix B. Supporting Information.

**Table 3.6.** Crystal data and structure refinement parameters for  $[\text{Cu}_2(\mu\text{-Ph}_2\text{Ppyqn})_2(\text{CH}_3\text{CN})_2](\text{PF}_6)_2$  **1** and  $[\text{Cu}_2\{\mu\text{-Et(Ph)Pbpy}\}_2(\text{CH}_3\text{CN})_2](\text{PF}_6)_2$  **2**.

	<b>1</b>	<b>2</b>
Formula	$\text{Cu}_2\text{C}_{56}\text{H}_{44}\text{N}_6\text{P}_2\text{B}_2\text{F}_8$	$\text{Cu}_2\text{C}_{40}\text{N}_6\text{H}_{40}\text{F}_{12}\text{P}_4$
FW/amu	1163.61	1083.74
$a/\text{\AA}$	28.49(2)	11.267(4)
$b/\text{\AA}$	26.82(2)	39.95(2)
$c/\text{\AA}$	14.911(5)	40.371(2)
$\alpha/^\circ$	90	90
$\beta/^\circ$	90	90
$\gamma/^\circ$	90	90
$U/\text{\AA}^3$	11394(8)	1817(1)
Crystal system, space group	Orthorhombic, <i>Fdd2</i>	Orthorhombic, <i>Fddd</i>
Z	8	16
$D_c/\text{g cm}^3$	1.357	1.584
F(000)	4736	8768
$\mu/\text{mm}^{-1}$	0.870	1.164
Power and current settings	55 kV, 25 mA	55 kV, 25 mA
Increment/ $^\circ$	0.35	0.63
Crystal dimensions/mm	0.35 x 0.32 x 0.29	0.73 x 0.46 x 0.38
$\lambda(\text{Mo K}\alpha)/\text{\AA}$	0.71069	0.71069
Temperature/K	293(2)	293(2)
$\theta$ range for collected data/ $^\circ$	2.09 to 22.97	2.02 to 22.97
Index ranges	$-31 \leq h \leq 16$ $-1 \leq k \leq 29$ $-16 \leq l \leq 14$	$-1 \leq h \leq 12$ $-1 \leq k \leq 43$ $-1 \leq l \leq 44$
Total reflections collected	4614	3803
Absorption correction	Semi-empirical	semi-empirical
Relative transmission coefficients (I)	0.9997 and 0.8985	0.9997 and 0.9445
Unique data	3575 ( $R_{\text{int}} = 0.0582$ )	3166 ( $R_{\text{int}} = 0.0258$ )
Unique observed data [ $I > 2\sigma(I)$ ]	2616	2182
Refinement method		Full-matrix least-squares on $F^2$
Data / restraints / parameters	3575 / 7 / 345	3166 / 0 / 372
Goodness-of-fit (based on $F^2$ )	1.465	1.1173
Extinction coefficient	0.021(1)	none
$\text{Max}(\Delta\rho)/\text{e.\AA}^{-3}$	1.330	0.586
$\text{Min}(\Delta\rho)/\text{e.\AA}^{-3}$	-0.897	-0.592
Final R indices [ $I > 2\sigma(I)$ ]	$R_1 = 0.1145$ , $wR_2 = 0.2613$	$R_1 = 0.0490$ , $wR_2 = 0.1145$
R indices (all data)	$R_1 = 0.1705$ , $wR_2 = 0.3506$	$R_1 = 0.0913$ , $wR_2 = 0.1495$

## Chapter 4. Homoleptic Dinuclear Complexes of Palladium(I) and Platinum(I) Bridged by 6-diphenylphosphino-2,2'-bipyridine, 6-(diphenylphosphino)-2-(2-quinolyl)pyridine and 6-[ethyl(phenyl)phosphino]-2,2'-bipyridine

---

### 4.1. Introduction

A number of complexes of palladium(I) and platinum(I) in which the metal atoms are linked by a metal-metal bond as well as being bridged by a bidentate ligand are known.<sup>121,122,123</sup> Their method of preparation involved a comproportionation reaction between the appropriate M(II) and M(0) complexes. A.L. Balch *et al.* adopted such an approach in the stepwise construction of both homodinuclear and heterodinuclear Pd(I) and Pt(I) complexes bridged by 2-(diphenylphosphino)pyridine (Ph<sub>2</sub>Ppy).<sup>124,125</sup> Thus [Pd(Ph<sub>2</sub>Ppy)<sub>2</sub>Cl<sub>2</sub>] was reacted with Pd<sub>2</sub>(dba)<sub>3</sub>.CHCl<sub>3</sub> to afford [Pd<sub>2</sub>(μ-Ph<sub>2</sub>Ppy)<sub>2</sub>Cl<sub>2</sub>] and with Pt(dba)<sub>2</sub> to form a mixture of [Pd<sub>2</sub>(μ-Ph<sub>2</sub>Ppy)<sub>2</sub>Cl<sub>2</sub>] and [PtPd(μ-Ph<sub>2</sub>Ppy)<sub>2</sub>Cl<sub>2</sub>]. Likewise [Pt(Ph<sub>2</sub>Ppy)<sub>2</sub>Cl<sub>2</sub>] was reacted with Pd<sub>2</sub>(dba)<sub>3</sub>.CHCl<sub>3</sub> to produce [PtPd(μ-Ph<sub>2</sub>Ppy)<sub>2</sub>Cl<sub>2</sub>] and with Pt(dba)<sub>2</sub> to give [Pt<sub>2</sub>(μ-Ph<sub>2</sub>Ppy)<sub>2</sub>Cl<sub>2</sub>] respectively; in both cases the bridging ligands adopt a head-to-tail configuration. J. Fujita *et al.* have used a similar approach to prepare an analogous series of complexes with 2-(dimethylphosphino)pyridine (Me<sub>2</sub>Ppy) as the bridging ligand.<sup>126,127</sup> The first step in the above approach to the preparation of dinuclear ligand-bridged complexes was to synthesise the mononuclear derivative [M(Ph<sub>2</sub>Ppy)<sub>2</sub>Cl<sub>2</sub>] (M = Pd, Pt) where Ph<sub>2</sub>Ppy is bonded to the metal through the phosphorus atom. The pyridine nitrogen is then available for coordination to a second metal atom that is in the zero oxidation state. The short bite and rigidity of Ph<sub>2</sub>Ppy ensures the oxidative addition of the M-Cl bond to this second metal centre and a dinuclear complex is formed in what is best described as a comproportionation reaction.<sup>128</sup>

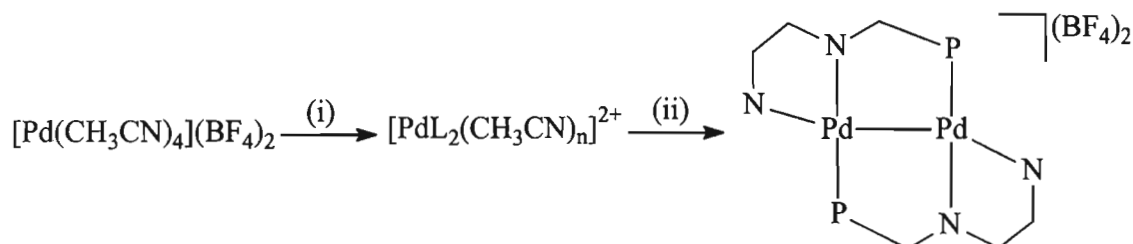
The same approach was considered for the synthesis of dinuclear complexes bridged by the phosphorus bipyridyl ligands Ph<sub>2</sub>Pbpy, Ph<sub>2</sub>Ppyqn and Et(Ph)Pbpy. Indeed, it has already been shown that the reaction of [M(PhCN)<sub>2</sub>Cl<sub>2</sub>] (M = Pt, Pd) with Ph<sub>2</sub>Pbpy in dichloromethane affords the mononuclear complexes [M(Ph<sub>2</sub>Pbpy)<sub>2</sub>Cl<sub>2</sub>] (M = Pt, Pd) in which each Ph<sub>2</sub>Pbpy ligand bonds pendently through the phosphorus atom to the metal atom.<sup>129</sup> The latter are expected to react with platinum and palladium zero-valent metal precursors to form the appropriate dinuclear ligand-bridged complexes via a comproportionation reaction. As described in the next section this proved to be the case.

## 4.2. Results and Discussion

### 4.2.1. Synthesis and Characterisation of the Dinuclear Complexes

#### 4.2.1.(i) $[\text{Pd}_2(\mu\text{-L})_2](\text{BF}_4)_2$ [L = Ph<sub>2</sub>Pbpy 3, Ph<sub>2</sub>Ppyqn 4 and Et(Ph)Pbpy 5]

The procedure adopted for the preparation of the dipalladium complexes  $[\text{Pd}_2(\mu\text{-L})_2](\text{BF}_4)_2$  [L = Ph<sub>2</sub>Pbpy 3, Ph<sub>2</sub>Ppyqn 4 and Et(Ph)Pbpy 5] is outlined in Scheme 4.1.



**Scheme 4.1.** Synthesis of the dipalladium complexes  $[\text{Pd}_2(\mu\text{-L})_2](\text{BF}_4)_2$  [L = Ph<sub>2</sub>Pbpy 3, Ph<sub>2</sub>Ppyqn 4 and Et(Ph)Pbpy 5]. (i) 2 eq. L,  $\text{CH}_3\text{CN}$ ; (ii) 0.5 eq.  $\text{Pd}_2(\text{dba})_3$ .

The palladium(II) precursor selected for the initial reaction with the phosphorus-polypyridyl ligands was the tetrakisacetonitrile Pd(II) complex,  $[\text{Pd}(\text{CH}_3\text{CN})_4](\text{BF}_4)_2$ , as the tridentate P,N,N ligands require an additional coordination site over Ph<sub>2</sub>Ppy. Reaction of the tetrakisacetonitrile Pd(II) cation with Ph<sub>2</sub>Pbpy and Et(Ph)Pbpy led to product mixtures that exhibited four singlets in their  $^{31}\text{P}\text{-}\{^1\text{H}\}$  NMR spectrum recorded in acetonitrile; at 26, 22, 21 and 0, and 32, 27, 17 and 0 ppm respectively. The Ph<sub>2</sub>Ppyqn ligand, on the other hand, afforded a product mixture for which only two phosphorus resonances at 20 and 19 ppm were observed. Assignments of these resonances were made as follows.

The reaction of  $[\text{Pd}(\text{PhCN})_2\text{Cl}_2]$  with Ph<sub>2</sub>Pbpy,<sup>129</sup> Ph<sub>2</sub>Ppy<sup>124</sup> and Me<sub>2</sub>Ppy<sup>126</sup> has been investigated previously and shown to afford a mixture of the P-ligated *cis* and *trans* isomers of  $[\text{Pd}(\eta^1\text{-L})_2\text{Cl}_2]$  (L = Ph<sub>2</sub>Pbpy, Ph<sub>2</sub>Ppy and Me<sub>2</sub>Ppy). The  $^{31}\text{P}\text{-}\{^1\text{H}\}$  NMR spectra of these products were found to exhibit two singlets, as expected, with  $[\text{Pd}(\text{Ph}_2\text{Pbpy})_2\text{Cl}_2]$  for example exhibiting peaks at 29.05 and 23.14 ppm, while the spectrum of  $[\text{Pd}(\text{Ph}_2\text{Ppy})_2\text{Cl}_2]$  measured in  $\text{CD}_2\text{Cl}_2$  displays peaks at 29.29 and 23.79 ppm. On the other hand, when the Ph<sub>2</sub>Ppy and Me<sub>2</sub>Ppy ligands are reacted with  $[\text{Pd}(\text{PhCN})_2\text{Cl}_2]$  in the presence of a halide abstractor the complexes *cis*- $[\text{Pd}(\eta^1\text{-Ph}_2\text{Ppy})(\eta^2\text{-Ph}_2\text{Ppy})\text{Cl}]\text{PF}_6$ <sup>130</sup> and *cis*- $[\text{Pd}(\eta^1\text{-Me}_2\text{Ppy})(\eta^2\text{-Me}_2\text{Ppy})\text{Cl}]\text{ClO}_4$ <sup>126</sup> are formed in which the ligands form four-membered ring chelates with palladium. The  $^{31}\text{P}\text{-}\{^1\text{H}\}$  NMR spectrum of the former complex exhibits peaks at 42.7 and -42.3 ppm, while the latter similarly has two broad peaks at 18.3 and -52.9 ppm. As can be deduced from these spectra, the  $^{31}\text{P}$



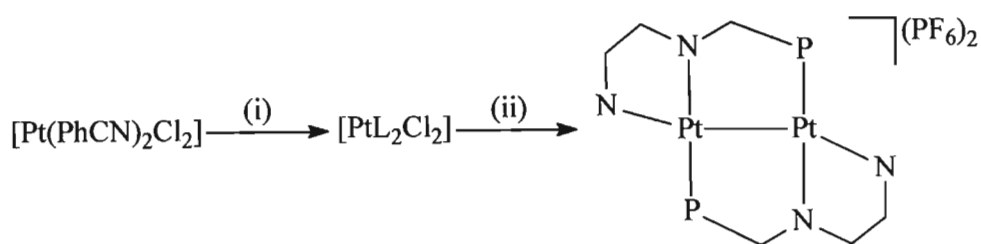
resonance of phosphine ligands that form a chelate ring shifts to a higher field upon chelate coordination.<sup>131</sup>

On the basis of the above <sup>31</sup>P NMR spectral data tentative assignments can be made to the peaks observed in the <sup>31</sup>P-<sup>1</sup>H NMR spectra recorded of the reaction product mixtures obtained in this work. The <sup>31</sup>P resonances at 26 and 22 ppm (for Ph<sub>2</sub>Pbpy), 32 and 17 ppm [for Et(Ph)Pbpy] and 20 and 19 ppm (for Ph<sub>2</sub>Ppyqn) are best assigned to the mononuclear, P-ligated *cis* and *trans* isomers. The resonances at 0 ppm, displayed in the <sup>31</sup>P-<sup>1</sup>H NMR spectra of the reaction mixtures obtained with the Ph<sub>2</sub>Pbpy and Et(Ph)Pbpy ligands are consistent with their coordination in a chelating mode. The lower field resonances at 21 and 17 ppm are probably due to the pendant coordinated Ph<sub>2</sub>Pbpy and Et(Ph)Pbpy ligands in complexes of the type [Pd(η<sup>1</sup>-L)(η<sup>2</sup>-L)(CH<sub>3</sub>CN)]<sup>2+</sup> [L = Ph<sub>2</sub>Pbpy and Et(Ph)Pbpy]. The extra steric demands of the quinoline fragment possibly preclude a chelating mode in the case of the Ph<sub>2</sub>Ppyqn ligand.

Addition of the zero valent palladium complex, Pd<sub>2</sub>(dba)<sub>3</sub>.CHCl<sub>3</sub>,<sup>132</sup> to the reaction mixture affords, after a period of 12 h, a species which exhibits only one singlet at *ca.* 4 ppm in its <sup>31</sup>P NMR spectra recorded in acetonitrile. This is similar in shift to the phosphorus resonance of [Pd<sub>2</sub>(μ-Ph<sub>2</sub>Ppy)<sub>2</sub>Cl<sub>2</sub>] observed at 4.47 ppm in dichloromethane. The reaction mixture was filtered through glass microfibre filter paper and the orange crystalline product precipitated from the solution by the addition of excess diethyl ether. Characteristic aromatic stretches of the ligands, and a very strong broad signal at 1062 cm<sup>-1</sup> due to BF<sub>4</sub><sup>-</sup>, are observed in the IR absorption spectrum recorded in the solid state as a KBr pellet. The <sup>1</sup>H NMR spectrum displays resonances in the aromatic region of the spectrum arising from the phosphorus-polypyridyl ligands. The microanalytical results correspond to the formalism of the products as the homoleptic, dinuclear complexes [Pd<sub>2</sub>(μ-L)<sub>2</sub>](BF<sub>4</sub>)<sub>2</sub> [L = Ph<sub>2</sub>Pbpy **3**, Ph<sub>2</sub>Ppyqn **4** and Et(Ph)Pbpy **5**].

#### 4.2.1.(ii) [Pt<sub>2</sub>(μ-L)<sub>2</sub>](PF<sub>6</sub>)<sub>2</sub> [L = Ph<sub>2</sub>Pbpy **6**, Ph<sub>2</sub>Ppyqn **7** and Et(Ph)Pbpy **8**]

The procedure used for the preparation of the dinuclear complexes [Pt<sub>2</sub>(μ-L)<sub>2</sub>](PF<sub>6</sub>)<sub>2</sub> [L = Ph<sub>2</sub>Pbpy **6**, Ph<sub>2</sub>Ppyqn **7** and Et(Ph)Pbpy **8**] is summarized in Scheme 4.2. Treatment of [Pt(PhCN)<sub>2</sub>Cl<sub>2</sub>] with the respective ligand affords a reaction mixture believed to contain the P-ligated mononuclear substitution product [Pt(η<sup>1</sup>-L)<sub>2</sub>Cl<sub>2</sub>]. Subsequent addition of Pt<sub>2</sub>(dba)<sub>3</sub><sup>133</sup> and two molar equivalents of TlPF<sub>6</sub> led to, via a conproportionation reaction, a mixture of the desired product, TlCl and presumably unreacted Pt<sub>2</sub>(dba)<sub>3</sub>. The pure product was separated from the latter by repeated fractional crystallization from an acetonitrile-diethyl ether solution.



**Scheme 4.2.** Synthesis of the dinuclear complexes  $[\text{Pt}_2(\mu\text{-L})_2](\text{PF}_6)_2$  [ $\text{L} = \text{Ph}_2\text{Pbpy}$  **6**,  $\text{Ph}_2\text{Ppyqn}$  **7** and  $\text{Et}(\text{Ph})\text{Pbpy}$  **8**]. (i) 2 eq. L,  $\text{CH}_3\text{CN}$ ; (ii) 0.5 eq.  $\text{Pt}_2(\text{dba})_3$ , 2 eq.  $\text{TlPF}_6$ .

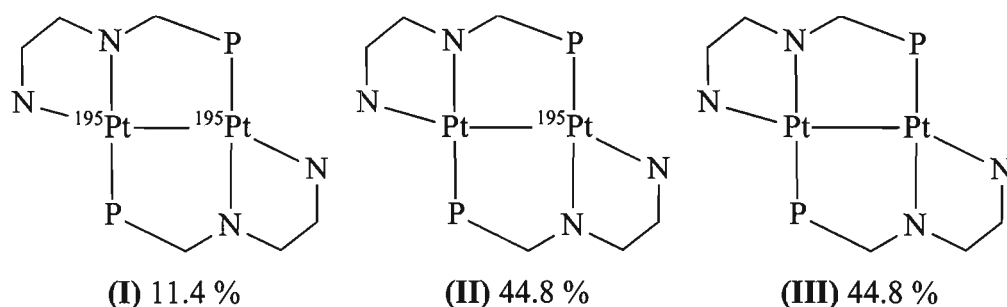
The  $^{31}\text{P}\{-^1\text{H}\}$  NMR data for complexes **6** – **8** are summarised in Table 4.1. Their interpretation enables conclusions to be drawn as to the structures of the complexes in solution, as will now be discussed.

**Table 4.1.**  $^{31}\text{P}\{-^1\text{H}\}$ <sup>a</sup> NMR spectral data for the complexes  $[\text{Pt}_2(\mu\text{-L})_2](\text{PF}_6)_2$  [ $\text{L} = \text{Ph}_2\text{Pbpy}$  **6**,  $\text{Ph}_2\text{Ppyqn}$  **7** and  $\text{Et}(\text{Ph})\text{Pbpy}$  **8**] and  $[\text{PtPd}(\mu\text{-L})_2](\text{PF}_6)_2$  [ $\text{L} = \text{Ph}_2\text{Pbpy}$  **9**,  $\text{Ph}_2\text{Ppyqn}$  **10** and  $\text{Et}(\text{Ph})\text{Pbpy}$  **11**].

Complex	$\delta$		J/Hz		
	P–Pt	P–Pd	$^1\text{J}(\text{PtP})$	$^2\text{J}(\text{PtP})$	$^3\text{J}(\text{PP})$
$[\text{Pt}_2(\mu\text{-Ph}_2\text{Pbpy})_2](\text{PF}_6)_2$ <b>6</b>	3.3		3981	206	21.0
$[\text{Pt}_2(\mu\text{-Ph}_2\text{Ppyqn})_2](\text{PF}_6)_2$ <b>7</b>	3.0		3961	219	21.9
$[\text{Pt}_2\{\mu\text{-Et}(\text{Ph})\text{Pbpy}\}_2](\text{PF}_6)_2$ <b>8</b>	4.8		4027	184	20.5
$[\text{PtPd}(\mu\text{-Ph}_2\text{Pbpy})_2](\text{PF}_6)_2$ <b>9</b>	–5.6	9.13	3962	158	19.1
$[\text{PtPd}\{\mu\text{-Ph}_2\text{Ppyqn}\}_2](\text{PF}_6)_2$ <b>10</b>	–7.5	7.67	3960	182	18.3
$[\text{PtPd}\{\mu\text{-Et}(\text{Ph})\text{Pbpy}\}_2](\text{PF}_6)_2$ <b>11</b>	–4.9	6.81	3959	126	18.7
	–5.5	5.67	4000	133	19.7

<sup>a</sup>  $^{31}\text{P}\{-^1\text{H}\}$  spectra (202 MHz) were measured in  $\text{CD}_3\text{CN}$  against  $(\text{CH}_3\text{O})_3\text{P}$  ( $\delta_{\text{P}} = 141.0$  ppm) as a secondary reference and are quoted relative to 85% phosphoric acid.

The only isotope of platinum with a non-zero nuclear spin is  $^{195}\text{Pt}$ , which has a spin quantum number of a half and comprises 33.8% of the naturally occurring element. The other isotopes can be grouped together as having no magnetic moment and therefore exhibiting no spin-spin coupling. The  $^{31}\text{P}\{-^1\text{H}\}$  spectral pattern can be interpreted as a composite of the individual spectrums of the three natural isotopomers that would thus arise, these are illustrated below. The  $^{31}\text{P}\{-^1\text{H}\}$  NMR spectrum of **6** (Figure 4.1) is discussed as a representative example.



Isotopomer **(III)**, containing no  $^{195}\text{Pt}$ , gives rise to the large central singlet as heteronuclear spin-spin coupling is absent. The two doublets of doublets arise from isotopomer **(II)**, in which one platinum centre is spin-active. The outermost doublet of doublets is due to the phosphorus bonded directly to the  $^{195}\text{Pt}$  and shows a  $^1\text{J}(\text{PtP})$  of 3981 Hz consistent with one-bond platinum-phosphorus coupling. The innermost doublet of doublets is due to the phosphorus bonded to the spin inactive platinum and shows a smaller  $^2\text{J}(\text{PtP})$  of 206 Hz. The phosphorus nuclei in this isotopomer are magnetically inequivalent and a three-bond spin-spin interaction further splits each doublet by a  $^3\text{J}(\text{PP})$  of 21 Hz.

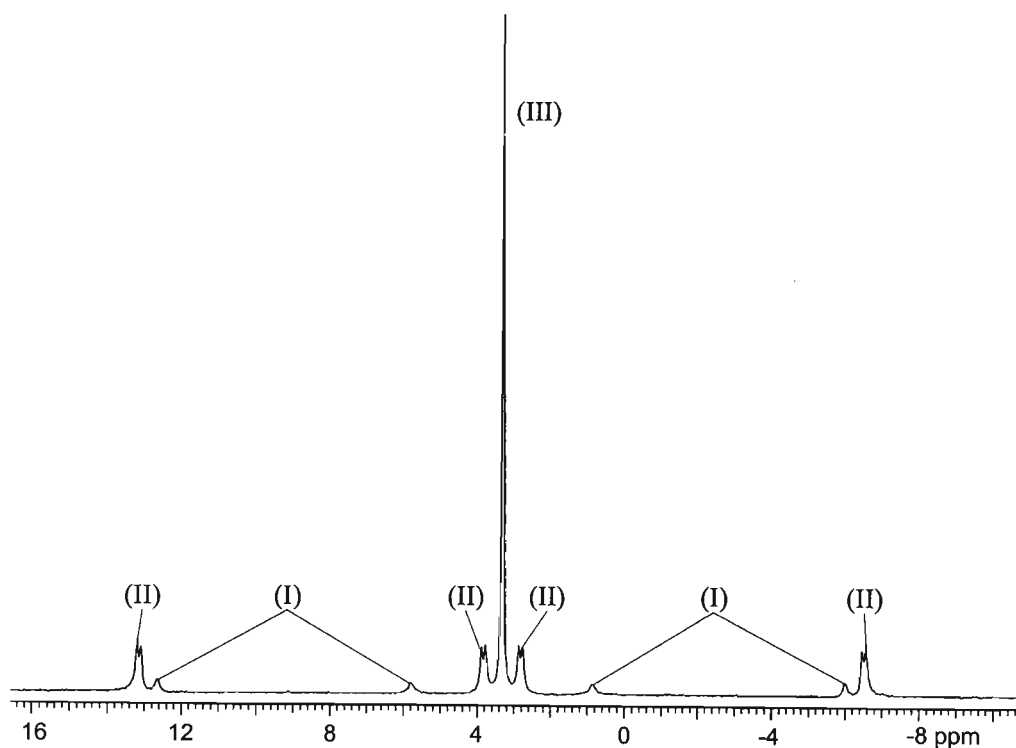


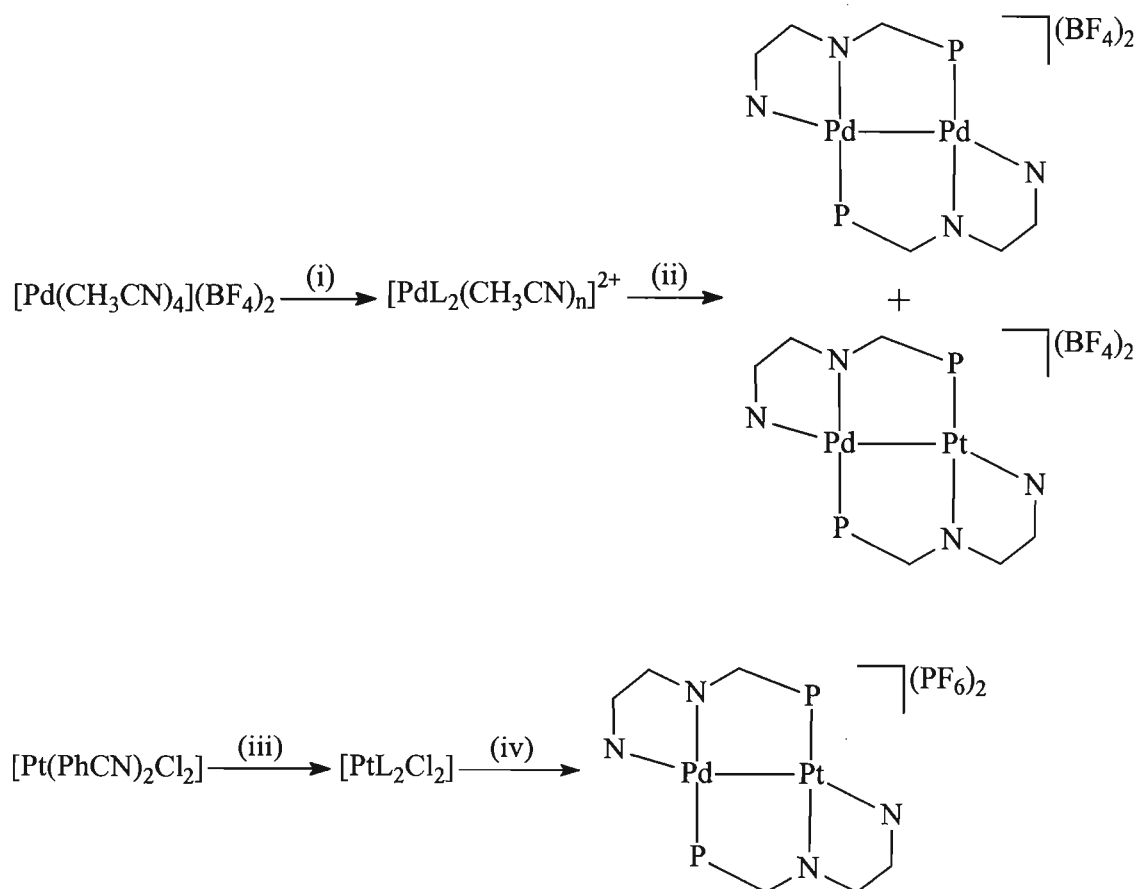
**Figure 4.1.** The  $^{31}\text{P}\{-^1\text{H}\}$  NMR spectrum of  $[\text{Pt}_2(\mu\text{-Ph}_2\text{Pbpy})_2](\text{PF}_6)_2$  **6**. The resonances are labelled according to the isotopomer from which they arise.

The remaining four resonances in the spectrum arise from isotopomer **(I)**, which has an AA'XX' spin system.<sup>134</sup> A simulation of this was attempted in the following manner; as a consequence of symmetry,  $J_{\text{AX}}$  is equivalent to  $J_{\text{A'X'}}$ , and  $J_{\text{AX'}}$  to  $J_{\text{A'X}}$ . Hence of the six coupling

constants for the AA'XX' system, it is necessary to take into consideration only four;  $J_{AX}$ ,  $J_{AX'}$ ,  $J_{AA'}$  and  $J_{XX'}$ . These correspond to the spectral parameters  $^1J(\text{PPt})$ ,  $^2J(\text{PPt})$ ,  $^3J(\text{PP})$  and  $^1J(\text{PtPt})$ . Using the previously obtained coupling constants a simulated spectrum was calculated that corresponded to the experimental one shown in Figure 4.1. However, due to the low intensity of the latter and the complexity of the spin system, the platinum-platinum coupling could not be evaluated with any degree of accuracy.

#### 4.2.1.(iii) [PtPd( $\mu$ -L) $_2$ ](PF $_6$ ) $_2$ [L = Ph $_2$ Pbpy 9, Ph $_2$ Ppyqn 10 and Et(Ph)Pbpy 11]

Two approaches may be used to prepare the heterodinuclear complexes [PtPd( $\mu$ -L) $_2$ ](PF $_6$ ) $_2$  [L = Ph $_2$ Pbpy 9, Ph $_2$ Ppyqn 10 and Et(Ph)Pbpy 11], that differ in whether the bridging ligand is initially bound to Pd(II) or Pt(II). These are outlined in Scheme 4.3.



**Scheme 4.3.** Synthesis of [PtPd( $\mu$ -L) $_2$ ](PF $_6$ ) $_2$  [L = Ph $_2$ Pbpy 9, Ph $_2$ Ppyqn 10 and Et(Ph)Pbpy 11]. (i) 2 eq. Ph $_2$ Pbpy, CH $_3$ CN; (ii) 0.5 eq. Pt $_2$ (dba) $_3$ ; (iii) 2 eq. L, CH $_3$ CN; (iv) 0.5 eq. Pd $_2$ (dba) $_3$ , 2 eq. TlPF $_6$ .

Treatment of tetrakisacetonitrile Pd(II) with two molar equivalents of Ph $_2$ Pbpy and the resulting intermediate with Pt $_2$ (dba) $_3$  produced a mixture that, on the basis of the  $^{31}\text{P}$  NMR spectrum, contained both the mixed metal species 9 and the dipalladium complex 3. The redox

condensation of  $[\text{Pt}(\text{Ph}_2\text{Pbpy})_2\text{Cl}_2]$  with  $\text{Pd}_2(\text{dba})_3$ , in contrast, gave **9** as the major product. As Pt(II) is substitutionally less labile than Pd(II), the ligand exchange which must occur in order to form the homonuclear dipalladium complex will take place to a lesser degree where the  $\text{Ph}_2\text{Pbpy}$  ligand is initially bound to Pt(II). While microanalytically pure crystals of **9** were obtained by fractional crystallization, inevitably in solution a small amount of dipalladium complex was seen to form. The analogous P,N,N ligand bridged complexes  $[\text{PtPd}(\mu\text{-L})_2](\text{PF}_6)_2$  [ $\text{L} = \text{Ph}_2\text{Ppyqn}$  **10** and  $\text{Et}(\text{Ph})\text{Pbpy}$  **11**] were similarly prepared by the conproportionation reaction of  $[\text{Pt}(\text{L})_2\text{Cl}_2]$  [ $\text{L} = \text{Ph}_2\text{Ppyqn}$  and  $\text{Et}(\text{Ph})\text{Pbpy}$ ] with  $\text{Pd}_2(\text{dba})_3$ .

The  $^{31}\text{P}\{-^1\text{H}\}$  NMR spectral data of complexes **9** - **11** are summarised in Table 4.1. The  $^{31}\text{P}\{-^1\text{H}\}$  NMR spectra of **9** and **10** are discussed using that of **10** (Figure 4.2) as a representative example.

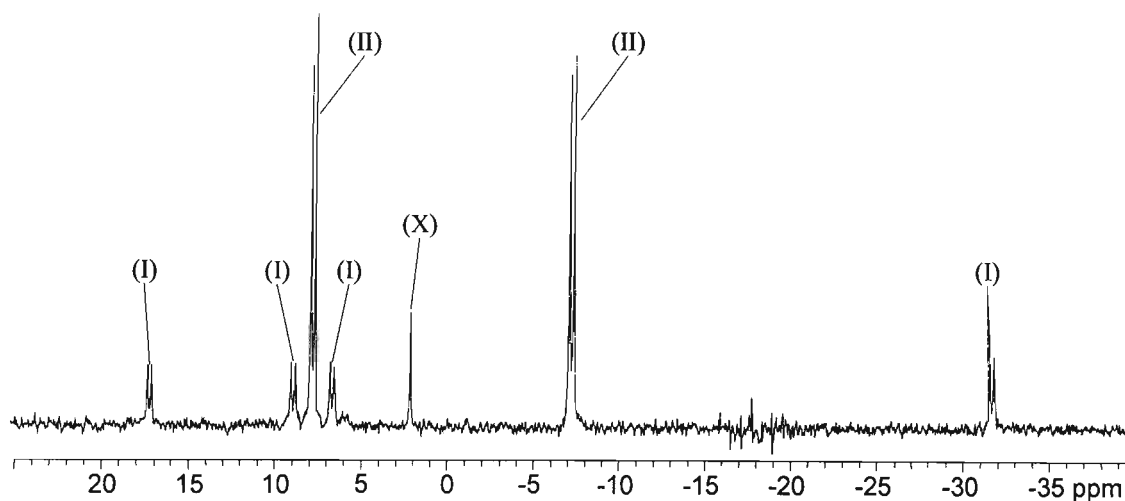
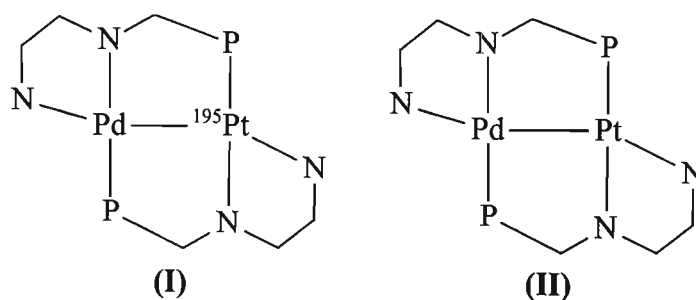


**Figure 4.2.** The  $^{31}\text{P}\{-^1\text{H}\}$  NMR spectrum of  $[\text{PtPd}(\mu\text{-Ph}_2\text{Ppyqn})_2](\text{PF}_6)_2$  **10**. The resonances are labelled according to the isotopomer from which they arise. The singlet labelled X is due to the  $[\text{Pd}_2(\mu\text{-Ph}_2\text{Ppyqn})_2]^{2+}$  impurity.



The spectrum of **10** is a combination of the spectra of two isotopomers (**I**) and (**II**). The presence of two chemically distinct phosphine ligands is reflected by the two major doublets at 7.7 and  $-7.5$  ppm, arising from isotopomer (**II**). Each is split by a three-bond phosphorus-

phosphorus coupling of 18.3 Hz. The spectrum of isotopomer (**I**) can be analysed as an AMX spin system. The doublet of doublets centred at  $-7.5$  ppm show a separation of 3960 Hz. This is within the range for one-bond platinum-phosphorus coupling and these peaks can be assigned to the phosphorus bonding to the platinum. The resonances centred at 7.7 ppm exhibit a  ${}^2J(\text{PtP})$  of 182 Hz and arise from the phosphorus bonded directly to the palladium centre.

The phosphorus atom of Et(Ph)Pbpy is chiral and as a result **11**, containing two different metal centres, will form four diastereomers. The  ${}^{31}\text{P}\{-\text{H}\}$  NMR spectrum of **11** presented in Figure 4.3 is interpreted in terms of the presence of the two pairs of enantiomers. The diastereotopic shifts of 91 (for P-Pd) and 49 Hz (for P-Pt) are significant enough for the two spectra to be resolved from one another.

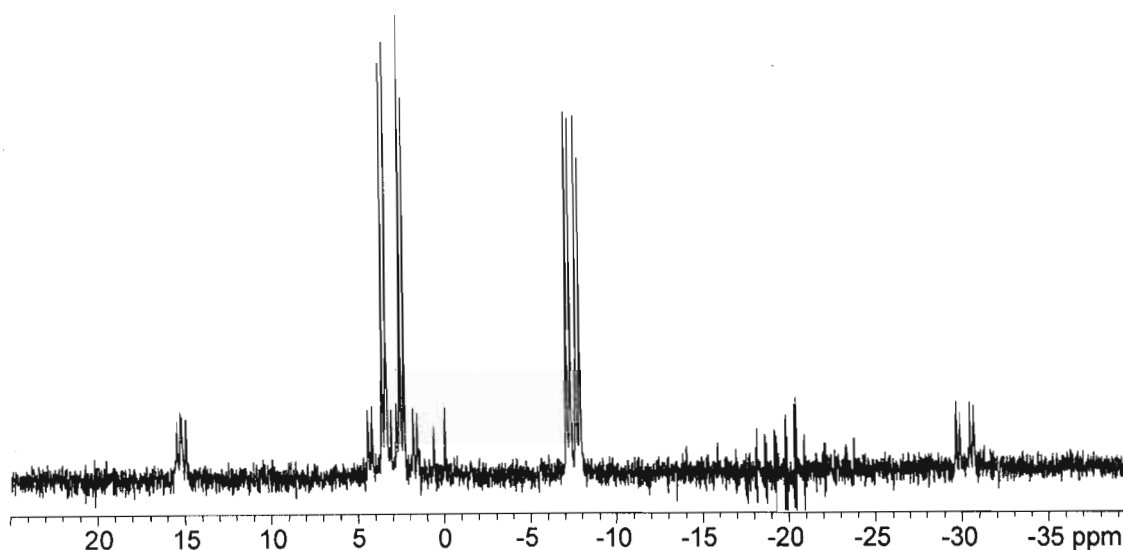


**Figure 4.3.** The  ${}^{31}\text{P}\{-\text{H}\}$  NMR spectrum of  $[\text{PtPd}\{\mu\text{-Et(Ph)Pbpy}\}_2](\text{PF}_6)_2$  **11**.

#### 4.2.2. Crystal Structure Determination of $[\text{Pd}_2(\mu\text{-Ph}_2\text{Pbpy})_2](\text{BF}_4)_2$ **3**

The molecular structure of **3** and its atom number scheme are depicted in Figure 4.4 while selected bond distances and angles are given in Table 4.2. The compound exists as discrete  $[\text{Pd}_2(\mu\text{-Ph}_2\text{Pbpy})_2]^{2+}$  cations and tetrafluoroborate anions in the crystal, there being no unusual intermolecular contact distances. The cation of **3** possesses a crystallographically imposed centre of symmetry midway between the two palladium atoms. These are bridged by two Ph<sub>2</sub>Pbpy ligands bonded in a head-to-tail configuration. Each metal ion is square-planar, being coordinated by the other metal ion and the phosphorus and nitrogen donor atoms. The geometry about the palladium centre is distorted from the ideal in that the angles subtended at the Pd atom are very different from  $90^\circ$  as a consequence of the small bite bipyridyl fragment. As illustrated in Figure 4.5, there is no major deviation of any one atom from the mean squares plane defined

by the metal, phosphorus and bipyridyl atoms; the phenyl rings are subtended above and below this plane.

**Table 4.2.** Selected interatomic distances(Å) and angles(°) for  $[\text{Pd}_2(\mu\text{-Ph}_2\text{Pbpy})_2](\text{BF}_4)_2$  **3**.

Pd–Pd <sup>a</sup>	2.568(2)	Pd–N(1)	2.06(2)
Pd–P <sup>a</sup>	2.218(4)	Pd–N(2)	2.18(2)
N(1)–Pd–N(2)	77.9(4)	N(1)–Pd–Pd <sup>a</sup>	97.7(3)
N(1)–Pd–P <sup>a</sup>	176.3(3)	N(2)–Pd–Pd <sup>a</sup>	175.4(3)
N(2)–Pd–P <sup>a</sup>	99.5(3)	P <sup>a</sup> –Pd–Pd <sup>a</sup>	84.9(2)

<sup>a</sup> Symmetry transformations used to generate equivalent atoms:  $(-x+1, -y+2, -z+1)$ .

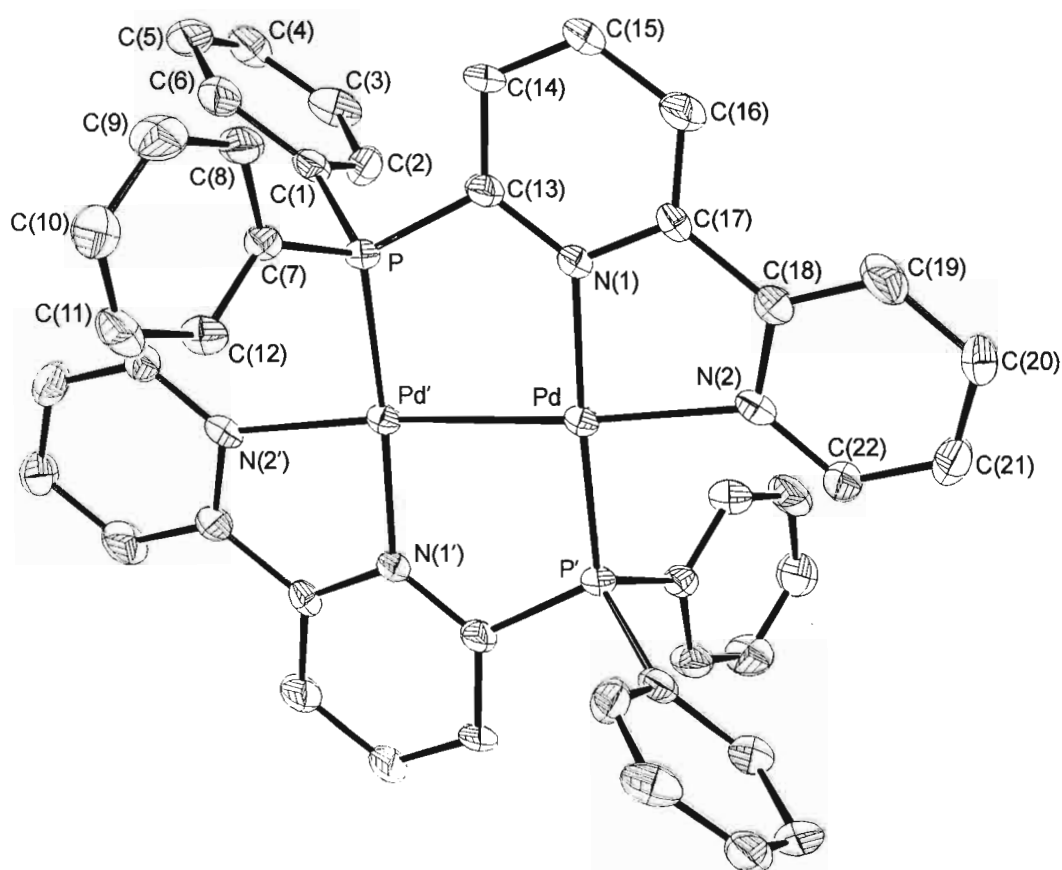


**Figure 4.4.** Perspective view of  $[\text{Pd}_2(\mu\text{-Ph}_2\text{Pbpy})_2](\text{BF}_4)_2$  **3**. Atoms are represented as thermal ellipsoids with a 25% probability surface.

The Pd–Pd bond lengths in dinuclear palladium(I) complexes normally lie in the range 2.57(1) to 2.699(5) Å.<sup>135</sup> The metal-metal distance of 2.568(2) Å observed in **3** is comparable to that of 2.594(1) Å observed for  $[\text{Pd}_2(\mu\text{-Ph}_2\text{Ppy})_2]\text{Cl}_2$ .<sup>136</sup> In these two complexes, the relatively short metal-metal bond length in comparison to those measured for other dinuclear complexes of

Pd(I) can be ascribed to the short 'bite' associated with the rigid PCN bridging fragment of the phosphorus-pyridyl ligand. The Pd–N distance of 2.181(12) Å for the bond *trans* to the palladium [N(2)] is larger than the value of 2.064(11) Å for the P–N bond *trans* to the phosphorus atom [N(1)]. This difference is consistent with palladium having a greater *trans* influence than phosphorus, as has been previously observed.<sup>15,137,138</sup>

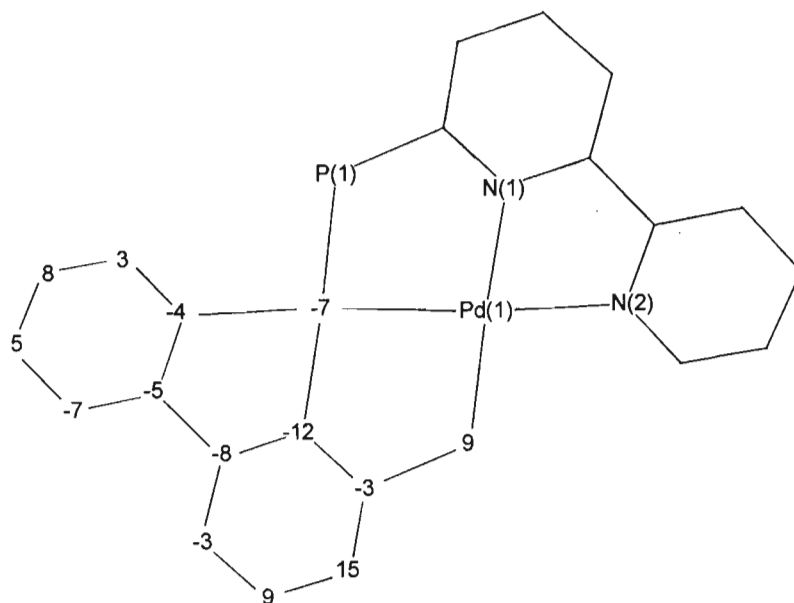
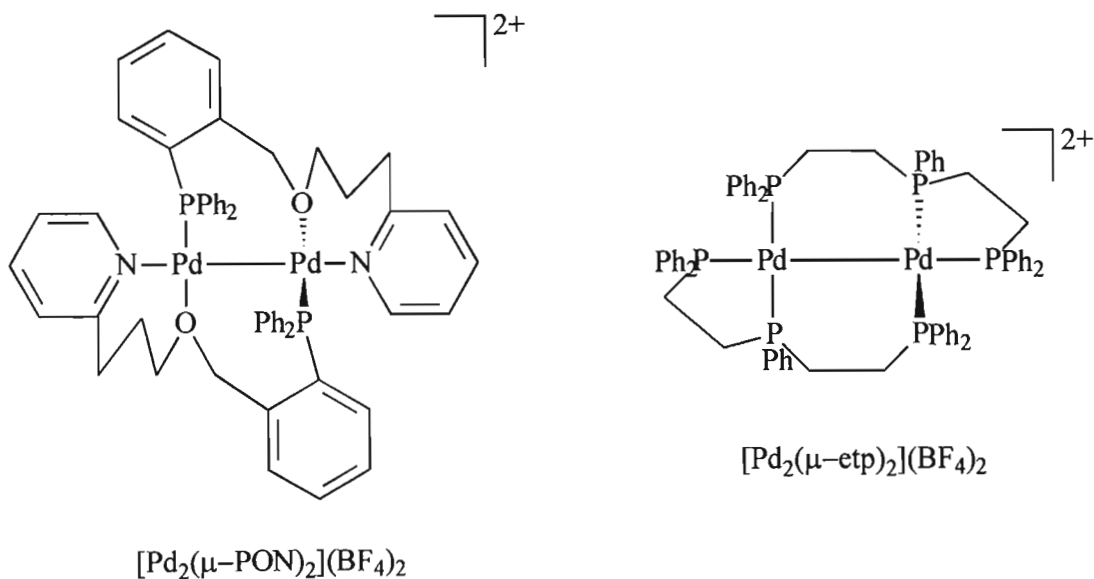


**Figure 4.5.** Pictorial representation of the deviation, measured in picometres, of the palladium, phosphorus and bipyridyl moiety atoms from the least-squares plane defined by these atoms in  $[\text{Pd}_2(\mu\text{-Ph}_2\text{Pbpy})_2](\text{BF}_4)_2$  **3**.

Two other examples of homoleptic dipalladium(I) complexes with tridentate bridging ligands exist, namely  $[\text{Pd}_2(\mu\text{-etp})_2](\text{BF}_4)_2$  (etp =  $\text{PhP}(\text{CH}_2\text{CH}_2\text{PPh}_2)_2$ )<sup>15</sup> and  $[\text{Pd}_2(\mu\text{-PN})_2](\text{BF}_4)_2$  [PON = *o*- $\text{PPh}_2\text{C}_6\text{H}_4\text{CH}_2\text{O}(\text{CH}_2)_3\text{-2-C}_5\text{H}_4\text{N}$ ].<sup>138</sup> The cations of these complexes have the same basic structure as **3**, the dimers consisting of two approximately square-planar molecules joined by Pd–Pd bonds. The dihedral angle between the best-fit planes of the two square-planar coordination planes is 67° in  $[\text{Pd}_2(\mu\text{-etp})_2](\text{BF}_4)_2$  and 58° in  $[\text{Pd}_2(\mu\text{-PN})_2](\text{BF}_4)_2$ . The equivalent dihedral angles measured for dimers with no bridging ligands exhibit a wide range of values between 60° and 90°. The dihedral angle between the best fit planes of Pd(I) and its four ligands and the coordination plane defined by the second palladium and its four ligands in **3** is 0°. We suggest that the dihedral angle between the metal coordination planes in dinuclear complexes of this type is a function of the number of atoms that make up the ring comprising the two Pd atoms and the ligand atoms that link them. For the tridentate PON and etp ligands the rings contain seven and six atoms respectively, which allows some degree of rotational freedom about the Pd–Pd bond and hence larger dihedral angles. On the other hand when  $\text{Ph}_2\text{Pbpy}$  bridges the Pd



atoms a five-membered ring is formed that constrains the two square-planar bonding units to planarity as a result of the rigidity of the PCN fragment and the ensuing short bite of the ligand.



The square planar complexes **3** - **11** are coordinatively saturated. However, this does not rule them out as potential electrocatalysts for the reduction of carbon dioxide. In fact a number of palladium complexes catalyse the electrochemical reduction of  $\text{CO}_2$  through what is thought to be a five coordinate intermediate.<sup>12,16</sup> Moreover, palladium and platinum pentacoordinate complexes are established to be of mechanistic and synthetic interest in organometallic chemistry.<sup>139</sup> The restriction of the dihedral angle between the Pd coordination planes of the palladium dimer by the bridging P,N,N ligand is therefore of relevance as it will ensure the unhindered axial approach of the  $\text{CO}_2$  substrate to both metal sites.

### 4.2.3. Electrochemical Behaviour of the Dinuclear Complexes

#### 4.2.3.(i) $[\text{Pd}_2(\mu\text{-L})_2](\text{BF}_4)_2$ [**L** = **Ph<sub>2</sub>Pbpy** **3**, **Ph<sub>2</sub>Ppyqn** **4** and **Et(Ph)Pbpy** **5**]

The redox properties of the dipalladium complexes are summarised in Table 4.3. The CV of the dipalladium complex **3** (Figure 4.6) consists of an electrochemically reversible one-electron reduction followed by a second irreversible reduction. Several irreversible reductions are seen at more negative potentials. A small return anodic wave appears at *ca.*  $-0.20$  V when the potential is scanned to the second cathodic reduction peak. As this feature is absent when the potential is reversed just beyond the first cathodic wave it must correspond to the oxidation of the decomposition product formed upon the second reduction. The CV of the analogous **Ph<sub>2</sub>Ppyqn** ligand-bridged complex **4** displays the same features as those illustrated in Figure 4.6.

The initial one-electron reduction of complex **5** is observed to be chemically irreversible. All three complexes are irreversibly oxidised at *ca.* 1.20 V.

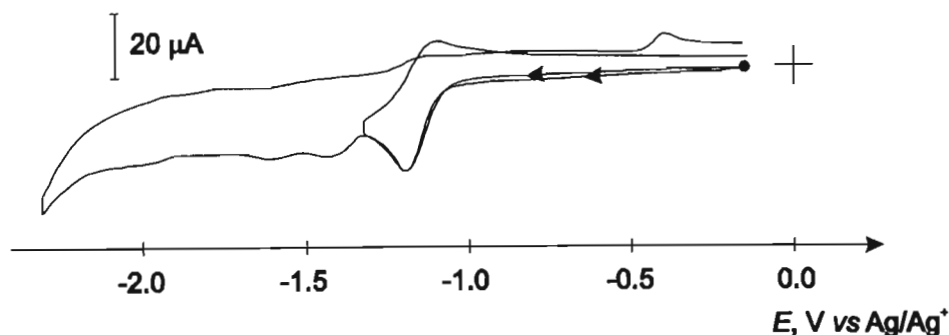


**Figure 4.6.** CV of  $[\text{Pd}_2(\mu\text{-Ph}_2\text{Pbpy})_2](\text{BF}_4)_2$  **3**, measured in  $\text{CH}_3\text{CN}$  (0.1 M TBAP). (Pt electrode,  $r = 1.0$  mm;  $\nu = 100$   $\text{mVs}^{-1}$ ).

**Table 4.3.** Cyclic voltammetric data of  $[\text{Pd}_2(\mu\text{-L})_2](\text{BF}_4)_2$  [L =  $\text{Ph}_2\text{Pbpy}$  **3**,  $\text{Ph}_2\text{Ppyqn}$  **4** and  $\text{Et(Ph)Pbpy}$  **5**].<sup>a</sup>

Complex	$E_{\text{pa}}^{\text{ox}}/\text{V}$	$E_{1/2}^{\text{red I}}/\text{V}$ ( $\Delta E_p/\text{mV}$ )	$E_{\text{pc}}^{\text{red II}}/\text{V}$
$[\text{Pd}_2(\mu\text{-Ph}_2\text{Pbpy})_2](\text{BF}_4)_2$ <b>3</b>	1.30	-1.14(80)	-1.39
$[\text{Pd}_2(\mu\text{-Ph}_2\text{Ppyqn})_2](\text{BF}_4)_2$ <b>4</b>	1.32	-1.00(55)	-1.40
$[\text{Pd}_2\{\mu\text{-Et(Ph)Pbpy}\}_2](\text{BF}_4)_2$ <b>5</b>	1.29	-1.33 <sup>b</sup>	–

<sup>a</sup> Potentials vs.  $\text{Ag}/\text{Ag}^+$ , measured in  $\text{CH}_3\text{CN}$  (0.1 M TBAP) using a  $\text{Ag}/\text{AgCl}$  wire pseudo-reference electrode, scan rate  $100$   $\text{mVs}^{-1}$ ,  $T = 298$  K. Definitions:  $E_{\text{pa}}^{\text{ox}}$ ,  $E_{\text{pc}}^{\text{red}}$  = anodic and cathodic peak potentials of chemically irreversible oxidation and reductions respectively;  $E_{1/2} = (E_{\text{pc}} + E_{\text{pa}})/2$ ;  $\Delta E_p = E_{\text{pc}} - E_{\text{pa}}$ .<sup>b</sup> Cathodic peak potential of chemically irreversible reduction.

The reductive electrochemistry of low-valent palladium  $\alpha$ -diimine complexes resembles that of a number of copper(I) complexes in that it is characterized by the dissociation of the bidentate ligand from the reduced palladium species.<sup>140</sup> The exception to this is the two reversible one-electron reductions exhibited by palladium(0) complexes that contain both olefin and  $\alpha$ -diimine ligands e.g.  $[\text{Pd}(\text{dmf})\text{L}]$  (dmf = dimethyl fumarate, L = 1,10-phenanthroline or 2,2'-bipyridine). In these cases the site of electron addition is the vacant  $\pi^*$ -orbital of the  $\alpha$ -diimine ligand.<sup>141</sup> The dimesityl Pd(II) complex  $[\text{Pd}(\text{bpy})(\text{Mes})_2]$  (Mes = mesityl = 2,4,6-trimethyl phenyl) and the related complex  $[\text{Pd}(\text{bpy})(\text{FMes})_2]$  [FMes = 2,4,6-tris(trifluoromethyl)phenyl] are also reported to undergo two reversible one-electron reductions centred mainly on the bpy ligand.<sup>142</sup> On this basis it is probable that the reversible, initial reductions of **3** and **4** are principally based on the  $\alpha$ -diimine fragments of the bridging ligands. The second irreversible reductions of **3** and **4** and the first irreversible reduction of **5** may essentially be metal based, leading to the dissociation of the reduced metal from the ligands.

The potentials at which complexes **3** - **5** are reduced follows a sequence that one would expect from the nature of the ligands; **4** is the most easily reduced while **5** exhibits the most cathodic potential. In contrast to the analogous dicopper(I) complexes (see Section 3.2.3), the potential at which the dipalladium species are first-reduced shows a significantly larger variation with the ligand type. In particular the dipalladium(I) complexes of Ph<sub>2</sub>Pbpy and Et(Ph)Pbpy, that contain the same  $\alpha$ -diimine moiety, show a 150 mV difference in their first reduction potentials. This is in comparison to the 20 mV differences in the  $E_{1/2}^{0/-}$  observed for the two free ligands. These observations and the general lack of chemical reversibility shown by the reduction processes imply that the reducing electrons are accepted into an unoccupied molecular orbital which possesses both metal and ligand orbital character.

**4.2.3.(ii) [Pt<sub>2</sub>( $\mu$ -L)<sub>2</sub>](PF<sub>6</sub>)<sub>2</sub> [L = Ph<sub>2</sub>Pbpy **6**, Ph<sub>2</sub>Ppyqn **7** and Et(Ph)Pbpy **8**] and [PtPd( $\mu$ -L)<sub>2</sub>](PF<sub>6</sub>)<sub>2</sub> [L = Ph<sub>2</sub>Pbpy **9**, Ph<sub>2</sub>Ppyqn **10** and Et(Ph)Pbpy **11**].**

The redox properties of the homoleptic diplatinum(I) complexes **6** - **8** and the heterodinuclear complexes **9** - **11** were investigated using cyclic voltammetry, the results being summarised in Table 4.4. The cathodic CV of **6** (Figure 4.7) epitomizes the form shown by the dinuclear complexes **8** - **11**, which also exhibit four reduction waves in their CVs. These meet the diagnostic criteria for chemically and electrochemically reversible processes;  $i_{pa}/i_{pc} \sim 1$ ,  $i_p$  varies linearly with  $\nu^{1/2}$ ,  $\Delta E_p$  is approximately that for a reversible one electron transfer and is independent of  $\nu$  from 20 to 500 mVs<sup>-1</sup>. The RDE voltammograms of the complexes, by comparison with that of ferrocene present in a known concentration, confirm that each wave corresponds to a one-electron transfer process.

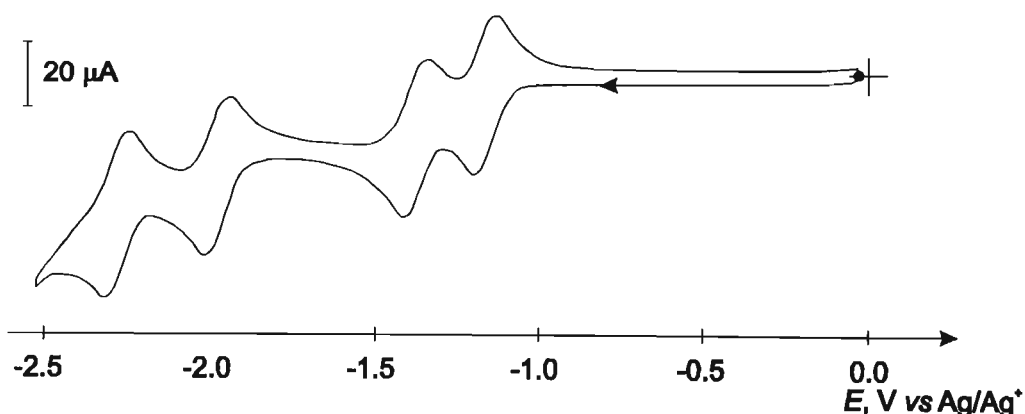


**Figure 4.7.** CV of [Pt<sub>2</sub>( $\mu$ -Ph<sub>2</sub>Pbpy)<sub>2</sub>](PF<sub>6</sub>)<sub>2</sub> **6**, measured in CH<sub>3</sub>CN (0.1 M TBAP). (Pt electrode,  $r = 1.0$  mm;  $\nu = 100$  mVs<sup>-1</sup>).

**Table 4.4.** Cyclic voltammetric data of  $[\text{Pt}_2(\mu\text{-L})_2](\text{PF}_6)_2$  [ $\text{L} = \text{Ph}_2\text{Pbpy}$  **6**,  $\text{Ph}_2\text{Ppyqn}$  **7** and  $\text{Et}(\text{Ph})\text{Pbpy}$  **8**] and  $[\text{PtPd}(\mu\text{-L})_2](\text{PF}_6)_2$  [ $\text{L} = \text{Ph}_2\text{Pbpy}$  **9**,  $\text{Ph}_2\text{Ppyqn}$  **10** and  $\text{Et}(\text{Ph})\text{Pbpy}$  **11**].<sup>a</sup>

Complex	$E_{1/2}/\text{V}$ ( $\Delta E_p/\text{mV}$ )				
	$E_{1/2}^{+2/+}$	$E_{1/2}^{+/0}$	$E_{1/2}^{0/-}$	$E_{1/2}^{-/-2}$	$E_{1/2}^{-2/-3}$
$[\text{Pt}_2(\mu\text{-Ph}_2\text{Pbpy})_2](\text{PF}_6)_2$ <b>6</b>	-1.28(80)	-1.46(80)	-2.02(80)	-2.28(80)	
$[\text{Pt}_2(\mu\text{-Ph}_2\text{Ppyqn})_2](\text{PF}_6)_2$ <b>7</b>	-1.10(50)	-1.30(50)	-1.80(40)	-2.06(50)	-2.23(100)
$[\text{Pt}_2\{\mu\text{-Et}(\text{Ph})\text{Pbpy}\}_2](\text{PF}_6)_2$ <b>8</b>	-1.36(50)	-1.54(80)	-2.09(60)	-2.36(80)	
$[\text{PtPd}(\mu\text{-Ph}_2\text{Pbpy})_2](\text{PF}_6)_2$ <b>9</b>	-1.36(60)	-1.68(70)	-2.07(70)	-2.47(90)	
$[\text{PtPd}(\mu\text{-Ph}_2\text{Ppyqn})_2](\text{PF}_6)_2$ <b>10</b>	-1.09(60)	-1.44(40)	-1.70(40)	-2.24(120)	
$[\text{PtPd}\{\mu\text{-Et}(\text{Ph})\text{Pbpy}\}_2](\text{PF}_6)_2$ <b>11</b>	-1.35(60)	-1.66(80)	-2.06(80)	-2.44(120)	

<sup>a</sup> Potentials vs.  $\text{Ag}/\text{Ag}^+$ , measured in  $\text{CH}_3\text{CN}$  (0.1 M TBAP), scan rate  $100 \text{ mVs}^{-1}$ ,  $T = 298 \text{ K}$ . Definitions:  $E_{\text{pa}}^{\text{ox}}$  = anodic peak potential of chemically irreversible oxidation;  $E_{1/2} = (E_{\text{pc}} + E_{\text{pa}})/2$ ;  $\Delta E_p = E_{\text{pc}} - E_{\text{pa}}$ .<sup>b</sup> Cathodic peak potential of quasi-reversible reduction.

In addition to the four reversible reduction processes exhibited by **6** and **8** - **11**, the CV of the diplatinum(I) complex **7**, illustrated in Figure 4.8, displays a further one-electron reduction wave at  $-1.80 \text{ V}$ , the anodic return of which is broad and ill-defined. This reduction is thus defined as quasi-reversible. When the potential is repeatedly scanned between  $-0.37$  and  $-2.27 \text{ V}$ , the form of the CV is completely unaltered, with no new peaks developing. The same observations are made when the potential scan is held beyond the third and fifth waves for *ca.* 30 seconds. Moreover, an estimate of the  $i_{\text{pa}}/i_{\text{pc}}$  ratio of the first, second, fourth and fifth redox couples remains essentially one. Thus one must conclude that this third redox process is in fact chemically reversible.

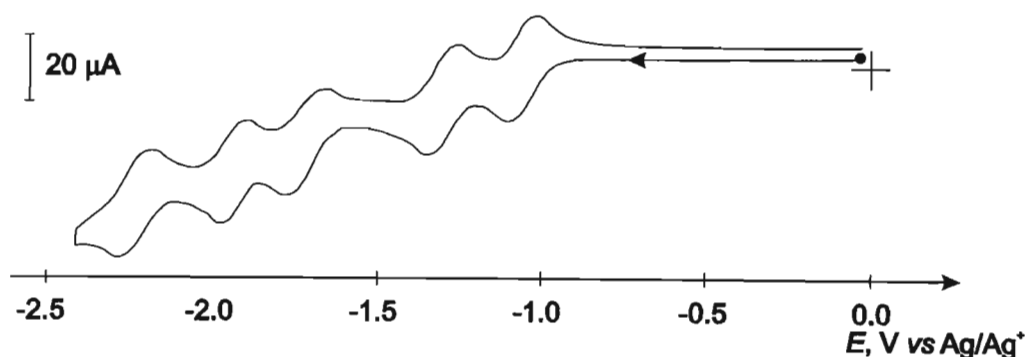


**Figure 4.8.** CV of  $[\text{Pt}_2(\mu\text{-Ph}_2\text{Ppyqn})_2](\text{PF}_6)_2$  **7**, measured in  $\text{CH}_3\text{CN}$  (0.1 M TBAP). (Pt electrode,  $r = 1.0 \text{ mm}$ ;  $\nu = 100 \text{ mVs}^{-1}$ ).

As few monomeric platinum(I) complexes are known and the phosphorus-polypyridyl diplatinum(I) complexes described here are novel, examples of the redox behaviour of this type

of complex in the literature are scant. The unusual 2,2'-bipyridyl ligand-bridged dication  $[\text{Pt}_2(\mu\text{-bpy})(\text{bpy})_2]^{2+}$ , electrosynthesised by the reduction of  $[\text{Pt}(\text{bpy})_2]^{2+}$  in aprotic media, represents the only example of a homoleptic platinum(I) dimeric cation.<sup>143</sup> This complex undergoes two successive one-electron reductions, separated by 600 mV, believed to be centred on one of the 2,2'-bipyridyl ligands.

A useful comparison can be made with related mononuclear square-planar platinum(II)  $\alpha$ -diimine complexes, whose electrochemical properties have received much attention.<sup>144,145,146</sup> The reductive electrochemistry of a number of these complexes is characterised by two reversible one-electron reductions with the  $\alpha$ -diimine as the predominant site of electron addition.<sup>144,145</sup> The separation between the first and second reduction potentials is typically about 700 mV and is associated with the spin-pairing energy of the two electrons added into the same localised orbital.<sup>144</sup> Such a separation is observed between the first and third, second and fourth reduction potentials of the complexes **6** and **8** - **11**. Likewise this difference is maintained between the first and fourth, and second and fifth reductions of **7**. Furthermore the reduction potentials of the complexes follow closely the sequence  $\text{Ph}_2\text{Ppyqn}$  (least cathodic) <  $\text{Ph}_2\text{Pbpy}$  <  $\text{Et}(\text{Ph})\text{Pbpy}$  (most cathodic) observed for the free ligands, demonstrating the comparable electronic character of the redox-active orbital in the ligands and their complexes. The pattern that thus emerges in the reductive electrochemistry of the dinuclear complexes is that of the addition of the first-electron to an empty MO on the  $\alpha$ -diimine fragment of one P,N,N ligand and the second to an empty MO on the  $\alpha$ -diimine fragment of the second P,N,N ligand; the third and fourth electrons are added in the same order to the same MOs.

The small potential separation of, on average, 225 mV between the first and second, and the third and fourth reduction peaks of the diplatinum complexes shows the presence of two almost degenerate acceptor orbitals into which the reducing electrons are localised. Conversely, the average separation between the equivalent reduction peaks of the heterodinuclear complexes **9** - **11** is 385 mV (Figure 4.9). While the inter-ligand repulsion must be responsible for the smaller peak separation that exists in the diplatinum complexes, the reductive patterns of **9** - **11** reflect the presence of two distinct, primarily  $\alpha$ -diimine ligand based redox orbitals that are stabilized, relative to the free ligand, to different extents by the metal to which they coordinate. By comparison with **6**, it is likely that the first and third reductions represent the addition of two electrons to the  $\alpha$ -diimine fragment coordinated to the platinum centre, while the second and fourth reductions are to the 2,2'-bipyridyl ring coordinated to the palladium atom. The electrochemical behaviour of **9** - **11** strongly supports a reductive mechanism where the reducing electrons are localised to  $\pi^*$  orbitals of individual  $\alpha$ -diimine fragments present in the complex.

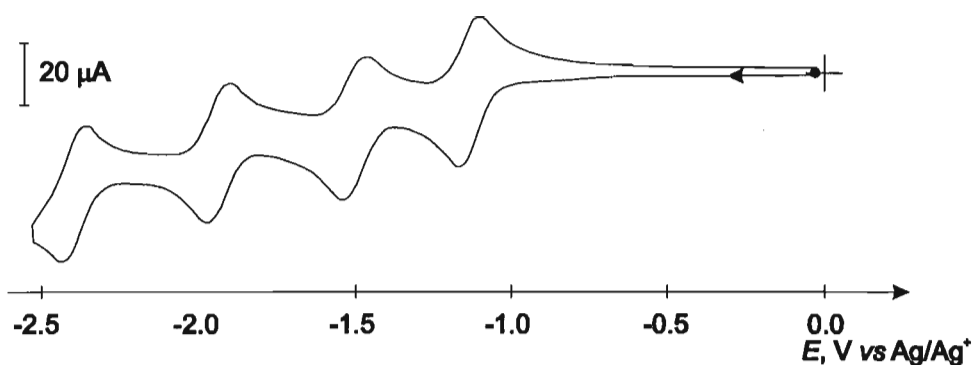


**Figure 4.9.** CV of  $[\text{PtPd}(\mu\text{-Ph}_2\text{Pbpy})_2](\text{PF}_6)_2$  **9**, measured in  $\text{CH}_3\text{CN}$  (0.1 M TBAP). (Pt electrode,  $r = 1.0$  mm;  $\nu = 100$   $\text{mVs}^{-1}$ ).

That the heterodinuclear complexes exhibit chemically reversible CVs whereas those of the homonuclear dipalladium(I) analogue do not, can be attributed to the presence of the stabilizing platinum nucleus. The bridging ligand and metal-metal bonds anchor the labile palladium to the platinum centre, preventing the decomposition observed in the dipalladium species. This example illustrates the utility of the phosphorus-polypyridyl ligand in curtailing the fragmentation of a dinuclear complex during a redox process.

The additional quasi-reversible reduction wave exhibited by **7** at  $-1.80$  V presents an anomaly in the series of dinuclear complexes. The poor electrochemical reversibility of this wave in comparison to the ligand based processes indicates that this reduction corresponds to the addition of an electron to an orbital containing a large metal component, the energetic availability of which is unique to **7**.

Exhaustive electrolysis experiments were carried out on the dinuclear complexes **6** - **11** at an applied potential corresponding to their first reduction peaks. The electrolysis required the passage of one Faraday per mole of complex and showed that the one-electron reduction products of the complexes are chemically unstable on an electrosynthetic time scale. In each case a dark red coloured solution was formed and a grey-black tarnishing of the electrode surface observed. CVs recorded after exhaustive electrolysis of the complexes show the presence of several new redox systems. Considering their complexity, a full characterisation of the decomposition products was not attempted. However, the absence of distinct free ligand reduction peaks in the solutions of the  $\text{Pt}_2$  and PtPd complexes after electrolysis is noteworthy. The converse is true of the Cu(I) complexes, the electrochemistry of these complexes after exhaustive electrolysis at their first reduction potentials being characterised by the predominance of free ligand in solution (see Section 3.2.3). The chemistry of tertiary phosphine complexes of Pd(0) and Pt(0) has been extensively studied and such complexes can be electrochemically

synthesised.<sup>77,147,148</sup> For example, the two-electron electrochemical reduction of the  $d^9-d^9$  complexes  $[M_2(dppm)_2Cl_2]$  ( $M = Pt$  or  $Pd$ ) in the presence of  $dppm$  leads to the formation of the  $M(0)$  dimers  $[M_2(dppm)_3]$ .<sup>149,150</sup> It is also reported that the two-electron electrochemical reduction of  $[PdM(dppm)_2Cl_2]$  ( $M = Pd$  and  $Pt$ ) results in the cleavage of the metal-metal bond, leading to the formation of  $[Pd(dppm)_2]$  and other uncharacterised fragments.<sup>151</sup> It is possible that the one-electron reduction of the dinuclear  $Pt$  and the binuclear  $PtPd$  complexes brings about the formation of  $M(0)$  species stabilised by  $\eta^1-P$  bound phosphorus-polypyridyl ligands.

In their anodic CVs the complexes **6** - **11** show an irreversible oxidation, the anodic peak potential varying from 1.26 V for **8** to 1.42 V for **9**. The data is given in Table 4.5 below while Figure 4.10 shows a typical CV.

**Table 4.5.** Anodic cyclic voltammetric data of  $[Pt_2(\mu-L)_2](PF_6)_2$  [ $L = Ph_2Pbpy$  **6**,  $Ph_2Ppyqn$  **7** and  $Et(Ph)Pbpy$  **8**] and  $[PtPd(\mu-L)_2](PF_6)_2$  [ $L = Ph_2Pbpy$  **9**,  $Ph_2Ppyqn$  **10** and  $Et(Ph)Pbpy$  **11**].<sup>a</sup>

Complex	$E_{pa}^{ox}/V$	$E_{pc}^{ox}/V$
$[Pt_2(\mu-Ph_2Pbpy)_2](PF_6)_2$ <b>6</b>	1.36	
$[Pt_2(\mu-Ph_2Ppyqn)_2](PF_6)_2$ <b>7</b>	1.29	
$[Pt_2\{\mu-Et(Ph)Pbpy\}_2](PF_6)_2$ <b>8</b>	1.26	-0.38
$[PtPd(\mu-Ph_2Pbpy)_2](PF_6)_2$ <b>9</b>	1.42	-0.09
$[PtPd(\mu-Ph_2Ppyqn)_2](PF_6)_2$ <b>10</b>	1.36	-0.12
$[PtPd\{\mu-Et(Ph)Pbpy\}_2](PF_6)_2$ <b>11</b>	1.36	-0.10

<sup>a</sup> Potentials vs.  $Ag/Ag^+$ , measured in  $CH_3CN$  (0.1 M TBAP), scan rate  $100\text{ mVs}^{-1}$ ,  $T = 298\text{ K}$ . Definitions:  $E_{pa}^{ox}$ ,  $E_{pc}^{ox}$  = anodic and cathodic peak potentials respectively of chemically irreversible oxidation.

The oxidations of **6** - **11** must be metal based as it would be expected that the HOMO of the complexes would be metal-metal bond in character. It is probable that oxidation leads to the irreversible rupture of the metal-metal bond. The oxidation potentials at which the complexes are oxidised reflect a greater stabilisation of the metal-metal bond in the heteronuclear complexes over their homonuclear analogues, the oxidation of **9** - **11** taking place at a potential *ca.* 75 mV more positive than that of **6** - **8**. The stronger  $\sigma$ -donor effect of  $Et(Ph)Pbpy$  relative to  $Ph_2Pbpy$ , and the consequent increased electron density on the metal centres, is clear in the less positive oxidation potentials of **8** and **11** relative to those recorded for the  $Ph_2Pbpy$  analogues **6** and **9** (Table 4.5). Perhaps unexpectedly, the complexes of the stronger  $\pi$ -acceptor ligand  $Ph_2Ppyqn$  are more easily oxidised than their  $Ph_2Pbpy$  analogues. In transition metal complexes of the  $\alpha$ -diimine ligands 2,2'-biquinoyl and 2-(2-pyridyl)quinoline, the quinoline fragment almost encases the metal centre, hindering the coordination of further ligands in the plane of the metal-

quinoline fragment.<sup>152,153</sup> A high degree of steric crowding must exist around the four coordinate, square planar metal centres in **7** and **10**, giving rise to a destabilisation of the M–M bond.

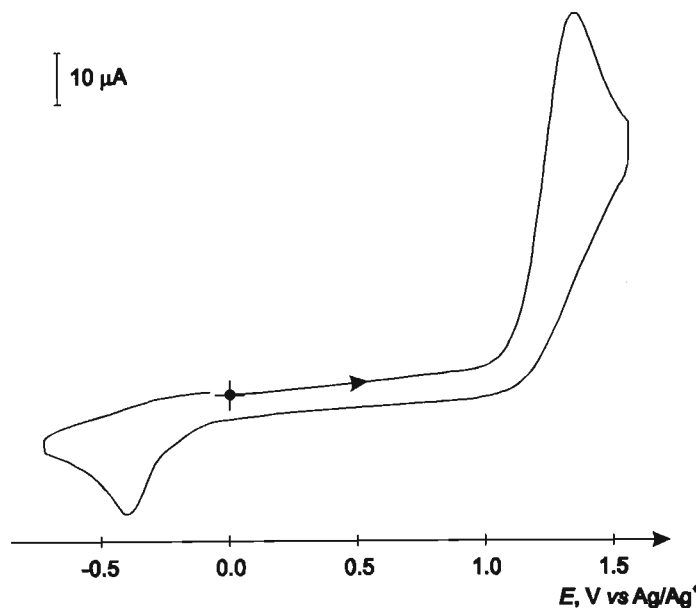


**Figure 4.10.** CV of  $[\text{Pt}_2\{\mu\text{-Et(Ph)Pbpy}\}_2](\text{PF}_6)_2$  **8**, measured in  $\text{CH}_3\text{CN}$  (0.1 M TBAP). (Pt electrode,  $r = 2.5$  mm;  $\nu = 100$   $\text{mVs}^{-1}$ ).

#### 4.2.4. Catalytic Properties Towards $\text{CO}_2$ Electrochemical Reduction

The redox behaviour of **6** and **8** - **11** in the presence of  $\text{CO}_2$  is exemplified by the CV of **6** shown in Figure 4.11. The CV of **6** measured in a  $\text{CO}_2$  saturated acetonitrile electrolyte exhibits an enhancement in current at the onset of the third reduction peak. Moreover the corresponding anodic peak is absent in the reverse scan. The form of the first two redox systems remains unchanged in the presence of  $\text{CO}_2$ . The evidence indicates that the tri-reduced complexes  $[\text{Pt}_2(\mu\text{-L})_2]^-$  or  $[\text{PtPd}(\mu\text{-L})_2]^-$  catalyse the electrochemical reduction of  $\text{CO}_2$ . Notably the behaviour of the heterodinuclear complexes does not differ from that of their homonuclear analogues. If the potential of the working electrode is cycled between the onset of the third and the fourth reduction peaks an immediate decrease in current is observed which continues to diminish with each cycle. Furthermore, a microelectrolysis (Pt disc working electrode,  $r = 2.5$  mm) at the potential of the onset of the third reduction peak shows a marked decrease of current with time. This behaviour is displayed by all the complexes and it indicates that the catalytically active species is rapidly transformed at this potential. The same behaviour of the complexes is observed on Pt disc, glassy carbon disc and carbon felt electrodes.



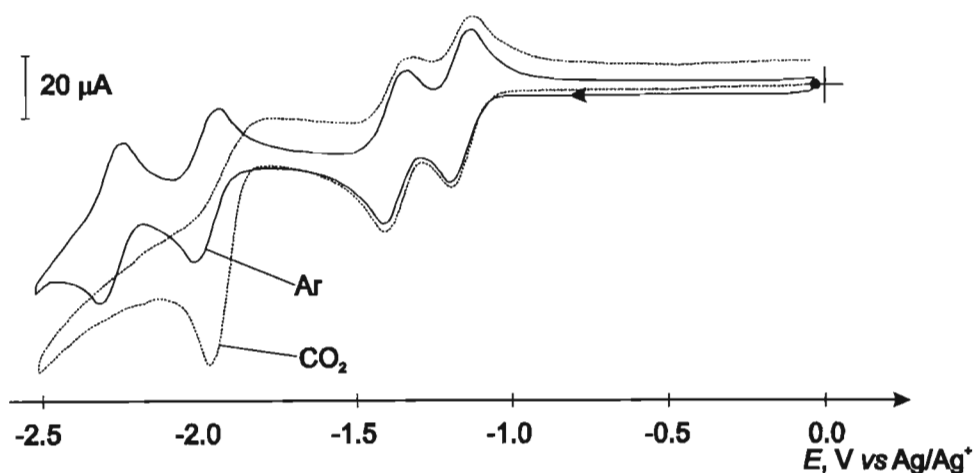


**Figure 4.11.** CVs of  $[\text{Pt}_2(\mu\text{-Ph}_2\text{Pbpy})_2](\text{PF}_6)_2$  **6** in  $\text{CO}_2$  and Ar saturated acetonitrile (0.1 M TBAP) electrolyte. (Pt electrode,  $r = 1.0$  mm;  $\nu = 100$   $\text{mVs}^{-1}$ ).

A similar pattern is likewise seen in the CV of **7** in the presence of  $\text{CO}_2$  (Figure 4.12), with a current enhancement being observed at the onset of the third reduction wave of the complex. The first two redox couples are unperturbed by the presence of  $\text{CO}_2$ . Notably, when the potential scan is extended to beyond the third reduction wave a further enhancement in current is observed coincident with fifth reduction peak, while in the return scan the fifth and third anodic waves disappear. An anodic response corresponding to the fourth reduction wave, although diminished, does still exist. When the switching potential is such that the scan is reversed just beyond the third wave the return anodic peak corresponding to that wave is still absent. Thus, it does not appear that the transfer of the first electron to  $\text{CO}_2$  is coupled to the transfer of the second, as is observed in the dicopper(I) complexes (see Section 3.2.4), the implication being that **7** catalyses the reduction of  $\text{CO}_2$  in two independent pathways.

In the presence of trace amounts of water, the current response just beyond the third reduction wave in the CVs of **6** - **11** is greatly magnified. This is shown for complex **8** in Figure 4.13. As is observed in the CVs of **6** - **11** measured under anhydrous conditions, the third anodic response is absent, while the anodic peaks of the first two reduction processes are retained. As opposed to the dicopper(I) complexes earlier described in Section 3.2.4, the diplatinum complexes show no signs of decomposition under these conditions.

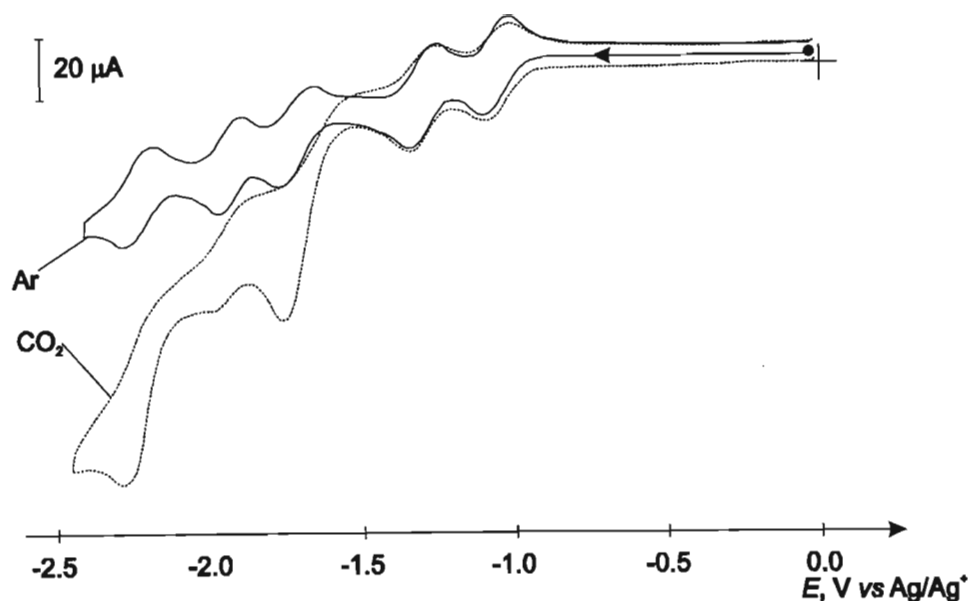


**Figure 4.12.** CVs of  $[\text{Pt}_2(\mu\text{-Ph}_2\text{Ppyqn})_2](\text{PF}_6)_2$  **7** in  $\text{CO}_2$  and Ar saturated acetonitrile (0.1 M TBAP) solution. (Pt electrode,  $r = 1.0$  mm;  $\nu = 100$   $\text{mVs}^{-1}$ ).

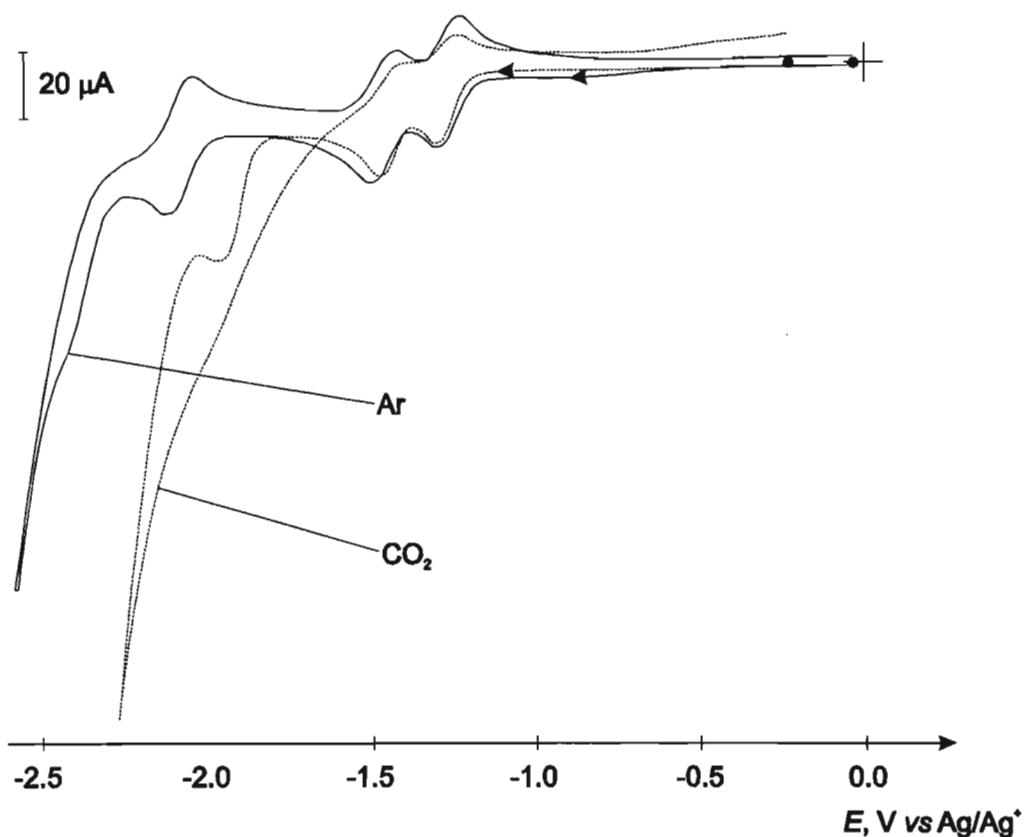


**Figure 4.13.** CVs of  $[\text{Pt}_2\{\mu\text{-Et(Ph)Pbpy}\}_2](\text{PF}_6)_2$  **8** in  $\text{CO}_2$  and Ar saturated acetonitrile (0.1 M TBAP) solution with water (0.5 %) present. (Pt electrode,  $r = 1.0$  mm;  $\nu = 100$   $\text{mVs}^{-1}$ ).

Preparative scale electrolysis experiments were carried out in  $\text{CO}_2$  saturated  $\text{CH}_3\text{CN} + 0.1$  M TBAP using carbon felt working electrodes and a 1 mM concentration of complex. The

results of these experiments are summarised in Table 4.5. A number of observations common to all the complexes can be made: (i) The start of the electrolysis experiment is accompanied by a rapid fall in the initial current to a small value. The colour of the solution begins to change immediately upon application of the applied potential, becoming progressively lighter during the course of the experiment. (ii). For the mixed metal Pt–Pd complexes, analyses show that CO is produced in small quantities while no formate is formed. For the diplatinum complexes the very low currents did not warrant an analysis of the possible CO<sub>2</sub> reduction products. (iii) After each electrolysis the solution was sufficiently purged with argon to remove completely the CO<sub>2</sub> and CVs then recorded. These show no sign of the original complex in solution.

As would be anticipated from the exhaustive electrolysis experiments carried out under an inert atmosphere, the complexes are not stable under the conditions of the preparative scale electrolysis in the presence of CO<sub>2</sub>. At the potential at which a catalytic current is observed the complexes rapidly decompose to a species that is no longer catalytically active. For this reason the complexes would not serve as practical electrocatalysts. Given the evident instability of the complexes under reducing conditions and the negative potentials required to bring about a catalytic effect, it was decided not to further examine their electrocatalytic properties in an aqueous-organic medium.

**Table 4.5.** Summary of preparative scale electrocatalysis experiments carried out with [Pt<sub>2</sub>(μ-L)<sub>2</sub>](PF<sub>6</sub>)<sub>2</sub> [L = Ph<sub>2</sub>Pbpy **6**, Ph<sub>2</sub>Ppyqn **7** and Et(Ph)Pbpy **8**] and [PtPd(μ-L)<sub>2</sub>](PF<sub>6</sub>)<sub>2</sub> [L = Ph<sub>2</sub>Pbpy **9**, Ph<sub>2</sub>Ppyqn **10** and Et(Ph)Pbpy **11**]

Complex	E <sub>app</sub> / V	i / mA (change in i per 10 C)	Coulombs / C	Faradaic Yield / %	
				CO	HCOO <sup>-</sup>
[Pt <sub>2</sub> (μ-Ph <sub>2</sub> Pbpy) <sub>2</sub> ](PF <sub>6</sub> ) <sub>2</sub> <b>6</b>	-1.95	1.2 (-0.6)	12	–	–
[Pt <sub>2</sub> (μ-Ph <sub>2</sub> Ppyqn) <sub>2</sub> ](PF <sub>6</sub> ) <sub>2</sub> <b>7</b>	-1.95	0.5 (-0.4)	8	–	–
[Pt <sub>2</sub> {μ-Et(Ph)Pbpy} <sub>2</sub> ](PF <sub>6</sub> ) <sub>2</sub> <b>8</b>	-1.95	1.2 (-0.8)	12	–	–
[PtPd(μ-Ph <sub>2</sub> Pbpy) <sub>2</sub> ](PF <sub>6</sub> ) <sub>2</sub> <b>9</b>	-1.90	1.7 (-0.1)	34	5	0
[PtPd(μ-Ph <sub>2</sub> Ppyqn) <sub>2</sub> ](PF <sub>6</sub> ) <sub>2</sub> <b>10</b>	-1.90	0.9 (-0.1)	15	0	0
[PtPd{μ-Et(Ph)Pbpy} <sub>2</sub> ](PF <sub>6</sub> ) <sub>2</sub> <b>11</b>	-1.90	1.6 (-0.7)	18	2	0

#### 4.2.5. Extended Hückel Molecular Orbital Calculation On [Pd<sub>2</sub>(μ-Ph<sub>2</sub>Pbpy)<sub>2</sub>](BF<sub>4</sub>)<sub>2</sub> **3**

An extended Hückel molecular orbital calculation was carried out on **3** using the bond lengths and angles obtained from its single crystal X-ray data. The form of the resulting frontier

molecular orbitals are pictorially represented in Figure 4.14, their calculated energies and the relative percent atomic contributions of the palladium and ligand donor atoms to them being given in Table 4.5.

The HOMO of **3** lies predominantly between the two palladium metals and is indeed the  $\sigma$ -bonding molecular orbital forming the metal-metal bond. The third lowest unoccupied molecular orbital (TLUMO) forms the corresponding  $\sigma^*$  antibonding molecular orbital. The irreversible oxidation of **3** can be logically interpreted in terms of the molecular orbital model; the oxidative process consists of the removal of both electrons from the  $\sigma$  bonding molecular orbital between the two metals, a non-bonding interaction between the two palladium centres develops and the metal-metal bond is broken leading to the decomposition of the complex.

**Table 4.6.** Calculated energies of the frontier MOs and relative percent atomic contribution<sup>a</sup> of the metal, phosphine and  $\alpha$ -diimine atoms of  $[\text{Pd}_2(\mu\text{-Ph}_2\text{Pbpy})_2](\text{BF}_4)_2$  **3**.

Molecular Orbital	Eigenvalue /eV	Percent Relative Atomic Contribution		
		Pd	$\alpha$ -diimine	phosphine
HOMO	-10.87	57	36	5
LUMO	-9.76	1	83	16
SLUMO	-9.73	2	88	10
TLUMO	-9.63	60	25	15

<sup>a</sup>Atomic contributions do not add up to 100 % since atomic contributions to the MOs of less than 1 % are neglected.

The LUMO is of  $\pi$  symmetry and chiefly of phosphorus-bipyridyl ligand in nature, containing little metal contribution. The chemical reversibility displayed by the first one-electron reduction of **3** is therefore explained on the basis that the process is ligand based. The reduction of the metal centre and its inevitable dissociation from the ligand is thus averted. In contrast to the P,N,N bridged dicopper(I) complexes, where the phosphorus admixture to the LUMO is negligible, the LUMO of **3** has a noticeable amount of phosphorus character. Thus it is not unexpected that the first reduction potential shows a more marked difference between **3** and **5**.

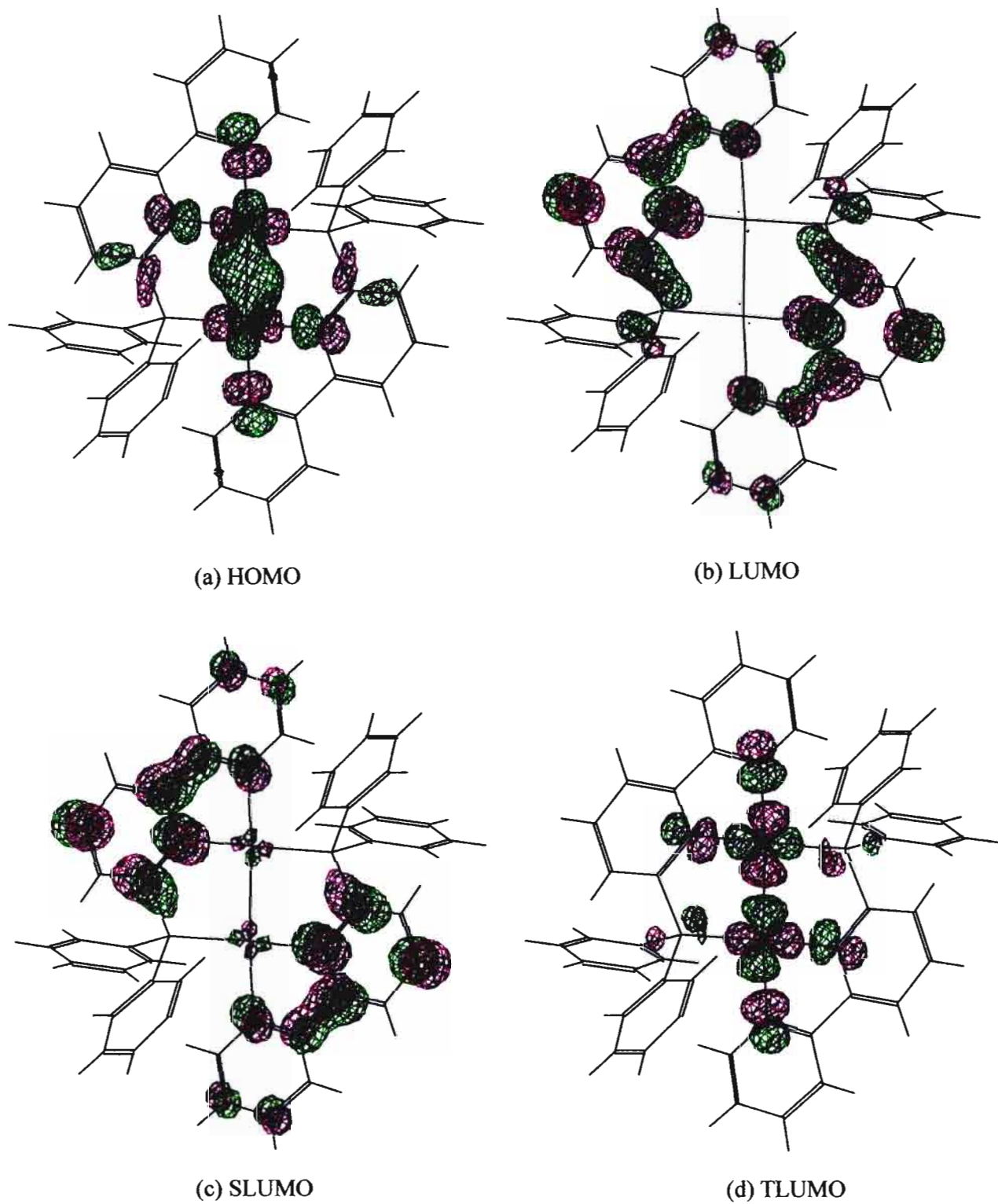


**Figure 4.14.** Molecular orbital representation of the (a) HOMO, (b) LUMO, (c) SLUMO and (d) TLUMO of  $[\text{Pd}_2(\mu\text{-Ph}_2\text{Pbpy})_2](\text{BF}_4)_2 \mathbf{3}$ .

### 4.3. Experimental

**[Pd<sub>2</sub>(μ-Ph<sub>2</sub>Pbpy)<sub>2</sub>](BF<sub>4</sub>)<sub>2</sub> 3.** A solution of [Pd(CH<sub>3</sub>CN)<sub>4</sub>](BF<sub>4</sub>)<sub>2</sub> (44 mg, 0.10 mmol) in CH<sub>3</sub>CN (5 cm<sup>3</sup>) was added drop wise to Ph<sub>2</sub>Pbpy (68 mg, 0.20 mmol) in CH<sub>3</sub>CN (5 cm<sup>3</sup>) and the resulting yellow solution maintained at 25°C for 1 h. The volume of solvent was reduced under vacuum to *ca.* 3 cm<sup>3</sup> and Et<sub>2</sub>O (15 cm<sup>3</sup>) added. A white precipitate formed after the solution was stored overnight at -25°C in a refrigerator. This precipitate was washed with Et<sub>2</sub>O (2 x 5 cm<sup>3</sup>) and redissolved in CH<sub>3</sub>CN (5 cm<sup>3</sup>). To this solution Pd<sub>2</sub>(dba)<sub>3</sub>.CHCl<sub>3</sub> (50 mg, 0.05 mmol) was introduced and the suspension stirred for 12 h at room temperature. The reaction mixture was filtered through glass microfibre, the volume reduced *in vacuo* and excess Et<sub>2</sub>O added. The precipitate which formed was recrystallised from CH<sub>3</sub>CN/Et<sub>2</sub>O to give an orange crystalline product (0.15 g, 68 %). (Found: C, 49.38; H, 3.57; N, 5.21. Pd<sub>2</sub>C<sub>44</sub>H<sub>34</sub>N<sub>4</sub>P<sub>2</sub>B<sub>2</sub>F<sub>8</sub> requires C, 49.52; H, 3.21; N, 5.25 %); λ<sub>max</sub>/nm (CH<sub>3</sub>CN) 231 (sh) (ε/dm<sup>3</sup> mol<sup>-1</sup> cm<sup>-1</sup> 85 300), 249 (sh) (73 300), 310 (53 800) and 435 (6 680); ν<sub>max</sub>/cm<sup>-1</sup> (KBr) 1710w, 1598w, 1485w, 1438s, 1062vs (BF<sub>4</sub>), 782w, 752w, 698w, 610w, 536s and 518w; δ<sub>H</sub> (200 MHz, CD<sub>3</sub>CN, CHD<sub>2</sub>CN) 8.48 (2H, dm), 8.28 (4H, m), 8.19 (2H, tm), 8.08 to 7.54 (22H, br m), 7.10 (2H, tm), 6.73 (2H, dm); δ<sub>P</sub> (32.2 MHz, CD<sub>3</sub>CN, 85% H<sub>3</sub>PO<sub>4</sub>) 3.4 (s).

**[Pd<sub>2</sub>(μ-Ph<sub>2</sub>Ppyqn)<sub>2</sub>](BF<sub>4</sub>)<sub>2</sub> 4.** [Pd(CH<sub>3</sub>CN)<sub>4</sub>](BF<sub>4</sub>)<sub>2</sub> (44 mg, 0.10 mmol) and Ph<sub>2</sub>Ppyqn (78 mg, 0.20 mmol) were dissolved in CH<sub>3</sub>CN (10 cm<sup>3</sup>) and the solution maintained at 25°C for 12 h. Pd<sub>2</sub>(dba)<sub>3</sub>.CHCl<sub>3</sub> (50 mg, 0.05 mmol) was added and the suspension stirred for a further 24 h. CH<sub>3</sub>CN (5 cm<sup>3</sup>) and Et<sub>2</sub>O (20 cm<sup>3</sup>) were added in succession and the solution stood overnight at -25°C. The clear orange/red supernatant was filtered from the black solid that formed through glass microfibre. The residue was washed with CH<sub>3</sub>CN (3 x 5 cm<sup>3</sup>), the washings being filtered through glass microfibre and combined with the supernatant. The solvent was removed from the combined solutions under reduced pressure and the remaining residue dissolved in CH<sub>3</sub>CN (5 cm<sup>3</sup>). The crude product was precipitated from this solution by the addition of excess Et<sub>2</sub>O. The pure red crystalline dipalladium complex was obtained by recrystallisation of this precipitate from CH<sub>3</sub>CN/Et<sub>2</sub>O (0.13 g, 56 %). (Found: C, 53.52; H, 3.24; N, 4.92. Pd<sub>2</sub>C<sub>52</sub>H<sub>38</sub>N<sub>4</sub>P<sub>2</sub>B<sub>2</sub>F<sub>8</sub> requires C, 53.51; H, 3.28; N, 4.80 %); λ<sub>max</sub>/nm (CH<sub>3</sub>CN) 224 (sh) (ε/dm<sup>3</sup> mol<sup>-1</sup> cm<sup>-1</sup> 73 500), 260 (48 900), 289 (sh) (30 700), 330 (23 100), 356 (21 800) and 467 (3510); ν<sub>max</sub>/cm<sup>-1</sup> (KBr) 1589w, 1515w, 1469w, 1440s, 1330w, 1060vs (BF<sub>4</sub>), 814w, 784w, 742w, 696w, 526s and 509w; δ<sub>H</sub> (200 MHz, CD<sub>3</sub>CN, CHD<sub>2</sub>CN) 8.85 (2H, tm), 8.84 (2H, d), 8.64 (2H, d), 8.41 (2H, tm), 7.86

(2H, dm), 7.84 (4H, m), 7.61 (6H, m), 7.40 (2H, tm), 7.28 (2H, dm), 7.24 (2H, dm), 6.90 (2H, tm);  $\delta_P$  (32.2 MHz, CD<sub>3</sub>CN, 85% H<sub>3</sub>PO<sub>4</sub>) 3.7 (s).

**[Pd<sub>2</sub>{ $\mu$ -Et(Ph)Pbpy}<sub>2</sub>](BF<sub>4</sub>)<sub>2</sub> 5.** The complex was synthesized in the same manner as [Pd<sub>2</sub>( $\mu$ -Ph<sub>2</sub>Ppyqn)<sub>2</sub>](BF<sub>4</sub>)<sub>2</sub>, thus [Pd(CH<sub>3</sub>CN)<sub>4</sub>](BF<sub>4</sub>)<sub>2</sub> (115 mg, 0.258 mmol) was reacted with Et(Ph)Pbpy (151 mg, 0.516 mmol). Subsequently Pd<sub>2</sub>(dba)<sub>3</sub>.CHCl<sub>3</sub> (129 mg, 0.129 mmol) was introduced to the reaction mixture. The product was purified as described above, affording the complex as a yellow crystalline material (0.32 g, 63 %) (Found: C, 44.15; H, 3.28; N, 5.98. Pd<sub>2</sub>C<sub>36</sub>H<sub>34</sub>N<sub>4</sub>P<sub>2</sub>B<sub>2</sub>F<sub>8</sub> requires C, 44.53; H, 3.53; N, 5.77 %);  $\lambda_{\max}/\text{nm}$  (CH<sub>3</sub>CN) 245 (sh) ( $\epsilon/\text{dm}^3 \text{ mol}^{-1} \text{ cm}^{-1}$  44 600), 308 (37 100) and 424 (4370);  $\nu_{\max}/\text{cm}^{-1}$  (KBr) 1597w, 1562w, 1486w, 1448w, 1438w (sh), 1250w, 1062vs (BF<sub>4</sub>), 781s, 754s, 600w and 523w;  $\delta_H$  (200 MHz, CD<sub>3</sub>CN, CHD<sub>2</sub>CN) 8.60 to 8.10 (12H, br m), 7.90 to 7.70 (8H, br m), 7.50 (2H, m), 7.30 (2H, m), 2.85 (4H, m, PCH<sub>2</sub>CH<sub>3</sub>), 1.53 (6H, m, PCH<sub>2</sub>CH<sub>3</sub>);  $\delta_P$  (32.2 MHz, CD<sub>3</sub>CN, 85% H<sub>3</sub>PO<sub>4</sub>) 3.1 (s).

**[Pt<sub>2</sub>( $\mu$ -Ph<sub>2</sub>Pbpy)<sub>2</sub>](PF<sub>6</sub>)<sub>2</sub> 6.** PtCl<sub>2</sub>(PhCN)<sub>2</sub> (47 mg, 0.10 mmol) and Ph<sub>2</sub>Pbpy (68 mg, 0.20 mmol) were dissolved in CH<sub>2</sub>Cl<sub>2</sub> (10 cm<sup>3</sup>) and stirred for 1 h at room temperature. Next Pt<sub>2</sub>(dba)<sub>3</sub>.CHCl<sub>3</sub> (60 mg, 0.05 mmol) and TIPF<sub>6</sub> (79 mg, 0.20 mmol) were added and the reaction mixture stirred for a further 24 h at room temperature. The solvent was then completely removed under reduced pressure and the remaining residue dissolved in CH<sub>3</sub>CN (5 cm<sup>3</sup>). To this solution was added Et<sub>2</sub>O (20 cm<sup>3</sup>). Upon leaving the solution to stand overnight at -25°C a dark brown solid residue formed, from which an orange supernatant was filtered through glass microfibre. A further portion of CH<sub>3</sub>CN (5 cm<sup>3</sup>) was added to the brown residue, followed by Et<sub>2</sub>O (20 cm<sup>3</sup>) and the solution stood overnight again at -25°C. The orange supernatant that formed was filtered through glass microfibre and the above procedure repeated once more on the remaining brown residue. The three filtered supernatants were combined, reduced in volume to ca. 3cm<sup>3</sup> and an excess of Et<sub>2</sub>O added. Orange crystalline material was obtained from this solution after leaving it to stand for 12 h at -25°C (0.14 g, 52 %). (Found: C, 38.94; H, 2.41; N, 4.12. Pt<sub>2</sub>C<sub>44</sub>H<sub>34</sub>N<sub>4</sub>P<sub>4</sub>F<sub>12</sub> requires C, 38.84; H, 2.52; N, 4.12 %);  $\lambda_{\max}/\text{nm}$  (CH<sub>3</sub>CN) 232 ( $\epsilon/\text{dm}^3 \text{ mol}^{-1} \text{ cm}^{-1}$  96 400), 288 (sh) (34 000), 315 (sh) (24 100), 329 (sh) (20 800), 360 (sh) (6 220) and 436 (3 860);  $\nu_{\max}/\text{cm}^{-1}$  (KBr) 1602w, 1451w (sh), 1438w, 1398w, 1253w, 1102w, 840vs (PF<sub>6</sub>), 776w, 752w, 696w, 610w, 558s and 526w;  $\delta_H$  (200 MHz, CD<sub>3</sub>CN, CHD<sub>2</sub>CN) 8.51 (2H, m), 8.35 (4H, m), 8.22 (2H, m), 7.68 (22H, br m), 7.15 (4H, m);  $\delta_P$  (202 MHz, CD<sub>3</sub>CN, 85% H<sub>3</sub>PO<sub>4</sub>) 3.3 (s), 3.3 (dd, <sup>1</sup>J(PtP) 3981 and <sup>3</sup>J(PP) 21.0), 3.3 (dd, <sup>2</sup>J(PtP) 206 and <sup>3</sup>J(PP) 21.0).

**[Pt<sub>2</sub>(μ-Ph<sub>2</sub>Ppyqn)<sub>2</sub>](PF<sub>6</sub>)<sub>2</sub> 7.** A suspension of PtCl<sub>2</sub>(PhCN)<sub>2</sub> (94 mg, 0.20 mmol) and Ph<sub>2</sub>Ppyqn (160 mg, 0.40 mmol) in CH<sub>3</sub>CN (20 cm<sup>3</sup>) was stirred for 12 h at room temperature. A white colloid-like suspension formed, to which was added Pt<sub>2</sub>(dba)<sub>3</sub>.CHCl<sub>3</sub> (120 mg, 0.10 mmol) and TlPF<sub>6</sub> (160 mg, 0.40 mmol), and the suspension stirred for 48 h. The green/black reaction mixture was filtered through glass microfibre and a large excess, *ca.* 25 cm<sup>3</sup>, of Et<sub>2</sub>O added to the filtrate. This was refrigerated overnight and the black solid that subsequently formed was removed by filtration through glass microfibre. The light red coloured filtrate was evaporated to dryness under vacuum and the resultant solid residue dissolved in CH<sub>3</sub>CN (2.5 cm<sup>3</sup>). Addition of diethyl ether (15 cm<sup>3</sup>) and standing overnight at -25°C furnished the complex in a red crystalline form (0.26 g, 44 %). (Found: C, 42.38; H, 2.66; N, 3.74. Pt<sub>2</sub>C<sub>52</sub>H<sub>38</sub>N<sub>4</sub>P<sub>4</sub>F<sub>12</sub> requires C, 42.75; H, 2.62; N, 3.83 %); λ<sub>max</sub>/nm (CH<sub>3</sub>CN) 242 (sh) (ε/dm<sup>3</sup> mol<sup>-1</sup> cm<sup>-1</sup> 57 200), 284 (40 900), 351 (sh) (21 100), 366 (sh) (19 400) and 465 (2670); ν<sub>max</sub>/cm<sup>-1</sup> (KBr) 1621w, 1592w, 1470w, 1440w, 1331w, 1104w, 842vs (PF<sub>6</sub>), 808w (sh), 698w, 610w and 558s; δ<sub>H</sub> (200 MHz, CD<sub>3</sub>CN, CHD<sub>2</sub>CN) 8.81 (2H, d), 8.53 (2H, dm), 8.35 (2H, d), 8.23 (6H, m), 7.85 (8H, m), 7.72 (2H, m) 7.48 (4H, m), 7.32 (2H, tm), 7.17 (8H, m) 6.89 (2H, tm); δ<sub>P</sub> (202 MHz, CD<sub>3</sub>CN, 85% H<sub>3</sub>PO<sub>4</sub>) 3.0 (s), 3.0 (dd, <sup>1</sup>J(PtP) 3961 and <sup>3</sup>J(PP) 21.9), 3.0 (dd, <sup>2</sup>J(PtP) 219 and <sup>3</sup>J(PP) 21.9).

**[Pt<sub>2</sub>{μ-Et(Ph)Pbpy}<sub>2</sub>](PF<sub>6</sub>)<sub>2</sub> 8.** This complex was prepared as for 7. Thus Pt(PhCN)<sub>2</sub>Cl<sub>2</sub> (260 mg, 0.55 mmol) was treated with Et(Ph)Pbpy (320 mg, 1.10 mmol) in CH<sub>3</sub>CN (30 cm<sup>3</sup>). Subsequently Pt<sub>2</sub>(dba)<sub>3</sub>.CH<sub>2</sub>Cl<sub>2</sub> (360 mg, 0.55 mmol) and TlPF<sub>6</sub> (383 mg, 1.10 mmol) were added and the suspension stirred for 48 h at room temperature. Purification procedure as described above led to the complex in a yellow crystalline form (1.00 g, 72 %). (Found: C, 34.03; H, 2.44; N, 4.29. Pt<sub>2</sub>C<sub>36</sub>H<sub>34</sub>N<sub>4</sub>P<sub>4</sub>F<sub>12</sub> requires C, 34.19; H, 2.71; N, 4.43 %); λ<sub>max</sub>/nm (CH<sub>3</sub>CN) 235 (ε/dm<sup>3</sup> mol<sup>-1</sup> cm<sup>-1</sup> 59 600), 289 (sh) (29 500), 316 (sh) (20 000), 330 (sh) (16 400), 365 (4610) and 445 (3860); ν<sub>max</sub>/cm<sup>-1</sup> (KBr) 1602w, 1450w, 1438w (sh), 1398w, 1250w, 1106w, 1034w, 840vs (PF<sub>6</sub>), 774w, 752w (sh), 696w 558s and 526w; δ<sub>H</sub> (200 MHz, CD<sub>3</sub>CN, CHD<sub>2</sub>CN) 8.50 (2H, br d), 8.30 (6H, m), 8.15 (4H, m), 8.00 (2H, br d), 7.70 (8H, m), 7.45 (2H, br t), 2.85 (4H, m, PCH<sub>2</sub>CH<sub>3</sub>), 1.36 (6H, m, PCH<sub>2</sub>CH<sub>3</sub>); δ<sub>P</sub> (202 MHz, CD<sub>3</sub>CN, 85% H<sub>3</sub>PO<sub>4</sub>) 4.8 (s), 4.8 (dd, <sup>1</sup>J(PtP) 4027 and <sup>3</sup>J(PP) 20.5), 4.8 (dd, <sup>2</sup>J(PtP) 184 and <sup>3</sup>J(PP) 20.5).

**[PtPd(μ-L)<sub>2</sub>](PF<sub>6</sub>)<sub>2</sub> (L = Ph<sub>2</sub>Pbpy 9, Ph<sub>2</sub>Ppyqn 10 and Et(Ph)Pbpy 11).** Pt(PhCN)<sub>2</sub>Cl<sub>2</sub> (47 mg, 0.10 mmol), dissolved in CH<sub>2</sub>Cl<sub>2</sub> (3 cm<sup>3</sup>), was added drop wise to a solution of L [L = Ph<sub>2</sub>Pbpy (68 mg, 0.20 mmol), Ph<sub>2</sub>Ppyqn (80 mg, 0.21 mmol) or Et(Ph)Pbpy (59 mg, 0.20 mmol)] in CH<sub>2</sub>Cl<sub>2</sub> (2 cm<sup>3</sup>) and the reaction mixture maintained at room temperature for one hour [for



Ph<sub>2</sub>Pbpy and Et(Ph)Pbpy] or three hours (for Ph<sub>2</sub>Ppyqn). The solvent was removed under reduced pressure and the residue dissolved in CH<sub>3</sub>CN (8 cm<sup>3</sup>). Pd<sub>2</sub>(dba)<sub>3</sub>.CH<sub>2</sub>Cl<sub>2</sub> (60 mg, 0.05 mmol) and TlPF<sub>6</sub> (79 mg, 0.20 mmol) in CH<sub>2</sub>Cl<sub>2</sub> were introduced and the reaction mixture stirred overnight. The mixture was filtered through glass microfibre to remove TlCl and unreacted Pd<sub>2</sub>(dba)<sub>3</sub>. The resulting red solution was reduced *in vacuo* to ca. 2 cm<sup>3</sup> and the product precipitated from the solution by the addition of excess EtOH. The product was then dissolved in acetone (2 cm<sup>3</sup>) and filtered through glass microfibre, removing a small amount of fine white precipitate. Recrystallisation of the crude product from acetone/EtOH yielded the binuclear complex as red crystals; [PtPd(μ-Ph<sub>2</sub>Pbpy)<sub>2</sub>](PF<sub>6</sub>)<sub>2</sub> **9** (0.10 g, 40 %). (Found: C, 41.78; H, 2.76; N, 4.08. PtPdC<sub>44</sub>H<sub>34</sub>N<sub>4</sub>P<sub>4</sub>F<sub>12</sub> requires C, 41.54; H, 2.69; N, 4.40 %); λ<sub>max</sub>/nm (CH<sub>3</sub>CN) 240 (ε/dm<sup>3</sup> mol<sup>-1</sup> cm<sup>-1</sup> 45 200), 295 (sh) (22 100), 324 (sh) (14 200) and 365 (sh) (3 680); ν<sub>max</sub>/cm<sup>-1</sup> (KBr) 1602w, 1485w, 1448w (sh), 1438s, 1398w, 1250w, 1158w, 1098s, 843vs (PF<sub>6</sub>), 774s, 750s, 694s, 558s, 544s (sh) and 522s; δ<sub>H</sub> (200 MHz, CD<sub>3</sub>CN, CHD<sub>2</sub>CN) 8.50 to 8.26 (9H, br m), 7.80 to 7.53 (21H, br m), 7.14 (3H, br d), 6.68 (1H, br d); δ<sub>P</sub> (202 MHz, CD<sub>3</sub>CN, 85% H<sub>3</sub>PO<sub>4</sub>) -5.6 (d, <sup>3</sup>J(PtP) 19.1, Pt-P), -5.6 (dd, <sup>1</sup>J(PtP) 3962 and <sup>3</sup>J(PtP) 19.1, Pt-P), 9.1 (d, <sup>3</sup>J(PtP) 19.1, Pd-P), 9.1 (dd, <sup>2</sup>J(PtP) 158 and <sup>3</sup>J(PtP) 19.1, Pd-P); [PtPd(μ-Ph<sub>2</sub>Ppyqn)<sub>2</sub>](PF<sub>6</sub>)<sub>2</sub> **10** (85 mg, 62 %); δ<sub>H</sub> (200 MHz, CD<sub>3</sub>CN, CHD<sub>2</sub>CN) 8.72 (4H, qm), 8.53 (2H, tm), 8.39 (2H, tm), 8.22 (2H, m), 7.79 (8H, m), 7.49 (6H, m) 7.32 (6H, m), 7.09 (4H, m), 6.91 (4H, m); δ<sub>P</sub> (80.96 MHz, CD<sub>3</sub>CN, 85% H<sub>3</sub>PO<sub>4</sub>) -7.5 (d, <sup>3</sup>J(PtP) 18.3, Pt-P), -7.5 (dd, <sup>1</sup>J(PtP) 3960 and <sup>3</sup>J(PtP) 18.3, Pt-P), 7.7 (d, <sup>3</sup>J(PtP) 18.3, Pd-P), 7.7 (dd, <sup>2</sup>J(PtP) 182 and <sup>3</sup>J(PtP) 18.3, Pd-P); [PtPd{μ-Et(Ph)Pbpy}<sub>2</sub>](PF<sub>6</sub>)<sub>2</sub> **11** (76 mg, 65 %); δ<sub>H</sub> (200 MHz, CD<sub>3</sub>CN, CHD<sub>2</sub>CN) 8.40 (4H, br m), 8.3 to 8.0 (8H, br m), 7.68 (8H, m), 7.44 (2H, m), 7.26 (2H, m), 2.81 (4H, br m, PCH<sub>2</sub>CH<sub>3</sub>), 1.67 to 1.31 (6H, br m, PCH<sub>2</sub>CH<sub>3</sub>); δ<sub>P</sub> (80.96 MHz, CD<sub>3</sub>CN, 85% H<sub>3</sub>PO<sub>4</sub>) -5.5 (d, <sup>3</sup>J(PtP) 19.7, Pt-P), -5.5 (dd, <sup>1</sup>J(PtP) 4000 and <sup>3</sup>J(PtP) 19.7, Pt-P), -4.9 (d, <sup>3</sup>J(PtP) 18.7, Pt-P), -4.9 (dd, <sup>1</sup>J(PtP) 3959 and <sup>3</sup>J(PtP) 18.7, Pt-P), 5.7 (d, <sup>3</sup>J(PtP) 19.7, Pd-P), 5.7 (dd, <sup>2</sup>J(PtP) 133 and <sup>3</sup>J(PtP) 19.7, Pd-P), 6.8 (d, <sup>3</sup>J(PtP) 18.7, Pd-P), 6.8 (dd, <sup>2</sup>J(PtP) 126 and <sup>3</sup>J(PtP) 18.7, Pd-P).

**X-ray Data Collection and Structure Solution for 3.** Yellow, hexagonal crystals of **3** were grown by the careful 'layering' of Et<sub>2</sub>O over an acetonitrile solution of the complex in 5 mm diameter schlenck tubes. Complete diffusion of the two solvent layers into one another brought about the crystallisation of the complex. Details of the crystal data, data collection and structure refinement of **3** are summarized in Table 4.7. The complete crystallographic data of **3** is presented in Appendix B. Supporting Information.

**Table 4.7.** Crystal data and structure refinement parameters for [Pd<sub>2</sub>(μ-Ph<sub>2</sub>Pbpy)<sub>2</sub>](BF<sub>4</sub>)<sub>2</sub> **3**.

Formula	Pd <sub>2</sub> C <sub>44</sub> H <sub>34</sub> B <sub>2</sub> F <sub>8</sub> N <sub>4</sub> P <sub>2</sub>
FW/amu	1067.11
<i>a</i> /Å	8.962(3)
<i>b</i> /Å	11.155(4)
<i>c</i> /Å	12.605(5)
$\alpha$ /°	66.16(3)
$\beta$ /°	79.95(3)
$\gamma$ /°	82.53(3)
<i>U</i> /Å <sup>3</sup>	1132.5(7)
Crystal system, space group	Triclinic, P $\bar{1}$
<i>Z</i>	1
<i>D</i> <sub>c</sub> /g cm <sup>3</sup>	1.565
F(000)	530
$\mu$ /mm <sup>-1</sup>	0.933
Power and current settings	55 kV, 25 mA
Increment/°	0.48
Crystal dimensions/mm	0.35 x 0.34 x 0.19
$\lambda$ (Mo K $\alpha$ )/Å	0.71069
Temperature/K	293(2)
$\theta$ range for collected data/°	2.00 to 22.97
Index ranges	-9 ≤ <i>h</i> ≤ 9 -11 ≤ <i>k</i> ≤ 12 -1 ≤ <i>l</i> ≤ 13
Total reflections collected	3646
Completeness to 2 $\theta$	100.0
Absorption correction	Semi-empirical
Relative transmission coefficients (I)	0.9650 and 0.9254
Unique data	3138 ( <i>R</i> <sub>int</sub> = 0.0251)
Unique observed data [ <i>I</i> > 2 $\sigma$ ( <i>I</i> )]	2389
Refinement method	Full-matrix least-squares on <i>F</i> <sup>2</sup>
Data / restraints / parameters	3138 / 0 / 281
Goodness-of-fit (based on <i>F</i> <sup>2</sup> )	1.159
Extinction coefficient	none
Max( $\Delta\rho$ )/e.Å <sup>-3</sup>	4.408
Min( $\Delta\rho$ )/e.Å <sup>-3</sup>	-0.545
Final <i>R</i> indices [ <i>I</i> > 2 $\sigma$ ( <i>I</i> )]	<i>R</i> <sub>1</sub> = 0.0852, <i>wR</i> <sub>2</sub> = 0.2487
<i>R</i> indices (all data)	<i>R</i> <sub>1</sub> = 0.1195, <i>wR</i> <sub>2</sub> = 0.2929

### 5.1. Introduction

As has been recounted in Chapter One, Section 1.3.3.(viii), electrodes modified by  $[\text{Ru}(\text{L})(\text{CO})_2]_n$  ( $\text{L} = \alpha$ -diimine) polymers are highly active catalytic systems for the selective electroreduction of  $\text{CO}_2$  in hydro-organic and pure aqueous electrolytes.<sup>42</sup> To gain insight into the mechanism of the formation of the  $\text{Ru}(0)$  polymer the study of related dimeric  $\text{Ru}(\text{I})$  polypyridyl complexes has been undertaken. The electrochemical properties of *trans*(Cl)- $[\text{Ru}_2(\text{bpy})_2(\text{CO})_4\text{Cl}_2]$  imply that the electropolymerisation of  $[\text{Ru}(\text{bpy})(\text{CO})_2\text{Cl}_2]$  to  $[\text{Ru}(\text{bpy})(\text{CO})_2]_n$  must proceed via the initial formation of a  $\text{Ru}(\text{I})$  intermediate, rather than through the direct reduction of  $\text{Ru}(\text{II})$  to  $\text{Ru}(0)$ .<sup>38</sup> The one-electron reduction of *trans*(Cl)- $[\text{Ru}_2(\text{bpy})_2(\text{CO})_4\text{Cl}_2]$  in DMSO leads to what is believed to be the soluble tetramer  $[\text{Ru}_4(\text{bpy})_4(\text{CO})_8\text{Cl}_2]$ , which is further reduced to the polymer  $[\text{Ru}(\text{bpy})(\text{CO})_2]_n$ .<sup>38</sup> On the other hand the  $\text{Ru}(\text{I})$  complex  $[\text{Ru}_2(\text{bpy})_2(\text{CO})_4\{\text{C}(\text{O})\text{OCH}_3\}_2]$ , which is formed by the one-electron reduction of  $[\text{Ru}(\text{bpy})(\text{CO})_2(\text{C}(\text{O})\text{OCH}_3)\text{Cl}]$  with the concomitant loss of  $\text{Cl}^-$ , does not polymerise upon its reduction.<sup>38,43</sup> Here further oligomerisation of the dimer under reducing conditions is prevented by the presence of the methoxycarbonyl poor leaving group. The air sensitive and insoluble polymeric nature of  $[\text{Ru}(\text{bpy})(\text{CO})_2]_n$  precludes its full structural characterisation. In addition, the poor solubility of  $[\text{Ru}_2(\text{bpy})_2(\text{CO})_4\text{Cl}_2]$ <sup>154</sup> prevented the study of its electrochemistry in common organic solvents. It was therefore decided to investigate the dicationic complex  $[\text{Ru}_2(\text{bpy})_2(\text{CO})_4(\text{CH}_3\text{CN})_2](\text{PF}_6)_2$  **12**, which represents both a model of the polymer in its simplest form and an intermediate in its formation. This complex is also a potentially interesting dinuclear electrocatalyst in its own right. The synthesis, crystal structure and electrochemical properties of **12** are reported here. The electrocatalytic activity towards  $\text{CO}_2$  reduction of the polymer obtained by the two-electron reduction of **12** is also reported.

### 5.2. Results and Discussion

#### 5.2.1. Synthesis and Characterisation of $[\text{Ru}_2(\text{bpy})_2(\text{CO})_4(\text{CH}_3\text{CN})_2](\text{PF}_6)_2$ **12**

Reaction of  $[\text{Ru}_2(\text{CO})_4(\text{CH}_3\text{CN})_6](\text{PF}_6)_2$ <sup>155</sup> with 2.5 equiv. of bpy at room temperature (rt) for 2 h in acetonitrile, followed by precipitation of the product by the addition of diethyl ether, led to the diruthenium(I) complex **12** (Figure 5.1) in a 65 % yield.

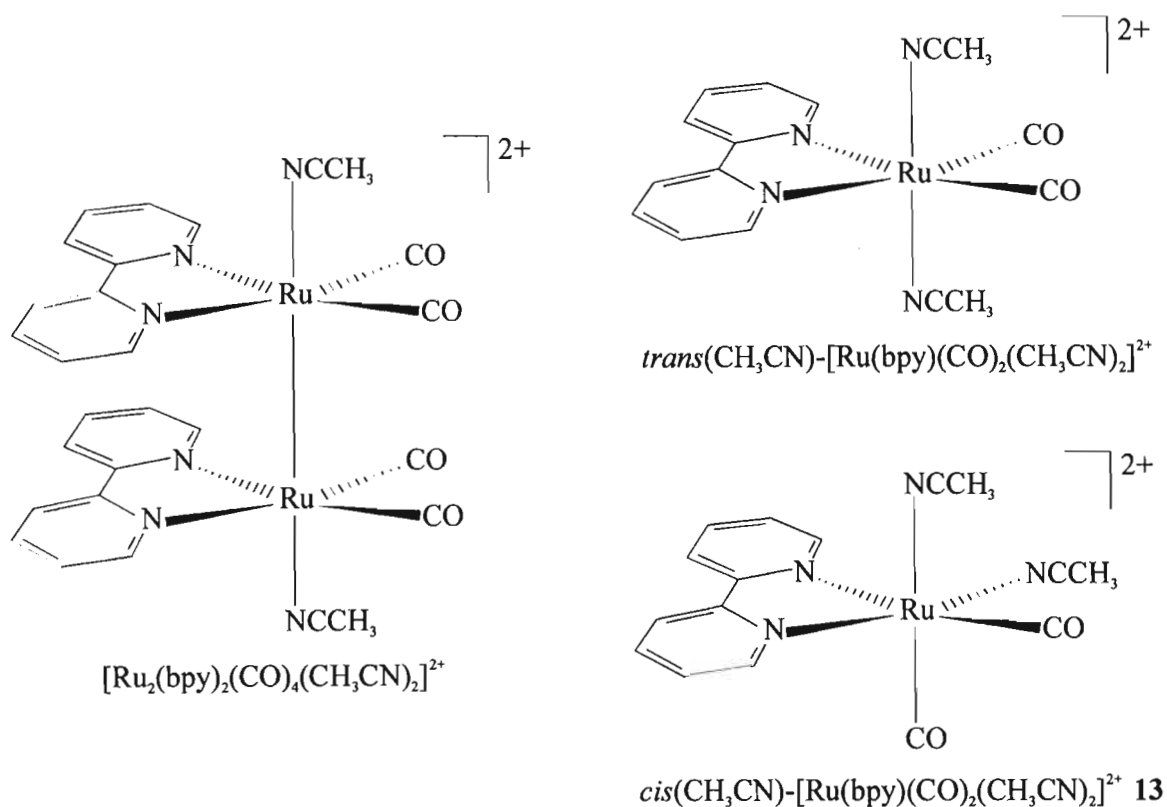


**Figure 5.1.** The structural formula of the dication of  $[\text{Ru}_2(\text{bpy})_2(\text{CO})_4(\text{CH}_3\text{CN})_2](\text{PF}_6)_2$  **12**, and  $\text{cis}(\text{CH}_3\text{CN})\text{-}[\text{Ru}(\text{bpy})(\text{CO})_2(\text{CH}_3\text{CN})_2]^{2+}$  **13** and  $\text{trans}(\text{CH}_3\text{CN})\text{-}[\text{Ru}(\text{bpy})(\text{CO})_2(\text{CH}_3\text{CN})_2]^{2+}$ .

The FT-IR absorption spectrum of **12**, recorded in the solid state, displays three strong absorption bands at 2044, 2003 and 1969  $\text{cm}^{-1}$  and an associated shoulder at 1948  $\text{cm}^{-1}$  in the terminal CO region. This pattern in the CO stretching region closely resembles that of a large number of diruthenium(I) compounds of the type  $[\text{Ru}_2(\text{CO})_4\text{L}_6]^{2+}$ .<sup>154,156,157</sup> In these complexes the equatorial coordinated carbonyl ligands occupy *cis* positions at each octahedral ruthenium centre and adopt either a *cis* or *trans*-staggered conformation relative to one another about the Ru–Ru bond.

The molecular structure of **12** together with its atomic numbering Scheme is depicted in Figure 5.2(a) while selected bond distances and angles are given in Table 5.1.<sup>†</sup> The compound exists in the crystal as discrete cations and hexafluorophosphate anions, together with acetonitrile solvates, there being no unusual intermolecular contact distances between them. An approximately octahedral geometry is described about each ruthenium atom by a formal metal-metal bond, the donor atoms of the axial acetonitrile and the equatorial carbonyl and bpy ligands.

<sup>†</sup> The crystal growth and data collection for this structure solution were performed by Dr. F. Southway at Natal University, Pietermaritzburg. This contribution is fully acknowledged by the author.

The dication  $12 \cdot (\text{CH}_3\text{CN})_2$  possesses a crystallographically imposed two-fold rotation axis that bisects the Ru–Ru bond. In comparison to the 2.829(2) Å Ru–Ru bond length observed for  $12 \cdot (\text{CH}_3\text{CN})_2$ , those measured for  $[\text{Ru}_2(\text{bpy})_2(\text{CO})_4\text{Cl}_2]$  (2.860 Å)<sup>154</sup> and  $[\text{Ru}_2(\text{dmbpy})_2(\text{CO})_4\text{Cl}_2]$  (dmbpy = 4,4'-dimethyl 2,2'-bipyridine) (2.854 Å)<sup>158</sup> are noticeably longer. This is a consequence of the effect on the metal-metal bond of the relatively high *trans*-influence of the chloride ligand present in the latter examples.

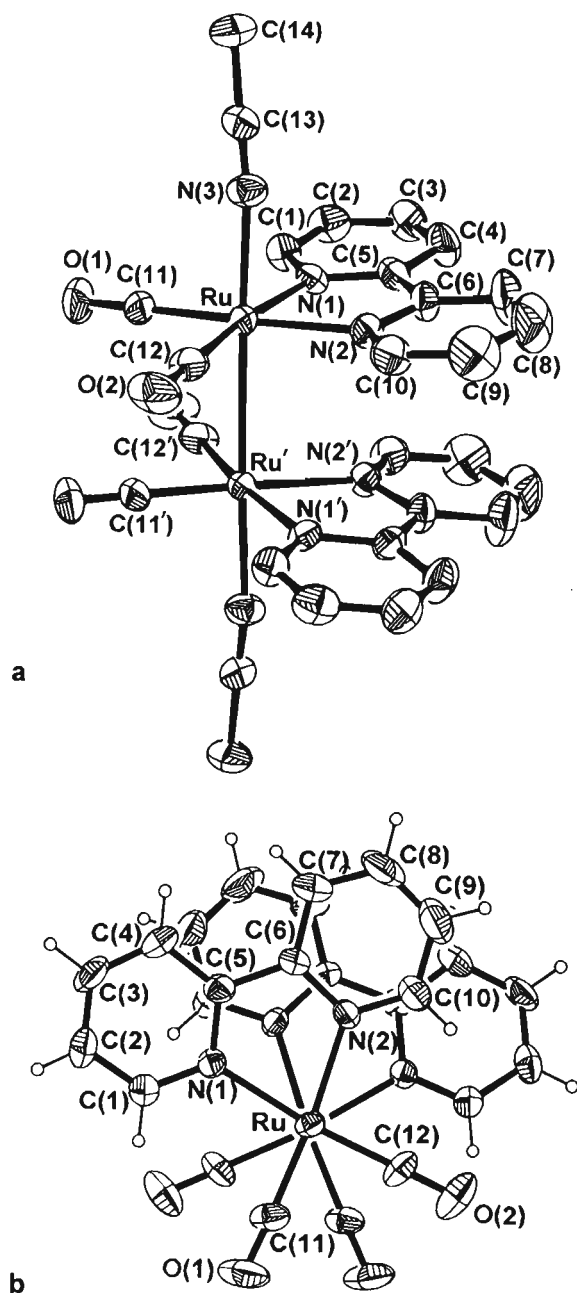


**Figure 5.2.** The molecular structure and atomic numbering scheme of the dication of  $12 \cdot (\text{CH}_3\text{CN})_2$ ; (a) view showing the equatorial substituents; (b) view down the Ru–Ru bond axis. The atoms are represented by their thermal ellipsoids at a 25% probability level.

**Table 5.1.** Selected interatomic distances (Å) and angles (°) for  $[\text{Ru}_2(\text{bpy})_2(\text{CO})_4(\text{CH}_3\text{CN})_2](\text{PF}_6)_2 \cdot 12 \cdot (\text{CH}_3\text{CN})_2$ .<sup>a</sup>

Ru–Ru <sup>b</sup>	2.829(2)	Ru–N(2)	2.110(8)
Ru–C(11)	1.86(2)	Ru–N(3)	2.145(9)
Ru–C(12)	1.86(2)	O(1)–C(11)	1.13(2)
Ru–N(1)	2.107(8)	O(2)–C(12)	1.15(2)
C(11)–Ru–Ru <sup>b</sup>	87.2(4)	N(1)–Ru–N(2)	77.0(3)
C(12)–Ru–Ru <sup>b</sup>	85.9(3)	N(1)–Ru–N(3)	85.7(3)
N(1)–Ru–Ru <sup>b</sup>	92.1(2)	N(2)–Ru–N(3)	86.0(3)
N(2)–Ru–Ru <sup>b</sup>	92.9(2)	C(12)–Ru–C(11)	87.3(6)
N(3)–Ru–Ru <sup>b</sup>	177.7(2)	C(13)–N(3)–Ru	172(1)
C(11)–Ru–N(1)	98.2(4)	C(1)–N(1)–Ru	127.2(7)
C(12)–Ru–N(1)	174.0(4)	C(5)–N(1)–Ru	115.7(6)
C(11)–Ru–N(2)	175.2(4)	C(6)–N(2)–Ru	116.3(6)
C(12)–Ru–N(2)	97.5(5)	C(10)–N(2)–Ru	125.4(8)
C(11)–Ru–N(3)	93.7(5)	O(1)–C(11)–Ru	178(2)
C(12)–Ru–N(3)	96.2(4)	O(2)–C(12)–Ru	180(2)

<sup>a</sup> The esd's of the least significant digits are given in parentheses. <sup>b</sup> Symmetry transformation used to generate equivalent atoms:  $-x+1, y, -z+3/2$ .

Figure 5.2(b) illustrates the conformation of the cation of  $12 \cdot (\text{CH}_3\text{CN})_2$ , wherein the equatorial ligands adopt what can be described as a *syn*-staggered conformation<sup>†</sup> relative to one another about the Ru–Ru bond. This is in contrast to the molecular structure of the closely related complex  $[\text{Ru}_2(\text{bpy})_2(\text{CO})_4\text{Cl}_2]$  reported by T.A. Pakkanen *et al.*<sup>154</sup> In the crystal structure of the latter complex two rotamers are observed; one with the equatorial bpy and CO ligands describing an *anti*-staggered arrangement and the other an *anti*-eclipsed arrangement about the Ru–Ru bond. In the diruthenium complexes axially substituted by phosphine ligands,  $[\text{Ru}_2(\text{CO})_4(\text{CH}_3\text{CN})_4(\text{L})_2](\text{X})_2$  [ $\text{L} = \text{PPh}_3$ ,  $\text{X} = \text{PF}_6$ ;  $\text{L} = \text{PPh}_2(\text{allyl})$ ,  $\text{X} = \text{BF}_4$ ], described by Klemperer<sup>155</sup> and Shiu,<sup>159</sup> the equatorial acetonitrile and CO groups occupy *cis* positions at each ruthenium centre and adopt a symmetrical *anti*-staggered conformation relative to one another about the Ru–Ru bond. That this strong precedent of an *anti* arrangement of the equatorial ligands is not preserved in the conformation of **12** is attributable to an intramolecular  $\pi$ - $\pi$  interaction between the two bpy groups. This stacking of the bpy rings, given the cylindrical

<sup>†</sup> The *syn/anti* notation is adopted to differentiate between the further two possible conformations of each staggered or eclipsed rotamer. *Syn* describes the conformation in which like equatorial ligands are on the same side of the molecule when it is viewed down the Ru–Ru axis.

symmetry of the M–M bond, may be the dominant electronic factor in the formation of this geometry. Indeed such an interaction would favour the *syn* arrangement of the equatorial ligands, where the orientation of the bpy ligands relative to one another will allow a favourable overlap of their molecular orbitals. Clearly this argument does not appear to apply to the conformation of  $[\text{Ru}_2(\text{bpy})_2(\text{CO})_4\text{Cl}_2]$ . However, as T.A. Pakkanen *et al.*<sup>154</sup> have noted, this complex is barely soluble in contrast to **12**, crystals of which can be grown by slow vapour diffusion of diethyl ether into an acetonitrile solution of the dimer **12**. This difference in the method of crystallization would permit the most energetically favourable conformation to be attained, *viz.* the *syn*-staggered conformation of  $[\text{Ru}_2(\text{bpy})_2(\text{CO})_4(\text{CH}_3\text{CN})_2]^{2+}$ . Significantly the conformation assumed by  $[\text{Ru}_2(\text{dmbpy})_2(\text{CO})_4\text{Cl}_2]$ ,<sup>158</sup> is the same as that observed for **12**. The exclusive formation of a staggered rotamer in this complex was attributed to steric and electronic interactions between the bulky methyl substituents of the bpy rings and the opposing carbonyl ligands.<sup>158</sup>

Evidence for the conformation of **12** in solution is provided by  $^1\text{H}$  NMR spectral data.  $^1\text{H}$  NMR spectra of **12** recorded in  $\text{CD}_2\text{Cl}_2$  or  $\text{CD}_3\text{CN}$  at room temperature exhibit the same pattern of a single resonance for the acetonitrile ligand methyl protons. The bpy signals displayed in the  $^1\text{H}$  NMR spectra of **12** show that the bpy ligands chelate in a symmetrical environment with only four sets of aromatic proton resonances being observed.<sup>43</sup> In addition the  $^{13}\text{C}$  NMR spectrum recorded at  $-80^\circ\text{C}$  in  $\text{CD}_2\text{Cl}_2$  exhibits single resonances for the acetonitrile methyl and nitrile carbons at 3.05 and 119.26 ppm respectively. The carbons of the carbonyl ligands are evident in this spectrum as a single resonance at 201.25 ppm.

A comparison between the chemical shifts of the bpy protons in **12** and three ruthenium(II) mononuclear analogues,<sup>†</sup> all of which possess the same geometrical arrangement of bpy and carbonyl ligands about the metal centre, is made in Table 5.2. While protons  $\text{H}_{4,4'}$  and  $\text{H}_{5,5'}$  do not exhibit a large difference in chemical shift across the series of complexes,  $\text{H}_{3,3'}$  and  $\text{H}_{6,6'}$  display noticeably higher field resonances in the dinuclear complex. The examination of Figure 5.2(b) shows that in a *syn*-staggered conformation protons  $\text{H}_{3,3'}$  and  $\text{H}_{6,6'}$  will be in closest proximity to the anisotropic magnetic field of the second bpy ligand. Protons  $\text{H}_{5,5'}$  and to the greatest extent  $\text{H}_{4,4'}$  will be located more to the periphery of the bpy shielding cone. The pattern observed with respect to the extent to which the individual proton resonances of **12** are shifted upfield relative to those of the mononuclear complexes is thus in keeping with the predominance of a *syn*-staggered conformation of **12** in solution and with the oxidation state of the metal. One

---

<sup>†</sup> To our knowledge no NMR spectra of Ru(I) dinuclear analogues have been published yet.

would anticipate that at lower temperatures rotation about Ru–Ru bond would become more restricted and the anisotropic effect more pronounced. The chemical shifts of H<sub>3,3'</sub> and H<sub>6,6'</sub> in the spectrum of **12** recorded in CD<sub>2</sub>Cl<sub>2</sub> at –80 °C thus display a slightly more marked upfield shift, with these resonances being observed at 7.91 and 8.27 ppm respectively, in comparison to those in the spectrum recorded at rt. The chemical shifts of H<sub>5,5'</sub> and H<sub>4,4'</sub> are affected to a lesser extent.

**Table 5.2.** Comparison between the proton chemical shifts of bpy in [Ru<sub>2</sub>(bpy)<sub>2</sub>(CO)<sub>4</sub>(CH<sub>3</sub>CN)<sub>2</sub>](PF<sub>6</sub>)<sub>2</sub> **12** and related ruthenium(II) mononuclear analogues.<sup>a</sup>

	$\delta/\text{ppm}^b$			
	H <sub>3,3'</sub>	H <sub>4,4'</sub>	H <sub>5,5'</sub>	H <sub>6,6'</sub>
<b>12</b>	8.00	8.11	7.49	8.42
<b>13</b>	8.39 (0.39)	8.23 (0.12)	7.70 (0.21)	8.92 (0.50)
<i>trans</i> (Cl)-[Ru(bpy)(CO) <sub>2</sub> Cl <sub>2</sub> ] <sup>c</sup>	8.47 (0.47)	8.24 (0.13)	7.74 (0.25)	9.17 (0.75)
<i>cis</i> (CO)-[Ru(bpy)(CO) <sub>2</sub> {C(O)OCH <sub>3</sub> }Cl] <sup>c</sup>	8.40 (0.40)	8.18 (0.07)	7.64 (0.15)	8.96 (0.54)

<sup>a</sup> Recorded in CD<sub>3</sub>CN at rt. <sup>b</sup> The change in chemical shift relative to that of **12** is given in brackets Given in reference 44.

## 5.2.2. Electrochemical Behaviour of [Ru<sub>2</sub>(bpy)<sub>2</sub>(CO)<sub>4</sub>(CH<sub>3</sub>CN)<sub>2</sub>](PF<sub>6</sub>)<sub>2</sub> **12**

### 5.2.2.(i) Oxidation

The CV of **12** reveals that the complex is irreversibly oxidised at E<sub>pc</sub> = 0.98 V (Figure 5.3).

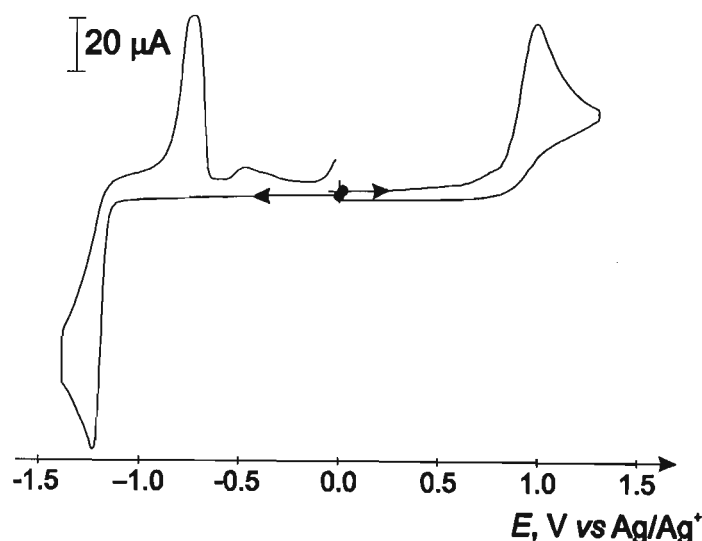
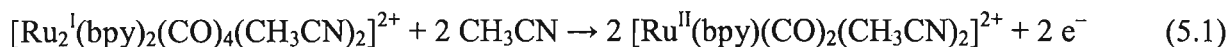


**Figure 5.3.** CV of [Ru<sub>2</sub>(bpy)<sub>2</sub>(CO)<sub>4</sub>(CH<sub>3</sub>CN)<sub>2</sub>](PF<sub>6</sub>)<sub>2</sub> **12** 1.0 mM in CH<sub>3</sub>CN + 0.1 M TBAP. (Pt electrode, r = 2.5 mm;  $\nu$  = 100 mVs<sup>-1</sup>).



Exhaustive oxidation at 1.10 V requires the exchange of two electrons per mole of dimer and leads to the Ru(II) monomer complex *cis*(CH<sub>3</sub>CN)-[Ru(bpy)(CO)<sub>2</sub>(CH<sub>3</sub>CN)<sub>2</sub>]<sup>2+</sup> **13**, formed from the oxidatively induced breakage of the metal-metal bond and coordination of CH<sub>3</sub>CN with an 80% electrical yield (reaction 5.1).



This Ru(II) complex was characterised by cyclic voltammetry and *in situ* FT-IR, UV-vis and <sup>1</sup>H NMR measurements described below. All characterisations are consistent with the unexpected and novel *cis*(CH<sub>3</sub>CN)-[Ru(bpy)(CO)<sub>2</sub>(CH<sub>3</sub>CN)<sub>2</sub>]<sup>2+</sup> **13** structural isomer schematically represented in Figure 5.1. This shows that a structural rearrangement takes place during the associated Ru–Ru bond breaking and acetonitrile coordination. While the structural isomer *trans*(CH<sub>3</sub>CN)-[Ru(bpy)(CO)<sub>2</sub>(CH<sub>3</sub>CN)<sub>2</sub>]<sup>2+</sup> has been described and well characterised,<sup>39,160</sup> it appears that only one publication mentions the *cis*(CH<sub>3</sub>CN) isomer.<sup>160</sup> Unfortunately, attempts to isolate this complex, either by extraction of the oxidation product of **12** from the electrolyte or through classical chemical synthesis, failed. Therefore it was not possible to compare the properties of the electrochemically synthesized *cis*(CH<sub>3</sub>CN) complex **13** with those of a chemically prepared and isolated sample.

In keeping with what is observed for *trans*(CH<sub>3</sub>CN)-[Ru(bpy)(CO)<sub>2</sub>(CH<sub>3</sub>CN)<sub>2</sub>]<sup>2+</sup>, the absorption spectrum recorded after oxidation of **12** exhibits no absorption bands in the visible region.<sup>37</sup>

The IR absorption spectrum of **13** exhibits two intense carbonyl absorption bands at 2117 and 2063 cm<sup>-1</sup>. The form and wavenumbers of these absorption bands are similar to those of *trans*(CH<sub>3</sub>CN)-[Ru(bpy)(CO)<sub>2</sub>(CH<sub>3</sub>CN)<sub>2</sub>]<sup>2+</sup>.<sup>160</sup> As is observed for both [Ru(bpy)(CO)<sub>2</sub>Cl<sub>2</sub>] isomers,<sup>38,43</sup> no striking difference is seen between the FT-IR properties of *trans*- and *cis*(CH<sub>3</sub>CN)-[Ru(bpy)(CO)<sub>2</sub>(CH<sub>3</sub>CN)<sub>2</sub>]<sup>2+</sup>. In comparison to the solution IR absorption spectrum of the initial dimer **12**, which showed absorption bands at 2021, 1985 (shoulder), 1978, 1944, and 1927 (shoulder) cm<sup>-1</sup>, that of **13** displays a simplified absorption envelope in the terminal carbonyl stretching region and a shift of the ν(CO) frequencies towards higher wavenumbers. This shift, which is due to a decrease of the electronic density on the metal, is in accordance with the shift observed previously between the ν(CO) frequencies of the dimer [Ru<sub>2</sub>(bpy)<sub>2</sub>(CO)<sub>4</sub>Cl<sub>2</sub>] and the monomer [Ru(bpy)(CO)<sub>2</sub>Cl<sub>2</sub>].<sup>43,154</sup>

The oxidation of **12** in a deuterated electrolyte (CD<sub>3</sub>CN + LiClO<sub>4</sub>) permitted an *in situ* <sup>1</sup>H NMR characterization of the oxidation product. The assignment of the aromatic

resonances of complexes **12**, **13** and  $\text{trans}(\text{CH}_3\text{CN})\text{-}[\text{Ru}(\text{bpy})(\text{CO})_2(\text{CH}_3\text{CN})_2]^{2+}$  are shown in Figure 5.4.

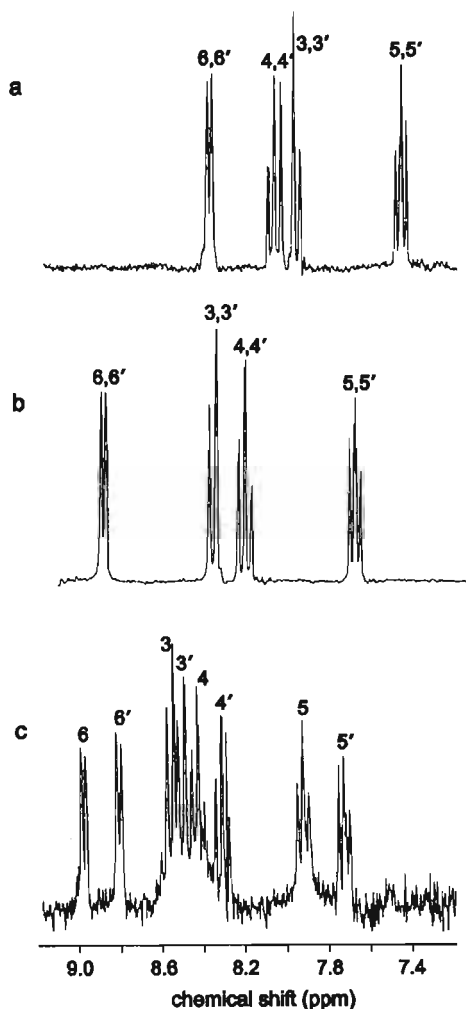


**Figure 5.4.** Aromatic region of  $^1\text{H}$  NMR spectra in  $\text{CD}_3\text{CN}$  of (a)  $[\text{Ru}_2(\text{bpy})_2(\text{CO})_4(\text{CH}_3\text{CN})_2](\text{PF}_6)_2$  **12**, (b)  $\text{trans}(\text{CH}_3\text{CN})\text{-}[\text{Ru}(\text{bpy})(\text{CO})_2(\text{CH}_3\text{CN})_2]^{2+}$  and (c) **13** in the presence of electrolyte.

The aromatic region of the  $^1\text{H}$  NMR spectrum of **13** contrasts those of the starting dimer **12** and the mononuclear isomer  $\text{trans}(\text{CH}_3\text{CN})\text{-}[\text{Ru}(\text{bpy})(\text{CO})_2(\text{CH}_3\text{CN})_2]^{2+}$ . The resonances of the bpy ligand protons between 7.2 and 9.2 ppm change from four {**12** and  $\text{trans}(\text{CH}_3\text{CN})\text{-}[\text{Ru}(\text{bpy})(\text{CO})_2(\text{CH}_3\text{CN})_2]^{2+}$ } to eight (**13**) well resolved signals, each integrating for one proton. This latter pattern reflects a non-symmetrical arrangement of ligands about the Ru(II) centre in the equatorial plane of the bpy ligand.<sup>38</sup> It allows a *cis*( $\text{CH}_3\text{CN}$ ) conformation to be unequivocally assigned to **13**.

The synthesis of an original sample of **13** from *cis*(Cl)-[Ru(bpy)(CO)<sub>2</sub>Cl<sub>2</sub>] using a procedure similar to that of Deacon *et al.*<sup>160</sup> was unsuccessful. However, during these fruitless synthetic attempts it was possible to characterise the intermediate monosubstituted acetonitrile complex *cis*(CO)-[Ru(bpy)(CO)<sub>2</sub>(CH<sub>3</sub>CN)Cl](PF<sub>6</sub>), as well as a mixture of it with the desired compound **13**. (Details of the synthetic conditions and characterisations of these reactions are given in the experimental section). The FT-IR, <sup>1</sup>H NMR and electrochemical properties of **13** in the crude product agree with those of the complex resulting from the electrochemical oxidation of **12**.

An indirect proof of the nature of **13** was obtained by adding a small excess of Cl<sup>-</sup> anions [2.2 equiv. per Ru(II)] to the electrolyte solution. This afforded the corresponding *cis*(Cl)-[Ru(bpy)(CO)<sub>2</sub>Cl<sub>2</sub>] complex, the complete coordination of chloride being reached after 15 h stirring at rt [FT-IR: ν(CO) 2067, 2001 cm<sup>-1</sup>; E<sub>p</sub>(Ru(II)/Ru(0)) = -1.54 V, E<sub>1/2</sub>(Ru(III)/Ru(II)) = 1.56 V] with a 90% yield. It should be noted that a monochloride complex is formed intermediately during this chemical reaction [ν(CO) = 2093 and 2035 cm<sup>-1</sup>; E<sub>p</sub>(Ru(II)/Ru(0)) = -1.30 V].

The electrochemical behaviour of **13** is essentially that of the *trans*(CH<sub>3</sub>CN)-[Ru(bpy)(CO)<sub>2</sub>(CH<sub>3</sub>CN)<sub>2</sub>]<sup>2+</sup> complex.<sup>39</sup> As illustrated in Figure 5.5 it is irreversibly reduced at the first reduction peak [E<sub>pc</sub> = -1.18 V, Ru(II)/Ru(0)], but is not electroactive between 0 and 1.30 V. The height of the reduction peak in comparison to that of the dimer **12** (Figure 5.3) is in agreement with a mononuclear Ru(II) structure. This irreversible Ru(II)/Ru(0) redox couple is shifted positively (+0.04 V) versus that of the *trans*(CH<sub>3</sub>CN)- isomer. The small change in E<sub>pc</sub> values is in agreement with that observed between the isomers of the corresponding *bis* chloride complex.<sup>38</sup> Clearly the reduction process is not significantly influenced by the stereochemistry of the complex and must be located on the bpy ligand.

Electroactive [Ru(bpy)(CO)<sub>2</sub>]<sub>n</sub> polymer films could be obtained from **13** by cycling the potential or by potentiostating the working electrode in a solution of the electrosynthesised complex. The resulting polymer film possesses exactly the same electroactivity and physico-chemical properties as those obtained from other bpy *bis* carbonyl Ru(II) precursor complexes. Thus, as for both [Ru(bpy)(CO)<sub>2</sub>Cl<sub>2</sub>] isomers,<sup>38</sup> the two-electron reduction of [Ru(bpy)(CO)<sub>2</sub>(CH<sub>3</sub>CN)<sub>2</sub>]<sup>2+</sup> leads to the formation of the same organometallic polymer irrespective of the initial monomer stereochemistry.

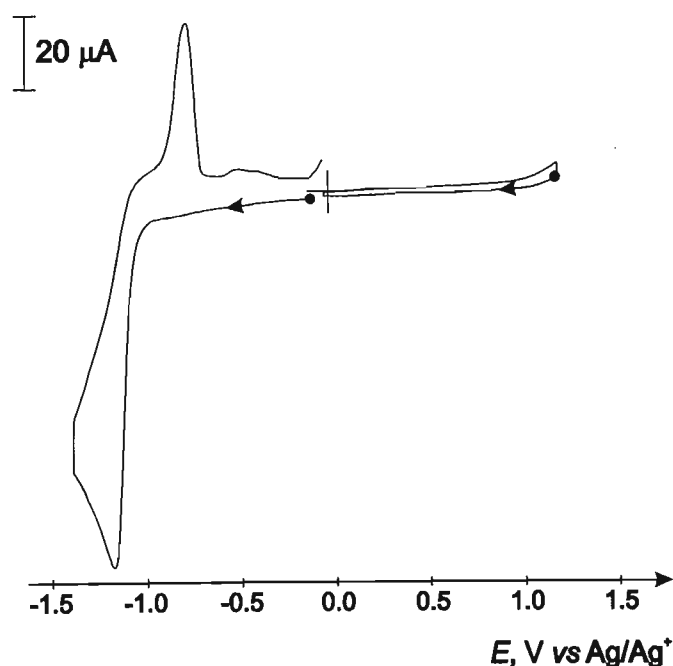


**Figure 5.5.** CV of **13** 1.0 mM in CH<sub>3</sub>CN + 0.1 M TBAP, formed by exhaustive oxidation at 1.1 V of **12**, between 0 and -1.4 V. (Pt electrode, r = 2.5 mm;  $\nu = 100 \text{ mVs}^{-1}$ ).

### 5.2.2.(ii) Reduction

In the cathodic CV of **12** (Figure 5.3) an irreversible reduction at -1.24 V with a corresponding return anodic peak at 0.73 V are seen. The shape of the CV is characteristic of an electroprecipitation-redissolution phenomenon due to the polymer film formation described by the overall reaction 5.2.



It is noted that the potential of this cathodic peak is the same as that of *trans*(CH<sub>3</sub>CN)-[Ru(bpy)(CO)<sub>2</sub>(CH<sub>3</sub>CN)<sub>2</sub>]<sup>2+</sup>.<sup>39</sup> It is shifted positively (+0.22 V) compared to that of the corresponding bis chloride dimer recorded in DMSO + 0.1 M TBAP,<sup>38</sup> in agreement with the cationic nature of the complex. By analogy with the mechanism of the polymerisation process previously proposed and in part demonstrated for *trans*(Cl)-[Ru(bpy)(CO)<sub>2</sub>Cl<sub>2</sub>],<sup>38</sup> it is suggested that the electropolymerisation of **12** proceeds via propagation reactions initiated by the one-electron bpy ligand reduction and CH<sub>3</sub>CN ligand decoordination.

Reductive electropolymerisation of the dimer **12** to [Ru(bpy)(CO)<sub>2</sub>]<sub>n</sub> can be accomplished by iterative potential cycles (Figure 5.6) or by applying a constant potential ( $E_{\text{app}} = -1.30 \text{ V}$ ). Both techniques generate a strongly adherent polymer film on the working electrode surface. The growth of the polymer is shown in Figure 5.6(b), the electroactive film becoming

progressively thicker with each successive potential scan between  $-0.90$  and  $-1.80$  V. Two clear redox systems emerge at  $E_{1/2} = -0.98$  V and  $E_{1/2} = -1.51$  V and increase in size continuously.

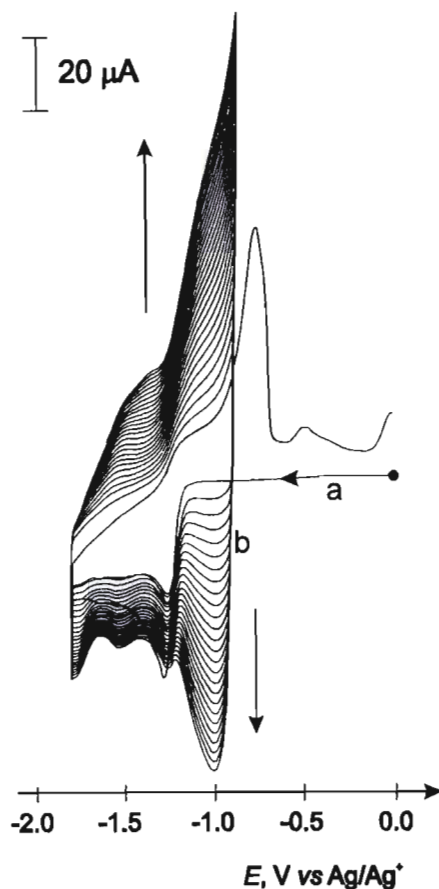
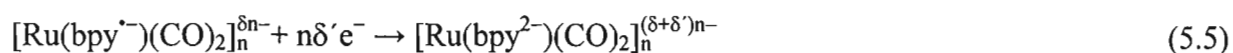
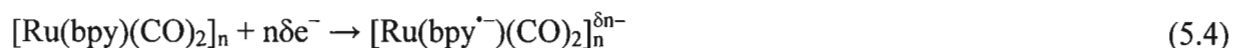
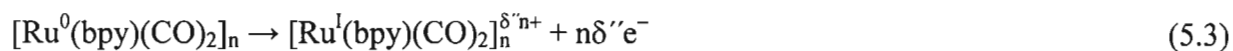


**Figure 5.6.** Repetitive CVs in  $\text{CH}_3\text{CN} + 0.1$  M TBAP of 1 mM of  $[\text{Ru}_2(\text{bpy})_2(\text{CO})_4(\text{CH}_3\text{CN})_2](\text{PF}_6)_2$  **12**; (a) 1st scan and (b) 2nd to the 26th successive scans between  $-0.9$  and  $-1.8$  V. (Pt electrode,  $r = 2.5$  mm;  $\nu = 100$   $\text{mVs}^{-1}$ ).

When the resulting modified electrode is transferred to a clean electrolyte both redox systems at  $E_{1/2} = -0.98$  V and  $E_{1/2} = -1.51$  V persist, attesting to the electrochemical stability of the film [Figure 5.7(a)]. As has been described by Deronzier *et al.*,<sup>44</sup> the redox process at  $E_{1/2} = -0.98$  V corresponds to the partial oxidation of the ruthenium centres in the film (Equation 5.3). The redox couple at  $E_{1/2} = -1.51$  V arises from the first of two consecutive one-electron bpy based reductions (Equations 5.4 and 5.5). The doping levels  $\delta$ ,  $\delta'$  and  $\delta''$  represent that restricted part of the total polymer that is electroactive.



At potentials higher than  $-0.90$  V the polymer is irreversibly oxidised ( $E_{pa} = -0.70$  V), subsequently detaching from the electrode surface to form soluble oligomeric species in solution. As is shown in Figure 5.6(b), consecutive scans beyond the oxidation-desorption potential bring about the rapid and complete desorption of the film.

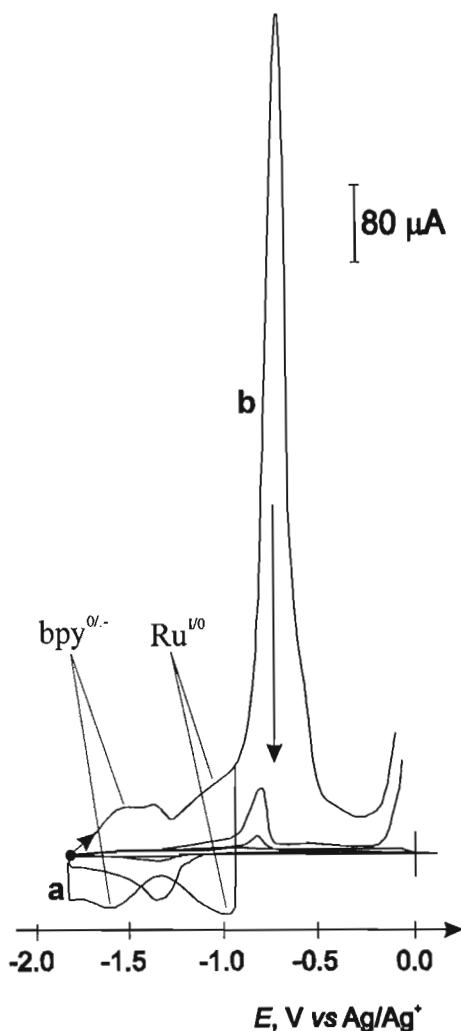
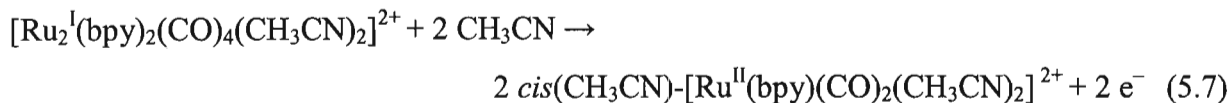
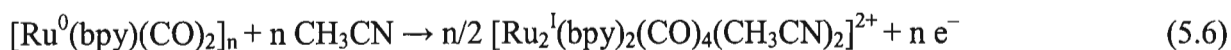


**Figure 5.7.** CVs of  $[\text{Ru}(\text{bpy})(\text{CO})_2]_n$  deposited on a Pt electrode in  $\text{CH}_3\text{CN} + 0.1$  M TBAP; (a) 1st scan between  $-0.90$  and  $-1.80$  V; (b) 2nd to the 4th scans between  $0.00$  and  $-1.80$  V. (Pt electrode,  $r = 2.5$  mm;  $\nu = 100$   $\text{mVs}^{-1}$ ).

The complete oxidation of the organometallic polymer  $[\text{Ru}(\text{bpy})(\text{CO})_2]_n$  can be carried out by either a direct two-electron oxidation or by two successive one-electron ruthenium centred oxidations (reactions 5.6 and 5.7). Both exhaustive oxidations induce the breakage of all Ru–Ru bonds in the polymer and lead quasi-quantitatively to the formation of the soluble mononuclear complex **13**.



The first exhaustive one-electron oxidation of the polymer was carried out at 0.6 V and resulted in the quantitative formation of the soluble dimer **12**. This indicates that there is no structural rearrangement during the partial Ru–Ru polymer bond breaking process. As expected, a subsequent one-electron exhaustive oxidation at 1.1 V induces the cleavage of the metal-metal bond of the dimer and leads to the Ru(II) monomer **13**. The sequential formation of **12** and **13** was confirmed by characterising the two products *in situ* by FT-IR and <sup>1</sup>H NMR spectroscopies.

The  $[\text{Ru}(\text{bpy})(\text{CO})_2]_n$  film formed from **12** was characterised by UV-vis spectroelectrochemical experiments by depositing it onto optically transparent electrodes. The steady increase in the intensities of low-energy absorption bands reflects the thickening of the film [Figure 5.8(a)]. The UV-vis spectrum of the polymer in clean electrolyte [Figure 5.8(b)] shows one major absorption band in the region of 790 nm in agreement with the presence of Ru–Ru bonds in the polymeric matrix, as previously described.<sup>161</sup>

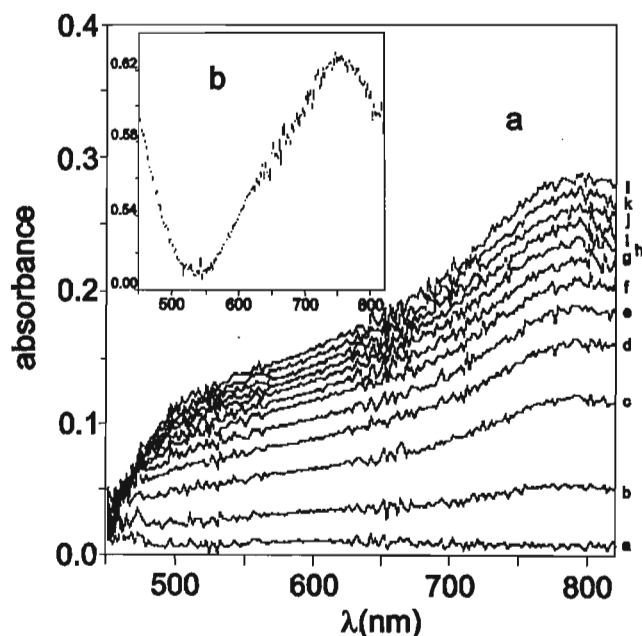


**Figure 5.8.** (a) Development of the UV-vis spectra of  $[\text{Ru}(\text{bpy})(\text{CO})_2]_n$  on an optically transparent electrode during the electropolymerisation of  $[\text{Ru}_2(\text{bpy})_2(\text{CO})_4(\text{CH}_3\text{CN})_2](\text{PF}_6)_2$  **12** in  $\text{CH}_3\text{CN} + 0.1 \text{ M TBAP}$ . (b) UV-vis spectrum of the resulting polymer film.

### 5.2.3. Catalytic Properties of $[\text{Ru}_2(\text{bpy})_2(\text{CO})_4(\text{CH}_3\text{CN})_2](\text{PF}_6)_2$ **12** and the Resulting $[\text{Ru}(\text{bpy})(\text{CO})_2]_n$ Polymer Towards $\text{CO}_2$ Electrochemical Reduction

In order to examine the electrocatalytic properties of **12** and the polymer formed from it, analytical and preparative electrolysis studies were performed in the presence of  $\text{CO}_2$ . The bubbling of  $\text{CO}_2$  into a homogeneous solution of **12** ( $\text{CH}_3\text{CN} + 0.1\text{M TBAP}$ ) causes an important modification in its CV. In particular a strong catalytic current beginning at  $-1.90\text{ V}$  is observed. This potential value corresponds closely to that for the direct reduction of  $\text{CO}_2$  on a glassy carbon electrode.<sup>162</sup> The progressive addition of  $\text{H}_2\text{O}$  causes an increase in the intensity of this  $\text{CO}_2$  reduction peak, while its foot potential becomes less and less negative, reaching an optimum value of *ca.*  $-1.40\text{ V}$  at a 5% concentration of  $\text{H}_2\text{O}$ . Cyclic voltammograms of glassy carbon $[\text{Ru}(\text{bpy})(\text{CO})_2]_n$  electrodes, prepared by the reduction of **12** as described in section 5.2.2.(ii), in clean electrolyte solution (either  $\text{CH}_3\text{CN} + 5\% \text{H}_2\text{O}$  or pure  $\text{H}_2\text{O}$ ), show a typical catalytic current in the presence of  $\text{CO}_2$ . This behaviour is represented in Figure 5.9. It demonstrates that the polymer derived from **12** is also an electrocatalyst for  $\text{CO}_2$  reduction, in keeping with the properties of the same polymer, prepared by electroreduction of *trans*(Cl)- $[\text{Ru}(\text{bpy})(\text{CO})_2\text{Cl}_2]$  as previously published.<sup>38,39</sup>

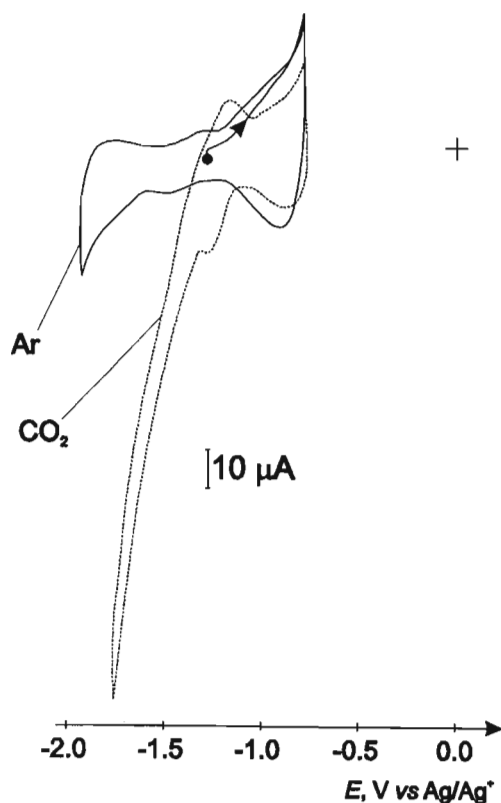


**Figure 5.9.** CVs in  $\text{CH}_3\text{CN} + 0.1\text{ M TBAP} + 5\% \text{H}_2\text{O}$  of a glassy carbon $[\text{Ru}(\text{bpy})(\text{CO})_2]_n$  electrode ( $r = 1.5\text{ mm}$ ) recorded in the presence of Ar and  $\text{CO}_2$ .



Controlled-potential electrolysis of CO<sub>2</sub> saturated hydro-organic and aqueous electrolytes using polymer-modified carbon felt electrodes confirm the efficacy of the electrocatalyst for the reduction of CO<sub>2</sub>. In these experiments, summarised in Table 5.3, CO is formed in high yields at moderate potentials while the formation of formate is minimal. Moreover, the catalytic currents are relatively stable. All of these results are in keeping with those obtained during previous electrocatalytic studies of Ru(II) monomers and Ru(0) polymers.<sup>37,38</sup>

**Table 5.3.** Summary of the electrocatalytic experiments carried out with [Ru<sub>2</sub>(bpy)<sub>2</sub>(CO)<sub>4</sub>(CH<sub>3</sub>CN)<sub>2</sub>](PF<sub>6</sub>)<sub>2</sub> **12** and its resulting polymer [Ru(bpy)(CO)<sub>2</sub>]<sub>n</sub> as catalysts.

Catalyst (electrolyte)	E <sub>app</sub> / V	i / mA (Δ i per 10 C)	Coulombs / C	Faradaic Yield / %	
				CO	HCOO <sup>-</sup>
[Ru <sub>2</sub> (bpy) <sub>2</sub> (CO) <sub>4</sub> (CH <sub>3</sub> CN) <sub>2</sub> ](PF <sub>6</sub> ) <sub>2</sub> <b>12</b> (CH <sub>3</sub> CN + 0.1 M TBAP + 10% H <sub>2</sub> O)	-1.40	7.7 (-0.3)	88	89	5
[Ru(bpy)(CO) <sub>2</sub> ] <sub>n</sub> (CH <sub>3</sub> CN + 0.1 M TBAP + 10% H <sub>2</sub> O)	-1.60	6.7 (+1.1)	113	92	1
[Ru(bpy)(CO) <sub>2</sub> ] <sub>n</sub> (H <sub>2</sub> O + 0.1 M LiClO <sub>4</sub> )	-1.30	6.3 (-0.2)	87	90	5

#### 5.2.4. *In situ* Synthesis of [Ru<sub>2</sub>(bpy)<sub>2</sub>(CO)<sub>4</sub>(CH<sub>3</sub>CN)<sub>2</sub>](PF<sub>6</sub>)<sub>2</sub> **12**

The coordination of bpy to [Ru<sub>2</sub>(CO)<sub>4</sub>(CH<sub>3</sub>CN)<sub>6</sub>](PF<sub>6</sub>)<sub>2</sub> (Equation 5.8) can be followed *in situ* by IR and <sup>1</sup>H NMR spectroscopic and cyclic voltammetric techniques. For these experiments reagents were used in exactly the same proportions as for the chemical preparation but at a lower concentration (*ca.* 2 mM).

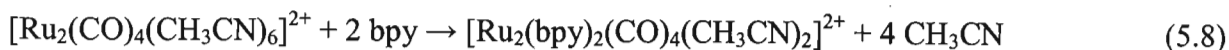
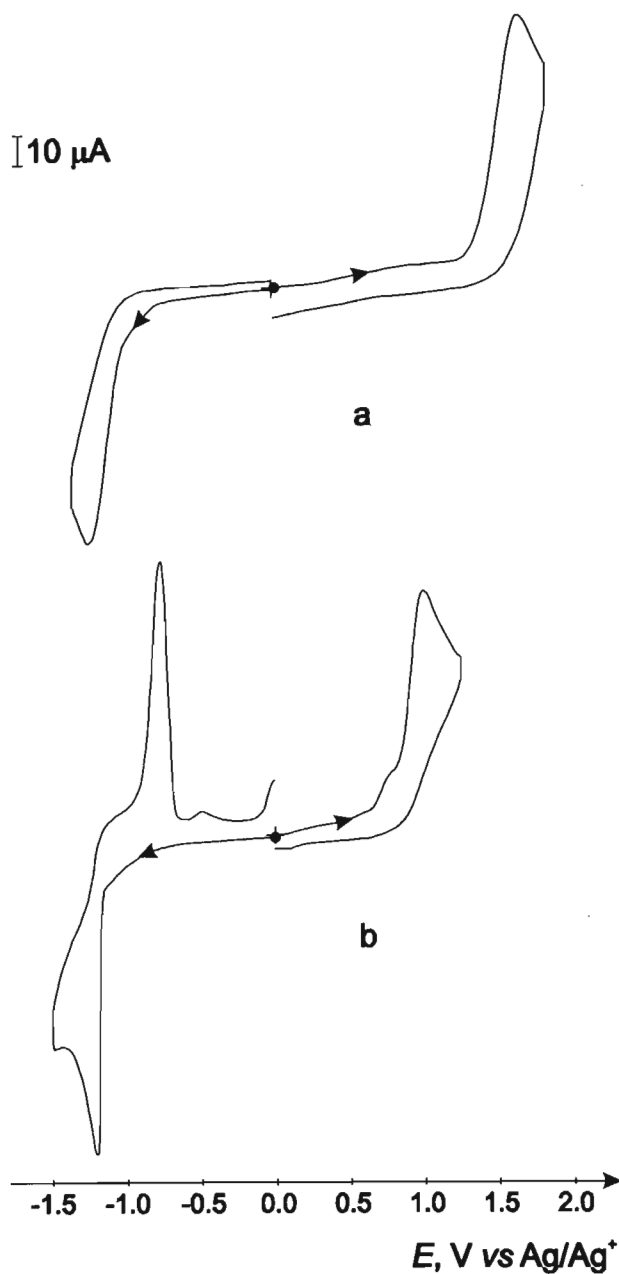
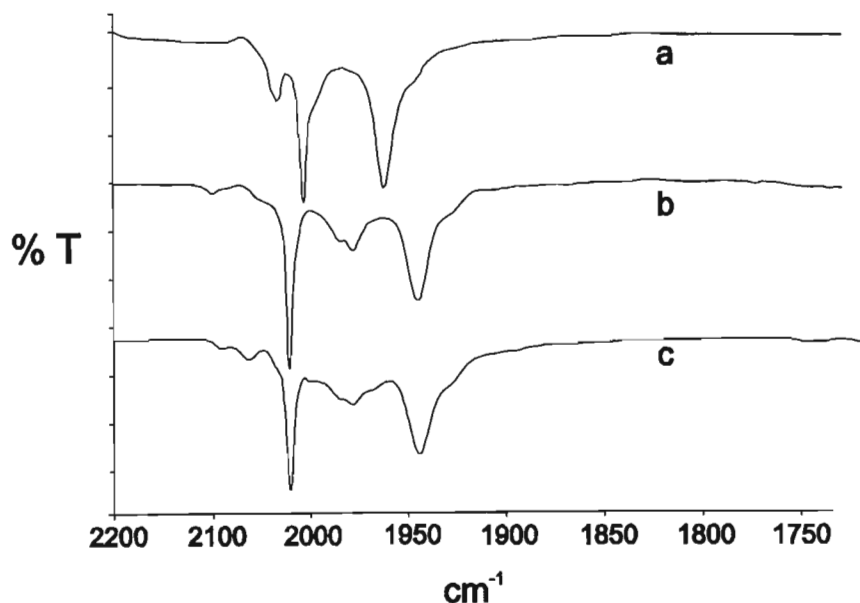


Figure 5.10(a) presents the CV of the Ru(I) precursor [Ru<sub>2</sub>(CO)<sub>4</sub>(CH<sub>3</sub>CN)<sub>6</sub>](PF<sub>6</sub>)<sub>2</sub>. This shows two irreversible redox processes at -1.64 and 1.22 V. Interestingly these features are comparable to those observed in the CV of Ru<sub>3</sub>(CO)<sub>12</sub>.<sup>163</sup> The addition of bpy to the electrolyte leads to a solution that shows a CV [Figure 5.10(b)] which mirrors that of **12**; an irreversible oxidation is seen at 1.04 V, while in the cathodic region of the CV an irreversible reduction at -1.24 V with a corresponding anodic return peak at -0.76 V are evident. As is expected, [Ru(bpy)(CO)<sub>2</sub>]<sub>n</sub> polymer films can be electrosynthesised from this solution by repetitive scanning of the electrode potential.



**Figure 5.10.** CVs of  $[\text{Ru}_2(\text{CO})_4(\text{CH}_3\text{CN})_6](\text{PF}_6)_2$  1.0 mM in  $\text{CH}_3\text{CN} + 0.1$  M TBAP; (a) before the addition of bpy; (b) 30 mins after the addition of bpy. (Pt electrode,  $r = 2.5$  mm;  $\nu = 100$   $\text{mVs}^{-1}$ ).

The IR spectrum of the unsubstituted Ru(I) precursor recorded in  $\text{CH}_3\text{CN} + 0.1$  M TBAP electrolyte displays in the terminal carbonyl stretching region two strong absorption bands at  $2006$  and  $1961$   $\text{cm}^{-1}$ , the latter being associated with a shoulder at  $1945$   $\text{cm}^{-1}$ , and a weak absorption at  $2031$   $\text{cm}^{-1}$  [Figure 5.11(a)]. The IR spectrum of this solution is modified by the addition of bpy [Figure 5.11(b)] and corresponds to that of an authentic sample of **12** in electrolyte solution, as is shown Figure 5.11(c).



**Figure 5.11.** CO stretching region of FT-IR spectrum recorded in electrolyte ( $\text{CH}_3\text{CN} + 0.1 \text{ M TBAP}$ ) of  $[\text{Ru}_2(\text{CO})_4(\text{CH}_3\text{CN})_6](\text{PF}_6)_2$  before (a) and 60 min after (b) the addition of bpy; (c)  $[\text{Ru}_2(\text{bpy})_2(\text{CO})_4(\text{CH}_3\text{CN})_2](\text{PF}_6)_2$  **12**.

Likewise,  $^1\text{H}$  NMR spectra recorded during the complexation show a simple transition of the free aromatic proton bpy signals to those of the coordinated bpy ligand when  $\text{CD}_3\text{CN}$  solutions of the two reactants are mixed at rt for 30 min (Figure 5.12). It should be noted that a stoichiometric excess of bpy was used in these experiments, this excess of free ligand being evident in the  $^1\text{H}$  NMR spectrum.

The results of these studies show that the substitution of the acetonitrile ligands of  $[\text{Ru}_2(\text{CO})_4(\text{CH}_3\text{CN})_6](\text{PF}_6)_2$  by a  $\alpha$ -diimine bidentate ligand can be readily monitored in the electrochemical cell. As will be described in the next chapter, this '*in situ*' methodology has been extended to substituted bpy ligands. For example, the reaction of  $[\text{Ru}_2(\text{CO})_4(\text{CH}_3\text{CN})_6](\text{PF}_6)_2$  with N-pyrrole substituted bpy ligands in electrolyte solution at room temperature leads to the formation of complexes exhibiting the same electrochemical properties as those of the isolated and fully characterised complexes. Through this approach diverse Ru(I) dimer complexes substituted by functionalised bpy ligands may be prepared *in situ*, allowing for the rapid assessment of their electrochemical properties without the necessity of a complete classical synthesis.

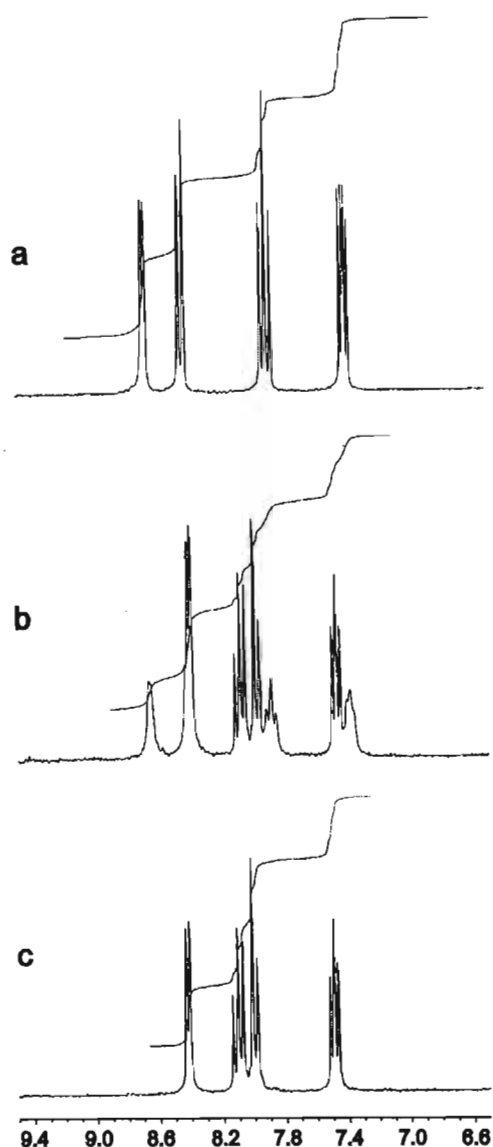


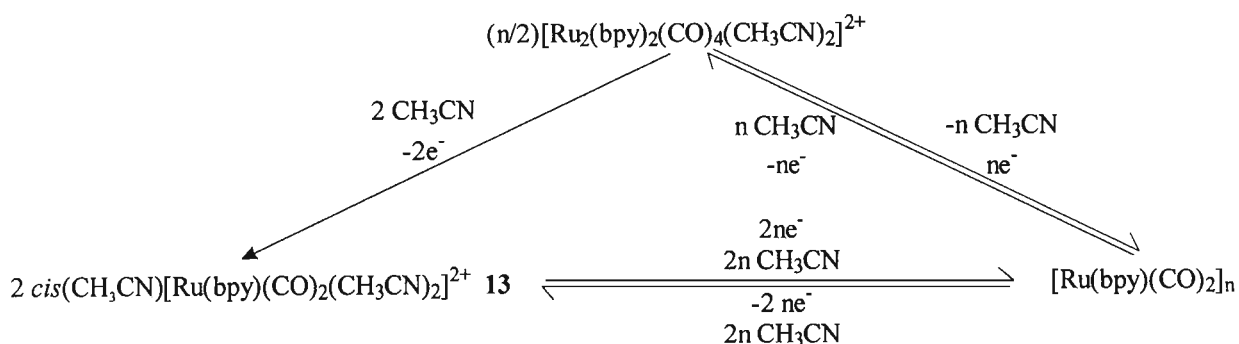
**Figure 5.12.** Aromatic region of the  $^1\text{H}$  NMR spectra recorded in  $\text{CD}_3\text{CN}$  at rt; (a) bpy; (b)  $[\text{Ru}_2(\text{CO})_4(\text{CH}_3\text{CN})_6](\text{PF}_6)_2 + \text{bpy}$  after 60 min; (c)  $[\text{Ru}_2(\text{bpy})_2(\text{CO})_4(\text{CH}_3\text{CN})_2](\text{PF}_6)_2$  **12**.

### 5.3. Summary

The study of **12** has provided a deeper understanding on how Ru(0) polymers form and their structures: (1) from the conformation of **12** revealed in its X-ray crystal structure it could be envisaged that a similar  $\pi$ - $\pi$  interaction will exist in the Ru(0) polymer; (2) the electrochemical behaviour of **12**, summarised in Scheme 5.1, is proof that both the electrogeneration and the oxidation of  $[\text{Ru}(\text{bpy})(\text{CO})_2]_n$  proceeds through a dinuclear Ru(I) intermediate.

Dinuclear bipyridyl ligand complexes of Ru(I) **12** can be conveniently formed under mild conditions from  $[\text{Ru}_2(\text{CO})_4(\text{CH}_3\text{CN})_6]^{2+}$  in electrolyte solution. Furthermore the oxidation of **12** results in a breakage of the M-M bond and affords the new mononuclear Ru(II) complex

*cis*(CH<sub>3</sub>CN)-[Ru(bpy)(CO)<sub>2</sub>(CH<sub>3</sub>CN)<sub>2</sub>]<sup>2+</sup> **13**. The successful use of these reactions to prepare bipyridyl complexes of ruthenium will be exploited in Chapter 6.



**Scheme 5.1.** Overview of the electrochemical behaviour of the dication of [Ru<sub>2</sub>(bpy)<sub>2</sub>(CO)<sub>4</sub>(CH<sub>3</sub>CN)<sub>2</sub>](PF<sub>6</sub>)<sub>2</sub> **12**.

#### 5.4. Experimental

[Ru<sub>2</sub>(bpy)<sub>2</sub>(CO)<sub>4</sub>(CH<sub>3</sub>CN)<sub>2</sub>](PF<sub>6</sub>)<sub>2</sub> **12**. Reaction vessels were covered with aluminium foil during the synthetic preparations in order to minimise exposure to light. A solution of [Ru<sub>2</sub>(CO)<sub>4</sub>(CH<sub>3</sub>CN)<sub>6</sub>](PF<sub>6</sub>)<sub>2</sub> (170 mg, 0.20 mmol) and bpy (78 mg, 0.50 mmol) in CH<sub>3</sub>CN (8 cm<sup>3</sup>) was maintained at room temperature for 2 h. The resulting red coloured solution was reduced in volume to *ca.* 3 cm<sup>3</sup> under vacuum and an excess of Et<sub>2</sub>O (20 cm<sup>3</sup>) slowly added with stirring. Upon standing for 12 h at -25°C the solution yielded orange needle-shaped crystals. The mother liquor was decanted and the crystals washed with Et<sub>2</sub>O (2 x 5 cm<sup>3</sup>). The product was recrystallised from CH<sub>3</sub>CN/Et<sub>2</sub>O a second time in the same manner described above. The material obtained was dried *in vacuo* for 30 min and then dissolved in CH<sub>3</sub>CN (5 cm<sup>3</sup>). The solvent was completely removed under reduced pressure and the solid product dried under vacuum for 36 h to afford the pure diruthenium complex **12** as an orange/red powder (130 mg, 65 %). (Found: C, 34.66; H, 2.42; N, 9.24; Ru, 19.44. Ru<sub>2</sub>C<sub>28</sub>H<sub>22</sub>N<sub>6</sub>P<sub>2</sub>F<sub>12</sub>O<sub>4</sub> requires C, 34.42; H, 2.34; N, 9.43; Ru, 19.19 %); λ<sub>max</sub>/nm (CH<sub>3</sub>CN) 244 (ε/dm<sup>3</sup> mol<sup>-1</sup> cm<sup>-1</sup> 30 800), 297 (26 100), 312 (sh) (20 700), 425 (sh) (2 200); ν<sub>max</sub>/cm<sup>-1</sup> (KBr) 2313w (CN), 2285w (CN), 2044s (CO), 2003m (CO), 1969s (CO), 1948m (sh) (CO), 839vs (PF), 558m (PF); ν<sub>max</sub>/cm<sup>-1</sup> (CH<sub>3</sub>CN) 2021s (CO), 1985 (sh) (CO), 1978w (CO), 1944s (CO), 1927 (sh) (CO); δ<sub>H</sub> (250 MHz, CD<sub>3</sub>CN, CD<sub>2</sub>H<sub>2</sub>CN) 8.42 (4H, d, H<sub>6,6'</sub>), 8.11 (4H, td, H<sub>4,4'</sub>), 8.00 (4H, d, H<sub>3,3'</sub>), 7.49 (4H, td, H<sub>5,5'</sub>), 1.98 (6H, s, H<sub>CH<sub>3</sub>CN</sub>); δ<sub>H</sub> (500 MHz, CD<sub>2</sub>Cl<sub>2</sub>, CDHCl<sub>2</sub>, rt.) 8.38 (4H, d, H<sub>6,6'</sub>), 8.17 (4H, t, H<sub>4,4'</sub>), 8.05 (4H, d, H<sub>3,3'</sub>), 7.52 (4H, t, H<sub>5,5'</sub>), 1.92 (6H, s, H<sub>CH<sub>3</sub>CN</sub>); δ<sub>H</sub> (500 MHz, CD<sub>2</sub>Cl<sub>2</sub>, CDHCl<sub>2</sub>, -80 °C) 8.27 (4H, s, H<sub>6,6'</sub>), 8.10 (4H, t, H<sub>4,4'</sub>), 7.91 (4H, d, H<sub>3,3'</sub>), 7.45 (4H, t, H<sub>5,5'</sub>), 1.92 (6H, s, H<sub>CH<sub>3</sub>CN</sub>); δ<sub>C</sub>

(500 MHz, CD<sub>2</sub>Cl<sub>2</sub>, CDHCl<sub>2</sub>, -80 °C) 201.25 (CO), 151.72 (C-6), 150.59 (C-2), 139.07 (C-4), 127.00 (C-5), 123.07 (C-3), 119.26 (CH<sub>3</sub>CN), 3.05 (CH<sub>3</sub>CN); ES<sup>+</sup>MS, mobile phase: CH<sub>3</sub>CN (z = 2): m/z 326.8 with the calculated isotopic patterns for [M - 2 CO]<sup>2+</sup>; 313.7 [M - 2 CH<sub>3</sub>CN]<sup>2+</sup>; 285.8 [M - 2 CH<sub>3</sub>CN - 2CO]<sup>2+</sup>.

**Attempted Chemical Synthesis of *cis*(CH<sub>3</sub>CN)-[Ru(bpy)(CO)<sub>2</sub>(CH<sub>3</sub>CN)<sub>2</sub>](PF<sub>6</sub>)<sub>2</sub> 13.** Reaction vessels were covered with aluminium foil during the synthetic preparations in order to minimise exposure to light. (a) *Cis*(Cl)-[Ru(bpy)(CO)<sub>2</sub>Cl<sub>2</sub>] (32 mg, 0.080 mmol) prepared as previously described<sup>38</sup> and two molar equivalents of TlPF<sub>6</sub> (63 mg, 0.18 mmol) were refluxed together in CH<sub>3</sub>CN (10 cm<sup>3</sup>) for 2 h 15 min. The fine white precipitate which formed was removed by filtration and the solvent evaporated from the filtrate under vacuum with gentle heating, yielding a crude light green powder *cis*(CO)-[Ru(bpy)(CO)<sub>2</sub>(CH<sub>3</sub>CN)Cl](PF<sub>6</sub>) containing TlPF<sub>6</sub> salt.  $\nu_{\max}/\text{cm}^{-1}$  (CsI) 2094s (CO), 2037s (CO), 839vs (PF), 323w (RuCl);  $\nu_{\max}/\text{cm}^{-1}$  (CH<sub>3</sub>CN) 2091s (CO), 2035s (CO);  $\delta_{\text{H}}$  (250 MHz, CD<sub>3</sub>CN, CD<sub>2</sub>H<sub>2</sub>CN) 9.49 (1H, d, H<sub>6</sub>), 8.87 (1H, d, H<sub>6'</sub>), 8.50 (2H, 2 d, H<sub>3,3'</sub>), 8.38 (1H, t, H<sub>4</sub>), 8.27 (1H, t, H<sub>4'</sub>), 7.92 (1H, t, H<sub>5</sub>), 7.68 (1H, t, H<sub>5'</sub>); FAB<sup>+</sup> (m/z) : 390 [M - PF<sub>6</sub>], 349 [M - PF<sub>6</sub> - CH<sub>3</sub>CN], 321 [M - PF<sub>6</sub> - CH<sub>3</sub>CN - CO]. In order to decoordinate the remaining chloride ligand the sample was then redissolved in CH<sub>3</sub>CN (20 cm<sup>3</sup>) and refluxed in the presence of the residual TlPF<sub>6</sub> for a further 72 h. The IR absorption spectra recorded of the reaction solution show no marked change in the carbonyl region. Therefore, in an attempt to obtain the bis acetonitrile monomer **13**, the experimental conditions were change. (b) *Cis*(Cl)-[Ru(bpy)(CO)<sub>2</sub>Cl<sub>2</sub>] (32 mg, 0.083 mmol) and four molar equivalents of TlPF<sub>6</sub> (117 mg, 0.330 mmol) were refluxed together in CH<sub>3</sub>CN (20 cm<sup>3</sup>) continuously for 72 h under a nitrogen atmosphere. The resulting pale yellow solution was filtered from the white precipitate that had formed and the solvent removed under vacuum to give a light tan coloured residue. This consisted, as estimated from the integrals of the proton signals in the <sup>1</sup>H NMR spectrum of the crude product, of a mixture of 45 % *cis*(CO)-[Ru(bpy)(CO)<sub>2</sub>(CH<sub>3</sub>CN)Cl](PF<sub>6</sub>) and 65 % *cis*(CH<sub>3</sub>CN)-[[Ru(bpy)(CO)<sub>2</sub>(CH<sub>3</sub>CN)<sub>2</sub>](PF<sub>6</sub>)<sub>2</sub> **13**. The <sup>1</sup>H NMR and FT-IR spectra of *cis*(CH<sub>3</sub>CN)-[Ru(bpy)(CO)<sub>2</sub>(CH<sub>3</sub>CN)<sub>2</sub>](PF<sub>6</sub>)<sub>2</sub> listed here were extracted from the crude product spectrum.  $\nu_{\max}/\text{cm}^{-1}$  (CH<sub>3</sub>CN) 2117s (CO), 2063s (CO);  $\delta_{\text{H}}$  (250 MHz, CD<sub>3</sub>CN, CD<sub>2</sub>H<sub>2</sub>CN) 9.01 (1H, d, H<sub>6</sub>), 8.82 (1H, d, H<sub>6'</sub>), 8.56 (1H, t, H<sub>3</sub>), 8.51 (2H, t, H<sub>3'</sub>), 8.45 (1H, td, H<sub>4</sub>), 8.33 (1H, td, H<sub>4'</sub>), 7.94 (1H, t, H<sub>5</sub>), 7.74 (1H, td, H<sub>5'</sub>).

**X-ray Data Collection and Structure Solution for 12.** Suitable crystals of **12** were grown by the slow vapour diffusion of diethyl ether into an acetonitrile solution of the complex.

The loss of occluded solvent from the crystal during data collection necessitated the application of a linear decay correction using the mean value linear curves fitted through three intensity control reflections, measured at regular time intervals. Details of the crystal data, data collection and structure refinement are summarized in Table 5.4. The complete crystallographic data of **12** are presented in Appendix B. Supporting Information.

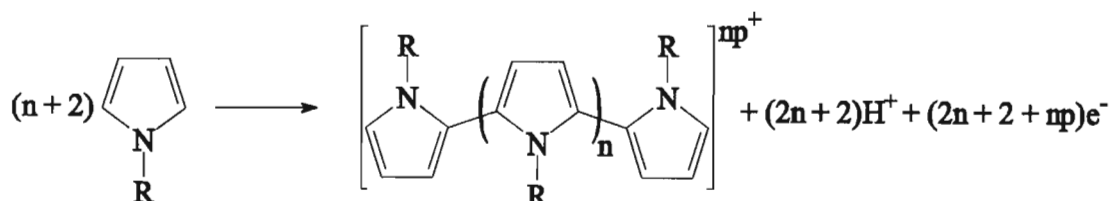
**Table 5.4.** Summary of the crystal data of  $[\text{Ru}_2(\text{bpy})_2(\text{CO})_4(\text{CH}_3\text{CN})_2](\text{PF}_6)_2 \cdot (\text{CH}_3\text{CN})_2$  **12**.

Formula	$\text{Ru}_2\text{C}_{32}\text{H}_{28}\text{F}_{12}\text{N}_8\text{O}_4\text{P}_2$
FW/amu	1080.70
Crystal system, space group	Monoclinic, $C2/c$
$a/\text{\AA}$	15.259(4)
$b/\text{\AA}$	17.754(4)
$c/\text{\AA}$	15.937(3)
$\alpha/^\circ$	90
$\beta/^\circ$	104.15(2)
$\gamma/^\circ$	90
$U/\text{\AA}^3$	4187(2)
$Z$	4
$D_c/\text{g cm}^3$	1.715
$F(000)$	2136
$\mu/\text{mm}^{-1}$	0.897
Crystal dimensions/mm	0.70 x 0.34 x 0.15
$\lambda(\text{Mo K}\alpha)/\text{\AA}$	0.71069
Temperature/K	293(3)
$\theta$ range for collected data/ $^\circ$	2.01 to 22.98
Index ranges	$-16 \leq h \leq 16$ $-1 \leq k \leq 19$ $-1 \leq l \leq 17$
Total reflections collected	3170
Absorption correction	Empirical
Relative transmission coefficients (I)	0.9973 and 0.7696
Unique data	2897 ( $R_{\text{int}} = 0.0272$ )
Unique observed data [ $I > 2\sigma(I)$ ]	1964
Refinement method	Full-matrix least-squares on $F^2$
Data / restraints / parameters	2897 / 0 / 273
Goodness-of-fit (based on $F^2$ )	1.036
Extinction coefficient	none
$\text{Max}(\Delta\rho)/e. \text{\AA}^{-3}$	0.865
$\text{Min}(\Delta\rho)/e. \text{\AA}^{-3}$	-0.643
Final R indices [ $I > 2\sigma(I)$ ]	$R_1 = 0.0587$ , $wR_2 = 0.1430$
R indices (all data)	$R_1 = 0.0967$ , $wR_2 = 0.1831$

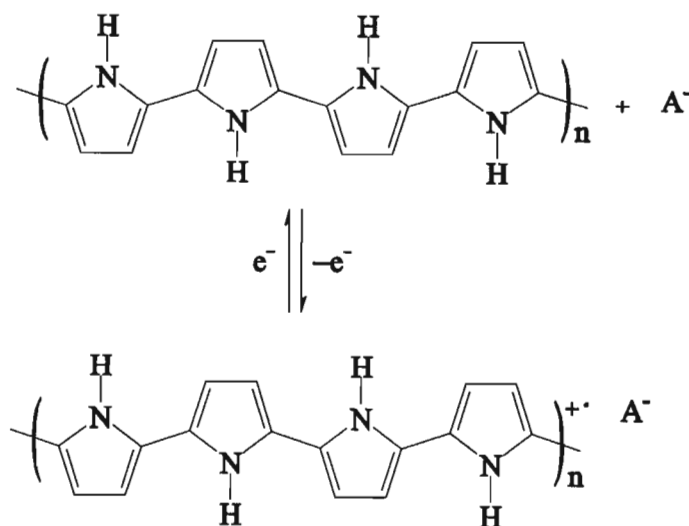
## Chapter 6. Dinuclear Pyrrole-substituted 2,2'-bipyridine Ligand Complexes of Ruthenium(I)

### 6.1. Introduction

The modification of electrode surfaces by organic conducting polymer films functionalised by metal complexes has received much interest. Particularly, these polymer coated electrodes have potential applications in electrocatalysis.<sup>164</sup> Pyrrole, a commercially available monomer, can be electropolymerised by anodic oxidation to a stable electroactive polypyrrole film on the working electrode surface.<sup>165,166</sup> Simplistically, the initial oxidation of the monomer leads to the formation of its radical cation which reacts with other monomers present in solution to form oligomeric species. Due to their extended conjugation these oligomers are immediately oxidised at the oxidation potential of the monomer,<sup>167</sup> thus propagating the reaction and ultimately leading to the formation of the polymer.<sup>168,169</sup> The global polymerisation reaction is presented in Scheme 6.1.



**Scheme 6.1.** Global reaction for the anodic polymerisation of pyrrole. (R = H, R, Ar).<sup>168</sup>



**Scheme 6.2.** Positively charged and neutral states of polypyrrole. (A = electrolyte anion).<sup>168</sup>



The conductivity of the conjugated film varies with applied potential, existing between a neutral essentially insulating form and an oxidised conducting state in which it is formed. In the latter 'p-doped' form the polymer chain carries a positive charge every three to four pyrrole units that is balanced by the movement of the supporting electrolyte anions into the film.<sup>168,170</sup> The change between these redox states is depicted in Scheme 6.2. The electropolymerisation of pyrroles with pendant functional groups allows the chemical anchoring of redox-active groups, such as transition metal complexes, to electrode surfaces. This is an extensively used and convenient method of modifying the electrode surface with a desired functionality, fine tuning its electroactivity.<sup>170,171,172</sup>

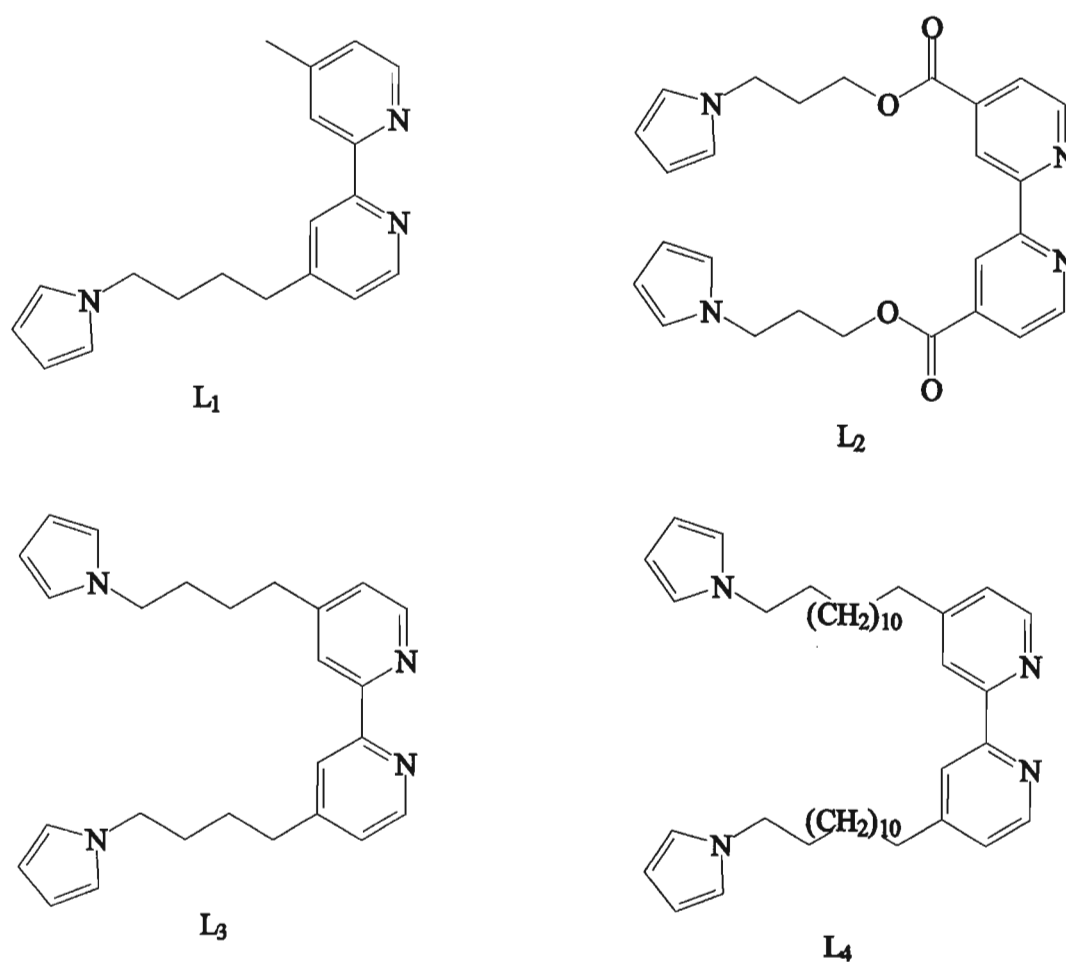


**Figure 6.1.** N-substituted pyrrole functionalised 2,2'-bipyridine ligands L<sub>1-4</sub>. [L<sub>1</sub> = 4-(4-pyrrol-1-ylbutyl)-4'-methyl-2,2'-bipyridine; L<sub>2</sub> = 4,4'-bis((3-pyrrol-1-ylpropyloxy)carbonyl)-2,2'-bipyridine; L<sub>3</sub> = 4,4'-bis(4-pyrrol-1-ylbutyl)-2,2'-bipyridine; L<sub>4</sub> = 4,4'-bis(13-pyrrol-1-yltridecyl)-2,2'-bipyridine]

The rapid oxidation of [Ru(bpy)(CO)<sub>2</sub>]<sub>n</sub> (E ≥ 0.8 V vs. Ag/Ag<sup>+</sup>) upon exposure to air limits the practical applications of this electrocatalyst. This has been overcome by immobilisation of the Ru(II) precursors [Ru(L)(CO)<sub>2</sub>Cl<sub>2</sub>], for which the ligands L are the N-

pyrrole functionalised bpy ligands  $L_1$  and  $L_2$  (Figure 6.1), by their anodic polymerisation into a polypyrrole film.<sup>37,42,172</sup> The subsequent reduction of the Ru(II) monomer leads to a Ru(0) polymer anchored to the electrode surface by the preformed polypyrrole film. The proposed final ppyr-[Ru( $L_1$ )(CO) $_2$ ] $_n$  composite material is illustrated in Figure 6.2. In the event of oxidation of the Ru–Ru metal bonds the organometallic polymer can be conveniently regenerated by reduction. In addition to increasing the robustness of the electrocatalyst its immobilisation has other inherent advantages; it facilitates the recovery and separation of the electrocatalyst; as the rate of the catalytic reaction is not limited by the rate of mass transfer of the catalyst to and from the electrode surface, lower quantities of catalyst, highly concentrated at the reaction site can be used.

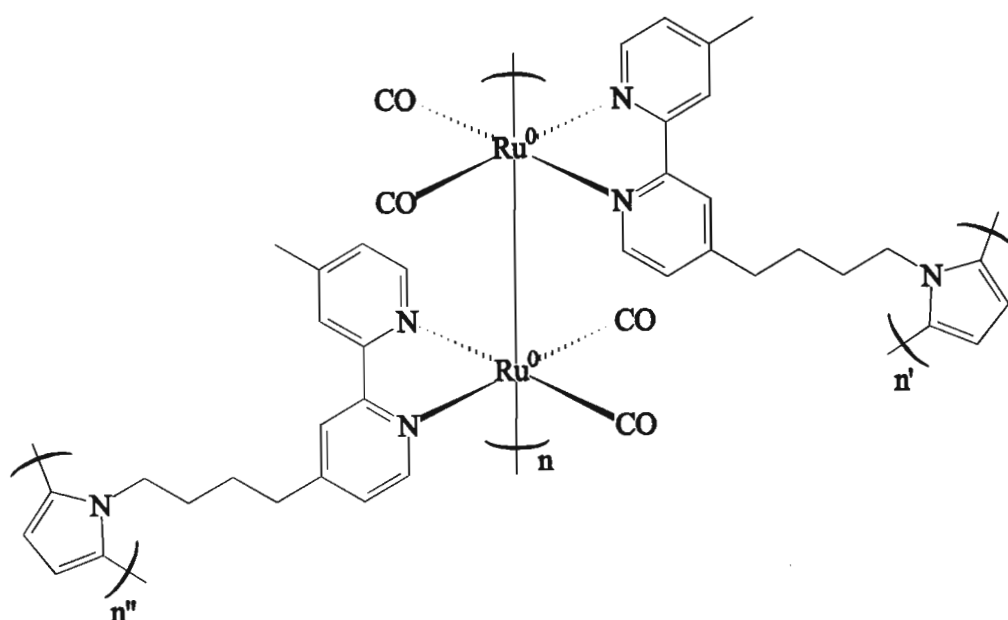


**Figure 6.2.** Proposed structure of ppyr-[Ru( $L_1$ )(CO) $_2$ ] $_n$ , a Ru(0) polymer immobilised in a preformed polypyrrole film.

Based on the work described in the previous chapter it is anticipated that the acetonitrile ligands in  $[Ru_2(CO)_4(CH_3CN)_6](PF_6)_2$  will be easily substituted by pyrrole-substituted  $\alpha$ -diimine ligands in an electrolyte medium. This suggests a convenient route to Ru(0) polymers immobilised in a polypyrrole matrix. Furthermore, it is envisaged that the electrochemical oxidation of  $[Ru_2(CO)_4(CH_3CN)_6](PF_6)_2$  and the subsequent *in situ* reaction of the intermediate with the appropriate ligand will provide a simple synthetic route to pyrrole-substituted bpy ligand complexes of Ru(II) under mild conditions. The work described in this chapter was thus motivated by the advantages of immobilising the electrocatalyst in a polypyrrole matrix and aimed to establish a rapid method for the preparation of the appropriate precursor. In the first part, the synthesis and electrochemical properties of the diruthenium(I) complexes

$[\text{Ru}_2(\text{L})_2(\text{CO})_4(\text{CH}_3\text{CN})_2](\text{PF}_6)_2$  ( $\text{L} = \text{L}_{1-4}$ ) are presented. In the second part, the electrochemical synthesis of the mononuclear complexes  $\text{trans}(\text{CH}_3\text{CN})\text{-}[\text{Ru}(\text{L})(\text{CO})_2(\text{CH}_3\text{CN})_2]^{2+}$  ( $\text{L} = \text{bpy}$  and  $\text{L}_1$ ) and their electrochemical properties are described. Finally the electrocatalytic properties of  $\text{ppyr}\text{-}[\text{Ru}(\text{L})(\text{CO})_2]_n$  ( $\text{L} = \text{L}_1, \text{L}_2, \text{and } \text{L}_4$ ) towards  $\text{CO}_2$  reduction are examined.

## 6.2. Results and Discussion

### 6.2.1. Synthesis and Characterisation of $[\text{Ru}_2(\text{L})_2(\text{CO})_4(\text{CH}_3\text{CN})_2](\text{PF}_6)_2$ ( $\text{L} = \text{L}_{1-2}$ )

Following the synthetic approach used for  $[\text{Ru}_2(\text{bpy})_2(\text{CO})_4(\text{CH}_3\text{CN})_2](\text{PF}_6)_2$  **12**, the diruthenium(I) complexes  $[\text{Ru}_2(\text{L})_2(\text{CO})_4(\text{CH}_3\text{CN})_2](\text{PF}_6)_2$  ( $\text{L} = \text{L}_1$  **14** and  $\text{L}_2$  **15**) were prepared by the reaction of the ruthenium(I) precursor,  $[\text{Ru}_2(\text{CO})_4(\text{CH}_3\text{CN})_6](\text{PF}_6)_2$ , with the appropriate ligand in acetonitrile at room temperature.

The solid state IR absorption spectra of **14** and **15**, which display three strong absorption bands with an associated shoulder in the terminal CO stretching region, closely resemble that of **12**. On the basis of the pattern of  $\nu(\text{CO})$  peaks one can infer that they have the same  $\text{Ru}_2(\text{CO})_4$  core fragment described for **12** (see Figure 5.1), wherein each pair of equatorial carbonyl ligands coordinate in *cis* positions at each octahedral Ru(I) centre. In comparison to **12**, the wave numbers of the terminal carbonyl stretches of **14** are consistently shifted to smaller values, while those of **15** appear at longer wavenumbers. This reflects the opposing donor-acceptor effects of the bpy substituents in each N-pyrrole functionalised ligand. While the alkyl moiety in  $\text{L}_1$  would lead to a less electron withdrawing bpy ligand, the ester linkage in  $\text{L}_2$  would increase the acceptor properties of the bpy ring. Consequently the electron density on the Ru(I) centre would be greater in **14** than in **15**, while that of **12** would be intermediate between the two. The IR absorption spectra further exhibit two weak  $\nu_{\text{CN}}$  bands in the region of  $2313 - 2289 \text{ cm}^{-1}$  and a very strong absorption band at *ca*  $840 \text{ cm}^{-1}$  assigned to the  $\text{PF}_6^-$  counter ion.

The  $^1\text{H}$  NMR spectrum of complex **14**, recorded at  $24^\circ\text{C}$  in  $\text{CD}_2\text{Cl}_2$ , shows a single resonance assigned to the methyl protons of the acetonitrile ligands at 1.91 ppm. The  $^{13}\text{C}$  NMR spectrum of **14**, recorded at  $-80^\circ\text{C}$  in  $\text{CD}_2\text{Cl}_2$ , shows single resonances for the acetonitrile alkyl and nitrile carbons at 3.86 and 119.61 ppm respectively. The carbonyl ligands are evident in the spectra as a single resonance at about 202.38 ppm. The multiplicities and chemical shifts of these resonances are alike to those of **12** and one can conclude that the  $\text{CH}_3\text{CN}$  and CO ligands adopt the same positions in the ruthenium coordination spheres.

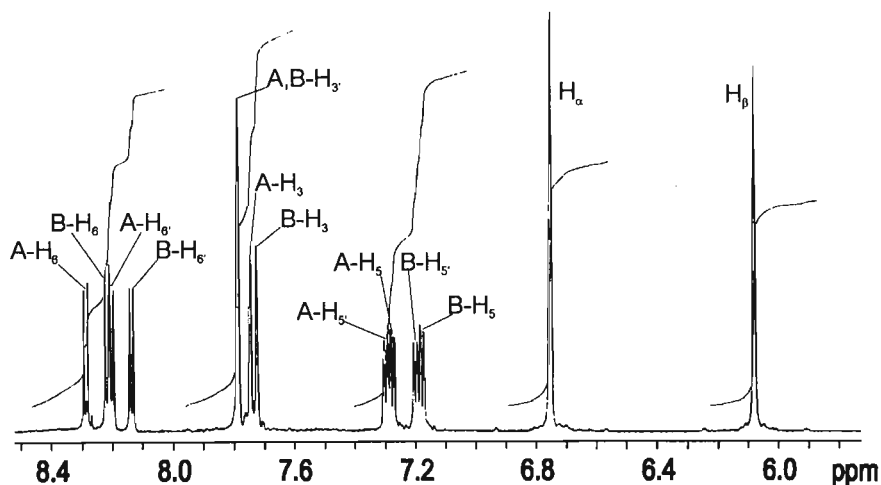


**Figure 6.3.** Expanded  $^1\text{H}$  NMR spectrum of  $[\text{Ru}_2(\text{L}_1)_2(\text{CO})_4(\text{CH}_3\text{CN})_2](\text{PF}_6)_2$  **14** depicting the aromatic resonances.

However, examination of the aromatic region of the  $^1\text{H}$  NMR spectrum of **14** (Figure 6.3) shows that  $\text{L}_1$  ligand is coordinated in two distinct chemical environments. While this is not clear in the proton signals of the pyrrole group and  $\text{C}_4$  alkyl chain it is manifested in the signals of the substituted 2,2'-bipyridyl moiety: specifically the signals due to  $\text{H}_6$  and  $\text{H}_6'$  appear as four sets of doublets, two of which overlap to form a virtual triplet;  $\text{H}_3$  and  $\text{H}_3'$  are observed as a pair of overlapping singlets and two pairs of doublets respectively; the resonances due to  $\text{H}_5$  and  $\text{H}_5'$  appear as four sets of closely spaced doublets; two singlets are observed at 2.544 and 2.537 ppm for the methyl groups substituted at  $\text{C}-4'$  of each ligand. The  $^{13}\text{C}$  NMR signals of  $\text{L}_1$  in **14** are observed as pairs of peaks and confirm the presence of two inequivalent  $\text{L}_1$  ligands. As is illustrated in Figure 6.4 two structural isomers of **14** can form, with equal probability, as a consequence of  $\text{L}_1$  being an asymmetrically substituted derivative of 2,2'-bipyridine. The pattern observed in the NMR spectra of **14** can be interpreted in terms of the presence of these two isomers in solution.

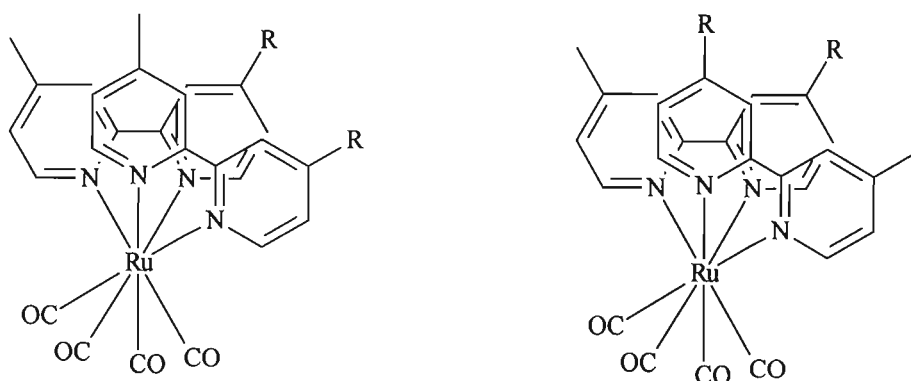


**Figure 6.4.** View along the Ru–Ru bond axis of the structural isomers of  $[\text{Ru}_2(\text{L}_1)_2(\text{CO})_4(\text{CH}_3\text{CN})_2](\text{PF}_6)_2$  **14**.

$^1\text{H}$  COSY-90 and NOESY experiments were performed on **14** to establish from which of the two possible structural isomers (arbitrarily labelled A and B) the resonances originate. The proton chemical shifts and their assignments are listed in Table 6.1. The two-dimensional NOESY spectrum of **14** provides evidence for a through-space interaction between the  $(\text{CH}_2)_a$  protons of chemical shift 2.77 ppm and the two sets of  $\text{H}_5$  bpy resonances observed at 7.28 and 7.18 ppm. The low field signal is arbitrarily assigned as A- $\text{H}_5$  and the higher field signal as B- $\text{H}_5$  respectively. The  $(\text{CH}_2)_a$  protons further show a Nuclear Overhauser Effect (NOE) with the two  $\text{H}_3$  bipyridyl doublets of shift 7.75 and 7.73 ppm. The COSY spectrum displays correlation peaks between the low field doublet and A- $\text{H}_5$  and between the high field doublet and B- $\text{H}_5$ . These resonances are thus assigned to A- $\text{H}_3$  and B- $\text{H}_3$  respectively. Likewise the COSY spectrum shows a spin-spin coupling of A- $\text{H}_5$  with a doublet at 8.29 ppm that is therefore assigned to A- $\text{H}_6$ . A similar argument allows the assignment of the doublet at 8.22 ppm, which couples with B- $\text{H}_5$ , to B- $\text{H}_6$ .

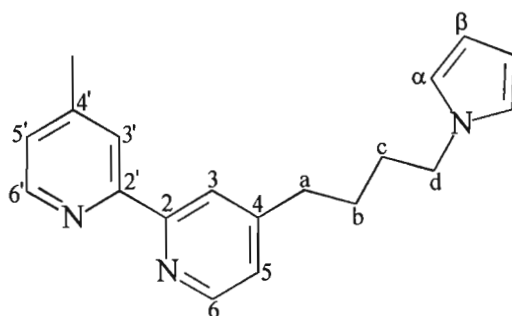


**Table 6.1.**  $^1\text{H}$  NMR spectral data of  $[\text{Ru}_2(\text{L}_1)_2(\text{CO})_4(\text{CH}_3\text{CN})_2](\text{PF}_6)_2$  **14**.<sup>a,b</sup>

8.29 (2H, d, J 5.89 Hz, A- $\text{H}_6$ ), 8.22 (2H, d, J 5.72 Hz, B- $\text{H}_6$ ), 8.20 (2H, d, J 5.69 Hz, A- $\text{H}_6'$ ), 8.14 (2H, d, J 5.71 Hz, B- $\text{H}_6'$ ), 7.79 (4H, s, A or B- $\text{H}_3$ ), 7.75 (2H, d, J 1.79 Hz, A- $\text{H}_3$ ), 7.73 (2H, d, J 1.82 Hz, B- $\text{H}_3$ ), 7.30 (2H, ddd, J 5.69, 1.78 and 0.74 Hz, A- $\text{H}_5$ ), 7.28 (2H, dd, J 5.89 and 1.79 Hz, A- $\text{H}_5$ ), 7.20 (2H, ddd, J 5.71, 1.72 and 0.80 Hz, B- $\text{H}_5$ ), 7.18 (2H, dd, J 5.72 and 1.82 Hz, B- $\text{H}_5$ ), 6.75 (8H, m, $\text{H}_\alpha$ ), 6.08 (8H, m, $\text{H}_\beta$ ), 4.02 (8H, t, J 6.86 Hz, $(\text{CH}_2)_d$ ), 2.77 (8H, m, $(\text{CH}_2)_a$ ), 2.54 (6H, s, A- or B- $\text{CH}_3$ ), 2.54 (6H, s, A- or B- $\text{CH}_3$ ), 1.98 (6H, s, $\text{CH}_3\text{CN}$ ), 1.88 (8H, m, $(\text{CH}_2)_c$ ), 1.66 (8H, m, $(\text{CH}_2)_b$ )
--

<sup>a</sup> Recorded in  $\text{CD}_3\text{CN}$  at 298 K. Data given as chemical shift ( $\delta$ ) (number of equivalent nuclei (by integration), multiplicity,  $J/\text{Hz}$ , assignment), s = singlet, d = doublet, t = triplet, m = multiplet. <sup>b</sup>  $\text{CD}_2\text{HCN}$  was used as a reference for the  $^1\text{H}$  (500 MHz) spectrum.

At this point an assumption had to be made. Though a NOE is observed between  $\text{H}_3$  and  $\text{H}_3'$  of the bipyridyl moiety, the  $\text{H}_3'$  signals of isomers A and B are superimposed over one another. Thus it is not possible to establish whether the proton signals of the methyl substituted pyridyl ring are of isomer A or B. It was therefore assumed that, as they are closest in chemical shift to

the corresponding protons of the C<sub>4</sub>pyr substituted pyridyl ring, that the resonance at 7.30 ppm arises from of A-H<sub>5'</sub> and that at 7.20 ppm from B-H<sub>5'</sub>. The close proximity of the H<sub>5'</sub> protons, as well as the H<sub>3'</sub> protons, to those of the CH<sub>3</sub> group is manifested in the NOESY spectrum and confirms their assignment to the methyl substituted pyridyl ring. Using a combination of the NOESY and COSY spectrum the remaining H<sub>6'</sub> protons were logically assigned to isomer A or B.

Which of the isomers labelled A and B corresponds to the *syn* confirmation and which to the *anti* confirmation? The NOESY spectrum shows that a weak dipole-dipole interaction exists between A-H<sub>5</sub> and (CH<sub>2</sub>)<sub>c</sub>. Inspection of a molecular model confirms that an inter-ligand interaction between these groups is feasible in the *syn* confirmation (but not in the *anti* confirmation) provided the alkyl chain is allowed to freely rotate. However, such an interaction is also possible intra-ligand and one cannot assign a confirmation in solution on this basis.

Variable temperature experiments were carried out to see if a dynamic interchange takes place between the two isomeric forms. <sup>1</sup>H NMR spectra of **14** were recorded at 24, 30, 40, 50 and 60 °C in CD<sub>3</sub>CN with a view to monitoring the CH<sub>3</sub>(bpy) resonances, these presenting well defined signals. The separation between the CH<sub>3</sub>(bpy) resonance of each isomer changed by an insignificant amount from 3.45 Hz at 24°C to 3.48 Hz at 60°C. Likewise the separation between the resonances of A-H<sub>3</sub> and B-H<sub>3</sub> show no marked shift from 10.98 Hz at 24°C to 10.06 Hz at 60°C. It appears that, in the temperature range examined, no dynamic exchange process takes place. It is noted that for coalescence to occur, the dynamic process would have to involve the dissociation-reassociation of L<sub>1</sub> from the ruthenium centre. A simple rotation about the ruthenium-ruthenium bond would not change the orientation of the ligands relative to one another. Considering the bonding properties of chelating bpy a high temperature may be required to force the dissociation of L<sub>1</sub>.

The NMR spectral data of **15** bears a close resemblance to that of **12**. The <sup>1</sup>H NMR spectrum shows a single resonance assigned to the acetonitrile methyl protons and three sets of aromatic proton resonances due to the pyrrole-substituted bpy ligand L<sub>2</sub>. This pattern is characteristic of a symmetrically substituted bpy ligand coordinated to the Ru atoms in an arrangement equivalent to that observed for **12**. The <sup>13</sup>C NMR spectrum is consistent with this, displaying a single CO resonance and five aromatic bpy carbon resonances.

The formulation of the complexes as [Ru<sub>2</sub>(L)<sub>2</sub>(CO)<sub>4</sub>(CH<sub>3</sub>CN)<sub>2</sub>](PF<sub>6</sub>)<sub>2</sub> (L = L<sub>1-2</sub>) indicated by the IR and NMR data was confirmed by the micro-analytical results.

## 6.2.2. Electrochemical Behaviour of $[\text{Ru}_2(\text{L})_2(\text{CO})_4(\text{CH}_3\text{CN})_2](\text{PF}_6)_2$ ( $\text{L} = \text{L}_{1-4}$ )

Following the procedure described for  $[\text{Ru}_2(\text{bpy})_2(\text{CO})_4(\text{CH}_3\text{CN})_2](\text{PF}_6)_2$  **12**, the synthesis of the complexes  $[\text{Ru}_2(\text{L})_2(\text{CO})_4(\text{CH}_3\text{CN})_2](\text{PF}_6)_2$  ( $\text{L} = \text{L}_1$  **14** and  $\text{L}_2$  **15**) were also carried out *in situ* in the electrochemical cell. The IR spectra and electrochemical properties (described below) of **14** and **15** synthesised by this method agreed exactly with those of the conventionally synthesised and isolated samples. For convenience, the complexes  $[\text{Ru}_2(\text{L})_2(\text{CO})_4(\text{CH}_3\text{CN})_2](\text{PF}_6)_2$  ( $\text{L} = \text{L}_3$  **16** and  $\text{L}_4$  **17**) were synthesised *in situ*. As the electrochemical properties of **14** and **15** prepared *in situ* were in exact agreement with those of authentic samples of these complexes the licence has been taken here to discuss the complexes prepared *in situ* together with those previously synthesised.

### 6.2.2.(i) Reduction

As is shown for **14** in Figure 6.4, the dimer complexes **14** - **17** show an irreversible reduction peak in their cathodic CVs. In comparison to  $[\text{Ru}_2(\text{bpy})_2(\text{CO})_4(\text{CH}_3\text{CN})_2](\text{PF}_6)_2$  **12**, which is irreversibly reduced at  $-1.24$  V, the reduction potentials of the pyrrole substituted bpy  $\text{Ru}(\text{I})$  adducts reflect the electronic effects of the substituents on the bpy ring (Table 6.2). Where  $\text{L}$  is  $\text{L}_1$ ,  $\text{L}_3$  and  $\text{L}_4$  the potential of the reduction peak is measured to be  $-1.32$  V, while in the case of  $\text{L}_2$  a less negative value of  $-0.95$  V is seen, a consequence of the electron withdrawing ester moiety.

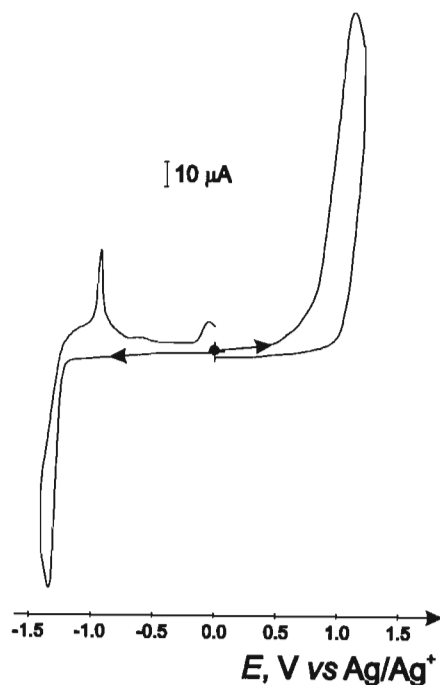


**Figure 6.4.** CV of  $[\text{Ru}_2(\text{L}_1)_2(\text{CO})_4(\text{CH}_3\text{CN})_2](\text{PF}_6)_2$  **14** 1.0 mM in  $\text{CH}_3\text{CN} + 0.1$  M TBAP. (Pt electrode,  $r = 2.5$  mm;  $\nu = 100$   $\text{mVs}^{-1}$ ).

**Table 6.2.** Cyclic voltammetric data of  $[\text{Ru}_2(\text{L})_2(\text{CO})_4(\text{CH}_3\text{CN})_2](\text{PF}_6)_2$  ( $\text{L} = \text{L}_{1-4}$ ) **14 - 17.**<sup>a</sup>

Complex $[\text{Ru}_2(\text{L})_2(\text{CO})_4(\text{CH}_3\text{CN})_2](\text{PF}_6)_2$	$\text{Ru}^{\text{I/0}}$		$\text{Ru}^{\text{II/I}}$ and $\text{Ru}^{\text{pyr/ppyr}}$
	$E_{\text{pc}} / \text{V}$	$E_{\text{pa}} / \text{V}$	$E_{\text{pa}} / \text{V}$
$\text{L}_1$ <b>14</b>	-1.32	-0.94	1.06
$\text{L}_2$ <b>15</b>	-0.95	-	1.02
$\text{L}_3$ <b>16</b>	-1.32	-0.88	1.01
$\text{L}_4$ <b>17</b>	-1.32	-0.92	1.10

<sup>a</sup> Potentials vs.  $\text{Ag}/\text{Ag}^+$ , measured in  $\text{CH}_3\text{CN}$  (0.1 M TBAP), scan rate  $100 \text{ mV s}^{-1}$ ,  $T = 298 \text{ K}$ . Definitions:  $E_{\text{pc}}$  and  $E_{\text{pa}}$  irreversible anodic and cathodic peak potentials.

As has been described for **12**, the reduction of the Ru(I) dimer complexes **14 - 17** substituted by pyrrole functionalised bpy ligands induces the formation of a Ru(0) polymer. With the exception of **14**, which shows a sharp but less intense dissolution peak at  $-0.94 \text{ V}$ , the complexes do not exhibit the classical electroprecipitation-redissolution form of the CV observed for **12** (see Figure 5.3). Instead, a broad ill-defined ‘daughter’ peak of the first reduction is seen for the complexes. This is probably due to the difference in solubility and adherence of the deposited Ru–Ru polymer containing the substituted bpy ligands compared to that of the standard  $[\text{Ru}(\text{bpy})(\text{CO})_2]_n$  polymer.

The direct electropolymerisation of the Ru(I) dimers in exclusion of a polypyrrole matrix can be brought about by repetitive reductive potential scans between chosen potential limits, or by an applied potential technique, to give adherent Ru–Ru bonded films. A summary of the cyclic voltammetric properties of the Ru(0) polymers is presented in Table 6.3.

**Table 6.3.** Electrochemical data of the  $[\text{Ru}(\text{L})(\text{CO})_2]_n$  ( $\text{L} = \text{L}_{1-4}$ ) polymers.<sup>a</sup>

Complex $[\text{Ru}(\text{L})(\text{CO})_2]_n$	$\text{Ru}^{\text{I/0}}$		$\text{L}^{\text{0/-}}$
	$E_{1/2}^{\text{b}}$	$E_{\text{pa}}^{\text{b,c}}$	$E_{1/2}^{\text{b}}$
bpy	-0.98	-0.73	-1.51
$\text{L}_1$	-1.07	-0.88	-1.34
$\text{L}_2$	-0.55 <sup>d</sup>	-0.50	-1.38
$\text{L}_3$	-1.10	-0.76	-1.31
$\text{L}_4$	-1.02	-0.80	-1.21

<sup>a</sup> Potentials vs.  $\text{Ag}/\text{Ag}^+$ , measured in  $\text{CH}_3\text{CN}$  (0.1 M TBAP), scan rate  $100 \text{ mV s}^{-1}$ ,  $T = 298 \text{ K}$ . Definitions:  $E_{1/2} = (E_{\text{pc}} + E_{\text{pa}})/2$ , where  $E_{\text{pc}}$  and  $E_{\text{pa}}$  are anodic and cathodic peak potentials. <sup>b</sup> See Figure 6.5. <sup>c</sup> Potential of the largest anodic peak observed during the anodic scan limited at 0 V. <sup>d</sup>  $E_{\text{pc}}$ , the return anodic wave is not observed.



The electroformation and cyclic voltammetric properties of  $[\text{Ru}(\text{L}_1)(\text{CO})_2]_n$ , shown in Figures 6.5(a) and (b), are representative of those of the complexes  $[\text{Ru}_2(\text{L})_2(\text{CO})_4(\text{CH}_3\text{CN})_2](\text{PF}_6)_2$  ( $\text{L} = \text{L}_1$  14,  $\text{L}_3$  16 and  $\text{L}_4$  17). During the electropolymerisation process two new reversible redox systems emerge with each successive cycle at  $E_{1/2} = -1.10$  and  $E_{1/2} = -1.32$  (Figure 6.5a). These correspond to the  $\text{Ru}^{\text{I/0}}$  and  $\text{L}^{\text{0/-}}$  couples respectively. When the polymer modified electrode is transferred to a clean electrolyte solution [Figure 6.5b(i)] the form of the CV is unchanged, attesting to the stability of the electroactivity of the Ru–Ru polymer. At potentials more positive of  $-1.00$  V the film is irreversibly oxidised ( $E_{\text{pa}} = -0.88$  V) leading to its oxidation and desorption [Figure 6.5b(ii)].

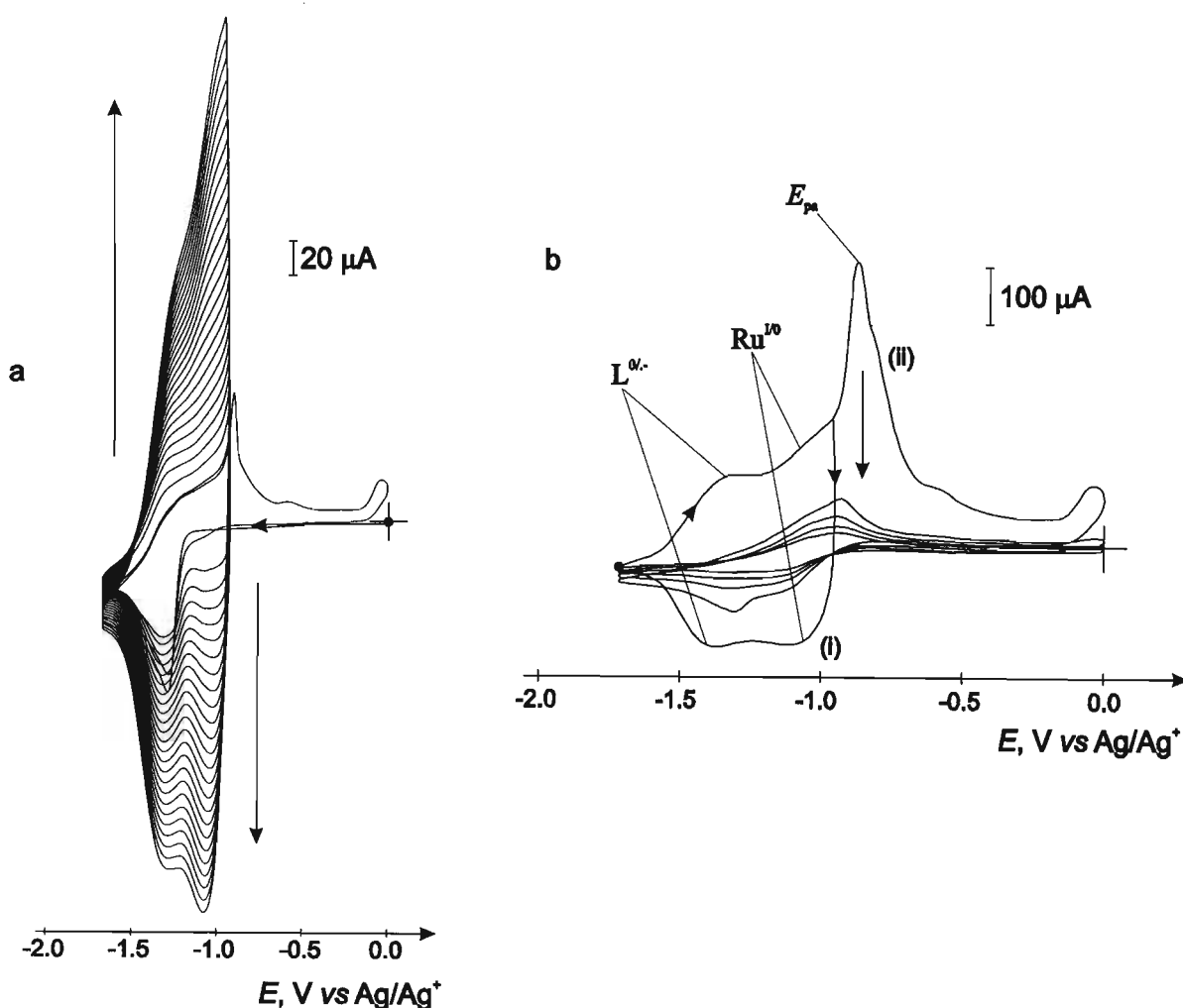


**Figure 6.5.** (a) 26 successive CVs between  $-0.94$  and  $-1.70$  V on a Pt electrode ( $r = 2.5$  mm) of  $[\text{Ru}_2(\text{L}_1)_2(\text{CO})_4(\text{CH}_3\text{CN})_2](\text{PF}_6)_2$  14 1.0 mM in  $\text{CH}_3\text{CN} + 0.1$  M TBAP. (b) CV of the resulting modified electrode in clean electrolyte; (i) first scan between  $-0.94$  and  $-1.70$  V; (ii) second to fifth scans between  $0.00$  and  $-1.70$  V.

The electrochemical properties of the Ru(0) polymers show the same features displayed by  $[\text{Ru}(\text{bpy})(\text{CO})_2]_n$  described earlier (see Section 5.2.2). A slight cathodic shift in the  $\text{Ru}^{I/0}$  redox potentials of  $[\text{Ru}(\text{L})(\text{CO})_2]_n$  ( $\text{L} = \text{L}_1, \text{L}_3$  and  $\text{L}_4$ ) relative to that of  $[\text{Ru}(\text{bpy})(\text{CO})_2]_n$  is seen, in keeping with the presence of the alkyl substituents on the bpy rings. On the other hand, the  $\text{L}^{0/-}$  couples of  $[\text{Ru}(\text{L})(\text{CO})_2]_n$  ( $\text{L} = \text{L}_1, \text{L}_3$  and  $\text{L}_4$ ) show an anodic shift relative to that of  $[\text{Ru}(\text{bpy})(\text{CO})_2]_n$ . Given the electron donating effects of the alkyl substituents this pattern is contrary to what one may expect. This difference in redox potentials has been observed previously between the polymer formed from  $[\text{Ru}(\text{bpy})(\text{CO})_2\text{Cl}_2]$  and those formed from  $[\text{Ru}(\text{L})(\text{CO})_2\text{Cl}_2]$  ( $\text{L} =$  diversely alkyl-substituted bpy).<sup>44</sup> Indeed the cyclic voltammetric properties of  $[\text{Ru}(\text{L})(\text{CO})_2]_n$  ( $\text{L} = \text{L}_1, \text{L}_3$  and  $\text{L}_4$ ) are very similar to those of the Ru(0) polymers containing the alkyl-substituted bpy ligands. Caix-Cecillon *et al.* proposed that in  $[\text{Ru}(\text{bpy})(\text{CO})_2]_n$  a stronger stacking effect of the unsubstituted bpy rings takes place, leading to a more compact structure of the polymer and a greater Ru(0) stabilization. It is reasonable to draw an analogy between this example and the Ru(0) polymers discussed here, in which the 4,4' substituents on the bipyridyl ring would prevent an ordered stacking of the bpy rings.

The influence of the bpy substituents on the physico-chemical properties of the polymer is also evident when the dissolution peak of the polymers is considered. This is very intense in the case of  $[\text{Ru}(\text{bpy})(\text{CO})_2]_n$  [see Figure 5.7(b)] while for  $[\text{Ru}(\text{L}_1)(\text{CO})_2]_n$ , though it has the same sharp form, it is much less intense [Figure 6.5(b)(ii)]. For the ligands  $[\text{Ru}(\text{L})(\text{CO})_2]_n$  ( $\text{L} = \text{L}_3$  and  $\text{L}_4$ ) it is broad and of the same magnitude as the reversible redox systems of the polymer. This change in the form of the oxidation-dissolution peak, which represents the further oxidation of the partially oxidized polymer  $[\{\text{Ru}(\text{L})(\text{CO})_2\}^{\delta+}]_n$  and its subsequent detachment from the electrode surface to soluble oligomeric species in solution, probably reflects an increased solubility of the partially oxidized polymer caused by the alkyl-pyrrole substituents.

Figure 6.6(a) shows the formation of  $[\text{Ru}(\text{L}_2)(\text{CO})_2]_n$  on a Pt electrode by repetitive scan cyclic voltammetry of a  $\text{CH}_3\text{CN}$  solution of **15**. The cathodic electroactivity of the resulting Ru(0) polymer modified electrode in clean electrolyte is shown in Figure 6.6b(i), the potential limits of the cathodic scan being chosen so as to avoid decomposition of the polymer film. The metal based process  $\text{Ru}^{I/0}$  is partially visible at  $-0.55$  V, while the ligand based redox system  $\text{L}^{0/-}$  is observable at  $-1.38$  V. The potentials of the  $\text{Ru}^{I/0}$  and  $\text{L}^{0/-}$  couples of  $[\text{Ru}(\text{L}_2)(\text{CO})_2]_n$  show a noticeable anodic shift in comparison to those of  $[\text{Ru}(\text{bpy})(\text{CO})_2]_n$ . This must be due to the more electron-withdrawing nature of the carboxylic substituent in  $\text{L}_2$ . Two additional peaks are seen at  $-1.24$  and  $-0.76$  V in the CV of  $[\text{Ru}(\text{L}_2)(\text{CO})_2]_n$ , the sharp forms of which are alike to 'pre-peaks' previously observed in polypyrrole films.<sup>173,174</sup> They may arise from the sudden

oxidation or reduction of a layer of polymer by a neighbouring layer which is in a different oxidation state. When the potential is scanned to less negative than  $-0.55$  V, two intense dissolution peaks which arise from the irreversible oxidation and dissolution of the polymer are seen at  $-0.50$  and  $-0.44$  V [Figure 6.6b(ii)].

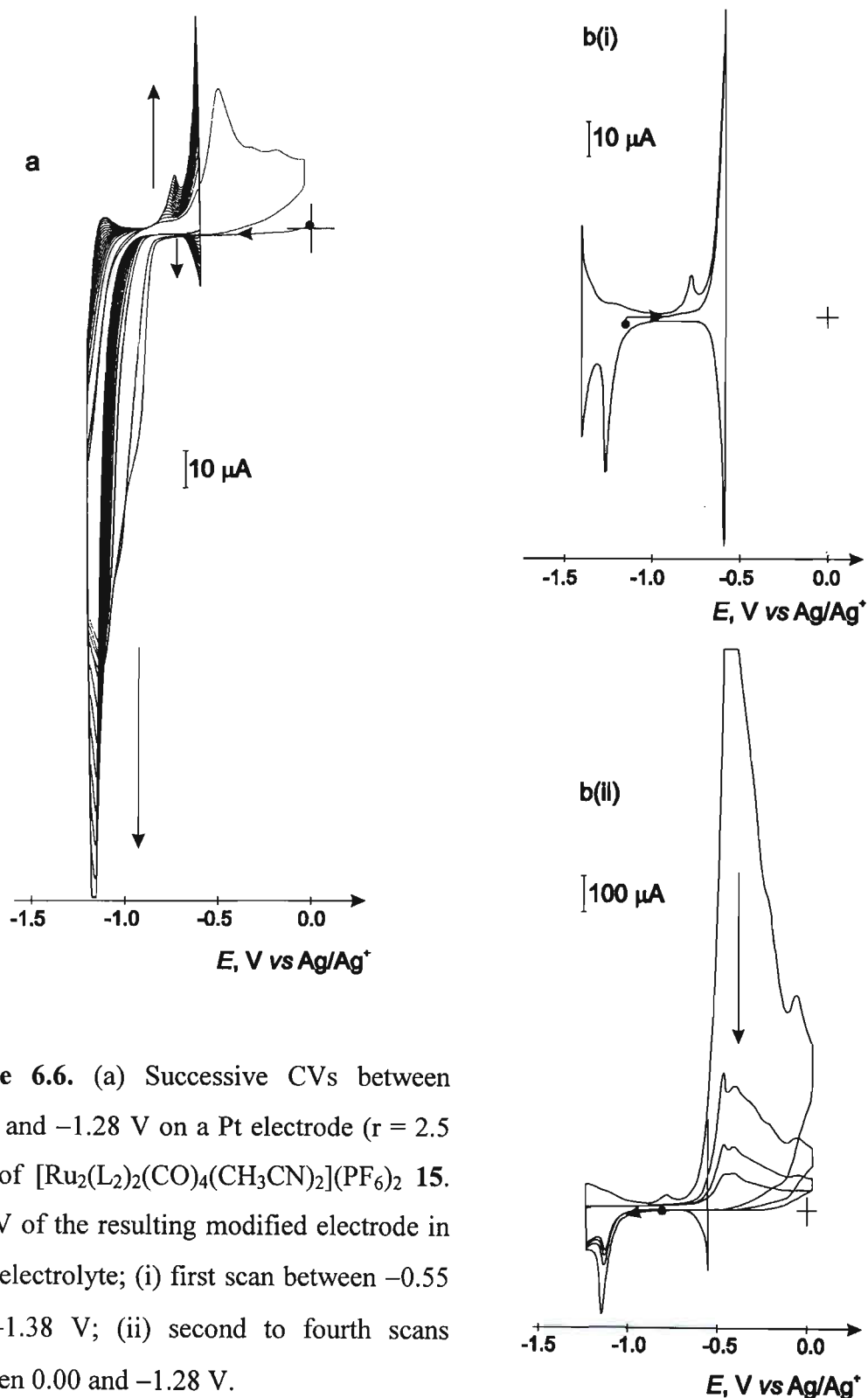


**Figure 6.6.** (a) Successive CVs between  $-0.55$  and  $-1.28$  V on a Pt electrode ( $r = 2.5$  mm) of  $[\text{Ru}_2(\text{L}_2)_2(\text{CO})_4(\text{CH}_3\text{CN})_2](\text{PF}_6)_2$  **15**. (b) CV of the resulting modified electrode in clean electrolyte; (i) first scan between  $-0.55$  and  $-1.38$  V; (ii) second to fourth scans between  $0.00$  and  $-1.28$  V.

### 6.2.2.(ii) Oxidation

The complexes **14** – **17** show an intense irreversible oxidation peak in the anodic region of their CVs (Table 6.2 and Figure 6.4). Both the irreversible oxidation of the pyrrole group<sup>175</sup> and the Ru–Ru bond in  $[\text{Ru}_2(\text{bpy})_2(\text{CO})_4(\text{CH}_3\text{CN})_2](\text{PF}_6)_2$  **12** occur at approximately this potential. It is probable that both these processes give rise to the oxidation peak observed here.

The complexes **15** and **17** could be oxidatively electropolymerised to give electrodes modified by polypyrrole films containing the pendant ruthenium complexes. The redox properties of these polypyrrole films are presented in Table 6.4. However, the electropolymerisation of **16** was inefficient, while **14** showed no polypyrrole formation despite numerous attempts under different conditions.

**Table 6.4.** Cyclic voltammetric data of ppyr- $[\text{Ru}_2(\text{L})_2(\text{CO})_4(\text{CH}_3\text{CN})_2](\text{PF}_6)_2$  (L = L<sub>2-4</sub>) **15** - **17**.<sup>a</sup>

Complex	Ru <sup>II</sup>		ppyr
	$E_{\text{pc}}^{\text{b}} / \text{V}$	$E_{\text{pa}}^{\text{b}} / \text{V}$	
ppyr- $[\text{Ru}_2(\text{L})_2(\text{CO})_4(\text{CH}_3\text{CN})_2](\text{PF}_6)_2$			$E_{\frac{1}{2}}^{\text{c}}$
L <sub>2</sub> <b>15</b>	-1.06	0.11	0.28
L <sub>3</sub> <b>16</b>	-1.66	0.42	0.35
L <sub>4</sub> <b>17</b>	-2.16	0.33	0.40

<sup>a</sup> Potentials vs. Ag/Ag<sup>+</sup>, measured in CH<sub>3</sub>CN (0.1 M TBAP), scan rate 100 mV s<sup>-1</sup>, T = 298 K. Definitions: <sup>b</sup>  $E_{\text{pc}}$  and  $E_{\text{pa}}$  are the irreversible cathodic and anodic peak potentials. <sup>c</sup>  $E_{\frac{1}{2}} = (E_{\text{pc}} + E_{\text{pa}})/2$ , where  $E_{\text{pc}}$  and  $E_{\text{pa}}$  are anodic and cathodic peak potentials.

A possible reason for this difference in the tendency of the complexes to form polypyrrole films lies in the oxidation potentials of the pyrrole moiety and the metal-metal bond in the various dimers. It would be anticipated that the alkyl substituted bpy ligands L<sub>1</sub>, L<sub>3</sub> and L<sub>4</sub> would stabilise the Ru–Ru bond to a lesser extent than L<sub>2</sub>. It is likely that at the anodic potentials required to initiate polymerisation of the pyrrole moiety in the complexes  $[\text{Ru}_2(\text{L})_2(\text{CO})_4(\text{CH}_3\text{CN})_2](\text{PF}_6)_2$  (L = L<sub>1</sub> and L<sub>3</sub>) the irreversible oxidation of the Ru–Ru bond will predominate, leading to an inefficient polymerisation. On the other hand, the applied potentials required to polymerise  $[\text{Ru}_2(\text{L})_2(\text{CO})_4(\text{CH}_3\text{CN})_2](\text{PF}_6)_2$  (L = L<sub>2</sub> and L<sub>4</sub>), of 0.85 and 0.73 V for L<sub>2</sub> and L<sub>4</sub> respectively, are less anodic than the potential that could be anticipated for oxidation of the metal-metal bond. The greater stabilisation of the Ru–Ru bond in  $[\text{Ru}_2(\text{L}_2)_2(\text{CO})_4(\text{CH}_3\text{CN})_2](\text{PF}_6)_2$ , coordinated by the more electron-accepting ligand L<sub>2</sub>, allows for the efficient polymerisation of the complex.

In the case of the mononuclear complexes  $[\text{Ru}(\text{bpy})_2(\text{L})_2]^{2+}$  (L = pyrrole substituted pyridyl ligand) and  $[\text{Ru}(\text{bpy})_n(\text{L})_{3-n}]^{2+}$  (L = pyrrole substituted bipyridyl ligand), it has been

shown that the efficiency of polymerisation and the stability of the resulting film increases with the number of pyrrole groups per metal centre.<sup>170,176</sup> In comparison to **14**, the additional pyrrole units in **16** permit its weak polymerisation absent in the former complex. This same argument can be applied to **17**, where the higher insolubility of the polymer would provide an additional driving force to the polymerisation process.

Electrodeposition of the ppyr-[Ru<sub>2</sub>(L)<sub>2</sub>(CO)<sub>4</sub>(CH<sub>3</sub>CN)<sub>2</sub>](PF<sub>6</sub>)<sub>2</sub> (L = L<sub>2</sub> and L<sub>4</sub>) films was performed using repetitive scan cyclic voltammetry or chronoamperometry at an optimised potential value. Figure 6.8a illustrates the formation of ppyr-[Ru<sub>2</sub>(L<sub>2</sub>)<sub>2</sub>(CO)<sub>4</sub>(CH<sub>3</sub>CN)<sub>2</sub>](PF<sub>6</sub>)<sub>2</sub>, with the reversible oxidation couple of the polypyrrole film becoming more prominent with each scan. When ppyr-[Ru<sub>2</sub>(L)<sub>2</sub>(CO)<sub>4</sub>(CH<sub>3</sub>CN)<sub>2</sub>](PF<sub>6</sub>)<sub>2</sub> (L = L<sub>2</sub> and L<sub>4</sub>) modified electrodes were transferred to clean electrolyte they showed the electroactivity typical of N-substituted polypyrroles in which a quasi-reversible oxidation of the polypyrrole is observed (Figure 6.8b).<sup>175</sup> In the case of ppyr-[Ru<sub>2</sub>(L<sub>3</sub>)<sub>2</sub>(CO)<sub>4</sub>(CH<sub>3</sub>CN)<sub>2</sub>](PF<sub>6</sub>)<sub>2</sub> only a poorly defined system is seen, reflecting an inferior formation of this film.

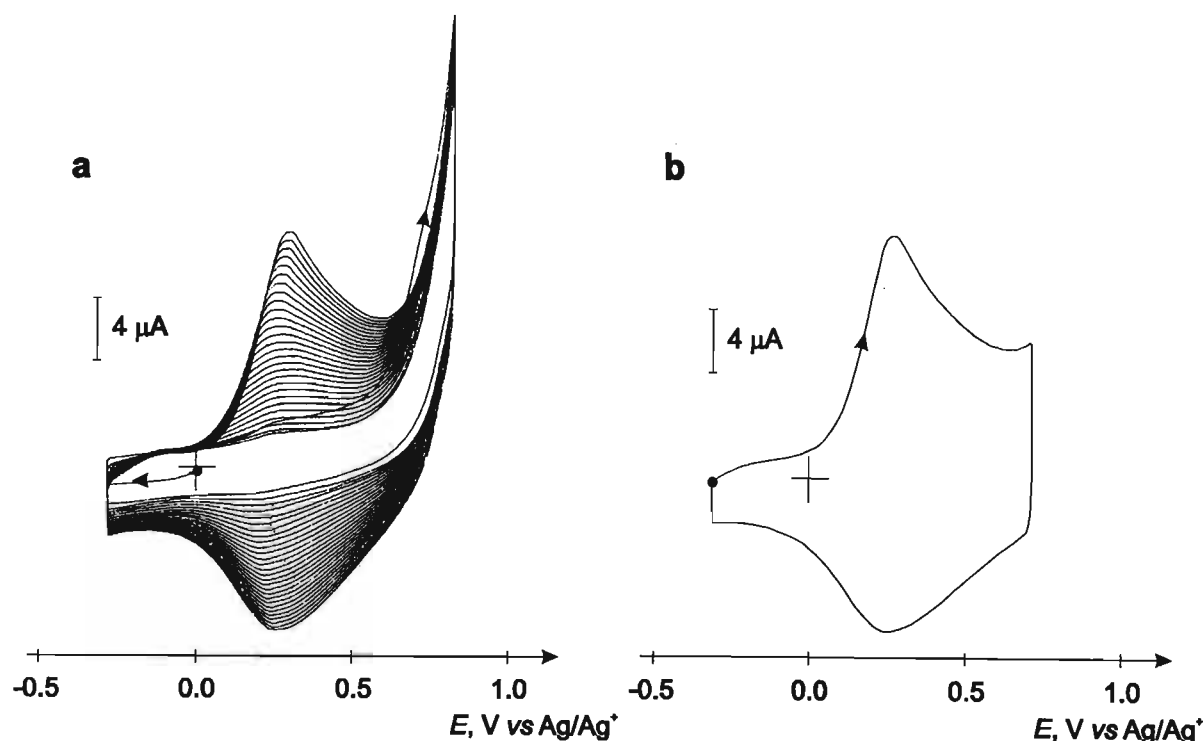


**Figure 6.8.** (a) Successive CVs ( $\nu = 100 \text{ mVs}^{-1}$ ), on a Pt electrode ( $r = 2.5 \text{ mm}$ ), of [Ru<sub>2</sub>(L<sub>2</sub>)<sub>2</sub>(CO)<sub>4</sub>(CH<sub>3</sub>CN)<sub>2</sub>](PF<sub>6</sub>)<sub>2</sub> **15** 1.0 mM in CH<sub>3</sub>CN + 0.1 M TBAP, showing the growth of the polypyrrole film by repeated potential scans between  $-0.30$  and  $0.85 \text{ V}$ . (b) Resulting ppyr-[Ru<sub>2</sub>(L<sub>2</sub>)<sub>2</sub>(CO)<sub>4</sub>(CH<sub>3</sub>CN)<sub>2</sub>](PF<sub>6</sub>)<sub>2</sub> modified electrode in pure electrolyte scanned between  $-0.30$  and  $0.85 \text{ V}$ .

The thickness of the ppyr-[Ru<sub>2</sub>(L)<sub>2</sub>(CO)<sub>4</sub>(CH<sub>3</sub>CN)<sub>2</sub>](PF<sub>6</sub>)<sub>2</sub> (L = L<sub>2</sub> and L<sub>4</sub>) films, as measured by apparent surface coverages  $\Gamma_{\text{Ru}}$  (mol cm<sup>-2</sup>) (calculation of  $\Gamma_{\text{Ru}}$  is detailed in Section 6.4.) of the order of 10<sup>-9</sup> to 10<sup>-8</sup>, is comparable to films obtained from similar Ru(II) mononuclear complexes prepared under similar conditions.<sup>177,178</sup> The efficiency of the formation of the polypyrrole films was typical of a N-functionalised pyrrole monomer precursor containing a metal complex; after the passage of 5, 10 and 15 mC the electropolymerisation yields were 31, 16 and 12 % for ppyr-[Ru<sub>2</sub>(L<sub>2</sub>)<sub>2</sub>(CO)<sub>4</sub>(CH<sub>3</sub>CN)<sub>2</sub>](PF<sub>6</sub>)<sub>2</sub>, and 41, 34 and 31 % for ppyr-[Ru<sub>2</sub>(L<sub>4</sub>)<sub>2</sub>(CO)<sub>4</sub>(CH<sub>3</sub>CN)<sub>2</sub>](PF<sub>6</sub>)<sub>2</sub>. The charge transport through the film becomes rate limiting as the film thickness increases. As a result, a poorer yield and electrochemical response were observed with increasing film thickness.

### 6.2.2.(iii) Electroactivity of ppyr-[Ru<sub>2</sub>(L)<sub>2</sub>(CO)<sub>4</sub>(CH<sub>3</sub>CN)<sub>2</sub>](PF<sub>6</sub>)<sub>2</sub> (L = L<sub>2</sub> and L<sub>4</sub>)

Cathodic scans reveal the different electroactivities of the immobilised ruthenium complexes in the polypyrrole films (Table 6.4). Common to both ppyr-[Ru<sub>2</sub>(L)<sub>2</sub>(CO)<sub>4</sub>(CH<sub>3</sub>CN)<sub>2</sub>](PF<sub>6</sub>)<sub>2</sub> (L = L<sub>2</sub> and L<sub>4</sub>) is the presence on the first scan of an intense irreversible reduction peak, which decreases in intensity when the potential of the electrode is repetitively scanned. If the potential is scanned to more positive values an intense oxidation peak is observed. This is illustrated by the behaviour of ppyr-[Ru<sub>2</sub>(L<sub>2</sub>)<sub>2</sub>(CO)<sub>4</sub>(CH<sub>3</sub>CN)<sub>2</sub>](PF<sub>6</sub>)<sub>2</sub>, depicted in Figure 6.9(a). This behaviour shows that the metal complex is encapsulated in the polypyrrole film. Furthermore, it supports the formation of Ru<sup>0</sup>-Ru<sup>0</sup> bonds upon reduction of the Ru(I) dimers, leading to a polypyrrole immobilised Ru(0) polymer ppyr-[Ru(L)(CO)<sub>2</sub>]<sub>n</sub>, through a mechanism probably similar to that described for the formation of [Ru(bpy)(CO)<sub>2</sub>]<sub>n</sub> from 12. The structural nature of the Ru(0) polymer chains is uncertain and will be constrained by the morphology of the polypyrrole film. It is expected that reduction of the Ru(I) dimers supported in the polypyrrole film will lead to the formation of shorter Ru<sup>0</sup>-Ru<sup>0</sup> bonded units than those formed in the absence of a polypyrrole film.

The electroactivity of ppyr-[Ru<sub>2</sub>(L<sub>2</sub>)<sub>2</sub>(CO)<sub>4</sub>(CH<sub>3</sub>CN)<sub>2</sub>](PF<sub>6</sub>)<sub>2</sub> in particular is reminiscent of that previously observed for Ru(II) polypyrrole supported complexes,<sup>37,172</sup> repetitive cycling of the potential giving rise to several stable electrochemical systems. The CV of the final ppyr-[Ru(L<sub>2</sub>)(CO)<sub>2</sub>]<sub>n</sub> polymer shows two reversible processes at  $E_{1/2}$  -1.07 and -1.42 V, followed by a quasi-reversible process at  $E_{1/2}$  -1.83 [Figure 6.9(b)].

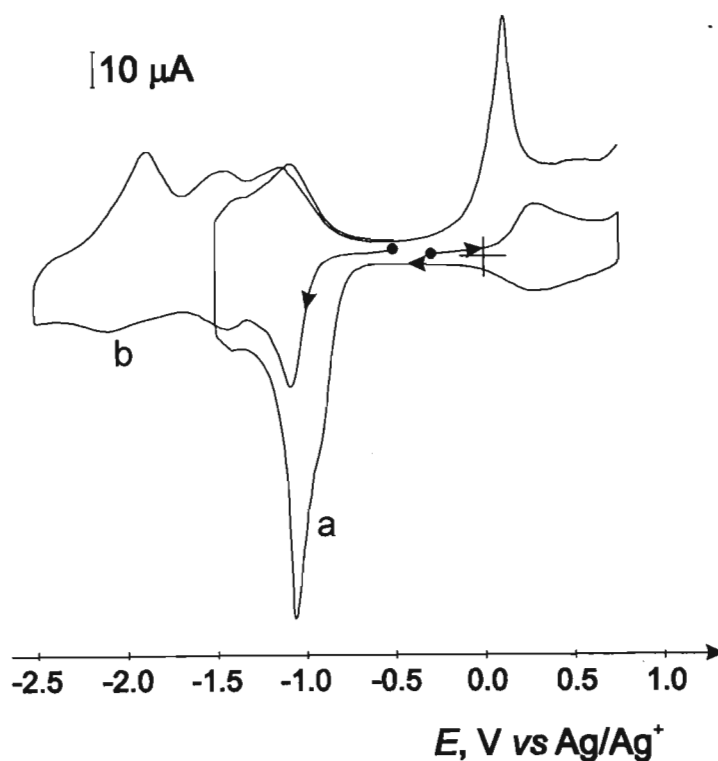


**Figure 6.9.** Pt electrode ( $r = 2.5$  mm) modified by  $\text{ppyr-}[\text{Ru}_2(\text{L}_2)_2(\text{CO})_4(\text{CH}_3\text{CN})_2](\text{PF}_6)_2$  in  $\text{CH}_3\text{CN} + 0.1$  M TBAP; (a) initial CV scan from  $-0.30$  to  $0.74$  V; (b) CV between  $-0.50$  and  $-2.50$  V of  $\text{ppyr-}[\text{Ru}(\text{L}_2)(\text{CO})_2]_n$ , formed by repetitive scans between  $-0.50$  and  $-1.35$  V.

On the other hand the cathodic scan of  $\text{ppyr-}[\text{Ru}_2(\text{L}_4)_2(\text{CO})_4(\text{CH}_3\text{CN})_2](\text{PF}_6)_2$  shows a single intense reduction peak at  $-2.16$  V [Figure 6.10(a)]. Repetitive scanning of the electrode potential leads to a CV showing a reduction peak at  $-2.16$  and an oxidation peak at  $-1.02$  V on the reverse scan. A marked increase in the potential required to reduce the Ru(I) complex is seen between  $\text{ppyr-}[\text{Ru}_2(\text{L}_2)_2(\text{CO})_4(\text{CH}_3\text{CN})_2](\text{PF}_6)_2$  and  $\text{ppyr-}[\text{Ru}_2(\text{L}_4)_2(\text{CO})_4(\text{CH}_3\text{CN})_2](\text{PF}_6)_2$ , as could be anticipated from the opposing electron donor / acceptor properties of their respective bpy substituents. Furthermore, in replacing the ester linkage between the pyrrole and bpy rings by a  $\text{C}_{13}$  alkyl chain in  $\text{ppyr-}[\text{Ru}_2(\text{L}_4)_2(\text{CO})_4(\text{CH}_3\text{CN})_2](\text{PF}_6)_2$  the electron-transfer properties of the film would be expected to decrease. This difference in conductivity of the polypyrrole film must also contribute to the difference in electrochemical properties shown by  $\text{ppyr-}[\text{Ru}(\text{L}_2)(\text{CO})_2]_n$  and  $\text{ppyr-}[\text{Ru}(\text{L}_4)(\text{CO})_2]_n$ .

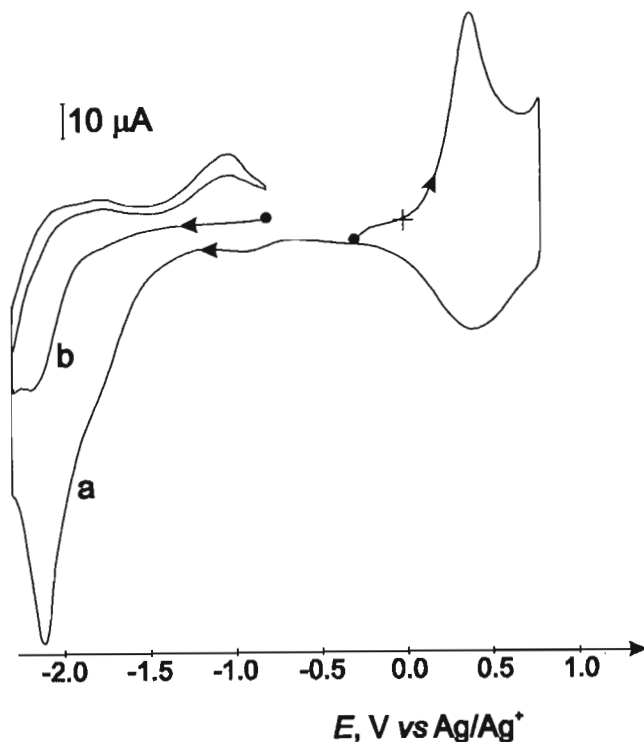


**Figure 6.10.** Pt electrode ( $r = 2.5$  mm) modified by  $\text{ppyr-}[\text{Ru}_2(\text{L}_4)_2(\text{CO})_4(\text{CH}_3\text{CN})_2](\text{PF}_6)_2$  in  $\text{CH}_3\text{CN} + 0.1$  M TBAP; (a) initial CV scan from  $-0.30$  to  $-0.80$  V; (b) CV between  $-0.80$  and  $-2.30$  V of  $\text{ppyr-}[\text{Ru}(\text{L}_4)(\text{CO})_2]_n$ , formed by repetitive scans between  $-0.80$  and  $-2.30$  V.

### 6.2.3. Catalytic Properties Towards $\text{CO}_2$ Electrochemical Reduction of $\text{ppyr-}[\text{Ru}(\text{L})(\text{CO})_2]_n$ ( $\text{L} = \text{L}_2$ and $\text{L}_4$ )

The CV of a glassy carbon electrode modified by  $\text{ppyr-}[\text{Ru}_2(\text{L}_2)_2(\text{CO})_4(\text{CH}_3\text{CN})_2](\text{PF}_6)_2$  in  $\text{CO}_2$  saturated  $\text{CH}_3\text{CN} + 0.1$  M TBAP showed a strong enhancement in current beginning at *ca.*  $-1.2$  V, revealing its catalytic activity towards the electrochemical reduction of  $\text{CO}_2$ . The stepwise addition of  $\text{H}_2\text{O}$  from 1 to 10 % leads to a parallel increase in catalytic current and a slight shift to less negative values of the threshold potential to *ca.*  $-1.1$  V. In  $\text{CO}_2$  saturated  $\text{H}_2\text{O} + 0.1$  M  $\text{LiClO}_4$  the CV of a  $\text{ppyr-}[\text{Ru}_2(\text{L}_2)_2(\text{CO})_4(\text{CH}_3\text{CN})_2](\text{PF}_6)_2$  modified glassy carbon electrode also exhibits a catalytic effect, the enhancement in current beginning at  $-0.76$  V vs.  $\text{Ag}/\text{AgCl}$ .

Conversely the CV of a  $\text{ppyr-}[\text{Ru}_2(\text{L}_4)_2(\text{CO})_4(\text{CH}_3\text{CN})_2](\text{PF}_6)_2$  modified glassy carbon electrode in a  $\text{CO}_2$  saturated  $\text{CH}_3\text{CN} + 0.1$  M TBAP medium showed no catalytic current when the potential is scanned to  $-2.10$  V. However, a catalytic current appeared immediately upon the addition of 1 %  $\text{H}_2\text{O}$ . With the stepwise addition of  $\text{H}_2\text{O}$  to a optimal concentration of 10 %, the catalytic current increased in intensity and its threshold potential became less negative, giving a



final value of *ca.* -1.60 V. In pure aqueous electrolyte (H<sub>2</sub>O + 0.1 M LiClO<sub>4</sub>) under an atmosphere of Ar, the CV of a ppyr-[Ru<sub>2</sub>(L<sub>4</sub>)<sub>2</sub>(CO)<sub>4</sub>(CH<sub>3</sub>CN)<sub>2</sub>](PF<sub>6</sub>)<sub>2</sub> modified glassy carbon electrode showed a catalytic current at -1.80 V due to H<sup>+</sup> reduction. Unexpectedly, the CV recorded in the same electrolyte saturated with CO<sub>2</sub> showed a strong enhancement in current only at a more negative potential of -2.00 V. This differing behaviour in comparison to ppyr-[Ru<sub>2</sub>(L<sub>2</sub>)<sub>2</sub>(CO)<sub>4</sub>(CH<sub>3</sub>CN)<sub>2</sub>](PF<sub>6</sub>)<sub>2</sub> must be a consequence of the hydrophobic nature of the long alkyl chains that anchor the metal complex to the polypyrrole film.

Preparative scale electrolysis using ppyr-[Ru<sub>2</sub>(L)<sub>2</sub>(CO)<sub>4</sub>(CH<sub>3</sub>CN)<sub>2</sub>](PF<sub>6</sub>)<sub>2</sub> (L = L<sub>2</sub> and L<sub>4</sub>) modified carbon felt electrodes in CO<sub>2</sub> saturated CH<sub>3</sub>CN / 10 % H<sub>2</sub>O + 0.1 M TBAP demonstrated their catalytic behaviour and allowed for the analysis of the CO<sub>2</sub> reduction products (Table 6.5). Ru(0) polymers are formed in the polypyrrole matrix during the course of the controlled potential electrolysis. Ultimately the active catalytic species will therefore be the Ru-Ru bonded polymers ppyr-[Ru(L)(CO)<sub>2</sub>]<sub>n</sub> (L = L<sub>2</sub> and L<sub>4</sub>). While the dominant product of reduction catalysed by ppyr-[Ru(L<sub>4</sub>)(CO)<sub>2</sub>(CH<sub>3</sub>CN)]<sub>2</sub>(PF<sub>6</sub>) is CO, that of the reduction catalysed by ppyr-[Ru(L<sub>2</sub>)(CO)<sub>2</sub>(CH<sub>3</sub>CN)]<sub>2</sub>(PF<sub>6</sub>) is HCOO<sup>-</sup>. As has been previously observed, this product distribution is a result of the opposite donor / acceptor properties of the 4,4' bpy ring substituents in L<sub>2</sub> and L<sub>4</sub>.<sup>42,179</sup>

**Table 6.5.** Electrocatalytic properties of ppyr-[Ru(L)(CO)<sub>2</sub>]<sub>n</sub> (L = L<sub>2</sub> and L<sub>4</sub>) towards CO<sub>2</sub> electrochemical reduction.

ppyr-[Ru(L)(CO) <sub>2</sub> ] <sub>n</sub>	<i>E</i> <sub>app</sub> / V	Q / C	<i>i</i> / mA	Faradaic Yield / %	
			(change in <i>i</i> per 10 C)	HCOO <sup>-</sup>	CO
L <sub>2</sub>	-1.40	73	5.1 (-0.3)	9	80
L <sub>4</sub>	-1.10	118	7.5 (-0.1)	77	0

#### 6.2.4. [Ru<sub>2</sub>(CO)<sub>4</sub>(CH<sub>3</sub>CN)<sub>6</sub>](PF<sub>6</sub>)<sub>2</sub> - a Potential Precursor for the Electrosynthesis of Mononuclear 2,2'-bipyridine Ligand Complexes of Ruthenium(II)

##### 6.2.4.(i) *trans*(CH<sub>3</sub>CN)-[Ru(bpy)(CO)<sub>2</sub>(CH<sub>3</sub>CN)<sub>2</sub>]<sup>2+</sup>

The CV of the ruthenium dimer [Ru<sub>2</sub>(CO)<sub>4</sub>(CH<sub>3</sub>CN)<sub>6</sub>](PF<sub>6</sub>)<sub>2</sub> shows an irreversible, poorly defined reduction peak at -1.70 V with no associated anodic peak and an irreversible oxidation peak at 1.26 V. The exhaustive electrolysis of this complex at 1.30 V in CH<sub>3</sub>CN + 0.1 M TBAP consumes 2.2 equivalents of electrons per mole of dimer. It leads to a solution which shows in its

CV an irreversible reduction peak at  $-1.44$  V, while no electroactivity is observed in the anodic region of the scan [Figure 6.11(a)].

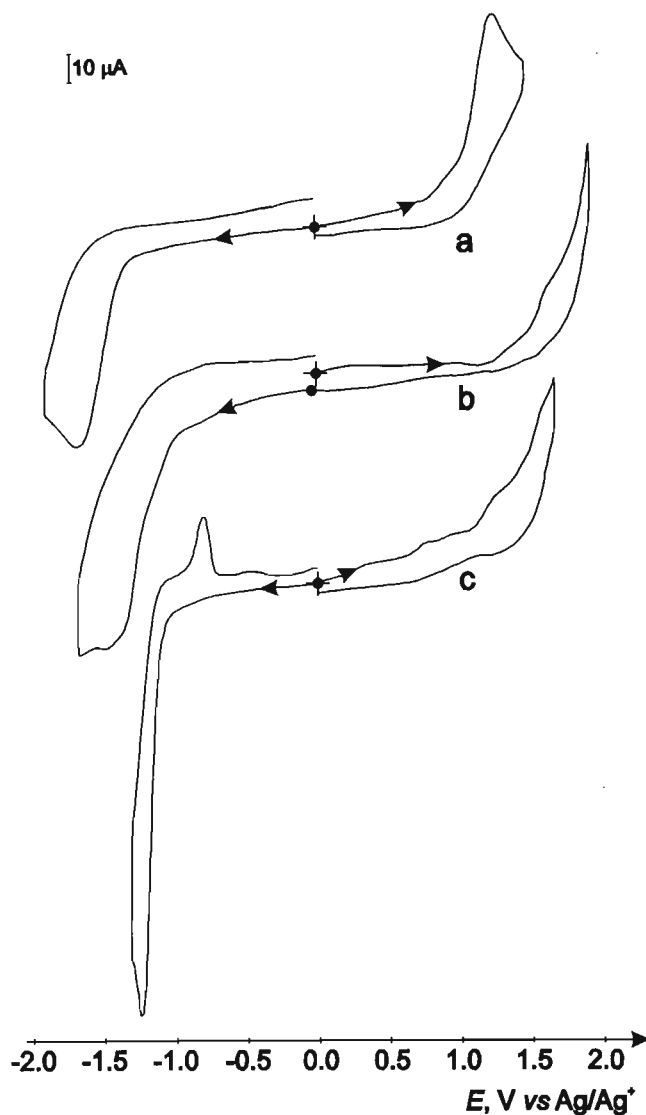
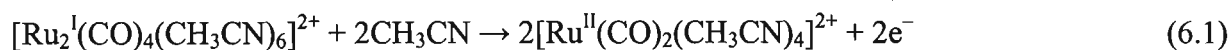


**Figure 6.11.** CVs ( $v = 100 \text{ mVs}^{-1}$ ), on a Pt electrode ( $r = 2.5 \text{ mm}$ ); (a)  $[\text{Ru}_2(\text{CO})_4(\text{CH}_3\text{CN})_6](\text{PF}_6)_2$  1.0 mM in  $\text{CH}_3\text{CN} + 0.1 \text{ M TBAP}$ ; (b) after exhaustive electrolysis at  $E_{\text{app}} 1.30 \text{ V}$ ; (c) 15 h after the addition of 1 equivalent of bpy to the oxidized solution.

The IR spectrum of this solution exhibits two major absorption bands at  $2135$  and  $2091 \text{ cm}^{-1}$  in the terminal CO stretching region. In comparison, that of  $[\text{Ru}_2(\text{CO})_4(\text{CH}_3\text{CN})_6](\text{PF}_6)_2$  recorded in the same electrolyte shows four absorption bands at  $2033$ ,  $2006$ ,  $1961$  and  $1946 \text{ cm}^{-1}$ . The coulometry of the exhaustive oxidation, the absence of any anodic electroactivity, the shift to higher wavenumbers of the  $\nu_{\text{CO}}$  absorption bands and the simplification of the IR absorption envelope suggest that the electrochemical oxidation of the Ru(I) dimer affords a Ru(II) mononuclear complex. The breakage of the metal-metal bond

induced by oxidation would be accompanied by the coordination of the acetonitrile solvent, giving the proposed intermediate complex  $[\text{Ru}(\text{CO})_2(\text{CH}_3\text{CN})_4]^{2+}$  (Equation 6.1).



One equivalent of bpy was added to the Ru(II) intermediate species [assuming 100 % conversion of Ru(I) to Ru(II)] and the progress of the reaction followed *in situ* by cyclic voltammetry and IR spectroscopy. It is found to go to completion after 15 h of stirring at room temperature. The IR spectrum of the final solution shows two major absorbances at 2116 and 2069  $\text{cm}^{-1}$  in the terminal carbonyl region. The CV of this solution, shown in Figure 6.11(b), displays a reduction peak at  $-1.24$  V and a corresponding anodic peak at  $-0.86$  V, while the anodic cyclic voltammetric scan shows that the resulting complex is not oxidised within the solvent limit of 1.5 V. The cyclic voltammetric properties and IR absorption spectrum of the final complex match those of the Ru(II) mononuclear complex  $[\text{Ru}(\text{bpy})(\text{CO})_2(\text{CH}_3\text{CN})_2](\text{PF}_6)_2$  reported previously.<sup>39</sup> In keeping with the electrochemical properties reported for  $[\text{Ru}(\text{bpy})(\text{CO})_2(\text{CH}_3\text{CN})_2](\text{PF}_6)_2$ , repetitive scanning of the electrode potential between  $-0.80$  and  $-1.70$  V leads to the progressive formation of the Ru–Ru bonded polymer  $[\text{Ru}(\text{bpy})(\text{CO})_2]_n$ . The use of a  $\text{CD}_3\text{CN} + \text{LiClO}_4$  electrolyte allowed for the  $^1\text{H}$  NMR analysis of the product and to deduce the confirmation of the isomer formed. This is as reported for *trans*( $\text{CH}_3\text{CN}$ )- $[\text{Ru}(\text{bpy})(\text{CO})_2(\text{CH}_3\text{CN})_2](\text{PF}_6)_2$ , the  $^1\text{H}$  NMR spectrum of the complex showing four sets of aromatic proton signals due to the bpy ligand; the latter implies that the bpy ligand shares the equatorial plane with the two CO ligands.

#### 6.2.4.(ii) *trans*( $\text{CH}_3\text{CN}$ )- $[\text{Ru}(\text{L}_1)(\text{CO})_2(\text{CH}_3\text{CN})_2]^{2+}$

The electrosynthetic approach described above was extended to the synthesis of the Ru(II) monomer complex substituted by the N-pyrrole functionalised bpy ligand  $\text{L}_1$ .

To an electrolyte solution of  $[\text{Ru}(\text{CO})_2(\text{CH}_3\text{CN})_4]^{2+}$ , obtained by the exhaustive oxidation of  $[\text{Ru}_2(\text{CO})_4(\text{CH}_3\text{CN})_6](\text{PF}_6)_2$ , was added one equivalent of  $\text{L}_1$ . The FT-IR spectrum of the resultant solution obtained after 18 h of stirring at room temperature exhibited two strong terminal carbonyl absorbances at 2115 and 2067  $\text{cm}^{-1}$ , while its CV (Figure 6.12) exhibited an irreversible reduction peak at  $-1.32$  V. These FT-IR and electrochemical features are characteristic of a Ru(II) mononuclear complex  $[\text{Ru}(\text{L})(\text{CO})_2(\text{CH}_3\text{CN})_2](\text{PF}_6)_2$ , where L is a bpy type ligand.<sup>39</sup> Under the conditions of this electrochemical synthesis and on the time scale of the cyclic voltammetric scan the typical anodic peak corresponding to the redissolution of the Ru(0)

polymer formed upon reduction is not observed. This could be a consequence of the difference in solubility of the polymer species caused by the bpy alkyl-pyrrole substitution. Nevertheless, in this medium the complex could be electropolymerised to a stable blue-grey Ru–Ru bonded polymer on the electrode surface by repetitive scan cyclic voltammetry. The electroactivity of this Ru(0) polymer in clean electrolyte reflects that of  $[\text{Ru}(\text{L}_1)(\text{CO})_2]_n$ , prepared by reduction of  $[\text{Ru}_2(\text{L}_1)_2(\text{CO})_4(\text{CH}_3\text{CN})_2](\text{PF}_6)_2$  [section 5.2.2.(ii)] or the equivalent bis-chloro Ru(II) precursor  $[\text{Ru}(\text{L}_1)(\text{CO})_2\text{Cl}_2]$ .<sup>37,39</sup>

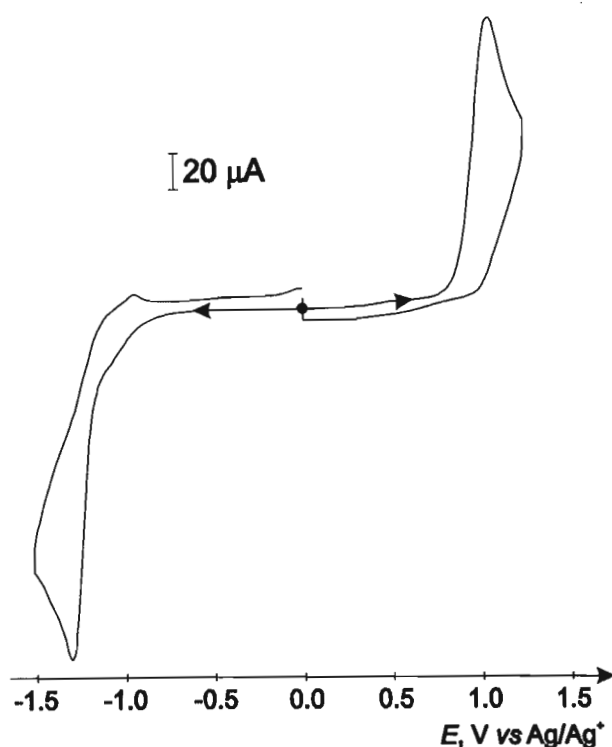


**Figure 6.12.** CV ( $\nu = 100 \text{ mVs}^{-1}$ ), on a Pt electrode ( $r = 2.5 \text{ mm}$ ), of  $[\text{Ru}(\text{L}_1)(\text{CO})_2(\text{CH}_3\text{CN})_2]^{2+}$ , formed 18 h after the addition of  $\text{L}_1$  to an oxidized solution of  $[\text{Ru}_2(\text{CO})_4(\text{CH}_3\text{CN})_6](\text{PF}_6)_2$  1.0 mM in  $\text{CH}_3\text{CN} + 0.1 \text{ M TBAP}$ .

In the anodic region the irreversible oxidation of the N-pyrrole substituted group gives rise to a peak at 0.97 V (Figure 6.12). Films of  $\text{ppyr}-[\text{Ru}(\text{L}_1)(\text{CO})_2(\text{CH}_3\text{CN})_2]^{2+}$  could be efficiently electrodeposited by cycling the working electrode potential between  $-0.30$  and  $1.10 \text{ V}$  [Figure 6.13(b)] or by controlled-potential electrolysis at  $0.90 \text{ V}$  on both Pt and glassy carbon surfaces. To obtain an efficient pyrrole polymerisation of  $[\text{Ru}(\text{L}_1)(\text{CO})_2(\text{CH}_3\text{CN})_2]^{2+}$  it was demonstrated that the reaction of the Ru(II) intermediate  $[\text{Ru}(\text{CO})_2(\text{CH}_3\text{CN})_4]^{2+}$  with an amount of  $\text{L}_1$  less than that required stoichiometrically was necessary. A maximum ratio of ligand to Ru(II) of 0.8:1 was used. These synthetic conditions probably prevented the presence of free

ligand in the solution that would have passivated the electrode surface through its own electropolymerisation. In fresh electrolyte, the electroactivity of  $\text{ppyr-}[\text{Ru}(\text{L}_2)(\text{CO})_2(\text{CH}_3\text{CN})_2]^{2+}$  in the anodic region of the CV is characteristic of a N-substituted polypyrrole film, a quasi-reversible oxidation being observed at 0.27 V [Figure 6.13(c)]. The apparent surface coverages ( $\Gamma_{\text{Ru}}$ ) for polypyrrole films obtained by the latter method are comparable to those of equivalent polypyrrole supported polypyridyl coordinated Ru(II) complexes.<sup>177,178</sup> Typical values of  $6.2 \times 10^{-8}$ ,  $9.8 \times 10^{-7}$  and  $1.5 \times 10^{-7}$  mol  $\text{cm}^{-2}$  on a Pt electrode, formed by the consumption of 5, 10 and 15 mC respectively, were obtained.

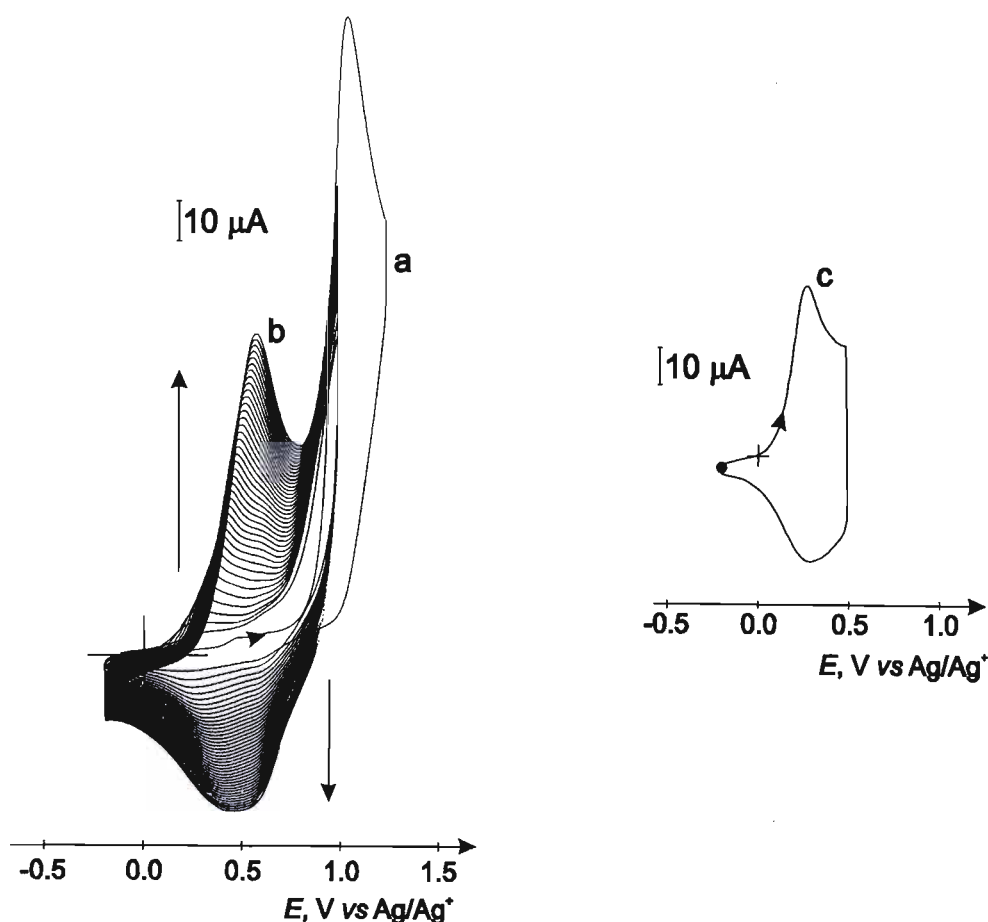


**Figure 6.13.** CVs ( $\nu = 100 \text{ mVs}^{-1}$ ), on a Pt electrode ( $r = 2.5 \text{ mm}$ ), of  $[\text{Ru}(\text{L}_1)(\text{CO})_2(\text{CH}_3\text{CN})_2]^{2+}$ ; (a) initial scan between 0.00 and 1.25 V; (b) subsequent repeated potential scans between  $-0.20$  and 1.00 V showing the growth of the polypyrrole film; (c) resulting ppyr- $[\text{Ru}(\text{L}_1)(\text{CO})_2(\text{CH}_3\text{CN})_2]^{2+}$  modified electrode in pure electrolyte scanned between  $-0.20$  and 0.50 V.

The cathodic CV of  $\text{ppyr-}[\text{Ru}(\text{L}_1)(\text{CO})_2(\text{CH}_3\text{CN})_2]^{2+}$  [Figure 6.14(a)] shows an intense irreversible reduction peak at  $-2.00 \text{ V}$  corresponding to the  $\text{Ru}^{\text{II}/0}$  couple. Cycling of the electrode potential allows for the generation of Ru–Ru bonds in the polypyrrole film [Figure

6.14(b)], the initial intense irreversible reduction evolving to a stable form in the CV. The electroactivity of the resulting polymer ppyr-[Ru(L<sub>1</sub>)(CO)<sub>2</sub>]<sub>n</sub> is shown in Figure 6.14(c). Two quasi-reversible redox systems are seen at  $E_{1/2} = -1.06$  and  $-1.90$  V. In addition an anodic peak is seen at  $-1.26$  V. The appearance of this peak is similar to that of a 'pre-peak', previously reported by various authors and originating from the heterogeneous conductivity of the film.

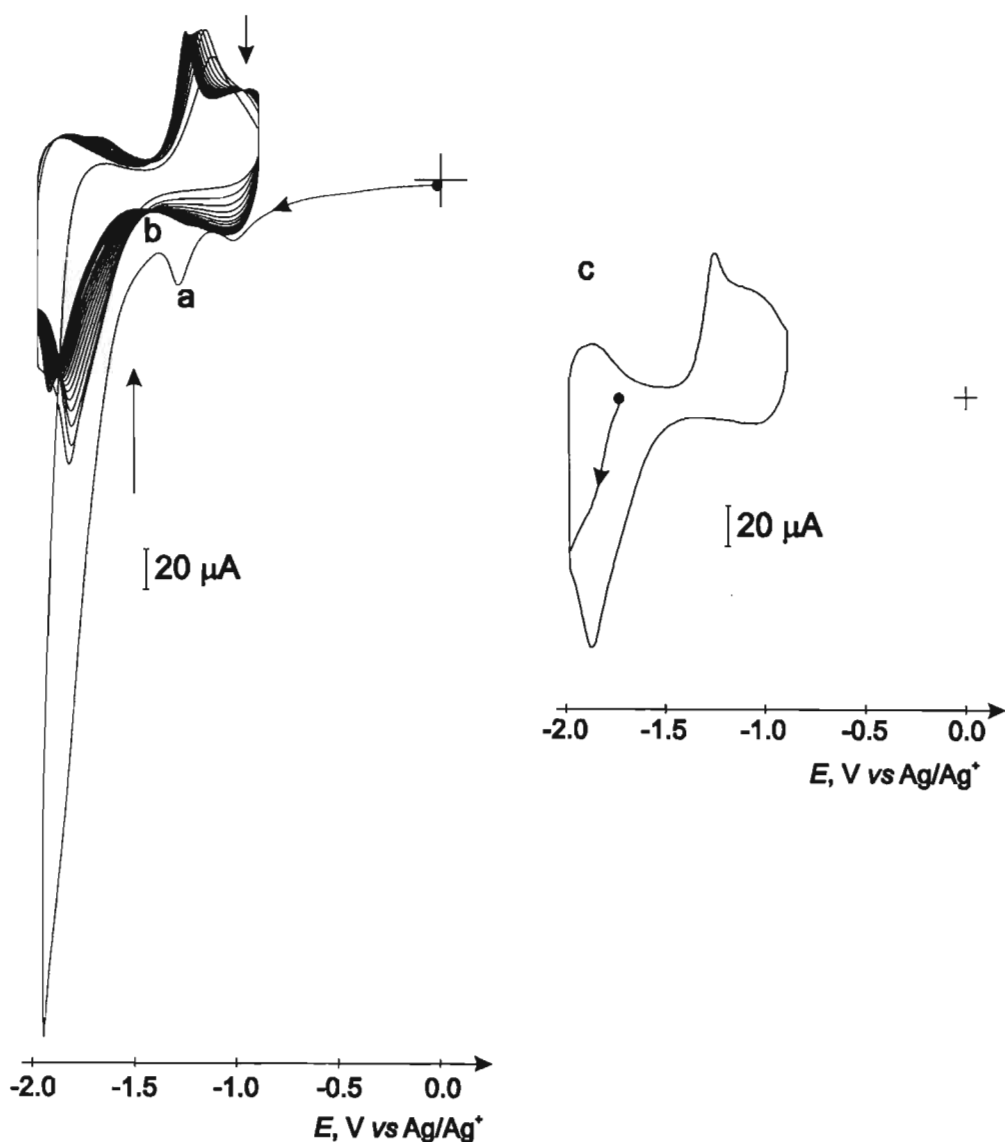


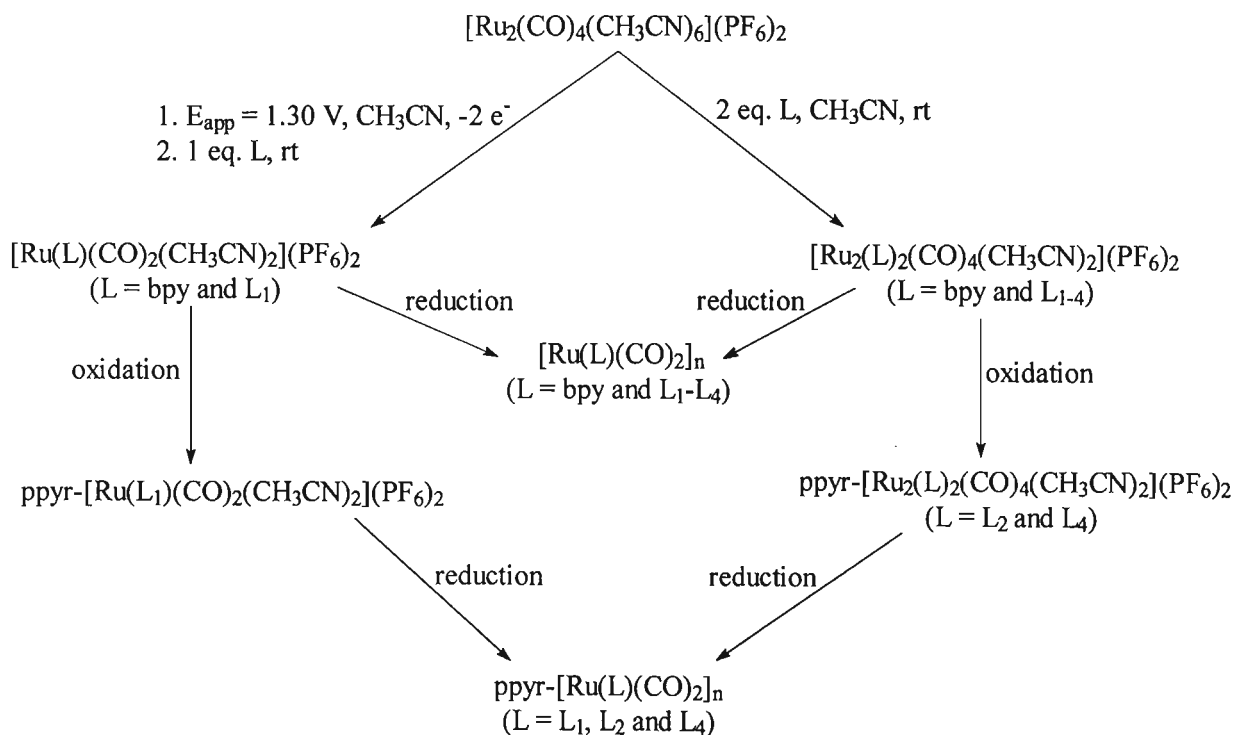
**Figure 6.14.** CVs of a ppyr-[Ru(L<sub>1</sub>)(CO)<sub>2</sub>(CH<sub>3</sub>CN)<sub>2</sub>]<sup>2+</sup> modified Pt electrode ( $r = 2.5$  mm) in CH<sub>3</sub>CN + 0.1 M TBAP; (a) initial scan from 0.00 to  $-0.90$  V; (b) subsequent successive scans between  $-0.90$  and  $-2.00$  V; (c) scan between  $-0.90$  and  $-2.00$  V of the resulting ppyr-[Ru(L<sub>1</sub>)(CO)<sub>2</sub>]<sub>n</sub>.

### 6.2.4.(iii) Catalytic Properties Towards CO<sub>2</sub> Electrochemical Reduction of ppyr-[Ru(L<sub>1</sub>)(CO)<sub>2</sub>]<sub>n</sub>

In CO<sub>2</sub> saturated CH<sub>3</sub>CN + 0.1 M TBAP, CVs of a glassy carbon electrode modified by ppyr-[Ru(L<sub>1</sub>)(CO)<sub>2</sub>(CH<sub>3</sub>CN)<sub>2</sub>]<sup>2+</sup> showed that the intensity of the catalytic current increases and its threshold potential shifts to less negative values with the stepwise addition of H<sub>2</sub>O from 1 to 10 %. At a 10 % concentration of H<sub>2</sub>O, the onset of this catalytic current is at approximately -1.40 V. The CV of ppyr-[Ru(L<sub>1</sub>)(CO)<sub>2</sub>(CH<sub>3</sub>CN)<sub>2</sub>]<sup>2+</sup> modified GC electrodes in CO<sub>2</sub> saturated H<sub>2</sub>O + 0.1 M LiClO<sub>4</sub> manifests a very similar catalytic effect towards CO<sub>2</sub> reduction, the enhancement in current beginning at -1.10 V.

Preparative scale electrolysis experiments performed in hydro-organic media (CH<sub>3</sub>CN + 10% H<sub>2</sub>O + 0.1 M TBAP) confirm that ppyr-[Ru(L<sub>1</sub>)(CO)<sub>2</sub>(CH<sub>3</sub>CN)<sub>2</sub>]<sup>2+</sup> catalyses the electrochemical reduction of CO<sub>2</sub> to CO and formate with Faradaic yields of 87 and 13 % respectively.

### 6.3. Summary



**Scheme 6.1.** Synthesis of bipyridyl ligand complexes of Ru(I) and Ru(II) from  $[\text{Ru}_2(\text{CO})_4(\text{CH}_3\text{CN})_6](\text{PF}_6)_2$  and their subsequent electrochemical elaboration.

Scheme 6.1 summarises the use of the diruthenium species  $[\text{Ru}_2(\text{CO})_4(\text{CH}_3\text{CN})_6](\text{PF}_6)_2$  as a precursor for the synthesis of both dinuclear bipyridyl ligand complexes of Ru(I) and

mononuclear bipyridyl ligand complexes of Ru(II). Shown in the Scheme are the electrochemical methods employed for the preparation of two types of Ru(0) polymers; one directly bonded to the electrode surface and the other embedded in a polypyrrole matrix. The Ru(0) polymers are obtained by the direct two-electron reduction of either the monomers  $[\text{Ru}(\text{L})(\text{CO})_2(\text{CH}_3\text{CN})_2](\text{PF}_6)_2$  ( $\text{L} = \text{bpy}$  and  $\text{L}_1$ ) or the Ru(I) dimers **14** – **17**. In order to obtain the Ru(0) polymer embedded in a polypyrrole matrix the polypyrrole film is first formed by oxidation of the dimer or monomer, following which reduction affords the desired ppyr- $[\text{Ru}(\text{L})(\text{CO})_2]_n$ . Noteworthy is that attempts to form polypyrrole films by oxidation of **14** and **16** (where  $\text{L} = \text{L}_1$  and  $\text{L}_3$ ) were unsuccessful because of the competitive oxidation of the metal-metal bond in the dimer. However, this problem was overcome for  $\text{L} = \text{L}_1$  by electrochemical oxidation of a monomer containing a Ru(II) centre,  $[\text{Ru}(\text{L}_1)(\text{CO})_2(\text{CH}_3\text{CN})_2](\text{PF}_6)_2$ . Electrodes modified by ppyr- $[\text{Ru}(\text{L})(\text{CO})_2]_n$  ( $\text{L} = \text{L}_1, \text{L}_2$  and  $\text{L}_4$ ) are effective catalysts for  $\text{CO}_2$  reduction, leading mainly to CO (for  $\text{L}_1$  and  $\text{L}_4$ ) and formate (for  $\text{L}_2$ ) with high Faradaic yields.

#### 6.4. Experimental

The substituted 2,2'-bipyridine ligands  $\text{L}_1$ ,<sup>180</sup>  $\text{L}_2$ ,<sup>181</sup>  $\text{L}_3$  and  $\text{L}_4$ <sup>178</sup> were synthesised according to procedures previously described.

**[Ru<sub>2</sub>(L<sub>1</sub>)<sub>2</sub>(CO)<sub>4</sub>(CH<sub>3</sub>CN)<sub>2</sub>](PF<sub>6</sub>)<sub>2</sub> **14**.**  $[\text{Ru}_2(\text{CO})_4(\text{CH}_3\text{CN})_6](\text{PF}_6)_2$  (0.170 g, 0.2 mmol) and  $\text{L}_1$  (0.145 g, 0.5 mmol) were dissolved in  $\text{CH}_3\text{CN}$  (8 cm<sup>3</sup>), affording a red coloured solution that was maintained at room temperature for 2 h. The volume of the solution was reduced to *ca.* 3 cm<sup>3</sup> *in vacuo* and an excess of  $\text{Et}_2\text{O}$  (20 cm<sup>3</sup>) added with stirring. Standing the solution for 12 h at  $-25^\circ\text{C}$  resulted in the formation of an orange coloured precipitate. The supernatant was decanted and the precipitate washed with  $\text{Et}_2\text{O}$  (2 x 5 cm<sup>3</sup>). The solid was dissolved in  $\text{CH}_2\text{Cl}_2$  (3 cm<sup>3</sup>) and a large excess of  $\text{Et}_2\text{O}$  (30 cm<sup>3</sup>) added to the solution with stirring. The orange precipitate thus formed was isolated by decanting the supernatant and washed with  $\text{Et}_2\text{O}$  (2 x 5 cm<sup>3</sup>). The crude product was dissolved in  $\text{CH}_3\text{CN}$  (3 cm<sup>3</sup>) and an excess of  $\text{Et}_2\text{O}$  added to the concentrated solution with stirring. Standing the solution at  $-25^\circ\text{C}$  for 12 h afforded orange crystals of  $[\text{Ru}_2(\text{L}_1)_2(\text{CO})_4(\text{CH}_3\text{CN})_2](\text{PF}_6)_2$  (165 mg, 66 %). (Found: C, 41.49; H, 3.61; N, 8.12.  $\text{Ru}_2\text{C}_{44}\text{H}_{48}\text{N}_8\text{P}_2\text{F}_{12}\text{O}_4$  requires C, 42.45; H, 3.89; N, 9.00 %);  $\lambda_{\text{max}}/\text{nm}$  ( $\text{CH}_3\text{CN}$ ) 249 (sh) (28 500  $\epsilon/\text{dm}^3\text{mol}^{-1}\text{cm}^{-1}$ ), 295 (23 500), 310 (sh) (17 400) 425 (sh) (1200);  $\nu_{\text{max}}/\text{cm}^{-1}$  (KBr)  $\nu_{\text{CN}}$ , 2313w, 2289w;  $\nu_{\text{CO}}$ , 2037s, 1998s, 1963s, 1944s (sh);  $\nu_{\text{PF}}$ , 841vs;  $\delta_{\text{H}}$  (500 MHz,  $\text{CD}_2\text{Cl}_2$ ,  $\text{CDHCl}_2$ ) 8.24 (1H, d, J 5.26,  $\text{H}_6$  or  $6'$ ), 8.16 (2H, m,  $\text{H}_6$  or  $6'$ ), 8.07 (1H, d, J 5.49,  $\text{H}_6$  or  $6'$ ), 7.92 (1H, s  $\text{H}_3$  or  $3'$ ),



7.91 (1H, s, H<sub>3</sub> or 3'), 7.89 (1H, s, H<sub>3</sub> or 3'), 7.86 (1H, s, H<sub>3</sub> or 3'), 7.28 (1H, d, J 4.80 Hz, H<sub>5</sub> or 5'), 7.25 (1H, d, J 5.26, H<sub>5</sub> or 5'), 7.21 (1H, d, J 5.03 Hz, H<sub>5</sub> or 5'), 7.18 (1H, d, J 5.03 Hz, H<sub>5</sub> or 5'), 6.68 (4H, s, H<sub>α</sub>), 6.01 (4H, s, H<sub>β</sub>), 3.91 (4H, br s, (CH<sub>2</sub>)<sub>d</sub>), 2.82 (4H, m, (CH<sub>2</sub>)<sub>a</sub>), 2.61 (3H, s, CH<sub>3</sub>), 2.60 (3H, s, CH<sub>3</sub>), 1.91 (6H, s, CH<sub>3</sub>CN), 1.88 (4H, m, (CH<sub>2</sub>)<sub>c</sub> or b), 1.68 (4H, m, (CH<sub>2</sub>)<sub>c</sub> or b); δ<sub>C</sub> (125 MHz, CD<sub>2</sub>Cl<sub>2</sub>, CDHCl<sub>2</sub>, -80°C) 202.38 (CO), 156.26 (C-2 and 2'), 152.96, 152.89, 152.73 and 152.67 (C-6 and 6'), 151.23, 151.06 and 150.67 (C-4 and 4'), 128.01 and 127.00 (C-5 and 5'), 124.41, 124.31, 123.84 and 123.62 (C-3 and 3'), 120.32 (C-α), 119.61 (CH<sub>3</sub>CN), 107.64 and 107.47 (C-β), 48.85 and 48.79 (C-d), 34.43 (C-c), 31.16 (C-b), 27.78 and 27.45 (C-a), 21.0 and 20.91 (CH<sub>3</sub>), 3.86 (CH<sub>3</sub>CN).

**[Ru<sub>2</sub>(L<sub>2</sub>)<sub>2</sub>(CO)<sub>4</sub>(CH<sub>3</sub>CN)<sub>2</sub>](PF<sub>6</sub>)<sub>2</sub> 15.** To a solution of [Ru<sub>2</sub>(CO)<sub>4</sub>(CH<sub>3</sub>CN)<sub>6</sub>](PF<sub>6</sub>)<sub>2</sub> (0.170 g, 0.2 mmol) in CH<sub>3</sub>CN (12 cm<sup>3</sup>) was added L<sub>2</sub> (206 mg, 0.5 mmol). The ligand took a couple of minutes to completely dissolve, resulting in a dark red solution. The solution was stirred at room temperature for 2 h, reduced in volume under vacuum to ca 3 cm<sup>3</sup> and an excess of Et<sub>2</sub>O added with stirring. Upon standing overnight the solution yielded dark orange crystals. The mother liquor was decanted and the product washed with Et<sub>2</sub>O (2 x 5 cm<sup>3</sup>). The material was then recrystallised from CH<sub>3</sub>CN/Et<sub>2</sub>O as just described. The material was redissolved in CH<sub>3</sub>CN (5 cm<sup>3</sup>), which was subsequently completely removed under vacuum during several hours to give a dark red product (228 mg, 70 %). (Found: C, 44.02; H, 4.09; N, 8.80. Ru<sub>2</sub>C<sub>60</sub>H<sub>58</sub>N<sub>10</sub>P<sub>2</sub>F<sub>12</sub>O<sub>12</sub> requires C, 44.95; H, 3.65; N, 8.74 %); λ<sub>max</sub>/nm (CH<sub>3</sub>CN) 245 (sh) (25 800 ε/dm<sup>3</sup>mol<sup>-1</sup>cm<sup>-1</sup>), 283 (17 700), 313 (19 300), 366 (5 700), 479 (sh) (2 300); ν<sub>max</sub>/cm<sup>-1</sup> (CsI) ν<sub>CO</sub>, 2050s, 2014s, 1983s, 1955m (sh), ν<sub>COOR</sub>, 1733s; δ<sub>H</sub> (250 MHz, CD<sub>3</sub>CN, CD<sub>2</sub>H<sub>2</sub>CN) 8.61 (4H, d, H<sub>6,6'</sub>), 8.57 (4H, s, H<sub>3,3'</sub>), 7.96 (4H, d, H<sub>5,5'</sub>), 6.78 (8H, s, H<sub>α, α'</sub>), 6.06 (8H, s, H<sub>β, β'</sub>), 4.40 (8H, t, (CH<sub>2</sub>)<sub>a,a'</sub>), 4.14 (8H, t, (CH<sub>2</sub>)<sub>c,c'</sub>), 2.29 (8H, t, (CH<sub>2</sub>)<sub>b,b'</sub>); δ<sub>C</sub> (125 MHz, CD<sub>2</sub>Cl<sub>2</sub>, CDHCl<sub>2</sub>, -80°C) 201.22 (CO), 162.67 (C(O)O), 154.12 (C-6 and 6'), 153.41 (C-2 and 2'), 140.51 (C-4 and 4'), 126.79 (C-5 and 5'), 123.88 (C-3 and 3'), 121.11 (CH<sub>3</sub>CN), 120.42 (C-α), 107.77 (C-β), 64.28 (C-a), 45.95 (C-c), 29.84 (C-b), 3.79 (CH<sub>3</sub>CN).

**Electrochemical Details.** The potential value used for pyrrole electropolymerisation was optimised by choosing a potential on the threshold of the pyrrole oxidation wave that gave a stable current during the passage of 5 mC. The electroactivity of the resulting films was also taken into consideration. The electrochemical response of the resulting polypyrrole modified electrode in pure electrolyte was also taken into account. The apparent surface coverages Γ<sub>Ru</sub> (mol cm<sup>-2</sup>), presented in Table 6.6, were determined from the charge measured at a scan rate of

10 mVs<sup>-1</sup> under the polypyrrole oxidation wave, assuming that one in three pyrrole units is oxidised.<sup>182</sup>

The conditions used to prepare the ppyr-[Ru(L)(CO)<sub>2</sub>]<sub>n</sub> (L = L<sub>2</sub> and L<sub>4</sub>) modified glassy carbon electrodes for the electrocatalytic studies are those presented in Table 6.6. Polypyrrole modified carbon felt electrodes for preparative scale electrolysis experiments were prepared by controlled-potential electrolysis under Ar from an CH<sub>3</sub>CN + 0.1 M TBAP electrolyte with a 1.0 mM concentration of complex as follows; for ppyr-[Ru<sub>2</sub>(L<sub>2</sub>)<sub>2</sub>(CO)<sub>4</sub>(CH<sub>3</sub>CN)<sub>2</sub>](PF<sub>6</sub>)<sub>2</sub>, E<sub>app</sub> = 0.80 V, Q = 2.34 C, Γ<sub>Ru</sub> = 1.7 x 10<sup>-6</sup> mol cm<sup>-2</sup>; for ppyr-[Ru(L<sub>4</sub>)(CO)<sub>2</sub>(CH<sub>3</sub>CN)]<sub>2</sub>(PF<sub>6</sub>)<sub>2</sub>, E<sub>app</sub> = 0.73 V, Q = 4.50 C, Γ<sub>Ru</sub> = 3.3 x 10<sup>-6</sup> mol cm<sup>-2</sup>. The electrodes were rinsed with CH<sub>3</sub>CN, then transferred to fresh CH<sub>3</sub>CN / 10 % H<sub>2</sub>O + 0.1 M TBAP electrolyte. The procedure used to carry out the electrocatalytic experiments using the modified electrodes is described in the appendix, section A.4.2.

**Table 6.6.** Apparent surface coverages of ppyr-[Ru<sub>2</sub>(L)<sub>2</sub>(CO)<sub>4</sub>(CH<sub>3</sub>CN)<sub>2</sub>](PF<sub>6</sub>)<sub>2</sub> (L = L<sub>2</sub> and L<sub>4</sub>) and the conditions used to prepare the Pt modified electrodes from CH<sub>3</sub>CN + 0.1 M TBAP electrolyte with a 1.0 mM concentration of complex.

Complex	Potentiodynamique		Potentiostatique		
	Potential Scan Range / V	Γ <sub>Ru</sub> / mol cm <sup>-2</sup> (no. cycles)	E <sub>app</sub> / V	Γ <sub>Ru</sub> / mol cm <sup>-2</sup> (C / mC)	% Yield
L <sub>2</sub>	-0.3 to 0.95	6.8 x 10 <sup>-9</sup> (15)	0.80	2.3 x 10 <sup>-8</sup> (5)	41
		9.9 x 10 <sup>-9</sup> (30)		3.9 x 10 <sup>-8</sup> (10)	34
		1.5 x 10 <sup>-8</sup> (60)		5.3 x 10 <sup>-8</sup> (15)	31
L <sub>4</sub>	-0.3 to 0.85	1.5 x 10 <sup>-8</sup> (60)	0.73	1.8 x 10 <sup>-8</sup> (5)	31
		3.5 x 10 <sup>-8</sup> (40)		1.9 x 10 <sup>-8</sup> (10)	16
		9.0 x 10 <sup>-8</sup> (125)		2.1 x 10 <sup>-8</sup> (15)	12

## Chapter 7. Dinuclear Complexes of Ruthenium(I) Bridged by 6-diphenylphosphino-2,2'-bipyridine and 6-(diphenylphosphino)-2-(2-quinolyl)pyridine

---

### 7.1. Introduction

A survey of the literature reveals three principle routes for the synthesis of dinuclear complexes of low-valent ruthenium. These are now briefly considered.

The ruthenium(0) carbonyl,  $[\text{Ru}_3\text{CO}_{12}]$ , has been used as a synthetic precursor in the formation of ligand-bridged diruthenium(0) complexes. Thus the diphosphazane ligand-bridged derivatives  $[\text{Ru}_2(\mu\text{-CO})(\text{CO})_4(\mu\text{-etdp})_2]$  (etdp =  $(\text{RO})_2\text{PN}(\text{Et})\text{P}(\text{OR})_2$ ; R = Me, Et, Pr<sup>i</sup> or Ph) have been obtained by UV irradiation of cyclohexane solutions of  $[\text{Ru}_3(\text{CO})_{12}]$  and the diphosphazane ligand.<sup>183</sup> The corresponding diphosphine derivatives  $[\text{Ru}_2(\mu\text{-CO})(\text{CO})_4(\mu\text{-dmpm})_2]$  (dmpm =  $\text{Me}_2\text{PCH}_2\text{PMe}_2$ ) and  $[\text{Ru}_2(\mu\text{-CO})(\text{CO})_4(\mu\text{-dppm})_2]$  are similarly synthesized.<sup>184</sup> These compounds can be considered as ligand stabilized derivatives of the labile diruthenium carbonyl  $[\text{Ru}_2(\text{CO})_9]$ . However attempts to synthesize phosphoruspyridyl and phosphorusbipyridyl bridged diruthenium complexes using this methodology were unsuccessful as the reaction conditions required *viz.* high temperatures and or pressures as well as UV irradiation, lead to decomposition of the ligand.<sup>185</sup>

The ruthenium carboxylate polymer  $[\{\text{Ru}\{\mu\text{-}\eta^2\text{-OC}(\text{R})\text{O}\}(\text{CO})_2\}_n]$ , first synthesized by Lewis *et al.*,<sup>186</sup> can be solubilised in donor solvents such as acetonitrile or THF, affording the solvated species  $[\text{Ru}_2\{\mu\text{-}\eta^2\text{-OC}(\text{R})\text{O}\}_2(\text{CO})_4(\text{solv})_2]$  (solv =  $\text{CH}_3\text{CN}$  and THF).<sup>187</sup> As the carboxylate and acetonitrile ligands are displaceable, both  $[\{\text{Ru}\{\mu\text{-}\eta^2\text{-OC}(\text{R})\text{O}\}(\text{CO})_2\}_n]$  and  $[\text{Ru}_2\{\mu\text{-}\eta^2\text{-OC}(\text{R})\text{O}\}_2(\text{CO})_4(\text{CH}_3\text{CN})_2]$  are useful synthons in the preparation of dinuclear ruthenium(I) complexes.<sup>157,188</sup> Thus the P,N ligand-bridged complexes  $[\text{Ru}_2\{\mu\text{-}\eta^2\text{-OC}(\text{R})\text{O}\}(\text{CO})_4(\mu\text{-L})_2](\text{PF}_6)$  (L =  $\text{Ph}_2\text{Ppy}$ ,  $\text{Ph}_2\text{Pquin}$  or  $\text{Ph}_2\text{Pbpy}$ ) can be prepared by the reaction of the ruthenium carboxylate polymer with two mole equivalents of the ligand and  $\text{NH}_4\text{PF}_6$  in refluxing toluene (where L is  $\text{Ph}_2\text{Ppy}$  and  $\text{Ph}_2\text{Pquin}$ ), or 1-butanol (where L is  $\text{Ph}_2\text{Pbpy}$ ).<sup>185</sup>

The complex  $[\text{Ru}_2(\text{CO})_4(\text{CH}_3\text{CN})_6](\text{PF}_6)_2$  represents an excellent precursor for the synthesis of dinuclear ruthenium(I) complexes in view of the six labile acetonitrile ligands.<sup>155,189</sup> Klemperer and Zhong describe the synthesis of  $[\text{Ru}_2(\text{CO})_4(\text{CH}_3\text{CN})_4(\text{PPh}_3)_2](\text{PF}_6)_2$ ,  $[\text{Ru}_2(\text{CO})_4(\text{py})_6](\text{PF}_6)_2$  (py = pyridine) and  $[\text{Ru}_2\{\mu\text{-OC}(\text{Me})\text{O}\}_2(\text{CO})_4(\text{CH}_3\text{CN})_2](\text{PF}_6)_2$  through the facile substitution of the coordinated acetonitriles in  $[\text{Ru}_2(\text{CO})_4(\text{CH}_3\text{CN})_6](\text{PF}_6)_2$  by the relevant ligand.<sup>155</sup> Treatment of  $[\text{Ru}_2(\text{CO})_4(\text{CH}_3\text{CN})_6](\text{PF}_6)_2$  with two equivalents of the appropriate P,N ligand in refluxing acetonitrile affords  $[\text{Ru}_2(\mu\text{-Ph}_2\text{Ppy})_2(\mu\text{-CO})_2(\text{CH}_3\text{CN})_4](\text{PF}_6)_2$

and  $[\text{Ru}_2(\mu\text{-Ph}_2\text{Pbpy})_2(\text{CO})_2(\text{CH}_3\text{CN})_2](\text{PF}_6)_2$  respectively, in which the P,N ligand has adopted a bridging mode of coordination.<sup>185</sup> In contrast, reaction of the same precursor with  $\text{Ph}_2\text{Pquin}$ , even under more forcing conditions, led to  $[\text{Ru}_2(\eta^1\text{-Ph}_2\text{Pquin})_2(\text{CO})_4(\text{CH}_3\text{CN})_4](\text{PF}_6)_2$ , where the  $\text{Ph}_2\text{Pquin}$  ligands are bonded in a P-ligated fashion collinear with the Ru–Ru bond axis. Presumably the steric bulkiness of the quinoline ring prevents the ligand from coordinating in a bridging mode.<sup>185</sup>

Figure 7.1 depicts the molecular structure of the dication in  $[\text{Ru}_2(\mu\text{-Ph}_2\text{Pbpy})_2(\text{CO})_2(\text{EtCN})_2](\text{PF}_6)_2$ .<sup>185</sup> A notable feature is the *cis* coordination of the bridging  $\text{Ph}_2\text{Pbpy}$  ligands with respect to one another. As a consequence of this the labile nitrile ligands are on the exposed side of the molecule. Thus the approach of a substrate to the active sites of the molecule will be sterically unhindered.

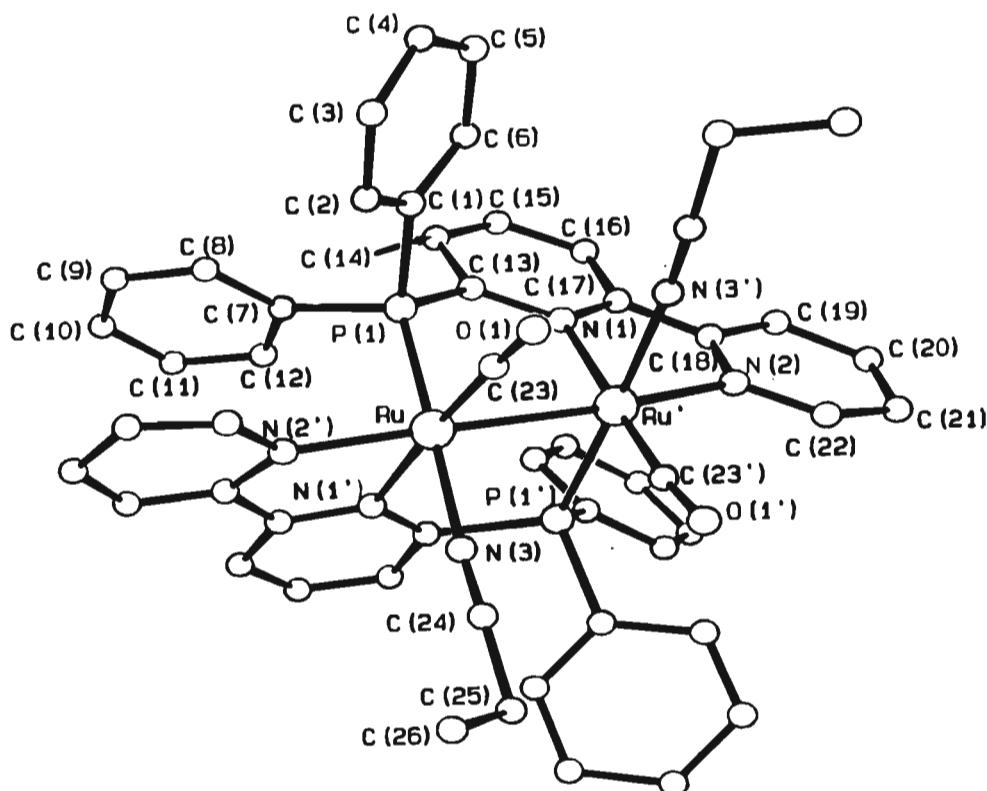


**Figure 7.1.** Molecular structure of the dication of *cis*( $\text{Ph}_2\text{Pbpy}$ )- $[\text{Ru}_2(\mu\text{-Ph}_2\text{Pbpy})_2(\text{CO})_2(\text{EtCN})_2](\text{PF}_6)_2$ .

The electrochemistry of  $[\text{Ru}_2(\mu\text{-Ph}_2\text{Pbpy})_2(\text{CO})_2(\text{CH}_3\text{CN})_2](\text{PF}_6)_2$  **18** as well as the first synthesis and electrochemistry of the  $\text{Ph}_2\text{Ppyqn}$  analogue  $[\text{Ru}_2(\mu\text{-Ph}_2\text{Ppyqn})_2(\text{CO})_2(\text{CH}_3\text{CN})_2](\text{PF}_6)_2$  **19** are described in this chapter.

## 7.2. Results and Discussion

### 7.2.1. Synthesis and Characterisation of the Dinuclear Ruthenium Complexes

The synthesis of  $[\text{Ru}_2(\mu\text{-Ph}_2\text{Pbpy})_2(\text{CO})_2(\text{CH}_3\text{CN})_2](\text{PF}_6)_2$  **18** was carried out as described by Parry.<sup>185</sup> By monitoring the progress of the reaction by IR and  $^{31}\text{P}\text{-}\{^1\text{H}\}$  NMR spectroscopy he noted the formation of an intermediate containing both terminal and bridging carbonyl ligands. The intermediate exhibits a singlet at 57.54 ppm in its  $^{31}\text{P}$  NMR spectrum, that is observed to shift upfield to 55.20 ppm as the reaction proceeds to completion. The bridging carbonyl bands due to the intermediate and present in the IR spectrum disappear, while the terminal carbonyl bands, observed as a strong absorption at  $1938\text{ cm}^{-1}$  with a shoulder at  $1914\text{ cm}^{-1}$ ,<sup>185</sup> remain unaffected.

The reaction of two equivalents of  $\text{Ph}_2\text{Pbpy}$  with  $[\text{Ru}_2(\text{CO})_4(\text{CH}_3\text{CN})_6](\text{PF}_6)_2$  in refluxing acetonitrile for 12 h initially produced a yellow solution that changed colour to purple-brown and finally to a deep-purple characteristic of the product. The progress of the reaction was monitored by  $^{31}\text{P}\text{-}\{\text{H}\}$  NMR and IR spectroscopy. The  $^{31}\text{P}$  NMR spectrum, recorded on external-lock, of the final deep purple solution exhibited two singlets at 57.0 and 54.6 ppm, implying the presence of two different species. An intense terminal carbonyl band at  $1946\text{ cm}^{-1}$ , with a shoulder at  $1924\text{ cm}^{-1}$ , was observed in the IR spectrum of the  $\text{CH}_3\text{CN}$  solution. Both the  $^{31}\text{P}$  NMR and IR absorption spectrums of the reaction mixture were unaltered upon refluxing the solution for a further 12 h.

Careful addition of diethyl ether to the solution and standing of the resultant mixture at  $-25^\circ\text{C}$  afforded a deep purple crystalline material. The  $^{31}\text{P}\text{-}\{^1\text{H}\}$  NMR spectrum measured in acetonitrile of this material exhibited the same two signals of approximately equal intensity, at 57.0 and 54.6 ppm, that are observed in the reaction mixture. The solid state IR absorption spectrum of this material, recorded as a KBr pellet, displayed the same features as the  $[\text{Ru}_2(\mu\text{-Ph}_2\text{Pbpy})_2(\text{CO})_2(\text{CH}_3\text{CN})_2](\text{PF}_6)_2$  compound isolated by Parry: an intense terminal carbonyl stretch at  $1943\text{ cm}^{-1}$  with a shoulder at  $1916\text{ cm}^{-1}$ , and a very strong absorption band at  $839\text{ cm}^{-1}$ , due to the P–F stretches within the  $\text{PF}_6^-$  counter ion. No bridging carbonyl absorption bands were observed. This is in contrast to the intense band at  $1715\text{ cm}^{-1}$  observed in the infrared spectrum recorded for the closely related complex  $[\text{Ru}_2(\mu\text{-Ph}_2\text{Ppy})_2(\mu\text{-CO})_2(\text{CH}_3\text{CN})_4](\text{PF}_6)$ . Furthermore the microanalytical results obtained for the material are consistent with the formulation  $[\text{Ru}_2(\mu\text{-Ph}_2\text{Pbpy})_2(\text{CO})_2(\text{CH}_3\text{CN})_2](\text{PF}_6)_2$  **18**. The  $^{31}\text{P}\text{-}\{^1\text{H}\}$  NMR spectrum does,

however, unambiguously show that two species are present in the product solution. As discussed below these two species are structural isomers.

The procedure was repeated using propionitrile instead of acetonitrile as a solvent and the reaction monitored by IR and  $^{31}\text{P}$  NMR spectroscopies. The spectral and microanalytical data, given in Section 7.3, present the same pattern as is observed for when the solvent is acetonitrile.

The reaction of two equivalents of  $\text{Ph}_2\text{Ppyqn}$  with the diruthenium(I) precursor  $[\text{Ru}_2(\text{CO})_4(\text{CH}_3\text{CN})_6](\text{PF}_6)_2$  in refluxing acetonitrile for 24 h afforded a deep purple solution. The  $^{31}\text{P}$ - $\{^1\text{H}\}$  NMR spectrum of this reaction mixture, as is similarly observed in the reaction of  $\text{Ph}_2\text{Pbpy}$  with  $[\text{Ru}_2(\text{CO})_4(\text{CH}_3\text{CN})_6](\text{PF}_6)_2$ , displayed two singlets of approximately equal intensity at 51.1 and 60.9 ppm. Further refluxing of the reaction mixture for 12 h brought about no change in the form of the spectrum. Purple crystalline material was precipitated from the acetonitrile solution by the addition of diethyl ether and by allowing the resulting solution to stand at  $-25\text{ }^\circ\text{C}$ . The crude product was recrystallised by the careful 'layering' of diethyl ether over a saturated acetonitrile solution of the material in narrow glass tubes. Two types of dark purple crystals were observed to form; one was of an irregular leaf-like shape while the second was cubic in shape. The two different crystal types were separated by hand.

The  $^{31}\text{P}$ - $\{^1\text{H}\}$  spectrum of the cubic shaped crystals exhibits a single resonance at 60.9 ppm. A strong terminal carbonyl stretch at  $1944\text{ cm}^{-1}$  with a shoulder at  $1922\text{ cm}^{-1}$  was observed in the infrared spectrum, run as a KBr disk. The presence of the  $\text{PF}_6^-$  counter ion was confirmed by the presence of a very strong absorption band at  $843\text{ cm}^{-1}$ . A complex pattern arising from the aromatic protons of the  $\text{Ph}_2\text{Ppyqn}$  ligand was observed from 9.43 to 5.98 ppm in the  $^1\text{H}$  NMR spectrum. A singlet, due to the methyl protons of the acetonitrile ligand, is displayed at 1.36 ppm. On the basis of this spectral evidence and the microanalytical results, the compound is formulated as  $[\text{Ru}_2(\mu\text{-Ph}_2\text{Ppyqn})_2(\text{CO})_2(\text{CH}_3\text{CN})_2](\text{PF}_6)_2$  **19**. This is confirmed by a crystal structure determination that shows these crystals to contain the *cis*( $\text{Ph}_2\text{Ppyqn}$ ) isomer *i.e.* *cis*( $\text{Ph}_2\text{Ppyqn}$ )-**19** (see below).

The  $^{31}\text{P}$ - $\{^1\text{H}\}$  spectrum of the irregular shaped crystals exhibited two singlets at 51.1 and 60.9 ppm, as was observed for the parent reaction mixture. The infrared spectral data recorded for these crystals is the same as that described above for the cubic form. Thus the IR spectrum, recorded as a KBr disc, confirms the presence of a terminal carbonyl and the  $\text{PF}_6^-$  counter ion. No stretches corresponding to a bridging carbonyl are observed in the region of  $1715\text{ cm}^{-1}$ . The microanalytical data of these crystals corresponds to their formulation as  $[\text{Ru}_2(\mu\text{-Ph}_2\text{Ppyqn})_2(\text{CO})_2(\text{CH}_3\text{CN})_2](\text{PF}_6)_2$  **19**.

The pattern that emerges is that two stable structural isomers are formed on the reaction of the phosphorus-polypyridyl ligands with  $[\text{Ru}_2(\text{CO})_4(\text{CH}_3\text{CN})_6](\text{PF}_6)_2$ . In the case of the reaction of  $\text{Ph}_2\text{Ppyqn}$  with  $[\text{Ru}_2(\text{CO})_4(\text{CH}_3\text{CN})_6](\text{PF}_6)_2$  the one isomer *viz.* *cis*( $\text{Ph}_2\text{Ppyqn}$ )-**19** can be selectively crystallized from the mixture. This configuration is also observed in the molecular structure of *cis*( $\text{Ph}_2\text{Pbpy}$ )- $[\text{Ru}_2(\mu\text{-Ph}_2\text{Pbpy})_2(\text{CO})_2(\text{EtCN})_2](\text{PF}_6)_2$ .<sup>185</sup> The second structural isomer of the diruthenium complexes is probably one in which the two bridging ligands coordinate in a *trans* fashion. Such an arrangement of the  $\text{Ph}_2\text{Pbpy}$  ligands is adopted in the related complex  $[\text{Ru}_2\{\mu\text{-}\eta^2\text{-OC}(\text{Me})\text{O}\}(\text{CO})_2(\mu\text{-Ph}_2\text{Pbpy})_2](\text{PF}_6)$ .<sup>190</sup> It can be concluded that the second product present in the reaction mixture is the *trans* structural isomer and that the product precipitated from the reaction mixture contains both the *cis* and *trans* isomers. The microanalytical and spectroscopic data lend weight to this argument.

A simple modification of the preparation described by Parry permitted the selective synthesis of *cis*( $\text{Ph}_2\text{Pbpy}$ )- $[\text{Ru}_2(\mu\text{-Ph}_2\text{Pbpy})_2(\text{CO})_2(\text{CH}_3\text{CN})_2](\text{PF}_6)_2$ , *cis*( $\text{Ph}_2\text{Pbpy}$ )-**18**. Instead of immediately refluxing the acetonitrile solution of  $\text{Ph}_2\text{Pbpy}$  and  $[\text{Ru}_2(\text{CO})_4(\text{CH}_3\text{CN})_6](\text{PF}_6)_2$ , the reactants were first stirred together at room temperature for 1.5 h. In addition an excess of ligand to metal was used *viz.* 2.5 equivalents of  $\text{Ph}_2\text{Pbpy}$  to one of  $[\text{Ru}_2(\text{CO})_4(\text{CH}_3\text{CN})_6](\text{PF}_6)_2$ . This approach led to an orange coloured solution that showed in its <sup>31</sup>P NMR spectrum two singlets at 25.0 and 3.7 ppm. The IR spectrum of the intermediate recorded in  $\text{CH}_3\text{CN}$  showed three strong  $\nu_{\text{CO}}$  absorption bands at 2048 (medium), 2027 (strong) and 1992 (strong, broad)  $\text{cm}^{-1}$  with a shoulder at 1976  $\text{cm}^{-1}$ . The reaction mixture was then refluxed for 24 h in  $\text{CH}_3\text{CN}$ , leading to a dark purple solution that showed in its <sup>31</sup>P NMR spectrum a major peak at 57.0 ppm and a minor peak at 54.6 ppm. From this, the product was precipitated out by the addition of excess diethyl ether and recrystallised from acetonitrile/diethyl ether, affording dark purple crystals that exhibited a single <sup>31</sup>P NMR signal at 57.0 ppm. The microanalytical data of the product corresponded to the formulation  $[\text{Ru}_2(\mu\text{-Ph}_2\text{Pbpy})_2(\text{CO})_2(\text{CH}_3\text{CN})_2](\text{PF}_6)_2$  **18**. The NMR spectral data of this product, presented in Section 7.2.2., is in agreement with a *cis*( $\text{Ph}_2\text{Pbpy}$ )-**18** confirmation.

The reaction in  $\text{CH}_2\text{Cl}_2$  of  $[\text{Ru}_2(\text{CO})_4(\text{CH}_3\text{CN})_6](\text{PF}_6)_2$  with 9.5 equivalents of  $\text{PPh}_3$  is reported to afford the Ru(I) complex  $[\text{Ru}_2(\text{CO})_4(\text{CH}_3\text{CN})_4(\eta\text{-PPh}_3)_2](\text{PF}_6)_2$  wherein the  $\text{PPh}_3$  ligands are axially coordinated.<sup>155</sup> The <sup>31</sup>P NMR and IR spectral data of this complex bear a close resemblance to that of the intermediate species formed at room temperature from the reaction of  $\text{Ph}_2\text{Pbpy}$  with  $[\text{Ru}_2(\text{CO})_4(\text{CH}_3\text{CN})_6](\text{PF}_6)_2$ : in the <sup>31</sup>P NMR spectrum a single peak at 22.4 ppm is observed while in the IR spectrum  $\nu_{\text{CO}}$  absorption bands are seen at 2048 (medium), 2026 (strong), 1992 (strong, broad) and 1975 (shoulder)  $\text{cm}^{-1}$ .<sup>155</sup> The initial reaction of  $\text{Ph}_2\text{Pbpy}$

with  $[\text{Ru}_2(\text{CO})_4(\text{CH}_3\text{CN})_6](\text{PF}_6)_2$  at room temperature evidently generates the P-ligated species  $[\text{Ru}_2(\text{CO})_4(\text{CH}_3\text{CN})_4(\eta\text{-Ph}_2\text{Pbpy})_2](\text{PF}_6)_2$ , the coordination of the ligand being transformed to a bridging mode during refluxing. The transformation of this intermediate complex to the *cis* isomer appears to be more favourable than to the *trans*. The mild conditions initially employed here would permit a more complete formation of the P-ligated species and therefore a more selective synthesis of the target complex.

In contrast to what was found for  $\text{Ph}_2\text{Pbpy}$ , a similar approach using  $\text{Ph}_2\text{Ppyqn}$  did not lead to the selective formation of *cis*( $\text{Ph}_2\text{Ppyqn}$ )-**19**. The reaction of  $\text{Ph}_2\text{Ppyqn}$  with  $[\text{Ru}_2(\text{CO})_4(\text{CH}_3\text{CN})_6](\text{PF}_6)_2$  in  $\text{CH}_3\text{CN}$  at room temperature gave a yellow solution that exhibited in its  $^{31}\text{P}$  NMR spectrum a major peak at 24.7 ppm and a minor peak at 3.4 ppm. The IR spectrum of the solution showed four  $\nu_{\text{CO}}$  absorption bands at 2050 (medium), 2027 (strong), 1992 (strong, broad) and 1977 (medium, shoulder)  $\text{cm}^{-1}$ . It can be concluded, in keeping with the behaviour of  $\text{Ph}_2\text{Pbpy}$ , that the intermediate complex  $[\text{Ru}_2(\text{CO})_4(\text{CH}_3\text{CN})_4(\eta\text{-Ph}_2\text{Ppyqn})_2](\text{PF}_6)_2$  is formed. The refluxing of the solution for 36 h led to the appearance of two peaks at 60.9 ppm and 51.1 ppm in the  $^{31}\text{P}$  NMR spectrum. Refluxing of the solution for up to a further 12 h did not bring about a change in the relative intensities of the two  $^{31}\text{P}$  resonances. The addition of diethyl ether yielded a crystalline precipitate that exhibited two peaks in its  $^{31}\text{P}$  NMR spectrum, consistent with the presence of both *cis* and *trans* isomers.

### 7.2.2. Crystal Structure Determination of *cis*( $\text{Ph}_2\text{Ppyqn}$ )- $[\text{Ru}_2(\mu\text{-Ph}_2\text{Ppyqn})_2(\text{CO})_2(\text{CH}_3\text{CN})_2](\text{PF}_6)_2$ , *cis*( $\text{Ph}_2\text{Ppyqn}$ )-**19**

The structure of the cation of *cis*( $\text{Ph}_2\text{Ppyqn}$ )-**19** together with its atomic numbering scheme is depicted in Figure 7.2. Selected bond distances and angles are given in Table 7.1.

The crystal structure of *cis*( $\text{Ph}_2\text{Ppyqn}$ )-**19** consists of non-interacting  $[\text{Ru}_2(\mu\text{-Ph}_2\text{Ppyqn})_2(\text{CO})_2(\text{CH}_3\text{CN})_2]^{2+}$  dications and hexafluorophosphate anions. The molecular structure of *cis*( $\text{Ph}_2\text{Ppyqn}$ )-**19** displays the same features found in that of *cis*( $\text{Ph}_2\text{Pbpy}$ )- $[\text{Ru}_2(\mu\text{-Ph}_2\text{Pbpy})_2(\text{CO})_2(\text{EtCN})_2](\text{PF}_6)_2$ .<sup>185</sup> An approximately octahedral geometry is described about each ruthenium atom by a formal metal-metal bond, the phosphorus and two nitrogen donor atoms of the bridging ligands, the carbonyl ligand and acetonitrile molecule. The geometric constraints imposed by the small bite polypyridyl unit distorts the bond angles from the idealized value of  $90^\circ$  (see Table 7.1). The two  $\text{Ph}_2\text{Ppyqn}$  ligands bridge the metal atoms in a head-to-tail fashion and are coordinated *cis* to one another. The crystal structure of *cis*( $\text{Ph}_2\text{Pbpy}$ )- $[\text{Ru}_2(\mu\text{-Ph}_2\text{Pbpy})_2(\text{CO})_2(\text{EtCN})_2]^{2+}$  shows the carbonyl and nitrile ligands are staggered about the metal-



metal bond to different extents.<sup>185</sup> This is also observed in *cis*(Ph<sub>2</sub>Ppyqn)-**19**, where the C(57)–Ru(1)–Ru(2)–C(58) torsion angle of 69.8° is significantly smaller than the corresponding torsion angle N(5)–Ru(1)–Ru(2)–N(6) for the acetonitrile ligands of 112.4°.

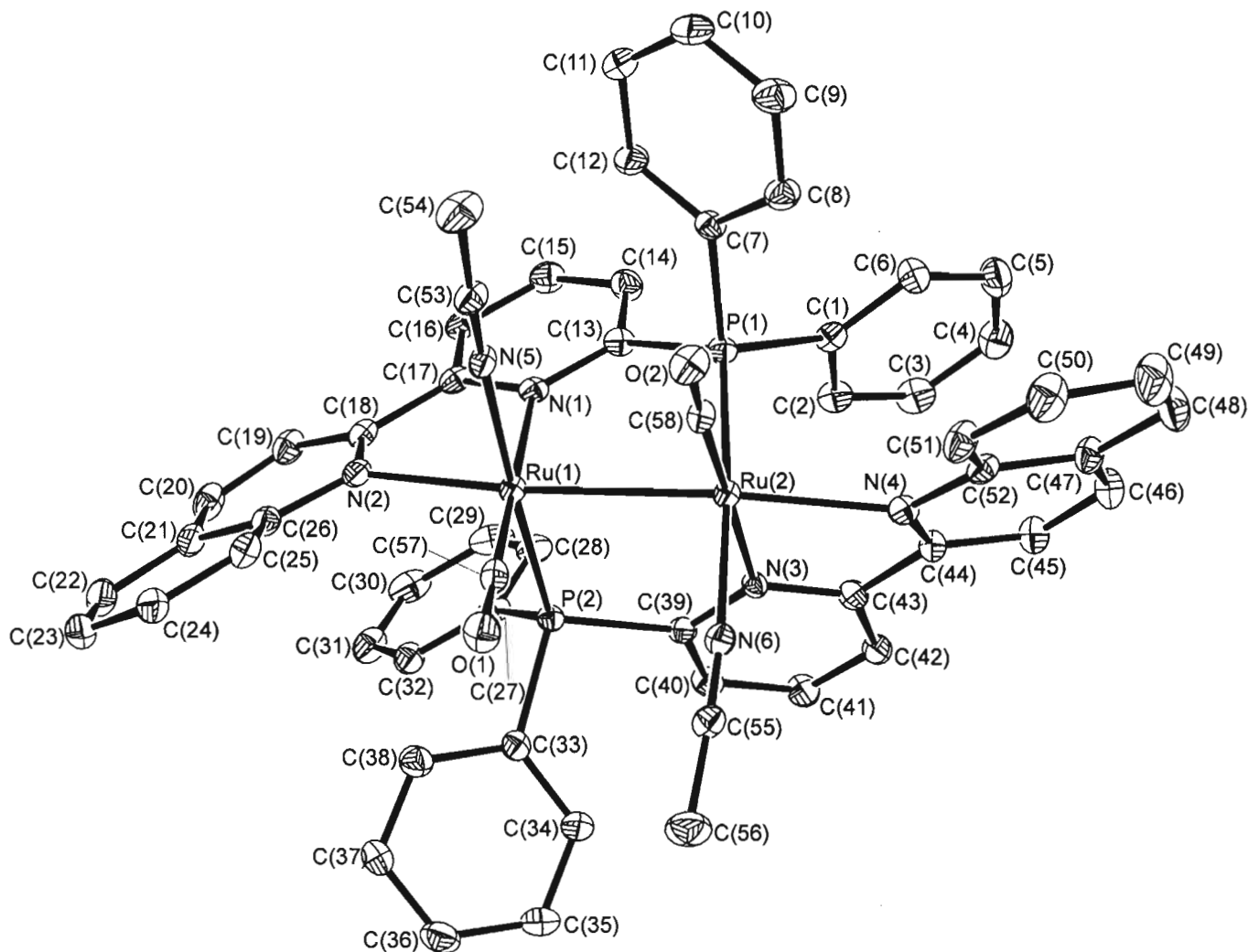


**Figure 7.2.** Perspective view of *cis*(Ph<sub>2</sub>Ppyqn)-[Ru<sub>2</sub>(μ-Ph<sub>2</sub>Ppyqn)<sub>2</sub>(CO)<sub>2</sub>(CH<sub>3</sub>CN)<sub>2</sub>]<sup>2+</sup>. The atoms are represented by their 20 % probability thermal ellipsoids.

**Table 7.1.** Selected interatomic distances (Å) and angles (°) for *cis*(Ph<sub>2</sub>Ppyqn)-[Ru<sub>2</sub>(μ-Ph<sub>2</sub>Ppyqn)<sub>2</sub>(CO)<sub>2</sub>(CH<sub>3</sub>CN)<sub>2</sub>](PF<sub>6</sub>)<sub>2</sub>, *cis*(Ph<sub>2</sub>Ppyqn)-**19**.

Ru(1)–Ru(2)	2.778(2)	Ru(1)–C(57)	1.828(7)
Ru(1)–N(5)	2.096(5)	Ru(2)–C(58)	1.836(6)
Ru(1)–N(1)	2.132(5)	Ru(2)–N(6)	2.103(6)
Ru(1)–N(2)	2.225(5)	Ru(2)–N(3)	2.148(4)
Ru(1)–P(2)	2.275(2)	Ru(2)–N(4)	2.235(5)
C(57)–Ru(1)–N(5)	88.6(2)	C(57)–Ru(1)–Ru(2)	86.2(2)
C(57)–Ru(1)–N(1)	178.3(2)	N(5)–Ru(1)–Ru(2)	93.4(2)
N(5)–Ru(1)–N(1)	89.8(2)	N(1)–Ru(1)–Ru(2)	93.3(2)
C(57)–Ru(1)–N(2)	105.6(2)	N(2)–Ru(1)–Ru(2)	167.8(2)
N(5)–Ru(1)–N(2)	90.3(2)	P(2)–Ru(1)–Ru(2)	84.23(7)
N(1)–Ru(1)–N(2)	75.1(2)	C(58)–Ru(2)–N(6)	94.0(2)
C(57)–Ru(1)–P(2)	91.6(2)	C(58)–Ru(2)–N(3)	177.5(2)
N(5)–Ru(1)–P(2)	177.6(2)	N(6)–Ru(2)–N(3)	83.6(2)
N(1)–Ru(1)–P(2)	90.0(2)	C(58)–Ru(2)–N(4)	104.7(2)
N(2)–Ru(1)–P(2)	92.0(2)	N(6)–Ru(2)–N(4)	88.8(2)

In the dinuclear complex [Ru<sub>2</sub>(CH<sub>3</sub>CN)<sub>6</sub>(CO)<sub>4</sub>](PF<sub>6</sub>)<sub>2</sub>, of which *cis*(Ph<sub>2</sub>Ppyqn)-**19** is a derivative, the carbonyl groups occupy *cis* positions at each ruthenium centre and adopt a *trans*-staggered conformation relative to one another about the ruthenium-ruthenium bond (Figure 7.3).<sup>155</sup> A similar conformation is observed in the crystal structure of the equatorially substituted triphenylphosphine adduct of this dinuclear precursor, [Ru<sub>2</sub>(CH<sub>3</sub>CN)<sub>4</sub>(CO)<sub>4</sub>(PPh<sub>3</sub>)<sub>2</sub>](PF<sub>6</sub>)<sub>2</sub>.<sup>155</sup>

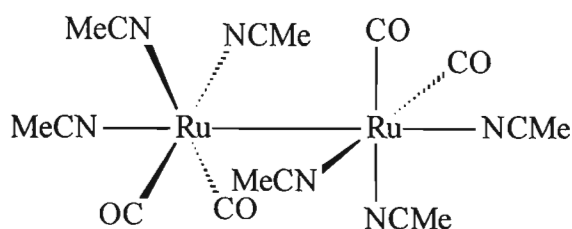


**Figure 7.3.** Orientation of the carbonyl and acetonitrile ligands about the ruthenium centre and Ru–Ru bond in [Ru<sub>2</sub>(CH<sub>3</sub>CN)<sub>6</sub>(CO)<sub>4</sub>](PF<sub>6</sub>)<sub>2</sub>.

Within the constraints imposed by the rigid N–C–P bridging fragment, this *trans*-staggered conformation of the equatorial ligands found in the dinuclear ruthenium precursor is preserved in both *cis*(Ph<sub>2</sub>Pbpy)-[Ru<sub>2</sub>(μ-Ph<sub>2</sub>Pbpy)<sub>2</sub>(CO)<sub>2</sub>(EtCN)<sub>2</sub>](PF<sub>6</sub>)<sub>2</sub> and *cis*(Ph<sub>2</sub>Ppyqn)-**19**. The view down the Ru–Ru bond axis shown in Figure 7.4 illustrates the orientation of the equatorial bonds relative to one another. The dihedral angles N(1)–Ru(1)–Ru(2)–P(1) and

N(3)–Ru(2)–Ru(1)–P(2) are found to have fairly large values of 19.0 and 25.7° respectively, reflecting how the rigid P–C–N plane is twisted as the molecule tries to attain a staggered conformation of the equatorial ligands about the Ru–Ru bond.

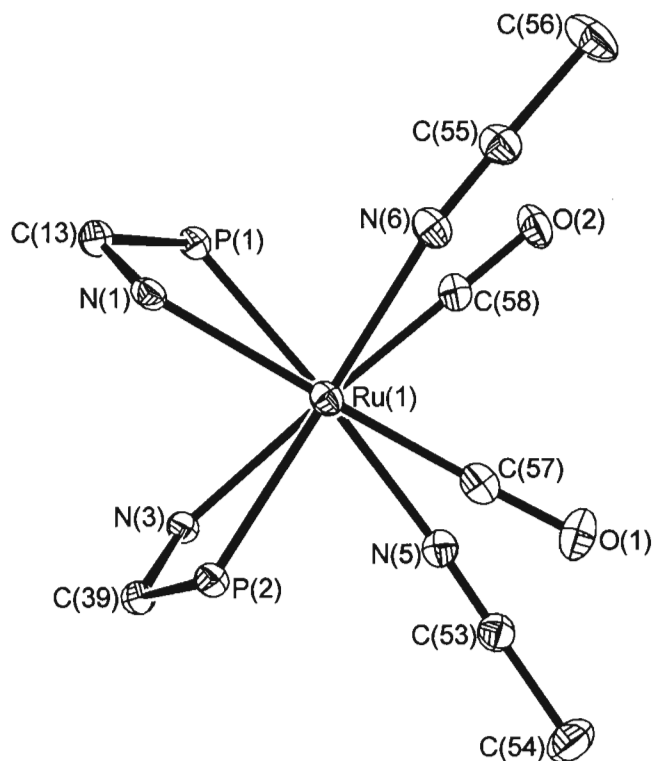


**Figure 7.4.** Perspective showing the axial substituents of the dication of *cis*(Ph<sub>2</sub>Ppyqn)-[Ru<sub>2</sub>(μ-Ph<sub>2</sub>Ppyqn)<sub>2</sub>(CO)<sub>2</sub>(CH<sub>3</sub>CN)<sub>2</sub>](PF<sub>6</sub>)<sub>2</sub>, *cis*(Ph<sub>2</sub>Ppyqn)-**19**, viewed down the Ru(1)–Ru(2) bond axis. The atoms are represented by their thermal ellipsoids at a 20 % probability level.

A significant twisting of the quinoline ring relative to that of the pyridyl about the intramolecular bond is observed in the coordinated Ph<sub>2</sub>Ppyqn ligands, the angle formed between the mean planes defined by the non-hydrogen atoms of each heteroaromatic ring being 18.4 and 19.1° for each ligand. Furthermore the Ru–N(quinoline) bond length of *cis*(Ph<sub>2</sub>Ppyqn)-**19** is longer, by almost 0.2 Å, than the corresponding Ru–N(pyridine) interatomic distance in *cis*(Ph<sub>2</sub>Pbpy)-[Ru(μ-Ph<sub>2</sub>Pbpy)<sub>2</sub>(CO)<sub>2</sub>(EtCN)<sub>2</sub>](PF<sub>6</sub>)<sub>2</sub>.<sup>185</sup> These effects can be ascribed to the steric crowding caused by the additional fused benzoid ring of the quinoline fragment in Ph<sub>2</sub>Ppyqn. A lengthening of the M–N(quinoline) bond distance is observed in manganese,<sup>153</sup> gold,<sup>191</sup> ruthenium and osmium<sup>192</sup> complexes of the likewise sterically hindered 2-(2'-pyridyl)quinoline ligand. The Ru–Ru bond distance of 2.778(2) Å is comparable to that of [Ru(μ-Ph<sub>2</sub>Pbpy)<sub>2</sub>(CO)<sub>2</sub>(EtCN)<sub>2</sub>](PF<sub>6</sub>)<sub>2</sub> [2.765 (2) Å]. It lies within the range exhibited by other similar diruthenium(I) complexes, where the metal-metal bond distance is seen to vary from 2.677(1) Å,

in  $[\text{Ru}(\mu\text{-Ph}_2\text{Ppy})_2(\mu\text{-CO})_2(\text{CH}_3\text{CN})_2](\text{PF}_6)_2$ <sup>185</sup> to 2.873(8) Å in  $[\text{Ru}(\text{CO})_4(\text{CH}_3\text{CN})_2(\text{PPh}_3)_2](\text{PF}_6)_2$ .<sup>155</sup>

The aromatic regions of the <sup>1</sup>H NMR spectra of *cis*(Ph<sub>2</sub>Pbpy)-**18** and *cis*(Ph<sub>2</sub>Ppyqn)-**19**, shown in Figure 7.5, were assigned with the aid of two-dimensional spectroscopy experiments. Table 7.2 gives the peak assignments of *cis*(Ph<sub>2</sub>Pbpy)-**18** and *cis*(Ph<sub>2</sub>Ppyqn)-**19** and compares the proton chemical shifts of the free ligands Ph<sub>2</sub>Pbpy and Ph<sub>2</sub>Ppyqn with those coordinated in the complexes. As will be argued below, these spectra can be interpreted in terms of the conformations shown by *cis*(Ph<sub>2</sub>Pbpy)-[Ru<sub>2</sub>(μ-Ph<sub>2</sub>Pbpy)<sub>2</sub>(CO)<sub>2</sub>(EtCN)<sub>2</sub>](PF<sub>6</sub>)<sub>2</sub> and *cis*(Ph<sub>2</sub>Ppyqn)-**19** in their crystal structures.

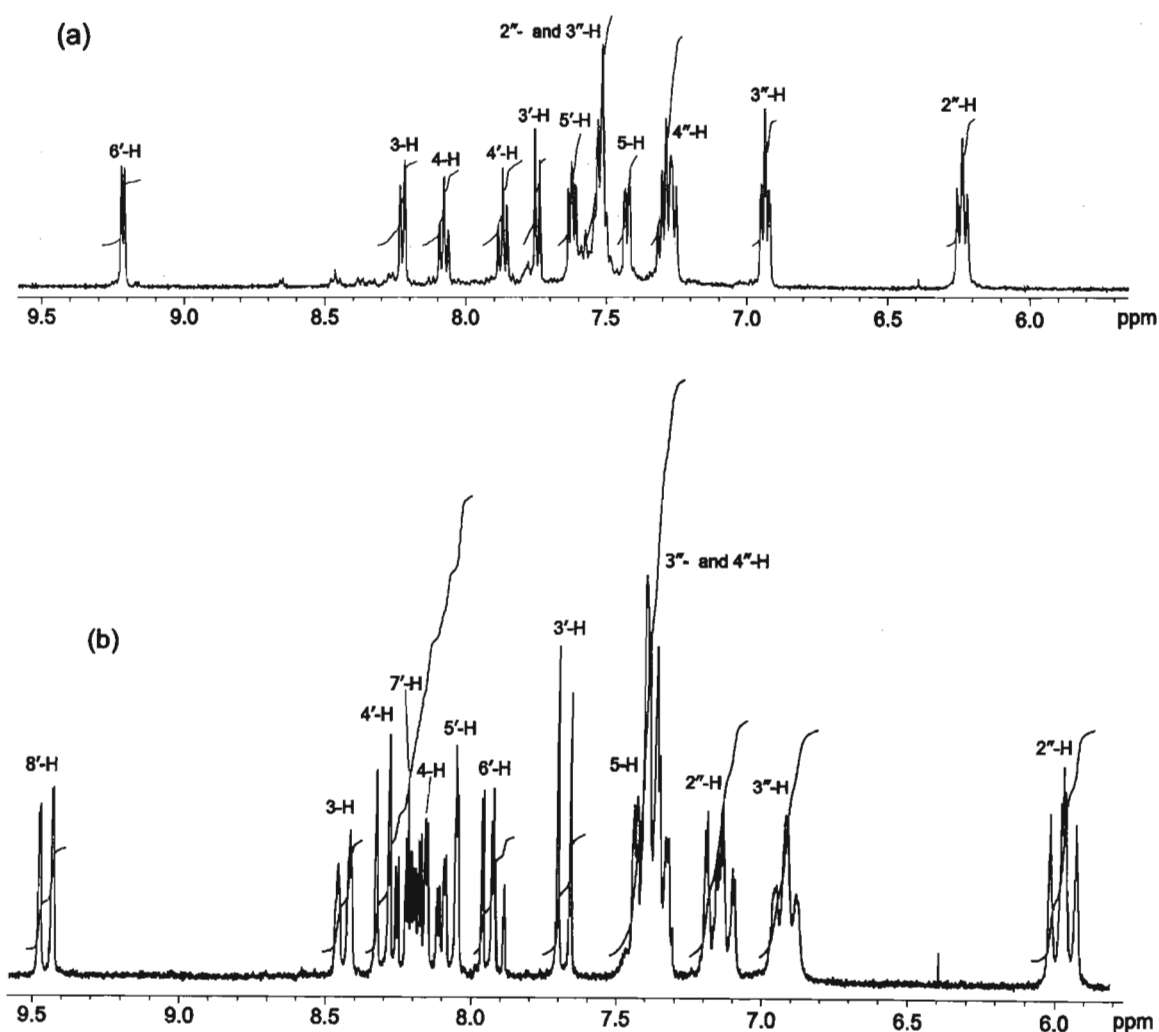


**Figure 7.5.** Aromatic regions of the <sup>1</sup>H NMR spectra of (a) *cis*(Ph<sub>2</sub>Pbpy)-[Ru<sub>2</sub>(μ-Ph<sub>2</sub>Pbpy)<sub>2</sub>(CO)<sub>2</sub>(CH<sub>3</sub>CN)<sub>2</sub>](PF<sub>6</sub>)<sub>2</sub>, *cis*(Ph<sub>2</sub>Pbpy)-**18** and (b) *cis*(Ph<sub>2</sub>Ppyqn)-[Ru<sub>2</sub>(μ-Ph<sub>2</sub>Ppyqn)<sub>2</sub>(CO)<sub>2</sub>(CH<sub>3</sub>CN)<sub>2</sub>](PF<sub>6</sub>)<sub>2</sub>, *cis*(Ph<sub>2</sub>Ppyqn)-**19**.

**Table 7.2.** Comparison between the proton chemical shifts of the free and coordinated P,N,N ligands in *cis*(L)-[Ru<sub>2</sub>(μ-L)<sub>2</sub>(CO)<sub>2</sub>(CH<sub>3</sub>CN)<sub>2</sub>](PF<sub>6</sub>)<sub>2</sub> (L = Ph<sub>2</sub>Pbpy **18** and Ph<sub>2</sub>Ppyqn **19**).<sup>a</sup>

Assignment	δ/ppm (Δδ vs. free ligand)				
	Ph <sub>2</sub> Pbpy	<i>cis</i> (Ph <sub>2</sub> Pbpy)- <b>18</b>	Ph <sub>2</sub> Ppyqn	<i>cis</i> (Ph <sub>2</sub> Ppyqn)- <b>19</b>	
3-H	8.31	8.23 (0.08)	8.56	8.42 (0.14)	
3'-H	8.25	7.75 (0.50)	8.40	7.68 (0.72)	
4-H	7.70	8.08 (-0.38)	7.76	8.15 (-0.39)	
4'-H	7.74	7.87 (-0.13)	8.20	8.29 (-0.09)	
5-H	7.15	7.43 (-0.28)	7.20	7.42 (-0.22)	
5'-H	7.28	7.63(-0.35)	7.84	8.06 (-0.22)	
6'-H	8.63	9.22(-0.59)	7.72	7.93 (-0.21)	
7'-H			7.54	8.21 (-0.67)	
8'-H			8.11	9.43 (-1.32)	
2''-H	unperturbed	7.44	7.52 (-0.08)	7.46	7.15 (0.31)
3''-H	} phenyl	7.44	7.52 (-0.08)	7.46	7.37 (0.09)
4''-H		ring	7.36	7.27 (0.09)	7.37
2''-H	shielded		6.24 (1.20)		5.98 (1.48)
3''-H	} phenyl		6.94 (0.50)		6.92 (0.54)
4''-H		ring		7.29 (0.07)	

<sup>a</sup>Recorded in CD<sub>2</sub>Cl<sub>2</sub> at 298 K using CDHCl<sub>2</sub> as an internal reference.

Four sets of phenyl proton resonances are observed in the <sup>1</sup>H NMR spectra of *cis*(Ph<sub>2</sub>Pbpy)-**18** and *cis*(Ph<sub>2</sub>Ppyqn)-**19**, the integrals of these signals corresponding to 8, 4, 4 and 4 protons respectively. Examination of the crystal structures (Figure 7.1 and 7.2) reveals that the two phenyl rings of the P,N,N ligands each possess a distinct chemical environment: while one is projected away from the rest of the molecule [phenyl rings C(1) – C(6), for *cis*(Ph<sub>2</sub>Pbpy)-[Ru<sub>2</sub>(μ-Ph<sub>2</sub>Pbpy)<sub>2</sub>(CO)<sub>2</sub>(EtCN)<sub>2</sub>](PF<sub>6</sub>)<sub>2</sub>, and C(7) – C(12) and C(33) – C(38), for *cis*(Ph<sub>2</sub>Ppyqn)-**19**], the other lies coplanar with the polypyridyl fragment of the second P,N,N ligand [phenyl rings C(7) – C(12), for *cis*(Ph<sub>2</sub>Pbpy)-[Ru<sub>2</sub>(μ-Ph<sub>2</sub>Pbpy)<sub>2</sub>(CO)<sub>2</sub>(EtCN)<sub>2</sub>](PF<sub>6</sub>)<sub>2</sub>, and C(1) – C(6) and C(27) – C(32), for *cis*(Ph<sub>2</sub>Ppyqn)-**19**]. The angles formed between the mean planes defined by the non-hydrogen atoms of the latter phenyl rings and the respective polypyridyl fragments are measured to be 16.7° for *cis*(Ph<sub>2</sub>Pbpy)-[Ru<sub>2</sub>(μ-Ph<sub>2</sub>Pbpy)<sub>2</sub>(CO)<sub>2</sub>(EtCN)<sub>2</sub>](PF<sub>6</sub>)<sub>2</sub>, and 9.4(3) and 14.9(1)° for *cis*(Ph<sub>2</sub>Ppyqn)-**19**. Table 7.3 lists the shortest contact distances between the carbon atoms of the coplanar phenyl rings and those of the polypyridyl fragment of the second ligand. The values show that the hydrogen atoms of these phenyl rings would be expected to be shielded by the polypyridyl fragment. Furthermore, this effect would be most marked for the *ortho* and *meta* protons. The proton chemical shifts of the four phenyl rings present in the complexes are

commensurate with this model. The four *ortho* (2''-H) and four *meta* (3''-H) protons of the shielded phenyl rings are shifted strongly upfield, appearing as triplets at 6.24 and 6.94 ppm [for *cis*(Ph<sub>2</sub>Pbpy)-18], and 5.98 and 6.92 ppm [for *cis*(Ph<sub>2</sub>Ppyqn)-19] respectively. In the case of *cis*(Ph<sub>2</sub>Pbpy)-18, the four *ortho* and four *meta* protons of the unperturbed phenyl rings are manifested as a complex multiplet centred at 7.52 ppm. Their chemical shift and pattern do not differ markedly from that exhibited by the free ligand. For *cis*(Ph<sub>2</sub>Ppyqn)-19, the *ortho* protons of the unperturbed phenyl ring are shifted upfield, appearing as a triplet centred at 7.15 ppm, while the *meta* protons show only a marginal change in chemical shift from what is observed in the free ligand. The chemical shifts of the *para* (4''-H) protons in *cis*(Ph<sub>2</sub>Pbpy)-18 and *cis*(Ph<sub>2</sub>Ppyqn)-19 do not differ markedly between the shielded and unperturbed phenyl rings, nor between the free and coordinated ligands. The *para* protons of the phenyl rings would be expected to be furthest to the periphery of the polypyridyl fragment shielding field; the small difference between the chemical shifts of the two types of *para* protons present can thus be expected.

**Table 7.3.** Shortest contact distances between the atoms of the coplanar phenyl rings and those of the polypyridyl fragment of the other P,N,N ligand in *cis*(Ph<sub>2</sub>Pbpy)-[Ru<sub>2</sub>(μ-Ph<sub>2</sub>Pbpy)<sub>2</sub>(CO)<sub>2</sub>(EtCN)<sub>2</sub>](PF<sub>6</sub>)<sub>2</sub> and *cis*(Ph<sub>2</sub>Ppyqn)-[Ru<sub>2</sub>(μ-Ph<sub>2</sub>Ppyqn)<sub>2</sub>(CO)<sub>2</sub>(CH<sub>3</sub>CN)<sub>2</sub>](PF<sub>6</sub>)<sub>2</sub>, *cis*(Ph<sub>2</sub>Ppyqn)-19.

<i>cis</i> (Ph <sub>2</sub> Pbpy)-[Ru <sub>2</sub> (μ-Ph <sub>2</sub> Pbpy) <sub>2</sub> (CO) <sub>2</sub> (EtCN) <sub>2</sub> ](PF <sub>6</sub> ) <sub>2</sub>			
C(7') ...N(2)	3.292	C(10') ...C(19)	3.877
C(8') ...N(2)	3.563	C(11') ...C(17)	3.630
C(9') ...C(19)	3.893	C(12') ...C(17)	3.107
<i>cis</i> (Ph <sub>2</sub> Ppyqn)-[Ru <sub>2</sub> (μ-Ph <sub>2</sub> Ppyqn) <sub>2</sub> (CO) <sub>2</sub> (CH <sub>3</sub> CN) <sub>2</sub> ](PF <sub>6</sub> ) <sub>2</sub> , <i>cis</i> (Ph <sub>2</sub> Ppyqn)-19			
C(1) ...C(44)	3.277	C(27) ...C(18)	3.154
C(2) ...C(43)	3.065	C(28) ...C(17)	3.015
C(3) ...C(45)	3.505	C(29) ...C(16)	3.515
C(4) ...C(45)	3.526	C(30) ...C(19)	3.567
C(5) ...C(46)	3.674	C(31) ...C(19)	3.415
C(6) ...N(4)	3.690	C(32) ...C(19)	3.422

In bipyridyl ligand complexes of Ru(II) the <sup>1</sup>H NMR signal of 3-H / 3'-H is often the lowest field resonance because of the close 3-H...3'-H contacts that give rise to van der Waals deshielding of these protons.<sup>63</sup> The opposite is true of 3'-H in *cis*(Ph<sub>2</sub>Pbpy)-18 and *cis*(Ph<sub>2</sub>Ppyqn)-19, where this proton is shifted upfield relative to the free ligand by 0.50 ppm in *cis*(Ph<sub>2</sub>Pbpy)-18 and 0.72 ppm in *cis*(Ph<sub>2</sub>Ppyqn)-19. However, all the other protons of the

polypyridyl fragments in *cis*(Ph<sub>2</sub>Pbpy)-**18** and *cis*(Ph<sub>2</sub>Ppyqn)-**19** are consistently shifted downfield. In particular, the resonances of protons 6'-H in *cis*(Ph<sub>2</sub>Pbpy)-**18** and 8'-H in *cis*(Ph<sub>2</sub>Ppyqn)-**19** are seen to be shifted downfield upon coordination by 0.59 and 1.32 ppm respectively. Inspection of Table 7.3 confirms that 3'-H, and to a lesser extent 3-H, would be strongly shielded in the complexes due to their position relative to the atoms of the coplanar phenyl rings.

The average distance of the shielded phenyl ring atoms from the mean planes defined by the non-hydrogen atoms of the polypyridyl fragments is 3.5(3) Å for [Ru<sub>2</sub>(μ-Ph<sub>2</sub>Pbpy)<sub>2</sub>(CO)<sub>2</sub>(EtCN)<sub>2</sub>](PF<sub>6</sub>)<sub>2</sub>, and 3.2(2) and 3.6(4) Å for *cis*(Ph<sub>2</sub>Ppyqn)-**19**. This interplanar separation of the two essentially parallel π-systems that are offset relative to one another is consistent with a favourable net π-π interaction.<sup>193</sup>

### 7.2.3. Cyclic Voltammetry of the Dinuclear Ruthenium Complexes

The redox properties of *cis*(L)-[Ru<sub>2</sub>(μ-L)<sub>2</sub>(CO)<sub>2</sub>(CH<sub>3</sub>CN)<sub>2</sub>](PF<sub>6</sub>)<sub>2</sub> (L = Ph<sub>2</sub>Pbpy **18** and Ph<sub>2</sub>Ppyqn **19**) are summarised in Table 7.4.

**Table 7.4.** Cyclic voltammetric data of the diruthenium complexes *cis*(L)-[Ru<sub>2</sub>(μ-L)<sub>2</sub>(CO)<sub>2</sub>(CH<sub>3</sub>CN)<sub>2</sub>](PF<sub>6</sub>)<sub>2</sub> (L = Ph<sub>2</sub>Pbpy **18** and Ph<sub>2</sub>Ppyqn **19**).<sup>a</sup>

Complex	$E_{1/2}/V$ ( $\Delta E_p/mV$ )					
	$E_{pa}^{ox}$	$E_{pc}^{ox}$	$E_{1/2}^{+3/+2}$	$E_{1/2}^{+2/+}$	$E_{1/2}^{+/0}$	$E_{1/2}^{0/-2}$
<i>cis</i> (Ph <sub>2</sub> Pbpy)- <b>18</b>	1.18	0.92	0.28(80)	-1.68 <sup>b</sup>		
<i>cis</i> (Ph <sub>2</sub> Ppyqn)- <b>19</b> <sup>c</sup>	1.44	1.34	0.43(65)	-1.48(70)	-1.62(70)	-1.90(115)

<sup>a</sup> Potentials vs. Ag/Ag<sup>+</sup>, measured in CH<sub>3</sub>CN (0.1 M TBAP), scan rate 100 mV s<sup>-1</sup>, T = 298 K. Definitions:  $E_{pa}^{ox}$ ,  $E_{pc}^{ox}$  = anodic and cathodic peak potentials of chemically irreversible oxidation;  $E_{1/2} = (E_{pc} + E_{pa})/2$ ;  $\Delta E_p = E_{pc} - E_{pa}$ . <sup>b</sup> Cathodic peak potential of chemically irreversible reduction. <sup>c</sup> Corresponds to the average of the two half-wave potentials,  $E_{1/2} = (E_{1/2}^{0/-} + E_{1/2}^{-/2})/2$ . <sup>d</sup> Measured using a Ag/AgCl wire pseudo-reference electrode.

The CV of *cis*(Ph<sub>2</sub>Pbpy)-**18**, shown in Figure 7.6, exhibits an irreversible reduction peak at  $E_{pc} = -1.68$  V [Figure 7.6(a)]. Corresponding anodic return peaks are seen at  $E_{pa} = -1.38$  and  $-0.24$  V. When the potential scan is extended to  $-2.28$  V two further and reversible reductions are observed at  $E_{1/2} = -1.90$  and  $-2.08$  V [Figure 7.6(b) and (c)]. The relative intensities of the first irreversible and second and third reversible systems are 2:1:1. It should be noted that when the potential scan is reversed just after the second reduction peak [curve (b)], the anodic peaks at  $-1.38$  and  $-0.24$  V become more prominent while an additional anodic peak is observed at

-1.64 V. The variation of the scan rate from 10 to 500 mVs<sup>-1</sup> leads to an increase in the relative heights of the anodic peaks at -1.38 and -1.64 V, these systems becoming more clearly defined. Cathodic electropolymerisation of the complex, as has been described in Sections 5.2.2.(ii) and 6.2.2.(i) for [Ru<sub>2</sub>(L)<sub>2</sub>(CO)<sub>4</sub>(CH<sub>3</sub>CN)<sub>2</sub>](PF<sub>6</sub>)<sub>2</sub> (L = bpy or L<sub>1-4</sub>), was attempted by cycling the potential between various potential limits on both Pt and glassy carbon electrodes. No formation of a film on the electrode surface was observed.

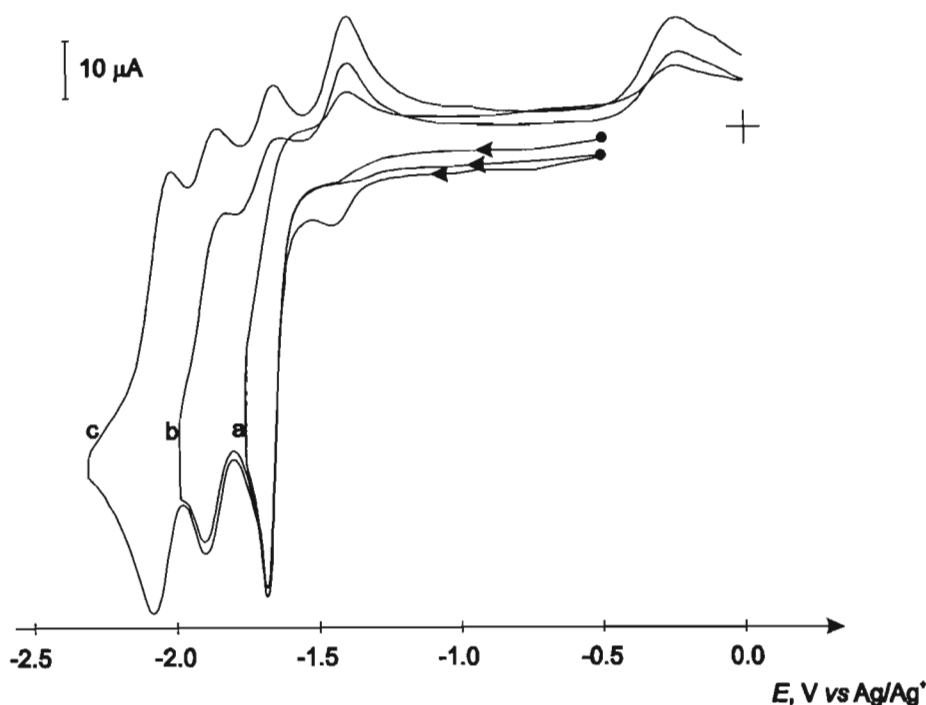


**Figure 7.6.** CV of *cis*(Ph<sub>2</sub>Pbpy)-18, measured in CH<sub>3</sub>CN (0.1 M TBAP); (a) first scan between 0 and -1.74 V; (b) second scan between 0 and -1.98 V; (c) third scan between 0 and -2.28 V. (Pt electrode, r = 2.5 mm;  $\nu$  = 100 mVs<sup>-1</sup>).

An exhaustive electrolysis of a CH<sub>3</sub>CN (0.1 M TBAP) solution of *cis*(Ph<sub>2</sub>Pbpy)-18 at  $E_{app}$  = -1.66 V consumes two electrons per complex and leads to the formation of new species in solution. The CV of this solution shows a reversible reduction process with  $E_{1/2}$  = -1.85 V, followed by irreversible cathodic peaks. An anodic peak is observed at  $E_{pa}^{ox}$  = -0.28 V. Though there was no deposition of Ru metal onto the electrode surface, it was observed that the green-brown coloured solution contained suspended black material. The characterisation of these reduction products was not attempted.

The cathodic CV of *cis*(Ph<sub>2</sub>Ppyqn)-19 (Figure 7.7) consists of three reversible reduction waves that, from a RDE experiment, are shown to be two one-electron steps followed by a third two-electron reduction. The extension of the potential scan to -2.60 V revealed no further reduction peaks. Although it is difficult to estimate the  $i_{pa}/i_{pc}$  ratio for the first two waves, that of



the third is unity. All three show a linear relationship of  $i_p$  with  $\nu^{1/2}$ , the scan rate being varied from 20 to 500  $\text{mVs}^{-1}$ . The peak splitting  $\Delta E_p$  shows no variation with scan rate between 20 and 500  $\text{mVs}^{-1}$  and, for the first two waves, is of the magnitude expected for a reversible one-electron reduction. The peak-to-peak separation of 115 mV for the third wave points towards this being the combination of two unresolved, one-electron reductions.

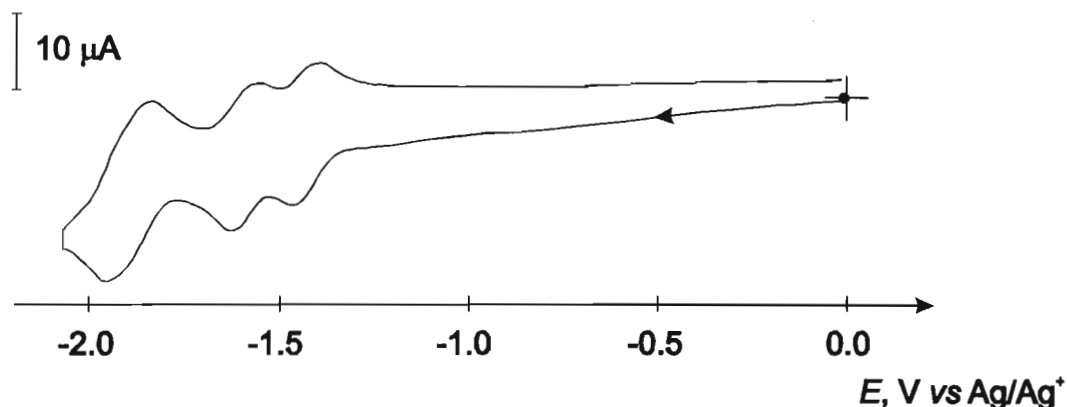


**Figure 7.7.** CV of *cis*(Ph<sub>2</sub>Ppyqn)-19, measured in CH<sub>3</sub>CN (0.1 M TBAP). (Pt electrode,  $r = 1.0$  mm;  $\nu = 100$   $\text{mVs}^{-1}$ ).

Figure 7.8 illustrates a structural difference between *cis*(Ph<sub>2</sub>Pbpy)-18 and *cis*(Ph<sub>2</sub>Ppyqn)-19 that may contribute towards their different electrochemical behaviour upon reduction. Using space-filling diagrams the donor atoms of the interlocking phosphorus-polypyridyl rings can be shown to form a shallow cavity in which the ruthenium centres are held. In *cis*(Ph<sub>2</sub>Pbpy)-18 this is open sided, while in *cis*(Ph<sub>2</sub>Ppyqn)-19 the presence of the extra benzoid atoms of the quinoline rings serves to deepen the cavity and form more of a steric constriction on the open side. This spatial ‘gate’ may sufficiently retard the decomposition that occurs for the reduced forms of *cis*(Ph<sub>2</sub>Ppyqn)-19, so stabilizing the reduction products of *cis*(Ph<sub>2</sub>Ppyqn)-19. Thus the electrochemical stability of the Ph<sub>2</sub>Ppyqn diruthenium(I) species over that of the Ph<sub>2</sub>Pbpy analogue appears to derive from both the more extended  $\alpha$ -diimine  $\pi^*$  system and the unique topography of the Ph<sub>2</sub>Ppyqn ligand.

The additional stability on reduction lent to complexes of Ph<sub>2</sub>Ppyqn by the particular topography of this ligand has also been demonstrated by its dicopper(I) and diplatinum(I) complexes [see sections 3.2.3 and 4.2.3.(ii)]. While the Ph<sub>2</sub>Pbpy and Et(Ph)Pbpy formally metal(-1) complexes are unstable on a time scale beyond that of cyclic voltammetric measurement, the Ph<sub>2</sub>Ppyqn analogues are chemically robust. Indeed, the examination of the space-filling models of [Cu<sub>2</sub>( $\mu$ -Ph<sub>2</sub>Ppyqn)<sub>2</sub>(CH<sub>3</sub>CN)<sub>2</sub>](BF<sub>4</sub>)<sub>2</sub> 1 and [Cu<sub>2</sub>( $\mu$ -

$\text{Ph}_2\text{Pbpy})_2(\text{CH}_3\text{CN})_2](\text{PF}_6)_2$  shows that they have the same topography as the analogous Ru(I) complexes.

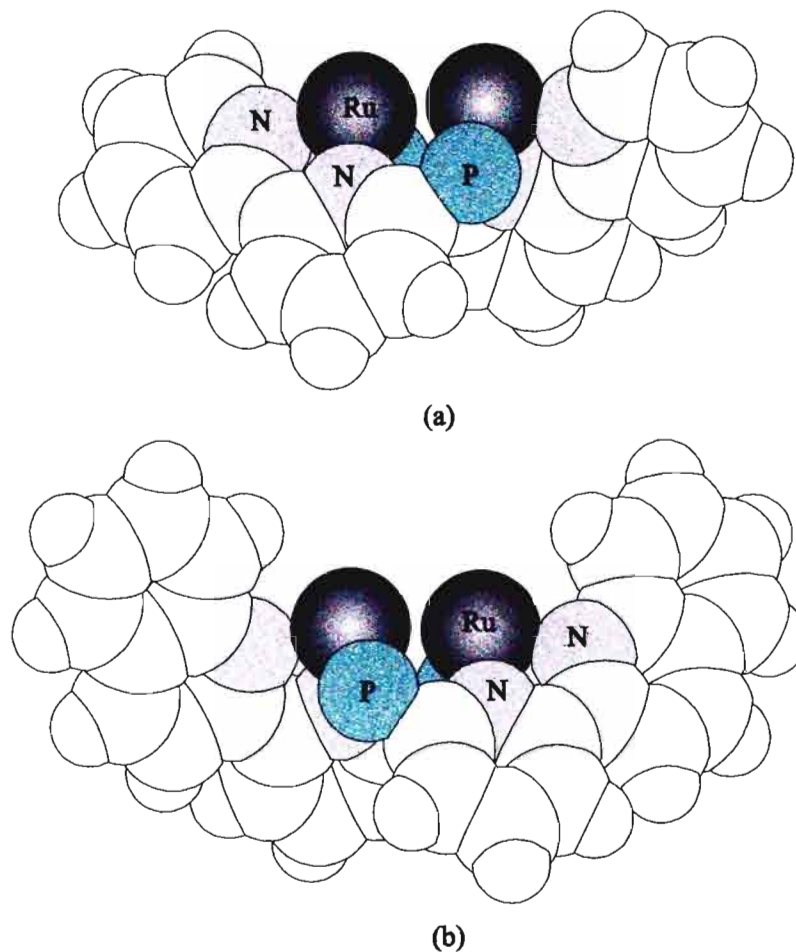


**Figure 7.8.** Space-filling model representation of the molecular structures of the dications (a)  $\text{cis}(\text{Ph}_2\text{Pbpy})\text{-}[\text{Ru}_2(\mu\text{-Ph}_2\text{Pbpy})_2(\text{CO})_2(\text{CH}_3\text{CN})_2]^{2+}$  and (b)  $\text{cis}(\text{Ph}_2\text{Ppyqn})\text{-}[\text{Ru}_2(\mu\text{-Ph}_2\text{Ppyqn})_2(\text{CO})_2(\text{CH}_3\text{CN})_2]^{2+}$ . For clarity only the ruthenium, phosphorus and  $\alpha$ -diimine ring atoms are shown. The atoms are represented by their van der Waal radii.

The electrochemistry of previously studied  $\alpha$ -diimine diruthenium(I) complexes shows that the nature of the axial ligand influences the reductive electrochemistry. Where it is suitably labile, for example  $\text{Cl}^-$  and  $\text{CH}_3\text{CN}$  in  $[\text{Ru}_2(\text{bpy})_2(\text{CO})_4(\text{CH}_3\text{CN})_2](\text{PF}_6)_2$  [see Section 5.2.2.(ii)] and  $[\text{Ru}_2(\text{bpy})_2(\text{CO})_4\text{Cl}_2]$ ,<sup>38,43</sup> reduction leads to the formation a Ru–Ru polymer through the loss of two axial leaving ligands. On the other hand, the complex  $[\text{Ru}_2(\text{bpy})_2(\text{CO})_4(\text{COOMe})_2]$ , containing the non-labile axial ligand COOMe, exhibits a quasi-reversible one-electron reduction.<sup>38,43</sup> The complexes  $[\text{Ru}_2(\text{L})_2(\text{CO})_4(i\text{Pr-DAB})_2]$  ( $\text{L} = \text{SnPh}_3, \text{PbPh}_3$ ;  $i\text{Pr-DAB} = 1,4$ -diisopropyl-1,4-diaza-1,3-butadiene), wherein the L–Ru–Ru–L bond axis is strongly stabilised by the Ru–L bonds, undergo an irreversible two-electron reduction to give the five coordinate

anion  $[\text{Ru}(\text{L})(\text{CO})_2(i\text{Pr-DAB})]^-$ .<sup>194</sup> In the case of *cis*(Ph<sub>2</sub>Pbpy)-18 and *cis*(Ph<sub>2</sub>Ppyqn)-19, the coordination mode of the tridentate ligand presents an axial ligand which is non-labile. On the other hand, the bridging nature of the P,N,N ligands would hinder the rupture of the metal-metal bond to form a mononuclear radical anion, as is observed for  $[\text{Ru}_2(\text{L})_2(\text{CO})_4(i\text{Pr-DAB})_2]$  (L = SnPh<sub>3</sub>, PbPh<sub>3</sub>). The sharp shape of the first reduction peak of *cis*(Ph<sub>2</sub>Pbpy)-18 is typical of the form of CV observed for those Ru complexes giving species with Ru–Ru bonds on reduction. It is noted that a black suspension is present at the end of the exhaustive electrolysis. It is possible therefore, that the reduction of the complex leads to some oligomer formation. The structural nature of the Ph<sub>2</sub>Pbpy ligand would sterically obstruct an efficient formation of Ru–Ru bonded chains, giving rise to species that would not be adherent to the electrode but would form a partially soluble material in solution. In *cis*(Ph<sub>2</sub>Ppyqn)-19 the Ph<sub>2</sub>Ppyqn ligand would further encapsulate the reduced ruthenium centres, so preventing the formation of Ru–Ru chains and thereby permitting the chemically reversible reduction of this complex.

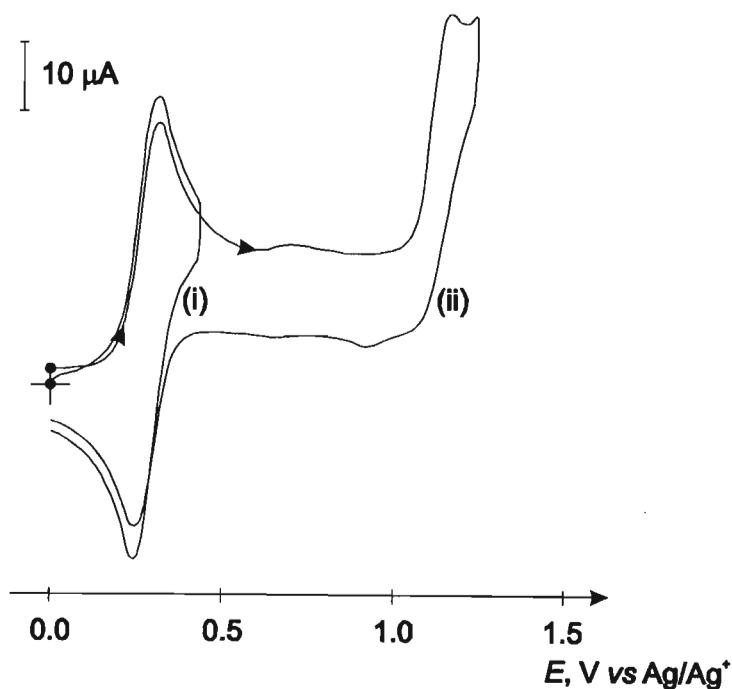


**Figure 7.9.** CVs of *cis*(Ph<sub>2</sub>Pbpy)-18 measured in acetonitrile (0.1 M TBAP) solution. (Pt electrode,  $r = 2.5$  mm;  $\nu = 100$  mVs<sup>-1</sup>).

The anodic CVs of the phosphorus-polypyridyl ligand-bridged diruthenium complexes *cis*(Ph<sub>2</sub>Pbpy)-18 and *cis*(Ph<sub>2</sub>Ppyqn)-19 consist of two one-electron oxidation waves (Figure 7.9 and 7.10 respectively). The first redox couple of both complexes is fully reversible, meeting the criteria for a reversible process previously described. The second oxidation of *cis*(Ph<sub>2</sub>Pbpy)-18 is

irreversible, with only a small return cathodic wave being observed 249 mV negative of the second anodic peak potential [Figure 7.9(ii)]. The second oxidation of *cis*(Ph<sub>2</sub>Ppyqn)-**19** is observed to be quasi-reversible, as is evident from the presence of a corresponding cathodic peak (Figure 7.10).

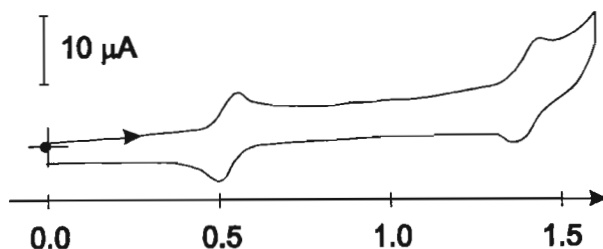


**Figure 7.10.** CV of *cis*(Ph<sub>2</sub>Ppyqn)-**19** measured in acetonitrile (0.1 M TBAP) solution. (Pt electrode,  $r = 1.0$  mm;  $\nu = 100$  mVs<sup>-1</sup>).

The exhaustive electrolysis of an acetonitrile solution of *cis*(Ph<sub>2</sub>Pbpy)-**18** at  $E_{app} = 0.36$  V with the consumption of one electron per mole of dimer resulted in a change in colour of the solution from dark purple to yellow. CV and RDE plots confirm the reversibility of this couple. Upon exhaustive bulk electrolysis at  $E_{app} = 0.00$  V of the product solution, with the coulometric measurement showing the passage of one electron per mole of dimer, the original complex was reformed. The yields of both transformations are around 80 - 90 %. UV-vis and IR spectroscopies confirm the complete reversibility of the oxidation-reduction processes.

As discussed in Section 5.2.2.(i), the oxidation of [Ru(bpy)(CO)<sub>2</sub>(CH<sub>3</sub>CN)]<sub>2</sub>(PF<sub>6</sub>)<sub>2</sub> **12** is a two-electron process resulting in a breakage of the metal-metal bond and a concurrent coordination of acetonitrile solvent to form *cis*(CH<sub>3</sub>CN)-[Ru(bpy)(CO)<sub>2</sub>(CH<sub>3</sub>CN)<sub>2</sub>](PF<sub>6</sub>)<sub>2</sub> **13**. It is reasonable to anticipate that a similar metal-based oxidation would take place in *cis*(Ph<sub>2</sub>Pbpy)-**18**. However, the phosphorus-polypyridyl ligand would impede the rupture of the M-M bond and associated CH<sub>3</sub>CN coordination initiated by oxidation. The IR spectrum of the one-electron oxidation product shows, in addition to the two absorption bands of the starting complex, two new bands of exactly the same pattern at longer wavenumbers of 1988 and 2016 cm<sup>-1</sup> (Figure 7.11). Clearly the oxidation product associated with these bands would have to be fully characterised, but this preliminary infrared data does suggest that the initial coordination sphere of the ruthenium centres is essentially unchanged while the electron density on one of the metal centres has been decreased.

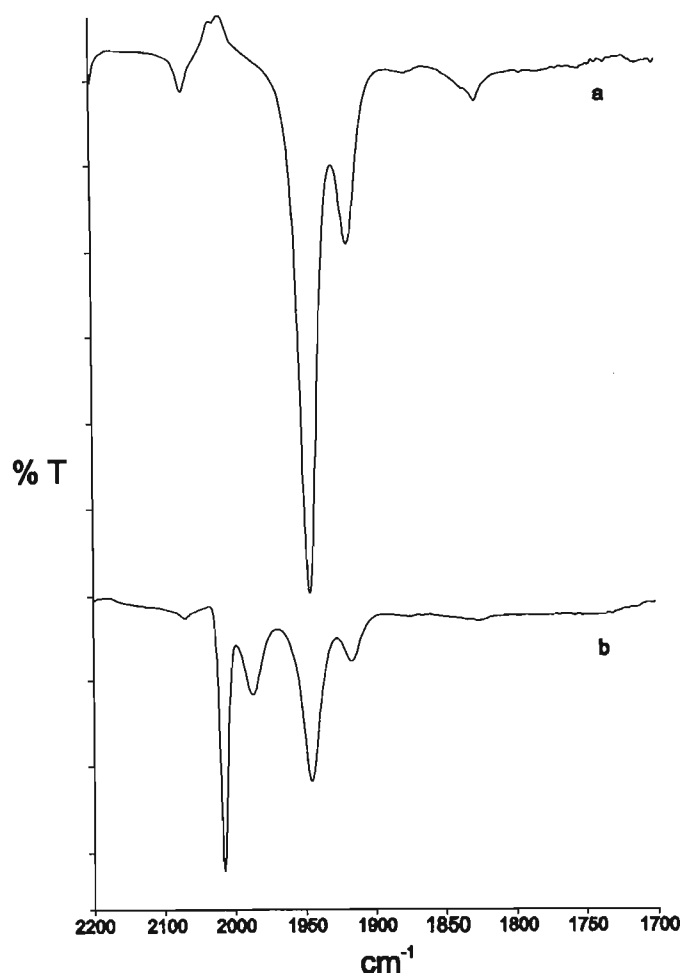


**Figure 7.11.** CO stretching region of FT-IR spectrum recorded in electrolyte ( $\text{CH}_3\text{CN} + 0.1 \text{ M TBAP}$ ) of *cis*( $\text{Ph}_2\text{Pbpy}$ )- $[\text{Ru}_2(\mu\text{-Ph}_2\text{Pbpy})_2(\text{CO})_2(\text{CH}_3\text{CN})_2](\text{PF}_6)_2$  **18** before (a) and after (b) exhaustive electrolysis at  $E_{\text{app}} = 0.36 \text{ V}$ .

#### 7.2.4. Catalytic Properties Towards $\text{CO}_2$ Electrochemical Reduction

The presence of  $\text{CO}_2$  in the electrolyte solution influences the electrochemical behaviour of *cis*( $\text{Ph}_2\text{Pbpy}$ )-**18** (Figure 7.12), producing an augmentation in current of the first reduction peak. Significantly, when the potential is repetitively scanned between  $-1.40$  and  $-1.80 \text{ V}$  a constant height of the first reduction peak is seen.

To examine further the potential catalytic properties of *cis*( $\text{Ph}_2\text{Pbpy}$ )-**18**, a preparative scale electrolysis experiment was carried out using a carbon felt working electrode in  $\text{CH}_3\text{CN} + 0.1 \text{ M TBAP}$  with a  $1 \text{ mM}$  concentration of complex. At a working electrode potential of  $E_{\text{app}} = -1.80 \text{ V}$  the initial constant current was  $2.6 \text{ mA}$ , this diminished to  $2.2 \text{ mA}$  after the consumption of  $42 \text{ C}$ . Carbon monoxide and formate were found to form with  $10$  and  $30 \%$  Faradaic yields respectively. During the course of the electrolysis the colour of the solution changed from purple

to a blood red colour. Furthermore a black precipitate was present at the end of the experiment. A CV of this solution, purged with Ar to remove the CO<sub>2</sub>, showed that the starting ruthenium complex *cis*(Ph<sub>2</sub>Pbpy)-18 was no longer present.

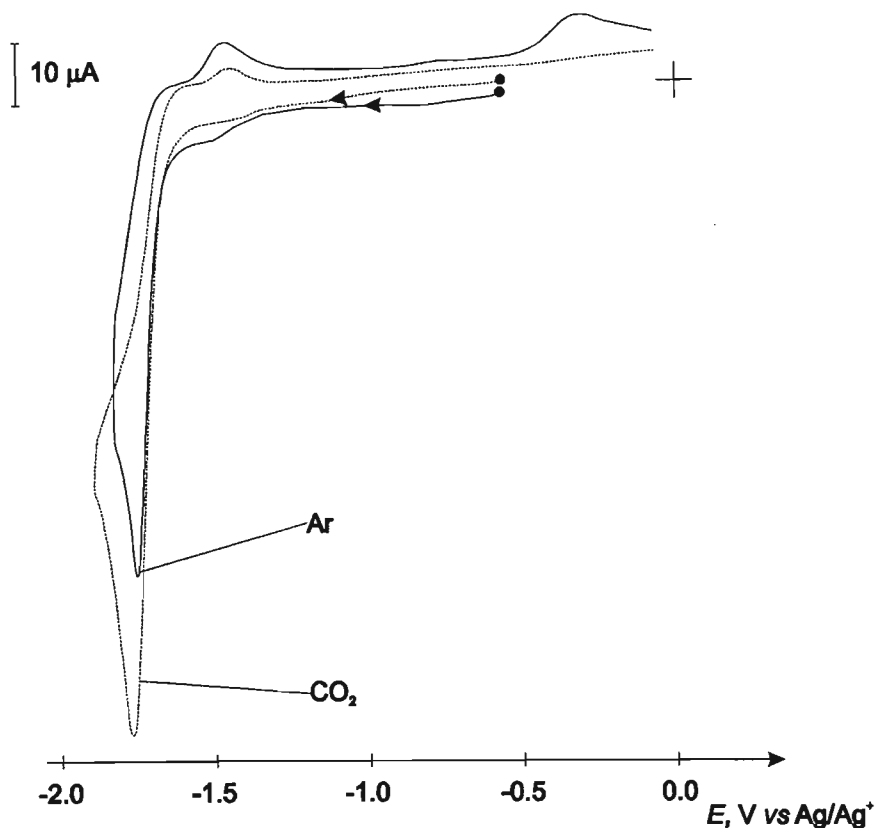


**Figure 7.12.** CVs of *cis*(Ph<sub>2</sub>Pbpy)-18 measured in carbon dioxide or argon saturated acetonitrile (0.1 M TBAP) solution. (Pt electrode,  $r = 2.5$  mm;  $\nu = 100$  mVs<sup>-1</sup>).

The electrochemistry of *cis*(Ph<sub>2</sub>Ppyqn)-19 has also been measured in the presence of carbon dioxide. As shown in Figure 7.13, there is an enhancement in current at the onset of the third wave in the CV of *cis*(Ph<sub>2</sub>Ppyqn)-19. Significantly, the return anodic peak of this wave is absent, while the first two redox couples remain essentially intact. Thus the triply reduced form of *cis*(Ph<sub>2</sub>Ppyqn)-19 catalyses the electrochemical reduction of carbon dioxide.

To assess the catalytic properties of 19 a preparative scale electrolysis experiment was carried out using the following conditions: a carbon felt working electrode; a CO<sub>2</sub> saturated CH<sub>3</sub>CN + 0.1 M TBAP electrolyte; a 0.5 mM concentration of complex; a working electrode potential of  $E_{app} = -1.80$  V; a total consumption of 46.61 C.<sup>†</sup> An initial constant current of 3 mA

<sup>†</sup> Due to inadequate amounts of *cis*(Ph<sub>2</sub>Ppyqn)-19, this experiment was carried out using a sample of 19 that consisted of a mixture of *cis* and *trans* isomers.

was observed. During the course of the electrolysis experiment this increased to give a final value of 4.5 mA, with the solution correspondingly changing from dark purple to brown-orange in colour. Carbon monoxide and formate were seen to form with Faradaic yields of 1.5 and 4.8 % respectively.

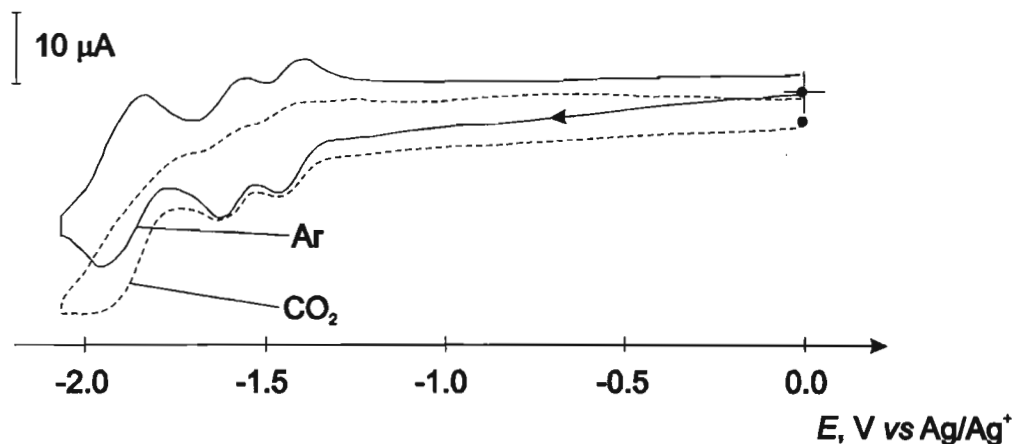


**Figure 7.13.** CVs of *cis*(Ph<sub>2</sub>Ppyqn)-**19** measured in carbon dioxide or argon saturated acetonitrile (0.1 M TBAP) solution. (Pt electrode,  $r = 2.5$  mm;  $\nu = 100$  mVs<sup>-1</sup>).

It is clear that the reduced forms of the diruthenium complexes **18** and **19** are not stable on an electrochemical time scale in the presence of CO<sub>2</sub>. This behaviour is consistent with what has been observed for the phosphorus polypyridyl complexes of Cu(I), Pt(I) and Pt(I)-Pd(I) discussed in Sections 3.2.4. and 4.2.4. The long-term stability of **18** and **19** under reducing conditions would have to be improved if they are to be considered as viable catalytic systems.

### 7.2.5. Extended Hückel Molecular Orbital Calculations

The energies and form of the frontier molecular orbitals of *cis*(Ph<sub>2</sub>Pbpy)-[Ru<sub>2</sub>(μ-Ph<sub>2</sub>Pbpy)<sub>2</sub>(CO)<sub>2</sub>(EtCN)<sub>2</sub>](PF<sub>6</sub>)<sub>2</sub> and *cis*(Ph<sub>2</sub>Ppyqn)-**19** and were calculated by the Extended Hückel method. The bond angles and distances used were those obtained from the crystal structures of the complexes. Table 7.5 summarises the results of the EHMO calculations.

The distribution of the lowest unoccupied and highest occupied MOs of *cis*(Ph<sub>2</sub>Pbpy)-[Ru<sub>2</sub>(μ-Ph<sub>2</sub>Pbpy)<sub>2</sub>(CO)<sub>2</sub>(EtCN)<sub>2</sub>](PF<sub>6</sub>)<sub>2</sub> and *cis*(Ph<sub>2</sub>Ppyqn)-**19** are depicted in Figures 7.14 and 7.15. In each example the HOMO is of σ symmetry and contains a large metal-metal bond component. The LUMO of these complexes is the σ\* anti-bonding interaction of the metal-metal bond. Thus the reductive electrochemical behaviour of *cis*(Ph<sub>2</sub>Pbpy)-**18** can be rationalised; the

addition of an electron to the  $\sigma^*$  anti-bonding orbital will destabilize the metal-metal bond and the complex decomposes upon reduction.

**Table 7.5.** Calculated energies of the frontier MOs and relative percent atomic contribution<sup>a</sup> of the metal, phosphine and  $\alpha$ -diimine atoms to them, for *cis*(Ph<sub>2</sub>Pbpy)-[Ru<sub>2</sub>( $\mu$ -Ph<sub>2</sub>Pbpy)<sub>2</sub>(CO)<sub>2</sub>(EtCN)<sub>2</sub>](PF<sub>6</sub>)<sub>2</sub> and *cis*(Ph<sub>2</sub>Ppyqn)-[Ru<sub>2</sub>( $\mu$ -L)<sub>2</sub>(CO)<sub>2</sub>(CH<sub>3</sub>CN)<sub>2</sub>](PF<sub>6</sub>)<sub>2</sub>, *cis*(Ph<sub>2</sub>Ppyqn)-**19**.

Complex	Molecular Orbital	Eigenvalue /eV	Percent Relative Atomic Contribution			
			Ru	$\alpha$ -diimine	phosphine	CO
Ph <sub>2</sub> Pbpy	HOMO	-12.02	12	70	8	4
	LUMO	-10.35	48	38	5	4
	SLUMO	-9.64	5	85	7	1
	TLUMO	-9.63	1	95	2	2
Ph <sub>2</sub> Ppyqn	HOMO	-12.04	9	74	8	3
	LUMO	-10.69	45	44	4	3
	SLUMO	-9.92	1	97	1	-
	TLUMO	-9.87	5	92	3	-

<sup>a</sup> Atomic contributions do not add up to 100 % since atomic contributions to the MOs of less than 1 % are neglected.

The reversible nature of the first two one-electron reductions of *cis*(Ph<sub>2</sub>Ppyqn)-**19** is seemingly in contradiction to what one would expect. The stabilization energy gained from the fill  $\sigma$  bonding orbital would be offset by the destabilisation energy arising from occupation of the  $\sigma^*$  anti-bonding orbital. A non-bonding interaction would arise. This anomalous behaviour can be explained by considering the additional stability lent to complexes of Ph<sub>2</sub>Ppyqn by the particular topography of this ligand, as elaborated in Section 7.2.3.

A similar trend of an enhanced stability for the oxidised forms of the diruthenium complex of the Ph<sub>2</sub>Ppyqn ligand is also observed. The oxidative processes that take place consist of the successive removal of two electrons from the  $\sigma$  bonding molecular orbital between the two metals. Not unexpectedly the second oxidation of *cis*(Ph<sub>2</sub>Pbpy)-**18** is irreversible as the metal-metal bond is broken. On the other hand the second oxidation of *cis*(Ph<sub>2</sub>Ppyqn)-**19** is quasi-reversible (Figure 7.13).

The energies of the second and third lower unoccupied molecular orbitals of *cis*(Ph<sub>2</sub>Pbpy)-[Ru<sub>2</sub>( $\mu$ -Ph<sub>2</sub>Pbpy)<sub>2</sub>(CO)<sub>2</sub>(EtCN)<sub>2</sub>](PF<sub>6</sub>)<sub>2</sub> and *cis*(Ph<sub>2</sub>Ppyqn)-**19** are found to be almost degenerate. The form of these MOs, illustrated in Figure 7.16, is of  $\pi$  symmetry and they



are localised chiefly on the  $\alpha$ -diimine fragment of the bridging ligand, with the SLUMO predominating on one ligand, the TLUMO on the second. Thus the third, two-electron redox process involves the addition of an electron to the  $\pi^*$  orbital of each of the two  $\alpha$ -diimine fragments. The small difference in the reduction potentials, resulting in the two waves overlapping, implies the presence of two similar redox centres in the molecule that do not interact strongly with one another. The form and energies of the SLUMO and TLUMO support this argument.

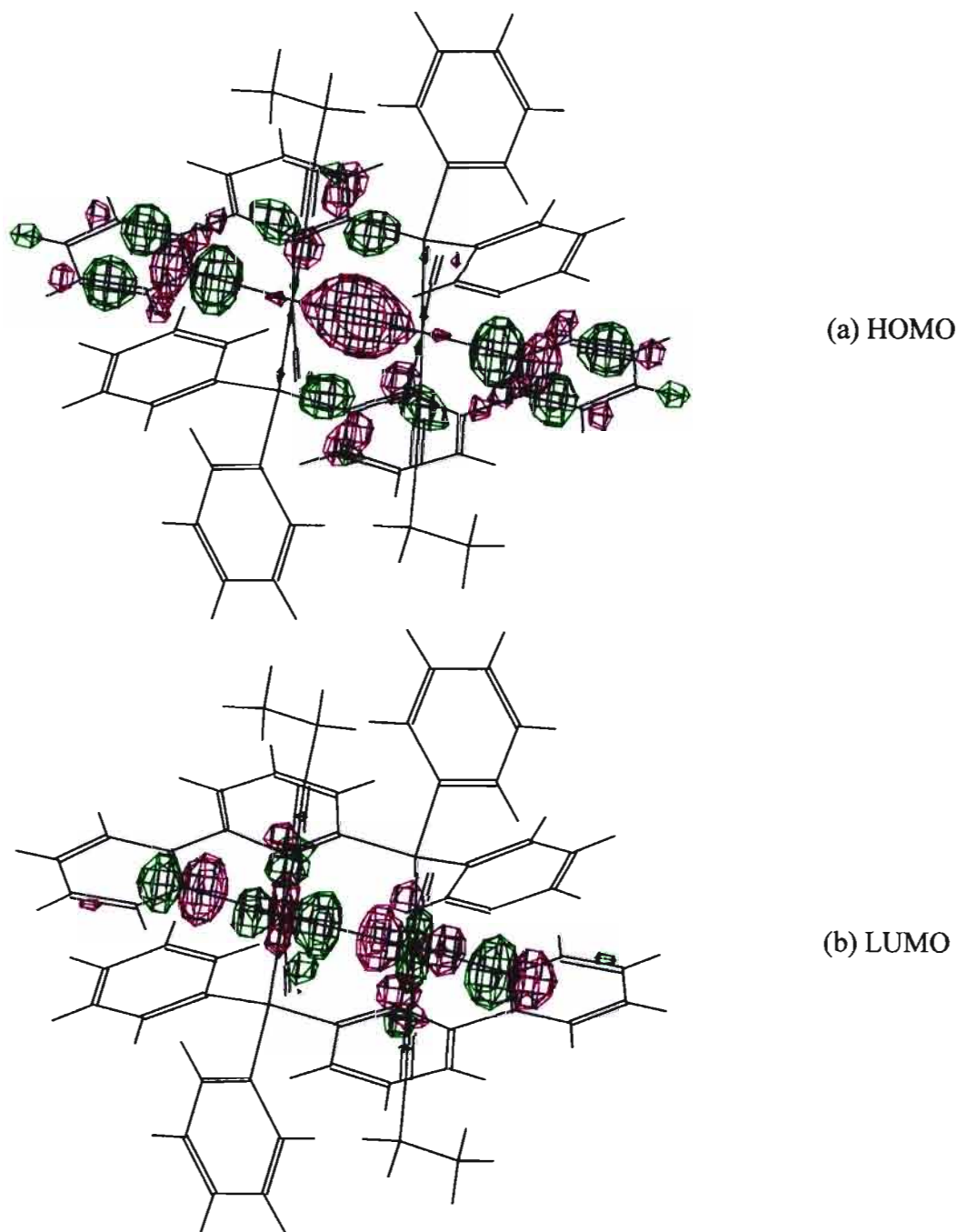


**Figure 7.14.** Molecular orbital representation for the (a) HOMO and (b) LUMO of *cis*(Ph<sub>2</sub>Pbpy)-[Ru<sub>2</sub>( $\mu$ -Ph<sub>2</sub>Pbpy)<sub>2</sub>(CO)<sub>2</sub>(EtCN)<sub>2</sub>](PF<sub>6</sub>)<sub>2</sub>.

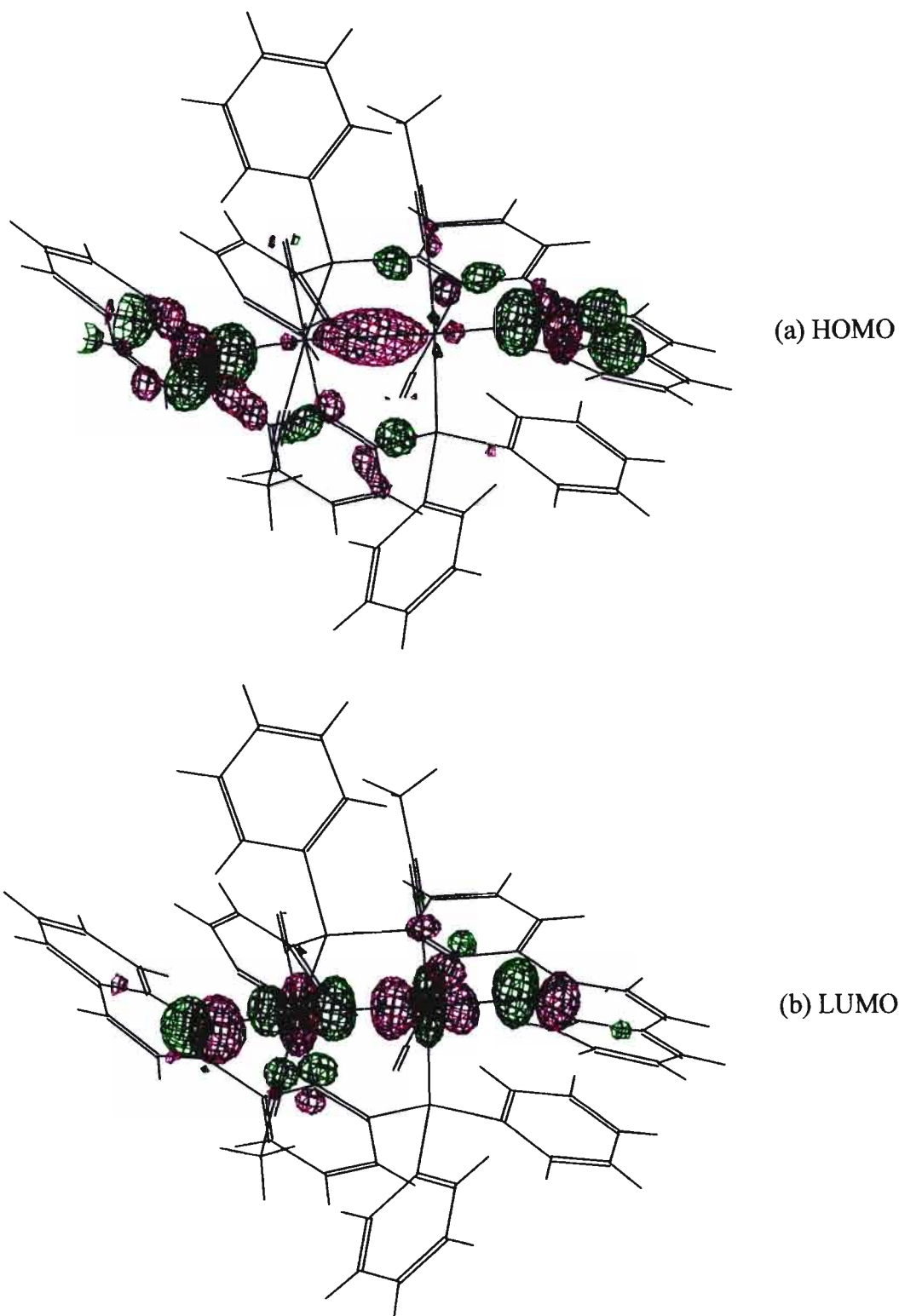


**Figure 7.15.** Molecular orbital representation for the (a) HOMO and (b) LUMO of *cis*(Ph<sub>2</sub>Ppyqn)-[Ru<sub>2</sub>(μ-Ph<sub>2</sub>Ppyqn)<sub>2</sub>(CO)<sub>2</sub>(CH<sub>3</sub>CN)<sub>2</sub>](PF<sub>6</sub>)<sub>2</sub>, *cis*(Ph<sub>2</sub>Ppyqn)-19.

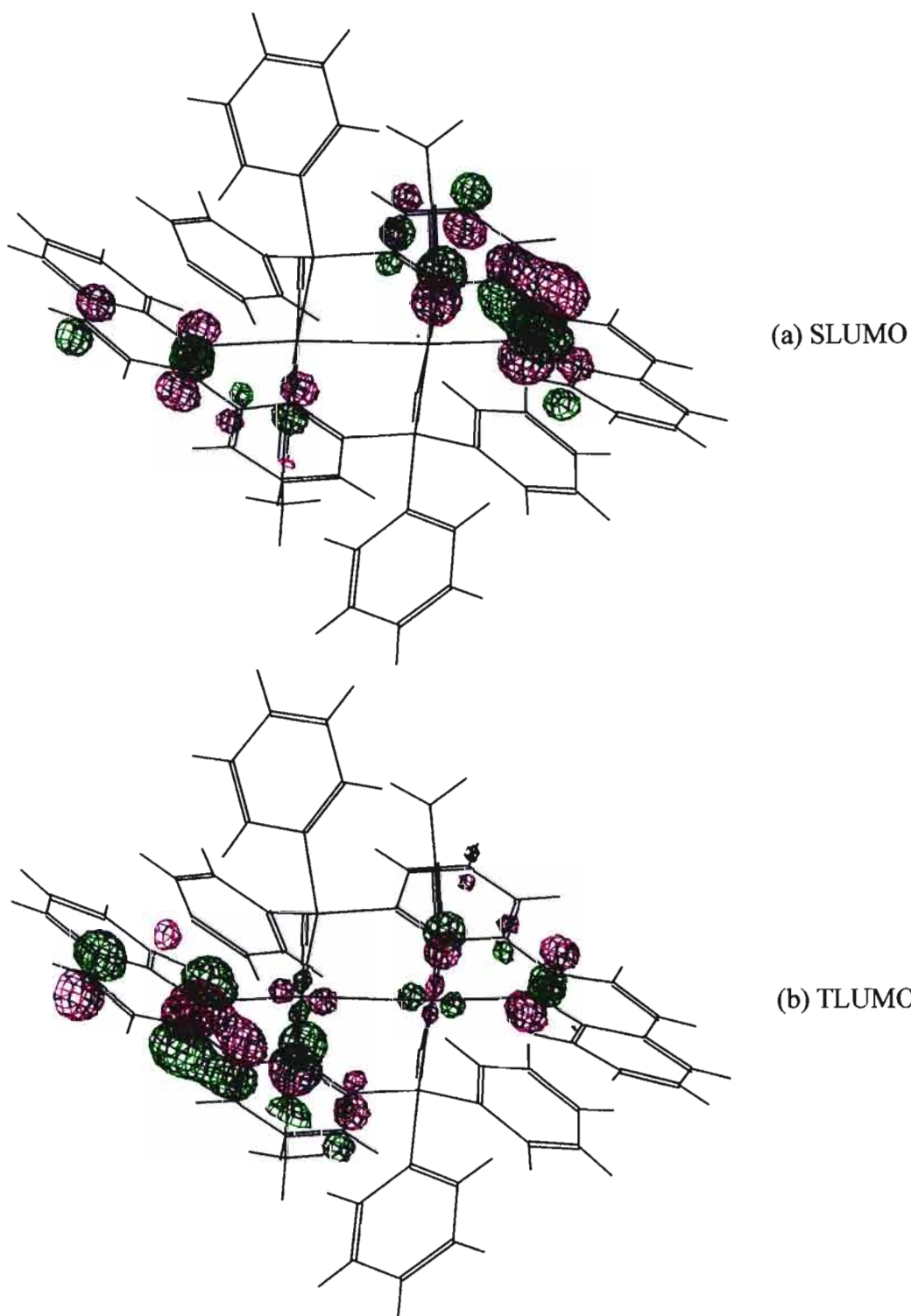


**Figure 7.16.** Molecular orbital representation for the (a) SLUMO and (b) TLUMO of *cis*(Ph<sub>2</sub>Ppyqn)-[Ru<sub>2</sub>(μ-Ph<sub>2</sub>Ppyqn)<sub>2</sub>(CO)<sub>2</sub>(CH<sub>3</sub>CN)<sub>2</sub>](PF<sub>6</sub>)<sub>2</sub>, *cis*(Ph<sub>2</sub>Ppyqn)-19.

### 7.3. Experimental

**[Ru<sub>2</sub>(μ-Ph<sub>2</sub>Pbpy)<sub>2</sub>(CO)<sub>2</sub>(CH<sub>3</sub>CN)<sub>2</sub>](PF<sub>6</sub>)<sub>2</sub> 18.** (a) A solution of [Ru<sub>2</sub>(CO)<sub>4</sub>(CH<sub>3</sub>CN)<sub>6</sub>](PF<sub>6</sub>)<sub>2</sub> (85 mg, 0.10 mmol) and Ph<sub>2</sub>Pbpy (78 mg, 0.21 mmol) in CH<sub>3</sub>CN (10 cm<sup>3</sup>) was refluxed for 12 h. The purple/black solution that formed was filtered through glass microfibre. Careful addition of diethyl ether to the solution and standing of the resultant mixture at -25°C afforded a deep purple microcrystalline material which contained a mixture of compounds [Ru<sub>2</sub>(μ-Ph<sub>2</sub>Pbpy)<sub>2</sub>(CO)<sub>2</sub>(CH<sub>3</sub>CN)<sub>2</sub>](PF<sub>6</sub>)<sub>2</sub> 18 (81 mg, 62 %). (Found: C, 46.12; H, 3.25; N, 6.06. Ru<sub>2</sub>C<sub>50</sub>H<sub>40</sub>N<sub>6</sub>P<sub>4</sub>F<sub>12</sub>O<sub>2</sub> requires C, 45.81; H, 3.08; N, 6.41 %);  $\nu_{\max}/\text{cm}^{-1}$  (KBr) 1943s (CO), 1916s (sh) (CO), 1437m, 1092w, 839vs (PF<sub>6</sub>), 773w, 698m, 558m (PF<sub>6</sub>) and 531m;  $\nu_{\max}/\text{cm}^{-1}$  (CH<sub>3</sub>CN) 1946s (CO), 1924s (sh) (CO);  $\delta_{\text{H}}$  (200 MHz, CD<sub>2</sub>Cl<sub>2</sub>, CDHCl<sub>2</sub>) 9.32 (2H, d), 8.55 (1H, t), 8.37 (1H, d), 8.24 (3H, t), 8.05 (3H, t), 7.91 (2H, t), 7.81 (2H, d), 7.68 (3H, t), 7.41 (20H, m), 6.93 (4H, t), 6.34 (4H, t);  $\delta_{\text{P}}$  (32.2 MHz, CD<sub>2</sub>Cl<sub>2</sub>, 85% H<sub>3</sub>PO<sub>4</sub>) 58.8 (s), 57.0 (s).

(b) A solution of [Ru<sub>2</sub>(CO)<sub>4</sub>(CH<sub>3</sub>CN)<sub>6</sub>](PF<sub>6</sub>)<sub>2</sub> (170 mg, 0.20 mmol) and Ph<sub>2</sub>Pbpy (170 mg, 0.50 mmol) in CH<sub>3</sub>CN (15 cm<sup>3</sup>) was maintained at rt for 1.5 h. The yellow coloured solution that formed was refluxed for 24 h. The purple/black solution that formed was filtered through glass microfibre and reduced in volume to *ca.* 5 cm<sup>3</sup>. Addition of excess Et<sub>2</sub>O (20 cm<sup>3</sup>) with stirring led to the formation of a fine purple coloured precipitate that was filtered and washed with Et<sub>2</sub>O (2 x 5 cm<sup>3</sup>). Recrystallisation from CH<sub>3</sub>CN/Et<sub>2</sub>O afforded fine dark purple crystals of *cis*(Ph<sub>2</sub>Pbpy)-[Ru<sub>2</sub>(μ-Ph<sub>2</sub>Pbpy)<sub>2</sub>(CO)<sub>2</sub>(CH<sub>3</sub>CN)<sub>2</sub>](PF<sub>6</sub>)<sub>2</sub>, *cis*(Ph<sub>2</sub>Pbpy)-18 (145 mg, 55 %). (Found: C, 46.17; H, 3.18; N, 6.03, . Ru<sub>2</sub>C<sub>50</sub>H<sub>40</sub>N<sub>6</sub>P<sub>4</sub>F<sub>12</sub>O<sub>2</sub> requires C, 45.81; H, 3.08; N, 6.41 %);  $\lambda_{\max}/\text{nm}$  (CH<sub>3</sub>CN) 231 (sh) ( $\epsilon/\text{dm}^3 \text{ mol}^{-1} \text{ cm}^{-1}$  40 300), 250 (sh) (28 900), 279 (29 700), 314 (sh) (13 700), 353 (sh) (6450);  $\nu_{\max}/\text{cm}^{-1}$  (KBr) 1943s (CO), 1916s (sh) (CO), 1483w, 1437m, 1092w, 839vs (PF<sub>6</sub>), 773m, 744m, 698m, 614w, 558m (PF<sub>6</sub>) and 531m;  $\nu_{\max}/\text{cm}^{-1}$  (CH<sub>3</sub>CN) 1946s (CO), 1919s (sh) (CO);  $\delta_{\text{H}}$  (500 MHz, CD<sub>2</sub>Cl<sub>2</sub>, CDHCl<sub>2</sub>) 9.22 (2H, d, 6'-H), 8.23 (2H, d, 3-H), 8.08 (2H, t, 4-H), 7.87 (2H, dt, 4'-H), 7.75 (2H, d, 3'-H), 7.63 (2H, t, 5'-H), 7.52 (8, m, 3'' and 2''-H), 7.43 (2H, dd, 5-H), 7.29 (4H, m, 4''-H), 6.94 (4H, t, 3''-H), 6.24 (4H, t, 2''-H);  $\delta_{\text{H}}$  (250 MHz, CD<sub>3</sub>CN, CD<sub>2</sub>H<sub>2</sub>CN) 9.31 (2H, d), 8.25 (2H, d), 8.05 (2H, dt), 7.91 (2H, dt), 7.81 (2H, d), 7.68 (2H, dt), 7.56 – 7.27 (14H, br m), 6.94 (4H, t), 6.34 (4H, t);  $\delta_{\text{P}}$  (32.2 MHz, CD<sub>2</sub>Cl<sub>2</sub>, 85% H<sub>3</sub>PO<sub>4</sub>) 58.8 (s).

**[Ru<sub>2</sub>(μ-Ph<sub>2</sub>Pbpy)<sub>2</sub>(CO)<sub>2</sub>(EtCN)<sub>2</sub>](PF<sub>6</sub>)<sub>2</sub>.** A solution of [Ru<sub>2</sub>(CO)<sub>4</sub>(CH<sub>3</sub>CN)<sub>6</sub>](PF<sub>6</sub>)<sub>2</sub> (85 mg, 0.10 mmol) and Ph<sub>2</sub>Pbpy (78 mg, 0.21 mmol) in EtCN (10 cm<sup>3</sup>) was refluxed for 12 h. The purple/black solution that formed was filtered through glass microfibre. Careful addition of

diethyl ether to the solution and standing of the resultant mixture at  $-25^{\circ}\text{C}$  afforded a deep purple microcrystalline material which contained a mixture of compounds  $[\text{Ru}_2(\mu\text{-Ph}_2\text{Pbpy})_2(\text{CO})_2(\text{EtCN})_2](\text{PF}_6)_2$  (98 mg, 73 %). (Found: C, 46.49; H, 3.19; N, 6.18.  $\text{Ru}_2\text{C}_{52}\text{H}_{44}\text{N}_6\text{P}_4\text{F}_{12}\text{O}_2$  requires C, 46.65; H, 3.31; N, 6.28 %);  $\nu_{\text{max}}/\text{cm}^{-1}$  (KBr) 2928w, 1944s (CO), 1922s (sh) (CO), 1438w, 1094w, 843vs (PF<sub>6</sub>), 810w (sh), 744w, 699w, 560w (PF<sub>6</sub>) and 530w;  $\delta_{\text{H}}$  (200 MHz, CD<sub>2</sub>Cl<sub>2</sub>, CDHCl<sub>2</sub>) 9.32 (2H, dm), 8.55 (2H, br t), 8.37 (1H, dm), 8.24 (2H, tm), 8.08 (2H, m), 7.87 (3H, m), 7.67 (2H, qm), 7.40 (10H, br m), 6.94 (2H, tm), 6.34 (2H, tm), 2.34 (4H, q, CH<sub>3</sub>CH<sub>2</sub>CN), 1.22 (6H, t, CH<sub>3</sub>CH<sub>2</sub>CN);  $\delta_{\text{P}}$  (32.2 MHz, CD<sub>2</sub>Cl<sub>2</sub>, 85% H<sub>3</sub>PO<sub>4</sub>) 62.5 (s) and 60.1 (s).

**$[\text{Ru}_2(\mu\text{-Ph}_2\text{Ppyqn})_2(\text{CO})_2(\text{CH}_3\text{CN})_2](\text{PF}_6)_2$  19.** (a) A solution of  $[\text{Ru}_2(\text{CO})_4(\text{CH}_3\text{CN})_6](\text{PF}_6)_2$  (175 mg, 0.21 mmol) and Ph<sub>2</sub>Ppyqn (161 mg, 0.41 mmol) in CH<sub>3</sub>CN (15 cm<sup>3</sup>) was refluxed for 36 h. The purple/black solution that formed was filtered through glass microfibre and the crude product precipitated from it by the addition of excess Et<sub>2</sub>O. Purple/black crystalline material was obtained by carefully ‘layering’ Et<sub>2</sub>O over a CH<sub>3</sub>CN solution of the crude material in narrow glass tubes (8 x 300 mm). This afforded two different dark purple crystalline forms that were isolated by hand;

(1) A ‘leaf’ shaped crystals of **19** (151 mg, 52 %). (Found: C, 49.52; H, 3.21; N, 5.74.  $\text{Ru}_2\text{C}_{58}\text{H}_{44}\text{N}_6\text{P}_4\text{F}_{12}\text{O}_2$  requires C, 49.37; H, 3.14; N, 5.96 %);  $\nu_{\text{max}}/\text{cm}^{-1}$  (KBr) 1944s (CO), 1922s (sh) (CO), 1438w, 1094w, 843vs (PF<sub>6</sub>), 810w (sh), 744w, 699w, 560w (PF<sub>6</sub>) and 530w;  $\delta_{\text{H}}$  (500 MHz, CD<sub>2</sub>Cl<sub>2</sub>, CDHCl<sub>2</sub>) 9.43 (2H, d), 8.71 (1H, d), 8.66 (1H, d), 8.54 (1H, d), 8.42 (2H, d), 8.29 (2H, d), 8.21 (3H, t), 8.15 (2H, t), 8.06 (3H, d), 7.93 (3H, t), 7.68 (2H, d), 7.46 (2H, t), 7.42 (2H, d), 7.37 (8H, m), 7.31 (2H, t), 7.23 (4H, m), 7.15 (4H, t), 7.06 (2H, m), 6.97 (2H, t), 6.92 (4H, m), 5.98 (4H, t), 1.55 (8H, s), 1.36 (6H, s);  $\delta_{\text{P}}$  (32.2 MHz, CD<sub>2</sub>Cl<sub>2</sub>, 85% H<sub>3</sub>PO<sub>4</sub>) 60.9 (s) and 51.1 (s).

(2) Cube shaped crystals of *cis*(Ph<sub>2</sub>Ppyqn)-**19** (61 mg, 21 %). (Found: C, 49.49; H, 3.11; N, 5.77.  $\text{Ru}_2\text{C}_{58}\text{H}_{44}\text{N}_6\text{P}_4\text{F}_{12}\text{O}_2$  requires C, 49.37; H, 3.14; N, 5.96 %);  $\lambda_{\text{max}}/\text{nm}$  (CH<sub>3</sub>CN) 227.0 (sh) ( $\epsilon/\text{dm}^3 \text{ mol}^{-1} \text{ cm}^{-1}$  49 000), 266.1 (38 500), 332.3 (22 100), 511.7 (1960), 588.3 (1930);  $\nu_{\text{max}}/\text{cm}^{-1}$  (KBr) 1944s (CO), 1922s (sh) (CO), 1438w, 1094w, 843vs (PF<sub>6</sub>), 810w (sh), 744w, 699w, 560w (PF<sub>6</sub>) and 530w;  $\delta_{\text{H}}$  (200 MHz, CD<sub>2</sub>Cl<sub>2</sub>, CDHCl<sub>2</sub>) 9.43 (2H, dd), 8.42 (2H, dm), 8.29 (2H, d), 8.21 (2H, td), 8.15 (2H, td), 8.06 (2H, dd), 7.92 (2H, tm), 7.68 (2H, d), 7.38 (10H, br m), 7.14 (4H, tm), 6.92 (4H, tm), 5.98 (4H, tm), 1.36 (6H, s, CH<sub>3</sub>CN);  $\delta_{\text{H}}$  (500 MHz, CD<sub>2</sub>Cl<sub>2</sub>, CDHCl<sub>2</sub>) 9.43 (2H, d, 8'-H), 8.42 (2H, d, 3-H), 8.29 (2H, d, 4'-H), 8.21 (2H, t, 7'-H), 8.15 (2H, t, 4-H), 8.06 (2H, d, 5'-H), 7.93 (2H, t, 6'-H), 7.68 (2H, d, 3'-H), 7.42 (2H, d, 5-H), 7.37 (8H, m,

3''- and 4''-H), 7.15 (4H, t, 2''-H), 6.92 (4H, m, 3''-H), 5.98 (4H, t, 2''-H), 1.36 (6H,s, CH<sub>3</sub>CN);  $\delta_P$  (32.2 MHz, CD<sub>2</sub>Cl<sub>2</sub>, 85% H<sub>3</sub>PO<sub>4</sub>) 60.9 (s).

(b) A mixture of [Ru<sub>2</sub>(CO)<sub>4</sub>(CH<sub>3</sub>CN)<sub>6</sub>](PF<sub>6</sub>)<sub>2</sub> (192 mg, 0.23 mmol) and Ph<sub>2</sub>Ppyqn (190 mg, 0.49 mmol) in CH<sub>3</sub>CN (30 cm<sup>3</sup>) was stirred at rt for 3 h, the ligand dissolving completely during this time. The resulting yellow coloured solution was refluxed for 36 h. The purple/black solution that formed was filtered through glass microfibre and reduced in volume to *ca.* 10 cm<sup>3</sup>. Addition of excess Et<sub>2</sub>O (30 cm<sup>3</sup>) with stirring followed by the standing of the solution at -25°C for 12 h led to the formation of purple/black coloured precipitate. The mother liquor was decanted off and the precipitate washed with Et<sub>2</sub>O (2 x 5 cm<sup>3</sup>). Recrystallisation from CH<sub>3</sub>CN/Et<sub>2</sub>O afforded fine dark purple crystals of **19** (190 mg, 65 %). (Found: C, 49.58; H, 3.18; N, 5.84. Ru<sub>2</sub>C<sub>58</sub>H<sub>44</sub>N<sub>6</sub>P<sub>4</sub>F<sub>12</sub>O<sub>2</sub> requires C, 49.37; H, 3.14; N, 5.96 %);  $\lambda_{max}/nm$  (CH<sub>3</sub>CN) 227.0 (sh) ( $\epsilon/dm^3 mol^{-1} cm^{-1}$  49 000), 266.1 (38 500), 332.3 (22 100), 511.7 (1960), 588.3 (1930);  $\nu_{max}/cm^{-1}$  (KBr) 1944s (CO), 1922s (sh) (CO), 1438w, 1094w, 843vs (PF<sub>6</sub>), 810w (sh), 744w, 699w, 560w (PF<sub>6</sub>) and 530w;  $\delta_H$  (500 MHz, CD<sub>2</sub>Cl<sub>2</sub>, CDHCl<sub>2</sub>) 9.43 (2H, d), 8.71 (1H, d), 8.66 (1H, d), 8.54 (1H, d), 8.42 (2H, d), 8.29 (2H, d), 8.21 (3H, t), 8.15 (2H, t), 8.06 (3H, d), 7.93 (3H, t), 7.68 (2H, d), 7.46 (2H, t), 7.42 (2H, d), 7.37 (8H, m), 7.31 (2H, t), 7.23 (4H, m), 7.15 (4H, t), 7.06 (2H, m), 6.97 (2H, t), 6.92 (4H, m), 5.98 (4H, t), 1.55 (8H, s), 1.36 (6H, s);  $\delta_P$  (32.2 MHz, CD<sub>2</sub>Cl<sub>2</sub>, 85% H<sub>3</sub>PO<sub>4</sub>) 60.9 (s) and 51.1 (s).

**X-ray Data Collection and Structure Solution for *cis*(Ph<sub>2</sub>Ppyqn)-19.** Purple, cube-shaped crystals of **19** were grown by the slow vapour diffusion of diethyl ether into an acetonitrile solution of the complex. Details of the crystal data, data collection and structure refinement of **19** are summarized in Table 7.4. The complete crystallographic data of **19** are presented in Appendix B. Supporting Information.

**Table 7.6.** Crystal data and structure refinement parameters for *cis*(Ph<sub>2</sub>Ppyqn)-[Ru<sub>2</sub>(μ-Ph<sub>2</sub>Ppyqn)<sub>2</sub>(CO)<sub>2</sub>(CH<sub>3</sub>CN)<sub>2</sub>](PF<sub>6</sub>)<sub>2</sub>, *cis*(Ph<sub>2</sub>Ppyqn)-19.

Formula	Ru <sub>2</sub> C <sub>58</sub> H <sub>44</sub> N <sub>6</sub> O <sub>2</sub> P <sub>4</sub> F <sub>12</sub>
FW/amu	1411.01
<i>a</i> /Å	19.91(2)
<i>b</i> /Å	14.40(2)
<i>c</i> /Å	20.91(2)
$\alpha$ /°	90
$\beta$ /°	95.92(6)
$\gamma$ /°	90
<i>U</i> /Å <sup>3</sup>	5960(9)
Crystal system, space group	Monoclinic, P2 <sub>1</sub> /c
<i>Z</i>	4
<i>D</i> /g cm <sup>3</sup>	1.572
F(000)	2824
$\mu$ /mm <sup>-1</sup>	0.699
Power and current settings	55 kV, 25 mA
Increment/°	1.00
Crystal dimensions/mm	0.62 x 0.61 x 0.61
$\lambda$ (Mo K $\alpha$ )/Å	0.71069
Temperature/K	293(2)
$\theta$ range for collected data/°	1.03 to 23.00
Index ranges	-21 ≤ <i>h</i> ≤ 21 -1 ≤ <i>k</i> ≤ 15 -1 ≤ <i>l</i> ≤ 22
Total reflections collected	9887
Completeness to 2 $\theta$	99.7
Absorption correction	semi-empirical
Relative transmission coefficients (I)	0.9996 and 0.7494
Unique data	8263 ( <i>R</i> <sub>int</sub> = 0.0385)
Unique observed data [ <i>I</i> > 2 $\sigma$ ( <i>I</i> )]	6594
Refinement method	Full-matrix least-squares on <i>F</i> <sup>2</sup>
Data / restraints / parameters	8263 / 0 / 826
Goodness-of-fit (based on <i>F</i> <sup>2</sup> )	0.910
Extinction coefficient	none
Max( $\Delta\rho$ )/e.Å <sup>-3</sup>	0.708
Min( $\Delta\rho$ )/e.Å <sup>-3</sup>	-0.788
Final <i>R</i> indices [ <i>I</i> > 2 $\sigma$ ( <i>I</i> )]	<i>R</i> <sub>1</sub> = 0.0393, <i>wR</i> <sub>2</sub> = 0.0998
<i>R</i> indices (all data)	<i>R</i> <sub>1</sub> = 0.0601, <i>wR</i> <sub>2</sub> = 0.1330

## Chapter 8. Conclusions

---

It was envisaged that the combination of  $\alpha$ -diimine and phosphine fragments would lead to a tridentate bridging ligand with electron acceptor properties. The electrochemical properties of the P,N,N ligands show that the  $\pi$ -acceptor properties of the  $\alpha$ -diimine fragment are retained in the phosphorus-polypyridyl hybrid ligand. Furthermore the utility of the P,N,N ligands in the synthesis of low valent dinuclear complexes of Cu(I), Pd(I), Pt(I) and Ru(I) has been shown.

A summary of the electrochemical properties of the dinuclear complexes studied in this work is presented in Table 8.1. Where the site of electron addition is believed to be primarily ligand based the reduction process is seen to be reversible on a cyclic voltammetric time scale. Thus the Cu(I) complexes **1**, **2** and  $[\text{Cu}_2(\mu\text{-Ph}_2\text{Pbpy})_2(\text{CH}_3\text{CN})_2](\text{PF}_6)_2$ , the Pt(I) complexes **6** - **8** and the Pd(I)-Pt(I) heterodinuclear complexes **9** - **11** undergo four chemically and electrochemically reversible one-electron reductions.

As can be seen in Table 8.1, the first and second reductions of the dicopper complexes occur at potentials that are, on average, 444 and 315 mV more negative than the first and second reduction potentials of the diplatinum and platinum-palladium complexes **6** - **11**. On this basis one can conclude that the  $\alpha$ -diimine  $\pi^*$  orbitals of the P,N,N ligands are stabilised to a greater extent on coordination to platinum or palladium than to copper. On the other hand the average differences between the potentials of the third and fourth reductions of the copper and platinum complexes are only 207 and 33 mV respectively. The stabilisation of the  $\pi^*$  orbitals may be ascribed to the loss of negative charge from the  $\alpha$ -diimine ligand upon coordination, which occurs by  $\sigma$ -donation through the chelating nitrogen atoms.<sup>93</sup> In the formally metal(0) complexes this ability to accept the electron density from the ligand may be saturated to a certain extent. Hence the difference between the third and fourth reduction potentials of the two metals' complexes is not marked as the metal no longer plays such a significant role in stabilising the relevant redox orbitals.

Where the reduction involves the placement of an electron into an empty molecular orbital which contains a significant metal contribution the redox process is irreversible. Thus the Pd(I) complexes **3** and **4** undergo one reversible reduction followed by an irreversible reduction leading to the decomposition of the complex. The dinuclear Pd(I) and Ru(I) complexes **5** and **18** respectively each undergo one irreversible reduction. The exception to this pattern is the Ru(I) complex **19**, where it is believed that the topography of the  $\text{Ph}_2\text{Ppyqn}$  ligand stabilises the metal-based reduction product to decomposition.



In the case of the 2,2'-bipyridyl ligand complexes of Ru(I), **12** and **14** – **17**, the reduction of the complexes initiates the formation of Ru–Ru bonds, leading to the Ru(0) polymers  $[\text{Ru}(\text{L})(\text{CO})_2]_n$  (L = bpy, L<sub>1-4</sub>). By analogy with the electropolymerisation mechanism described for the formation of  $[\text{Ru}(\text{bpy})(\text{CO})_2]_n$  from  $[\text{Ru}(\text{bpy})(\text{CO})_2\text{Cl}_2]$ ,<sup>38</sup> the initial reduction of **12** and **14** – **17** would be bipyridyl based, forming an unstable bipyridyl radical anion. This would be followed by a rapid transfer of the electron density to the metal centre with the associated loss of an acetonitrile ligand, leading to a coordinatively unsaturated species that dimerises through the formation of M–M bonds.

A comparison is made in Table 8.1, for the P,N,N ligand-bridged dinuclear complexes between the cathodic peak potential of the peak at which an enhancement in current is observed in the presence of CO<sub>2</sub> and the 'corresponding' peak of the complex measured under argon. As the values show, the respective reduction peak of the complex is effectively coincidental with the catalytic peak for the reduction of CO<sub>2</sub>. This strongly supports the argument that it is the reduced form of the complex, in a formal oxidation state corresponding to that particular cathodic peak, which interacts with the CO<sub>2</sub>. Noticeably, while the doubly reduced dicopper complexes  $[\text{Cu}_2(\mu\text{-Ph}_2\text{Pbpy})_2(\text{CH}_3\text{CN})_2](\text{PF}_6)_2$  and **2** catalyse the reduction of CO<sub>2</sub>, it is only upon the third reduction of **1** that an enhancement of current is observed under CO<sub>2</sub>. Likewise, it is only the triply reduced forms of complexes **6** – **11** and **19** that show an interaction with CO<sub>2</sub>. The peak potentials of the second reduction of  $[\text{Cu}_2(\mu\text{-Ph}_2\text{Pbpy})_2(\text{CH}_3\text{CN})_2](\text{PF}_6)_2$  and **2**, with values of –1.92 and –1.94 V respectively, do not differ markedly from the third reduction potentials of complexes **1**, **6**, **8**, **9**, **11** and **19**, which range from –1.95 V (for **19**) to –2.18 V (for **9**). Indeed, the interaction CO<sub>2</sub> with these complexes as evidenced by an enhancement in current occurs over a narrow range of potentials. It is evident that, regardless of the metal type or formal oxidation state of the complex, a certain minimum potential must be attained in order to reduce the CO<sub>2</sub>. The small variation of the potential at which CO<sub>2</sub> reduction occurs further suggests (but does not prove) that the reaction proceeds through an outer-sphere mechanism, with the CO<sub>2</sub> not coordinating directly to the metal centre. Since the reducing electrons are localised on the phosphorus-polypyridyl ligands of these complexes, it is likely that electron transfer takes place directly from the reduced ligand to uncoordinated CO<sub>2</sub>. Though the experimental observations are not inconsistent with an outer-sphere mechanism, further studies are evidently required to establish the true mechanism of reduction.

An exception to this trend is observed for the diplatinum complex **7** and the platinum-palladium complex **10**, that both catalyse the reduction of CO<sub>2</sub> at –1.86 V. In these cases the reducing electron is believed to derive from a metal-based orbital. Thus the reaction of the

reduced forms of **7** and **10** with carbon dioxide may proceed through an inner-sphere mechanism, with the carbon dioxide binding to the metal centre. Certainly, this could account for the less cathodic potential of  $-1.86$  V at which electrocatalysis occurs.

In comparison, the reduction of  $\text{CO}_2$  catalysed by  $[\text{Ru}(\text{bpy})(\text{CO})_2]_n$  formed from **12** proceeds through the direct coordination of  $\text{CO}_2$  to the metal centre<sup>40</sup> and occurs at a relatively low overpotential of  $-1.40$  V.

If the reduction of  $\text{CO}_2$  by the complexes were to involve an outer-sphere mechanism one would expect this to involve the transfer of one electron to  $\text{CO}_2$  to give the  $\text{CO}_2^{\cdot-}$  radical anion. The potential for the reduction of  $\text{CO}_2$  to its radical anion  $\text{CO}_2^{\cdot-}$  in DMF has been estimated to be  $-2.21$  V vs. SCE by cyclic voltammetry on a mercury electrode.<sup>8</sup> In comparison to this, the potential at which the complexes catalyse the reduction of  $\text{CO}_2$  is significantly more positive, with typical values being  $-1.64$  V (for **2**) and  $-1.84$  V (for **8**) vs. SCE. This indicates, in the first instance, that the overpotential associated with the direct reduction of  $\text{CO}_2$  at an electrode surface has been reduced by use of the transition metal complex to facilitate the transfer of the electron from the electrode to the  $\text{CO}_2$ . Indeed, the standard potential of the  $\text{CO}_2/\text{CO}_2^{\cdot-}$  couple has been reported to be  $-1.90$  V vs. NHE ( $-1.66$  V vs. SCE)<sup>195</sup> and it therefore seems likely that the potentials recorded here approach the true thermodynamic value.

The utility of the phosphorus-polypyridyl ligands in the synthesis of dinuclear complexes that are stable under reducing conditions has been demonstrated in this work. By increasing the  $\pi$ -acceptor properties of the P,N,N ligands the potential at which their transition metal complexes are reduced can be lowered. Equally, the transition metal to which the ligands are complexed strongly influences the electrochemical properties of the ligands. The results presented in Table 8.1 suggest that a minimum potential must be attained to provide the driving force required for the reduction of carbon dioxide. Thus, although the reduction potentials of the complexes can be controlled through judicious choice of ligand and metal, it is not necessarily true that they will catalyse the reduction of  $\text{CO}_2$  at a more favourable potential and, in the final analysis, that potential will depend on the mechanism of activation of the  $\text{CO}_2$  molecule.

On a cyclic voltammetric time scale the phosphorus-polypyridyl ligands prevent the fragmentation of the dinuclear complexes under reducing conditions: with the exception of the Pd(I) complexes **3** – **4** and the Ru(I) complex **18** all the P,N,N ligand bridged complexes studied here are reversibly reduced to the formally dinuclear  $\text{M}(-1)$  species. However, on an electrosynthetic time scale under both Ar and  $\text{CO}_2$  atmospheres the singly reduced complexes are chemically unstable. For this reason they cannot be considered as viable homogeneous electrocatalysts. If this barrier was to be overcome it must still be borne in mind that the

potentials at which the P,N,N ligand-bridged complexes show an interaction with CO<sub>2</sub> are relatively cathodic in comparison to those reported for other catalysts reported e.g., [Ru(bpy)(CO)<sub>2</sub>]<sub>n</sub>.<sup>38,39</sup> The instability of the complexes in the presence of water also poses a serious limitation as the multiple electron reduction of CO<sub>2</sub> requires the formation of C–H bonds, necessitating a protic electrolyte.

Nevertheless, an understanding of the reductive electrochemistry of P,N,N ligand bridged complexes has been gained which can be used as a rationale to develop catalysts that are more durable. The use of more electron-accepting polypyridyl fragments in the P,N,N ligand may improve the stability of the reduced forms of their dinuclear complexes. In this regard diazine ligands present suitable candidates. In particular, 4,4'-bipyrimidine possesses the necessary combination of strong  $\pi$ -acceptor and  $\sigma$ -donor properties required to stabilise low-valent metals.<sup>196</sup> On the other hand, the phosphine fragment in the P,N,N ligand may be substituted by alkoxy and/or phenoxy groups to generate a softer phosphorus centre. This would assist in the prevention of the dissociation of the ligand from the metal in the reduced complex. Alternatively, the anionic 6-phenylphosphino-2,2'-bipyridyl ligand would provide a strong  $\sigma$ -donor phosphorus centre, while at the same time functioning as a bridging ligand. The neutrality of dinuclear M(I) complexes of this ligand should have as a result that they react more readily with CO<sub>2</sub>. Finally, it has been seen that the steric bulk provided by the fused phenyl ring system in Ph<sub>2</sub>Ppyqn plays a significant role in the complexes electrochemical behaviour. The incorporation of bulky substituents at the *ortho*-positions of the  $\alpha$ -diimine moiety of the P,N,N ligands will lend greater stability to the reduced complexes of these ligands.

**Table 8.1.** Summary of the reductive cyclic voltammetric properties of the dinuclear complexes studied in this work.<sup>a</sup>

Complex	$E_{1/2}/V(\Delta E_p/mV)$					$E_{pc}(\text{Ar})^b$	$E_{pc}(\text{CO}_2)^b$
	$E_{1/2}^{+2/+}$	$E_{1/2}^{+/0}$	$E_{1/2}^{0/-}$	$E_{1/2}^{-/-2}$	$E_{1/2}^{-2/-3}$		
$[\text{Cu}_2(\mu\text{-Ph}_2\text{Pbpy})_2(\text{CH}_3\text{CN})_2](\text{PF}_6)_2$ <sup>c</sup>	-1.68(75)	-1.88(75)	-2.18(75)	-2.34(70)		-1.92	-1.95
$[\text{Cu}_2(\mu\text{-Ph}_2\text{Ppyqn})_2(\text{CH}_3\text{CN})_2](\text{PF}_6)_2$ <b>1</b> <sup>c</sup>		-1.66(100) <sup>c</sup>	-2.04(75)	-2.23(85)		-2.08	-2.07
$[\text{Cu}_2\{\mu\text{-Et(Ph)Pbpy}\}_2(\text{CH}_3\text{CN})_2](\text{PF}_6)_2$ <b>2</b> <sup>c</sup>	-1.72(70)	-1.91(50)	-2.23(50)	-2.40(80)		-1.94	-1.95
$[\text{Pd}_2(\mu\text{-Ph}_2\text{Pbpy})_2](\text{BF}_4)_2$ <b>3</b> <sup>c</sup>	-1.14(80)	-1.39 <sup>d</sup>					
$[\text{Pd}_2(\mu\text{-Ph}_2\text{Ppyqn})_2](\text{BF}_4)_2$ <b>4</b> <sup>c</sup>	-1.00(55)	-1.40 <sup>d</sup>					
$[\text{Pd}_2\{\mu\text{-Et(Ph)Pbpy}\}_2](\text{BF}_4)_2$ <b>5</b> <sup>c</sup>	-1.33 <sup>d</sup>						
$[\text{Pt}_2(\mu\text{-Ph}_2\text{Pbpy})_2](\text{PF}_6)_2$ <b>6</b>	-1.28(80)	-1.46(80)	-2.02(80)	-2.28(80)		-2.06	-1.97
$[\text{Pt}_2(\mu\text{-Ph}_2\text{Ppyqn})_2](\text{PF}_6)_2$ <b>7</b>	-1.10(50)	-1.30(50)	-1.80(40)	-2.06(50)	-2.23(100)	-1.82	-1.86
$[\text{Pt}_2\{\mu\text{-Et(Ph)Pbpy}\}_2](\text{PF}_6)_2$ <b>8</b>	-1.36(50)	-1.54(80)	-2.09(60)	-2.36(80)		-2.12	-2.15
$[\text{PtPd}(\mu\text{-Ph}_2\text{Pbpy})_2](\text{PF}_6)_2$ <b>9</b>	-1.28(60)	-1.61(60)	-1.99(60)	-2.40(80)		-2.18	-2.14
$[\text{PtPd}(\mu\text{-Ph}_2\text{Ppyqn})_2](\text{PF}_6)_2$ <b>10</b>	-1.09(60)	-1.44(40)	-1.70(40)	-2.24(120)		-1.82	-1.86
$[\text{PtPd}\{\mu\text{-Et(Ph)Pbpy}\}_2](\text{PF}_6)_2$ <b>11</b>	-1.35(60)	-1.66(80)	-2.06(80)	-2.44(120)		-2.10	-2.06
$[\text{Ru}_2(\text{bpy})_2(\text{CO})_4(\text{CH}_3\text{CN})_2](\text{PF}_6)_2$ <b>12</b>	-1.24 <sup>d</sup>						
$[\text{Ru}_2(\text{L}_1)_2(\text{CO})_4(\text{CH}_3\text{CN})_2](\text{PF}_6)_2$ <b>14</b>	-1.32 <sup>d</sup>						
$[\text{Ru}_2(\text{L}_2)_2(\text{CO})_4(\text{CH}_3\text{CN})_2](\text{PF}_6)_2$ <b>15</b>	-0.95 <sup>d</sup>						
$[\text{Ru}_2(\text{L}_3)_2(\text{CO})_4(\text{CH}_3\text{CN})_2](\text{PF}_6)_2$ <b>16</b>	-1.32 <sup>d</sup>						
$[\text{Ru}_2(\text{L}_4)_2(\text{CO})_4(\text{CH}_3\text{CN})_2](\text{PF}_6)_2$ <b>17</b>	-1.32 <sup>d</sup>						
$[\text{Ru}_2(\mu\text{-Ph}_2\text{Pbpy})_2(\text{CO})_2(\text{EtCN})_2](\text{PF}_6)_2$ <b>18</b>	-1.64 <sup>d</sup>						
$[\text{Ru}_2(\mu\text{-Ph}_2\text{Ppyqn})_2(\text{CO})_2(\text{CH}_3\text{CN})_2](\text{PF}_6)_2$ <b>19</b> <sup>c</sup>	-1.48(70)	-1.62(70)	-1.90(115) <sup>c</sup>			-1.95	-1.97

<sup>a</sup> Potentials vs. Ag/Ag<sup>+</sup>, measured in CH<sub>3</sub>CN (0.1 M TBAP), scan rate 100 mV s<sup>-1</sup>, T = 298 K. <sup>b</sup> Peak potential of cathodic wave at which an enhancement in current is observed in the presence of CO<sub>2</sub> [ $E_{pc}(\text{CO}_2)$ ] and the “corresponding” wave measured under Ar [ $E_{pc}(\text{Ar})$ ]. <sup>c</sup> Overall transfer of 2e, where the half-wave potential corresponds to the average of the two half-wave potentials,  $E_{1/2} = (E_{1/2}^{\text{red I}} + E_{1/2}^{\text{red II}})/2$ . <sup>d</sup> Cathodic peak potential of chemically irreversible reduction. <sup>e</sup> Cathodic peak potential of quasi-reversible reduction. <sup>c</sup> Measurement made using a Ag/AgCl wire pseudo-reference electrode.

## Appendix A. General Experimental Details

---

### A.1. Instrumentation

Carbon, hydrogen and nitrogen analyses were performed by the Microanalytical Laboratory of the Chemistry Department at the University of Natal in Pietermaritzburg. Infrared spectra were recorded with a Perkin Elmer Spectrum GX FT-IR Spectrometer or a Shimadzu FT-1400 infrared spectrometer.  $^1\text{H}$ ,  $^{13}\text{C}$  NMR and  $^{31}\text{P}\{-^1\text{H}\}$  NMR spectra were recorded on either a Bruker AC-250, Varian Gemini, Varian Unity Inova or Varian FT-80 spectrometer. Mass spectra were recorded on a Hewlett-Packard Gas Chromatographic-Mass Spectrometer (HP5988A). Absorption spectra were recorded on a Shimadzu UV-2101PC uv/vis Spectrophotometer. Electrochemical measurements were performed using either; (a) a PAR 175 universal programmer, a PAR 173 potentiostat, fitted with a PAR 176 current follower and a Lloyd Instruments PL3 XY/t recorder; or (b) an EG & Princeton Applied Research model 273 or 173 potentiostat - galvanostat equipped with a Sefram TGM 164 X-Y recorder.

### A.2. Experimental Techniques

All reactions, unless otherwise stated, were performed under an atmosphere of dry nitrogen gas, using standard Schlenk techniques. All solvents were freshly distilled and dried prior to use, using standard procedures.<sup>197</sup>

### A.3. Crystal Structure Determination

#### A.3.1. Data Collection

The intensities of the reflections were measured using the variable-speed  $\omega$ - $2\theta$  scan method on an Enraf-Nonius CAD-4 diffractometer with graphite monochromated Mo-K $\alpha$  radiation. Cell constants were obtained by fitting the setting angles of 25 high-order reflections ( $\theta > 12^\circ$ ). An  $i$ - $2\theta$  scan with a variable speed up to a maximum of  $5.49^\circ\text{min}^{-1}$  was used. The  $i$ -angle changed as  $a_\omega + b_\omega \tan\theta$  ( $^\circ$ ) and the horizontal aperture as  $a_h + b_h \tan\theta$  (mm), but was limited to the range 1.3 to 5.9 mm. The vertical slit was fixed at 4 mm. Optimal values of  $a_\omega$ ,  $b_\omega$ ,  $a_h$  and  $b_h$  were determined for each crystal by a critical evaluation of the peak shape for several reflections with different values of  $\theta$  using the program OTPLOT (Omega-Theta plot; Enraf-

Nonius diffractometer control program, 1988). In most cases the crystals exhibited a rapid fall-off of scattering power above 23 degrees. Thus, as only a very small percentage of the data would be observed at higher theta values the collection of this data was not justified. Three standard reflections were measured every hour to check any possible decomposition of the crystal. Where applicable, a linear decay correction was applied using the mean value linear curves fitted through the three intensity control reflections. Data were corrected for absorption by the  $\psi$ -scan method.<sup>198</sup>

### A.3.2. Structural Solution Refinement

The structure was solved by either standard direct or Patterson methods and subsequently completed by Fourier recycling and full-matrix least-squares refinement based on  $F$ -squared. The residuals and weighting schemes are defined as follows:  $R = \sum(|F_o| - |F_c|) / \sum(|F_o|)$ ,  $wR2 = [\sum(|F_o| - |F_c|)^2 / \sum w|F_o|^2]^{1/2}$ ,  $w = 1 / (\sigma^2 F + 0.0005 F^2)$ . Non-hydrogen atoms were assigned anisotropic thermal factors and the hydrogen atoms a single common thermal factor, the latter being placed in calculated positions. The structure solution of **I** was an exception as hydrogen atoms were located in this structure. For all the structure solution and refinement calculations, SHELX-97<sup>199</sup> was employed in conjunction with ORTEX 6a.<sup>200</sup> ORTEP-III was used to produce the diagrams.<sup>201</sup> Mean plane and torsion angle calculations, and the tabulation of fractional coordinates, thermal parameters, interatomic distances and angles were done using SHELX-97.

### A.4. Electrochemistry

Cyclic voltammetry, rotating disc electrode voltammetry and controlled potential electrolysis experiments were performed in a conventional three-electrode cell under an argon atmosphere. The cell was equipped with a Ag/AgNO<sub>3</sub> 10 mM in CH<sub>3</sub>CN + 0.1 M TBAP reference electrode and a platinum wire counter electrode. The following working electrodes were used; platinum ( $r = 1.0$  or  $2.5$  mm) or glassy carbon ( $r = 1.5$  mm) discs polished with a 2 $\mu$ m diamond paste (Mecaprex Presi) for cyclic voltammetry; a Tacussel EDI rotating electrode to which is fixed a platinum ( $r = 1.0$  mm) or glassy carbon ( $r = 1.5$  mm) disc for RDE voltammetry; a platinum sheet of surface area 5 cm<sup>2</sup> for exhaustive controlled potential electrolysis. Tetrabutylammonium perchlorate (TBAP) and LiClO<sub>4</sub> supporting electrolytes from Fluka were used as received. Acetonitrile from Rathburn (HPLC grade) was used as received without further purification. Water was doubly distilled using a quartz apparatus. All experiments and the

preparation of electrodes were carried out in a dry box, except where the use of CO<sub>2</sub> or H<sub>2</sub>O did not permit this.

All potentials reported are relative to Ag|10 mM Ag<sup>+</sup> in CH<sub>3</sub>CN + 0.1M TBAP. They can be converted to other reference systems (see for instance, V.V. Pavlishchuk and A. Addison, *Inorg. Chim. Acta*, 2000, **298**, 97). The ferrocene/ferrocenium couple, which serves as an internal reference against which more universal comparisons can be made,<sup>202</sup> had a  $E_{1/2}$  of 0.07 V vs. Ag/Ag<sup>+</sup> reference electrode used here in CH<sub>3</sub>CN + 0.1M TBAP. A few cyclic voltammetry measurements were performed using a Ag/AgCl wire pseudo-reference electrode. This is clearly stated for those compounds for which this is the case. At the end of these experiments ferrocene was added to give a 10<sup>-3</sup> M solution and the  $E_{1/2}$  of the FeCp<sup>+0</sup> couple recorded. The ferrocene/ferrocenium couple in CH<sub>3</sub>CN + 0.1M TBAP had a  $E_{1/2}$  of 0.375 V vs. Ag/AgCl pseudo-reference electrode and a peak-to-peak separation of 65 mV. Potentials measured against the Ag/AgCl pseudo-reference electrode are reported relative to Ag|10 mM Ag<sup>+</sup> in CH<sub>3</sub>CN + 0.1M TBAP. They were converted by use of the ferrocene couple as an internal reference in each reference electrode system. The redox potentials of complexes measured against both reference electrode systems showed good agreement when converted as such. A Ag/AgCl (Metrohm 6-07240140 RA) reference electrode, furnished with a KCl 3M electrolytic bridge, was used for pure aqueous electrolytes.

#### A.4.1. Cyclic Voltammetry

The concentration of the substrates during measurements was about 10<sup>-3</sup> M, solutions being purged with a stream of argon prior to and during measurements. The electrochemical behaviour of the complexes in the presence of carbon dioxide was investigated by purging the acetonitrile solution with CO<sub>2</sub> for 20 mins. The cyclic voltammetric measurements were then performed in the carbon dioxide saturated solution.

The number of electrons transferred in a particular redox process was estimated in the following manner. A rotating disc electrode voltammogram of the complex being examined was measured ( $i$  500s<sup>-1</sup>;  $v$  10 mVs<sup>-1</sup>), after which an exact amount of ferrocene was introduced to the solution so as to give a concentration equivalent to that of the complex and the RDE voltammogram measurement repeated. Levich has derived the equation for the diffusion controlled limiting current  $i_l$  that can be simplified to:<sup>203</sup>

$$i_l \propto nD^{2/3}c$$

where  $n$  = number of electrons transferred in redox process,  $c$  = concentration of electroactive species/mol  $\text{cm}^{-3}$ ,  $D$  = diffusion coefficient of electroactive species/ $\text{cm}^2\text{s}^{-1}$ . The diffusion coefficients of ferrocene and the metal complex being examined are not expected to differ markedly. Furthermore each will be present in essentially equal concentrations. Thus,

$$i_l \propto n$$

Hence a comparison of the magnitude of the limiting currents in the RDE voltammograms of ferrocene and the metal complex allows a reasonable estimation of the number of electrons involved in the metal complexes reversible redox processes to be made.

#### A.4.2. Electrocatalytic Experiments

Electrocatalysis experiments were carried out in a conventional three-electrode cell made airtight with vacuum grease (M. Apiezon). The total volume of the cell was 208  $\text{cm}^3$ . The working electrodes used were carbon felt (10 x 10 x 4 mm, RVC 2000, 65  $\text{mg cm}^{-3}$ , from Le Carbon Lorraine) or platinum gauze. Electrodes modified by  $[\text{Ru}(\text{bpy})(\text{CO})_2]_n$ ,  $\text{ppyr}-[\text{Ru}(\text{L}_1)(\text{CO})_2(\text{CH}_3\text{CN})_2]^{2+}$  and  $\text{ppyr}-[\text{Ru}_2(\text{L})_2(\text{CO})_4(\text{CH}_3\text{CN})_2]^{2+}$  ( $\text{L} = \text{L}_2$  and  $\text{L}_4$ ) films were prepared under an argon atmosphere by potentiostating a carbon felt electrode dipped in a  $\text{CH}_3\text{CN}$  solution of the appropriate complex (1 mM). The electrodes were removed, rinsed with a pure  $\text{CH}_3\text{CN}$  solution and then placed in the appropriate pure electrolyte. Electrolytes were saturated with  $\text{CO}_2$  by purging continuously for 20 min with stirring. All experiments were stopped after a known amount of coulombs had been passed. The gas headspace was sampled through a septum with a Hamilton gas-tight syringe.  $\text{CO}$  was analysed for on a Delsi Model 30 Gas Chromatograph equipped with a FID detector, a 120 cm 5 Å molecular sieve column using hydrogen as the carrier gas. The sample chromatogram is compared with that of a gas standard containing known concentrations of  $\text{CO}$  and  $\text{CO}_2$ . Formate ions were analysed on a Perkin Elmer series 200 pump equipped with a Perkin Elmer 785A UV/vis detector ( $\lambda = 210$  nm) and a Bio-Rad 87H cation exchange resin column eluted with a  $10^{-2}$  M  $\text{H}_2\text{SO}_4$  solution.

#### A.4.3. UV-vis Spectroelectrochemical Measurements

Electronic absorption spectra were recorded with a Hewlett - Packard HP 8452 A diode array spectrometer controlled with a Compaq 286 computer equipped with a Citizen 120 D printer. Absorption spectroelectrochemical experiments were conducted in a dry box under an argon atmosphere. The cuvettes were inserted into an optical translator connected to the



spectrophotometer via an optical fibre system (Photonetics spectrofip system). The optical fibres pass through the wall of the dry box by means of seals. Spectroelectrochemical measurements on  $[\text{Ru}(\text{bpy})(\text{CO})_2]_n$  films were made by using a conventional sandwich-type cell.<sup>204</sup> The optical transparent conductive electrode (OTE) (diameter 1.1 cm) was doped with Indium Tin Oxide (ITO) (Balthracon Z 20 from Balzers).

#### A.5. Extended Hückel Molecular Orbital Calculations

Extended Hückel calculations were performed using HyperChem Lite<sup>205</sup> on X-ray crystal structures of the compounds. The orbital exponents and ionisation potentials used were the default values contained in HyperChem Lite. These are given in Table A.1. A valence shell minimum basis set was used in the calculations.

Observations drawn from the EHMO calculations are of a purely qualitative value. The extended Hückel approach is the crudest semi-empirical method and has no explicit treatment of electron-electron interactions. Thus the energies of the lower unoccupied MO's are seen to be insensitive to the addition of electrons as would occur during a reduction process. Higher level semi-empirical and *ab initio* methods, which take into account coulombic repulsion and electron-electron correlation, would be required to describe radical anions accurately. Nevertheless, there is a qualitative agreement between the experimental results and the calculations and it is reasonable to employ them in describing the gross features of the redox properties of the complexes and ligands studied in this work.

**Table A.1.** Parameters used in EHMO calculations.

	$\zeta_s$	$\zeta_p$	$\zeta_d$	$I_s$	$I_p$	$I_d$	$C_1$	$\zeta_{d2}$	$C_2$
H	1.300	0.000	0.000	13.600	0.000	-	-	-	-
C	1.625	1.625	0.000	21.400	11.400	-	-	-	-
N	1.950	1.950	0.000	26.000	13.400	-	-	-	-
O	2.275	2.275	0.000	32.300	14.800	-	-	-	-
P	1.600	1.600	1.400	18.600	14.000	7.000	1.0000	0.000	0.0000
Cu	1.950	1.200	5.950		6.060		0.5770	2.100	0.6168
Ru	2.080	2.040	5.380		6.870		0.5343	2.300	0.6368
Pd	2.190	2.152	5.983	<u>7.320</u>	<u>3.750</u>		0.5264	2.613	0.6373

Key:  $\zeta_s$ ,  $\zeta_p$  and  $\zeta_d$  are the s, p and d orbital Slater exponents (a.u.);  $I_s$ ,  $I_p$  and  $I_d$  are the s, p and d orbital ionisation potentials (eV);  $C_1$ , coefficient of Slater exponent  $\zeta_d$ ;  $\zeta_{d2}$ , d orbital Slater exponent (a.u.);  $C_2$ , coefficient of Slater exponent  $\zeta_{d2}$ .

## A. 6. Sources of Chemicals

### A.6.1. Commercially Available Chemicals

The following chemicals were purchased from the indicated commercial supplier and used without further purification;

**Aldrich:** ethyldiphenylphosphine,  $C_{14}H_{15}P$ ; diethylphenylphosphine,  $C_{10}H_{15}P$ ;

**E.Merk:** butyllithium,  $C_4H_9Li$ ; 2-chloro-2-methylpropane,  $C_4H_9Cl$ ; 1,2-ethanedithiol,  $C_2H_6S_2$ ; dichlorophenylphosphine oxide,  $C_6H_5Cl_2OP$ ; silica gel 60, particle size 0.063 - 0.200 nm (70 - 230 mesh ASTM);

**Fluka:** sodium ethanethiolate,  $CH_3CH_2SNa$ ; 2-chloroquinoline,  $C_9H_6ClN$ ; diphenylphosphine,  $C_{12}H_{11}P$ ; boron trifluoride ethyl etherate,  $BF_3 \cdot C_4H_{10}O$ ;

**SAARchem:** hydrogen peroxide,  $H_2O_2$ ; lithium metal;

**Strem Chemicals:** tetrakis(acetonitrile)palladium (II) tetrafluoroborate,  $[Pd(CH_3CN)_4](BF_4)_2$ ; dichlorobis(benzonitrile)platinum (II),  $PtCl_2(C_6H_5CN)_2$ ; thallium hexafluorophosphate,  $TlPF_6$ .

### A.6.2. Compounds Synthesised by Published Methods

The following chemicals were synthesised by literature methods.

Compound	Literature Reference
6-chloro-2,2'-bipyridine	62
6-diphenyl(phosphino)-2,2'-bipyridine	62
6-bromo-2-(2-quinolyl)pyridine	74
$[Cu(CH_3CN)_4](PF_6)$	120
$[Cu(CH_3CN)_4](BF_4)$	119
$[Cu_2(\mu-Ph_2Pbpy)_2(CH_3CN)_2](PF_6)_2$	99
$Pt_2(dba)_3(CHCl_3)$	133
$Pd_2(dba)_3(CHCl_3)$	132
4-(4-pyrrol-1-ylbutyl)-4'-methyl-2,2'-bipyridine	180
4,4'-bis((3-pyrrol-1-ylpropyloxy)carbonyl)-2,2'-bipyridine	181
4,4'-bis(13-pyrrol-1-yltridecyl)-2,2'-bipyridine	178
$[Ru_2(CO)_4(CH_3CN)_6](PF_6)_2$	155
$[Ru_2(\mu-Ph_2Pbpy)_2(CO)_2(EtCN)_2](PF_6)_2$	185

## Appendix B. Supporting Information

### B.1. Crystallographic Supporting Information

#### B.1.1. Ph<sub>2</sub>Ppyqn I

**Table B.1.** Atomic coordinates ( $\times 10^4$ ) and equivalent isotropic displacement parameters ( $\text{\AA}^2 \times 10^3$ ) for Ph<sub>2</sub>Ppyqn I.<sup>a</sup>

atom	<i>x</i>	<i>y</i>	<i>z</i>	U(eq)
P(1)	3257(1)	7701(1)	2413(1)	45(1)
N(1)	2477(1)	5950(1)	3220(1)	45(1)
N(2)	1404(1)	3745(1)	4473(1)	48(1)
C(1)	4328(1)	7966(2)	2752(2)	45(1)
C(2)	4794(1)	8706(2)	3692(2)	59(1)
C(3)	5601(1)	8843(2)	3862(2)	64(1)
C(4)	5953(1)	8251(2)	3091(2)	62(1)
C(5)	5501(1)	7516(3)	2165(2)	72(1)
C(6)	4696(1)	7379(2)	1990(2)	63(1)
C(7)	2922(1)	8943(2)	3242(2)	41(1)
C(8)	2819(1)	10124(2)	2709(2)	60(1)
C(9)	2495(1)	11083(2)	3209(2)	68(1)
C(10)	2257(1)	10889(2)	4234(2)	61(1)
C(11)	2360(1)	9731(2)	4783(2)	55(1)
C(12)	2692(1)	8766(2)	4292(2)	47(1)
C(13)	3227(1)	6329(2)	3367(2)	44(1)
C(14)	3877(1)	5716(2)	4140(2)	57(1)
C(15)	3751(1)	4664(2)	4764(2)	61(1)
C(16)	2989(1)	4276(2)	4629(2)	51(1)
C(17)	2361(1)	4957(2)	3863(2)	44(1)
C(18)	1518(1)	4636(2)	3742(2)	45(1)
C(19)	893(1)	5302(2)	2918(2)	57(1)
C(20)	132(1)	5034(2)	2868(2)	60(1)
C(21)	-24(1)	4101(2)	3629(2)	50(1)
C(22)	-800(1)	3780(2)	3648(2)	64(1)
C(23)	-913(1)	2880(2)	4407(2)	71(1)
C(24)	-260(2)	2248(3)	5187(3)	76(1)
C(25)	501(1)	2528(2)	5206(2)	66(1)
C(26)	638(1)	3469(2)	4423(2)	48(1)

<sup>a</sup> U(eq) is defined as one third of the trace of the orthogonalized U<sub>ij</sub> tensor. The esd's of the least significant digits are given in parentheses.

**Table B.2.** Interatomic lengths for Ph<sub>2</sub>Ppyqn I.<sup>a</sup>

bond	length/\AA	bond	length/\AA
P(1)-C(7)	1.8249(18)	C(10)-C(11)	1.374(3)

P(1)-C(1)	1.8268(18)	C(11)-C(12)	1.383(3)
P(1)-C(13)	1.8348(19)	C(13)-C(14)	1.379(3)
N(1)-C(17)	1.339(2)	C(14)-C(15)	1.382(3)
N(1)-C(13)	1.342(2)	C(15)-C(16)	1.368(3)
N(2)-C(18)	1.318(2)	C(16)-C(17)	1.388(3)
N(2)-C(26)	1.363(2)	C(17)-C(18)	1.488(2)
C(1)-C(6)	1.378(3)	C(18)-C(19)	1.404(3)
C(1)-C(2)	1.382(3)	C(19)-C(20)	1.352(3)
C(2)-C(3)	1.381(3)	C(20)-C(21)	1.400(3)
C(3)-C(4)	1.369(3)	C(21)-C(26)	1.412(3)
C(4)-C(5)	1.361(3)	C(21)-C(22)	1.415(3)
C(5)-C(6)	1.378(3)	C(22)-C(23)	1.346(3)
C(7)-C(12)	1.383(2)	C(23)-C(24)	1.395(4)
C(7)-C(8)	1.389(3)	C(24)-C(25)	1.364(3)
C(8)-C(9)	1.376(3)	C(25)-C(26)	1.411(3)
C(9)-C(10)	1.367(3)		

<sup>a</sup> The esd's of the least significant digits are given in parentheses.

**Table B.3.** Bond angles for Ph<sub>2</sub>Ppyqn I.<sup>a</sup>

angle	degree/°	angle	degree/°
C(7)-P(1)-C(1)	104.55(8)	C(9)-C(8)-C(7)	120.9(2)
C(7)-P(1)-C(13)	101.87(8)	C(10)-C(9)-C(8)	120.6(2)
C(1)-P(1)-C(13)	102.22(8)	C(9)-C(10)-C(11)	119.46(19)
C(17)-N(1)-C(13)	118.48(15)	C(10)-C(11)-C(12)	120.22(19)
C(18)-N(2)-C(26)	117.86(15)	C(7)-C(12)-C(11)	120.97(17)
C(6)-C(1)-C(2)	117.61(17)	N(1)-C(13)-C(14)	122.11(17)
C(6)-C(1)-P(1)	116.56(14)	N(1)-C(13)-P(1)	111.74(13)
C(2)-C(1)-P(1)	125.83(14)	C(14)-C(13)-P(1)	126.15(14)
C(3)-C(2)-C(1)	120.94(19)	C(13)-C(14)-C(15)	118.88(18)
C(4)-C(3)-C(2)	120.3(2)	C(16)-C(15)-C(14)	119.49(19)
C(5)-C(4)-C(3)	119.4(2)	C(15)-C(16)-C(17)	118.62(19)
C(4)-C(5)-C(6)	120.5(2)	N(1)-C(17)-C(16)	122.34(16)
C(5)-C(6)-C(1)	121.3(2)	N(1)-C(17)-C(18)	116.35(15)
C(12)-C(7)-C(8)	117.81(17)	C(16)-C(17)-C(18)	121.30(16)
C(12)-C(7)-P(1)	124.70(13)	N(2)-C(18)-C(19)	123.26(16)
C(8)-C(7)-P(1)	117.18(14)		

<sup>a</sup> The esd's of the least significant digits are given in parentheses.

**Table B.4.** Dihedral angles for Ph<sub>2</sub>Ppyqn I.<sup>a</sup>

dihedral angle	degree/°	dihedral angle	degree/°
C(7)-P(1)-C(1)-C(6)	-163.15(16)	P(1)-C(13)-C(14)-C(15)	-177.69(16)
C(13)-P(1)-C(1)-C(6)	90.96(17)	C(13)-C(14)-C(15)-C(16)	-1.8(3)
C(7)-P(1)-C(1)-C(2)	16.34(19)	C(14)-C(15)-C(16)-C(17)	0.0(3)
C(13)-P(1)-C(1)-C(2)	-89.55(18)	C(13)-N(1)-C(17)-C(16)	-2.9(2)
C(6)-C(1)-C(2)-C(3)	-0.3(3)	C(13)-N(1)-C(17)-C(18)	175.37(14)
P(1)-C(1)-C(2)-C(3)	-179.81(17)	C(15)-C(16)-C(17)-N(1)	2.4(3)
C(1)-C(2)-C(3)-C(4)	0.4(4)	C(15)-C(16)-C(17)-C(18)	-175.82(18)

dihedral angle	degree/°	dihedral angle	degree/°
C(2)-C(3)-C(4)-C(5)	-0.7(4)	C(26)-N(2)-C(18)-C(19)	-0.4(3)
C(3)-C(4)-C(5)-C(6)	0.9(4)	C(26)-N(2)-C(18)-C(17)	177.14(15)
C(4)-C(5)-C(6)-C(1)	-0.8(4)	N(1)-C(17)-C(18)-N(2)	-172.96(15)
C(2)-C(1)-C(6)-C(5)	0.5(3)	C(16)-C(17)-C(18)-N(2)	5.4(2)
P(1)-C(1)-C(6)-C(5)	-179.9(2)	N(1)-C(17)-C(18)-C(19)	4.6(2)
C(1)-P(1)-C(7)-C(12)	-108.16(16)	C(16)-C(17)-C(18)-C(19)	-177.02(18)
C(13)-P(1)-C(7)-C(12)	-2.02(17)	N(2)-C(18)-C(19)-C(20)	0.6(3)
C(1)-P(1)-C(7)-C(8)	78.40(16)	C(17)-C(18)-C(19)-C(20)	-176.81(18)
C(13)-P(1)-C(7)-C(8)	-175.46(15)	C(18)-C(19)-C(20)-C(21)	-0.2(3)
C(12)-C(7)-C(8)-C(9)	-0.3(3)	C(19)-C(20)-C(21)-C(26)	-0.3(3)
P(1)-C(7)-C(8)-C(9)	173.62(18)	C(19)-C(20)-C(21)-C(22)	178.9(2)
C(7)-C(8)-C(9)-C(10)	-0.9(4)	C(20)-C(21)-C(22)-C(23)	-179.5(2)
C(8)-C(9)-C(10)-C(11)	1.4(4)	C(26)-C(21)-C(22)-C(23)	-0.3(3)
C(9)-C(10)-C(11)-C(12)	-0.8(3)	C(21)-C(22)-C(23)-C(24)	-0.1(4)
C(8)-C(7)-C(12)-C(11)	0.9(3)	C(22)-C(23)-C(24)-C(25)	0.4(4)
P(1)-C(7)-C(12)-C(11)	-172.53(15)	C(23)-C(24)-C(25)-C(26)	-0.3(4)
C(10)-C(11)-C(12)-C(7)	-0.3(3)	C(18)-N(2)-C(26)-C(25)	-179.30(18)
C(17)-N(1)-C(13)-C(14)	1.0(3)	C(18)-N(2)-C(26)-C(21)	-0.2(3)
C(17)-N(1)-C(13)-P(1)	-179.81(12)	C(24)-C(25)-C(26)-N(2)	179.0(2)
C(7)-P(1)-C(13)-N(1)	73.95(13)	C(24)-C(25)-C(26)-C(21)	-0.1(3)
C(1)-P(1)-C(13)-N(1)	-178.10(12)	C(20)-C(21)-C(26)-N(2)	0.6(3)
C(7)-P(1)-C(13)-C(14)	-106.94(17)	C(22)-C(21)-C(26)-N(2)	-178.66(18)
C(1)-P(1)-C(13)-C(14)	1.02(18)	C(20)-C(21)-C(26)-C(25)	179.6(2)
N(1)-C(13)-C(14)-C(15)	1.3	C(22)-C(21)-C(26)-C(25)	0.4(3)

<sup>a</sup> The esd's of the least significant digits are given in parentheses.

**Table B.5.** Anisotropic displacement parameters ( $\text{\AA}^2 \times 10^3$ ) for Ph<sub>2</sub>Ppyqn I.<sup>a</sup>

atom	U <sub>11</sub>	U <sub>22</sub>	U <sub>33</sub>	U <sub>23</sub>	U <sub>13</sub>	U <sub>12</sub>
P(1)	44(1)	48(1)	46(1)	-6(1)	15(1)	-6(1)
N(1)	44(1)	36(1)	55(1)	-5(1)	14(1)	-3(1)
N(2)	45(1)	37(1)	62(1)	2(1)	18(1)	3(1)
C(1)	45(1)	44(1)	48(1)	-1(1)	20(1)	-4(1)
C(2)	51(1)	61(1)	68(1)	-19(1)	24(1)	-7(1)
C(3)	49(1)	62(1)	81(2)	-15(1)	18(1)	-10(1)
C(4)	45(1)	65(1)	79(1)	7(1)	24(1)	1(1)
C(5)	59(1)	89(2)	78(2)	-15(1)	35(1)	6(1)
C(6)	58(1)	72(1)	64(1)	-21(1)	25(1)	-2(1)
C(7)	36(1)	40(1)	46(1)	2(1)	11(1)	-1(1)
C(8)	73(1)	49(1)	65(1)	12(1)	29(1)	0(1)
C(9)	75(1)	40(1)	87(2)	12(1)	21(1)	6(1)
C(10)	51(1)	43(1)	89(2)	-10(1)	22(1)	3(1)
C(11)	61(1)	46(1)	66(1)	-8(1)	30(1)	-2(1)
C(12)	55(1)	38(1)	52(1)	2(1)	20(1)	2(1)
C(13)	44(1)	38(1)	53(1)	-10(1)	18(1)	-3(1)
C(14)	42(1)	53(1)	79(1)	-1(1)	20(1)	1(1)
C(15)	44(1)	53(1)	83(1)	10(1)	14(1)	9(1)
C(16)	49(1)	40(1)	65(1)	1(1)	18(1)	3(1)

atom	U <sub>11</sub>	U <sub>22</sub>	U <sub>33</sub>	U <sub>23</sub>	U <sub>13</sub>	U <sub>12</sub>
C(17)	45(1)	34(1)	53(1)	-7(1)	15(1)	-1(1)
C(18)	45(1)	34(1)	55(1)	-5(1)	15(1)	-2(1)
C(19)	49(1)	50(1)	67(1)	13(1)	10(1)	-3(1)
C(20)	43(1)	57(1)	71(1)	10(1)	2(1)	0(1)
C(21)	43(1)	47(1)	58(1)	-8(1)	12(1)	-4(1)
C(22)	44(1)	67(1)	78(1)	-9(1)	13(1)	-9(1)
C(23)	53(1)	78(2)	85(2)	-9(1)	29(1)	-17(1)
C(24)	76(2)	72(2)	89(2)	8(1)	38(1)	-16(1)
C(25)	61(1)	61(1)	79(2)	15(1)	26(1)	1(1)
C(26)	47(1)	41(1)	59(1)	-5(1)	19(1)	-2(1)

<sup>a</sup> The esd's of the least significant digits are given in parentheses. The anisotropic displacement factor exponent takes the form:  $-2 \pi^2 [h^2 a^{*2} U_{11} + \dots + 2 h k a^* b^* U_{12}]$ .

**Table B.6.** Hydrogen atom coordinates ( $\times 10^4$ ) and equivalent isotropic displacement parameters ( $\text{\AA}^2 \times 10^3$ ) for Ph<sub>2</sub>Ppyqn I.<sup>a</sup>

atom	x	y	z	U(eq)
H(1)	4561(14)	9090(2)	4250(2)	73(7)
H(2)	5932(16)	9380(3)	4570(3)	99(9)
H(3)	6487(14)	8320(2)	3180(2)	67(6)
H(4)	5762(17)	7100(3)	1650(2)	100(9)
H(5)	4383(16)	6870(3)	1320(2)	89(8)
H(6)	2952(14)	10220(2)	1950(2)	79(7)
H(7)	2408(15)	11850(3)	2790(2)	84(8)
H(8)	2009(14)	11550(2)	4540(2)	81(7)
H(9)	2191(13)	9580(2)	5520(2)	65(6)
H(10)	2751(12)	7994(19)	4688(18)	52(5)
H(11)	4427(15)	5980(2)	4210(2)	81(7)
H(12)	4184(16)	4240(2)	5310(2)	84(8)
H(13)	2886(12)	3600(2)	5080(2)	64(6)
H(14)	1001(14)	5900(2)	2410(2)	74(7)
H(15)	-293(14)	5430(2)	2360(2)	72(7)
H(16)	-1232(16)	4240(2)	3110(2)	87(8)
H(17)	-1443(16)	2660(2)	4450(2)	82(7)
H(18)	-314(16)	1620(3)	5700(2)	94(9)
H(19)	955(14)	2100(2)	5720(2)	72(7)

<sup>a</sup> U(eq) is defined as one third of the trace of the orthogonalized U<sub>ij</sub> tensor. The esd's of the least significant digits are given in parentheses.

### B.1.2. [Cu<sub>2</sub>(μ-Ph<sub>2</sub>Ppyqn)<sub>2</sub>(CH<sub>3</sub>CN)<sub>2</sub>](BF<sub>4</sub>)<sub>2</sub> 1

**Table B.7.** Atomic coordinates ( $\times 10^4$ ) and equivalent isotropic displacement parameters ( $\text{\AA}^2 \times 10^3$ ) for [Cu<sub>2</sub>(μ-Ph<sub>2</sub>Ppyqn)<sub>2</sub>(CH<sub>3</sub>CN)<sub>2</sub>](BF<sub>4</sub>)<sub>2</sub> 1.<sup>a</sup>

atom	x	y	z	U(eq)
Cu	-2603(1)	-1943(1)	1224(1)	52(1)

P	-3104(1)	-3024(2)	606(3)	47(1)
N(1)	-3124(6)	-2024(5)	244(11)	61(4)
N(2)	-2794(5)	-1189(5)	972(11)	57(4)
N(3)	-2841(5)	-2044(5)	2485(12)	60(4)
C(1)	-3141(8)	-3522(8)	-247(13)	69(5)
C(2)	-2903(8)	-3445(10)	-1057(16)	81(6)
C(3)	-2900(11)	-3821(12)	-1690(20)	106(9)
C(4)	-3115(8)	-4275(9)	-1420(19)	85(7)
C(5)	-3308(10)	-4353(12)	-653(18)	98(9)
C(6)	-3327(7)	-3968(7)	-48(14)	66(5)
C(7)	-3598(5)	-3139(6)	1356(14)	52(4)
C(8)	-4047(6)	-3208(7)	1043(16)	70(6)
C(9)	-4395(8)	-3352(9)	1651(19)	90(8)
C(10)	-4339(7)	-3447(7)	2518(18)	75(6)
C(11)	-3870(8)	-3322(9)	2851(17)	82(7)
C(12)	-3511(6)	-3214(7)	2250(13)	57(4)
C(13)	-3300(6)	-2470(7)	-40(12)	53(4)
C(14)	-3587(10)	-2470(8)	-720(20)	89(7)
C(15)	-3730(9)	-2019(8)	-1158(19)	87(7)
C(16)	-3588(8)	-1631(8)	-827(17)	75(6)
C(17)	-3254(6)	-1602(7)	-115(14)	61(5)
C(18)	-3068(8)	-1156(7)	253(14)	66(6)
C(19)	-3153(9)	-677(7)	-172(17)	78(6)
C(20)	-2906(9)	-242(8)	190(20)	93(7)
C(21)	-2657(7)	-302(6)	1012(19)	75(5)
C(22)	-2380(10)	104(8)	1460(20)	92(7)
C(23)	-2147(11)	28(12)	2120(30)	105(9)
C(24)	-2103(12)	-428(9)	2520(20)	111(8)
C(25)	-2338(6)	-789(7)	2141(15)	66(5)
C(26)	-2612(8)	-754(7)	1356(16)	74(5)
C(27)	-3007(7)	-2115(9)	3148(15)	74(6)
C(28)	-3189(10)	-2181(8)	4080(18)	97(9)
B	-1904(10)	-1364(16)	4810(40)	140(20)
F(1)	-1479(5)	-1646(6)	5097(11)	105(5)
F(2)	-2094(7)	-1277(8)	5722(13)	132(6)
F(3)	-2153(7)	-1661(7)	4361(16)	157(9)
F(4)	-1791(9)	-936(6)	4529(16)	149(9)

<sup>a</sup> U(eq) is defined as one third of the trace of the orthogonalized U<sub>ij</sub> tensor. The esd's of the least significant digits are given in parentheses.

**Table B.8.** Interatomic lengths for [Cu<sub>2</sub>(μ-Ph<sub>2</sub>Ppyqn)<sub>2</sub>(CH<sub>3</sub>CN)<sub>2</sub>](BF<sub>4</sub>)<sub>2</sub> **1**.<sup>a</sup>

bond	length/Å	bond	length/Å
Cu-N(3)	2.017(19)	C(9)-C(10)	1.33(3)
Cu-N(1)	2.096(17)	C(10)-C(11)	1.47(3)
Cu-N(2)	2.128(14)	C(11)-C(12)	1.39(3)
Cu-P <sup>b</sup>	2.217(4)	C(13)-C(14)	1.30(3)
Cu-Cu <sup>b</sup>	3.045(4)	C(14)-C(15)	1.43(3)
P-C(7)	1.823(17)	C(15)-C(16)	1.22(3)
P-C(1)	1.85(2)	C(16)-C(17)	1.43(3)

P-C(13)	1.86(2)	C(17)-C(18)	1.42(3)
P-Cu <sup>b</sup>	2.217(4)	C(18)-C(19)	1.45(3)
N(1)-C(17)	1.31(2)	C(19)-C(20)	1.47(4)
N(1)-C(13)	1.36(2)	C(20)-C(21)	1.42(4)
N(2)-C(18)	1.33(3)	C(21)-C(26)	1.32(3)
N(2)-C(26)	1.40(3)	C(21)-C(22)	1.50(4)
N(3)-C(27)	1.11(2)	C(22)-C(23)	1.20(4)
C(1)-C(6)	1.34(3)	C(23)-C(24)	1.37(4)
C(1)-C(2)	1.40(3)	C(24)-C(25)	1.31(4)
C(2)-C(3)	1.38(4)	C(25)-C(26)	1.41(3)
C(3)-C(4)	1.42(4)	C(27)-C(28)	1.49(3)
C(4)-C(5)	1.29(4)	B-F(3)	1.26(3)
C(5)-C(6)	1.37(3)	B-F(4)	1.26(5)
C(7)-C(12)	1.37(3)	B-F(2)	1.48(5)
C(7)-C(8)	1.37(3)	B-F(1)	1.49(4)
C(8)-C(9)	1.40(3)		

<sup>a</sup> The esd's of the least significant digits are given in parentheses. Symmetry transformations used to generate equivalent atoms: <sup>b</sup> (-x-1/2, -y-1/2, z).

**Table B.9.** Bond angles for [Cu<sub>2</sub>(μ-Ph<sub>2</sub>Ppyqn)<sub>2</sub>(CH<sub>3</sub>CN)<sub>2</sub>](BF<sub>4</sub>)<sub>2</sub> **1.**<sup>a</sup>

angle	degree/°	angle	degree/°
N(3)-Cu-N(1)	113.4(6)	C(10)-C(9)-C(8)	127(2)
N(3)-Cu-N(2)	101.9(6)	C(9)-C(10)-C(11)	113.3(18)
N(1)-Cu-N(2)	78.1(6)	C(12)-C(11)-C(10)	120(2)
N(3)-Cu-P <sup>b</sup>	133.5(4)	C(7)-C(12)-C(11)	121.8(19)
N(1)-Cu-P <sup>b</sup>	110.5(5)	C(14)-C(13)-N(1)	118.2(18)
N(2)-Cu-P <sup>b</sup>	101.4(4)	C(14)-C(13)-P	126.3(16)
N(3)-Cu-Cu <sup>b</sup>	86.1(4)	N(1)-C(13)-P	115.5(13)
N(1)-Cu-Cu <sup>b</sup>	91.9(4)	C(13)-C(14)-C(15)	122(2)
N(2)-Cu-Cu <sup>b</sup>	169.1(5)	C(16)-C(15)-C(14)	116(2)
P <sup>b</sup> -Cu-Cu <sup>b</sup>	77.68(13)	C(15)-C(16)-C(17)	125(2)
C(7)-P-C(1)	104.9(10)	N(1)-C(17)-C(18)	117.8(19)
C(7)-P-C(13)	102.9(7)	N(1)-C(17)-C(16)	116.5(18)
C(1)-P-C(13)	101.8(8)	C(18)-C(17)-C(16)	125.6(18)
C(7)-P-Cu <sup>b</sup>	116.0(6)	N(2)-C(18)-C(17)	118.3(16)
C(1)-P-Cu <sup>b</sup>	108.0(6)	N(2)-C(18)-C(19)	121(2)
C(13)-P-Cu <sup>b</sup>	121.3(5)	C(17)-C(18)-C(19)	121(2)
C(17)-N(1)-C(13)	122.0(17)	C(18)-C(19)-C(20)	117(2)
C(17)-N(1)-Cu	113.3(13)	C(21)-C(20)-C(19)	118.0(18)
C(13)-N(1)-Cu	124.6(11)	C(26)-C(21)-C(20)	119(2)
C(18)-N(2)-C(26)	119.5(16)	C(26)-C(21)-C(22)	116(2)
C(18)-N(2)-Cu	110.9(12)	C(20)-C(21)-C(22)	124.1(19)
C(26)-N(2)-Cu	128.7(14)	C(23)-C(22)-C(21)	122(2)
C(27)-N(3)-Cu	174.1(17)	C(22)-C(23)-C(24)	124(3)
C(6)-C(1)-C(2)	121(2)	C(25)-C(24)-C(23)	115(3)
C(6)-C(1)-P	120.9(17)	C(24)-C(25)-C(26)	127(2)
C(2)-C(1)-P	117.3(18)	C(21)-C(26)-N(2)	125(2)
C(3)-C(2)-C(1)	119(3)	C(21)-C(26)-C(25)	116(2)



angle	degree/°	angle	degree/°
C(5)-C(4)-C(3)	125(2)	N(3)-C(27)-C(28)	174(3)
C(4)-C(5)-C(6)	119(2)	F(3)-B-F(4)	123(5)
C(1)-C(6)-C(5)	121(2)	F(3)-B-F(2)	113(3)
C(12)-C(7)-C(8)	118.6(17)	F(4)-B-F(2)	105(2)
C(12)-C(7)-P	118.9(12)	F(3)-B-F(1)	107(3)
C(8)-C(7)-P	122.1(17)	F(4)-B-F(1)	110(2)
C(7)-C(8)-C(9)	118(2)	F(2)-B-F(1)	97(3)

<sup>a</sup> The esd's of the least significant digits are given in parentheses. Symmetry transformations used to generate equivalent atoms: <sup>b</sup> (-x-1/2, -y-1/2, z).

**Table B.10.** Dihedral angles for [Cu<sub>2</sub>(μ-Ph<sub>2</sub>Ppyqn)<sub>2</sub>(CH<sub>3</sub>CN)<sub>2</sub>](BF<sub>4</sub>)<sub>2</sub> **1**.<sup>a</sup>

dihedral angle	degree/°	dihedral angle	degree/°
N(3)-Cu-N(1)-C(17)	107.0(13)	Cu-N(1)-C(13)-C(14)	-172.8(17)
N(2)-Cu-N(1)-C(17)	9.1(13)	C(17)-N(1)-C(13)-P	-175.9(14)
P <sup>b</sup> -Cu-N(1)-C(17)	-88.8(13)	Cu-N(1)-C(13)-P	7.8(19)
Cu <sup>b</sup> -Cu-N(1)-C(17)	-166.3(13)	C(7)-P-C(13)-C(14)	-80(2)
N(3)-Cu-N(1)-C(13)	-76.4(15)	C(1)-P-C(13)-C(14)	29(2)
N(2)-Cu-N(1)-C(13)	-174.4(15)	Cu <sup>b</sup> -P-C(13)-C(14)	148.4(18)
P <sup>b</sup> -Cu-N(1)-C(13)	87.8(14)	C(7)-P-C(13)-N(1)	99.4(13)
Cu <sup>b</sup> -Cu-N(1)-C(13)	10.2(14)	C(1)-P-C(13)-N(1)	-152.1(14)
N(3)-Cu-N(2)-C(18)	-122.5(12)	Cu <sup>b</sup> -P-C(13)-N(1)	-32.3(15)
N(1)-Cu-N(2)-C(18)	-10.8(13)	N(1)-C(13)-C(14)-C(15)	-1(4)
P <sup>b</sup> -Cu-N(2)-C(18)	98.0(12)	P-C(13)-C(14)-C(15)	177.8(19)
Cu <sup>b</sup> -Cu-N(2)-C(18)	14(3)	C(13)-C(14)-C(15)-C(16)	-4(4)
N(3)-Cu-N(2)-C(26)	69.1(15)	C(14)-C(15)-C(16)-C(17)	7(4)
N(1)-Cu-N(2)-C(26)	-179.1(16)	C(13)-N(1)-C(17)-C(18)	177.2(17)
P <sup>b</sup> -Cu-N(2)-C(26)	-70.3(15)	Cu-N(1)-C(17)-C(18)	-6(2)
Cu <sup>b</sup> -Cu-N(2)-C(26)	-154.3(18)	C(13)-N(1)-C(17)-C(16)	0(3)
N(1)-Cu-N(3)-C(27)	12(17)	Cu-N(1)-C(17)-C(16)	176.3(14)
N(2)-Cu-N(3)-C(27)	94(17)	C(15)-C(16)-C(17)-N(1)	-6(4)
P <sup>b</sup> -Cu-N(3)-C(27)	-147(16)	C(15)-C(16)-C(17)-C(18)	177(3)
Cu <sup>b</sup> -Cu-N(3)-C(27)	-78(17)	C(26)-N(2)-C(18)-C(17)	-179.1(16)
C(7)-P-C(1)-C(6)	-29.2(18)	Cu-N(2)-C(18)-C(17)	11(2)
C(13)-P-C(1)-C(6)	-136.1(16)	C(26)-N(2)-C(18)-C(19)	4(3)
Cu <sup>b</sup> -P-C(1)-C(6)	95.1(17)	Cu-N(2)-C(18)-C(19)	-165.6(15)
C(7)-P-C(1)-C(2)	160.6(15)	N(1)-C(17)-C(18)-N(2)	-4(3)
C(13)-P-C(1)-C(2)	53.7(17)	C(16)-C(17)-C(18)-N(2)	173.5(18)
Cu <sup>b</sup> -P-C(1)-C(2)	-75.1(15)	N(1)-C(17)-C(18)-C(19)	173.1(19)
C(6)-C(1)-C(2)-C(3)	6(3)	C(16)-C(17)-C(18)-C(19)	-10(3)
P-C(1)-C(2)-C(3)	176.2(18)	N(2)-C(18)-C(19)-C(20)	3(3)
C(1)-C(2)-C(3)-C(4)	-5(3)	C(17)-C(18)-C(19)-C(20)	-173.5(19)
C(2)-C(3)-C(4)-C(5)	0(4)	C(18)-C(19)-C(20)-C(21)	-9(3)
C(3)-C(4)-C(5)-C(6)	2(5)	C(19)-C(20)-C(21)-C(26)	8(3)
C(2)-C(1)-C(6)-C(5)	-3(3)	C(19)-C(20)-C(21)-C(22)	178.5(19)
P-C(1)-C(6)-C(5)	-173(2)	C(26)-C(21)-C(22)-C(23)	-4(4)
C(4)-C(5)-C(6)-C(1)	-1(4)	C(20)-C(21)-C(22)-C(23)	-175(3)
C(1)-P-C(7)-C(12)	122.1(15)	C(21)-C(22)-C(23)-C(24)	1(5)

dihedral angle	degree/°	dihedral angle	degree/°
Cu <sup>b</sup> -P-C(7)-C(12)	3.1(16)	C(23)-C(24)-C(25)-C(26)	2(4)
C(1)-P-C(7)-C(8)	-50.5(16)	C(20)-C(21)-C(26)-N(2)	0(3)
C(13)-P-C(7)-C(8)	55.6(16)	C(22)-C(21)-C(26)-N(2)	-171.7(18)
Cu <sup>b</sup> -P-C(7)-C(8)	-169.6(13)	C(20)-C(21)-C(26)-C(25)	176.6(19)
C(12)-C(7)-C(8)-C(9)	0(3)	C(22)-C(21)-C(26)-C(25)	5(3)
P-C(7)-C(8)-C(9)	172.7(15)	C(18)-N(2)-C(26)-C(21)	-6(3)
C(7)-C(8)-C(9)-C(10)	-2(4)	Cu-N(2)-C(26)-C(21)	161.5(14)
C(8)-C(9)-C(10)-C(11)	8(3)	C(18)-N(2)-C(26)-C(25)	177.4(16)
C(9)-C(10)-C(11)-C(12)	-12(3)	Cu-N(2)-C(26)-C(25)	-15(2)
C(8)-C(7)-C(12)-C(11)	-5(3)	C(24)-C(25)-C(26)-C(21)	-5(3)
P-C(7)-C(12)-C(11)	-177.6(17)	C(24)-C(25)-C(26)-N(2)	172(2)
C(10)-C(11)-C(12)-C(7)	11(3)	Cu-N(3)-C(27)-C(28)	-169(14)
C(17)-N(1)-C(13)-C(14)	3(3)		

<sup>a</sup> The esd's of the least significant digits are given in parentheses. Symmetry transformations used to generate equivalent atoms: <sup>b</sup> (-x-1/2, -y-1/2, z).

**Table B.11.** Anisotropic displacement parameters ( $\text{\AA}^2 \times 10^3$ ) for  $[\text{Cu}_2(\mu\text{-Ph}_2\text{Ppyqn})_2(\text{CH}_3\text{CN})_2](\text{BF}_4)_2 \mathbf{1}^a$

atom	U <sub>11</sub>	U <sub>22</sub>	U <sub>33</sub>	U <sub>23</sub>	U <sub>13</sub>	U <sub>12</sub>
Cu	53(1)	51(1)	52(1)	3(1)	0(1)	-1(1)
P	51(2)	45(2)	46(3)	-3(2)	-1(2)	-5(2)
N(1)	64(9)	47(8)	71(12)	12(7)	-5(8)	13(7)
N(2)	63(8)	46(8)	63(11)	6(7)	22(7)	7(6)
N(3)	65(9)	39(7)	77(13)	-16(8)	-20(9)	11(7)
C(1)	89(14)	71(12)	48(12)	1(10)	-20(10)	34(11)
C(2)	77(13)	93(16)	72(16)	-34(13)	-4(10)	14(11)
C(3)	120(20)	110(20)	85(19)	-15(16)	9(15)	45(18)
C(4)	81(15)	91(16)	82(19)	-37(15)	-2(12)	2(12)
C(5)	97(18)	120(20)	75(18)	-2(16)	4(13)	-55(16)
C(6)	83(13)	58(12)	59(13)	-8(10)	2(10)	19(9)
C(7)	32(7)	59(9)	63(13)	-17(9)	5(7)	8(6)
C(8)	51(10)	78(13)	81(16)	-16(11)	7(9)	-9(8)
C(9)	67(14)	84(16)	120(20)	-3(15)	18(13)	38(11)
C(10)	83(14)	57(11)	84(17)	26(11)	24(12)	-19(10)
C(11)	77(13)	89(15)	80(16)	15(12)	33(12)	-19(11)
C(12)	47(9)	65(12)	60(13)	2(9)	7(8)	2(8)
C(13)	48(9)	70(12)	40(10)	-5(8)	12(8)	-7(8)
C(14)	120(20)	61(13)	85(18)	-13(12)	9(15)	-24(12)
C(15)	106(17)	66(13)	90(19)	7(14)	-30(14)	7(11)
C(16)	75(13)	55(12)	96(17)	21(11)	-8(11)	25(10)
C(17)	54(10)	63(12)	66(12)	5(10)	11(8)	-3(8)
C(18)	91(14)	51(11)	55(13)	16(9)	16(10)	36(10)
C(19)	110(17)	43(10)	82(17)	5(10)	18(12)	12(10)
C(20)	111(17)	38(11)	131(19)	23(12)	20(12)	39(11)
C(21)	69(12)	30(8)	127(17)	13(10)	39(9)	9(7)
C(22)	107(17)	42(10)	130(20)	22(12)	44(14)	-13(10)
C(23)	85(19)	110(30)	120(30)	0(19)	7(17)	-10(16)

atom	U <sub>11</sub>	U <sub>22</sub>	U <sub>33</sub>	U <sub>23</sub>	U <sub>13</sub>	U <sub>12</sub>
C(24)	150(20)	48(12)	140(20)	-19(14)	33(15)	-16(12)
C(25)	64(11)	46(9)	89(13)	30(8)	40(8)	-16(8)
C(26)	82(12)	58(11)	82(13)	8(10)	32(8)	50(10)
C(27)	71(12)	102(16)	51(13)	11(11)	32(10)	-9(11)
C(28)	140(20)	49(11)	100(20)	27(11)	57(15)	23(12)
B	63(16)	140(30)	220(50)	-150(40)	0(20)	-11(18)
F(1)	74(8)	126(11)	116(12)	-21(10)	-15(7)	29(7)
F(2)	122(12)	177(17)	98(13)	-33(12)	13(10)	38(12)
F(3)	138(14)	138(14)	200(20)	-98(14)	-98(15)	21(12)
F(4)	220(20)	69(10)	154(18)	-6(11)	-58(17)	-12(11)

<sup>a</sup> The esd's of the least significant digits are given in parentheses. The anisotropic displacement factor exponent takes the form:  $-2 \pi^2 [h^2 a^{*2} U_{11} + \dots + 2 h k a^* b^* U_{12}]$ .

**Table B.12.** Hydrogen atom coordinates ( $\times 10^4$ ) and equivalent isotropic displacement parameters ( $\text{\AA}^2 \times 10^3$ ) for  $[\text{Cu}_2(\mu\text{-Ph}_2\text{Ppyqn})_2(\text{CH}_3\text{CN})_2](\text{BF}_4)_2 \mathbf{1}$ .<sup>a</sup>

atom	x	y	z	U(eq)
H(2)	-2750	-3145	-1167	97
H(3)	-2766	-3780	-2252	127
H(4)	-3116	-4536	-1830	102
H(5)	-3432	-4664	-511	117
H(6)	-3470	-4016	506	80
H(8)	-4117	-3160	440	84
H(9)	-4697	-3384	1424	108
H(10)	-4575	-3579	2878	90
H(11)	-3812	-3314	3465	98
H(12)	-3205	-3192	2459	69
H(14)	-3703	-2773	-930	107
H(15)	-3920	-2022	-1665	105
H(16)	-3705	-1334	-1055	90
H(19)	-3356	-646	-657	94
H(20)	-2912	64	-99	112
H(22)	-2388	423	1214	111
H(23)	-1986	297	2364	126
H(24)	-1920	-476	3033	133
H(25)	-2324	-1100	2416	80
H(28A)	-3104	-2506	4297	146
H(28B)	-3524	-2149	4079	146
H(28C)	-3055	-1931	4463	146

<sup>a</sup> U(eq) is defined as one third of the trace of the orthogonalized  $U_{ij}$  tensor. The esd's of the least significant digits are given in parentheses.

### B.1.3. $[\text{Cu}_2\{\mu\text{-Et(Ph)Pbpy}\}_2(\text{CH}_3\text{CN})_2](\text{PF}_6)_2 \mathbf{2}$

**Table B.13.** Atomic coordinates ( $\times 10^4$ ) and equivalent isotropic displacement parameters ( $\text{\AA}^2 \times 10^3$ ) for  $[\text{Cu}_2\{\mu\text{-Et(Ph)Pbpy}\}_2(\text{CH}_3\text{CN})_2](\text{PF}_6)_2 \mathbf{2}$ .<sup>a</sup>

atom	x	y	z	U(eq)
Cu	6642(1)	1302(1)	2211(1)	57(1)
P(1)	9491(2)	1476(1)	2378(1)	58(1)
N(1)	7756(4)	1622(1)	1949(1)	54(1)
N(2)	5666(5)	1376(1)	1772(1)	62(1)
N(3)	7304(5)	847(1)	2127(1)	61(2)
C(1)	10298(6)	1152(2)	2157(2)	59(2)
C(2)	10529(8)	1157(2)	1820(2)	83(2)
C(3)	11168(8)	905(2)	1667(3)	92(3)
C(4)	11624(8)	652(2)	1848(3)	90(3)
C(5)	11394(11)	641(3)	2173(3)	113(4)
C(6)	10727(11)	884(2)	2326(2)	98(3)
C(7)	10725(8)	1739(2)	2522(3)	85(3)
C(8)	10321(17)	2054(3)	2692(4)	119(4)
C(9)	8852(6)	1720(2)	2036(2)	60(2)
C(10)	9449(8)	1965(2)	1868(2)	77(2)
C(11)	8925(8)	2111(2)	1594(2)	95(3)
C(12)	7838(8)	2005(2)	1501(2)	82(3)
C(13)	7256(6)	1756(2)	1678(2)	58(2)
C(14)	6090(6)	1618(2)	1580(2)	56(2)
C(15)	5461(8)	1729(2)	1309(2)	80(2)
C(16)	4410(9)	1591(3)	1239(2)	102(3)
C(17)	3985(8)	1336(2)	1425(2)	91(3)
C(18)	4643(7)	1238(2)	1692(2)	75(2)
C(19)	7800(6)	610(2)	2078(2)	59(2)
C(20)	8454(11)	303(2)	2006(4)	92(3)
P(2)	7500	2500	564(1)	70(1)
P(3)	5000	5000	1003(1)	91(1)
F(1)	6528(4)	2463(2)	844(1)	112(2)
F(2)	6524(5)	2478(2)	292(1)	144(2)
F(3)	7386(7)	2882(1)	573(2)	162(3)
F(4)	5000	5000	1347(3)	345(11)
F(5)	5000	5000	654(3)	365(14)
F(6)	6298(5)	4895(2)	985(3)	206(4)
F(7)	5319(8)	5356(2)	1003(4)	282(7)

<sup>a</sup> U(eq) is defined as one third of the trace of the orthogonalized U<sub>ij</sub> tensor. The esd's of the least significant digits are given in parentheses.

**Table B.14.** Interatomic lengths for [Cu<sub>2</sub>{μ-Et(Ph)Pbpy}<sub>2</sub>(CH<sub>3</sub>CN)<sub>2</sub>](PF<sub>6</sub>)<sub>2</sub> **2**.<sup>a</sup>

bond	length/Å	bond	length/Å
Cu-N(3)	1.994(6)	C(10)-C(11)	1.382(11)
Cu-N(1)	2.082(5)	C(11)-C(12)	1.351(12)
Cu-N(2)	2.109(5)	C(12)-C(13)	1.389(9)
Cu-P(1) <sup>b</sup>	2.203(2)	C(13)-C(14)	1.478(9)
Cu-Cu <sup>b</sup>	3.0283(17)	C(14)-C(15)	1.378(9)
P(1)-C(1)	1.817(7)	C(15)-C(16)	1.337(11)
P(1)-C(7)	1.836(8)	C(16)-C(17)	1.351(12)
P(1)-C(9)	1.838(6)	C(17)-C(18)	1.364(11)

bond	length/Å	bond	length/Å
N(1)-C(13)	1.341(7)	P(2)-F(3) <sup>c</sup>	1.532(5)
N(1)-C(9)	1.342(8)	P(2)-F(3)	1.532(5)
N(2)-C(18)	1.319(9)	P(2)-F(2)	1.557(5)
N(2)-C(14)	1.326(8)	P(2)-F(2) <sup>c</sup>	1.557(5)
N(3)-C(19)	1.117(8)	P(2)-F(1) <sup>c</sup>	1.580(5)
C(1)-C(6)	1.360(10)	P(2)-F(1)	1.580(5)
C(1)-C(2)	1.383(11)	P(3)-F(4)	1.390(12)
C(2)-C(3)	1.384(12)	P(3)-F(5)	1.410(11)
C(3)-C(4)	1.348(12)	P(3)-F(7) <sup>d</sup>	1.466(8)
C(4)-C(5)	1.338(14)	P(3)-F(7)	1.466(8)
C(5)-C(6)	1.372(13)	P(3)-F(6)	1.523(6)
C(7)-C(8)	1.505(16)	P(3)-F(6) <sup>d</sup>	1.523(6)
C(9)-C(10)	1.368(9)		

<sup>a</sup> The esd's of the least significant digits are given in parentheses. Symmetry transformations used to generate equivalent atoms: <sup>b</sup> (-x+3/2,y,-z+1/2) <sup>c</sup> (-x+3/2,-y+1/2,z) <sup>d</sup> (-x+1,-y+1,z)

**Table B.15.** Bond angles for [Cu<sub>2</sub>{μ-Et(Ph)Pbpy}<sub>2</sub>(CH<sub>3</sub>CN)<sub>2</sub>](PF<sub>6</sub>)<sub>2</sub> **2**.<sup>a</sup>

angle	degree/°	angle	degree/°
N(3)-Cu-N(1)	104.3(2)	C(12)-C(13)-C(14)	123.3(6)
N(3)-Cu-N(2)	100.3(2)	N(2)-C(14)-C(15)	120.8(6)
N(1)-Cu-N(2)	78.4(2)	N(2)-C(14)-C(13)	115.9(5)
N(3)-Cu-P(1) <sup>b</sup>	129.22(16)	C(15)-C(14)-C(13)	123.3(6)
N(1)-Cu-P(1) <sup>b</sup>	122.58(14)	C(16)-C(15)-C(14)	119.3(8)
N(2)-Cu-P(1) <sup>b</sup>	106.63(17)	C(15)-C(16)-C(17)	120.5(9)
N(3)-Cu-Cu <sup>b</sup>	83.85(15)	C(16)-C(17)-C(18)	117.6(8)
N(1)-Cu-Cu <sup>b</sup>	90.42(14)	N(2)-C(18)-C(17)	123.1(8)
N(2)-Cu-Cu <sup>b</sup>	168.73(15)	N(3)-C(19)-C(20)	178.7(9)
P(1) <sup>b</sup> -Cu-Cu <sup>b</sup>	77.94(6)	F(3) <sup>c</sup> -P(2)-F(3)	177.2(6)
C(1)-P(1)-C(7)	100.6(4)	F(3) <sup>c</sup> -P(2)-F(2)	91.1(4)
C(1)-P(1)-C(9)	101.7(3)	F(3)-P(2)-F(2)	90.8(4)
C(7)-P(1)-C(9)	103.3(4)	F(3) <sup>c</sup> -P(2)-F(2) <sup>c</sup>	90.8(4)
C(1)-P(1)-Cu <sup>b</sup>	115.8(2)	F(3)-P(2)-F(2) <sup>c</sup>	91.1(4)
C(7)-P(1)-Cu <sup>b</sup>	112.5(4)	F(2)-P(2)-F(2) <sup>c</sup>	90.2(4)
C(9)-P(1)-Cu <sup>b</sup>	120.4(2)	F(3) <sup>c</sup> -P(2)-F(1) <sup>c</sup>	91.0(4)
C(13)-N(1)-C(9)	119.0(5)	F(3)-P(2)-F(1) <sup>c</sup>	87.0(4)
C(13)-N(1)-Cu	114.0(4)	F(2)-P(2)-F(1) <sup>c</sup>	177.7(4)
C(9)-N(1)-Cu	126.8(4)	F(2) <sup>c</sup> -P(2)-F(1) <sup>c</sup>	90.6(3)
C(18)-N(2)-C(14)	118.6(6)	F(3) <sup>c</sup> -P(2)-F(1)	87.0(4)
C(18)-N(2)-Cu	127.1(5)	F(3)-P(2)-F(1)	91.0(4)
C(14)-N(2)-Cu	113.9(4)	F(2)-P(2)-F(1)	90.6(3)
C(19)-N(3)-Cu	171.9(6)	F(2) <sup>c</sup> -P(2)-F(1)	177.7(4)
C(6)-C(1)-C(2)	115.9(8)	F(1) <sup>c</sup> -P(2)-F(1)	88.7(4)
C(6)-C(1)-P(1)	119.5(6)	F(4)-P(3)-F(5)	180.000(2)
C(2)-C(1)-P(1)	124.6(6)	F(4)-P(3)-F(7) <sup>d</sup>	90.0(6)
C(1)-C(2)-C(3)	121.8(9)	F(5)-P(3)-F(7) <sup>d</sup>	90.0(6)
C(4)-C(3)-C(2)	120.1(10)	F(4)-P(3)-F(7)	90.0(6)
C(5)-C(4)-C(3)	118.7(10)	F(5)-P(3)-F(7)	90.0(6)
C(4)-C(5)-C(6)	121.7(10)	F(7) <sup>d</sup> -P(3)-F(7)	180.0(13)

angle	degree/°	angle	degree/°
C(1)-C(6)-C(5)	121.7(10)	F(4)-P(3)-F(6)	92.8(4)
C(8)-C(7)-P(1)	113.1(9)	F(5)-P(3)-F(6)	87.2(4)
N(1)-C(9)-C(10)	122.0(6)	F(7) <sup>d</sup> -P(3)-F(6)	88.2(5)
N(1)-C(9)-P(1)	113.8(5)	F(7)-P(3)-F(6)	91.8(4)
C(10)-C(9)-P(1)	124.1(6)	F(4)-P(3)-F(6) <sup>d</sup>	92.8(4)
C(9)-C(10)-C(11)	119.3(8)	F(5)-P(3)-F(6) <sup>d</sup>	87.2(4)
C(12)-C(11)-C(10)	118.5(8)	F(7) <sup>d</sup> -P(3)-F(6) <sup>d</sup>	91.8(4)
C(11)-C(12)-C(13)	120.7(8)	F(7)-P(3)-F(6) <sup>d</sup>	88.2(5)
N(1)-C(13)-C(12)	120.4(6)	F(6)-P(3)-F(6) <sup>d</sup>	174.4(9)
N(1)-C(13)-C(14)	116.3(5)		

<sup>a</sup> The esd's of the least significant digits are given in parentheses. Symmetry transformations used to generate equivalent atoms: <sup>b</sup> (-x+3/2,y,-z+1/2) <sup>c</sup> (-x+3/2,-y+1/2,z) <sup>d</sup> (-x+1,-y+1,z)

**Table B.16.** Dihedral angles for [Cu<sub>2</sub>{μ-Et(Ph)Pbpy}<sub>2</sub>(CH<sub>3</sub>CN)<sub>2</sub>](PF<sub>6</sub>)<sub>2</sub> **2**.<sup>a</sup>

dihedral angle	degree/°	dihedral angle	degree/°
N(3)-Cu-N(1)-C(13)	108.5(4)	C(13)-N(1)-C(9)-C(10)	3.6(10)
N(2)-Cu-N(1)-C(13)	10.6(4)	Cu-N(1)-C(9)-C(10)	-171.3(6)
P(1) <sup>b</sup> -Cu-N(1)-C(13)	-91.9(4)	C(13)-N(1)-C(9)-P(1)	-172.4(5)
Cu <sup>b</sup> -Cu-N(1)-C(13)	-167.8(4)	Cu-N(1)-C(9)-P(1)	12.6(7)
N(3)-Cu-N(1)-C(9)	-76.3(5)	C(1)-P(1)-C(9)-N(1)	92.7(5)
N(2)-Cu-N(1)-C(9)	-174.2(5)	C(7)-P(1)-C(9)-N(1)	-163.3(6)
P(1) <sup>b</sup> -Cu-N(1)-C(9)	83.3(5)	Cu <sup>b</sup> -P(1)-C(9)-N(1)	-36.9(6)
Cu <sup>b</sup> -Cu-N(1)-C(9)	7.4(5)	C(1)-P(1)-C(9)-C(10)	-83.3(7)
N(3)-Cu-N(2)-C(18)	74.7(6)	C(7)-P(1)-C(9)-C(10)	20.7(8)
N(1)-Cu-N(2)-C(18)	177.4(7)	Cu <sup>b</sup> -P(1)-C(9)-C(10)	147.1(6)
P(1) <sup>b</sup> -Cu-N(2)-C(18)	-61.8(6)	N(1)-C(9)-C(10)-C(11)	-1.6(12)
Cu <sup>b</sup> -Cu-N(2)-C(18)	-174.3(6)	P(1)-C(9)-C(10)-C(11)	174.1(7)
N(3)-Cu-N(2)-C(14)	-113.4(5)	C(9)-C(10)-C(11)-C(12)	-0.7(14)
N(1)-Cu-N(2)-C(14)	-10.7(5)	C(10)-C(11)-C(12)-C(13)	0.9(15)
P(1) <sup>b</sup> -Cu-N(2)-C(14)	110.1(5)	C(9)-N(1)-C(13)-C(12)	-3.4(10)
Cu <sup>b</sup> -Cu-N(2)-C(14)	-2.4(12)	Cu-N(1)-C(13)-C(12)	172.2(6)
N(1)-Cu-N(3)-C(19)	32(4)	C(9)-N(1)-C(13)-C(14)	175.2(6)
N(2)-Cu-N(3)-C(19)	112(4)	Cu-N(1)-C(13)-C(14)	-9.2(7)
P(1) <sup>b</sup> -Cu-N(3)-C(19)	-126(4)	C(11)-C(12)-C(13)-N(1)	1.2(13)
Cu <sup>b</sup> -Cu-N(3)-C(19)	-57(4)	C(11)-C(12)-C(13)-C(14)	-177.4(8)
C(7)-P(1)-C(1)-C(6)	85.5(8)	C(18)-N(2)-C(14)-C(15)	1.9(10)
C(9)-P(1)-C(1)-C(6)	-168.4(7)	Cu-N(2)-C(14)-C(15)	-170.7(6)
Cu <sup>b</sup> -P(1)-C(1)-C(6)	-36.0(8)	C(18)-N(2)-C(14)-C(13)	-178.2(6)
C(7)-P(1)-C(1)-C(2)	-93.9(7)	Cu-N(2)-C(14)-C(13)	9.2(7)
C(9)-P(1)-C(1)-C(2)	12.3(7)	N(1)-C(13)-C(14)-N(2)	-0.1(9)
Cu <sup>b</sup> -P(1)-C(1)-C(2)	144.7(6)	C(12)-C(13)-C(14)-N(2)	178.5(7)
C(6)-C(1)-C(2)-C(3)	-0.5(13)	N(1)-C(13)-C(14)-C(15)	179.8(7)
P(1)-C(1)-C(2)-C(3)	178.9(7)	C(12)-C(13)-C(14)-C(15)	-1.6(11)
C(1)-C(2)-C(3)-C(4)	-2.6(14)	N(2)-C(14)-C(15)-C(16)	0.0(13)
C(2)-C(3)-C(4)-C(5)	3.4(15)	C(13)-C(14)-C(15)-C(16)	-179.9(8)
C(3)-C(4)-C(5)-C(6)	-1.2(17)	C(14)-C(15)-C(16)-C(17)	-2.4(16)
C(2)-C(1)-C(6)-C(5)	2.8(14)	C(15)-C(16)-C(17)-C(18)	2.7(16)
P(1)-C(1)-C(6)-C(5)	-176.6(9)	C(14)-N(2)-C(18)-C(17)	-1.5(12)

dihedral angle	degree/°	dihedral angle	degree/°
C(4)-C(5)-C(6)-C(1)	-2.0(18)	Cu-N(2)-C(18)-C(17)	170.0(7)
C(1)-P(1)-C(7)-C(8)	174.6(9)	C(16)-C(17)-C(18)-N(2)	-0.7(15)
C(9)-P(1)-C(7)-C(8)	69.8(9)	Cu-N(3)-C(19)-C(20)	-70(45)
Cu <sup>b</sup> -P(1)-C(7)-C(8)	-61.5(9)		

<sup>a</sup> The esd's of the least significant digits are given in parentheses. Symmetry transformations used to generate equivalent atoms: <sup>b</sup> (-x+3/2,y,-z+1/2) <sup>c</sup> (-x+3/2,-y+1/2,z) <sup>d</sup> (-x+1,-y+1,z)

**Table B.17.** Anisotropic displacement parameters ( $\text{\AA}^2 \times 10^3$ ) for  $[\text{Cu}_2\{\mu\text{-Et(Ph)Pbpy}\}_2(\text{CH}_3\text{CN})_2](\text{PF}_6)_2 \mathbf{2}^a$

atom	U <sub>11</sub>	U <sub>22</sub>	U <sub>33</sub>	U <sub>23</sub>	U <sub>13</sub>	U <sub>12</sub>
Cu	66(1)	46(1)	58(1)	6(1)	-13(1)	-6(1)
P(1)	57(1)	49(1)	67(1)	4(1)	-19(1)	-8(1)
N(1)	58(3)	41(3)	62(3)	8(2)	-14(3)	-3(2)
N(2)	65(4)	56(3)	65(3)	8(3)	-19(3)	-13(3)
N(3)	80(4)	47(3)	54(3)	5(3)	-12(3)	-5(3)
C(1)	53(4)	60(4)	64(4)	8(3)	-16(3)	-5(3)
C(2)	77(6)	81(6)	90(6)	25(5)	0(5)	6(5)
C(3)	91(6)	99(7)	85(6)	4(6)	28(5)	7(5)
C(4)	78(6)	82(6)	111(8)	-18(6)	-5(6)	12(5)
C(5)	160(11)	82(7)	98(8)	-5(6)	-25(8)	43(7)
C(6)	154(10)	76(6)	64(6)	1(5)	-13(6)	37(6)
C(7)	82(6)	75(6)	99(7)	17(5)	-36(6)	-27(5)
C(8)	158(13)	75(7)	124(10)	-18(7)	-29(11)	-43(8)
C(9)	59(4)	46(4)	75(4)	9(3)	-20(4)	-3(3)
C(10)	70(5)	69(5)	94(6)	22(4)	-17(5)	-22(4)
C(11)	93(7)	76(6)	116(7)	46(5)	-23(6)	-34(5)
C(12)	74(6)	78(6)	95(6)	35(5)	-20(5)	-15(4)
C(13)	64(4)	46(4)	63(4)	11(3)	-11(4)	-3(3)
C(14)	55(4)	57(4)	56(4)	9(3)	-7(3)	-1(3)
C(15)	74(6)	98(6)	69(5)	37(5)	-20(4)	-15(5)
C(16)	76(6)	140(8)	90(7)	51(6)	-25(5)	-21(6)
C(17)	66(5)	128(7)	79(6)	17(5)	-24(5)	-29(5)
C(18)	78(6)	83(5)	62(5)	16(4)	-16(4)	-28(5)
C(19)	78(5)	48(4)	50(4)	5(3)	-13(4)	-11(4)
C(20)	84(8)	64(6)	126(9)	0(5)	-13(7)	13(5)
P(2)	83(2)	68(2)	60(2)	0	0	-13(2)
P(3)	69(2)	118(3)	84(2)	0	0	-6(2)
F(1)	84(3)	172(5)	81(3)	17(3)	6(3)	-20(3)
F(2)	129(4)	221(6)	83(3)	30(4)	-39(3)	-49(5)
F(3)	226(7)	70(3)	191(6)	15(4)	14(6)	-1(4)
F(4)	460(30)	470(30)	103(8)	0	0	40(30)
F(5)	460(30)	540(30)	93(8)	0	0	280(30)
F(6)	80(4)	170(7)	368(13)	-8(7)	3(6)	2(4)
F(7)	164(8)	116(6)	570(20)	-5(9)	44(11)	-36(5)

<sup>a</sup> The esd's of the least significant digits are given in parentheses. The anisotropic displacement factor exponent takes the form:  $-2\pi^2 [h^2 a^{*2} U_{11} + \dots + 2hk a^* b^* U_{12}]$ .

**Table B.18.** Hydrogen atom coordinates ( $\times 10^4$ ) and equivalent isotropic displacement parameters ( $\text{\AA}^2 \times 10^3$ ) for  $[\text{Cu}_2\{\mu\text{-Et(Ph)Pbpy}\}_2(\text{CH}_3\text{CN})_2](\text{PF}_6)_2 \mathbf{2}^a$

atom	<i>x</i>	<i>y</i>	<i>z</i>	U(eq)
H(2)	10310(70)	1317(19)	1708(18)	80(30)
H(3)	11360(80)	920(20)	1440(20)	110(30)
H(4)	12140(70)	480(20)	1750(19)	100(30)
H(5)	11650(100)	500(30)	2300(30)	160(50)
H(6)	10540(60)	869(17)	2511(18)	70(30)
H(7A)	11200(70)	1585(19)	2659(18)	90(20)
H(7B)	11150(60)	1802(17)	2346(17)	70(20)
H(8A)	10940(110)	2180(30)	2740(30)	180(50)
H(8B)	9690(90)	2060(30)	2820(30)	130(50)
H(8C)	9810(100)	2210(20)	2550(30)	140(40)
H(10)	10100(60)	2037(16)	1949(16)	70(20)
H(11)	9320(70)	2261(19)	1486(18)	90(30)
H(12)	7480(60)	2077(17)	1355(16)	70(20)
H(15)	5820(60)	1897(17)	1215(16)	70(20)
H(16)	3930(90)	1680(20)	1090(20)	140(40)
H(17)	3230(70)	1246(18)	1417(19)	100(30)
H(18)	4330(50)	1106(13)	1814(13)	39(17)
H(20A)	9200(100)	330(30)	1940(30)	140(40)
H(20B)	7820(90)	120(20)	2010(20)	150(40)
H(20C)	8860(90)	260(20)	2160(20)	90(40)

<sup>a</sup> U(eq) is defined as one third of the trace of the orthogonalized  $U_{ij}$  tensor.

#### B.1.4. $[\text{Pd}_2(\mu\text{-Ph}_2\text{Pbpy})_2](\text{BF}_4)_2 \mathbf{3}$

**Table B.19.** Atomic coordinates ( $\times 10^4$ ) and equivalent isotropic displacement parameters ( $\text{\AA}^2 \times 10^3$ ) for  $[\text{Pd}_2(\mu\text{-Ph}_2\text{Pbpy})_2](\text{BF}_4)_2 \mathbf{3}^a$

atom	<i>x</i>	<i>y</i>	<i>z</i>	U(eq)
Pd	5401(1)	9771(1)	5997(1)	37(1)
P	5514(4)	12176(3)	3454(3)	39(1)
N(1)	6181(13)	11588(11)	5585(10)	38(3)
N(2)	6080(13)	9552(12)	7649(11)	41(3)
C(1)	7205(15)	12374(13)	2387(12)	38(3)
C(2)	7669(16)	11409(15)	1952(14)	48(4)
C(3)	8910(20)	11513(19)	1135(17)	66(5)
C(4)	9790(20)	12580(20)	763(17)	69(5)
C(5)	9360(20)	13543(19)	1210(17)	70(5)
C(6)	8099(19)	13439(15)	1999(15)	55(4)
C(7)	4139(18)	13510(14)	2812(13)	45(4)
C(8)	4430(20)	14521(17)	1712(16)	65(5)
C(9)	3230(30)	15489(17)	1289(18)	77(6)
C(10)	1840(20)	15447(18)	1945(18)	64(5)
C(11)	1616(18)	14499(19)	3000(20)	67(5)
C(12)	2753(18)	13524(16)	3447(15)	55(4)



atom	x	y	z	U(eq)
C(13)	6065(17)	12628(14)	4559(13)	44(4)
C(14)	6360(20)	13892(15)	4357(15)	63(5)
C(15)	6960(30)	14080(18)	5219(16)	76(6)
C(16)	7120(20)	13001(17)	6293(16)	65(5)
C(17)	6667(18)	11807(15)	6451(13)	46(4)
C(18)	6611(17)	10655(15)	7583(13)	47(4)
C(19)	7140(20)	10710(20)	8535(17)	70(5)
C(20)	6980(20)	9620(20)	9590(16)	74(6)
C(21)	6400(20)	8535(17)	9642(15)	59(4)
C(22)	5977(18)	8539(16)	8648(13)	49(4)
B	8090(30)	7370(20)	12603(18)	65(6)
F(1)	9195(17)	8144(14)	11800(13)	113(5)
F(2)	8590(30)	6760(20)	13594(15)	172(8)
F(3)	7860(20)	6464(14)	12193(14)	127(5)
F(4)	6862(18)	8210(20)	12530(20)	166(8)

<sup>a</sup> U(eq) is defined as one third of the trace of the orthogonalized  $U_{ij}$  tensor. The esd's of the least significant digits are given in parentheses.

**Table B.20.** Interatomic lengths for  $[\text{Pd}_2(\mu\text{-Ph}_2\text{Pbpy})_2](\text{BF}_4)_2 \mathbf{3}^a$

bond	length/Å	bond	length/Å
Pd-N(1)	2.064(11)	C(7)-C(8)	1.40(2)
Pd-N(2)	2.181(12)	C(8)-C(9)	1.43(3)
Pd-P <sup>b</sup>	2.218(4)	C(9)-C(10)	1.37(3)
Pd-Pd <sup>b</sup>	2.568(2)	C(10)-C(11)	1.33(3)
P-C(7)	1.813(16)	C(11)-C(12)	1.40(2)
P-C(1)	1.814(14)	C(13)-C(14)	1.38(2)
P-C(13)	1.819(15)	C(14)-C(15)	1.39(2)
P-Pd <sup>b</sup>	2.218(4)	C(15)-C(16)	1.42(3)
N(1)-C(13)	1.354(19)	C(16)-C(17)	1.37(2)
N(1)-C(17)	1.360(18)	C(17)-C(18)	1.48(2)
N(2)-C(22)	1.307(19)	C(18)-C(19)	1.39(2)
N(2)-C(18)	1.342(19)	C(19)-C(20)	1.39(3)
C(1)-C(2)	1.38(2)	C(20)-C(21)	1.35(3)
C(1)-C(6)	1.39(2)	C(21)-C(22)	1.37(2)
C(2)-C(3)	1.36(2)	F(1)-B	1.38(3)
C(3)-C(4)	1.38(3)	F(2)-B	1.29(3)
C(4)-C(5)	1.39(3)	F(3)-B	1.36(3)
C(5)-C(6)	1.35(2)	F(4)-B	1.34(3)
C(7)-C(12)	1.36(2)		

<sup>a</sup> The esd's of the least significant digits are given in parentheses. Symmetry transformations used to generate equivalent atoms: <sup>b</sup> (-x+1,-y+2,-z+1).

**Table B.21.** Bond angles for  $[\text{Pd}_2(\mu\text{-Ph}_2\text{Pbpy})_2](\text{BF}_4)_2 \mathbf{3}^a$

angle	degree/°	angle	degree/°
N(1)-Pd-N(2)	77.9(4)	C(8)-C(7)-P	123.6(13)
N(1)-Pd-P <sup>b</sup>	176.3(3)	C(7)-C(8)-C(9)	118.1(18)

angle	degree/°	angle	degree/°
N(2)-Pd-P <sup>b</sup>	99.5(3)	C(10)-C(9)-C(8)	121.4(18)
N(1)-Pd-Pd <sup>b</sup>	97.7(3)	C(11)-C(10)-C(9)	118.7(16)
N(2)-Pd-Pd <sup>b</sup>	175.4(3)	C(10)-C(11)-C(12)	121.8(17)
P <sup>b</sup> -Pd-Pd <sup>b</sup>	84.88(11)	C(7)-C(12)-C(11)	121.3(16)
C(7)-P-C(1)	107.7(7)	N(1)-C(13)-C(14)	124.0(14)
C(7)-P-C(13)	101.7(7)	N(1)-C(13)-P	112.6(10)
C(1)-P-C(13)	104.0(7)	C(14)-C(13)-P	123.3(12)
C(7)-P-Pd <sup>b</sup>	111.9(5)	C(13)-C(14)-C(15)	117.7(16)
C(1)-P-Pd <sup>b</sup>	111.7(5)	C(14)-C(15)-C(16)	119.0(15)
C(13)-P-Pd <sup>b</sup>	118.9(5)	C(17)-C(16)-C(15)	118.9(15)
C(13)-N(1)-C(17)	117.4(12)	N(1)-C(17)-C(16)	122.6(15)
C(13)-N(1)-Pd	124.4(9)	N(1)-C(17)-C(18)	114.0(13)
C(17)-N(1)-Pd	117.7(10)	C(16)-C(17)-C(18)	123.4(13)
C(22)-N(2)-C(18)	119.1(13)	N(2)-C(18)-C(19)	121.1(16)
C(22)-N(2)-Pd	128.7(10)	N(2)-C(18)-C(17)	118.2(12)
C(18)-N(2)-Pd	112.2(10)	C(19)-C(18)-C(17)	120.7(15)
C(2)-C(1)-C(6)	117.5(13)	C(20)-C(19)-C(18)	118.1(18)
C(2)-C(1)-P	119.2(11)	C(21)-C(20)-C(19)	119.5(16)
C(6)-C(1)-P	123.3(11)	C(20)-C(21)-C(22)	118.7(16)
C(3)-C(2)-C(1)	121.9(15)	N(2)-C(22)-C(21)	123.3(15)
C(2)-C(3)-C(4)	119.5(16)	F(2)-B-F(4)	119(2)
C(3)-C(4)-C(5)	119.3(17)	F(2)-B-F(3)	107.8(19)
C(6)-C(5)-C(4)	120.3(17)	F(4)-B-F(3)	110(2)
C(5)-C(6)-C(1)	121.4(16)	F(2)-B-F(1)	110(2)
C(12)-C(7)-C(8)	118.7(15)	F(4)-B-F(1)	103.7(18)
C(12)-C(7)-P	117.7(12)	F(3)-B-F(1)	106.2(17)

<sup>a</sup> The esd's of the least significant digits are given in parentheses. Symmetry transformations used to generate equivalent atoms: <sup>b</sup> (-x+1,-y+2,-z+1).

**Table B.22.** Dihedral angles for [Pd<sub>2</sub>(μ-Ph<sub>2</sub>Pbpy)<sub>2</sub>](BF<sub>4</sub>)<sub>2</sub> **3**.<sup>a</sup>

dihedral angle	degree/°	dihedral angle	degree/°
N(2)-Pd-N(1)-C(13)	-173.0(12)	P-C(7)-C(12)-C(11)	-178.4(13)
P <sup>b</sup> -Pd-N(1)-C(13)	-129(5)	C(10)-C(11)-C(12)-C(7)	0(3)
Pd <sup>b</sup> -Pd-N(1)-C(13)	5.5(11)	C(17)-N(1)-C(13)-C(14)	-2(2)
N(2)-Pd-N(1)-C(17)	-1.8(10)	Pd-N(1)-C(13)-C(14)	169.2(13)
P <sup>b</sup> -Pd-N(1)-C(17)	42(6)	C(17)-N(1)-C(13)-P	176.5(10)
Pd <sup>b</sup> -Pd-N(1)-C(17)	176.8(10)	Pd-N(1)-C(13)-P	-12.2(15)
N(1)-Pd-N(2)-C(22)	178.3(13)	C(7)-P-C(13)-N(1)	137.7(11)
P <sup>b</sup> -Pd-N(2)-C(22)	0.9(13)	C(1)-P-C(13)-N(1)	-110.5(11)
Pd <sup>b</sup> -Pd-N(2)-C(22)	160(3)	Pd <sup>b</sup> -P-C(13)-N(1)	14.4(13)
N(1)-Pd-N(2)-C(18)	1.1(10)	C(7)-P-C(13)-C(14)	-43.7(16)
P <sup>b</sup> -Pd-N(2)-C(18)	-176.3(9)	C(1)-P-C(13)-C(14)	68.1(16)
Pd <sup>b</sup> -Pd-N(2)-C(18)	-17(4)	Pd <sup>b</sup> -P-C(13)-C(14)	-166.9(13)
C(7)-P-C(1)-C(2)	-117.5(12)	N(1)-C(13)-C(14)-C(15)	7(3)
C(13)-P-C(1)-C(2)	135.1(12)	P-C(13)-C(14)-C(15)	-171.8(15)
Pd <sup>b</sup> -P-C(1)-C(2)	5.7(13)	C(13)-C(14)-C(15)-C(16)	-5(3)
C(7)-P-C(1)-C(6)	64.3(14)	C(14)-C(15)-C(16)-C(17)	0(3)

dihedral angle	degree/°	dihedral angle	degree/°
Pd <sup>b</sup> -P-C(1)-C(6)	-172.5(12)	Pd-N(1)-C(17)-C(16)	-176.0(14)
C(6)-C(1)-C(2)-C(3)	-3(2)	C(13)-N(1)-C(17)-C(18)	174.0(13)
P-C(1)-C(2)-C(3)	178.9(13)	Pd-N(1)-C(17)-C(18)	2.1(17)
C(1)-C(2)-C(3)-C(4)	3(3)	C(15)-C(16)-C(17)-N(1)	5(3)
C(2)-C(3)-C(4)-C(5)	-1(3)	C(15)-C(16)-C(17)-C(18)	-172.6(17)
C(3)-C(4)-C(5)-C(6)	0(3)	C(22)-N(2)-C(18)-C(19)	4(2)
C(4)-C(5)-C(6)-C(1)	0(3)	Pd-N(2)-C(18)-C(19)	-178.4(13)
C(2)-C(1)-C(6)-C(5)	1(2)	C(22)-N(2)-C(18)-C(17)	-177.9(14)
P-C(1)-C(6)-C(5)	179.4(14)	Pd-N(2)-C(18)-C(17)	-0.3(17)
C(1)-P-C(7)-C(12)	177.3(12)	N(1)-C(17)-C(18)-N(2)	-1(2)
C(13)-P-C(7)-C(12)	-73.7(13)	C(16)-C(17)-C(18)-N(2)	177.0(16)
Pd <sup>b</sup> -P-C(7)-C(12)	54.2(13)	N(1)-C(17)-C(18)-C(19)	177.0(15)
C(1)-P-C(7)-C(8)	-3.3(16)	C(16)-C(17)-C(18)-C(19)	-5(3)
C(13)-P-C(7)-C(8)	105.7(14)	N(2)-C(18)-C(19)-C(20)	-6(3)
Pd <sup>b</sup> -P-C(7)-C(8)	-126.4(13)	C(17)-C(18)-C(19)-C(20)	176.4(17)
C(12)-C(7)-C(8)-C(9)	-3(2)	C(18)-C(19)-C(20)-C(21)	4(3)
P-C(7)-C(8)-C(9)	177.9(13)	C(19)-C(20)-C(21)-C(22)	-1(3)
C(7)-C(8)-C(9)-C(10)	1(3)	C(18)-N(2)-C(22)-C(21)	-1(2)
C(8)-C(9)-C(10)-C(11)	1(3)	Pd-N(2)-C(22)-C(21)	-177.8(12)
C(9)-C(10)-C(11)-C(12)	-2(3)	C(20)-C(21)-C(22)-N(2)	-1(3)
C(8)-C(7)-C(12)-C(11)	2(2)		

<sup>a</sup> The esd's of the least significant digits are given in parentheses. Symmetry transformations used to generate equivalent atoms: <sup>b</sup> (-x+1,-y+2,-z+1).

**Table B.23.** Anisotropic displacement parameters ( $\text{\AA}^2 \times 10^3$ ) for  $[\text{Pd}_2(\mu\text{-Ph}_2\text{Pbpy})_2](\text{BF}_4)_2 \mathbf{3}$ .<sup>a</sup>

atom	U <sub>11</sub>	U <sub>22</sub>	U <sub>33</sub>	U <sub>23</sub>	U <sub>13</sub>	U <sub>12</sub>
Pd	45(1)	32(1)	38(1)	-14(1)	-8(1)	-8(1)
P	45(2)	31(2)	40(2)	-13(2)	-5(2)	-6(2)
N(1)	44(7)	35(6)	37(7)	-17(5)	-6(5)	-5(5)
N(2)	40(7)	40(7)	51(8)	-26(6)	-6(6)	0(5)
C(1)	35(7)	37(8)	41(8)	-14(6)	-5(6)	2(6)
C(2)	34(8)	44(9)	64(10)	-22(8)	0(7)	-2(6)
C(3)	70(12)	69(12)	72(12)	-48(10)	-1(10)	4(10)
C(4)	61(11)	83(14)	59(11)	-26(10)	-2(9)	-5(10)
C(5)	65(12)	65(12)	78(13)	-19(10)	-8(10)	-28(9)
C(6)	61(10)	38(8)	59(10)	-17(8)	10(8)	-11(7)
C(7)	56(9)	39(8)	49(9)	-26(7)	-4(7)	-1(7)
C(8)	83(13)	52(10)	62(11)	-26(9)	-11(9)	7(9)
C(9)	121(18)	36(10)	66(12)	-11(9)	-32(13)	17(10)
C(10)	75(13)	57(11)	72(13)	-36(11)	-35(10)	22(9)
C(11)	36(9)	68(12)	108(17)	-51(13)	-1(9)	4(8)
C(12)	57(10)	49(9)	56(10)	-18(8)	-8(8)	-6(8)
C(13)	53(9)	37(8)	44(9)	-20(7)	1(7)	-11(7)
C(14)	115(15)	27(8)	49(10)	-17(7)	-4(10)	-18(9)
C(15)	140(19)	47(10)	55(11)	-27(9)	-14(11)	-28(11)
C(16)	93(13)	56(11)	57(11)	-30(9)	-6(10)	-30(10)
C(17)	61(10)	48(9)	39(8)	-25(7)	-8(7)	-9(7)

C(19)	78(13)	76(13)	70(13)	-37(11)	-33(10)	-2(10)
C(20)	106(16)	77(14)	45(10)	-19(10)	-37(10)	-3(11)
C(21)	72(12)	53(10)	49(10)	-12(8)	-19(9)	-6(9)
C(22)	58(10)	44(9)	47(9)	-18(8)	-12(7)	1(7)
B	91(16)	49(12)	42(11)	-12(10)	-3(11)	13(11)
F(1)	125(11)	94(10)	103(10)	-25(8)	11(9)	-33(9)
F(2)	260(20)	147(17)	91(12)	-6(11)	-58(14)	-38(16)
F(3)	191(16)	73(9)	127(12)	-48(9)	-5(11)	-32(9)
F(4)	98(11)	177(18)	220(20)	-102(16)	12(12)	37(12)

<sup>a</sup> The esd's of the least significant digits are given in parentheses. The anisotropic displacement factor exponent takes the form:  $-2 \pi^2 [h^2 a^{*2} U_{11} + \dots + 2 h k a^* b^* U_{12}]$ .

**Table B.24.** Hydrogen atom coordinates ( $\times 10^4$ ) and equivalent isotropic displacement parameters ( $\text{\AA}^2 \times 10^3$ ) for  $[\text{Pd}_2(\mu\text{-Ph}_2\text{Pbpy})_2](\text{BF}_4)_2 \mathbf{3}$ .<sup>a</sup>

atom	x	y	z	U(eq)
H(2)	7114	10668	2225	58
H(3)	9177	10870	829	79
H(4)	10655	12653	219	83
H(5)	9942	14263	966	84
H(6)	7823	14094	2289	66
H(8)	5386	14562	1267	78
H(9)	3406	16162	553	92
H(10)	1056	16071	1653	77
H(11)	681	14483	3462	80
H(12)	2556	12872	4191	66
H(14)	6167	14593	3668	75
H(15)	7256	14902	5093	91
H(16)	7527	13102	6880	77
H(19)	7584	11445	8468	83
H(20)	7261	9648	10256	89
H(21)	6297	7797	10340	71
H(22)	5596	7784	8686	59

<sup>a</sup> U(eq) is defined as one third of the trace of the orthogonalized  $U_{ij}$  tensor. The esd's of the least significant digits are given in parentheses.

### B.1.5. $[\text{Ru}_2(\text{bpy})_2(\text{CO})_4(\text{CH}_3\text{CN})_2](\text{PF}_6)_2 \cdot (\text{CH}_3\text{CN})_2 \mathbf{12}$ .

**Table B.25.** Atomic coordinates ( $\times 10^4$ ) and equivalent isotropic displacement parameters ( $\text{\AA}^2 \times 10^3$ ) for  $[\text{Ru}_2(\text{bpy})_2(\text{CO})_4(\text{CH}_3\text{CN})_2](\text{PF}_6)_2 \cdot (\text{CH}_3\text{CN})_2 \mathbf{12}$ .<sup>a</sup>

atom	x	y	z	U(eq)
Ru	4045(1)	5921(1)	7325(1)	52(1)
P	1721(2)	5300(2)	9421(2)	72(1)
N(1)	3927(5)	6527(4)	6166(5)	54(2)
N(2)	3998(5)	7051(5)	7721(5)	57(2)
N(3)	2597(6)	5957(5)	7024(5)	72(2)

atom	x	y	z	U(eq)
N(4)	8749(16)	2321(11)	2643(11)	200(9)
O(1)	4110(8)	4376(5)	6595(7)	132(4)
O(2)	4294(6)	5207(6)	9078(6)	118(4)
F(1)	2291(7)	4861(7)	8894(9)	190(5)
F(2)	1121(9)	5731(8)	9864(10)	224(7)
F(3)	955(8)	4751(6)	9162(13)	236(8)
F(4)	2464(9)	5837(9)	9645(15)	292(11)
F(5)	2113(12)	4806(14)	10107(11)	335(13)
F(6)	1274(10)	5715(12)	8642(9)	271(10)
C(1)	3872(7)	6243(7)	5375(7)	69(3)
C(2)	3748(8)	6658(8)	4641(7)	84(4)
C(3)	3666(9)	7410(8)	4712(9)	97(4)
C(4)	3698(9)	7748(8)	5507(9)	90(4)
C(5)	3830(7)	7288(6)	6224(7)	63(3)
C(6)	3854(7)	7574(6)	7088(7)	66(3)
C(7)	3728(11)	8324(7)	7264(10)	113(5)
C(8)	3734(13)	8525(10)	8076(13)	131(6)
C(9)	3878(12)	8007(11)	8721(11)	123(6)
C(10)	3998(8)	7274(8)	8508(8)	80(3)
C(11)	4080(8)	4955(7)	6883(8)	83(4)
C(12)	4198(7)	5479(7)	8407(8)	75(3)
C(13)	1857(8)	5895(6)	6850(7)	67(3)
C(14)	868(7)	5822(8)	6625(10)	99(4)
C(15)	8698(15)	2320(10)	1949(12)	139(7)
C(16)	8676(15)	2299(9)	1047(10)	162(9)

<sup>a</sup> U(eq) is defined as one third of the trace of the orthogonalized  $U_{ij}$  tensor. The esd's of the least significant digits are given in parentheses.

**Table B.26.** Interatomic lengths for  $[\text{Ru}_2(\text{bpy})_2(\text{CO})_4(\text{CH}_3\text{CN})_2](\text{PF}_6)_2 \cdot (\text{CH}_3\text{CN})_2$  **12**.<sup>a</sup>

bond	length/Å	bond	length/Å
Ru-C(11)	1.860(13)	N(3)-C(13)	1.101(12)
Ru-C(12)	1.858(11)	N(4)-C(15)	1.090(19)
Ru-N(1)	2.107(8)	O(1)-C(11)	1.132(14)
Ru-N(2)	2.110(8)	O(2)-C(12)	1.149(12)
Ru-N(3)	2.145(9)	C(1)-C(2)	1.357(15)
Ru-Ru <sup>b</sup>	2.8290(17)	C(2)-C(3)	1.349(17)
P-F(1)	1.557(10)	C(3)-C(4)	1.391(18)
P-F(2)	1.497(9)	C(4)-C(5)	1.379(15)
P-F(3)	1.500(11)	C(5)-C(6)	1.460(14)
P-F(4)	1.458(12)	C(6)-C(7)	1.383(16)
P-F(5)	1.416(12)	C(7)-C(8)	1.34(2)
P-F(6)	1.462(12)	C(8)-C(9)	1.36(2)
N(1)-C(1)	1.340(12)	C(9)-C(10)	1.37(2)
N(1)-C(5)	1.365(13)	C(13)-C(14)	1.469(16)
N(2)-C(6)	1.349(13)	C(15)-C(16)	1.43(2)
N(2)-C(10)	1.315(13)		

<sup>a</sup> The esd's of the least significant digits are given in parentheses. <sup>b</sup> Symmetry transformation used to generate equivalent atoms:  $-x+1, y, -z+3/2$

**Table B.27.** Bond angles for  $[\text{Ru}_2(\text{bpy})_2(\text{CO})_4(\text{CH}_3\text{CN})_2](\text{PF}_6)_2 \cdot (\text{CH}_3\text{CN})_2$  **12.**<sup>a</sup>

angle	degree/°	angle	degree/°
C(12)-Ru-C(11)	87.3(6)	F(6)-P-F(1)	90.0(9)
C(11)-Ru-N(1)	98.2(4)	F(6)-P-F(2)	86.0(9)
C(12)-Ru-N(1)	174.0(4)	F(6)-P-F(3)	85.6(10)
C(11)-Ru-N(2)	175.2(4)	C(1)-N(1)-C(5)	117.0(9)
C(12)-Ru-N(2)	97.5(5)	C(1)-N(1)-Ru	127.2(7)
N(1)-Ru-N(2)	77.0(3)	C(5)-N(1)-Ru	115.7(6)
C(11)-Ru-N(3)	93.7(5)	C(10)-N(2)-C(6)	117.9(10)
C(12)-Ru-N(3)	96.2(4)	C(10)-N(2)-Ru	125.4(8)
N(1)-Ru-N(3)	85.7(3)	C(6)-N(2)-Ru	116.3(6)
N(2)-Ru-N(3)	86.0(3)	N(1)-C(1)-C(2)	124.7(11)
C(11)-Ru-Ru <sup>b</sup>	87.2(4)	C(3)-C(2)-C(1)	117.5(12)
C(12)-Ru-Ru <sup>b</sup>	85.9(3)	C(2)-C(3)-C(4)	121.3(11)
N(1)-Ru-Ru <sup>b</sup>	92.1(2)	C(5)-C(4)-C(3)	117.8(12)
N(2)-Ru-Ru <sup>b</sup>	92.9(2)	N(1)-C(5)-C(4)	121.7(11)
N(3)-Ru-Ru <sup>b</sup>	177.7(2)	N(1)-C(5)-C(6)	115.5(9)
C(13)-N(3)-Ru	172.4(10)	C(4)-C(5)-C(6)	122.8(11)
F(2)-P-F(3)	86.3(7)	N(2)-C(6)-C(7)	121.1(11)
F(2)-P-F(1)	175.7(8)	N(2)-C(6)-C(5)	115.3(9)
F(3)-P-F(1)	91.5(6)	C(7)-C(6)-C(5)	123.6(11)
F(4)-P-F(1)	87.5(8)	C(8)-C(7)-C(6)	118.9(14)
F(4)-P-F(2)	94.5(8)	C(7)-C(8)-C(9)	120.9(15)
F(4)-P-F(3)	178.3(12)	C(8)-C(9)-C(10)	117.6(14)
F(4)-P-F(6)	93.0(12)	N(2)-C(10)-C(9)	123.6(13)
F(5)-P-F(1)	85.5(10)	O(1)-C(11)-Ru	177.9(14)
F(5)-P-F(2)	98.2(11)	O(2)-C(12)-Ru	179.7(13)
F(5)-P-F(3)	87.9(12)	N(3)-C(13)-C(14)	179.2(14)
F(5)-P-F(4)	93.4(12)	N(4)-C(15)-C(16)	177(3)
F(5)-P-F(6)	172.0(15)		

<sup>a</sup> The esd's of the least significant digits are given in parentheses. <sup>b</sup> Symmetry transformation used to generate equivalent atoms:  $-x+1, y, -z+3/2$

**Table B.28.** Dihedral angles for  $[\text{Ru}_2(\text{bpy})_2(\text{CO})_4(\text{CH}_3\text{CN})_2](\text{PF}_6)_2 \cdot (\text{CH}_3\text{CN})_2$  **12.**<sup>a</sup>

dihedral angle	degree/°	dihedral angle	degree/°
C(12)-Ru-N(3)-C(13)	-77(7)	Ru-N(1)-C(5)-C(4)	-176.5(9)
C(11)-Ru-N(3)-C(13)	10(7)	C(1)-N(1)-C(5)-C(6)	177.4(9)
N(1)-Ru-N(3)-C(13)	108(7)	Ru-N(1)-C(5)-C(6)	2.0(11)
N(2)-Ru-N(3)-C(13)	-175(7)	C(3)-C(4)-C(5)-N(1)	0.0(18)
Ru(1) <sup>b</sup> -Ru-N(3)-C(13)	125(7)	C(3)-C(4)-C(5)-C(6)	-178.5(12)
C(12)-Ru-N(1)-C(1)	159(4)	C(10)-N(2)-C(6)-C(7)	1.2(17)
C(11)-Ru-N(1)-C(1)	1.6(9)	Ru-N(2)-C(6)-C(7)	174.0(11)
N(2)-Ru-N(1)-C(1)	-178.4(8)	C(10)-N(2)-C(6)-C(5)	-177.9(9)
N(3)-Ru-N(1)-C(1)	-91.5(8)	Ru-N(2)-C(6)-C(5)	-5.1(12)
Ru(1) <sup>b</sup> -Ru-N(1)-C(1)	89.1(8)	N(1)-C(5)-C(6)-N(2)	2.0(14)
C(12)-Ru-N(1)-C(5)	-26(4)	C(4)-C(5)-C(6)-N(2)	-179.4(10)
C(11)-Ru-N(1)-C(5)	176.5(7)	N(1)-C(5)-C(6)-C(7)	-177.1(12)
N(2)-Ru-N(1)-C(5)	-3.5(7)	C(4)-C(5)-C(6)-C(7)	1.4(19)



dihedral angle	degree/°	dihedral angle	degree/°
N(3)-Ru-N(1)-C(5)	83.3(7)	N(2)-C(6)-C(7)-C(8)	-1(2)
Ru <sup>b</sup> -Ru-N(1)-C(5)	-96.0(7)	C(5)-C(6)-C(7)-C(8)	177.8(14)
C(12)-Ru-N(2)-C(10)	-5.4(9)	C(6)-C(7)-C(8)-C(9)	1(3)
C(11)-Ru-N(2)-C(10)	177(5)	C(7)-C(8)-C(9)-C(10)	-1(3)
N(1)-Ru-N(2)-C(10)	176.9(9)	C(6)-N(2)-C(10)-C(9)	-1.3(18)
N(3)-Ru-N(2)-C(10)	90.4(9)	Ru-N(2)-C(10)-C(9)	-173.4(11)
Ru(1) <sup>b</sup> -Ru-N(2)-C(10)	-91.6(8)	C(8)-C(9)-C(10)-N(2)	1(2)
C(12)-Ru-N(2)-C(6)	-177.6(8)	C(12)-Ru-C(11)-O(1)	-153(32)
C(11)-Ru-N(2)-C(6)	5(5)	N(1)-Ru-C(11)-O(1)	24(32)
N(1)-Ru-N(2)-C(6)	4.7(7)	N(2)-Ru-C(11)-O(1)	24(35)
N(3)-Ru-N(2)-C(6)	-81.8(7)	N(3)-Ru-C(11)-O(1)	110(32)
Ru(1) <sup>b</sup> -Ru-N(2)-C(6)	96.2(7)	Ru <sup>b</sup> -Ru-C(11)-O(1)	-67(32)
C(5)-N(1)-C(1)-C(2)	1.5(15)	C(11)-Ru-C(12)-O(2)	149(100)
Ru-N(1)-C(1)-C(2)	176.3(8)	N(1)-Ru-C(12)-O(2)	-8(100)
N(1)-C(1)-C(2)-C(3)	-0.6(19)	N(2)-Ru-C(12)-O(2)	-30(100)
C(1)-C(2)-C(3)-C(4)	-1(2)	N(3)-Ru-C(12)-O(2)	-117(100)
C(2)-C(3)-C(4)-C(5)	1(2)	Ru <sup>b</sup> -Ru-C(12)-O(2)	62(100)
C(1)-N(1)-C(5)-C(4)	-1.1(15)	Ru-N(3)-C(13)-C(14)	158(100)

<sup>a</sup> The esd's of the least significant digits are given in parentheses. Symmetry transformations used to generate equivalent atoms: <sup>b</sup> (-x+1,y,-z+3/2).

**Table B.29.** Anisotropic displacement parameters ( $\text{\AA}^2 \times 10^3$ ) for  $[\text{Ru}_2(\text{bpy})_2(\text{CO})_4(\text{CH}_3\text{CN})_2](\text{PF}_6)_2 \cdot (\text{CH}_3\text{CN})_2$  **12**.<sup>a</sup>

atom	U <sub>11</sub>	U <sub>22</sub>	U <sub>33</sub>	U <sub>23</sub>	U <sub>13</sub>	U <sub>12</sub>
Ru	52(1)	44(1)	54(1)	7(1)	0(1)	-4(1)
P	78(2)	61(2)	68(2)	-3(2)	-3(2)	12(2)
N(1)	51(4)	57(5)	52(5)	4(4)	7(4)	11(4)
N(2)	65(5)	55(5)	49(5)	-9(4)	13(4)	3(4)
N(3)	61(6)	89(7)	57(5)	17(5)	2(4)	-7(5)
N(4)	330(30)	181(18)	97(11)	-8(12)	69(15)	30(17)
O(1)	151(9)	48(5)	157(10)	-22(6)	-38(7)	-1(6)
O(2)	91(6)	152(10)	101(7)	68(7)	4(5)	-5(6)
F(1)	142(8)	177(11)	278(15)	-90(10)	104(9)	-11(8)
F(2)	191(11)	237(14)	265(15)	-156(12)	100(11)	15(10)
F(3)	137(9)	99(8)	490(30)	-96(12)	114(13)	-30(7)
F(4)	133(10)	208(14)	500(30)	-184(18)	-1(13)	-58(9)
F(5)	232(17)	520(30)	243(16)	270(20)	36(13)	110(20)
F(6)	195(13)	440(30)	175(12)	164(15)	38(10)	74(15)
C(1)	78(7)	67(7)	63(7)	1(6)	17(6)	4(6)
C(2)	90(8)	109(11)	49(7)	11(7)	9(6)	-6(8)
C(3)	119(11)	83(10)	74(9)	41(8)	-2(8)	0(8)
C(4)	112(10)	67(8)	86(9)	31(7)	18(8)	15(7)
C(5)	61(6)	58(7)	66(7)	2(6)	5(5)	13(5)
C(6)	84(7)	46(6)	67(7)	-6(5)	19(6)	5(5)
C(7)	170(15)	57(8)	115(12)	-6(8)	38(11)	29(9)
C(8)	175(17)	88(12)	135(15)	-48(11)	45(14)	29(11)
C(9)	151(15)	136(16)	85(11)	-32(11)	36(10)	19(12)

atom	U <sub>11</sub>	U <sub>22</sub>	U <sub>33</sub>	U <sub>23</sub>	U <sub>13</sub>	U <sub>12</sub>
C(10)	83(8)	84(9)	72(8)	-15(7)	15(6)	11(7)
C(11)	82(8)	52(7)	91(9)	3(7)	-28(6)	-7(6)
C(12)	61(6)	84(8)	73(8)	35(7)	1(6)	-18(6)
C(13)	60(7)	73(7)	64(7)	7(6)	10(5)	7(6)
C(14)	51(6)	114(11)	123(11)	0(9)	5(7)	-14(7)
C(15)	220(20)	102(13)	88(11)	13(10)	34(13)	51(13)
C(16)	300(30)	88(12)	97(12)	31(10)	41(14)	29(14)

<sup>a</sup> The esd's of the least significant digits are given in parentheses. The anisotropic displacement factor exponent takes the form:  $-2 \pi^2 [h^2 a^{*2} U_{11} + \dots + 2 h k a^* b^* U_{12}]$ .

**Table B.30.** Hydrogen coordinates ( $\times 10^4$ ) and isotropic displacement parameters ( $\text{\AA}^2 \times 10^3$ ) for  $[\text{Ru}_2(\text{bpy})_2(\text{CO})_4(\text{CH}_3\text{CN})_2](\text{PF}_6)_2 \cdot (\text{CH}_3\text{CN})_2$  **12**.<sup>a</sup>

atom	x	y	z	U(eq)
H(1)	3923	5723	5327	83
H(2)	3720	6432	4108	101
H(3)	3586	7709	4220	116
H(4)	3632	8266	5552	108
H(7)	3641	8682	6826	136
H(8)	3638	9026	8198	157
H(9)	3895	8145	9288	147
H(10)	4084	6913	8944	97
H(14A)	598	6305	6459	148
H(14B)	674	5638	7117	148
H(14C)	684	5475	6153	148
H(16A)	9256	2146	974	243
H(16B)	8533	2791	801	243
H(16C)	8225	1946	760	243

<sup>a</sup> U(eq) is defined as one third of the trace of the orthogonalized U<sub>ij</sub> tensor.

### B.1.6. *cis*(Ph<sub>2</sub>Ppyqn)-[Ru<sub>2</sub>(μ-Ph<sub>2</sub>Ppyqn)<sub>2</sub>(CO)<sub>2</sub>(CH<sub>3</sub>CN)<sub>2</sub>](PF<sub>6</sub>)<sub>2</sub>, *cis*(Ph<sub>2</sub>Ppyqn)-19

**Table B.31.** Atomic coordinates ( $\times 10^4$ ) and equivalent isotropic displacement parameters ( $\text{\AA}^2 \times 10^3$ ) for  $[\text{Ru}_2(\mu\text{-Ph}_2\text{Ppyqn})_2(\text{CO})_2(\text{CH}_3\text{CN})_2](\text{PF}_6)_2$  **19**.<sup>a</sup>

atom	x	y	z	U(eq)
Ru(1)	1575(1)	3120(1)	5584(1)	31(1)
Ru(2)	2783(1)	2439(1)	6188(1)	30(1)
P(1)	3106(1)	3936(1)	6100(1)	34(1)
P(2)	1866(1)	2307(1)	4721(1)	32(1)
N(1)	2038(2)	4331(3)	5240(2)	34(1)
N(2)	749(2)	3854(3)	4987(2)	39(1)
N(3)	3146(2)	2044(3)	5295(2)	31(1)
N(4)	3829(2)	1910(3)	6463(2)	37(1)
N(5)	1347(2)	3858(3)	6398(2)	39(1)
N(6)	2434(2)	1060(4)	6184(2)	40(1)



atom	x	y	z	U(eq)
O(1)	930(2)	1461(3)	6118(2)	57(1)
O(2)	2284(2)	2887(3)	7445(2)	51(1)
C(1)	3987(3)	4082(4)	5928(3)	40(1)
C(2)	4159(3)	3875(4)	5314(3)	49(2)
C(3)	4819(4)	3873(5)	5192(3)	58(2)
C(4)	5325(4)	4065(5)	5667(4)	62(2)
C(5)	5162(3)	4286(5)	6270(4)	63(2)
C(6)	4499(3)	4291(5)	6402(3)	50(2)
C(7)	3012(3)	4731(4)	6765(2)	36(1)
C(8)	3297(3)	4507(4)	7381(3)	49(2)
C(9)	3224(4)	5090(5)	7889(3)	61(2)
C(10)	2867(4)	5895(5)	7804(3)	63(2)
C(11)	2569(4)	6121(5)	7204(4)	62(2)
C(12)	2650(3)	5545(4)	6687(3)	52(2)
C(13)	2673(3)	4607(4)	5431(3)	38(1)
C(14)	2953(3)	5386(4)	5175(3)	48(2)
C(15)	2572(3)	5897(4)	4712(3)	52(2)
C(16)	1928(3)	5618(4)	4520(3)	48(2)
C(17)	1665(3)	4839(4)	4788(2)	38(1)
C(18)	972(3)	4502(4)	4614(3)	39(1)
C(19)	590(3)	4827(5)	4054(3)	52(2)
C(20)	-20(3)	4446(5)	3883(3)	57(2)
C(21)	-298(3)	3813(5)	4284(3)	50(2)
C(22)	-950(4)	3423(6)	4154(4)	66(2)
C(23)	-1214(4)	2862(6)	4570(4)	67(2)
C(24)	-842(3)	2665(5)	5164(4)	61(2)
C(25)	-203(3)	3000(4)	5309(3)	50(2)
C(26)	93(3)	3551(4)	4861(3)	41(1)
C(27)	1743(3)	2917(4)	3940(3)	40(1)
C(28)	2205(3)	3586(4)	3801(3)	49(2)
C(29)	2100(4)	4091(5)	3232(3)	63(2)
C(30)	1526(5)	3941(5)	2817(3)	68(2)
C(31)	1078(4)	3283(5)	2949(3)	60(2)
C(32)	1174(3)	2774(4)	3512(3)	47(2)
C(33)	1439(3)	1204(4)	4530(2)	37(1)
C(34)	1756(3)	415(4)	4343(3)	47(2)
C(35)	1385(4)	-351(4)	4129(3)	56(2)
C(36)	695(4)	-338(5)	4105(3)	62(2)
C(37)	374(3)	427(5)	4301(3)	59(2)
C(38)	742(3)	1194(4)	4523(3)	49(2)
C(39)	2762(3)	2006(4)	4725(3)	36(1)
C(40)	3042(3)	1752(4)	4169(3)	44(1)
C(41)	3708(3)	1509(5)	4201(3)	52(2)
C(42)	4092(3)	1516(4)	4785(3)	45(2)
C(43)	3805(3)	1798(4)	5329(3)	39(1)
C(44)	4186(3)	1820(4)	5964(3)	38(1)
C(45)	4899(3)	1763(4)	6032(3)	50(2)
C(46)	5240(3)	1786(5)	6620(3)	56(2)
C(47)	4883(3)	1805(4)	7161(3)	49(2)

atom	x	y	z	U(eq)
C(48)	5216(4)	1756(5)	7792(3)	66(2)
C(49)	4853(4)	1719(6)	8294(4)	78(2)
C(50)	4156(4)	1713(5)	8214(3)	68(2)
C(51)	3808(4)	1791(5)	7609(3)	55(2)
C(52)	4171(3)	1850(4)	7066(3)	40(1)
C(53)	1231(3)	4147(4)	6872(3)	45(1)
C(54)	1097(4)	4497(5)	7510(3)	68(2)
C(55)	2212(3)	347(4)	6135(3)	43(1)
C(56)	1896(4)	-564(5)	6062(4)	71(2)
C(57)	1181(3)	2095(4)	5903(3)	40(1)
C(58)	2459(3)	2725(4)	6955(3)	36(1)
P(3)	3429(1)	8536(2)	4926(1)	63(1)
P(4)	873(1)	7079(2)	2656(1)	69(1)
F(1)	3655(3)	7661(4)	4557(3)	123(2)
F(2)	3212(3)	9418(4)	5283(3)	117(2)
F(3)	2694(3)	8358(6)	4617(4)	152(3)
F(4)	4166(2)	8663(5)	5246(3)	118(2)
F(5)	3615(5)	9126(5)	4349(3)	153(3)
F(6)	3243(4)	7936(5)	5495(3)	146(3)
F(7)	1472(3)	7034(5)	2230(3)	119(2)
F(8A)	380(4)	7370(11)	3120(2)	160(2)
F(8B)	230(2)	6980(6)	3040(3)	145(14)
F(9A)	1405(13)	7460(3)	3230(2)	147(13)
F(9B)	1300(14)	6870(5)	3260(2)	145(19)
F(10)	373(4)	6948(7)	2051(3)	162(3)
F(11)	826(5)	8125(4)	2541(4)	173(3)
F(12)	944(8)	6053(6)	2764(7)	257(6)
O(3)	3873(4)	8976(6)	7405(3)	117(2)
C(59)	3209(6)	8805(11)	7454(6)	138(5)
C(60)	3059(5)	8559(8)	8124(5)	110(3)
C(61)	4039(7)	9217(9)	6797(5)	124(4)
C(62)	4783(7)	9309(7)	6807(5)	113(4)

<sup>a</sup> U(eq) is defined as one third of the trace of the orthogonalized  $U_{ij}$  tensor. The esd's of the least significant digits are given in parentheses.

**Table B.32.** Interatomic lengths for *cis*(Ph<sub>2</sub>Ppyqn)-[Ru<sub>2</sub>(μ-Ph<sub>2</sub>Ppyqn)<sub>2</sub>(CO)<sub>2</sub>(CH<sub>3</sub>CN)<sub>2</sub>](PF<sub>6</sub>)<sub>2</sub>, *cis*(Ph<sub>2</sub>Ppyqn)-19.<sup>a</sup>

bond	length/Å	bond	length/Å
Ru(1)-C(57)	1.828(7)	C(23)-C(24)	1.407(11)
Ru(1)-N(5)	2.096(5)	C(24)-C(25)	1.364(9)
Ru(1)-N(1)	2.132(5)	C(25)-C(26)	1.402(9)
Ru(1)-N(2)	2.225(5)	C(27)-C(32)	1.385(9)
Ru(1)-P(2)	2.2747(19)	C(27)-C(28)	1.383(9)
Ru(1)-Ru(2)	2.778(2)	C(28)-C(29)	1.391(9)
Ru(2)-C(58)	1.836(6)	C(29)-C(30)	1.379(11)
Ru(2)-N(6)	2.103(6)	C(30)-C(31)	1.349(11)
Ru(2)-N(3)	2.148(4)	C(31)-C(32)	1.381(9)

bond	length/Å	bond	length/Å
Ru(2)-N(4)	2.235(5)	C(33)-C(34)	1.375(8)
Ru(2)-P(1)	2.262(2)	C(33)-C(38)	1.387(8)
P(1)-C(7)	1.826(5)	C(34)-C(35)	1.377(9)
P(1)-C(1)	1.837(6)	C(35)-C(36)	1.369(10)
P(1)-C(13)	1.840(6)	C(36)-C(37)	1.360(10)
P(2)-C(33)	1.825(6)	C(37)-C(38)	1.378(9)
P(2)-C(39)	1.834(6)	C(39)-C(40)	1.389(8)
P(2)-C(27)	1.849(6)	C(40)-C(41)	1.366(9)
N(1)-C(13)	1.345(7)	C(41)-C(42)	1.373(9)
N(1)-C(17)	1.356(7)	C(42)-C(43)	1.386(8)
N(2)-C(18)	1.322(7)	C(43)-C(44)	1.459(8)
N(2)-C(26)	1.378(8)	C(44)-C(45)	1.413(8)
N(3)-C(39)	1.348(7)	C(45)-C(46)	1.342(9)
N(3)-C(43)	1.353(7)	C(46)-C(47)	1.398(9)
N(4)-C(44)	1.328(7)	C(47)-C(52)	1.412(9)
N(4)-C(52)	1.373(7)	C(47)-C(48)	1.415(9)
N(5)-C(53)	1.122(7)	C(48)-C(49)	1.336(11)
N(6)-C(55)	1.119(7)	C(49)-C(50)	1.379(11)
O(1)-C(57)	1.155(7)	C(50)-C(51)	1.383(9)
O(2)-C(58)	1.138(6)	C(51)-C(52)	1.410(9)
C(1)-C(6)	1.379(9)	C(53)-C(54)	1.475(9)
C(1)-C(2)	1.395(8)	C(55)-C(56)	1.455(9)
C(2)-C(3)	1.364(9)	P(3)-F(6)	1.547(6)
C(3)-C(4)	1.368(10)	P(3)-F(5)	1.551(6)
C(4)-C(5)	1.371(10)	P(3)-F(3)	1.559(6)
C(5)-C(6)	1.376(9)	P(3)-F(2)	1.556(5)
C(7)-C(12)	1.377(8)	P(3)-F(4)	1.559(5)
C(7)-C(8)	1.389(8)	P(3)-F(1)	1.567(5)
C(8)-C(9)	1.373(9)	P(4)-F(12)	1.499(8)
C(9)-C(10)	1.362(10)	P(4)-F(9B)	1.48(3)
C(10)-C(11)	1.371(10)	P(4)-F(11)	1.526(7)
C(11)-C(12)	1.384(9)	P(4)-F(10)	1.539(7)
C(13)-C(14)	1.384(8)	P(4)-F(7)	1.562(6)
C(14)-C(15)	1.380(9)	P(4)-F(8B)	1.58(3)
C(15)-C(16)	1.363(9)	P(4)-F(8A)	1.51(4)
C(16)-C(17)	1.381(8)	P(4)-F(9A)	1.611(19)
C(17)-C(18)	1.472(8)	F(8A)-F(8B)	0.64(11)
C(18)-C(19)	1.409(8)	F(9A)-F(9B)	0.88(3)
C(19)-C(20)	1.346(10)	F(9B)-F(12)	1.68(8)
C(20)-C(21)	1.390(10)	O(3)-C(59)	1.357(13)
C(21)-C(26)	1.418(8)	O(3)-C(61)	1.390(12)
C(21)-C(22)	1.415(10)	C(59)-C(60)	1.505(14)
C(22)-C(23)	1.334(11)	C(61)-C(62)	1.485(15)

<sup>a</sup> The esd's of the least significant digits are given in parentheses.

**Table B.33.** Bond angles for *cis*(Ph<sub>2</sub>Ppyqn)-[Ru<sub>2</sub>(μ-Ph<sub>2</sub>Ppyqn)<sub>2</sub>(CO)<sub>2</sub>(CH<sub>3</sub>CN)<sub>2</sub>](PF<sub>6</sub>)<sub>2</sub>, *cis*(Ph<sub>2</sub>Ppyqn)-19.<sup>a</sup>

angle	degree/°	angle	degree/°
C(57)-Ru(1)-N(5)	88.6(2)	C(32)-C(27)-P(2)	121.7(5)
C(57)-Ru(1)-N(1)	178.3(2)	C(28)-C(27)-P(2)	119.1(5)
N(5)-Ru(1)-N(1)	89.76(18)	C(29)-C(28)-C(27)	119.9(7)
C(57)-Ru(1)-N(2)	105.6(2)	C(28)-C(29)-C(30)	119.9(7)
N(5)-Ru(1)-N(2)	90.28(17)	C(31)-C(30)-C(29)	120.2(7)
N(1)-Ru(1)-N(2)	75.10(18)	C(30)-C(31)-C(32)	120.7(7)
C(57)-Ru(1)-P(2)	91.61(19)	C(27)-C(32)-C(31)	120.3(7)
N(5)-Ru(1)-P(2)	177.59(13)	C(34)-C(33)-C(38)	118.4(5)
N(1)-Ru(1)-P(2)	89.95(13)	C(34)-C(33)-P(2)	124.3(4)
N(2)-Ru(1)-P(2)	91.96(13)	C(38)-C(33)-P(2)	117.0(4)
C(57)-Ru(1)-Ru(2)	86.16(18)	C(33)-C(34)-C(35)	120.5(6)
N(5)-Ru(1)-Ru(2)	93.39(13)	C(34)-C(35)-C(36)	120.3(6)
N(1)-Ru(1)-Ru(2)	93.27(13)	C(37)-C(36)-C(35)	120.1(6)
N(2)-Ru(1)-Ru(2)	167.79(13)	C(36)-C(37)-C(38)	120.0(6)
P(2)-Ru(1)-Ru(2)	84.23(7)	C(37)-C(38)-C(33)	120.6(6)
C(58)-Ru(2)-N(6)	94.0(2)	N(3)-C(39)-C(40)	120.6(5)
C(58)-Ru(2)-N(3)	177.5(2)	N(3)-C(39)-P(2)	117.3(4)
N(6)-Ru(2)-N(3)	83.55(17)	C(40)-C(39)-P(2)	122.1(4)
C(58)-Ru(2)-N(4)	104.7(2)	C(41)-C(40)-C(39)	119.9(6)
N(6)-Ru(2)-N(4)	88.77(18)	C(40)-C(41)-C(42)	119.3(5)
N(3)-Ru(2)-N(4)	75.25(17)	C(41)-C(42)-C(43)	119.6(5)
C(58)-Ru(2)-P(1)	89.20(18)	N(3)-C(43)-C(42)	120.8(5)
N(6)-Ru(2)-P(1)	174.63(13)	N(3)-C(43)-C(44)	117.0(5)
N(3)-Ru(2)-P(1)	93.25(12)	C(42)-C(43)-C(44)	122.2(5)
N(4)-Ru(2)-P(1)	94.60(13)	N(4)-C(44)-C(45)	122.6(5)
C(58)-Ru(2)-Ru(1)	87.26(18)	N(4)-C(44)-C(43)	116.4(5)
N(6)-Ru(2)-Ru(1)	93.48(14)	C(45)-C(44)-C(43)	120.9(5)
N(3)-Ru(2)-Ru(1)	92.92(13)	C(46)-C(45)-C(44)	120.0(6)
N(4)-Ru(2)-Ru(1)	167.64(11)	C(45)-C(46)-C(47)	119.3(6)
P(1)-Ru(2)-Ru(1)	82.35(6)	C(46)-C(47)-C(52)	118.3(6)
C(7)-P(1)-C(1)	104.6(3)	C(46)-C(47)-C(48)	121.7(6)
C(7)-P(1)-C(13)	100.0(3)	C(52)-C(47)-C(48)	120.0(6)
C(1)-P(1)-C(13)	100.0(3)	C(49)-C(48)-C(47)	119.7(7)
C(7)-P(1)-Ru(2)	118.84(19)	C(48)-C(49)-C(50)	121.6(7)
C(1)-P(1)-Ru(2)	114.19(18)	C(49)-C(50)-C(51)	120.9(7)
C(13)-P(1)-Ru(2)	116.60(19)	C(52)-C(51)-C(50)	119.4(7)
C(33)-P(2)-C(39)	103.1(3)	N(4)-C(52)-C(47)	121.8(5)
C(33)-P(2)-C(27)	101.8(3)	N(4)-C(52)-C(51)	119.8(6)
C(39)-P(2)-C(27)	99.0(3)	C(47)-C(52)-C(51)	118.3(6)
C(33)-P(2)-Ru(1)	118.06(18)	N(5)-C(53)-C(54)	177.5(6)
C(39)-P(2)-Ru(1)	116.41(19)	N(6)-C(55)-C(56)	177.6(7)
C(27)-P(2)-Ru(1)	115.73(19)	O(1)-C(57)-Ru(1)	178.3(5)
C(13)-N(1)-C(17)	118.5(5)	O(2)-C(58)-Ru(2)	176.9(5)
C(13)-N(1)-Ru(1)	124.7(4)	F(6)-P(3)-F(5)	179.3(4)
C(17)-N(1)-Ru(1)	116.8(4)	F(6)-P(3)-F(3)	86.4(4)
C(18)-N(2)-C(26)	118.7(5)	F(5)-P(3)-F(3)	93.3(5)

angle	degree/°	angle	degree/°
C(18)-N(2)-Ru(1)	113.2(4)	F(6)-P(3)-F(2)	89.2(4)
C(26)-N(2)-Ru(1)	126.0(4)	F(5)-P(3)-F(2)	91.5(4)
C(39)-N(3)-C(43)	119.7(4)	F(3)-P(3)-F(2)	92.1(4)
C(39)-N(3)-Ru(2)	124.6(3)	F(6)-P(3)-F(4)	91.4(4)
C(43)-N(3)-Ru(2)	115.7(4)	F(5)-P(3)-F(4)	88.9(4)
C(44)-N(4)-C(52)	117.4(5)	F(3)-P(3)-F(4)	177.1(5)
C(44)-N(4)-Ru(2)	113.1(4)	F(2)-P(3)-F(4)	89.6(3)
C(52)-N(4)-Ru(2)	128.2(4)	F(6)-P(3)-F(1)	91.9(4)
C(53)-N(5)-Ru(1)	171.2(5)	F(5)-P(3)-F(1)	87.4(4)
C(55)-N(6)-Ru(2)	173.9(5)	F(3)-P(3)-F(1)	88.2(3)
C(6)-C(1)-C(2)	118.2(6)	F(2)-P(3)-F(1)	178.8(4)
C(6)-C(1)-P(1)	122.3(4)	F(4)-P(3)-F(1)	90.0(3)
C(2)-C(1)-P(1)	119.0(5)	F(12)-P(4)-F(9B)	69(3)
C(3)-C(2)-C(1)	120.5(6)	F(12)-P(4)-F(11)	178.0(7)
C(4)-C(3)-C(2)	120.9(6)	F(9B)-P(4)-F(11)	111(3)
C(3)-C(4)-C(5)	119.3(6)	F(12)-P(4)-F(10)	92.6(8)
C(6)-C(5)-C(4)	120.5(7)	F(9B)-P(4)-F(10)	161(3)
C(5)-C(6)-C(1)	120.6(6)	F(11)-P(4)-F(10)	88.1(5)
C(12)-C(7)-C(8)	117.8(5)	F(12)-P(4)-F(7)	88.8(5)
C(12)-C(7)-P(1)	122.4(4)	F(9B)-P(4)-F(7)	94.1(12)
C(8)-C(7)-P(1)	119.8(4)	F(11)-P(4)-F(7)	89.4(4)
C(7)-C(8)-C(9)	120.6(6)	F(10)-P(4)-F(7)	89.5(4)
C(10)-C(9)-C(8)	121.0(6)	F(12)-P(4)-F(8B)	85(3)
C(9)-C(10)-C(11)	119.5(6)	F(9B)-P(4)-F(8B)	89(2)
C(10)-C(11)-C(12)	119.9(6)	F(11)-P(4)-F(8B)	97(3)
C(7)-C(12)-C(11)	121.2(6)	F(10)-P(4)-F(8B)	85(3)
N(1)-C(13)-C(14)	122.0(5)	F(7)-P(4)-F(8B)	171(3)
N(1)-C(13)-P(1)	114.9(4)	F(12)-P(4)-F(8A)	103(6)
C(14)-C(13)-P(1)	122.9(5)	F(9B)-P(4)-F(8A)	82(3)
C(13)-C(14)-C(15)	119.2(6)	F(11)-P(4)-F(8A)	78(6)
C(16)-C(15)-C(14)	118.9(6)	F(10)-P(4)-F(8A)	99(3)
C(15)-C(16)-C(17)	120.2(6)	F(7)-P(4)-F(8A)	165(6)
N(1)-C(17)-C(16)	121.2(6)	F(8B)-P(4)-F(8A)	24(4)
N(1)-C(17)-C(18)	115.3(5)	F(12)-P(4)-F(9A)	100(2)
C(16)-C(17)-C(18)	123.5(5)	F(9B)-P(4)-F(9A)	32.8(12)
N(2)-C(18)-C(19)	122.7(6)	F(11)-P(4)-F(9A)	79(2)
N(2)-C(18)-C(17)	116.7(5)	F(10)-P(4)-F(9A)	166(2)
C(19)-C(18)-C(17)	120.5(5)	F(7)-P(4)-F(9A)	87.5(14)
C(20)-C(19)-C(18)	118.6(6)	F(8B)-P(4)-F(9A)	99(3)
C(19)-C(20)-C(21)	120.8(6)	F(8A)-P(4)-F(9A)	81(4)
C(20)-C(21)-C(26)	118.1(6)	F(8B)-F(8A)-P(4)	84(7)
C(20)-C(21)-C(22)	124.0(6)	F(8A)-F(8B)-P(4)	72(6)
C(26)-C(21)-C(22)	117.9(7)	F(9B)-F(9A)-P(4)	65(3)
C(23)-C(22)-C(21)	122.1(7)	F(9A)-F(9B)-P(4)	82(2)
C(22)-C(23)-C(24)	119.4(7)	F(9A)-F(9B)-F(12)	136(5)
C(25)-C(24)-C(23)	121.2(7)	P(4)-F(9B)-F(12)	56(2)
C(24)-C(25)-C(26)	119.9(6)	P(4)-F(12)-F(9B)	55.1(11)
N(2)-C(26)-C(25)	120.5(5)	C(59)-O(3)-C(61)	116.1(9)
N(2)-C(26)-C(21)	120.2(6)	O(3)-C(59)-C(60)	113.6(9)

angle	degree/°	angle	degree/°
C(25)-C(26)-C(21)	119.2(6)	O(3)-C(61)-C(62)	109.9(9)
C(32)-C(27)-C(28)	119.0(6)		

<sup>a</sup> The esd's of the least significant digits are given in parentheses.

**Table B.34.** Dihedral angles for *cis*(Ph<sub>2</sub>Ppyqn)-[Ru<sub>2</sub>(μ-Ph<sub>2</sub>Ppyqn)<sub>2</sub>(CO)<sub>2</sub>(CH<sub>3</sub>CN)<sub>2</sub>](PF<sub>6</sub>)<sub>2</sub>, *cis*(Ph<sub>2</sub>Ppyqn)-19.<sup>a</sup>

dihedral angle	degree/°	dihedral angle	degree/°
C(57)-Ru(1)-Ru(2)-C(58)	-69.8(3)	C(26)-N(2)-C(18)-C(17)	176.9(5)
N(5)-Ru(1)-Ru(2)-C(58)	18.6(2)	Ru(1)-N(2)-C(18)-C(17)	-18.8(6)
N(1)-Ru(1)-Ru(2)-C(58)	108.5(2)	N(1)-C(17)-C(18)-N(2)	11.5(7)
N(2)-Ru(1)-Ru(2)-C(58)	125.9(6)	C(16)-C(17)-C(18)-N(2)	-168.2(5)
P(2)-Ru(1)-Ru(2)-C(58)	-161.86(18)	N(1)-C(17)-C(18)-C(19)	-165.0(5)
C(57)-Ru(1)-Ru(2)-N(6)	24.0(2)	C(16)-C(17)-C(18)-C(19)	15.3(8)
N(5)-Ru(1)-Ru(2)-N(6)	112.41(18)	N(2)-C(18)-C(19)-C(20)	-1.7(9)
N(1)-Ru(1)-Ru(2)-N(6)	-157.64(17)	C(17)-C(18)-C(19)-C(20)	174.6(5)
N(2)-Ru(1)-Ru(2)-N(6)	-140.3(6)	C(18)-C(19)-C(20)-C(21)	6.5(9)
P(2)-Ru(1)-Ru(2)-N(6)	-68.02(14)	C(19)-C(20)-C(21)-C(26)	-2.8(9)
C(57)-Ru(1)-Ru(2)-N(3)	107.7(2)	C(19)-C(20)-C(21)-C(22)	176.4(6)
N(5)-Ru(1)-Ru(2)-N(3)	-163.89(17)	C(20)-C(21)-C(22)-C(23)	-175.7(7)
N(1)-Ru(1)-Ru(2)-N(3)	-73.93(16)	C(26)-C(21)-C(22)-C(23)	3.4(10)
N(2)-Ru(1)-Ru(2)-N(3)	-56.6(6)	C(21)-C(22)-C(23)-C(24)	1.5(11)
P(2)-Ru(1)-Ru(2)-N(3)	15.69(12)	C(22)-C(23)-C(24)-C(25)	-3.3(10)
C(57)-Ru(1)-Ru(2)-N(4)	124.2(6)	C(23)-C(24)-C(25)-C(26)	0.0(10)
N(5)-Ru(1)-Ru(2)-N(4)	-147.4(6)	C(18)-N(2)-C(26)-C(25)	-168.0(5)
N(1)-Ru(1)-Ru(2)-N(4)	-57.4(6)	Ru(1)-N(2)-C(26)-C(25)	29.9(7)
N(2)-Ru(1)-Ru(2)-N(4)	-40.1(8)	C(18)-N(2)-C(26)-C(21)	10.4(8)
P(2)-Ru(1)-Ru(2)-N(4)	32.2(5)	Ru(1)-N(2)-C(26)-C(21)	-151.8(4)
C(57)-Ru(1)-Ru(2)-P(1)	-159.41(18)	C(24)-C(25)-C(26)-N(2)	-176.6(5)
N(5)-Ru(1)-Ru(2)-P(1)	-71.00(14)	C(24)-C(25)-C(26)-C(21)	5.0(9)
N(1)-Ru(1)-Ru(2)-P(1)	18.96(12)	C(20)-C(21)-C(26)-N(2)	-5.8(8)
N(2)-Ru(1)-Ru(2)-P(1)	36.3(5)	C(22)-C(21)-C(26)-N(2)	175.0(5)
P(2)-Ru(1)-Ru(2)-P(1)	108.58(7)	C(20)-C(21)-C(26)-C(25)	172.6(6)
C(58)-Ru(2)-P(1)-C(7)	5.2(3)	C(22)-C(21)-C(26)-C(25)	-6.6(8)
N(6)-Ru(2)-P(1)-C(7)	131.8(14)	C(33)-P(2)-C(27)-C(32)	31.6(5)
N(3)-Ru(2)-P(1)-C(7)	-175.0(2)	C(39)-P(2)-C(27)-C(32)	137.1(5)
N(4)-Ru(2)-P(1)-C(7)	-99.5(2)	Ru(1)-P(2)-C(27)-C(32)	-97.7(5)
Ru(1)-Ru(2)-P(1)-C(7)	92.5(2)	C(33)-P(2)-C(27)-C(28)	-153.4(5)
C(58)-Ru(2)-P(1)-C(1)	129.4(3)	C(39)-P(2)-C(27)-C(28)	-47.9(5)
N(6)-Ru(2)-P(1)-C(1)	-104.0(14)	Ru(1)-P(2)-C(27)-C(28)	77.3(5)
N(3)-Ru(2)-P(1)-C(1)	-50.8(2)	C(32)-C(27)-C(28)-C(29)	-1.1(9)
N(4)-Ru(2)-P(1)-C(1)	24.7(2)	P(2)-C(27)-C(28)-C(29)	-176.3(5)
Ru(1)-Ru(2)-P(1)-C(1)	-143.3(2)	C(27)-C(28)-C(29)-C(30)	1.8(10)
C(58)-Ru(2)-P(1)-C(13)	-114.6(3)	C(28)-C(29)-C(30)-C(31)	-2.4(10)
N(6)-Ru(2)-P(1)-C(13)	12.0(14)	C(29)-C(30)-C(31)-C(32)	2.3(11)
N(3)-Ru(2)-P(1)-C(13)	65.2(2)	C(28)-C(27)-C(32)-C(31)	1.0(9)
N(4)-Ru(2)-P(1)-C(13)	140.7(2)	P(2)-C(27)-C(32)-C(31)	176.0(5)

dihedral angle	degree/°	dihedral angle	degree/°
Ru(1)-Ru(2)-P(1)-C(13)	-27.3(2)	C(30)-C(31)-C(32)-C(27)	-1.6(10)
C(57)-Ru(1)-P(2)-C(33)	17.3(3)	C(39)-P(2)-C(33)-C(34)	-8.7(5)
N(5)-Ru(1)-P(2)-C(33)	113(3)	C(27)-P(2)-C(33)-C(34)	93.6(5)
N(1)-Ru(1)-P(2)-C(33)	-163.4(2)	Ru(1)-P(2)-C(33)-C(34)	-138.6(4)
N(2)-Ru(1)-P(2)-C(33)	-88.3(2)	C(39)-P(2)-C(33)-C(38)	176.8(4)
Ru(2)-Ru(1)-P(2)-C(33)	103.3(2)	C(27)-P(2)-C(33)-C(38)	-80.9(5)
C(57)-Ru(1)-P(2)-C(39)	-106.1(3)	Ru(1)-P(2)-C(33)-C(38)	46.9(5)
N(5)-Ru(1)-P(2)-C(39)	-10(3)	C(38)-C(33)-C(34)-C(35)	2.7(9)
N(1)-Ru(1)-P(2)-C(39)	73.1(2)	P(2)-C(33)-C(34)-C(35)	-171.7(5)
N(2)-Ru(1)-P(2)-C(39)	148.2(2)	C(33)-C(34)-C(35)-C(36)	-0.5(10)
Ru(2)-Ru(1)-P(2)-C(39)	-20.2(2)	C(34)-C(35)-C(36)-C(37)	-1.0(11)
C(57)-Ru(1)-P(2)-C(27)	138.2(3)	C(35)-C(36)-C(37)-C(38)	0.3(11)
N(5)-Ru(1)-P(2)-C(27)	-126(3)	C(36)-C(37)-C(38)-C(33)	2.0(10)
N(1)-Ru(1)-P(2)-C(27)	-42.5(3)	C(34)-C(33)-C(38)-C(37)	-3.4(9)
N(2)-Ru(1)-P(2)-C(27)	32.5(3)	P(2)-C(33)-C(38)-C(37)	171.4(5)
Ru(2)-Ru(1)-P(2)-C(27)	-135.8(2)	C(43)-N(3)-C(39)-C(40)	-2.6(8)
C(57)-Ru(1)-N(1)-C(13)	59(7)	Ru(2)-N(3)-C(39)-C(40)	179.3(4)
N(5)-Ru(1)-N(1)-C(13)	82.1(4)	C(43)-N(3)-C(39)-P(2)	177.6(4)
N(2)-Ru(1)-N(1)-C(13)	172.5(4)	Ru(2)-N(3)-C(39)-P(2)	-0.4(6)
P(2)-Ru(1)-N(1)-C(13)	-95.5(4)	C(33)-P(2)-C(39)-N(3)	-112.7(4)
Ru(2)-Ru(1)-N(1)-C(13)	-11.3(4)	C(27)-P(2)-C(39)-N(3)	142.9(4)
C(57)-Ru(1)-N(1)-C(17)	-122(7)	Ru(1)-P(2)-C(39)-N(3)	18.2(5)
N(5)-Ru(1)-N(1)-C(17)	-99.4(4)	C(33)-P(2)-C(39)-C(40)	67.5(5)
N(2)-Ru(1)-N(1)-C(17)	-9.0(3)	C(27)-P(2)-C(39)-C(40)	-36.9(5)
P(2)-Ru(1)-N(1)-C(17)	83.0(4)	Ru(1)-P(2)-C(39)-C(40)	-161.6(4)
Ru(2)-Ru(1)-N(1)-C(17)	167.2(3)	N(3)-C(39)-C(40)-C(41)	2.2(9)
C(57)-Ru(1)-N(2)-C(18)	-166.6(4)	P(2)-C(39)-C(40)-C(41)	-178.1(5)
N(5)-Ru(1)-N(2)-C(18)	104.7(4)	C(39)-C(40)-C(41)-C(42)	0.2(10)
N(1)-Ru(1)-N(2)-C(18)	15.0(4)	C(40)-C(41)-C(42)-C(43)	-2.1(10)
P(2)-Ru(1)-N(2)-C(18)	-74.4(4)	C(39)-N(3)-C(43)-C(42)	0.7(8)
Ru(2)-Ru(1)-N(2)-C(18)	-2.9(8)	Ru(2)-N(3)-C(43)-C(42)	178.9(4)
C(57)-Ru(1)-N(2)-C(26)	-3.6(5)	C(39)-N(3)-C(43)-C(44)	-177.7(5)
N(5)-Ru(1)-N(2)-C(26)	-92.3(4)	Ru(2)-N(3)-C(43)-C(44)	0.5(6)
N(1)-Ru(1)-N(2)-C(26)	178.0(4)	C(41)-C(42)-C(43)-N(3)	1.6(9)
P(2)-Ru(1)-N(2)-C(26)	88.6(4)	C(41)-C(42)-C(43)-C(44)	180.0(6)
Ru(2)-Ru(1)-N(2)-C(26)	160.1(4)	C(52)-N(4)-C(44)-C(45)	-6.6(8)
C(58)-Ru(2)-N(3)-C(39)	81(5)	Ru(2)-N(4)-C(44)-C(45)	161.1(5)
N(6)-Ru(2)-N(3)-C(39)	80.5(4)	C(52)-N(4)-C(44)-C(43)	174.3(5)
N(4)-Ru(2)-N(3)-C(39)	170.9(4)	Ru(2)-N(4)-C(44)-C(43)	-17.9(6)
P(1)-Ru(2)-N(3)-C(39)	-95.2(4)	N(3)-C(43)-C(44)-N(4)	12.2(8)
Ru(1)-Ru(2)-N(3)-C(39)	-12.7(4)	C(42)-C(43)-C(44)-N(4)	-166.2(5)
C(58)-Ru(2)-N(3)-C(43)	-97(5)	N(3)-C(43)-C(44)-C(45)	-166.9(5)
N(6)-Ru(2)-N(3)-C(43)	-97.6(4)	C(42)-C(43)-C(44)-C(45)	14.7(9)
N(4)-Ru(2)-N(3)-C(43)	-7.2(4)	N(4)-C(44)-C(45)-C(46)	0.9(10)
P(1)-Ru(2)-N(3)-C(43)	86.7(4)	C(43)-C(44)-C(45)-C(46)	179.9(6)
Ru(1)-Ru(2)-N(3)-C(43)	169.2(4)	C(44)-C(45)-C(46)-C(47)	4.3(10)
C(58)-Ru(2)-N(4)-C(44)	-168.9(4)	C(45)-C(46)-C(47)-C(52)	-3.4(10)
N(6)-Ru(2)-N(4)-C(44)	97.3(4)	C(45)-C(46)-C(47)-C(48)	175.0(7)

dihedral angle	degree/°	dihedral angle	degree/°
N(3)-Ru(2)-N(4)-C(44)	13.6(4)	C(46)-C(47)-C(48)-C(49)	-175.9(7)
P(1)-Ru(2)-N(4)-C(44)	-78.5(4)	C(52)-C(47)-C(48)-C(49)	2.5(11)
Ru(1)-Ru(2)-N(4)-C(44)	-3.4(8)	C(47)-C(48)-C(49)-C(50)	0.9(13)
C(58)-Ru(2)-N(4)-C(52)	-2.7(5)	C(48)-C(49)-C(50)-C(51)	-3.2(13)
N(6)-Ru(2)-N(4)-C(52)	-96.5(5)	C(49)-C(50)-C(51)-C(52)	2.0(11)
N(3)-Ru(2)-N(4)-C(52)	179.8(5)	C(44)-N(4)-C(52)-C(47)	7.4(8)
P(1)-Ru(2)-N(4)-C(52)	87.7(4)	Ru(2)-N(4)-C(52)-C(47)	-158.3(4)
Ru(1)-Ru(2)-N(4)-C(52)	162.8(4)	C(44)-N(4)-C(52)-C(51)	-169.9(5)
C(57)-Ru(1)-N(5)-C(53)	28(3)	Ru(2)-N(4)-C(52)-C(51)	24.4(8)
N(1)-Ru(1)-N(5)-C(53)	-151(3)	C(46)-C(47)-C(52)-N(4)	-2.5(9)
N(2)-Ru(1)-N(5)-C(53)	134(3)	C(48)-C(47)-C(52)-N(4)	179.1(6)
P(2)-Ru(1)-N(5)-C(53)	-68(5)	C(46)-C(47)-C(52)-C(51)	174.9(6)
Ru(2)-Ru(1)-N(5)-C(53)	-58(3)	C(48)-C(47)-C(52)-C(51)	-3.6(9)
C(58)-Ru(2)-N(6)-C(55)	116(4)	C(50)-C(51)-C(52)-N(4)	178.8(6)
N(3)-Ru(2)-N(6)-C(55)	-65(4)	C(50)-C(51)-C(52)-C(47)	1.4(9)
N(4)-Ru(2)-N(6)-C(55)	-140(4)	Ru(1)-N(5)-C(53)-C(54)	34(19)
P(1)-Ru(2)-N(6)-C(55)	-11(5)	Ru(2)-N(6)-C(55)-C(56)	-36(19)
Ru(1)-Ru(2)-N(6)-C(55)	28(4)	N(5)-Ru(1)-C(57)-O(1)	-3(17)
C(7)-P(1)-C(1)-C(6)	32.2(6)	N(1)-Ru(1)-C(57)-O(1)	20(22)
C(13)-P(1)-C(1)-C(6)	135.3(5)	N(2)-Ru(1)-C(57)-O(1)	-93(17)
Ru(2)-P(1)-C(1)-C(6)	-99.4(5)	P(2)-Ru(1)-C(57)-O(1)	175(100)
C(7)-P(1)-C(1)-C(2)	-155.0(5)	Ru(2)-Ru(1)-C(57)-O(1)	91(17)
C(13)-P(1)-C(1)-C(2)	-51.9(5)	N(6)-Ru(2)-C(58)-O(2)	85(10)
Ru(2)-P(1)-C(1)-C(2)	73.4(5)	N(3)-Ru(2)-C(58)-O(2)	84(11)
C(6)-C(1)-C(2)-C(3)	0.6(9)	N(4)-Ru(2)-C(58)-O(2)	-5(10)
P(1)-C(1)-C(2)-C(3)	-172.5(5)	P(1)-Ru(2)-C(58)-O(2)	-99(10)
C(1)-C(2)-C(3)-C(4)	0.5(10)	Ru(1)-Ru(2)-C(58)-O(2)	179(100)
C(2)-C(3)-C(4)-C(5)	-1.7(11)	F(12)-P(4)-F(8A)-F(8B)	-39(9)
C(3)-C(4)-C(5)-C(6)	1.7(11)	F(9B)-P(4)-F(8A)-F(8B)	-105(10)
C(4)-C(5)-C(6)-C(1)	-0.5(11)	F(11)-P(4)-F(8A)-F(8B)	142(9)
C(2)-C(1)-C(6)-C(5)	-0.6(9)	F(10)-P(4)-F(8A)-F(8B)	56(9)
P(1)-C(1)-C(6)-C(5)	172.2(5)	F(7)-P(4)-F(8A)-F(8B)	178.6(17)
C(1)-P(1)-C(7)-C(12)	107.3(5)	F(9A)-P(4)-F(8A)-F(8B)	-138(10)
C(13)-P(1)-C(7)-C(12)	4.1(6)	F(12)-P(4)-F(8B)-F(8A)	142(9)
Ru(2)-P(1)-C(7)-C(12)	-123.9(5)	F(9B)-P(4)-F(8B)-F(8A)	73(10)
C(1)-P(1)-C(7)-C(8)	-74.5(5)	F(11)-P(4)-F(8B)-F(8A)	-38(9)
C(13)-P(1)-C(7)-C(8)	-177.7(5)	F(10)-P(4)-F(8B)-F(8A)	-125(9)
Ru(2)-P(1)-C(7)-C(8)	54.3(5)	F(7)-P(4)-F(8B)-F(8A)	-177(4)
C(12)-C(7)-C(8)-C(9)	-0.8(9)	F(9A)-P(4)-F(8B)-F(8A)	42(9)
P(1)-C(7)-C(8)-C(9)	-179.1(5)	F(12)-P(4)-F(9A)-F(9B)	-13(5)
C(7)-C(8)-C(9)-C(10)	0.5(11)	F(11)-P(4)-F(9A)-F(9B)	168(5)
C(8)-C(9)-C(10)-C(11)	0.9(11)	F(10)-P(4)-F(9A)-F(9B)	-179(100)
C(9)-C(10)-C(11)-C(12)	-2.0(12)	F(7)-P(4)-F(9A)-F(9B)	-102(4)
C(8)-C(7)-C(12)-C(11)	-0.3(10)	F(8B)-P(4)-F(9A)-F(9B)	73(5)
P(1)-C(7)-C(12)-C(11)	177.9(5)	F(8A)-P(4)-F(9A)-F(9B)	89(7)
C(10)-C(11)-C(12)-C(7)	1.7(11)	P(4)-F(9A)-F(9B)-F(12)	17(5)
C(17)-N(1)-C(13)-C(14)	-0.5(8)	F(12)-P(4)-F(9B)-F(9A)	166(5)
Ru(1)-N(1)-C(13)-C(14)	178.0(4)	F(11)-P(4)-F(9B)-F(9A)	-12(5)



dihedral angle	degree/°	dihedral angle	degree/°
C(17)-N(1)-C(13)-P(1)	174.4(4)	F(10)-P(4)-F(9B)-F(9A)	179.2(15)
Ru(1)-N(1)-C(13)-P(1)	-7.1(6)	F(7)-P(4)-F(9B)-F(9A)	79(4)
C(7)-P(1)-C(13)-N(1)	-101.0(4)	F(8B)-P(4)-F(9B)-F(9A)	-109(5)
C(1)-P(1)-C(13)-N(1)	152.1(4)	F(8A)-P(4)-F(9B)-F(9A)	-86(8)
Ru(2)-P(1)-C(13)-N(1)	28.4(5)	F(11)-P(4)-F(9B)-F(12)	-178.0(6)
C(7)-P(1)-C(13)-C(14)	73.8(5)	F(10)-P(4)-F(9B)-F(12)	13(5)
C(1)-P(1)-C(13)-C(14)	-33.1(5)	F(7)-P(4)-F(9B)-F(12)	-87.1(7)
Ru(2)-P(1)-C(13)-C(14)	-156.7(4)	F(8B)-P(4)-F(9B)-F(12)	85(3)
N(1)-C(13)-C(14)-C(15)	0.1(9)	F(8A)-P(4)-F(9B)-F(12)	108(7)
P(1)-C(13)-C(14)-C(15)	-174.4(5)	F(9A)-P(4)-F(9B)-F(12)	-166(5)
C(13)-C(14)-C(15)-C(16)	0.1(9)	F(11)-P(4)-F(12)-F(9B)	73(22)
C(14)-C(15)-C(16)-C(17)	0.1(9)	F(10)-P(4)-F(12)-F(9B)	-175.6(12)
C(13)-N(1)-C(17)-C(16)	0.8(7)	F(7)-P(4)-F(12)-F(9B)	94.9(12)
Ru(1)-N(1)-C(17)-C(16)	-177.9(4)	F(8B)-P(4)-F(12)-F(9B)	-91(3)
C(13)-N(1)-C(17)-C(18)	-178.9(5)	F(8A)-P(4)-F(12)-F(9B)	-76(4)
Ru(1)-N(1)-C(17)-C(18)	2.5(6)	F(9A)-P(4)-F(12)-F(9B)	8(2)
C(15)-C(16)-C(17)-N(1)	-0.6(8)	F(9A)-F(9B)-F(12)-P(4)	-20(6)
C(15)-C(16)-C(17)-C(18)	179.1(5)	C(61)-O(3)-C(59)-C(60)	-179.3(11)
C(26)-N(2)-C(18)-C(19)	-6.7(8)	C(59)-O(3)-C(61)-C(62)	-175.5(11)
Ru(1)-N(2)-C(18)-C(19)	157.6(4)		

<sup>a</sup> The esd's of the least significant digits are given in parentheses.

**Table B.35.** Anisotropic displacement parameters ( $\text{\AA}^2 \times 10^3$ ) for *cis*(Ph<sub>2</sub>Ppyqn)-[Ru<sub>2</sub>(μ-Ph<sub>2</sub>Ppyqn)<sub>2</sub>(CO)<sub>2</sub>(CH<sub>3</sub>CN)<sub>2</sub>](PF<sub>6</sub>)<sub>2</sub>, *cis*(Ph<sub>2</sub>Ppyqn)-19.<sup>a</sup>

Atom	U <sub>11</sub>	U <sub>22</sub>	U <sub>33</sub>	U <sub>23</sub>	U <sub>13</sub>	U <sub>12</sub>
Ru(1)	33(1)	34(1)	26(1)	1(1)	3(1)	4(1)
Ru(2)	32(1)	32(1)	27(1)	2(1)	4(1)	2(1)
P(1)	39(1)	36(1)	27(1)	-1(1)	3(1)	-1(1)
P(2)	33(1)	35(1)	28(1)	-1(1)	3(1)	0(1)
N(1)	44(3)	35(2)	21(2)	-3(2)	2(2)	3(2)
N(2)	41(3)	39(3)	36(3)	-4(2)	1(2)	11(2)
N(3)	26(2)	36(2)	32(2)	-4(2)	4(2)	-1(2)
N(4)	42(3)	37(3)	31(3)	1(2)	4(2)	1(2)
N(5)	34(3)	47(3)	35(3)	0(2)	5(2)	10(2)
N(6)	39(3)	41(3)	40(3)	4(2)	4(2)	3(2)
O(1)	47(3)	56(3)	69(3)	19(2)	15(2)	-7(2)
O(2)	61(3)	61(3)	33(2)	5(2)	18(2)	9(2)
C(1)	41(3)	34(3)	45(3)	6(3)	13(3)	-1(3)
C(2)	54(4)	50(4)	46(4)	0(3)	15(3)	-2(3)
C(3)	65(5)	61(4)	52(4)	2(3)	27(4)	-2(4)
C(4)	49(4)	67(5)	71(5)	13(4)	18(4)	0(3)
C(5)	44(4)	72(5)	72(5)	3(4)	-1(3)	-1(3)
C(6)	43(4)	62(4)	44(4)	0(3)	4(3)	-3(3)
C(7)	39(3)	42(3)	28(3)	-3(2)	4(2)	-2(3)
C(8)	58(4)	46(4)	43(4)	-1(3)	3(3)	5(3)
C(9)	84(5)	59(4)	39(4)	-5(3)	4(3)	2(4)

Atom	$U_{11}$	$U_{22}$	$U_{33}$	$U_{23}$	$U_{13}$	$U_{12}$
C(10)	78(5)	60(4)	52(4)	-23(3)	9(4)	2(4)
C(11)	61(4)	54(4)	70(5)	-19(4)	-1(4)	15(3)
C(12)	59(4)	55(4)	40(4)	-15(3)	-2(3)	12(3)
C(13)	47(4)	37(3)	31(3)	3(2)	4(3)	-1(3)
C(14)	45(4)	44(3)	54(4)	3(3)	4(3)	-7(3)
C(15)	63(4)	37(3)	55(4)	10(3)	7(3)	-2(3)
C(16)	72(5)	35(3)	36(3)	7(3)	7(3)	12(3)
C(17)	52(4)	35(3)	27(3)	1(2)	8(3)	9(3)
C(18)	44(3)	39(3)	33(3)	0(3)	4(3)	14(3)
C(19)	56(4)	56(4)	44(4)	6(3)	6(3)	19(3)
C(20)	59(4)	75(5)	35(3)	3(3)	-4(3)	29(4)
C(21)	42(4)	64(4)	41(3)	-16(3)	-6(3)	19(3)
C(22)	45(4)	76(5)	76(5)	-18(4)	-7(4)	18(4)
C(23)	37(4)	75(5)	87(6)	-30(5)	-2(4)	4(4)
C(24)	39(4)	53(4)	91(6)	-9(4)	8(4)	1(3)
C(25)	42(4)	50(4)	58(4)	1(3)	8(3)	12(3)
C(26)	41(3)	46(3)	35(3)	-8(3)	-2(3)	11(3)
C(27)	52(4)	36(3)	33(3)	-1(2)	9(3)	6(3)
C(28)	66(4)	46(4)	36(3)	-2(3)	11(3)	3(3)
C(29)	101(6)	45(4)	50(4)	2(3)	34(4)	-7(4)
C(30)	108(7)	57(5)	39(4)	1(3)	4(4)	21(5)
C(31)	73(5)	70(5)	35(4)	0(3)	-6(3)	26(4)
C(32)	50(4)	54(4)	37(3)	-3(3)	-1(3)	9(3)
C(33)	41(3)	44(3)	25(3)	1(2)	-3(2)	3(3)
C(34)	46(4)	40(3)	56(4)	-1(3)	3(3)	-2(3)
C(35)	69(5)	40(4)	59(4)	-9(3)	7(3)	-4(3)
C(36)	65(5)	47(4)	72(5)	-1(3)	-1(4)	-16(4)
C(37)	38(4)	59(4)	79(5)	-6(4)	-1(3)	-7(3)
C(38)	46(4)	51(4)	48(4)	-9(3)	5(3)	-2(3)
C(39)	34(3)	35(3)	39(3)	-3(2)	9(3)	-2(2)
C(40)	47(4)	52(4)	33(3)	-7(3)	7(3)	-4(3)
C(41)	45(4)	68(4)	44(4)	-19(3)	14(3)	3(3)
C(42)	34(3)	53(4)	49(4)	-13(3)	10(3)	2(3)
C(43)	38(3)	42(3)	39(3)	1(3)	4(3)	-3(3)
C(44)	33(3)	44(3)	38(3)	3(3)	2(3)	4(3)
C(45)	43(4)	61(4)	46(4)	8(3)	3(3)	5(3)
C(46)	39(4)	72(5)	57(4)	10(3)	-4(3)	6(3)
C(47)	47(4)	50(4)	46(4)	10(3)	-6(3)	11(3)
C(48)	52(4)	88(5)	55(5)	4(4)	-14(4)	8(4)
C(49)	84(6)	105(6)	40(4)	12(4)	-13(4)	27(5)
C(50)	79(5)	83(5)	41(4)	13(4)	6(4)	24(4)
C(51)	60(4)	64(4)	42(4)	9(3)	6(3)	25(3)
C(52)	49(4)	35(3)	37(3)	3(2)	4(3)	10(3)
C(53)	51(4)	43(3)	40(4)	2(3)	5(3)	11(3)
C(54)	94(6)	78(5)	31(3)	-3(3)	11(3)	28(4)
C(55)	43(3)	41(4)	47(4)	1(3)	10(3)	4(3)
C(56)	75(5)	44(4)	95(6)	-2(4)	16(4)	-13(4)
C(57)	33(3)	51(4)	36(3)	1(3)	2(3)	8(3)

Atom	U <sub>11</sub>	U <sub>22</sub>	U <sub>33</sub>	U <sub>23</sub>	U <sub>13</sub>	U <sub>12</sub>
C(58)	32(3)	40(3)	36(3)	6(3)	5(3)	5(2)
P(3)	52(1)	75(1)	62(1)	-8(1)	9(1)	7(1)
P(4)	75(1)	74(1)	59(1)	21(1)	11(1)	3(1)
F(1)	92(4)	109(4)	174(6)	-68(4)	39(4)	-4(3)
F(2)	118(4)	106(4)	133(5)	-43(4)	37(4)	16(3)
F(3)	65(3)	201(7)	184(7)	-66(6)	-25(4)	20(4)
F(4)	57(3)	198(6)	97(4)	-40(4)	-5(3)	-8(3)
F(5)	261(9)	124(5)	78(4)	25(4)	38(5)	-16(5)
F(6)	167(7)	146(6)	133(5)	36(5)	52(5)	-29(5)
F(7)	99(4)	163(5)	99(4)	0(4)	33(3)	9(4)
F(8A)	100(2)	300(6)	99(14)	-30(3)	50(15)	10(3)
F(8B)	97(13)	250(3)	99(17)	60(2)	35(13)	-11(17)
F(9A)	133(13)	180(2)	116(19)	-64(15)	-24(12)	12(15)
F(9B)	99(14)	230(4)	98(18)	90(2)	-17(11)	20(2)
F(10)	110(5)	267(10)	104(5)	-21(5)	-15(4)	-50(6)
F(11)	239(10)	78(4)	211(9)	4(5)	58(8)	11(5)
F(12)	391(18)	94(6)	306(14)	89(8)	130(14)	37(8)
O(3)	109(6)	157(7)	80(5)	-9(4)	-11(4)	-9(5)
C(59)	97(9)	211(15)	100(9)	-32(9)	-21(7)	8(9)
C(60)	80(7)	128(9)	121(9)	5(7)	5(6)	10(6)
C(61)	179(13)	130(10)	59(6)	-1(6)	-9(7)	-11(9)
C(62)	153(11)	87(7)	96(8)	0(6)	2(7)	-8(7)

<sup>a</sup> The esd's of the least significant digits are given in parentheses. The anisotropic displacement factor exponent takes the form:  $-2 \pi^2 [h^2 a^{*2} U_{11} + \dots + 2 h k a^* b^* U_{12}]$ .

**Table B.36.** Hydrogen atom coordinates ( $\times 10^4$ ) and equivalent isotropic displacement parameters ( $\text{\AA}^2 \times 10^3$ ) for *cis*(Ph<sub>2</sub>Ppyqn)-[Ru<sub>2</sub>( $\mu$ -Ph<sub>2</sub>Ppyqn)<sub>2</sub>(CO)<sub>2</sub>(CH<sub>3</sub>CN)<sub>2</sub>](PF<sub>6</sub>)<sub>2</sub>, *cis*(Ph<sub>2</sub>Ppyqn)-19.<sup>a</sup>

atom	x	y	z	U(eq)
H(2)	3822	3738	4987	59
H(3)	4926	3739	4779	70
H(4)	5774	4047	5582	74
H(5)	5503	4433	6593	76
H(6)	4395	4437	6814	60
H(8)	3539	3958	7449	59
H(9)	3420	4932	8297	73
H(10)	2826	6288	8150	76
H(11)	2313	6660	7144	75
H(12)	2456	5711	6279	62
H(14)	3394	5564	5314	57
H(15)	2751	6421	4533	62
H(16)	1665	5955	4207	57
H(19)	755	5296	3807	62
H(20)	-258	4608	3493	68
H(22)	-1202	3561	3766	80
H(23)	-1639	2604	4468	80

atom	x	y	z	U(eq)
H(24)	-1035	2300	5463	73
H(25)	35	2864	5704	60
H(28)	2586	3698	4087	59
H(29)	2416	4529	3132	76
H(30)	1447	4294	2445	82
H(31)	700	3170	2659	72
H(32)	856	2333	3603	57
H(34)	2225	399	4362	57
H(35)	1603	-880	4000	67
H(36)	446	-854	3953	74
H(37)	-95	434	4286	71
H(38)	521	1709	4669	58
H(40)	2777	1748	3776	53
H(41)	3899	1340	3830	62
H(42)	4543	1333	4816	54
H(45)	5131	1709	5670	60
H(46)	5710	1790	6667	68
H(48)	5685	1751	7857	80
H(49)	5075	1696	8708	93
H(50)	3918	1655	8572	81
H(51)	3338	1806	7561	66
H(54A)	1341	4128	7839	102
H(54B)	622	4460	7552	102
H(54C)	1242	5132	7555	102
H(56A)	1700	-722	6448	107
H(56B)	2231	-1019	5983	107
H(56C)	1550	-553	5706	107
H(59A)	3063	8298	7167	166
H(59B)	2949	9351	7313	166
H(60A)	3328	8034	8275	165
H(60B)	2589	8408	8121	165
H(60C)	3165	9079	8404	165
H(61A)	3824	9801	6665	149
H(61B)	3876	8744	6489	149
H(62A)	4941	9793	7101	169
H(62B)	4895	9460	6384	169
H(62C)	4995	8733	6944	169

<sup>a</sup> U(eq) is defined as one third of the trace of the orthogonalized  $U_{ij}$  tensor.

## B.2. Extended Hückel Molecular Orbital Calculations<sup>†</sup>

### B.2.1. Ph<sub>2</sub>Pbpy

**Table B.37.** Molecular orbital coefficients of Ph<sub>2</sub>Pbpy.

Atomic Orbitals ↓	Molecular Orbitals→ Eigenvalue/eV→	<i>trans</i> -Ph <sub>2</sub> Pbpy		<i>cis</i> -Ph <sub>2</sub> Pbpy	
		HOMO -9.31	LUMO -9.08	HOMO -9.33	LUMO -8.93
P 3s		-0.032	0.054	0.006	0.001
3p <sub>x</sub>		0.011	0.075	0.046	-0.053
3p <sub>y</sub>		0.038	-0.166	0.036	-0.111
3p <sub>z</sub>		-0.056	0.158	-0.024	-0.021
3d <sub>z<sup>2</sup></sub>		-0.094	0.350	-0.106	0.219
3d <sub>xz</sub>		0.122	-0.209	0.060	-0.234
3d <sub>yz</sub>		-0.018	0.044	-0.064	0.113
3d <sub>x<sup>2</sup>-y<sup>2</sup></sub>		0.045	0.004	0.060	-0.191
3d <sub>xy</sub>		-0.048	0.262	0.024	0.156
N 2s		0.005	-0.012	-0.004	0.017
2p <sub>x</sub>		0.466	-0.230	0.400	-0.188
2p <sub>y</sub>		-0.138	0.035	-0.078	0.031
2p <sub>z</sub>		-0.047	-0.018	-0.210	0.133
N' 2s		-0.000	0.001	0.000	-0.001
2p <sub>x</sub>		0.379	0.165	0.359	0.140
2p <sub>y</sub>		-0.124	-0.055	-0.072	-0.027
2p <sub>z</sub>		-0.051	-0.020	-0.182	-0.075
C-2 2s		-0.001	0.005	-0.000	-0.002
2p <sub>x</sub>		-0.376	-0.100	-0.347	-0.099
2p <sub>y</sub>		0.122	0.033	0.070	0.023
2p <sub>z</sub>		0.046	0.033	0.177	0.046
C-3 2s		0.001	-0.000	-0.001	0.001
2p <sub>x</sub>		0.080	0.403	0.092	0.399
2p <sub>y</sub>		-0.021	-0.148	-0.018	-0.080
2p <sub>z</sub>		-0.009	-0.059	-0.048	-0.203
C-4 2s		-0.003	0.013	-0.001	0.002
2p <sub>x</sub>		0.342	-0.158	0.311	-0.174

<sup>†</sup> The following abbreviations are used in the tables; HOMO = highest occupied molecular orbital, LUMO = lowest unoccupied molecular orbital, SLUMO = second lowest unoccupied molecular orbital, TLUMO = third lowest unoccupied molecular orbital.

Atomic Orbitals ↓	Molecular Orbitals→ Eigenvalue/eV→	<i>trans</i> -Ph <sub>2</sub> Pbpy		<i>cis</i> -Ph <sub>2</sub> Pbpy	
		HOMO -9.31	LUMO -9.08	HOMO -9.33	LUMO -8.93
2p <sub>y</sub>		-0.113	0.049	-0.067	0.037
2p <sub>z</sub>		-0.054	0.049	-0.162	0.093
C-5 2s		0.005	-0.022	0.003	-0.008
2p <sub>x</sub>		-0.257	-0.333	-0.253	-0.292
2p <sub>y</sub>		0.096	0.062	0.065	0.057
2p <sub>z</sub>		0.049	-0.016	0.138	0.132
C-6 2s		-0.009	0.041	-0.002	-0.013
2p <sub>x</sub>		-0.180	0.344	-0.154	0.323
2p <sub>y</sub>		0.061	-0.106	0.025	-0.050
2p <sub>z</sub>		-0.009	0.102	0.068	-0.188
C-2' 2s		-0.001	0.001	-0.000	0.001
2p <sub>x</sub>		-0.369	-0.150	-0.340	-0.152
2p <sub>y</sub>		0.122	0.045	0.070	0.026
2p <sub>z</sub>		0.049	0.020	0.173	0.080
C-3' 2s		0.000	-0.001	0.000	-0.001
2p <sub>x</sub>		0.167	0.013	0.143	0.044
2p <sub>y</sub>		-0.055	-0.003	-0.029	-0.008
2p <sub>z</sub>		-0.023	-0.000	-0.073	-0.024
C-4' 2s		0.000	0.000	-0.000	0.000
2p <sub>x</sub>		0.284	0.158	0.282	0.113
2p <sub>y</sub>		-0.093	-0.052	-0.056	-0.024
2p <sub>z</sub>		-0.038	-0.021	-0.144	-0.058
C-5' 2s		-0.000	0.000	0.000	-0.000
2p <sub>x</sub>		-0.319	-0.109	-0.292	-0.118
2p <sub>y</sub>		0.104	0.035	0.058	0.024
2p <sub>z</sub>		0.042	0.015	0.149	0.060
C-6' 2s		-0.000	0.000	-0.000	0.000
2p <sub>x</sub>		-0.097	-0.083	-0.112	-0.028
2p <sub>y</sub>		0.032	0.027	0.023	0.004
2p <sub>z</sub>		0.013	0.011	0.057	0.015
C-1'' 2s		0.023	-0.069	0.007	-0.020
2p <sub>x</sub>		-0.027	0.124	0.020	-0.191
2p <sub>y</sub>		0.063	-0.157	0.020	-0.113
2p <sub>z</sub>		-0.008	0.020	-0.003	0.003
C-2'' 2s		0.004	0.010	0.003	-0.003
2p <sub>x</sub>		-0.022	-0.019	-0.034	0.214
2p <sub>y</sub>		-0.024	0.036	-0.012	0.081
2p <sub>z</sub>		-0.040	0.060	-0.021	0.036

Atomic Orbitals ↓	Molecular Orbitals→ Eigenvalue/eV→	<i>trans</i> -Ph <sub>2</sub> Pbpy		<i>cis</i> -Ph <sub>2</sub> Pbpy	
		HOMO -9.31	LUMO -9.08	HOMO -9.33	LUMO -8.93
C-3" 2s		0.003	-0.013	-0.000	-0.001
2p <sub>x</sub>		-0.017	0.023	-0.013	0.079
2p <sub>y</sub>		-0.011	-0.014	-0.006	0.027
2p <sub>z</sub>		-0.003	0.001	0.001	0.006
C-4" 2s		0.005	-0.010	0.002	-0.004
2p <sub>x</sub>		0.032	-0.012	0.044	-0.273
2p <sub>y</sub>		0.045	-0.033	0.018	-0.105
2p <sub>z</sub>		0.012	-0.009	0.001	-0.024
C-3" 2s		0.003	-0.009	0.000	-0.002
2p <sub>x</sub>		-0.010	0.022	-0.010	0.103
2p <sub>y</sub>		-0.002	-0.001	-0.004	0.035
2p <sub>z</sub>		-0.005	0.011	-0.002	0.013
C-2" 2s		-0.001	0.001	0.001	0.003
2p <sub>x</sub>		-0.032	0.021	-0.039	0.202
2p <sub>y</sub>		-0.042	0.035	-0.010	0.071
2p <sub>z</sub>		0.006	-0.055	0.001	-0.008
C-1" 2s		0.001	0.001	-0.008	0.029
2p <sub>x</sub>		-0.007	0.042	0.044	-0.080
2p <sub>y</sub>		0.000	-0.064	0.036	-0.086
2p <sub>z</sub>		0.012	0.097	-0.028	0.032
C-2" 2s		0.005	0.001	0.005	-0.001
2p <sub>x</sub>		-0.005	-0.031	-0.063	0.070
2p <sub>y</sub>		-0.007	0.041	-0.033	0.054
2p <sub>z</sub>		-0.006	-0.076	0.055	-0.099
C-3" 2s		-0.002	0.000	-0.002	0.003
2p <sub>x</sub>		0.005	-0.058	-0.010	0.005
2p <sub>y</sub>		-0.001	0.067	-0.000	-0.004
2p <sub>z</sub>		0.008	-0.110	0.014	-0.005
C-4" 2s		0.001	-0.001	-0.000	0.005
2p <sub>x</sub>		-0.002	0.075	0.068	-0.094
2p <sub>y</sub>		0.001	-0.089	0.029	-0.043
2p <sub>z</sub>		-0.002	0.147	-0.069	0.089
C-3" 2s		0.001	0.001	-0.001	0.003
2p <sub>x</sub>		-0.004	0.010	-0.024	0.054
2p <sub>y</sub>		0.003	-0.017	-0.008	0.020
2p <sub>z</sub>		-0.006	0.021	0.026	-0.060
C-2" 2s		-0.005	-0.004	0.001	-0.000
2p <sub>x</sub>		0.015	-0.080	-0.060	0.070

Atomic Orbitals ↓	Molecular Orbitals→ Eigenvalue/eV→	<i>trans</i> -Ph <sub>2</sub> Pbpy		<i>cis</i> -Ph <sub>2</sub> Pbpy	
		HOMO	LUMO	HOMO	LUMO
		-9.31	-9.08	-9.33	-8.93
2p <sub>y</sub>		0.000	0.106	-0.020	0.011
2p <sub>z</sub>		0.003	-0.152	0.047	-0.037

### B.2.2. Ph<sub>2</sub>Ppyqn I

**Table B.38.** Molecular orbital coefficients of Ph<sub>2</sub>Ppyqn I.

Atomic Orbitals ↓	Molecular Orbitals→ Eigenvalue/eV→	<i>trans</i> -Ph <sub>2</sub> Ppyqn		<i>cis</i> -Ph <sub>2</sub> Ppyqn	
		HOMO	LUMO	HOMO	LUMO
		-9.68	-9.11	-9.30	-9.14
P 3s		-0.015	0.062	0.004	-0.004
3p <sub>x</sub>		-0.008	0.189	-0.017	0.064
3p <sub>y</sub>		-0.008	0.139	0.004	-0.018
3p <sub>z</sub>		0.026	-0.012	0.020	-0.047
3d <sub>z<sup>2</sup></sub>		-0.027	0.117	-0.012	0.060
3d <sub>xz</sub>		0.003	-0.278	-0.030	0.023
3d <sub>yz</sub>		0.045	-0.370	0.065	-0.221
3d <sub>x<sup>2</sup>-y<sup>2</sup></sub>		-0.017	-0.042	0.003	0.010
3d <sub>xy</sub>		-0.002	-0.118	0.005	-0.051
N 2s		0.002	-0.012	-0.001	0.007
2p <sub>x</sub>		0.061	-0.051	0.022	-0.030
2p <sub>y</sub>		0.139	-0.216	0.045	-0.060
2p <sub>z</sub>		0.280	-0.330	0.273	-0.423
N' 2s		0.000	0.001	0.000	-0.000
2p <sub>x</sub>		0.091	0.009	-0.013	-0.036
2p <sub>y</sub>		0.190	0.018	-0.025	-0.072
2p <sub>z</sub>		0.400	0.034	-0.151	-0.414
C-2 2s		-0.000	0.005	-0.000	-0.000
2p <sub>x</sub>		-0.055	0.014	-0.023	0.025
2p <sub>y</sub>		-0.115	0.040	-0.043	0.049
2p <sub>z</sub>		-0.240	0.044	-0.255	0.291
C-3 2s		0.000	-0.001	-0.000	0.001
2p <sub>x</sub>		0.038	0.092	0.008	0.009
2p <sub>y</sub>		0.081	0.155	0.016	0.015
2p <sub>z</sub>		0.170	0.344	0.099	0.084
C-4 2s		-0.001	0.012	-0.001	0.002
2p <sub>x</sub>		0.040	-0.055	0.019	-0.034
2p <sub>y</sub>		0.080	-0.107	0.031	-0.057
2p <sub>z</sub>		0.173	-0.286	0.196	-0.362



Atomic Orbitals ↓	Molecular Orbitals→ Eigenvalue/eV→	<i>trans</i> -Ph <sub>2</sub> Ppyqn		<i>cis</i> -Ph <sub>2</sub> Ppyqn	
		HOMO -9.68	LUMO -9.11	HOMO -9.30	LUMO -9.14
C-5 2s		0.001	-0.021	0.001	-0.005
2p <sub>x</sub>		-0.059	-0.014	-0.025	0.022
2p <sub>y</sub>		-0.110	-0.145	-0.030	0.009
2p <sub>z</sub>		-0.243	-0.158	-0.204	0.130
C-6 2s		-0.003	0.037	-0.002	0.000
2p <sub>x</sub>		-0.018	0.103	-0.004	0.014
2p <sub>y</sub>		-0.037	0.283	-0.018	0.051
2p <sub>z</sub>		-0.060	0.287	-0.068	0.246
C-2' 2s		-0.000	0.002	-0.000	0.001
2p <sub>x</sub>		-0.084	-0.002	-0.022	0.018
2p <sub>y</sub>		-0.175	-0.013	-0.043	0.032
2p <sub>z</sub>		-0.369	-0.027	-0.252	0.188
C-3' 2s		-0.000	-0.000	0.000	-0.000
2p <sub>x</sub>		-0.013	-0.020	0.041	-0.000
2p <sub>y</sub>		-0.028	-0.036	0.081	0.001
2p <sub>z</sub>		-0.058	-0.082	0.480	0.005
C-4' 2s		0.000	0.000	-0.000	0.000
2p <sub>x</sub>		0.089	0.020	-0.002	-0.018
2p <sub>y</sub>		0.186	0.041	-0.003	-0.038
2p <sub>z</sub>		0.392	0.087	-0.020	-0.224
C-4a 2s		-0.000	0.000	-0.000	-0.000
2p <sub>x</sub>		-0.022	0.007	-0.034	-0.009
2p <sub>y</sub>		-0.046	0.015	-0.069	-0.018
2p <sub>z</sub>		-0.097	0.030	-0.407	-0.106
C-5' 2s		0.000	0.000	-0.000	0.000
2p <sub>x</sub>		-0.061	-0.015	0.021	0.025
2p <sub>y</sub>		-0.128	-0.031	0.041	0.050
2p <sub>z</sub>		-0.270	-0.065	0.242	0.295
C-6' 2s		-0.000	0.000	0.000	-0.000
2p <sub>x</sub>		0.047	0.002	0.025	-0.006
2p <sub>y</sub>		0.099	0.004	0.050	-0.011
2p <sub>z</sub>		0.208	0.008	0.292	-0.066
C-7' 2s		-0.000	0.000	-0.000	0.000
2p <sub>x</sub>		0.045	0.014	-0.033	-0.021
2p <sub>y</sub>		0.095	0.030	-0.065	-0.042
2p <sub>z</sub>		0.200	0.063	-0.385	-0.247
C-8' 2s		0.000	0.000	0.000	-0.000
2p <sub>x</sub>		-0.062	-0.010	-0.007	0.017
2p <sub>y</sub>		-0.130	-0.021	-0.014	0.035

Atomic Orbitals ↓	Molecular Orbitals→ Eigenvalue/eV→	<i>trans</i> -Ph <sub>2</sub> Ppyqn		<i>cis</i> -Ph <sub>2</sub> Ppyqn	
		HOMO	LUMO	HOMO	LUMO
		-9.68	-9.11	-9.30	-9.14
2p <sub>z</sub>		-0.274	-0.045	-0.080	0.205
C-8a' 2s		-0.000	0.000	0.000	0.000
2p <sub>x</sub>		-0.018	-0.007	0.036	0.030
2p <sub>y</sub>		-0.038	-0.016	0.072	0.059
2p <sub>z</sub>		-0.080	-0.034	0.424	0.350
C-1" 2s		0.007	-0.071	0.003	-0.012
2p <sub>x</sub>		-0.014	0.171	-0.006	0.044
2p <sub>y</sub>		-0.008	0.060	0.003	-0.031
2p <sub>z</sub>		-0.008	0.109	0.005	-0.037
C-2" 2s		0.004	0.007	0.002	-0.003
2p <sub>x</sub>		0.001	-0.042	0.000	-0.025
2p <sub>y</sub>		-0.020	0.069	-0.014	0.065
2p <sub>z</sub>		0.003	-0.047	-0.001	0.036
C-3" 2s		0.000	-0.012	-0.000	-0.000
2p <sub>x</sub>		0.008	0.003	0.003	-0.009
2p <sub>y</sub>		-0.005	0.020	-0.002	0.015
2p <sub>z</sub>		-0.003	0.023	-0.004	0.018
C-4" 2s		0.002	-0.011	0.001	-0.003
2p <sub>x</sub>		-0.016	0.063	-0.006	0.036
2p <sub>y</sub>		0.010	-0.046	0.008	-0.060
2p <sub>z</sub>		0.005	-0.009	0.010	-0.062
C-3" 2s		0.001	-0.010	0.000	-0.001
2p <sub>x</sub>		-0.003	-0.007	0.001	-0.010
2p <sub>y</sub>		0.000	0.031	-0.002	0.021
2p <sub>z</sub>		0.000	0.015	-0.001	0.018
C-2" 2s		0.000	0.002	0.001	-0.001
2p <sub>x</sub>		0.016	-0.072	0.003	-0.023
2p <sub>y</sub>		-0.010	-0.007	-0.007	0.042
2p <sub>z</sub>		-0.007	0.050	-0.010	0.057
C-1" 2s		0.002	0.003	-0.003	0.013
2p <sub>x</sub>		0.008	0.065	-0.020	0.063
2p <sub>y</sub>		0.002	0.062	0.003	-0.013
2p <sub>z</sub>		-0.010	-0.004	0.024	-0.079
C-2" 2s		0.003	-0.002	0.002	-0.004
2p <sub>x</sub>		0.003	-0.040	0.021	-0.058
2p <sub>y</sub>		-0.006	-0.048	0.001	-0.010
2p <sub>z</sub>		0.000	0.006	-0.039	0.113
C-3" 2s		-0.001	0.001	-0.001	0.002
2p <sub>x</sub>		-0.003	-0.066	0.002	-0.006

Atomic Orbitals ↓	Molecular Orbitals→ Eigenvalue/eV→	<i>trans</i> -Ph <sub>2</sub> Ppyqn		<i>cis</i> -Ph <sub>2</sub> Ppyqn	
		HOMO	LUMO	HOMO	LUMO
		-9.68	-9.11	-9.30	-9.14
2p <sub>y</sub>		-0.002	-0.099	0.002	-0.005
2p <sub>z</sub>		0.000	0.002	-0.009	0.024
C-4" 2s		0.000	-0.001	-0.000	0.002
2p <sub>x</sub>		0.003	0.082	-0.020	0.059
2p <sub>y</sub>		0.003	0.116	-0.005	0.013
2p <sub>z</sub>		-0.000	-0.005	0.046	-0.132
C-3" 2s		0.002	0.001	-0.000	0.001
2p <sub>x</sub>		0.004	0.025	0.006	-0.022
2p <sub>y</sub>		-0.000	0.026	0.002	-0.008
2p <sub>z</sub>		-0.001	-0.000	-0.016	0.056
C-2" 2s		-0.004	-0.002	0.000	-0.001
2p <sub>x</sub>		-0.009	-0.101	0.014	-0.036
2p <sub>y</sub>		0.000	-0.127	0.000	0.004
2p <sub>z</sub>		0.007	-0.001	-0.037	0.099

### B.2.3. Et(Ph)Pbpy II

**Table B.39.** Molecular orbital coefficients of Et(Ph)Pbpy II.

Atomic Orbitals ↓	Molecular Orbitals→ Eigenvalue/eV→	<i>trans</i> -Et(Ph)Pbpy		<i>cis</i> - Et(Ph)Pbpy	
		HOMO	LUMO	HOMO	LUMO
		-9.31	-9.03	-9.32	-8.91
P 3s		-0.027	-0.045	-0.010	0.002
3p <sub>x</sub>		0.018	-0.036	-0.048	-0.007
3p <sub>y</sub>		0.011	0.222	-0.056	-0.114
3p <sub>z</sub>		-0.058	-0.032	-0.020	-0.070
3d <sub>z<sup>2</sup></sub>		-0.058	-0.066	0.009	-0.052
3d <sub>xz</sub>		0.147	0.306	-0.110	-0.358
3d <sub>yz</sub>		0.008	-0.101	0.013	0.073
3d <sub>x<sup>2</sup>-y<sup>2</sup></sub>		0.011	0.164	-0.026	-0.171
3d <sub>xy</sub>		-0.008	-0.301	-0.024	0.131
N 2s		0.007	-0.002	0.005	0.015
2p <sub>x</sub>		0.471	0.247	-0.440	-0.234
2p <sub>y</sub>		-0.073	-0.003	-0.053	-0.041
2p <sub>z</sub>		0.045	0.028	0.011	0.030
N' 2s		-0.000	0.000	-0.000	-0.000
2p <sub>x</sub>		0.400	-0.165	-0.418	0.132
2p <sub>y</sub>		-0.068	0.026	-0.041	0.014
2p <sub>z</sub>		0.019	-0.010	0.004	-0.004

Atomic Orbitals ↓	Molecular Orbitals→ Eigenvalue/eV→	<i>trans</i> -Et(Ph)Pbpy		<i>cis</i> -Et(Ph)Pbpy	
		HOMO	LUMO	HOMO	LUMO
		-9.31	-9.03	-9.32	-8.91
C-2 2s		-0.002	-0.001	-0.000	-0.002
2p <sub>x</sub>		-0.396	0.089	0.400	-0.092
2p <sub>y</sub>		0.068	-0.019	0.041	-0.005
2p <sub>z</sub>		-0.026	-0.003	-0.004	-0.003
C-3 2s		0.001	0.003	0.000	-0.000
2p <sub>x</sub>		0.097	-0.425	-0.137	0.424
2p <sub>y</sub>		-0.012	0.078	-0.015	0.044
2p <sub>z</sub>		0.007	-0.017	0.002	-0.005
C-4 2s		-0.003	-0.009	0.001	0.001
2p <sub>x</sub>		0.355	0.195	-0.344	-0.202
2p <sub>y</sub>		-0.060	-0.027	-0.032	-0.020
2p <sub>z</sub>		0.012	-0.011	0.007	0.006
C-5 2s		0.003	0.019	-0.003	-0.007
2p <sub>x</sub>		-0.285	0.304	0.322	-0.292
2p <sub>y</sub>		0.059	-0.044	0.022	-0.023
2p <sub>z</sub>		-0.003	0.059	-0.013	-0.007
C-6 2s		-0.012	-0.006	-0.001	-0.016
2p <sub>x</sub>		-0.169	-0.358	0.147	0.362
2p <sub>y</sub>		0.036	0.054	0.020	0.055
2p <sub>z</sub>		-0.047	-0.075	0.003	-0.031
C-2' 2s		-0.000	-0.002	0.001	0.002
2p <sub>x</sub>		-0.389	0.144	0.399	-0.145
2p <sub>y</sub>		0.067	-0.018	0.037	-0.020
2p <sub>z</sub>		-0.019	0.006	-0.004	0.003
C-3' 2s		0.000	-0.000	-0.000	-0.001
2p <sub>x</sub>		0.176	0.002	-0.165	0.044
2p <sub>y</sub>		-0.031	-0.001	-0.016	0.006
2p <sub>z</sub>		0.008	-0.003	0.001	-0.002
C-4' 2s		0.000	-0.000	0.000	0.001
2p <sub>x</sub>		0.300	-0.164	-0.329	0.105
2p <sub>y</sub>		-0.052	0.029	-0.033	0.009
2p <sub>z</sub>		0.015	-0.008	0.004	-0.001
C-5' 2s		-0.000	-0.000	0.000	-0.000
2p <sub>x</sub>		-0.336	0.101	0.340	-0.113
2p <sub>y</sub>		0.058	-0.017	0.034	-0.011
2p <sub>z</sub>		-0.017	0.004	-0.004	0.001
C-6' 2s		-0.000	-0.000	0.000	0.000
2p <sub>x</sub>		-0.103	0.092	0.130	-0.023
2p <sub>y</sub>		0.018	-0.015	0.012	-0.003

Atomic Orbitals ↓	Molecular Orbitals→ Eigenvalue/eV→	<i>trans</i> -Et(Ph)Pbpy		<i>cis</i> - Et(Ph)Pbpy	
		HOMO -9.31	LUMO -9.03	HOMO -9.32	LUMO -8.91
2p <sub>z</sub>		-0.005	0.004	-0.001	0.000
C-1" 2s		0.018	0.062	-0.004	-0.017
2p <sub>x</sub>		-0.027	-0.091	-0.032	-0.187
2p <sub>y</sub>		0.045	0.211	-0.030	-0.182
2p <sub>z</sub>		0.004	0.096	-0.011	-0.073
C-2" 2s		0.002	-0.006	-0.005	-0.006
2p <sub>x</sub>		-0.002	-0.013	0.045	0.211
2p <sub>y</sub>		-0.007	-0.096	0.027	0.151
2p <sub>z</sub>		-0.028	-0.177	0.038	0.120
C-3" 2s		0.002	0.011	0.001	-0.001
2p <sub>x</sub>		-0.017	-0.040	0.013	0.073
2p <sub>y</sub>		-0.019	-0.023	0.012	0.052
2p <sub>z</sub>		-0.029	-0.049	0.005	0.038
C-4" 2s		0.003	0.009	-0.002	-0.003
2p <sub>x</sub>		0.013	0.065	-0.057	-0.265
2p <sub>y</sub>		0.031	0.145	-0.043	-0.200
2p <sub>z</sub>		0.037	0.181	-0.026	-0.138
C-3" 2s		0.003	0.010	-0.001	-0.004
2p <sub>x</sub>		0.000	-0.041	0.016	0.107
2p <sub>y</sub>		0.011	-0.036	0.011	0.072
2p <sub>z</sub>		0.008	-0.071	0.009	0.059
C-2" 2s		-0.001	-0.003	0.000	0.008
2p <sub>x</sub>		-0.021	-0.067	0.048	0.197
2p <sub>y</sub>		-0.043	-0.144	0.034	0.149
2p <sub>z</sub>		-0.032	-0.099	0.020	0.069
CH <sub>2</sub> 2s		0.006	-0.032	0.010	0.028
2p <sub>x</sub>		-0.013	0.063	0.025	0.047
2p <sub>y</sub>		-0.015	0.070	-0.012	-0.039
2p <sub>z</sub>		-0.002	0.028	-0.016	-0.063
CH <sub>3</sub> 2s		0.003	0.002	0.007	0.002
2p <sub>x</sub>		-0.010	-0.020	-0.005	0.009
2p <sub>y</sub>		0.002	0.006	-0.006	-0.007
2p <sub>z</sub>		0.003	-0.006	-0.008	0.015

**B.2.4. [Cu<sub>2</sub>(μ-Ph<sub>2</sub>Pbpy)<sub>2</sub>(CH<sub>3</sub>CN)<sub>2</sub>](PF<sub>6</sub>)<sub>2</sub>, [Cu<sub>2</sub>(μ-Ph<sub>2</sub>Ppyqn)<sub>2</sub>(CH<sub>3</sub>CN)<sub>2</sub>](BF<sub>4</sub>)<sub>2</sub> **1** and [Cu<sub>2</sub>{μ-Et(Ph)Pbpy}<sub>2</sub>(CH<sub>3</sub>CN)<sub>2</sub>](PF<sub>6</sub>)<sub>2</sub> **2**.**

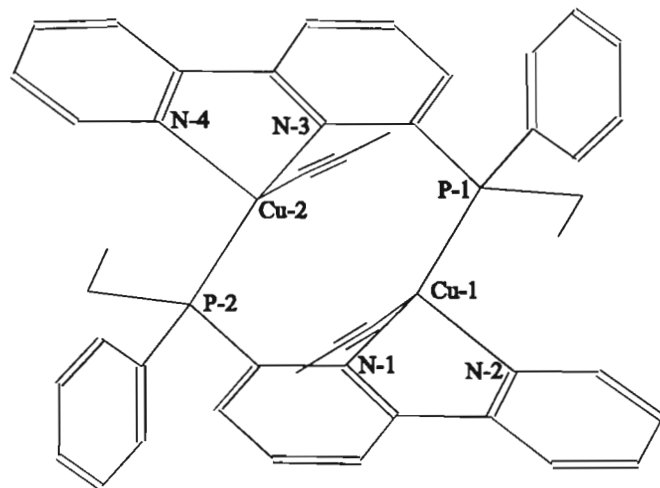


**Table B.40.** Molecular orbital coefficients of the metal and phosphorus-polypyridyl ligand donor atoms of [Cu<sub>2</sub>(μ-Ph<sub>2</sub>Pbpy)<sub>2</sub>(CH<sub>3</sub>CN)<sub>2</sub>](PF<sub>6</sub>)<sub>2</sub>, Cu<sub>2</sub>(μ-Ph<sub>2</sub>Ppyqn)<sub>2</sub>(CH<sub>3</sub>CN)<sub>2</sub>(BF<sub>4</sub>)<sub>2</sub> **1** and [Cu<sub>2</sub>{μ-Et(Ph)Pbpy}<sub>2</sub>(CH<sub>3</sub>CN)<sub>2</sub>](PF<sub>6</sub>)<sub>2</sub> **2**.

Atomic Orbitals ↓	Molecular Orbitals→ Eigenvalue/eV→	[Cu <sub>2</sub> (μ-Ph <sub>2</sub> Pbpy) <sub>2</sub> (CH <sub>3</sub> CN) <sub>2</sub> ](PF <sub>6</sub> ) <sub>2</sub>			<b>1</b>			<b>2</b>		
		HOMO	LUMO	SLUMO	HOMO	LUMO	SLUMO	HOMO	LUMO	SLUMO
		-11.62	-9.78	-9.62	-11.30	-9.96	-9.89	-11.23	-9.65	-9.57
Cu-1 3s		-0.007	-0.025	0.051	0.071	-0.009	0.016	0.067	-0.008	0.025
3p <sub>x</sub>		-0.015	-0.024	0.022	0.014	0.001	0.006	0.036	0.005	-0.013
3p <sub>y</sub>		-0.028	0.003	-0.015	0.085	0.005	0.004	-0.004	-0.007	-0.008
3p <sub>z</sub>		0.111	-0.009	0.008	0.057	-0.007	0.020	0.099	-0.007	0.012
3d <sub>z<sup>2</sup></sub>		-0.120	0.014	-0.009	-0.190	-0.022	-0.101	0.147	-0.051	-0.055
3d <sub>xz</sub>		0.182	0.041	-0.059	0.090	0.005	0.023	0.394	0.021	0.070
3d <sub>yz</sub>		-0.194	0.022	0.050	0.098	-0.020	-0.027	-0.073	-0.036	-0.017
3d <sub>x<sup>2</sup>-y<sup>2</sup></sub>		-0.182	-0.007	-0.074	-0.362	0.024	0.004	0.145	-0.013	-0.041

Atomic Orbitals ↓	Molecular Orbitals→ Eigenvalue/eV→	[Cu <sub>2</sub> (μ-Ph <sub>2</sub> Pbpy) <sub>2</sub> (CH <sub>3</sub> CN) <sub>2</sub> ](PF <sub>6</sub> ) <sub>2</sub>			<b>1</b>			<b>2</b>		
		HOMO	LUMO	SLUMO	HOMO	LUMO	SLUMO	HOMO	LUMO	SLUMO
		-11.62	-9.78	-9.62	-11.30	-9.96	-9.89	-11.23	-9.65	-9.57
3d <sub>xy</sub>		0.145	0.085	0.045	0.052	0.014	0.029	-0.008	0.005	-0.009
Cu-2 3s		-0.007	-0.025	-0.051	-0.071	0.007	-0.017	-0.067	-0.008	-0.025
3p <sub>x</sub>		0.015	0.024	0.022	-0.010	0.006	-0.004	0.036	-0.005	-0.013
3p <sub>y</sub>		0.028	-0.003	-0.015	0.084	-0.009	0.001	0.004	-0.007	0.008
3p <sub>z</sub>		-0.111	0.009	0.008	0.058	-0.009	0.019	0.099	0.007	0.012
3d <sub>z<sup>2</sup></sub>		-0.120	0.014	0.009	0.193	-0.086	0.058	-0.147	-0.051	0.055
3d <sub>xz</sub>		0.182	0.041	0.059	0.091	-0.017	0.012	-0.394	0.021	-0.070
3d <sub>yz</sub>		-0.194	0.022	-0.050	-0.094	-0.032	0.008	-0.073	0.036	-0.017
3d <sub>x<sup>2</sup>-y<sup>2</sup></sub>		-0.182	-0.007	0.074	0.356	0.015	0.015	-0.145	-0.013	0.041
3d <sub>xy</sub>		0.145	0.085	-0.045	0.047	-0.034	0.013	-0.008	-0.005	-0.009
N-1 2s		0.075	0.018	-0.015	-0.018	-0.006	-0.002	0.032	-0.003	0.005
2p <sub>x</sub>		0.212	-0.143	-0.247	-0.037	0.236	-0.091	-0.053	0.150	0.141
2p <sub>y</sub>		-0.185	-0.074	-0.026	0.032	0.022	-0.002	-0.073	-0.266	-0.263
2p <sub>z</sub>		-0.213	-0.157	-0.111	0.076	0.272	-0.100	0.104	-0.217	-0.195
N-2 2s		-0.064	0.012	-0.007	0.100	-0.002	0.010	-0.102	0.007	-0.008
2p <sub>x</sub>		-0.036	-0.305	-0.293	0.159	0.232	-0.092	-0.213	0.136	0.123
2p <sub>y</sub>		0.307	-0.090	-0.015	-0.380	0.040	-0.045	0.120	-0.182	-0.180
2p <sub>z</sub>		-0.019	-0.195	-0.208	-0.071	0.334	-0.156	-0.371	-0.119	-0.174
N-3 2s		0.075	0.018	0.015	0.019	-0.006	-0.002	-0.032	-0.003	-0.005
2p <sub>x</sub>		-0.212	0.143	-0.247	0.032	0.108	0.224	-0.053	-0.150	0.141
2p <sub>y</sub>		0.185	0.074	-0.026	0.034	-0.015	-0.017	0.073	-0.266	0.263
2p <sub>z</sub>		0.213	0.157	-0.111	0.074	-0.130	-0.261	0.104	0.217	-0.195
N-4 2s		-0.064	0.012	0.007	-0.098	0.007	-0.005	0.102	0.007	0.008

Atomic Orbitals ↓	Molecular Orbitals→ Eigenvalue/eV→	[Cu <sub>2</sub> (μ-Ph <sub>2</sub> Pbpy) <sub>2</sub> (CH <sub>3</sub> CN) <sub>2</sub> ](PF <sub>6</sub> ) <sub>2</sub>			1			2		
		HOMO	LUMO	SLUMO	HOMO	LUMO	SLUMO	HOMO	LUMO	SLUMO
		-11.62	-9.78	-9.62	-11.30	-9.96	-9.89	-11.23	-9.65	-9.57
2p <sub>x</sub>		0.036	0.305	-0.293	-0.172	0.108	0.228	-0.213	-0.136	0.123
2p <sub>y</sub>		-0.307	0.090	-0.015	-0.413	0.003	-0.065	-0.120	-0.182	0.180
2p <sub>z</sub>		0.019	0.195	-0.208	-0.076	-0.135	-0.338	-0.371	0.119	-0.174
P-1 3s		0.030	0.007	0.021	0.065	0.005	0.028	0.068	0.011	0.023
3p <sub>x</sub>		0.021	-0.039	-0.030	0.055	-0.002	0.033	0.116	0.031	0.027
3p <sub>y</sub>		-0.030	-0.040	0.071	0.035	0.003	0.010	-0.025	0.019	-0.041
3p <sub>z</sub>		-0.068	-0.040	0.017	-0.127	-0.022	-0.055	-0.082	-0.040	-0.013
3d <sub>z<sup>2</sup></sub>		-0.058	0.044	-0.027	-0.005	-0.025	-0.001	-0.036	-0.088	0.059
3d <sub>xz</sub>		-0.007	0.027	-0.034	-0.015	0.043	-0.010	-0.023	-0.002	0.014
3d <sub>yz</sub>		0.058	0.075	-0.039	-0.031	-0.039	-0.004	-0.009	-0.040	0.022
3d <sub>x<sup>2</sup>-y<sup>2</sup></sub>		0.037	-0.077	0.069	0.020	0.021	-0.000	0.006	-0.041	0.020
3d <sub>xy</sub>		-0.018	0.130	-0.116	0.023	-0.020	0.014	-0.021	0.074	-0.073
P-2 3s		0.030	0.007	-0.021	-0.067	0.022	-0.017	-0.068	0.011	-0.023
3p <sub>x</sub>		-0.021	0.039	-0.030	-0.058	0.022	-0.024	0.116	-0.031	0.027
3p <sub>y</sub>		0.030	0.040	0.071	0.034	-0.006	0.007	0.025	0.019	0.041
3p <sub>z</sub>		0.068	0.040	0.017	-0.131	0.053	-0.023	-0.082	0.040	-0.013
3d <sub>z<sup>2</sup></sub>		-0.058	0.044	0.027	0.002	-0.019	-0.016	0.036	-0.088	-0.059
3d <sub>xz</sub>		-0.007	0.027	0.034	-0.013	-0.022	-0.037	0.023	-0.002	-0.014
3d <sub>yz</sub>		0.058	0.075	0.039	0.030	-0.032	-0.022	-0.009	0.040	0.022
3d <sub>x<sup>2</sup>-y<sup>2</sup></sub>		0.037	-0.077	-0.069	-0.021	0.015	0.013	-0.006	-0.041	-0.020
3d <sub>xy</sub>		-0.018	0.130	0.116	0.021	0.008	0.027	-0.021	-0.074	-0.073



### B.2.5. $[\text{Pd}_2(\mu\text{-Ph}_2\text{Pbpy})_2](\text{BF}_4)_2 \mathbf{3}$

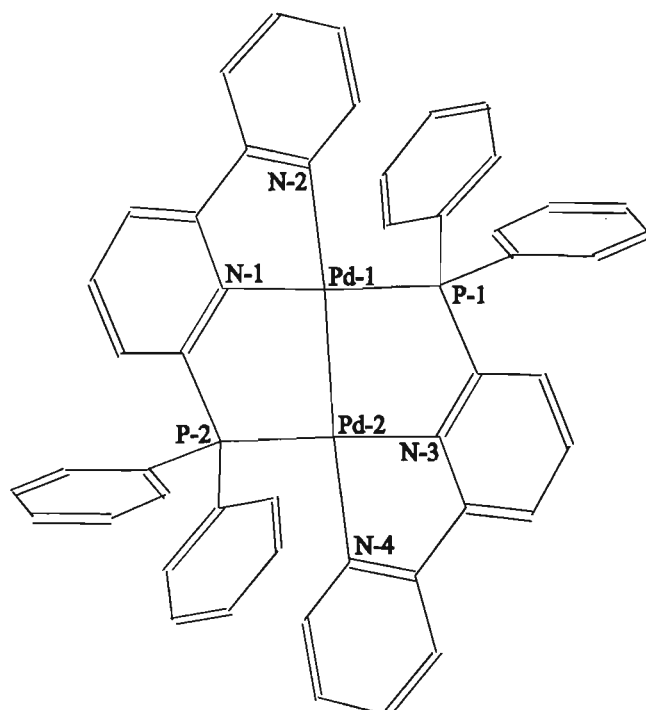


**Table B.41.** Molecular orbital coefficients of the metal and phosphorus-polypyridyl ligand donor atoms of  $[\text{Pd}_2(\mu\text{-Ph}_2\text{Pbpy})_2](\text{BF}_4)_2 \mathbf{3}$ .

Atomic Orbitals ↓	Molecular Orbitals→ Eigenvalue/eV→	HOMO -10.87	LUMO -9.76	SLUMO -9.73	TLUMO -9.63
Pd-1 4s		0.148	-0.018	0.013	-0.127
4p <sub>x</sub>		-0.019	0.039	0.017	0.043
4p <sub>y</sub>		0.005	-0.025	-0.027	0.036
4p <sub>z</sub>		-0.069	-0.002	-0.013	0.035
4d <sub>z<sup>2</sup></sub>		0.268	-0.001	0.048	-0.396
4d <sub>xz</sub>		0.156	-0.018	0.032	-0.280
4d <sub>yz</sub>		0.220	0.002	0.069	-0.212
4d <sub>x<sup>2</sup>-y<sup>2</sup></sub>		0.205	-0.054	-0.045	-0.221
4d <sub>xy</sub>		-0.282	-0.005	-0.044	0.180
Pd-2 4s		0.148	-0.018	-0.013	0.127
4p <sub>x</sub>		0.019	-0.039	0.017	0.043
4p <sub>y</sub>		-0.005	0.025	-0.027	0.036
4p <sub>z</sub>		0.069	0.002	-0.013	0.035
4d <sub>z<sup>2</sup></sub>		0.268	-0.001	-0.048	0.396
4d <sub>xz</sub>		0.156	-0.018	-0.032	0.280
4d <sub>yz</sub>		0.220	0.002	-0.069	0.212
4d <sub>x<sup>2</sup>-y<sup>2</sup></sub>		0.205	-0.054	0.045	0.221
4d <sub>xy</sub>		-0.282	-0.005	0.044	-0.180
P-1 3s		0.024	-0.002	0.013	-0.089

Atomic Orbitals	Molecular Orbitals→	HOMO	LUMO	SLUMO	TLUMO
↓	Eigenvalue/eV→	-10.87	-9.76	-9.73	-9.63
3p <sub>x</sub>		0.048	0.058	-0.010	-0.065
3p <sub>y</sub>		0.095	-0.032	0.032	-0.157
3p <sub>z</sub>		-0.008	-0.011	-0.005	0.115
3d <sub>z<sup>2</sup></sub>		0.041	0.091	-0.060	0.017
3d <sub>xz</sub>		-0.008	-0.139	0.085	-0.010
3d <sub>yz</sub>		-0.044	0.084	-0.055	-0.013
3d <sub>x<sup>2</sup>-y<sup>2</sup></sub>		0.011	-0.030	0.079	-0.041
3d <sub>xy</sub>		-0.047	-0.004	0.040	0.054
P-2 3s		0.024	-0.002	-0.013	0.089
3p <sub>x</sub>		-0.048	-0.058	-0.010	-0.065
3p <sub>y</sub>		-0.095	0.032	0.032	-0.157
3p <sub>z</sub>		0.008	0.011	-0.005	0.115
3d <sub>z<sup>2</sup></sub>		0.041	0.091	0.060	-0.017
3d <sub>xz</sub>		-0.008	-0.139	-0.085	0.010
3d <sub>yz</sub>		-0.044	0.084	0.055	0.013
3d <sub>x<sup>2</sup>-y<sup>2</sup></sub>		0.011	-0.030	-0.079	0.041
3d <sub>xy</sub>		-0.047	-0.004	-0.040	-0.054
N-1 2s		0.051	0.002	0.011	-0.076
2p <sub>x</sub>		-0.059	0.328	0.312	0.144
2p <sub>y</sub>		-0.213	-0.140	-0.163	0.171
2p <sub>z</sub>		0.017	-0.116	-0.117	-0.018
N-2 2s		-0.071	0.007	-0.011	0.075
2p <sub>x</sub>		0.144	0.147	0.194	-0.080
2p <sub>y</sub>		0.107	-0.100	-0.086	-0.127
2p <sub>z</sub>		0.223	-0.068	-0.029	-0.224
N-3 2s		0.051	0.002	-0.011	0.076
2p <sub>x</sub>		0.059	-0.328	0.312	0.144
2p <sub>y</sub>		0.213	0.140	-0.163	0.171
2p <sub>z</sub>		-0.017	0.116	-0.117	-0.018
N-4 2s		-0.071	0.007	0.011	-0.075
2p <sub>x</sub>		-0.144	-0.147	0.194	-0.080
2p <sub>y</sub>		-0.107	0.100	-0.086	-0.127
2p <sub>z</sub>		-0.223	0.068	-0.029	-0.224

**B.2.6.  $[\text{Ru}_2(\mu\text{-Ph}_2\text{Pbpy})_2(\text{CO})_2(\text{EtCN})_2](\text{PF}_6)_2$  **18** and  $[\text{Ru}_2(\mu\text{-Ph}_2\text{Ppyqn})_2(\text{CO})_2(\text{CH}_3\text{CN})_2](\text{PF}_6)_2$  **19****

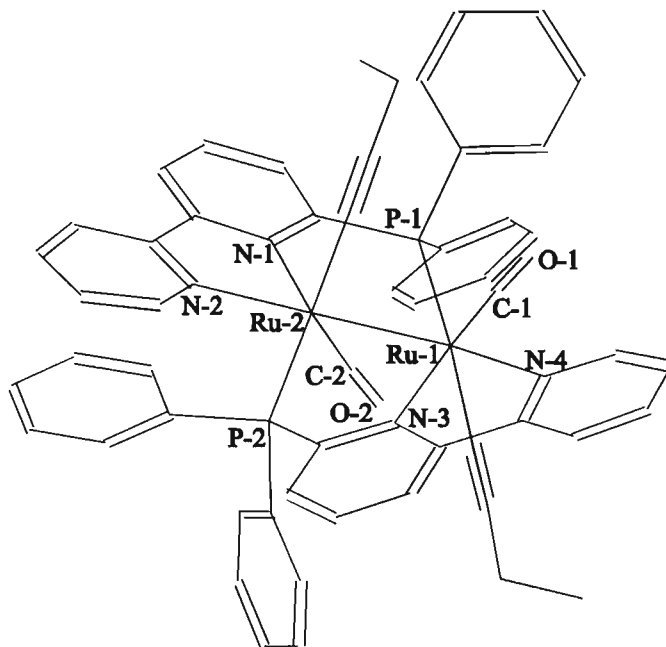


**Table B.42.** Molecular orbital coefficients of the metal, carbonyl and phosphorus-polypyridyl ligand donor atoms of  $[\text{Ru}_2(\mu\text{-L})_2(\text{CO})_2(\text{EtCN})_2](\text{PF}_6)_2$  (L = Ph<sub>2</sub>Pbpy **18** and Ph<sub>2</sub>Ppyqn **19**).

Atomic Orbitals	Molecular Orbitals→ Eigenvalue/eV→	$[\text{Ru}_2(\mu\text{-Ph}_2\text{Pbpy})_2(\text{CO})_2(\text{EtCN})_2](\text{PF}_6)_2$ <b>18</b>				$[\text{Ru}_2(\mu\text{-Ph}_2\text{Ppyqn})_2(\text{CO})_2(\text{CH}_3\text{CN})_2](\text{PF}_6)_2$ <b>19</b>			
		HOMO	LUMO	SLUMO	TLUMO	HOMO	LUMO	SLUMO	TLUMO
↓		-12.02	-10.35	-9.64	-9.63	-12.04	-10.69	-9.92	-9.87
Ru-1 4s		-0.036	-0.093	0.034	-0.005	-0.022	0.095	-0.003	-0.034
4p <sub>x</sub>		0.160	0.108	-0.024	0.007	-0.127	0.062	0.014	-0.020
4p <sub>y</sub>		-0.017	0.038	-0.012	-0.011	0.025	-0.062	0.006	0.023
4p <sub>z</sub>		0.026	-0.026	0.031	-0.017	-0.065	0.039	0.018	-0.030
		0.066	0.255	-0.053	-0.001	0.034	-0.059	0.034	-0.059

Atomic Orbitals	Molecular Orbitals→ Eigenvalue/eV→	[Ru <sub>2</sub> (μ-Ph <sub>2</sub> Pbpy) <sub>2</sub> (CO) <sub>2</sub> (EtCN) <sub>2</sub> ](PF <sub>6</sub> ) <sub>2</sub> <b>18</b>				[Ru <sub>2</sub> (μ-Ph <sub>2</sub> Ppyqn) <sub>2</sub> (CO) <sub>2</sub> (CH <sub>3</sub> CN) <sub>2</sub> ](PF <sub>6</sub> ) <sub>2</sub> <b>19</b>			
		HOMO	LUMO	SLUMO	TLUMO	HOMO	LUMO	SLUMO	TLUMO
↓		-12.02	-10.35	-9.64	-9.63	-12.04	-10.69	-9.92	-9.87
4d <sub>xz</sub>		0.021	0.059	-0.026	0.007	-0.072	0.365	-0.012	-0.099
4d <sub>yz</sub>		-0.010	-0.008	0.132	-0.057	0.053	-0.165	0.019	0.018
4d <sub>x<sup>2</sup>-y<sup>2</sup></sub>		-0.146	-0.468	0.094	0.010	-0.053	0.227	0.001	-0.102
4d <sub>xy</sub>		-0.019	-0.028	-0.033	0.043	0.071	-0.234	0.029	0.074
Ru-2 4s		-0.036	0.093	-0.034	-0.005	-0.032	-0.093	0.013	0.036
4p <sub>x</sub>		-0.160	0.108	-0.024	-0.007	0.109	0.079	-0.031	-0.027
4p <sub>y</sub>		0.017	0.038	-0.012	0.011	-0.035	-0.048	-0.005	0.011
4p <sub>z</sub>		0.026	0.026	-0.031	-0.017	0.085	0.010	-0.012	0.008
4d <sub>z<sup>2</sup></sub>		0.066	-0.255	0.053	-0.001	0.028	0.112	-0.018	-0.071
4d <sub>xz</sub>		-0.021	0.059	-0.026	-0.007	-0.083	-0.316	0.037	0.108
4d <sub>yz</sub>		0.010	-0.008	0.132	0.057	0.053	0.122	-0.020	-0.065
4d <sub>x<sup>2</sup>-y<sup>2</sup></sub>		-0.146	0.468	-0.094	0.010	-0.084	-0.296	0.034	0.075
4d <sub>xy</sub>		-0.019	0.028	0.033	0.043	0.093	0.225	0.054	-0.008
P-1 3s		0.003	-0.058	0.007	0.001	0.000	-0.055	0.007	0.015
3p <sub>x</sub>		-0.086	0.033	-0.044	-0.010	-0.056	0.051	-0.011	-0.028
3p <sub>y</sub>		-0.022	-0.104	-0.032	-0.016	0.052	0.095	-0.019	0.000
3p <sub>z</sub>		-0.037	-0.054	0.008	0.000	-0.059	0.021	-0.004	-0.003
3d <sub>z<sup>2</sup></sub>		-0.005	-0.037	0.019	-0.026	0.038	-0.026	0.022	-0.065
3d <sub>xz</sub>		0.061	0.020	-0.056	-0.024	0.015	0.027	-0.014	-0.006
3d <sub>yz</sub>		-0.011	0.036	0.104	0.024	-0.023	-0.013	0.020	-0.034
3d <sub>x<sup>2</sup>-y<sup>2</sup></sub>		0.008	0.009	-0.007	0.017	-0.034	-0.019	0.009	-0.012
3d <sub>xy</sub>		0.017	0.021	0.031	0.059	-0.031	-0.013	0.027	0.015
P-2 3s		0.003	0.058	-0.007	0.001	0.002	0.054	-0.001	-0.020
		0.086	0.033	-0.044	0.010	0.078	0.002	-0.003	-0.005

Atomic Orbitals	Molecular Orbitals→ Eigenvalue/eV→	<u>[Ru<sub>2</sub>(μ-Ph<sub>2</sub>Pbpy)<sub>2</sub>(CO)<sub>2</sub>(EtCN)<sub>2</sub>](PF<sub>6</sub>)<sub>2</sub> 18</u>				<u>[Ru<sub>2</sub>(μ-Ph<sub>2</sub>Ppyqn)<sub>2</sub>(CO)<sub>2</sub>(CH<sub>3</sub>CN)<sub>2</sub>](PF<sub>6</sub>)<sub>2</sub> 19</u>			
		HOMO	LUMO	SLUMO	TLUMO	HOMO	LUMO	SLUMO	TLUMO
↓		-12.02	-10.35	-9.64	-9.63	-12.04	-10.69	-9.92	-9.87
3p <sub>y</sub>		0.022	-0.104	-0.032	0.016	-0.024	0.056	0.017	0.008
3p <sub>z</sub>		-0.037	0.054	-0.008	0.000	0.015	0.099	0.003	-0.043
3d <sub>z<sup>2</sup></sub>		-0.005	0.037	-0.019	-0.026	-0.042	0.008	-0.011	-0.038
3d <sub>xz</sub>		-0.061	0.020	-0.056	0.024	-0.014	-0.006	0.002	0.007
3d <sub>yz</sub>		0.011	0.036	0.104	-0.024	0.013	-0.020	0.012	0.022
3d <sub>x<sup>2</sup>-y<sup>2</sup></sub>		0.008	-0.009	0.007	0.017	0.030	-0.011	0.013	0.021
3d <sub>xy</sub>		0.017	-0.021	-0.031	0.059	-0.013	0.039	0.068	0.043
N-1 2s		-0.026	0.049	-0.030	-0.006	-0.016	0.043	-0.005	-0.020
2p <sub>x</sub>		-0.089	0.028	0.025	0.023	-0.033	-0.018	-0.076	0.162
2p <sub>y</sub>		-0.083	0.148	0.187	0.252	0.104	-0.172	0.111	-0.100
2p <sub>z</sub>		-0.122	0.095	-0.297	-0.227	-0.095	0.018	0.143	-0.269
N-2 2s		0.070	-0.113	0.020	-0.006	0.063	-0.111	0.013	0.023
2p <sub>x</sub>		0.330	-0.373	0.078	-0.001	0.179	-0.192	-0.059	0.173
2p <sub>y</sub>		0.040	-0.009	0.207	0.222	-0.106	0.112	0.154	-0.306
2p <sub>z</sub>		0.110	-0.150	-0.099	-0.145	0.279	-0.342	0.159	-0.147
N-3 2s		-0.026	-0.049	0.030	-0.006	-0.018	-0.043	0.002	0.023
2p <sub>x</sub>		0.089	0.028	0.025	-0.023	0.121	0.071	-0.111	-0.105
2p <sub>y</sub>		0.083	0.148	0.187	-0.252	-0.050	-0.111	-0.298	-0.160
2p <sub>z</sub>		-0.122	-0.095	0.297	-0.227	-0.055	-0.102	0.086	0.108
N-4 2s		0.070	0.113	-0.020	-0.006	0.068	0.111	0.005	-0.026
2p <sub>x</sub>		-0.330	-0.373	0.078	0.001	-0.347	-0.396	-0.046	0.068
2p <sub>y</sub>		-0.040	-0.009	0.207	-0.222	0.028	0.002	-0.371	-0.226
2p <sub>z</sub>		0.110	0.150	0.099	-0.145	-0.043	-0.051	-0.008	0.006
		0.012	-0.067	0.047	-0.011	0.010	0.056	-0.003	-0.032

Atomic Orbitals	Molecular Orbitals→ Eigenvalue/eV→	<u>[Ru<sub>2</sub>(μ-Ph<sub>2</sub>Pbpy)<sub>2</sub>(CO)<sub>2</sub>(EtCN)<sub>2</sub>](PF<sub>6</sub>)<sub>2</sub> 18</u>				<u>[Ru<sub>2</sub>(μ-Ph<sub>2</sub>Ppyqn)<sub>2</sub>(CO)<sub>2</sub>(CH<sub>3</sub>CN)<sub>2</sub>](PF<sub>6</sub>)<sub>2</sub> 19</u>			
		HOMO	LUMO	SLUMO	TLUMO	HOMO	LUMO	SLUMO	TLUMO
↓		-12.02	-10.35	-9.64	-9.63	-12.04	-10.69	-9.92	-9.87
2p <sub>x</sub>		0.090	0.082	-0.010	0.031	-0.063	0.091	0.005	-0.014
2p <sub>y</sub>		0.007	0.008	0.062	-0.077	0.035	0.002	0.012	-0.036
2p <sub>z</sub>		-0.014	0.081	-0.014	-0.033	-0.041	-0.026	0.042	-0.018
C-2 2s		0.012	0.067	-0.047	-0.011	0.006	-0.059	0.009	0.035
2p <sub>x</sub>		-0.090	0.082	-0.010	-0.031	0.066	0.014	-0.033	0.003
2p <sub>y</sub>		-0.007	0.008	0.062	0.077	-0.026	-0.036	-0.033	-0.019
2p <sub>z</sub>		-0.014	-0.081	0.014	-0.033	0.024	0.080	-0.015	-0.031
O-1 2s		0.003	0.007	-0.006	0.003	0.001	-0.006	-0.001	0.005
2p <sub>x</sub>		-0.091	-0.057	0.006	-0.020	0.070	-0.069	-0.003	0.010
2p <sub>y</sub>		-0.002	-0.006	-0.040	0.050	-0.031	-0.001	-0.010	0.026
2p <sub>z</sub>		0.006	-0.057	0.011	0.019	0.040	0.019	-0.027	0.010
O-2 2s		0.003	-0.007	0.006	0.003	0.000	0.005	-0.002	-0.004
2p <sub>x</sub>		0.091	-0.057	0.006	0.020	-0.069	-0.012	0.020	-0.002
2p <sub>y</sub>		0.002	-0.006	-0.040	-0.050	0.028	0.028	0.024	0.012
2p <sub>z</sub>		0.006	0.057	-0.011	0.019	-0.031	-0.061	0.012	0.022

## References

---

1. K.A. Magrini and D. Boron, *Chem. & Ind.*, 1994, 997.
2. A. Behr, *Carbon Dioxide Activation by Metal Complexes*, VCH, Weinheim, 1988.
3. H. Arakawa, M. Aresta, J.N. Armor, M.A. Barteau, E.J. Beckman, A.T. Bell, J.E. Bercaw, C. Creutz, E. Dinjus, D.A. Dixon, K. Domen, D.L. DuBois, J. Eckert, E. Fujita, D.H. Gibson, W.A. Goddard, D.W. Goodman, J. Keller, G.J. Kubas, H.H. Kung, J.E. Lyons, L.E. Manzer, T.J. Marks, K. Morokuma, K.M. Nicholas, R. Periana, L. Que, J. Rostrup-Nielson, W.M.H. Sachtler, L.D. Schmidt, A. Sen, G.A. Somorjai, P.C. Stair, B.R. Stults and W. Tumas, *Chem. Rev.*, 2001, **101**, 953.
4. W. Leitner, *Angew. Chem., Int. Ed. Engl.*, 1995, **34**, 2207.
5. *Carbon Dioxide Chemistry: Environmental Issues*, Eds. J. Paul, C.-M. Pradier, Royal Society of Chemistry, London, 1994.
6. A. Gennaro, A.A. Isse, M.-G. Severin, E. Vianello, I. Bhugun and J.-M. Savéant, *J. Chem. Soc., Faraday Trans.*, 1996, **92**, 3963. (and references cited therein)
7. C. Amatore and J.M. Savéant, *J. Am. Chem. Soc.*, 1981, **103**, 5021, and references cited therein.
8. E. Lamy, L. Nadjo and J.-M. Savéant, *J. Electroanal. Chem.*, 1977, **78**, 403.
9. *Electrochemical and Electrocatalytic Reactions of Carbon Dioxide*, eds. B.P. Sullivan, K. Krist and H.E. Guard, Elsevier, Amsterdam, 1993, ch 1, p 7.
10. J.P. Collin and J.P. Sauvage, *Coord. Chem. Rev.*, 1989, **93**, 245.
11. R.J. Haines, R.E. Wittrig and C.P. Kubiak, *Inorg. Chem.*, 1994, **33**, 4723.
12. A.G.M. Mostafa Hossain, T. Nagoaka and K. Ogura, *Electrochimica Acta*, 1996, **41**, 2773.
13. A.G.M. Mostafa Hossain, T. Nagoaka and K. Ogura, *Electrochimica Acta*, 1997, **42**, 2577.
14. D.L. DuBois and A. Miedaner, *J. Am. Chem. Soc.*, 1987, **109**, 113.
15. D.L. DuBois, A. Miedaner and R.C. Haltiwanger, *J. Am. Chem. Soc.*, 1991, **113**, 8753
16. P.R. Bernatis, A. Miedaner, R.C. Haltiwanger and D.L. DuBois, *Organometallics*, 1994, **13**, 4835.
17. B.D. Steffey, A. Miedaner, M.L. Maciejewski-Farmer, P.R. Bernatis, A.M. Herring, V.S. Allured, V. Carperos and D.L. DuBois, *Organometallics*, 1994, **13**, 4844.
18. S.A. Wander, A. Miedaner, B.C. Noll, R.M. Barkley and D.L. DuBois, *Organometallics*, 1996, **15**, 3360.

19. A. Miedaner, B.C. Noll and D.L. DuBois, *Organometallics*, 1997, **16**, 5779.
20. A.M. Herruig, B.D. Steffey, A. Miedaner, S.A. Waneler and D.L. DuBois, *Inorg Chem.*, 1995, **34**, 1100.
21. BD Steffen, CJ Curtis, D.L. Dubois, *Organometallics*, 1995, **14**, 4937.
22. H. Ishida, K. Tanaka and T. Tanaka, *Organometallics*, 1987, **6**, 181; H. Ishida, K. Tanaka and T. Tanaka, *Chem. Lett.*, 1985, 405; H. Ishida, H. Tanaka, K. Tanaka and T. Tanaka, *J. Chem. Soc., Chem. Commun.*, 1987, 131.
23. J.-M. Lehn and R. Ziessel, *J. Organomet. Chem.*, 1990, **382**, 157.
24. H. Ishida, K. Fujiki, T. Ohba, K. Tanaka, T. Terada and T. Tanaka, *J. Chem. Soc., Dalton Trans.*, 1990, 2155.
25. J.R. Pugh, M.R.M. Bruce, B.P. Sullivan and T.J. Meyer, *Inorg. Chem.*, 1991, **30**, 86.
26. H. Nakajima, Y. Kushi, H. Nagao and K. Tanaka, *Organometallics*, 1995, **14**, 5093.
27. H. Nagao, T. Mizukawa and K. Tanaka, *Inorg. Chem.*, 1994, **33**, 3415.
28. T. Mizukawa, K. Tsuge, H. Nakajima and K. Tanaka, *Angew. Chem. Int. Ed.*, 1999, **38**, 362.
29. H. Tanaka, H. Nagao, S.-M. Peng and K. Tanaka, *Organometallics*, 1992, **11**, 1450; H. Tanaka, B.-C. Tzeng, H. Nagao, S.-M. Peng and K. Tanaka, *Inorg. Chem.*, 1993, **32**, 1508.
30. E. Fujita, M. Chou and K. Tanaka, *Appl. Organometal. Chem.*, 2000, **14**, 844.
31. K. Toyohara, H. Nagao, T. Adachi, T. Yoshida and K. Tanaka, *Chem. Lett.*, 1996, 27.
32. K. Toyohara, H. Nagao, T. Mizukawa and K. Tanaka, *Inorg. Chem.*, 1995, **34**, 5399.
33. K. Tanaka and T. Mizukwa, *Appl. Organometal. Chem.*, 2000, **14**, 863.
34. H. Nakajima and K. Tanaka, *Chem. Lett.*, 1995, **10**, 891.
35. Md.M. Ali, H. Sato, T. Mizukawa, K. Tsuge, M. Haga and K. Tanaka, *J. Chem. Soc. Chem. Commun.*, 1998, 249.
36. S. Rau, M. Ruben, T. Büttner, C. Temme, S. Dautz, H. Görls, M. Rudolph, D. Walther, A. Brodkorb, M. Duati, C. O'Connor and J.G. Vos, *J. Chem. Soc., Dalton Trans.*, 2000, 3649.
37. M.-N. Collomb-Dunand-Sauthier, A. Deronzier and R. Ziessel, *Inorg. Chem.*, 1994, **33**, 2961.
38. S. Chardon-Noblat, A. Deronzier, D. Zsoldos, R. Ziessel, M. Haukka, T. Pakkanen and T. Venäläinen, *J. Chem. Soc., Dalton Trans.*, 1996, 2581.
39. M.-N. Collomb-Dunand-Sauthier, A. Deronzier and R. Ziessel, *J. Electroanal. Chem.*, 1993, **350**, 43.



40. M.-N. Collomb-Dunand-Sauthier, A. Deronzier and R. Ziessel, *J. Chem. Soc., Chem. Commun.*, 1994, 189.
41. S. Chardon-Noblat, M.-N. Collomb-Dunand-Sauthier, A. Deronzier, R. Ziessel and D. Zsoldos, *Inorg. Chem.*, 1994, **33**, 4410.
42. S. Chardon-Noblat, A. Deronzier, R. Ziessel, D.J. Zsoldos, *J. Electroanal. Chem.*, 1998, **444**, 253.
43. S. Chardon-Noblat, P. Da Costa, A. Deronzier, M. Haukka, T.A. Pakkanen, R. Ziessel, *J. Electroanal. Chem.*, 2000, **490**, 62.
44. C. Caix-Cecillon, S. Chardon-Noblat, A. Deronzier, M. Haukka, T.A. Pakkanen, R. Ziessel, D. Zsoldos, *J. Electroanal. Chem.*, 1999, **466**, 187.
45. K.W. Frese and S. Leach, *J. Electrochem. Soc.*, 1985, 259.
46. CJ Stalder, S. Chao and M.S. Wrighton, *J. Am. Chem. Soc.*, 1984, **106**, 3673.
- 47 K. Hara and T. Sakata, *J. Electrochem.Soc.*, 1997, **144**, 539.
48. S. Kuwabata, R. Tsuda and H. Yoneyama, *J. Am. Chem. Soc.*, 1994, **116**, 5437; Y. Hori, K. Kikuchi, A. Murata, S. Suzuki, *Chem. Lett.*, 1986, 897; G. Kyriacou and A. Anagnostopoulos, *J. Electroanal. Chem.*, 1992, **328**, 233; Y. Hori, K. Kikuchi and S. Suzuki, *Chem. Lett.*, 1958, 1695; M. Azuma, K. Hashimoto, M. Hiromoto, M. Watanabe and T. Sakata, *J. Electrochem. Soc.*, 1990, **137**, 1772; A. Naitoh, K. Otha, T. Mizuno, H. Yoshida, M. Sakai and H. Noda, *Electrochim. Acta*, 1993, **38**, 2177.
49. J.S. Field, R.J. Haines, J. Sundermeyer and S.F. Woollam, *J. Chem. Soc., Chem. Commun.*, 1990, 985; J.S. Field, R.J. Haines, J. Sundermeyer and S.F. Woollam, *J. Chem. Soc., Dalton Trans.*, 1993, 2735.
50. D.H. Gibson, Y. Ding, B.A. Sleadd, J.O. Franco, J.F. Richardson and M.S. Mashuta, *J. Am. Chem. Soc.*, 1996, **118**, 11984; D.H. Gibson, Y. Ding, J.G. Andino, M.S. Mashuta and J.F. Richardson, *Organometallics*, 1998, **17**, 5178; D.H. Gibson, J.M. Mehta, B.A. Sleadd, M.S. Mashuta and J.F. Richardson, *Organometallics*, 1995, **14**, 4886; K.K. Pandey, *Coord. Chem. Rev.*, 1995, **140**, 37; W. Leitner, *Coord. Chem. Rev.*, 1996, **153**, 257.
51. M. Hammouche, D. Lexa, M.. Momenteau and J.-M. Savéant, *J. Am. Chem. Soc.*, 1991, **113**, 8455.
52. P. Espinet and K. Soulantica, *Coord. Chem. Rev.*, 1999, **193 – 195**, 499.
53. P. Molina, A.Arques, A. García and M.C. Ramírez de Arellanno, *Eur. J. Inorg. Chem.*, 1998, 1359; K. Tani, M. Yabuta, S. Nakamura and T. Yamagata, *J. Chem. Soc., Dalton Trans.*, 1993, 2781; M. Grassi, G. De Munno, F. Nicolo and S. Lo Schiave, *J. Chem. Soc., Dalton Trans.*, 1992, 2367; S. Stoccoro, G. Chelucci, A. Zucca, M.A. Cinellu, G. Minghetti and M. Manassero, *J. Chem. Soc., Dalton Trans.*, 1996, 1295.

54. A. Del Zotto, A. Mezzetti and P. Rigo, *J. Chem. Soc., Dalton Trans.*, 1994, 2257; M.P. Anderson, A.L. Casalnuovo, B.J. Johnson, B.M. Mattson, A.M. Mueting and L.H. Pignolet, *Inorg. Chem.*, 1988, **27**, 1649.
55. JM Brown, D.I. Hulmes and T.P. Layzell, *J. Chem. Soc., Chem. Commun.*, 1993, 1673; P. Vonmatt and A. Pfaltz, *Angew. Chem., Int. Ed. Engl.*, 1993, **32**, 566.
56. G.R. Newkome, *Chem. Rev.*, 1993, **93**, 2067.
57. R. Ziessel, *Tetrahedron Lett.*, 1989, **30**, 463.
58. R. Ziessel, L. Toupet, S. Chardon-Noblat, A. Deronzier and D. Matt, *J. Chem. Soc., Dalton Trans.*, 1997, 3777.
59. R. Ziessel, D. Matt and L. Toupet, *J. Chem. Soc., Chem. Commun.*, 1995, 2033.
60. S.M. Kuang, Z-Z. Zhang, Q-G. Wang and T.C.W. Mak, *J. Chem. Soc., Dalton Trans.*, 1997, 4477.
61. J.P. Farr, M.M. Olmstead, N.M. Rutherford, F.E. Wood and A.L. Balch, *Organometallics*, 1983, **2**, 1758; J.P. Farr, M.M. Olmstead and A.L. Balch, *J. Am. Chem. Soc.*, 1980, **102**, 6654; S. Lo Schiavo, E. Rotondo, G. Bruno and F. Faraone, *Organometallics*, 1991, **10**, 1613; A. Maisonnnet, J.P. Farr, M.M. Olmstead, C.T. Hunt and A.L. Balch, *Inorg. Chem.*, 1982, **21**, 3961; Z-Z. Zhang, H-P. Xi, W-J. Zhao, K-Y. Jiang, R-J. Wang H-G. Wang and Y. Wu, *J. Organomet. Chem.*, 1993, **454**, 221; S-L. Li, T.C.W. Mak and Z-Z. Zhang, *J. Chem. Soc., Dalton Trans.*, 1996, 3475; W.-H Chan, Z.-Z Zhang, T.C.W. Mak and C.-M Che, *J. Chem. Soc., Dalton Trans.*, 1998, 803.
62. J.S. Field, R.J. Haines, C.J. Parry and S.H. Sookraj, *S. Afr. J. Chem.*, 1993, **46**, 70.
63. E.C. Constable, *Adv. Inorg. Chem. Radiochem.*, 1989, **34**, 1.
64. N.S. Ramesar, M.Sc. Thesis, University of Natal, 1998.
65. T.E. Keyes, J.G. Vos, J.A. Kolnaar, J.G. Haasnoot, J. Reedijk and R. Hage, *Inorg. Chim. Acta*, 1996, **245**, 237.
66. H. Masuda, N. Fukushima and H. Einaga, *Bull. Chem. Soc. Jpn.*, 1993, **66**, 3643.
67. *Metal-Ligand Interactions: from Atoms, to Clusters, to Surfaces*, eds. D.R. Salahub and N. Russo, Kluwer Academic Publishers, Netherlands, 1992, p175.
68. D.H. Gibson, *Chem. Rev.*, 1996, **96**, 2063; M. Aresta and C.F. Nobile, *J. Chem. Soc., Chem. Com.*, 1975, 636.
69. B. Beilenson and F.M. Hamer, *J. Chem. Soc.*, 1939, 143.
70. N. Furukawa, F. Takahashi, T. Kawai, K. Kishimoto, S. Ogawa and S. Oae, *Phosphorus Sulfur*, 1983, **16**, 167.
71. A. Albert and G.B. Barlin, *J. Chem. Soc.*, 1959, 2384.

72. L. Testaferri, M. Tingoli and M. Tiecco, *J. Org. Chem.*, 1980, **45**, 4376; P. Cogolli, F. Maiolo, L. Testaferri, M. Tingoli and M. Tiecco, *J. Org. Chem.*, 1979, **44**, 2642; D. Chianelli, L. Testaferri, M. Tiecco and M. Tingoli, *Synthesis*, 1982, 475.
73. S. Oae, T. Kawai and N. Furukawa, *Tetrahedron Lett.*, 1983, **24**, 2957.
74. J. Uenishi, T. Tanaka, K. Nishiwaki, S. Wakabayashi, S. Oae and H. Tsukube, *J. Org. Chem.*, 1993, **58**, 4382.
75. S. Wakabayashi, T. Tanaka, Y. Kubo, J. Uenishi and S. Oae, *Bull. Chem. Soc. Jpn.*, 1989, **62**, 3848; N. Furukawa, T. Shibutani and H. Fujihara, *Tetrahedron Lett.*, 1987, **28**, 5845; S. Oae and N. Furukawa, *Adv. Heterocycl. Chem.*, 1990, **48**, 1.
76. P.A. MacNeil, N.K. Roberts and B. Bosnich, *J. Am. Chem. Soc.*, 1981, **103**, 2273; S.L. Li, Z-Z Zhang and T.C.W. Mak, *J. Organomet. Chem.*, 1997, **536-637**, 73; S-M. Kuang, Z-Z. Zhang, B-M. Wu and T.C.W. Mak, *J. Organomet. Chem.*, 1997, **540**, 55.
77. *Advanced Inorganic Chemistry* (5<sup>th</sup> Edition), F. A. Cotton and G. Wilkinson, John Wiley & Sons, New York, 1988.
78. J.B. Robert and J.D. Robert, *J. Am. Chem. Soc.*, 1972, **94**, 4902.
79. *Phosphorus-31 NMR Spectroscopy in Stereochemical Analysis, Organic Compounds and Metal Complexes*, Eds. J.G. Verkade and L.D. Quin, VCH Publishers, Weinheim, 1987.
80. J.B. Hendrickson, M.L. Maddox, J.J. Sims and H.D. Kaesz, *Tetrahedron*, 1964, **20**, 449; G. Mavel, *J. Chim. Phys.*, 1962, **59**, 683.
81. D. Gagnaire, J.B. Robert and J. Verrier, *Chem. Comm.*, 1967, 819.
82. F.A. Kramer and R. West, *J. Phys. Chem.*, 1965, **69**, 673, and references cited therein.
83. T.M. Spotswood and C.I. Tanzer, *Aust. J. Chem.*, 1967, **20**, 1227.
84. B.E. Mann, *J. Chem. Soc., Perkin Trans. II*, 1972, 30.
85. A. Marker, A.J. Canty and R.T.C. Brownlee, *Aust. J. Chem.*, 1978, **31**, 1255.
86. P.J. Black and M.L. Hefernan, *Aust. J. Chem.*, 1964, **17**, 558.
87. J.D. Memory and N.K. Wilson, *NMR of Aromatic Compounds*, Wiley, New York, 1982, p 56.
88. E. Breitmaier and W. Voelter, *Carbon-13 NMR Spectroscopy*, Weinheim, New York, 1987, p. 324.
89. K. Nakamoto, *J. Phys. Chem.*, 1960, **64**, 1420.
90. S. Castellano, H. Günther and S. Ebersole, *J. Phys. Chem.*, 1965, **69**, 4166.
91. L.L. Merritt and E.D. Schroeder, *Acta Crystallogr.*, 1956, **9**, 801.

92. S. Ernst and W. Kaim, *J. Am. Chem. Soc.*, 1986, **108**, 3578; S.D. Erust and W. Kaim, *Inorg. Chem.*, 1989, **28**, 1520; Y. Ohsawa, M-H Whang, K.W. Hanck and M.K. De Armond, *Inorg. Chem.*, 1984, **23**, 3427; W. Kaim and S. Kohlmann, *Inorg. Chem.*, 1987, **26**, 68; F. Barigelletti, A. Juris, V. Balzani, P. Belser and A. von Zelewsky, *Inorg. Chem.*, 1987, **26**, 4115; P. Chen, M. Curry and T.J. Meyer, *Inorg. Chem.*, 1989, **28**, 2271.
93. C.M. Elliott and E.J. Hershenhart, *J. Am. Chem. Soc.*, 1982, **104**, 7519.
94. P.T. Kissinger and W.R. Heineman, *J. Chem. Educ.*, 1983, **60**, 702; J. Heinze, *Angew. Chem., Int. Ed. Engl.*, 1984, **23**, 831.
95. M. Krejčík and A.A. Vlček, *J. Electroanal. Chem.*, 1991, **313**, 243.
96. M. Nakamura, M. Miki and T. Majima, *J. Chem. Soc., Perkin Trans. 2*, 2000, 1447.
97. M. Culcasi, Y. Berchadsky, G. Gronchi and P. Tordo, *J. Org. Chem.*, 1991, **56**, 3537.
98. J. Díez, M. Pilar Gamasa, J. Guineno, A. Tiripicchio and M. Tiripicchio Camellini, *J. Chem. Soc., Dalton Trans.*, 1987, 1275.
99. J.S. Field, R.J. Haines and B. Warwick, *Polyhedron*, 1996, **15**, 3741.
100. E. Lastra, M.P. Gamasa, J. Guineno, M. Lanfranchi and A. Tiripicchio, *J. Chem. Soc., Dalton Trans.*, 1989, 1499.
101. J.S. Field, R.J. Haines, C.J. Parry and S.H. Sookraj, *Polyhedron*, 1993, **12**, 2425.
102. M. Maekawa, M. Munakata, S. Kitagawa and T. Yonezawa, *Bull. Chem. Soc. Jpn.*, 1991, **64**, 2286.
103. A. Knödler, K. Hübler, T. Sixt and W. Kaim, *Inorg. Chem. Commun.*, 2000, **3**, 182.
104. A.M. Manotti Lanfredi, F. Ugozzoli, A.M. Camus and N. Marsich, *Inorg. Chim. Acta*, 1985, **99**, 111.
105. M. Munakato, S. Kitagawa, H. Simono, T. Emori and H. Masuda, *J. Chem. Soc., Chem. Comm.*, 1987, 1798.
106. M.J. Samide and D.G. Peters, *J. Electroanal. Chem.*, 1998, **443**, 95.
107. M.I. Pilo, G. Manca, M.A. Zoroddu and R. Seeber, *Inorg. Chim. Acta*, 1991, **180**, 225.
108. P. Federlin, J-M Keru and A. Rastegar, *New J. Chem.*, 1990, **14**, 9.
109. A.M. Leiva, L. Rivera and B. Loeb, *Polyhedron*, 1991, **10**, 347.
110. W. Kaim and S. Kohlmann, *Inorg. Chem.*, 1987, **26**, 1471; S.M. Scott, K.C. Gordon and A.K. Burrell, *Inorg. Chem.*, 1996, **35**, 2452; S.M. Scott, K.C. Gordon and A.K. Burrell, *J. Chem. Soc., Dalton Trans.*, 1998, 2873; S.E. Page, K.C. Gordon, A.K. Burrell, *Inorg. Chem.*, 1998, **37**, 4452; M. Glöckle, K. Hübler, H.-J. Kümmerer, G. Denninger and W. Kaim, *Inorg. Chem.*, 2001, **40**, 2263; J. Fees, M. Ketterle, A. Klein, J. Fielder and W. Kaim,

- J. Chem. Soc., Dalton Trans.*, 1999, 2595; C. Vogler, W. Kaim and H.-D. Hausen, *Z. Naturforsch.*, 1993, **48 b**, 1470; C. Vogler and W. Kaim, *Z. Naturforsch.*, 1992, **47 b**, 1057.
111. G. Sanna, M.I. Pilo, M.A. Zoroddu, R. Seeber and S. Mosca, *Inorg. Chim. Acta*, 1993, **208**, 153.
  112. C. Dietrich-Buchecker, J-P Sauvage and J-M Keru, *J. Am. Chem. Soc.*, 1989, **111**, 7791; C. Dietrich-Buchecker and J-P Sauvage, *J. Am. Chem. Soc.*, 1984, **106**, 3043.
  113. P. Federlin, J.-M. Kern and A. Rastegar, C. Dietrich-Buchecker, P.A. Marnot and J.-P. Sauvage, *New J. Chem.*, 1990, **14**, 9.
  114. Md. A. Masood and P.S. Zacharias, *J. Chem. Soc., Dalton Trans.*, 1991, 111.
  115. S. Sundararajan and E.L. Wehry, *J. Phys. Chem.*, 1972, **76**, 1528. P.M. Bush, J.P. Whitehead, C.C. Pink, E.C. Gramm, J.L. Eglin, S.P. Watton and L.E. Pence, *Inorg. Chem.*, 2001, **40**, 1871; B. Xie, T. Elder, L.J. Wilson, and D.M. Stanbury, *Inorg. Chem.*, 1999, **38**, 12; J.-M. Kern, L. Raehm, J.-P. Sauvage, B. Divisia-Blohorn and P.-L. Vidal, *Inorg. Chem.*, 2000, **39**, 1555; D.R. McMillin, J.R. Kirchoff, and K.V. Goodwin, *Coord. Chem. Rev.*, 1985, **64**, 83.
  116. M.T. Miller, P.K. Gantzel and T.B. Karpishin, *Angew. Chem. Int. Ed.*, 1998, **37**, 1556.
  117. E.C. Riesgo, Y.-Z. Hu, F. Bouvier, R.P. Thummel, D.V. Scaltrito and G.J. Meyer, *Inorg. Chem.*, 2001, **40**, 3413; Y. Jahng, J. Hazelrigg, D. Kimball, E. Riesgo, F. Wu and R.P. Thummel, *Inorg. Chem.*, 1997, **36**, 5390.
  118. H.V Balzani, A. Juris , M. Venturi, S. Campagua and S. Serroui, *Chem. Rev.*, 1996, **96**, 759, and references cited therein.
  119. B.J. Hathaway, D.G. Holah and J.D. Postlethwaite, *J. Chem. Soc.*, 1961, 3215.
  120. Kubas, *Inorg. Synth.*, 1979, **19**, 90.
  121. L.S Banner, AL. Bach., *J. Am. Chem. Soc.*, 1978, **100**, 6099; LS Banner, AL. Bach., *Inorg. Synth.*, 1982, **21**, 47.
  122. A. Miedanar and D.L. DuBois, *Inorg. Chem.*, 1988, **27**, 2479.
  123. P.G. Pringle, B.L. Shaw, *J. Chem. Soc., Chem. Commun.*, 1982, 81.
  124. A. Maisonnat, J.P. Farr and A.L. Balch, *Inorg. Chim. Acta.*, 1981, **53**, L217.
  125. J.P. Farr, F.E. Wood and A.L. Balch, *Inorg. Chem.*, 1983, **22**, 3387
  126. T. Suzuki, M. Kita, K. Kashiwabara and J. Fujita, *Bull. Chem. Soc. Jpn.*, 1990, **63**, 3434.
  127. T. Suzuki and J. Fujita, *Bull. Chem. Soc. Jpn.*, 1992, **65**, 1016.
  128. Z.Z. Zhang, H. Cheng, *Coord. Chem. Rev.*, 1996, **147**, 1.
  129. S.H. Sookraj, Ph.D. Thesis, University of Natal, 1994.

130. J.P. Farr, M.M. Olmstead and A.L. Balch, *Inorg. Chem.*, 1983, **22**, 1229.
131. P.E. Garren, *Chem. Rev.*, 1981, **81**, 229.
132. T. Ukai, H. Kawazura, Y. Ishi, J.J. Bonnet, J.A. Ibers, *J. Organomet. Chem.*, 1974, **65**, 253; Y. Takahashi, Ts. Ito and Y. Ishi, *J. Chem. Soc., Chem. Commun.*, 1970, 1065.
133. H. Tanaka and H. Kaezura, *Bull. Chem. Soc. Jpn.*, 1979, **52**, 2815; K. Moseley and P.M. Maitlis, *J. Chem. Soc., Chem. Commun.*, 1971, 1604; K. Moseley and P.M. Maitlis, *J. Chem. Soc., Dalton Trans.*, 1974, 169.
134. P. Sohár, *Nuclear Magnetic Resonance Spectroscopy*, CRC Press, Boca Raton, 1983, vol. 1, pp 126.
135. P.M. Maitlis, P. Espinet and M.J.H. Russel, in *Comprehensive Organometallic Chemistry*, Eds. G. Wilkinson, F.G.A. Stone and E.W. Abel, Pergamon Press, Oxford, England, 1982, Vol. 6, p 265.
136. T. Suzuki, N. Iitaka, S. Kurachi, M. Kita, K. Kashiwabara, S. Ohba and J. Fujita, *Bull. Chem. Soc. Jpn.*, 1992, **65**, 1817.
137. R.J. Blau, J.H. Espenson, *Inorg. Chem.*, 1986, **25**, 878; A. Miedaner, D.L. DuBois, *Inorg. Chem.*, 1988, **27**, 2479.
138. K. Tani, S. Nakamura, T. Yamagata and Y. Kataoka, *Inorg. Chem.*, 1993, **32**, 5398.
139. R. Garrone, A.M. Romano, R. Santi and R. Millini, *Organometallics*, 1998, **17**, 4519 and references cited therein.
140. P. Wehman, V.E. Kaasjager, W.G.J. de Lange, F. Hartl, P.C.J. Kramer and P.W.N.M. van Leeuwen, *Organometallics*, 1995, **14**, 3751.
141. N. Ito, T. Saji and S. Aoyagui, *Bull. Chem. Soc. Jpn.*, 1985, **58**, 2326.
142. A. Klein and M. Niemeyer, *Z. Anorg. Allg. Chem.*, 2000, **626**, 1191.
143. A.R. Brown, Z. Guo, F.W.J. Mosselmans, S. Parsons, M. Schröder and L.J. Yellowlees, *J. Am. Chem. Soc.*, 1998, **120**, 8805.
144. E.J.L. McInnes, R.D. Farley, C.C. Rowlands, A.L. Welch, L. Rovatti and L.J. Yellowlees, *J. Chem. Soc., Dalton Trans.*, 1999, 4203; E.J.L. McInnes, A.J. Welch and L.J. Yellowlees, *J. Chem. Soc., Chem. Commun.*, 1996, 2393.
145. E.J.L. McInnes, R.D. Farley, S.A. Macgregor, K.J. Taylor, L.J. Yellowlees and C.C. Rowlands, *J. Chem. Soc., Faraday Trans.*, 1998, **94**, 2985; Volger, B. Schwederski, A. Klein and W. Kaim, *J. Organomet. Chem.*, 1992, **436**, 367; A. Klein and W. Kaim, *Organometallics*, 1995, **14**, 1176; P.S. Braterman, J-I Song, F.M. Wimmer, S. Wimmer, W. Kaim, A. Klein and R.D. Peacock, *Inorg. Chem.*, 1992, **31**, 5084; P.S. Braterman, J-I Song, C. Volger and W. Kaim, *Inorg. Chem.*, 1992, **31**, 222.

146. G. Sanna, G. Minghetti, A. Zucca, M.I. Pilo, R. Seeber and F. Laschi, *Inorg. Chim. Acta*, 2000, **305**, 189; J.A. Zuleta, J.M. Bevilacqua, D.M. Proserpio, P.D. Harvey and R. Eisenberg, *Inorg. Chem.*, 1992, **31**, 2396; J.A. Zuleta, M.S. Burberry and R. Eisenberg, *Coord. Chem. Rev.*, 1990, **97**, 47; D. Collison, F.E. Mabbs, E.J.L. McInnes, K.J. Taylor, A.J. Welch and L.J. Yellowlees, *J. Chem. Soc., Dalton Trans.*, 1996, 329; L. Yang, F.L. Wimmer, S. Wimmer, J. Zhao and P.S. Braterman, *J. Organomet. Chem.*, 1996, **525**, 1.
147. *Comprehensive Organometallic Chemistry* (1<sup>st</sup> Edition), eds. E.W. Abel, F.G.A. Stone and G. Wilkinson, Pergamon Press Ltd, Oxford, 1982, Vol. 6.
148. C. Amatore, M. Azzabi and A. Jutand, *J. Organomet. Chem.*, 1989, **363**, 41.
149. I. Gauthron, Y. Mugnier, K. Hierso and P.D. Harvey, *New J. Chem.*, 1998, 237.
150. J.V. Zeile Krevor and L. Yee, *Inorg. Chem.*, 1990, **29**, 4305.
151. G. Nemra, P. Lemoine, P. Braunstein, C. de Meric de Bellefon and M. Ries, *J. Organomet. Chem.*, 1986, **304**, 245.
152. R.J. Charlton, C.M. Harris, H. Patil and N.C. Stephenson, *Inorg. Nucl. Chem. Letters*, 1966, **2**, 409.
153. R.J. Butcher and E. Sinn, *J. Chem. Soc., Dalton Trans.*, 1976, 1186.
154. M. Haukka, J. Kiviaho, M. Ahlgrén, T.A. Pakkanen, *Organometallics*, 1995, **14**, 825.
155. W.G. Klemperer and B. Zhong, *Inorg. Chem.*, 1993, **32**, 5821.
156. K.-B. Shiu, W.-M. Lee, C.-L. Wang, S.-L. Wang, F.-L. Liao, J.-C. Wang, L.-S. Liou, S.-M. Peng, G.-H. Lee, M.Y. Chiang, *Organometallics*, 1996, **15**, 2979; K.-B. Shiu, C.-H. Li, T.-J. Chan, S.-M. Peng, M.-C. Cheng, S.-L. Wang, F.-L. Liao, M.Y. Chang, *Organometallics*, 1995, **14**, 524; G.R. Crooks, B.F.G. Johnson, J. Lewis, I.G. Williams, G. Gamlen, *J. Chem. Soc. (A)*, 1969, 2761.
157. R.W. Hiltz, S.J. Sherlock, M. Cowie, E. Singleton and M.M. de V. Steyn, *Inorg. Chem.*, 1990, **29**, 3161; E. Singleton, P.H. van Rooyen and M.M. de V. Steyn, *S. Afr. J. Chem.*, 1989, **42**, 57; S.J. Sherlock, M. Cowie, E. Singleton and M.M. de V. Steyn, *Organometallics*, 1988, **7**, 1663.
158. P. Homanen, M. Haukka, M. Ahlgrén, T.A. Pakkanen, P.N.W. Baxter, R.E. Benfield, J.A. Connor, *J. Organomet. Chem.*, 1998, **552**, 205.
159. K.-B. Shiu, C.-H. Li, T.-J. Chan, S.-M. Peng, M.-C. Cheng, S.-L. Wang, F.-L. Liao, M.Y. Chang, *Organometallics*, 1995, **14**, 524.
160. D.St.C. Black, G.B. Deacon, N.C. Thomas, *Aust. J. Chem.* 1982, **35**, 2445.
161. M.-N. Collomb-Dunand-Sauthier, A. Deronzier, R. Ziessel, *J. Electroanal. Chem.*, 1991, **319**, 347.

162. H. Ishida, K. Kujiki, T. Ohba, K. Ohkubo, K. Tanaka, T. Terada, T. Tanaka, *J. Chem. Soc., Dalton Trans.*, 1990, 2155.
163. J.E. Cyr and P.H. Rieger, *Organometallics*, 1991, **10**, 2153.
164. see for example : M. Kaneko, D. Wörhle, in *Advances in Polymer Sciences*, Vol.84, Springer Verlag, Berlin, 1998, 141; H.D. Abruña, *Coord. Chem. Rev.*, 1988, **86**, 135; A. Mertz, in *Electrochemistry IV, Topics in Current Chemistry*, Vol. 152, Ed. Steckhan, E., Springer Verlag, Berlin, 1990, 51; A. Deronzier, J.-C. Moutet, *Coord. Chem. Rev.*, 1996, **147**, 339; D. Curran, J. Grimshaw, S.D. Perera, *Chem. Soc. Rev.*, 1991, **20**, 391.
165. A.F. Diaz, K. Kanazawa and G.P. Gardini, *J. Chem. Soc., Chem. Com.*, 1979, 635.
166. K.K. Kanazawa, A.F. Diaz, R.H. Geiss, W.D. Gill, J.F. Kwak, J.A. Logan, J.F. Robolt and G.B. Street, *J. Chem. Soc., Chem. Commun.*, 1979, 854.
167. A.F. Diaz, J. Crowley, J. Bargon, G.P. Gardini and J.B. Torrance, *J. Electroanal. Chem.*, 1981, **121**, 355.
168. S. Sadki, P. Schottland, N. Brodie and G. Sabouraud, *Chem. Soc. Rev.*, 2000, **29**, 283.
169. B.L. Funt and A.F. Diaz, *Organic Electrochemistry: an Introduction and a Guide*, Marcel Dekker, New York, 1991, 1337; E.M. Genies, G. Bidan and A.F. Diaz, *J. Electroanal. Chem.*, 1983, **149**, 101.
170. For reviews on this topic see A. Deronzier and J.-C. Moutet, *Coord. Chem. Rev.*, 1996, **147**, 339; D. Curran, J. Grimshaw and S.D. Perera, *Chem. Soc. Rev.*, 1991, **20**, 391; S.J. Higgins, *Chem. Soc. Revs.*, 1997, **26**, 247.
171. Examples of polypyrrole supported Ru(II) polypyridyl complexes; A.R. Guadalupe, X. Chen, B.P. Sullivan and T.J. Meyer, *Inorg. Chem.*, 1993, **32**, 5502; J.G. Eaves, H.S. Munro and D. Parker, *Inorg. Chem.*, 1987, **26**, 644; M.-N. Collomb Dunand-Sauthier, A. Deronzier, J.-C. Moutet and S. Tingry, *J. Chem. Soc., Dalton Trans.*, 1996, 2503; C. Lopez, J.-C. Moutet and E. Saint-Aman, *J. Chem. Soc., Faraday Trans.*, 1996, **92**, 1527; W.F.D. Giovani and A. Deronzier, *J. Chem. Soc., Chem. Commun.*, 1992, 1461; M.-N. Collomb-Dunand-Sauthier, A. Deronzier, H. Lebozec and M. Navarro, *J. Electroanal. Chem.*, 1996, **410**, 21.
172. M.-N. Collomb-Dunand-Sauthier, A. Deronzier, R. Ziessel, *J. Phys. Chem.*, 1993, **97**, 5973.
173. C. Caix, S. Chardon-Noblat, A. Deronzier and R. Ziessel, *J. Electroanal. Chem.*, 1996, **403**, 189.
174. S. Cosnier, A. Deronzier and J.-C. Moutet, *J. Electroanal. Chem.*, 1985, **193**, 193; S. Cosnier, A. Deronzier and J.-F. Roland, *J. Electroanal. Chem.*, 1990, **285**, 133
175. A. Deronzier, J.C. Moutet, *Acc. Chem. Res.*, 1989, **22**, 249.
176. F. Bedioui, J. Devynck and C. Bied-Charreton, *Acc. Chem. Res.*, 1995, **28**, 30.
177. J.G. Eaves, H.S. Munro and D. Parker, *Inorg. Chem.*, 1987, **26**, 644.



178. A. Deronzier, J.-C. Moutet and D. Zsoldos, *J. Phys. Chem.*, 1994, **98**, 3086.
179. S. Chardon-Noblat, M.-N. Collomb-Dunand-Sauthier, A. Deronzier, M. Orillon, R. Ziessel, D. Zsoldos, French Pat. Appl. 96.04840, 1996; U.S. Pat. WPB 39500, 1997.
180. S. Cosnier, A. Deronzier and J.-C. Moutet, *J. Electroanal. Chem.*, 1986, **207**, 315.
181. S. Cosnier, A. Deronzier and J.-C. Moutet, *J. Electroanal. Chem.*, 1990, **291**, 243.
182. G. K. Chandler and D. Pletcher, *Electrochemistry, Specialist Periodical Reports*, Royal Society of Chemistry, London, 1986, pp. 117-150.
183. G. de Leeuw, J.S. Field, R.J. Haines, B. McCulloch, E. Meintjies, C. Monberg, G.M. Olivier, P. Ramdial, C.N. Sampson, B. Sigwarth, N.D. Steen and K.G. Moodley, *J. Organomet. Chem.*, 1982, **228**, C66; G. de Leeuw, J.S. Field, R.J. Haines, C. McCulloch, E. Meintjies, C. Monberg, G.M. Olivier, P. Ramdial, C.N. Sampson, B. Sigwarth, N.D. Steen and K.G. Moodley, *ibid*, 1984, **275**, 99.
184. K.A. Johnson and W.L. Gladgeler, *Organometallics*, 1989, **8**, 2866; H.A. Mirza, J.J. Vittal and R.J. Puddephatt, *Inorg. Chem.*, 1993, **32**, 1327.
185. C.J. Parry, Ph.D. Thesis, University of Natal, 1994.
186. G.R. Crooks, B.F.G. Johnson, J. Lewis, I.G. Williams and G. Graham, *J. Chem. Soc.(A)*, 1969, 2761.
187. D.S. Bohle and H. Vahrenkamp, *Inorg. Chem.*, 1990, **29**, 1097.
188. R.J. Haines, in *Comprehensive Organometallic Chemistry II*, eds. E.W. Abel, F.G.A. Stone and G. Wilkinson, Pergamon, Oxford, 1995. Vol. 7. Ch 11.
189. K.-B. Shin, W.-M. Lee, C.-L. Wang, S.-L. Wang, F.-L. Liao, J.-C. Wang, L.-S. Liou, S.-M. Peng, G.-H. Lee and M.Y. Chiang, *Organometallics*, 1996, **15**, 2979.
190. J.S. Field, R.J. Haines, C.J. Parry, *J. Chem. Soc., Dalton Trans.*, 1997, 2843.
191. C.J.O'Connor and E. Sinn, *Inorg. Chem.*, 1978, **17**, 2067.
192. D.M. Klassen, *Inorg. Chem.*, 1976, **15**, 3166.
193. C.A. Hunter and J.K.M. Sanders, *J. Am. Chem. Soc.*, 1990, **112**, 5525.
194. M.P. Aarnts, F. Hartl, K. Peelen, D.J. Stufkens, C. Amatore and J.-N. Verpeaux, *Organometallics*, 1997, **16**, 4686.
195. H.A. Schwarz and R.W. Dodson, *J. Phys. Chem.*, 1989, **93**, 409; P.S. Surdhar, S.P. Mezyk and D.A. Armstrong, *J. Phys. Chem.*, 1989, **93**, 3360.
196. S. Ernst and W. Kaim, *J. Am. Chem. Soc.*, 1986, **108**, 3578

197. D.D. Perrin, W.L.F. Amarego, D.R. Perrin, in *Purification of Laboratory Chemicals*, 2<sup>nd</sup> Ed., Pergamon Press, New York, 1980.)
198. A.C.T. North, D.C. Philips, F.S. Mathews, *Acta Crystallogr., Sect. A*, 1968, **24**, 351.
199. SHELX-97, G.M. Sheldrick, Institut Anorg. Chemie, University of Gottingen, 1997.
200. P. McArdle, *J. Appl. Cryst.*, 1995, **28**, 65.
201. L.J. Farrugia, *J. Appl. Cryst.*, 1997, **30**, 565.
202. R.R. Cagné, C.A., Koval and C.G. Lisensky, *Inorg. Chem.*, 1980, **19**, 2854; G. Gritzner and J. Kuta, *Pure Appl. Chem.*, 1984, **56**, 461.
203. J.A. Bard and L.R. Faulkner, *Electrochemical Methods, Fundamentals and Applications*, John Wiley and Sons, New York, 1980.
204. G.A. Gruver, T. Kuwana, *J. Electroanal. Chem.*, 1972, **36**, 85.
- 205 Hypercube, Inc., 1115 NW 4<sup>th</sup> St., Gainesville, Florida 32601-4256.